AZOBENZENE-MODIFIED BETA-CYCLODEXTRIN: MOLECULES, MATERIALS AND MOLECULAR DEVICES

Noby Charn Keng Leong

Thesis submitted for the degree of

Doctor of Philosophy

In

The University of Adelaide

School of Physical Sciences

July, 2017

Contents

Abstract v
Declaration vii
Acknowledgments viii
Abbreviations ix

Chapter 1: Introduction

1.1 Supramolecular Chemistry 2
1.2 Cyclodextrins - General 4
1.2.1 Analysis of Host-Guest Complexes 6
1.2.2 Thermodynamics 7
1.2.3 Enthalpy-Entropy Compensation Effect 8
1.3 Modified Cyclodextrins 10
1.3.1 Cyclodextrin Oligomers 13
1.3.2 Polymeric Hydrogels 17
1.4 Mechanically Interlocked Molecules 25
1.4.1 Rotaxanes and Pseudorotaxanes 26
1.4.2 Polyrotaxanes and Polypseudorotaxanes 27
1.4.3 Daisy Chains 28
1.4.4 Towards Molecular Devices 31
1.5 Molecular Devices 32
1.5.1 Types of Device 32
1.5.2 Molecular Devices on Particles and Surfaces in Materials 34
1.5.3 Barriers to Success 37
1.6 Azobenzene 38
1.6.1 Mechanism of Isomerisation 39
1.6.2 Perturbations of Isomerisation 40
1.6.3 Effect of Cyclodextrin 41
1.7 Research Objectives 42
1.7.1 Aims and Sequence of this Research 43
1.8 References 44

Chapter 2: Synthesis and Photochemistry of Structural Isomers of Azobenzene-linked β-Cyclodextrin Dimers

2.1 Introduction 52
2.1.1 Aims of this study 53
2.2 Results and Discussion 54
2.2.1 Synthesis of β-CD Dimers 54
2.2.2 Characterisation of Photochemical Properties of the *p*-βCD$_2$az and *m*-βCD$_2$az Dimers 63
2.2.3 Effect of guest complexation on the isomerisation properties of the *p*-β-CD$_2$az and *m*-β-CD$_2$az Dimers 75
2.3 Conclusion 85
2.4 References 86
2.5 Appendix 88

Chapter 3: Host-Guest Chemistry of Modified β-Cyclodextrin Oligomers

3.1 Introduction 94
3.1.1 Organic Dyes 94
3.1.2 Dimerisation of CV^+, RB and EO^- 96
3.1.3 Complexation of CV^+, RB and EO^- by β-CD 97
3.1.4 Aims of this study 97
3.2 Results and Discussion 98
3.2.1 Complexation of CV^+, RB and EO^- by β-CD, *E*-*p*-βCD$_2$az and β-CDab 98
3.3 Conclusion 128
3.4 References 129
3.5 Appendix 131

Chapter 4: Complexation of Porphyrins by β-Cyclodextrin Oligomers

4.1 Introduction 148
4.1.1 Porphyrins 148
4.1.2 Porphyrin Speciation 149
4.1.3 Aggregation of Porphyrins 150
4.1.4 Complexation with Cyclodextrins 152
4.1.5 Aims of this study 153

4.2 Results and Discussion 155
4.2.1 Complexation of H_2TSPP^{4-}, H_3TCPP^{3-}/H_2TCPP^{4-}, H_2TMAP^{4+} and H_2TMPyP^{4+} by β-CD and β-CDab 155
4.3 Conclusion 209
4.4 References 210
4.5 Appendix 212

Chapter 5: Investigation of Polymeric Hydrogels using β-Cyclodextrin Oligomers and Adamantane- and Alkyl-substituted Poly(acrylate)s

5.1 Introduction to Polymeric Hydrogels 234
5.1.1 Aims of this study 236
5.2 Results and Discussion 238
5.2.1 Synthesis of polymers 238
5.2.2 Complexation of PAAADen, PAAADhn, PAAADddn and PAAC12 by β-CD, β-CDab, *E*-*p*-β-CD_2az and *E/Z*-*m*-β-CD_2az 239
5.2.3 Macroscopic properties studies 301
5.3 Conclusions 308
5.4 References 309
5.5 Appendix 311

Chapter 6: Synthesis of β-Cyclodextrin-based Molecular Muscles

6.1 Introduction 314
6.1.1 Molecular Muscles 314
6.1.2 Aims of this study 318
6.2 Results and Discussion 320
6.2.1 Synthesis of β-CDazpr 320
6.2.2 Self-Assembly of β-CDazpr 320
6.2.3 Synthesis of Molecular Muscles 323
6.2.4 Molecular Muscle Design Considerations 329
6.3 Conclusion 331
6.4 References 332

Chapter 7: Experimental

7.1 General Experimental 336
7.1.1 Materials 338
7.2 Chapter 2 Experimental 339
7.2.1 Syntheses 339
7.2.2 Sample Preparation 345
7.3 Chapter 3 Experimental 346
7.3.1 Sample Preparation 346
7.4 Chapter 4 Experimental 347
7.4.1 Sample Preparation 347
7.5 Chapter 5 Experimental 348
7.5.1 Syntheses 348
7.5.2 Sample Preparation 350
7.6 Chapter 6 Experimental 351
7.6.1 Syntheses 351
7.7 References 354

Chapter 8: Conclusion

8.1 Conclusion and Future Directions 356

Abstract

Cyclodextrins (CD) are naturally occurring macrocycles composed of α-1,4-linked *D*-glucopyranose units. CDs are common components in supramolecular chemistry owing to their ability to act as hosts to complex a wide variety of guests. Similarly, azobenzene has frequently been used in supramolecular chemistry as a photoswitchable moiety. We have explored the combined utility of CDs and azobenzene to explore supramolecular systems on the molecular, material and molecular device scale.

Chapter 1 summarises CD and azobenzene chemistry. The applications of CDs are explored, including its use as components of polymeric hydrogels, mechanically interlocked molecules and molecular devices.

Chapter 2 describes the attempted synthesis of three structural isomers of azobenzene-linked β-CD dimers, in which the β-CD substituent is attached to the *para*, *meta* or *ortho* position of both phenyl rings of azobenzene to give *bis*(6^{A}-deoxy-β-cyclodextrin-6^{A}-yl)-4,4'-aminocarbonylazobenzene (*p*-β-CD$_2$az), *bis*(6^{A}-deoxy-β-cyclodextrin-6^{A}-yl)-3,3'-aminocarbonylazobenzene (*m*-β-CD$_2$az) and *bis*(6^{A}-deoxy-β-cyclodextrin-6^{A}-yl)-2,2'-aminocarbonylazobenzene (*o*-β-CD$_2$az), respectively. The aim of this research was to determine the effect of structural isomerisation on the photochemical properties of β-CD dimers. The synthesis of *p*-β-CD$_2$az and *m*-β-CD$_2$az was successful, while the synthesis of *o*-β-CD$_2$az did not yield the desired compound. Instead, (6^{A}-deoxy-β-cyclodextrin-6^{A}-yl)-2-aminocarbonyl-aminobenzene (β-CDab) was produced. The photoisomerisation properties of *p*-β-CD$_2$az and *m*-β-CD$_2$az were examined by NMR and UV-vis spectroscopy.

Chapter 3 investigated the host-guest complexation properties of β-CD, β-CDab and *E*-*p*-β-CD$_2$az. Three dyes were chosen as guests: cationic crystal violet (CV^{+}), zwitterionic rhodamine B (RB) and anionic ethyl orange (EO^{-}). The host-guest complexes were qualitatively studied by NMR spectroscopy. The complexation constants and thermodynamic parameters were determined by UV-vis spectroscopy.

Chapter 4 explored the effect of guest modification on the host-guest complexation properties of β-CD and β-CDab. Four porphyrins were chosen as guests: *meso*-tetra(4-sulfonatophenyl)porphine (TSPP), *meso*-tetra(4-carboxyphenyl)porphine (TCPP), meso-tetra(4-*N*,*N*,*N*-trimethylanilinium)porphine (TMAP) and *meso*-tetra(*N*-methyl-4-pyridyl)porphine (TMPyP). The host-guest complexation properties were studied by NMR spectroscopy. The complexation constants and thermodynamic parameters were determined by UV-vis spectroscopy.

Chapter 5 investigated the complexation between β-CD, β-CDab, *E*-*p*-β-CD_2az and *E/Z*-*m*-β-CD_2az and hydrophobe-substituted poly(acrylates) (PAA) in the formation of polymer hydrogels. The molecular-scale complexation properties were investigated to understand the factors that influence the bulk-material properties of the solutions. Three adamantane (AD) substituted PAAs were chosen for study, in which the length of the alkyl tether connecting the AD group to the PAA backbone was an ethyl, hexyl or dodecyl group (PAAADen, PAAADhn and PAAADddn, respectively). One dodecyl substituted PAA (PAAC12) was also chosen for study. The host-polymer complexation was qualitatively investigated by NMR spectroscopy. The complexation constants and thermodynamic parameters were investigated by isothermal titration calorimetry. The macroscopic properties of the host-polymer solutions were investigated by rheology.

Chapter 6 describes the attempted synthesis of three azobenzene-modified β-CD-based molecular muscles, differing by the choice of blocking groups as either adamantane, aza-18-crown-6 and 1,4,7,10-tetraazacyclododecane-1,4,7,10-tetraacetic acid (DOTA). The synthesis of an azobenzene-linked β-CD compound was successful. However, the attachment of the blocking groups was not successful.

Chapter 7 describes detailed procedures for experiments in Chapters 2 – 6. The research presented in this thesis hopes to extend our understanding of azobenzene-modified β-CD compounds used on the molecular, material and molecular device scale, as summarised in Chapter 8.

Declaration

I certify that this work contains no material which has been accepted for the award of any other degree or diploma in my name, in any university or other tertiary institution and, to the best of my knowledge and belief, contains no material previously published or written by another person, except where due reference has been made in the text. In addition, I certify that no part of this work will, in the future, be used in a submission in my name, for any other degree or diploma in any university or other tertiary institution without the prior approval of the University of Adelaide and where applicable, any partner institution responsible for the joint-award of this degree.

I give consent to this copy of my thesis when deposited in the University Library, being made available for loan and photocopying, subject to the provisions of the Copyright Act 1968. I acknowledge that copyright of published works contained within this thesis resides with the copyright holder(s) of those works. I also give permission for the digital version of my thesis to be made available on the web, via the University's digital research repository, the Library Search and also through web search engines, unless permission has been granted by the University to restrict access for a period of time.

I acknowledge the support I have received for my research through the provision of an Australian Government Research Training Program Scholarship.

Noby Leong

18/07/2017

Acknowledgments

The PhD experience has been a defining episode in my life, filled with the complete set of intellectual battles and emotional hurdles one faces when embarking on a research career. Throughout a seemingly never-ending series of experiments and writings, I have relied on the support of many people. With my deepest sincerity, I must thank them. To my supervisor, Associate Professor Tak Kee, thank you for going on this journey and taking me to the finish line.

To the continually evolving Lab 8 Roster, I have many thanks, for I spent most of my days with you. To Dr Truc Pham, for showing me the ropes; you have defined my experimental skillset and helped me hone my scientific mind. To Trang Nguyen, Hamish McTernan, Liang Yan, Hillary Coleman, Jianjia Liu and the many other lab mates that came and went, I sincerely thank you. We shared a journey that was indescribable to the rest of our friends and family. We toiled together through failed experiments, scooped papers and much more. You were my scientific family that I continually relied on for advice, support and comradery.

Thank you to the many support staff and collaborators who have helped along the way. Thanks to Phil Clements, Matthew Bull and the Chemical Store for troubleshooting, bouncing off ideas and sourcing the all-important chemicals. Thanks to Professor Xuhong Guo and Wang Meng Xue from East China University of Science and Technology for your help with all aspects of rheology. Thanks to Dr Campbell Coghlan for lending your crystallographic knowledge.

To my chemistry cohort, I thank you also. To Justin Spence, Jack Evans, Andrew Tarzia and countless others, you were with me from the beginning of undergraduate uni to the final days of postgraduate life. We have truly gone on a unique journey together.

Finally, to my friends and family, not only for supporting me throughout these many years but for generally putting up with me. Throughout this PhD experience, I have been elated by successful experiments, discouraged by failed ones, depressed through terribly failed ones and non-plussed when asked “So how’s that PhD going?” Despite my many mood swings, you all stood by and encouraged me. Thank you Philip, for helping me over the line, thanks to my parents for always being there and feeding my self-worth and thank you to all the many faces - real-life, online and abroad - that helped me along the way. Couldn’t have done it without you!

Abbreviations

General

Å	Angstrom
Az	Aryl
δ	chemical shift (ppm)
ΔG	Gibbs free energy change
ΔH	enthalpy change
ΔS	entropy change
ε	molar absorptivitiy (mol-1 dm-3 cm-1)
E	heat of formation
et al.	et alia
Hz	hertz
I	ionic strength
ITC	isothermal titration calorimetry
J	coupling constant (Hz)
K_{xy}	stability constant for x:y host-guest compexation (dm-3 mol-1)
K_a	acid dissociation constant
K_D	dimerisation constant
λ	wavelength
m/z	mass:charge ratio
MALDI TOF	matrix-assisted laser desorption-ionisation time-of-flight
MS	mass spectrometry
NMR	nuclear magnetic resonance imaging
NOE	nuclear Overhauser effect
NOESY	nuclear Overhauser effect spectroscopy
pD	-log[D+]
pH	-log[H+]
p*Ka*	-log[Ka]

ppm	parts per million
PS	Photostationary state
QTOF	Quadropole time-of-flight
R_c	relative retention factor to native cyclodextrin (in TLC)
R_f	retention factor
ROESY	rotating-frame nuclear Overhauser effect correlation spectroscopy
TLC	thin layer chromatography
UV-vis	ultra violet-visible
wt	weight

Chemicals

6β-CDTs	6^A-O-(4-methylbenzenesulfonyl)-β-CD
6β-$CDNH_2$	6^A-amino-6^A-deoxy-β-CD
α-, β-, γ-CD	α-, β-, γ-cyclodextrin
AD	adamatane
ADC	1-adamantanecarboxylate
ADCA	1-adamantanecarboxylic acid
ADddn	*N*-(2-aminododecyl)-adamantane-1-carboxyamide
ADen	*N*-(2-aminoethyl)-adamantane-1-carboxyamide
ADhn	*N*-(2-aminohexyl)-adamantane-1-carboxyamide
ADnp	1-(4-nitrophenyloxylcarbonyl)adamantane
aza-18-crown-6	1,4,7,10,13-pentaoxa-16-azacyclooctadecane
aza-18-crown-6-COOH	2-(1,4,7,10,13-pentaoxa-16-azacyclooctadecan-16-yl)acetic acid
β-CDab	(6^A-deoxy-β-cyclodextrin-6^A-yl)-2-aminocarbonyl-aminobenzene
β-CDaz	(*E*)-*N*-(6^A-deoxy-β-cyclodextrin-6A-yl)-4-aminocarbonyl-4'-carboxyazobenzene
β-CDazpr	(*E*)-*N*-(6^A-deoxy-β-cyclodextrin-6^A-yl)-4-aminocarbonyl-4'-carboxyazobenzene
C12	dodecyl
CD	cyclodextrin
CV^+	crystal violet

DCC	dicyclohexylcarbodiimide
ddn	dodecyl
DMSO	dimethylsulfoxide
DMT-MM	4-(4,6-dimethoxy-1,3,5-triazin-2-yl)-4-methylmorpholinium chloride
DOTA	1,4,7,10-tetraazacyclododecane-1,4,7,10-tetraacetic acid
E-*m*-AzCOOH	*meta*-*E*-azobenzene-dicarboxylic acid
en	ethyl
EO^-	ethyl orange
E-*o*-AzCOOH	*ortho*-*E*-azobenzene-dicarboxylic acid
E-*o*-Aznp	*bis*(4-nitrophenyl)-*E*-2,2'-dicarboxyazobenzene
E-*p*-AzCOOH	*para*-*E*-azobenzene-dicarboxylic acid
hn	hexyl
HoBT	hydroxybenzotriazole
K_2.*E*-*p*-Az$(COO)_2$	*E*-4,4'-azobenzene-dicarboxylate
m-β-CD_2az	*bis*(6^A-deoxy-β-cyclodextrin-6^A-yl)-3,3'-aminocarbonylazobenzene
o-β-CD_2az	*bis*(6^A-deoxy-β-cyclodextrin-6^A-yl)-2,2'-aminocarbonylazobenzene
PAA	poly(acrylate)
PAAADddn	1-(12-aminododecyl)-adamantane-1-carboxyamide poly(acrylate)s
PAAADen	1-(2-aminoethyl)-adamantane-1-carboxyamide poly(acrylate)s
PAAADhn	1-(6-aminohexyl)-adamantane-1-carboxyamide poly(acrylate)s
PAAC12	dodecyl-substituted poly(acrylate)s
p-β-CD_2az	*bis*(6^A-deoxy-β-cyclodextrin-6^A-yl)-4,4'-aminocarbonylazobenzene
RB	rhodamine B
TCPP	*meso*-tetra(4-carboxyphenyl)porphine
TMAP	*meso*-tetra(4-*N,N,N*-trimethylanilinium)porphine
TMPyP	*meso*-tetra(*N*-methyl-4-pyridyl)porphine
TsCl	*para*-toluenesulfonyl chloride
TSPP	*meso*-tetra(4-sulfonatophenyl)porphine

This page is intentionally left blank

CHAPTER 1

Introduction

1.1 Supramolecular Chemistry

The sophistication and wizardry of natural biological processes have long inspired chemists. Biological systems engineer discrete subunits, which display diverse and efficient functionalities.[1] These pre-organised subunits self-assemble into highly ordered architectures to eventually form living organisms. The beauty of these natural processes is underpinned by the modularity of nature's approach, which has inspired a new field in science known as supramolecular chemistry.[2]

The term "supramolecular chemistry" was first coined in 1978 by Jean-Marie Lehn, who famously described the field as "chemistry beyond the molecule".[3] Supramolecular chemistry employs biologically inspired principles into the design and synthesis of molecules which can self-assemble into a single entity by intermolecular forces.

Supramolecular chemistry is underpinned by two fundamental concepts- *complementarity* and *pre-organisation*.[4] Broadly, these concepts involve the relationship between at least two molecules- a host and a guest, where a host is described as having convergent binding sites, while a guest, being more spherical in nature, has divergent binding sites.[5] The host and guest experience multiple, cooperative, intermolecular binding interactions (complementarity), with inherent specificity to allow self-assembly (pre-organisation) to form a complex, as summarised in Figure 1.1.

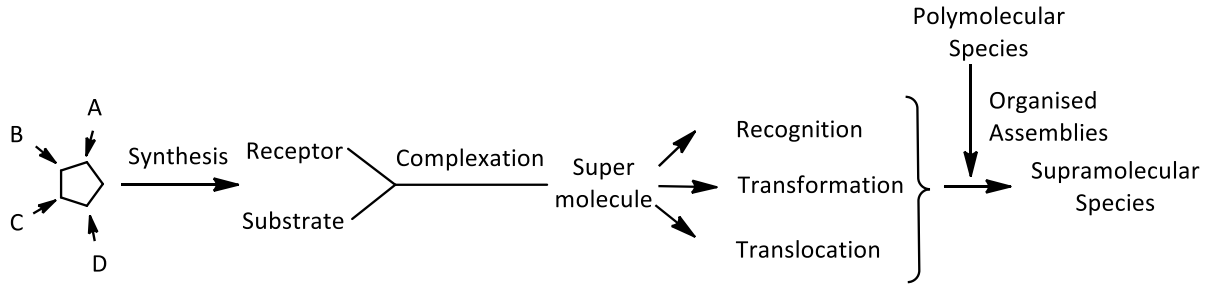

Figure 1.1: The formation of supramolecular species from the self-assembly of monomeric units A, B, C and D.[2]

As the components of supramolecular systems have their own discrete properties, the final utility of a self-assembled complex will be the sum of its individual parts, creating a system where information is intrinsically stored within chemical bonds.[3] Nature abounds with examples which confirm the potential of this approach. One such example is the tobacco mosaic virus (TMV), which may be decomposed into its constituent parts *in vitro* and, when exposed to physiological conditions, spontaneously reassemble through non-covalent interactions to reform a fully functional organism. The TMV system is modular and all information required to form the living TMV organism is encoded within the virus' DNA.[4]

The field of supramolecular chemistry was pioneered by Pedersen, Lehn and Cram. Pedersen and Lehn respectively made breakthroughs in designing structure-specific molecules, called crown ethers (or coronands) and cryptands that possess extraordinary selectivity in complexing metal ions.[2,6,7] This work was continued by Cram, who designed three-dimensional structures capable of selectively binding organic compounds.[5,8-10] For their efforts, Pedersen, Lehn and Cram were jointly awarded the Nobel Prize in Chemistry in 1987 "for their development and use of molecules with structure-specific interactions of high selectivity". Since the pioneering work of these three giants of supramolecular chemistry, the field has greatly expanded to create a vast range of supramolecular architectures with increasing diversity and functionality.

1.2 Cyclodextrins - General

Cyclodextrins (CD), also known as cycloamyloses, are naturally occurring homochiral macrocycles composed of α-1,4-linked D-glucopyranose units, as shown in Figure 1.2. (They are often referred to as native CDs to distinguish them from their modified forms.) The most frequently occurring CDs are α-CD, β-CD and γ-CD, composed of 6, 7 and 8 D-glucopyranose units, respectively, although larger CDs also exist.[11] Each D-glucopyranose unit of CD is labelled from A-H in a clockwise fashion around the annulus.

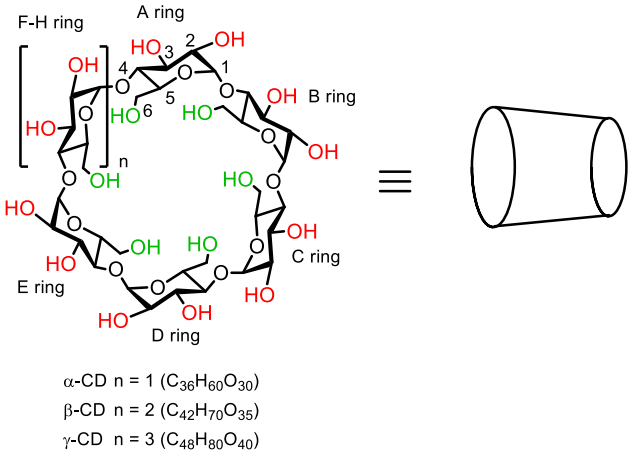

Figure 1.2: Structure of α-, β- and γ-CD, highlighting the primary hydroxyl groups (green) and secondary hydroxyl groups (red) (left) and the approximate molecular shape (right).

The linked D-glucopyranose units adopt a $^4C_1$ chair conformation and are oriented in-register (*cis*) to form a torus shape with a hollow internal annulus.[4] The number of D-glucopyranose units defines the diameter of a CD, with sizes increasing from α-CD to β-CD to γ-CD, as shown in Figure 1.3.

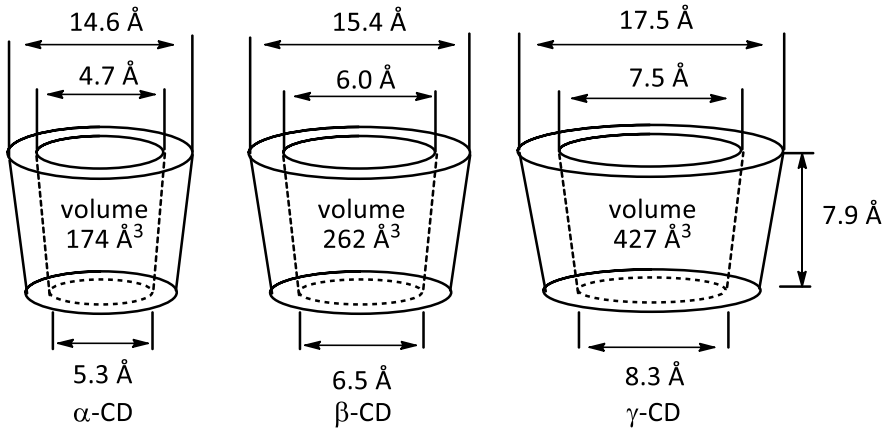

Figure 1.3: Dimensions of α-, β- and γ-CD.[11]

Cyclodextrins possess unique structural properties, which enable them to act as hosts to encapsulate a wide-variety of guests, and places them at the heart of supramolecular chemistry. The torus of a CD is flanked on either end by hydroxyl groups. The primary face, consisting of hydroxyl groups extending from the C6 carbon, is slightly smaller in diameter than the secondary face, which consists of hydroxyl groups attached to the C2 and C3 carbon;[12] these exterior hydroxyl groups give CDs high solubility in aqueous media. In contrast to the external hydrophilic characteristic of CDs, the annulus is lined with skeletal carbons, hydrogen atoms, glycosidic oxygen bridges and non-bonding electron pairs to create a hydrophobic micro-environment, as shown in Figure 1.4. The exterior hydrophilic and interior hydrophobic duality gives CDs their characteristic host-guest complexation properties, satisfying the *cooperativity* requirement of supramolecular chemistry.

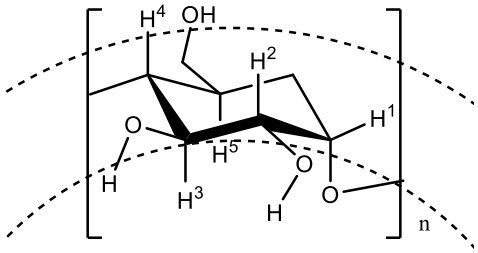

Figure 1.4: Position of one D-glucopyranose unit of CD relative to the macrocyclic structure.

In general, complexation occurs in aqueous media between a CD and hydrophobic guest molecule.[13] The main driving force is the hydrophobic effect, where the hydrophobic portion of the guest becomes dehydrated upon penetration into the CD annulus,[14] as shown in Figure 1.5. The guest and hydrophobic interior of CD experience favourable van der Waals interactions, as well as minimised unfavourable hydrophilic interactions between the hydrophobic guest segments and bulk water. The complexation process is further enhanced by the displacement of water molecules from the CD annulus. The displaced water molecules, which experience incomplete hydrogen bond potentials within the confined CD annulus and are therefore sometimes referred to as “high energy”, reform complete hydrogen bonds with the bulk aqueous media, contributing to favourable enthalpic and entropic gains.

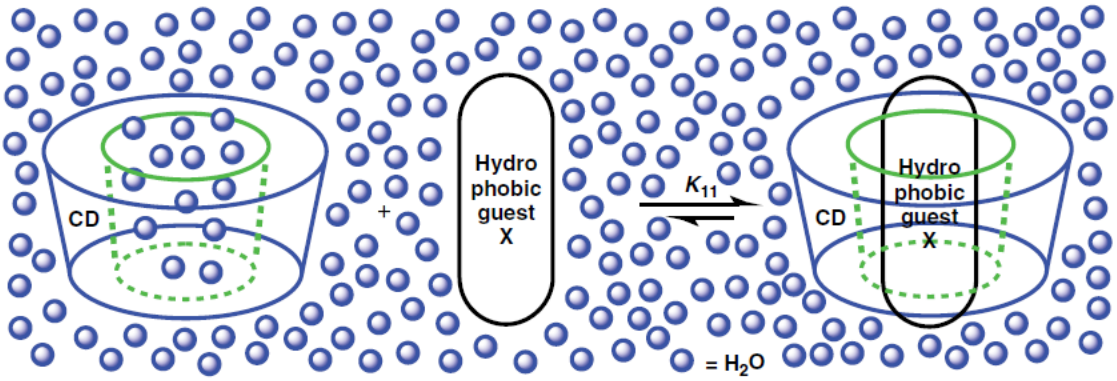

Figure 1.5:The formation of a 1:1 host-guest complex from CD either partially or fully encapsulating a hydrophobic guest in aqueous media.[4]

Other factors may fine tune or strengthen the complexation. Comparable size matching between the guest and CD annulus will enhance complexation as the van der Waals interactions are strongly dependent on the distance of separation. Guests that exhibit similar size profiles to the CD annulus can also reduce conformational strain of an otherwise hollow CD. Various other factors such as guest shape, dipole-dipole interactions, π-π stacking, presence of aliphatic chains or hydroxyl groups, functional groups on CD, solvent and temperature also influence the host-guest complexation.[14-17]

1.2.1 Analysis of Host-Guest Complexes

The formation of host-guest complexes by CDs may be studied both qualitatively and quantitatively. Several NMR techniques such as 2D ^{1}H rotating frame Overhauser enhancement spectroscopy (ROESY) and nuclear Overhauser enhancement spectroscopy (NOESY) are important techniques for qualitative determination of complexation.[18]

When a guest molecule is complexed within a CD annulus, the protons of the guest interact with the interior protons of CD (H3, H5 and H6). As the through-space interaction is less than 4 Å between these two sets of protons, cross-peaks arising from the nuclear Overhauser effect (NOE) occur and generate cross-peaks in the NMR spectrum.[18] As CDs are homochiral, the NMR peaks corresponding to H3, H5 and H6 protons are readily distinguished. However, modification of CDs (see Section 1.3 *Modified Cyclodextrins*) leads to a loss of equivalence between each D-glucopyranose unit and therefore, protons becomes inequivalent, causing superimposition of peaks. Nevertheless, cross-peaks arising from guest protons and H2 – H6 protons of modified CDs are generally found to indicate complexation.[18]

Many other techniques are used to give qualitative analysis of complexation. 2D diffusion-ordered NMR spectroscopy (DOSY) gives diffusion coefficients corresponding to individual proton resonances.[19,20] Identical diffusion coefficients between guest and CD resonances may indicate

complexation as both host and guest form a single entity that diffuses together in solution. Mass spectrometry may also be used to identify a host-guest complex if the complex is stable in the gas phase and soft ionisation techniques are used.[21,22]

However, beyond simple interpretations of the existence of host-guest complexes, chemists have sort to further quantify and understand the strength, stoichiometry and the thermodynamic and kinetic parameters of complexation.

1.2.2 Thermodynamics

Quantitative assessment is gained through host-guest complex stoichiometry and the magnitudes of the associated equilibrium constants (often called the complexation constant when referring to host-guest complexes) and thermodynamics. The simplest CD-guest complex is a 1:1 host-guest complex in which one CD complexes one guest. However, in principle, CDs may exhibit various complexation stoichiometries, as shown in Figure 1.6.

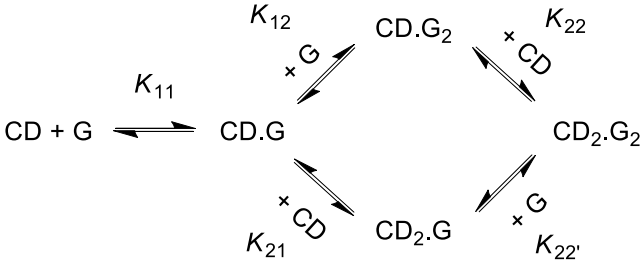

Figure 1.6: Equilibria describing various CD-guest complexation models.

For a 1:1 host-guest complex, the complexation constant, *K*, is given by Equation 1.1, where H is the host and G is the guest. The enthalpy change (ΔH), entropy change (ΔS) and Gibbs free energy change (ΔG) are given by Equations 1.2 and 1.3.

$$K = \frac{[HG]}{[H][G]} \tag{1.1}$$

$$\Delta G = -RTlnK \tag{1.2}$$

$$\Delta G = \Delta H - T\Delta S \tag{1.3}$$

Calorimetric techniques such as isothermal titration calorimetry (ITC) provide a direct determination of the thermodynamic parameters through measurement of heat changes upon complexation of a CD and a guest.[23-25] This is in contrast to indirect methods such as spectroscopic techniques (UV-vis, fluorescence, NMR, circular dichroism), which employ temperature-variable titrations to determine the complexation constants and thermodynamic parameters.

1.2.3 Enthalpy-Entropy Compensation Effect

The change in enthalpy and entropy for the complexation between various CD-guest complexes exhibits a linear relationship, as shown in Figure 1.7. While there is no necessary relationship requiring a linear relationship between the two thermodynamic parameters, such a relationship is often observed. An enthalpy-entropy linear relationship is observed for a series of CD-guest complexation reactions where factors such as the solvent or CD substituent are changed, which critically alter the equilibrium constant. However, the expected change in the equilibrium constant between the complexation reactions is generally smaller than expected when compared with the enthalpic change ($\Delta\Delta H$) alone (i.e. the change in K is not reflected in the change in ΔH). This is due to a compensatory effect of the entropy ($\Delta\Delta S$), which cancels out a large part of the effect of enthalpic change. Hence, the linear relationship between enthalpy and entropy is often called the enthalpy-entropy compensation effect.

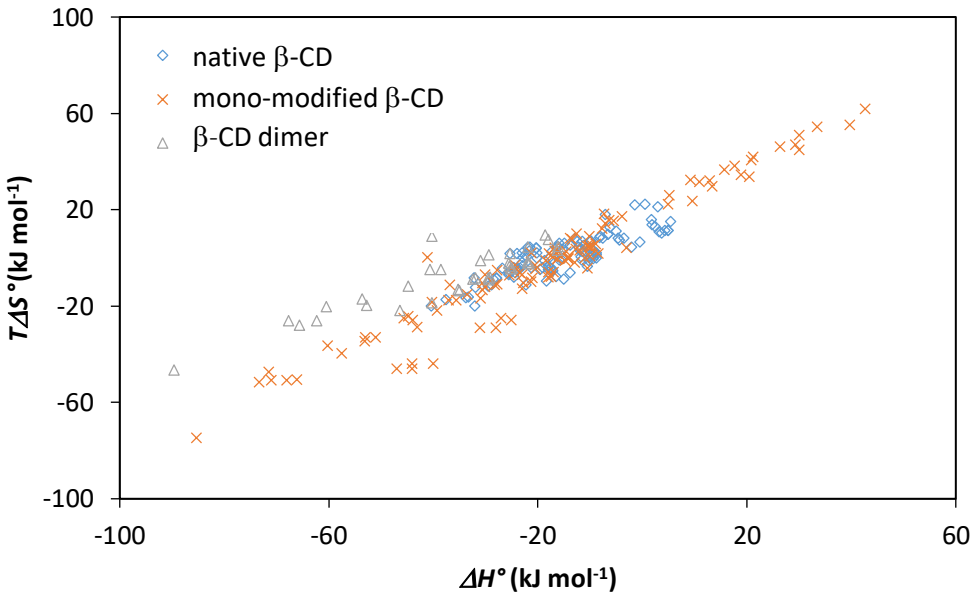

Figure 1.7: Enthalpy-entropy linear relationship for a series of host-guest complexes of various native and modified β-CD.[14]

Correlation analyses by Rekharsky and Inoue[14] describes the relationship between ΔH and ΔS by Equation 1.4, where T is the temperature, α is the slope of the plot and $T\Delta S_0$ (the intercept) represents the inherent complex stability (ΔG) when ΔH = 0. If $T\Delta S_0$ is positive, the complex is entropically stabilised even in the absence of enthalpic gains upon complexation.

$$T\Delta S = \alpha\Delta H + T\Delta S_0 \qquad (1.4)$$

The α value can be used to quantify the extent of compensation caused by modifications to the host or guest. For the native CDs, the α value is 0.79, 0.80 and 0.97 for α-CD, β-CD and γ-CD, respectively. These values proportionally represent the extent to which the entropy change cancels out the enthalpy change. For β-CD, an α value of 0.80 indicates that 80% of the $\Delta\Delta H$ (either positive or negative) is cancelled out by the $\Delta\Delta S$ while the remaining 20% is reflected in the net increased or decreased free energy of complexation, $\Delta\Delta G$.

Debate has arisen over the validity of this extra thermodynamic relationship as most determinations of ΔH or ΔS accrue from van't Hoff or Arrhenius equations, where the ΔH and ΔS values are not independent of each other. Therefore, any minor errors in the determination of ΔH may introduce compensatory errors in ΔS and vice-versa. However, this does not necessarily exclude the existence of a true enthalpy-entropy compensation effect.

1.3 Modified Cyclodextrins

While each individual interaction between a CD and a guest is weak and not sufficient to individually create stable complexes, their mutual and simultaneous action stabilises molecular assembly. In this way, CDs satisfy *cooperativity* requirements in supramolecular chemistry. However, *pre-organisation* to allow for guest selectivity is generally not observed in complexation by native CDs, which has led to the exploration of CD modification.

Cyclodextrins are modified for a variety of reasons which include solubility enhancement, increasing the strength or selectivity of complexation and a facilitation of attachment to other moieties or surfaces for synergistic functionality.[4,26] For example, Easton *et al*. used diamine-modified β-CD to coordinate to Cu(II), which acts as a catalyst for the hydrolysis of phosphate esters, as shown in Figure 1.8.[27] The CD acts to increase the effective concentration of the phosphate by forming a host-guest complex adjacent to the Cu(II) reaction site.

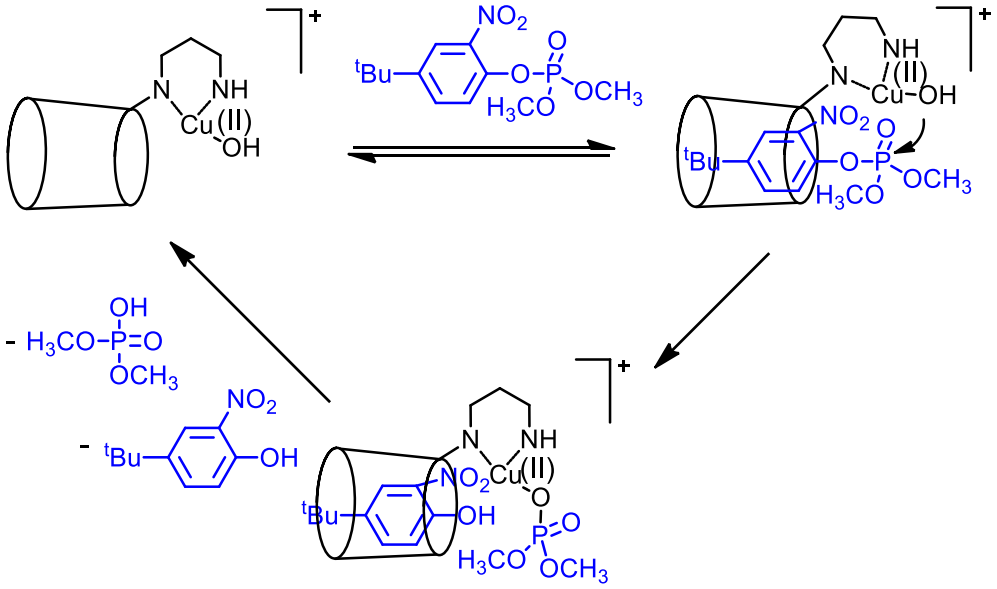

Figure 1.8: The catalytic hydrolysis of 4-*tert*-butyl-2-nitrophenyl phosphate by diamine-modified β-CD coordinated to Cu(II).[27]

Cyclodextrins can be modified on the primary or secondary face via the C2, C3 or C6 hydroxyl groups. Regioselective modification is possible as each hydroxyl group has different nucleophilicities and basicities.[28] The C6 hydroxyl group is the most basic and nucleophilic as the hydroxyl group can freely rotate. In contrast, the C2 and C3 hydroxyl groups form an intramolecular hydrogen bond network across the secondary face, restricting their rotation. As such, the C3 hydroxyl group is the least accessible and the C2 hydroxyl group is the most acidic. Given these differences, modification of CD via a mildly-reacting electrophilic substituent will selectively react with the C6 hydroxyl group.

Access to the C2 and C3 hydroxyl groups on the secondary face may be achieved through a series of protection and deprotection reactions, direct substitution by exploiting the greater acidity of the C2 hydroxyl group or utilising the complexation capabilities of CDs to direct an electrophilic reactant to the secondary face. Figure 1.9 gives an overview of common routes to regioselective CD modification.[28]

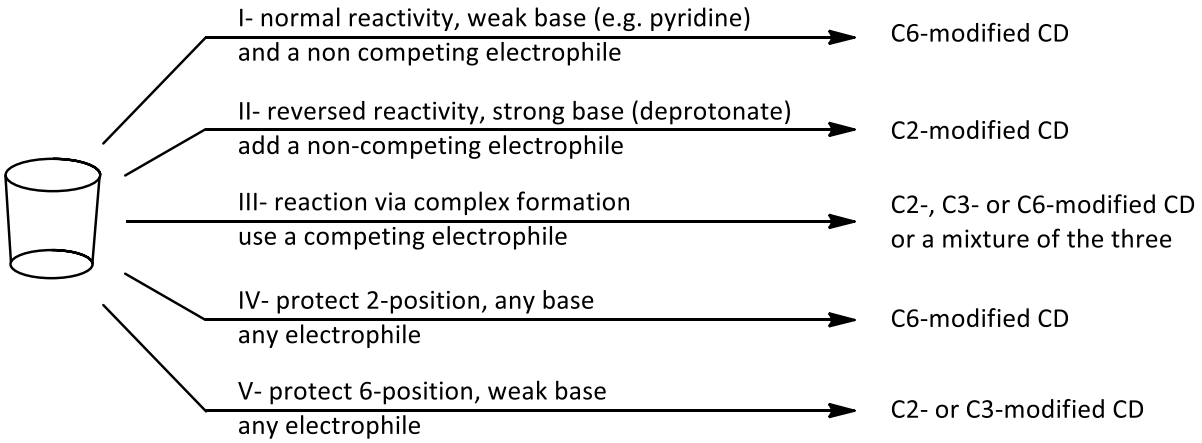

Figure 1.9: Overview of some methods for selective CD modification.[28]

The most common CD modification is the formation of mono-6-tosyl-CD from a reaction between native CD and *p*-toluenesulfonyl chloride.[29] The introduction of a sulfonate group opens up a vast range of possibilities for further modification as the sulfonate group is prone to nucleophilic substitution. In this way, mono-6-tosyl-CD is a precursor to a diverse range of functionalised CDs.

In principle, poly-functionalisation of a single CD is also possible. However, due to the high symmetry present in native CDs, regioselectivity in the second and subsequent modifications remains challenging and the prospect of generating multiple regioisomers is high, as shown in Figure 1.10.

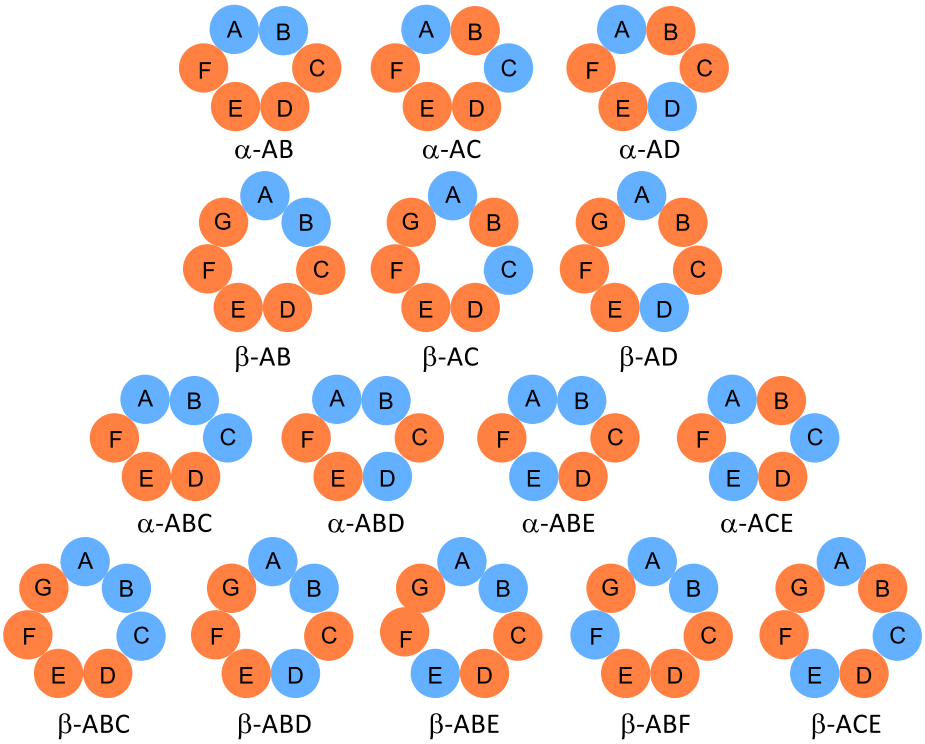

Figure 1.10: Possible regioisomers of homo-functionalised di and tri-substituted α- and β-CD.[28] Orange circles represent hydroxyl groups and blue circles represent a functionalised group on the primary face of CD.

The problem of selectivity is amplified when considering hetero-modification using at least two different substituents. However, achieving regioselective poly-hetero-functionalisation of CDs can open up new possibilities. For example, α-CD has six D-glucopyranose units, giving 7826 unique arrangements of six different functional groups on the primary face. Recently, Sollogoub *et al*. realised complete site selectivity through advances in post-synthetic modification[30-33] to create a poly-hetero-functionalised α-CD,[34] as shown in Figure 1.11.

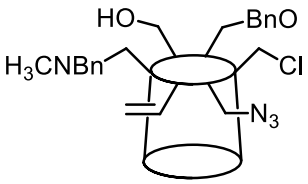

Figure 1.11: Hexa-hetero-functionalised α-CD.[34]

1.3.1 Cyclodextrin Oligomers

The synthesis of mono-modified CDs has logically been extended to create CD oligomers and polymers. The synthesis of CD oligomers has been, to some extent, in response to shortcomings in the supramolecular capabilities of their native counterparts. As native CDs lack a defined structure and have significant flexibility, guest selectivity is decreased. Consequently, native CDs often possess weaker complexation constants, making them less suited to several applications such as enzyme catalysis.[35] However, CDs can be linked to form more rigid and defined structures, optimised for specific guests, and this has led to the synthesis of CD dimers, trimers, tetramers and higher oligomeric and polymeric forms.

CD oligomers may exhibit cooperative binding, which is the simultaneous complexation of a guest by two or more CD entities within one oligomer.[35-38] The cooperative binding effect is analogous to the chelate effect in metal-ligand chemistry where, in this case, enhanced binding arises from increased van der Waals and hydrophobic interactions between host and guest. The strength of this type of complexation is dependent on the length of the linker connecting two CDs and the number of complexation sites on the guest. Complexation constants arising from the cooperative binding effect may be several orders of magnitude higher in CD oligomers than native CDs.

The variety of CD oligomers is enormous, with CD dimers alone exhibiting incredibly diversity.[39] The properties of CD dimers can easily be changed by alterations in the linker length, linker functionality, number of linkages and CD type (α-, β- or γ-CD).[38] Guest size may further be accommodated by considering the location of the link on either the primary or secondary face.[40] For a CD homo-dimer (containing one type of CD), there are six possible link combinations that can be formed from modifications on adjacent carbons: C6C6, C2C2, C3C3, C2C3, C2C6 or C3C6. The number of linker types increases when considering hetero-dimers, which consist of two different CDs linked together. Figure 1.12 describes a variety of CD dimers.

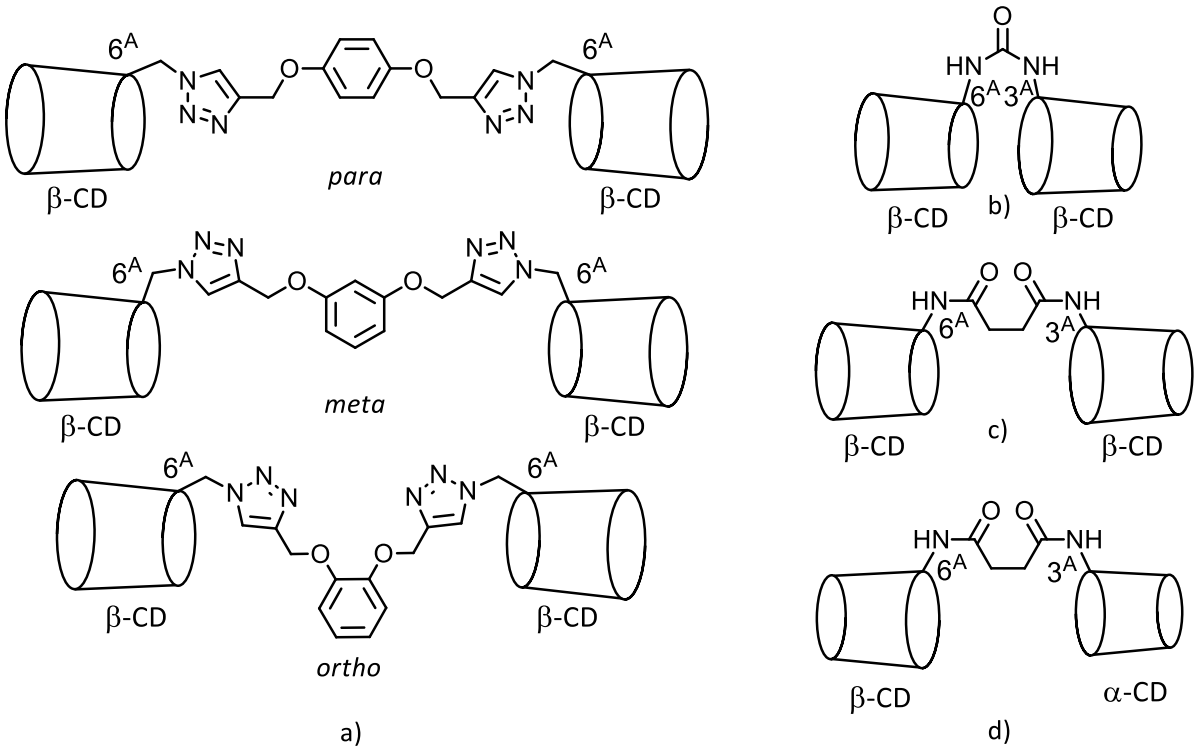

Figure 1.12: CD-dimers with various types of linkers including a) structural isomers of triazole containing β-CD dimers connected on the C6 position, each isomer representing a different length and degree of flexibility,[41] b) a urea-linked β-CD dimer connected via the C6 and C3 positions,[40] c) a succinimide-linked β-CD dimer connected via the C6 and C3 positions[40] and d) a succinimide-linked hetero-dimer connected via the C3 position of α-CD and C6 position β-CD.[42]

Cyclodextrin dimers may also be formed by connecting two CDs through multiple links, as shown in Figure 1.13.[43-47] Doubly-linked CD dimers, also called duplexes, are the most common, though triply-linked CD dimers have also been synthesised.[48] The structure that arises from these modifications further defines the dimer stereochemistry for increased pre-organised guest selectivity. The first CD duplex was synthesised by Tabushi *et al*. consisting of two β-CD units linked by two diamine groups, forming a tubular structure.[44] Bent-shaped CD duplexes were later synthesised by Breslow *et al*. using two linkers of differing lengths.[43]

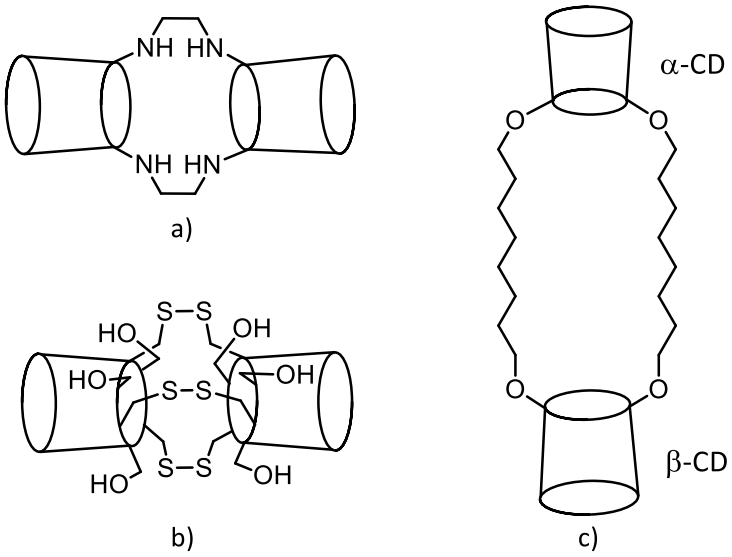

Figure 1.13: A range of CD duplexes including a) a doubly diamine-linked β-CD duplex,[44] b) a triply disulphide-linked α-CD duplex[48] and c) a hetero-duplex consisting of α-CD and β-CD.[49]

Aside from enhancing complexation strengths and guest selectivity, linkers connecting CD dimers may also possess intrinsic functionality. Thus, CD dimers linked by a ligand capable of binding a metal can, for example, act as sensitisers[50] or receptors,[51,52] as shown in Figure 1.14.

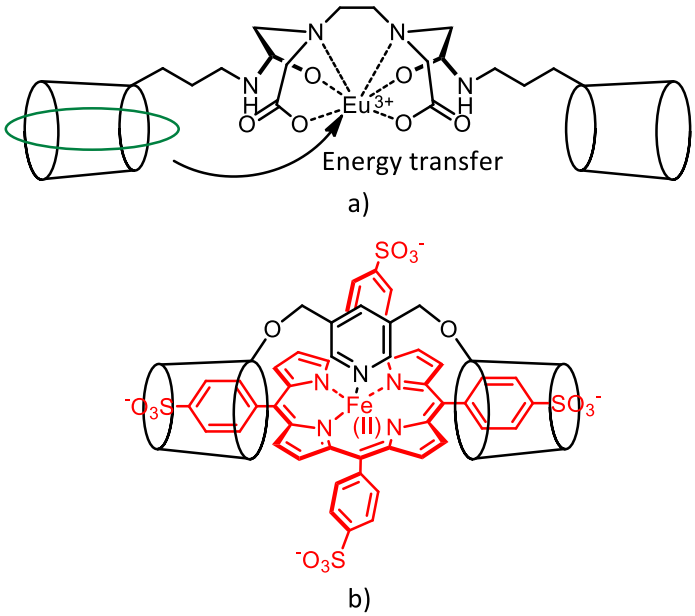

Figure 1.14: The use of CD-dimers as sensitisers and receptors from a) the association between an EDTA-linked β-CD dimer coordinated to Eu(III) and a guest molecule undergoing energy transfer[50] and b) the coordination of pyridine-linked β-CD dimer to a Fe(II)-centered porphyrin to create a haemoglobin mimic.[51] In both cases, CDs are increasing the effective concentration of the guests to the reactive centre.

Given the scope of CD dimer synthesis, it is not surprising the vast possibilities that extend to trimers,[53-56] tetramers[57] and higher oligomeric structures.[58] As the number of CD groups increases, so too does the diversity in architecture. Thus, CD trimers may exist as linear, triangular or branched/star-shaped structures, as shown in Figure 1.15. Similar structures are possible for tetramers and other oligomers, as shown in Figure 1.16.

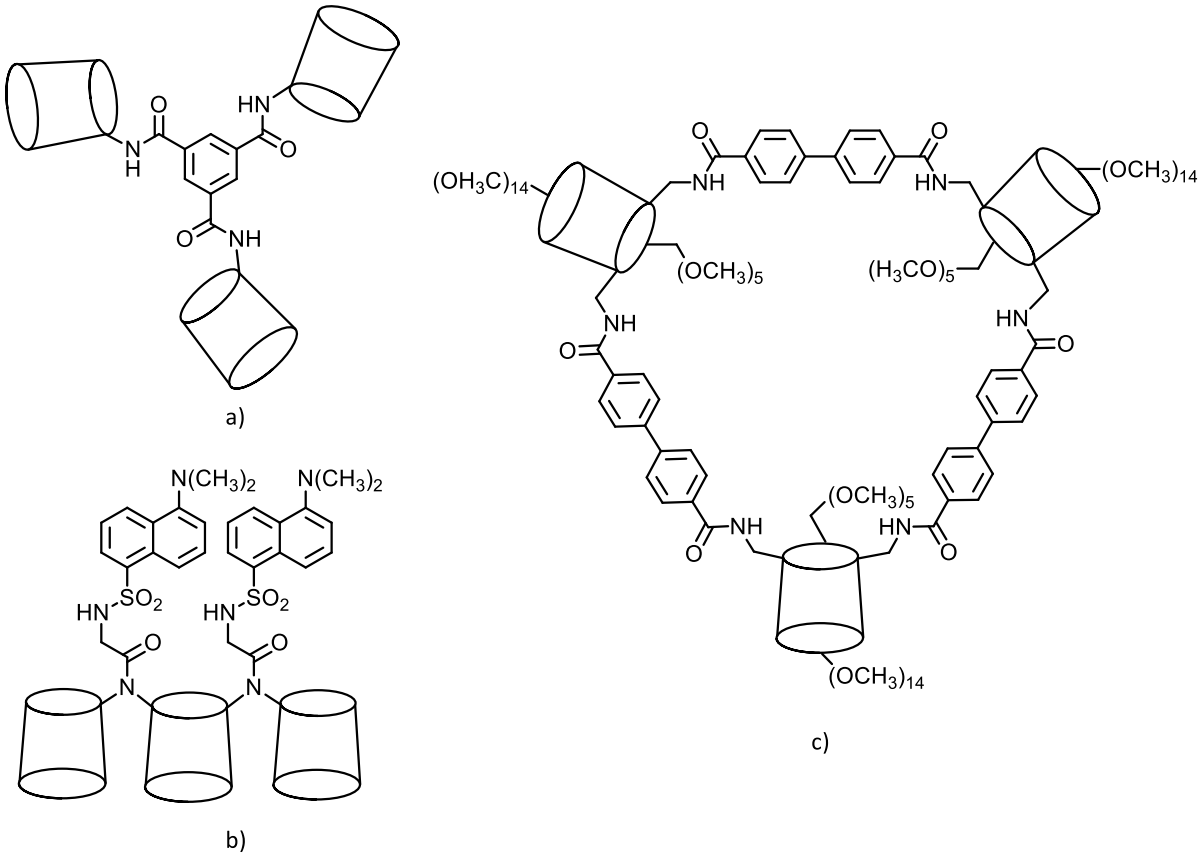

Figure 1.15: A range of CD trimers including a) a benzene-centred star shaped β-CD trimer,[53] b) a dansyl-modified fluorescent linear β-CD trimer[59] and c) a biphenyl-linked cyclic β-CD trimer.[56]

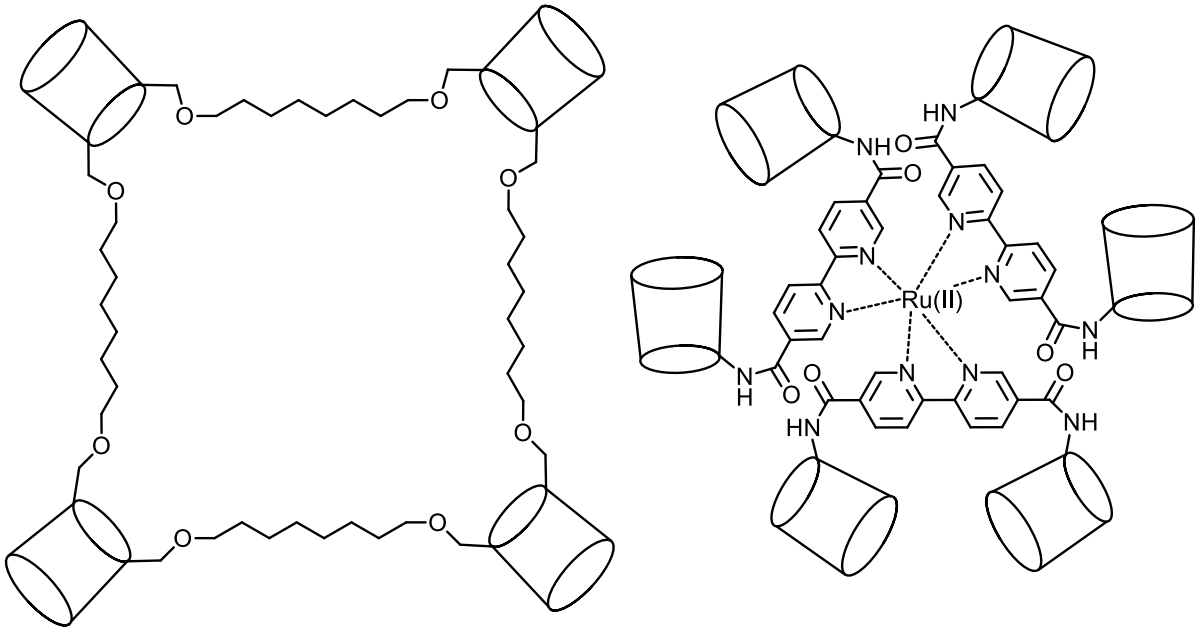

a) b)

Figure 1.16: Higher order CD oligomers including a) a cyclic β-CD tetramer[57] and b) a ruthenium-centred star-shaped β-CD hexamer.[58]

While CD oligomers have been extensively studied, there are almost limitless possibilities to explore and fine-tune the nature of these remarkable hosts. We do not yet fully understand the thermodynamics and kinetics of native CD complexation, let alone their oligomeric forms. Our incomplete understanding of CD oligomer properties may hamper their use in various applications such as drug-delivery, where drug release rates and mechanisms must be appreciated.[60] Consequently continuing research is essential.

1.3.2 Polymeric Hydrogels

Polymer chemistry is another area that has been permeated by CDs.[61,62] The incorporation of CDs into polymer networks enriches the possibility for the host properties of CDs to be employed on nano-, micro- and macroscopic scales.[63-66] Given the biocompatibility of CDs, much attention has been directed towards the use of CDs in hydrogel technology,[67-70] which as a consequence of its aqueous nature has considerable potential for medical application.

Hydrogels are 3D networks of cross-linked polymers that can entrap large proportions of water.[71] Cyclodextrins are particularly useful in the design of hydrogels as they are water soluble, highly biocompatible and can be used to both construct and functionalise the hydrogel.[72] Due to the large proportion of water, hydrogels can mimic the viscoelastic properties of biological tissue, making them particularly useful in biochemistry, having applications as a super absorbent material, medium for storage and delivery of substances in biomedicine and as scaffolds in tissue engineering.[73-78]

1.3.2.1 Chemical and Physical hydrogels

Cyclodextrin-based hydrogels may be classified as either chemical or physical according to the type of cross-link used to create the 3D polymer networks.[62] Chemical hydrogels may be created from directly cross-linking CDs to create an expansive network, as shown in Figure 1.17.[68,69,79]

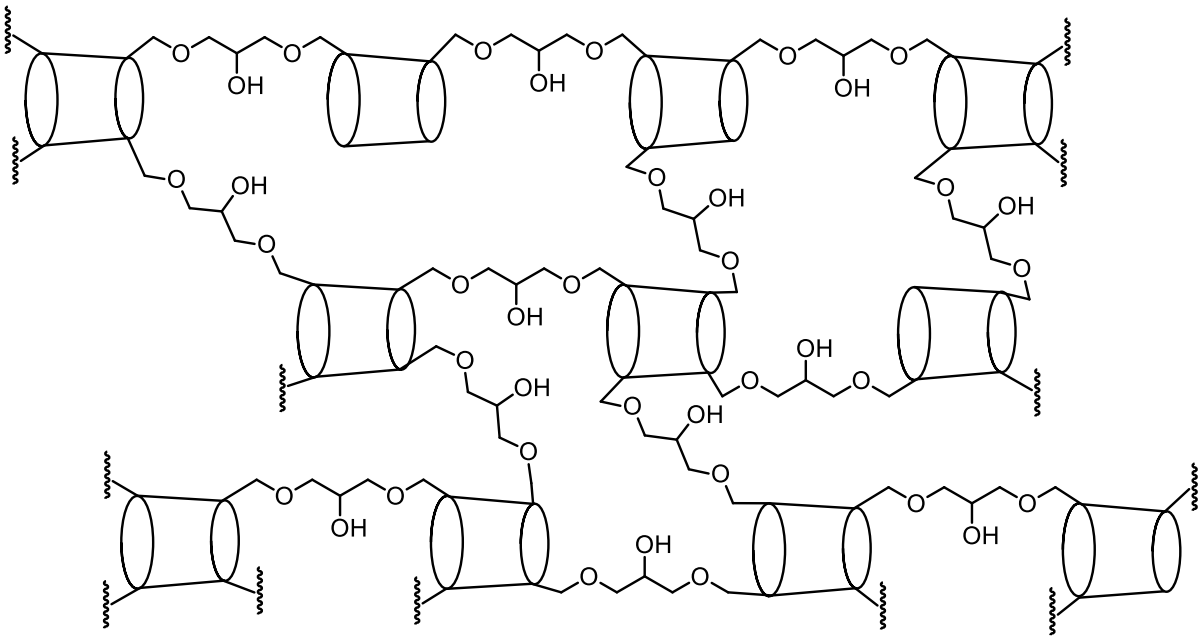

Figure 1.17: Representation of portions of a water-soluble β-CD polymer chemically cross-linked by epichlorohydrin.[79]

As the cross-links in chemical hydrogels are permanent, the gel can be made with considerable strength and stability. However, chemical hydrogels have several intrinsic disadvantages which may limit their application.[62,71,75] Firstly, the synthesis of chemical hydrogels often results in a poorly defined network; consequently, it is difficult to design a system with a predictable outcome. Additionally, the synthesis is often under harsh conditions, requiring organic solvents and metal catalysts. The use of covalent cross-links also prevents the hydrogel from self-healing, so any defects that arise within the network cause permanent damage.

Many of the disadvantages of chemical hydrogels may be circumvented by physical hydrogels, which may be defined as hydrogels with arrays of monomeric or polymeric units brought together by non-covalent interactions. The advantage of physical hydrogels over chemical hydrogels arises from the transient nature of the non-covalent crosslinks.[62,71,75,76] This makes the polymer network dynamic and able to respond to external stresses placed on the system. Due to the enormity of research into physical hydrogels, the field requires further sub-division to broadly describe the most prevalent types. However, given that there is no formal categorisation of CD-based physical hydrogels in the

literature, it remains convenient to designate the most common examples as either polypseudorotaxane hydrogels, host-guest linked hydrogels or supramolecular hydrogels.

1.3.2.2 Polypseudorotaxane Hydrogels

Polypseudorotaxane hydrogels are perhaps the most common type of CD-based hydrogel.[67,80,81] Polypseudorotaxanes are formed by the threading of CD groups onto a polymer chain (see Section 1.4.2 Polyrotaxanes and Polypseudorotaxanes), which may then form polymer networks through the interaction of CDs with adjacent chains. One of the first polypseudorotaxane hydrogels was synthesised by Harada, Kamachi *et al*.,[82,83] from the association of α-CD threaded through poly(ethylene glycol) (PEG), as shown in Figure 1.18. Since this discovery, various other polypseudorotaxanes hydrogels have been created with a diverse range of morphologies and physical properties, employing linear polymer chains,[84-86] star-shaped polymers,[87] brush polymers[88] and dual molecular recognition.[89]

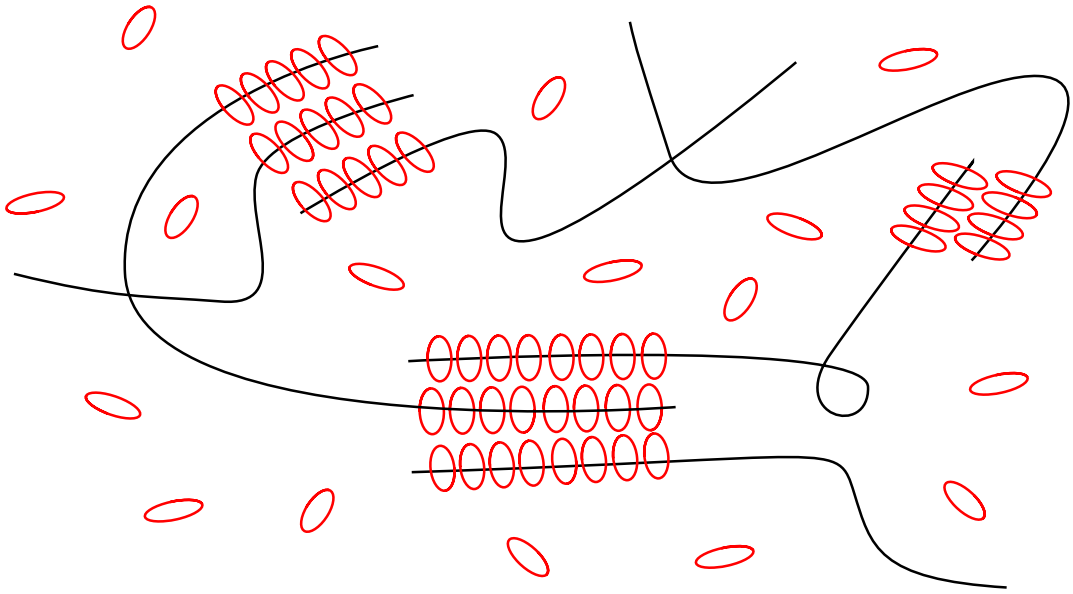

Figure 1.18: Formation of a polypseudorotaxane hydrogel from the association of adjacent α-CD moieties (red ovals) threaded through PEG chains (black lines).[83]

The maturing of polypseudorotaxane hydrogel chemistry eventually led to the investigation of stimuli-responsive polypseudorotaxanes hydrogels, which could alter their physical or chemical properties upon exposure to external stimuli. Yiu *et al*. created thermosensitive hydrogels using chitosan- and dextran-modified PEG and α-CD.[90,91] The hydrogel exists in the gel phase when α-CD is threaded onto the modified-PEG, but reverts to a solution phase upon heating. Polypseudorotaxane hydrogels exhibiting responsiveness from multiple stimuli have also been synthesised.[92]

1.3.2.3 Host-guest linked Hydrogels

Another type of CD-based hydrogel is the host-guest linked hydrogel, which utilises the host properties of a CD to non-covalently link polymer chains.[93-105] Host-guest linked hydrogels can form either from the interaction between a CD-modified polymer and guest-modified polymer, a CD-modified polymer and a guest oligomeric linker or a guest-modified polymer and CD oligomeric linker. Guo, Lincoln, Prud'homme *et al*. used adamantyl-functionalised poly(acrylate) (PAA) cross-linked with either a β-CD-functionalised PAA[106] or a β-CD oligomer,[53] as shown in Figure 1.19. In both cases, host-guest interactions connect adjacent polymer strands to create polymeric networks.

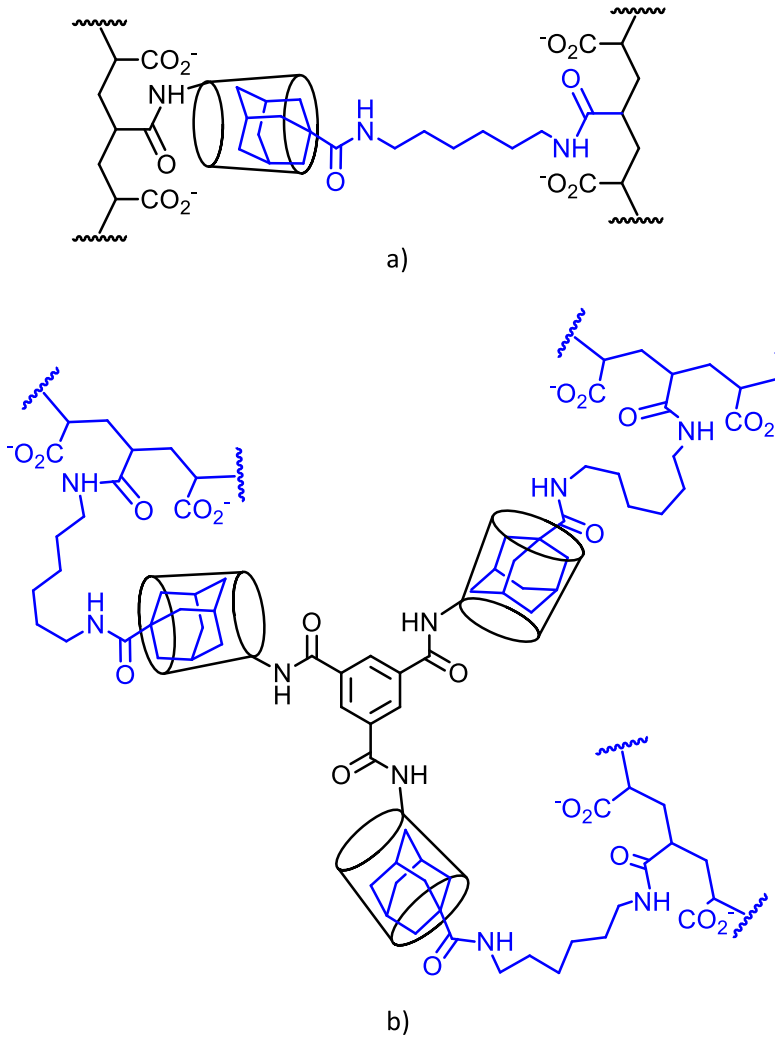

Figure 1.19: Host-guest linked hydrogels arising from the interaction between a) a CD-modified PAA and adamantane-modified PAA[106] and b) an adamantane-modified PAA and a β-CD trimer.[53]

As with polypseudorotaxane hydrogels, stimuli-responsive host-guest linked hydrogels have been investigated. There has been much interest in controlling the sol-gel phase transition of hydrogels using light, redox, pH and thermal stimuli. Stoddart *et al*. used azobenzene-functionalised PAA cross-linked with β-CD to create a light-responsive hydrogel system. Upon UV-irradiation, the azobenzene moiety isomerises from *E* to *Z* isomer, accompanied by a gel-sol phase transition.[107] Yuan and Harada created a redox-responsive hydrogel combining dodecyl-modified PAA, β-CD and ferrocene.[108,109] In its reduced state, ferrocene binds to β-CD, allowing dodecyl strands of adjacent PAA chains to associate to produce in a gel phase. However, in the oxidised state, ferrocene is charged and β-CD instead binds to the dodecyl groups of the modified PAA and a gel phase is not produced as a consequence. Yui *et al*. devised a pH-responsive hydrogel from the inclusion of γ-CD with two branches of linear poly(ethyleneimine) (PEI).[110] Under acidic conditions, the secondary amines of PEI become protonated, causing partial dethreading of γ-CD, which loosens the network and decreases the viscoelasticity. Aside from controlling sol-gel phase transitions, stimuli-responsive host-guest linked hydrogels have also been synthesised to exhibit controllable self-healing properties,[111,112] shape memory[113] and recognition capabilities.[114,115]

The host-guest linked hydrogels discussed so far have used linear polymer chains and oligomers as the basis of the polymeric network. However, there are a huge variety of other architectures. Star-shaped polymers have been used instead of linear chains to create a more expansive 3D network,[116,117] as well as an array of different linkers. Linkers composed of CD-functionalised CdS quantum dots,[118,119] CD-modified single- and multi-walled carbon nanotubes,[120-123] β-CD vesicles[124] and linearly linked CD-based molecular tubes[125] have all been used as junctions to accommodate guests of adjacent polymer chains. Many of these have also been made stimuli-responsive by the use of azobenzene[118,120] or ferrocene[119] as the guest.

1.3.2.4 Supramolecular Hydrogels

The third type of CD-based hydrogels are supramolecular hydrogels, which are characterised by the formation of polymer networks from host-guest interactions between small molecule subunits.[126-129] Supramolecular hydrogels differ from host-guest linked hydrogels as they are formed from small molecules, rather than polymer chains. Supramolecular hydrogels should be more applicable in biological and environmental settings as gels created without a polymeric backbone are more biodegradable.[130]

Harada *et al*. synthesised supramolecular hydrogels from the self-assembly of β-CD modified with a cinnamoyl and trinitrophenyl group, as shown in Figure 1.20.[130,131] In aqueous solution, the compound forms a head-to-tail channel-type structure. As the concentration is increased, these structures arrange to form supramolecular fibrils and eventually gels. Gel-sol transition was achieved by the addition of 1-adamantanecarboxylic acid, which acts as a competitive guest to displace the cinnamoyl group from the CD annulus.

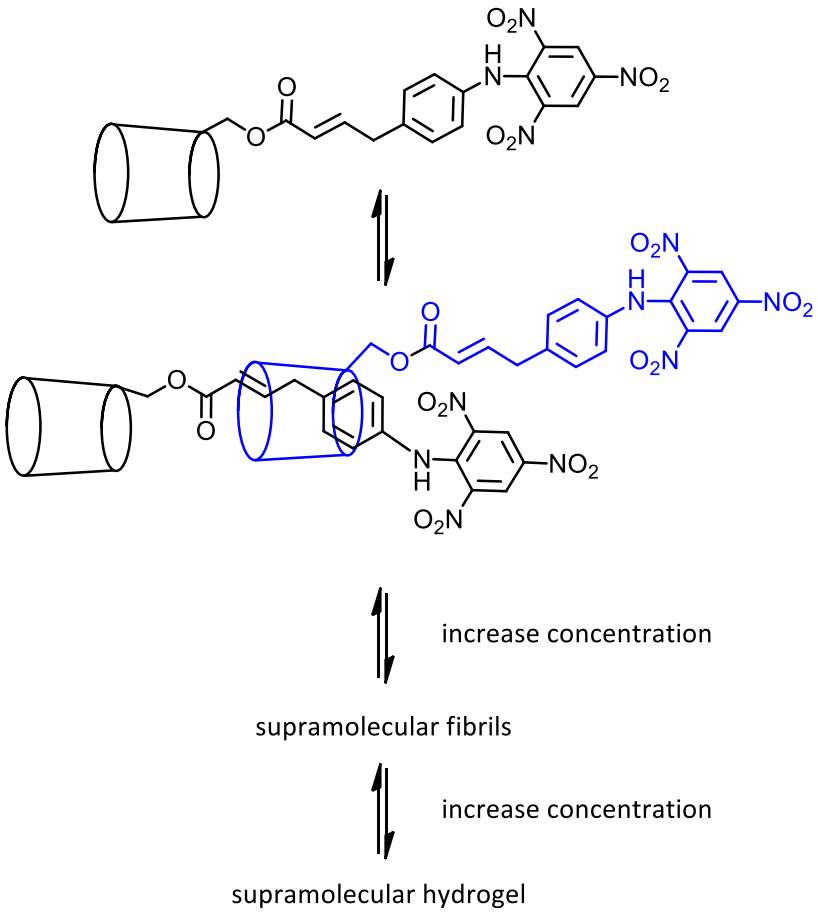

Figure 1.20: Formation of a supramolecular hydrogel from the self-assembly of cinnamoyl-modified β-CD monomers in water to form head-to-tail channel-type structures, which forms supramolecular fibrils and finally supramolecular hydrogels with increasing concentration.[130]

Tian *et al*. formed a supramolecular polymer from the interaction between γ-CD and a coumarin dimer, as shown in Figure 1.21.[132] As γ-CD has a large annulus, two coumarin moieties from two different dimers may be encapsulated at the same time. Photoirradiation at 365 nm fuses the two coumarin moieties, forming a gel, the effect of which is reversed upon photoirradiation at 254 nm, which separates the two coumarin entities to form a solution. Tian *et al*. furthered this work by synthesising a coumarin trimer to create a more expansive polymer network.[133]

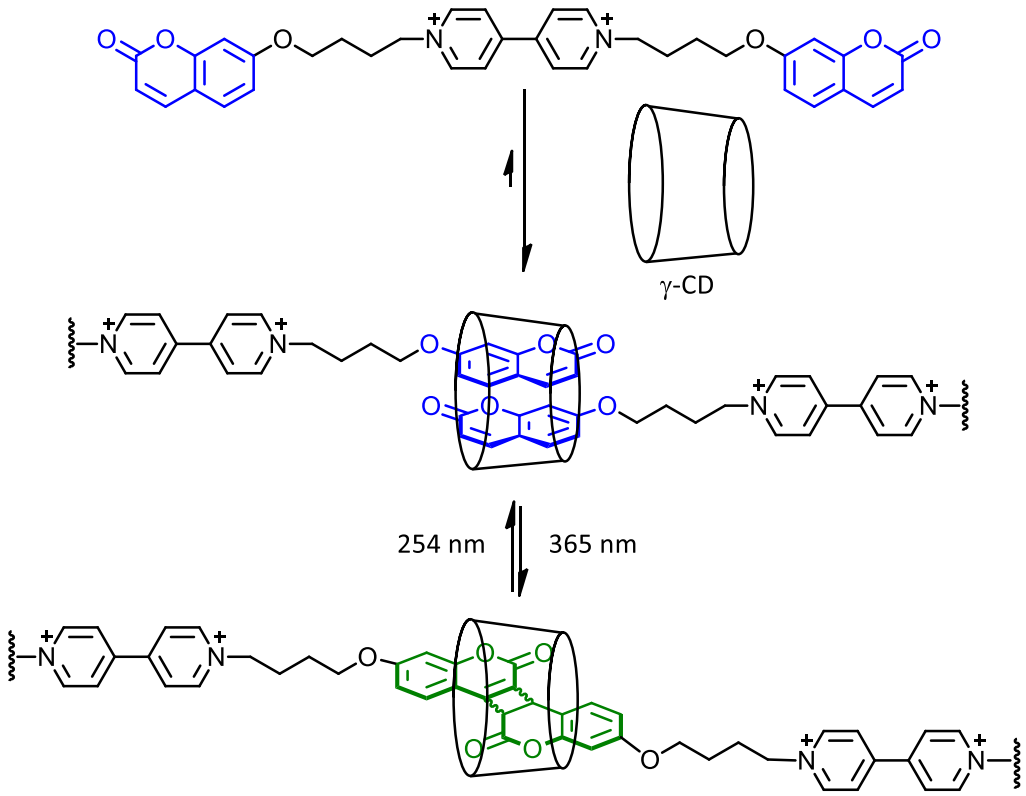

Figure 1.21: Formation of a supramolecular hydrogel from the host-guest interaction between coumarin dimers and γ-CDs. Gel-sol phase transition is controlled by photoirradiation, which can fuse or separate the coumarin entities, resulting in a gel and solution phase, respectively.[132]

1.3.2.5 Hybrid Hydrogels

The types of hydrogels so far described are by no means a comprehensive list. In principle, almost any linker or combination of linkers can be used to form a CD-based hydrogel. Therefore, a variety of hybrid hydrogels possessing a mixture of linker types has been investigated.

While there has been some interest in hybrid hydrogels possessing multiple types of non-covalent interactions (e.g. combining host-guest and polypseudorotaxane links),[134] much of the interest has centred on chemical-physical hybrid hydrogels, which possess both covalent and non-covalent links. Slide-ring gels, for example, consist of CD moieties threaded through a polymer chain and end-capped to created a polyrotaxane (see Section 1.4.2 Polyrotaxanes and Polypseudorotaxanes).[135-138] The CD groups are then covalently linked to create a hydrogel.

Various other types of chemical-physical hybrid hydrogels have been developed,[139,140] including those that exhibit stretching[141] and shape memory[142] properties. However, the potential of these types of hydrogels has been superbly demonstrated by Harada. Using a mixture of covalent and non-covalent cross-links, Harada *et al*. have demonstrated macroscopic recognition and self-assembly of hydrogels,[115,143] strong adhesion between hydrogels,[144] expansion and contraction of hydrogels and

directional movement of hydrogels,[145] as shown in Figure 1.22. This research has significantly demonstrated the main tenets of supramolecular chemistry - that an understanding of molecular behavior can directly influence macroscopic properties.

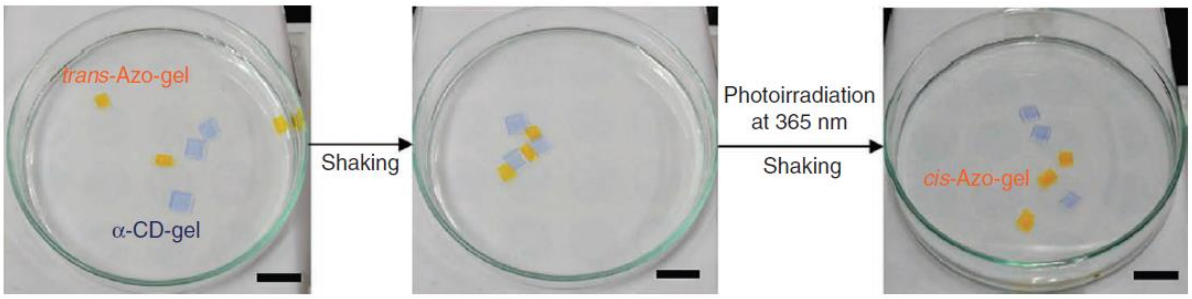

a)

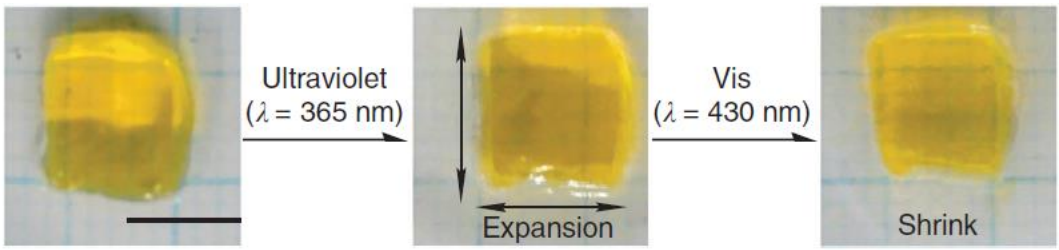

b)

c)

Figure 1.22: Photoresponsive hydrogels[115,145] consisting of covalent and non-covalent cross-links that demonstrate various macroscopic changes including a) recognition behavior of pure hydrogels which, upon gentle agitation and irradiation, predictably self-assemble and disassemble, respectively, b) expansion and contraction of a hydrogel upon successive irradiation, forming an artificial muscle and c) the directional movement of a hydrogel upon irradiation, replicating an actuator.

1.4 Mechanically Interlocked Molecules

The discussion of supramolecular chemistry has so far relied on two of chemistry's most prevalent chemical bonds: covalent and non-covalent. However, supramolecular chemistry also has a strong association with another special type of chemical bond: the mechanical bond.[146,147] The mechanical bond exists where two or more molecular components are mechanically interlocked with each other. The resulting compound is termed a mechanically interlocked molecule (MIM) as even though the components are not covalently bound, a covalent bond nevertheless must be broken to separate the components.

In many ways, mechanical bonds combine the strength of covalent bonds with the intricacies and subtleties of non-covalent and coordination bonds, to create robust molecules with controllable functionality. The mechanical bond has become a key feature in much of supramolecular chemistry as we continue to aspire to nature's benchmark. The prevalence of mechanical bonds in biological systems, human cultural enterprises and artistic endeavours provides endless inspiration for chemists' pursuit.[147]

Of the various types of MIMs that have been developed, rotaxanes and catenanes remain archetypal, as shown in Figure 1.23.[148,149] Catenanes, derived from the Latin word *catena,* meaning chain, consist of macrocycles mechanically linked, much like the links in a chain.[150-152] Rotaxanes, on the other hand, consist of a linear molecule (axle) threaded through a macrocycle.[153,154] The macrocycle is mechanically locked by the addition of blocking groups on either end of the axle, which is larger than the annulus of the macrocycle, preventing the dissociation of components. The word rotaxane is derived from Latin words *rota* and *axis*, meaning wheel and axle, respectively. The intriguing aspect of catenanes, rotaxanes and other MIMs is that even though components are linked and cannot dissociate, components are able to independently move, hence the superiority of MIMs from the combined advantages of covalent bonds and non-covalent bonds.

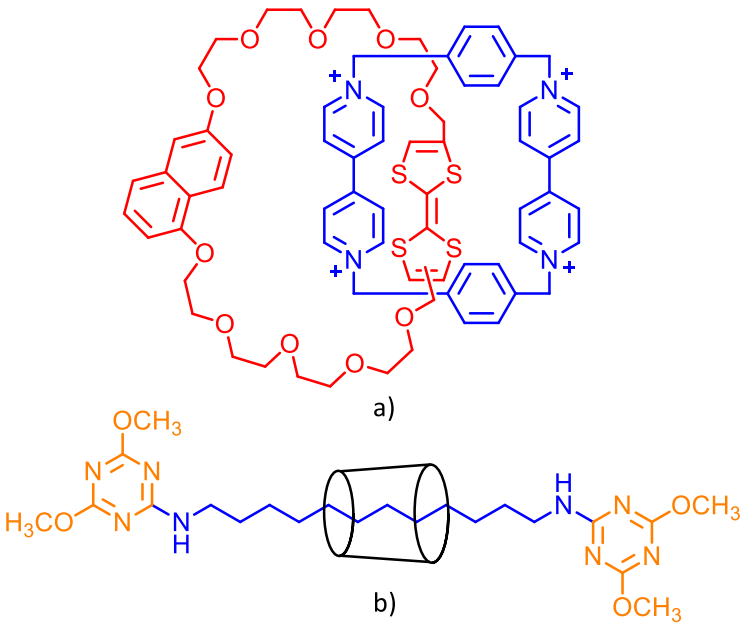

Figure 1.23: Structures of a) a catenane[150,151] and b) a rotaxane.[155]

1.4.1 Rotaxanes and Pseudorotaxanes

The exploration of MIMs has expanded to create architectures such as knots and Borromean rings, rotaxanes remain the most heavily researched MIMs.[154,156-158] Rotaxanes are named from the sum of the macrocycle and axle components. If the sum of the macrocycles and axles in a rotaxane, *n,* is well defined, this number is given in square brackets: [n]-rotaxane. If the rotaxane contains a macrocycle and axle, but no blocking group to mechanically lock the formation, it is termed a pseudorotaxane, as shown in Figure 1.24.

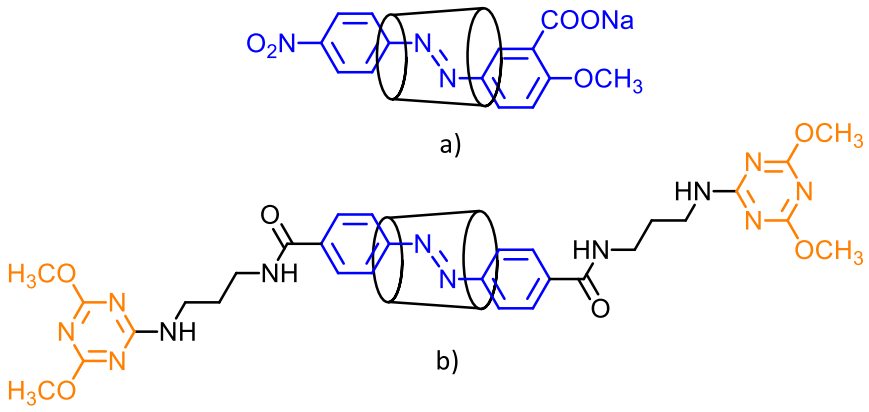

Figure 1.24: Structures of a) a pseudorotaxane[159] and b) a rotaxane[155] based upon an azobenzene axle and β-CD macrocycle.

Cyclodextrins are suitable components of rotaxanes and pseudorotaxanes as they inherently possess a macrocyclic structure suitable for threading linear molecules. The self-assembly behaviour of CDs also provides synthetic advantages as pseudorotaxanes can form spontaneously in aqueous media,

before a rotaxanation reaction is initiated to couple blocking groups to the axle. This synthetic route is known as the threading approach and is the most common mode of rotaxane formation.[160] Given the variety of CD compounds that can selectively bind a range of diverse guests, a huge catalogue of rotaxanes may be synthesised and, like the CD entities previously discussed, both oligomeric and polymeric species may be synthesised.

1.4.2 Polyrotaxanes and Polypseudorotaxanes

Polymeric forms of rotaxanes and pseudorotaxanes may arise in two common ways – through the condensation of monomeric pseudorotaxanes or through the threading of multiple macrocycles onto a pluritopic axle, to form polyrotaxanes or polypseudorotaxanes, depending on the absence or presence of a blocking group.[81,161-164] For CD-based polyrotaxanes and polypseudorotaxanes, the latter synthetic route is easier to achieve.

Various polyrotaxanes have been developed, often with biomedical applications. Vives, Hasenknopf *et al*. synthesised a polyrotaxane composed of γ-CD modified with either a fluorescent tag or a dia- or paramagnetic lanthanide, for use as a biomedical imaging tool.[165] Yui *et al*. established a drug delivery system based upon a polyrotaxane consisting of a modified α-CD, PEG chain and an amide-bound blocking group, as shown in Figure 1.25.[166] The polyrotaxane could act as a targeted drug delivery agent as the blocking group could be cleaved by a site-specific enzyme, releasing the modified α-CD load at the target site.[167]

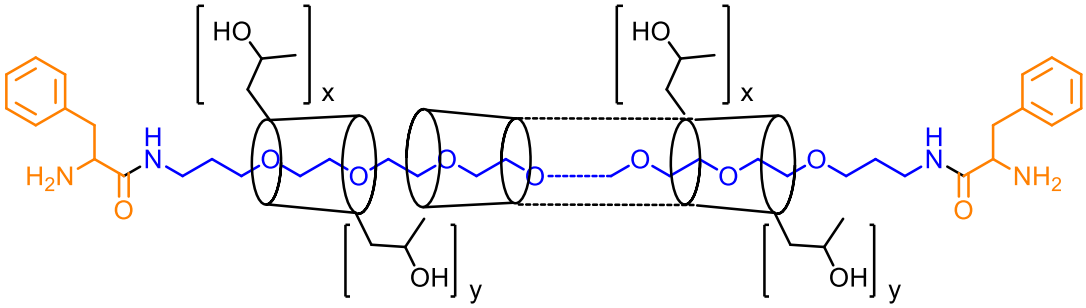

Figure 1.25: A polyrotaxane consisting of modified α-CD macrocycles threaded through a poly(ethylene glycol) axle, end capped by enzyme-cleavable blocking groups.[166]

Polyrotaxanes have also been used as templates for the formation of other architectures. Harada, Kamachi *et al*. used polyrotaxanes as the basis of forming an α-CD molecular tube, as shown in Figure 1.26.[168]

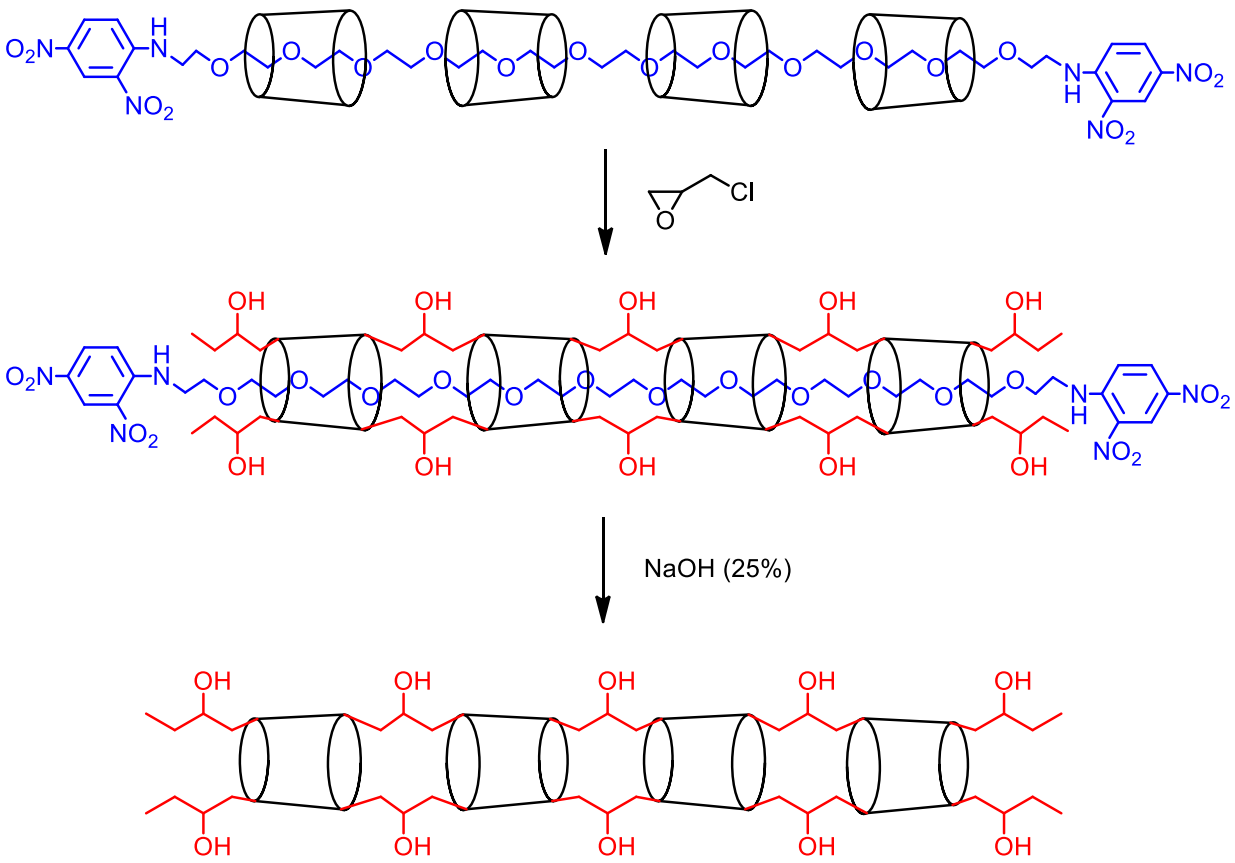

Figure 1.26: Formation of an α-CD molecular tube from a polyrotaxane.[168]

1.4.3 Daisy Chains

Special types of polyrotaxane and polypseudorotaxane arise from the interaction of a molecule in which the macrocycle and axle component are covalently linked. This molecule is given a variety of names in the literature including heteroditopic, hermaphrodite, plerotopic and self-complementary.[169] The axle component of a heteroditopic molecule may interlink with the macrocycle component of a second heteroditopic molecule and so on, creating a supramolecular polymer known as a daisy chain, named from the chains arising from interlinked stems of a daisy garland.[169-172] Daisy chains may form either cyclic or acyclic conformations, as shown in Figure 1.27, which may be mechanically locked with a suitable blocking group. Typically, cyclic daisy chains may be labelled [cn]-daisy chains, where n is the number of monomeric units. Additionally, a [c2]-daisy chain, the smallest possible cyclic daisy chain, is often given the name Janus, after the Roman god possessing two faces. Extensive research has been carried out into daisy chain chemistry, resulting in the synthesis of a diverse range of daisy chain architectures including daisy chains with alternating α-CD and β-CD subunits[173] and cyclic trimers,[174] as shown in Figure 1.28 and Figure 1.29, respectively.

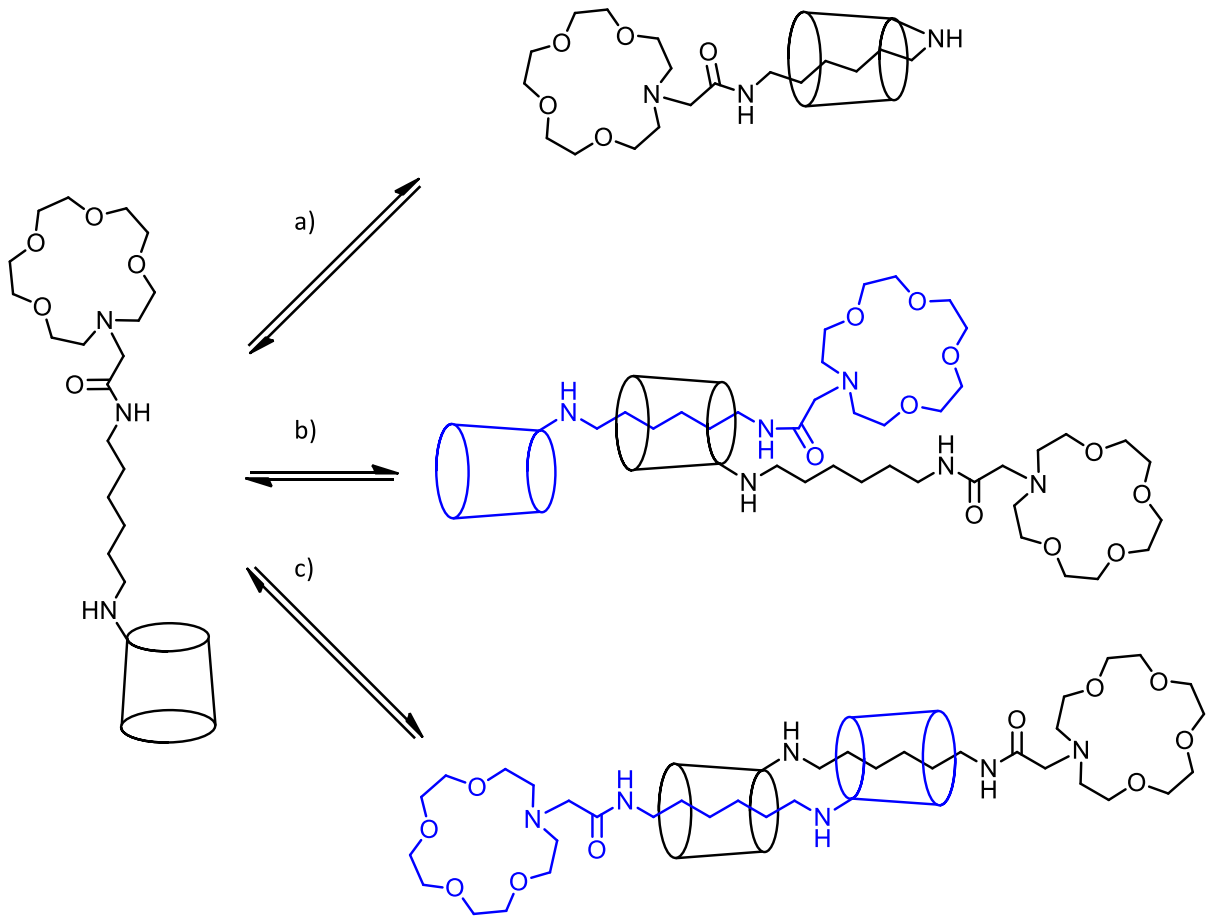

Figure 1.27: Structure of β-CD modified with an alkyl chain and crown ether. The final structure may be a) a self-included complex, b) an acyclic daisy chain or c) a cyclic daisy chain or Janus complex.[175]

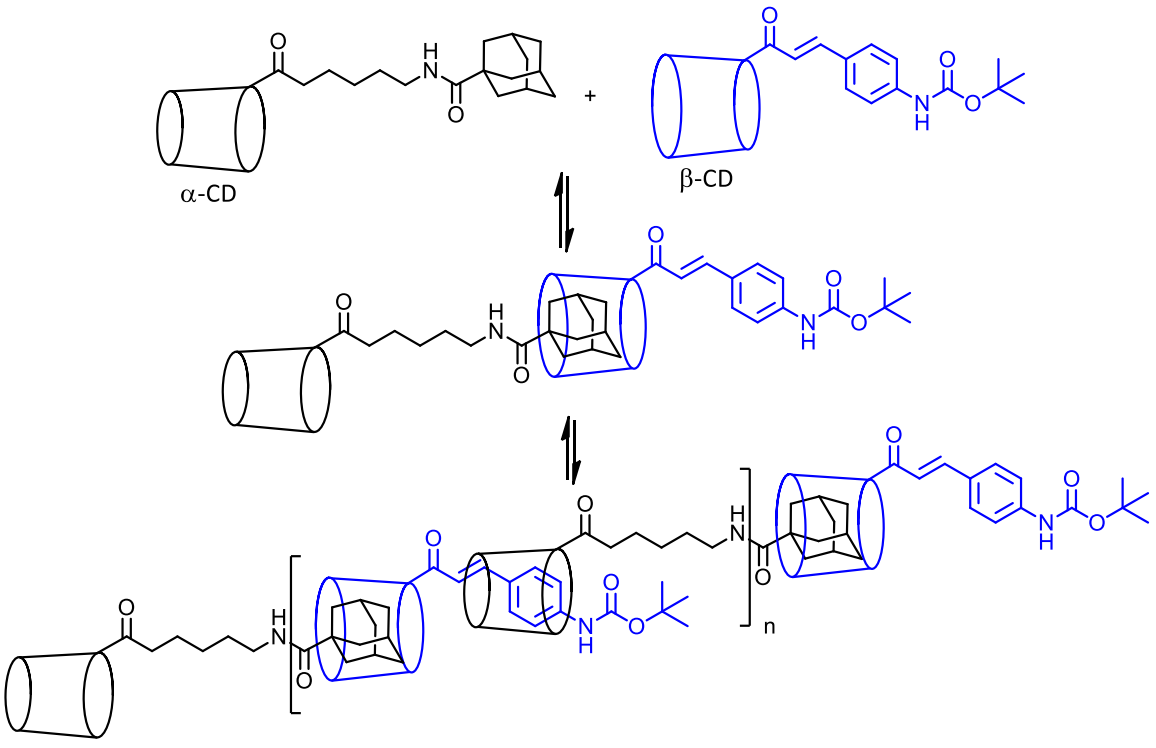

Figure 1.28: Construction of an acyclic daisy chain with alternating α-CD and β-CD groups.[173]

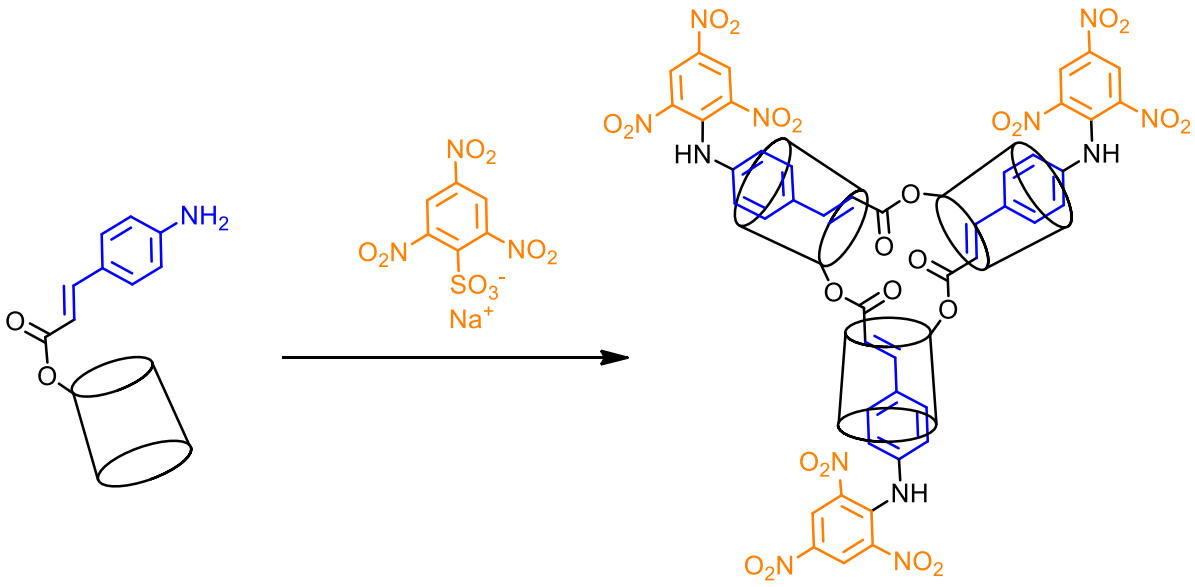

Figure 1.29: Formation of a trimeric cyclic daisy chain- tri[2]rotaxane.[174]

Despite the plethora of daisy chains now under investigation, vexed questions remain concerning the control of daisy-chain formation, namely, the preference for either the cyclic or acyclic form. Considering the thermodynamics of daisy chain assembly, we expect the Janus form to be the most favoured conformation in most systems as Janus formations consist of two stabilising host-guest interactions from two monomers. This is in contrast to the acyclic form, which always has one axle that is hindered from complexation, being exposed to unfavourable interactions with the bulk solvent media. Despite the apparent thermodynamic preference of cyclic daisy chains, the literature contains many examples of acyclic forms. Various factors such as the modification site and type of modification may influence the final architecture.[169]

Kaneda *et al*. discovered that an azobenzene-modified α-CD would competitively form either a 2-component or 4-component cyclic daisy chain, depending on the temperature.[176] Harada *et al*. demonstrated that α-CD modified with cinnamide on the C3 position led to an acyclic daisy chain, while modification on the C6 position led to a Janus complex, as shown in Figure 1.30. Stimuli-responsive daisy chains have also been investigated, establishing the use of light to alter the preference of either cyclic or acyclic forms.[177,178]

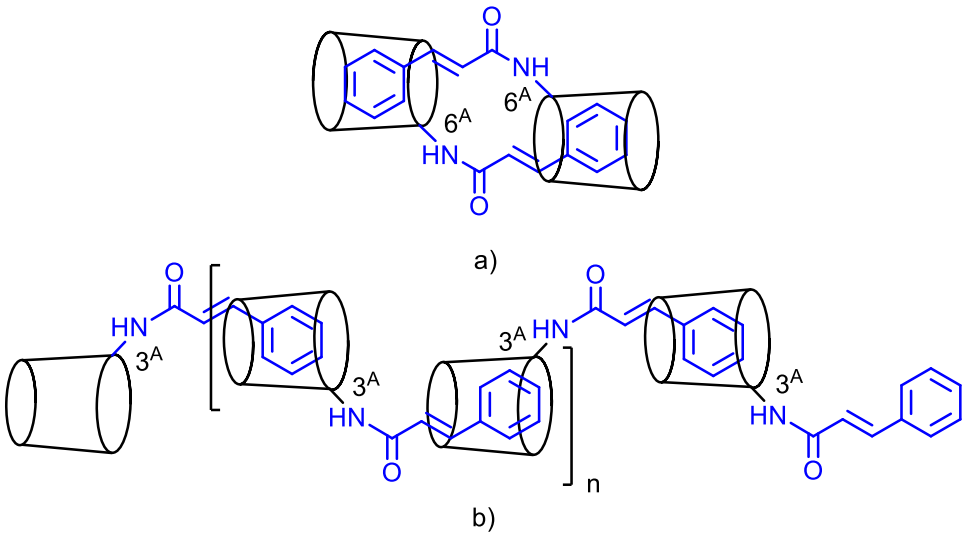

Figure 1.30: The self-assembly of a cinnamide-modified α-CD on either the a) C6 position to form a Janus or b) the C3 position to form an acyclic daisy chain.[179]

1.4.4 Towards Molecular Devices

Unlike rotaxanes and polyrotaxanes, the blocking group of daisy chains is an integral part of the molecule. While the mechanical bond present in rotaxanes and polyrotaxanes is, in many ways, a place holder, the mechanical bond in a daisy chain can regulate the size of the molecule.[169] Depending on the length of the axle, the independent movement of each monomer unit can cause an expansion or contraction of the daisy chain, as shown in Figure 1.31.

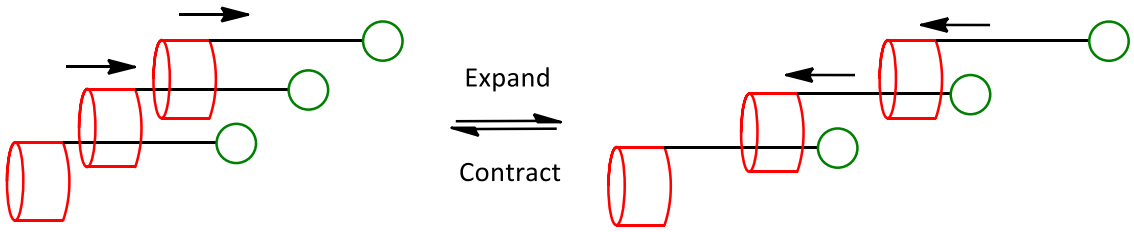

Figure 1.31: Expansion and contraction of an acyclic daisy chain from the sliding of individual monomer units.[169]

This elongation adaptability is the key to exploiting a structure-property relationship, where elongation on the molecular level may be translated to a physical macroscopic change. If the concept was expanded to include all molecular movements and if such movements could be controlled by an external stimulus, the resultant molecule would represent the promise of supramolecular chemistry – a self-assembled system from pre-organised subunits that performs a function based on intrinsic molecular information. Such molecules do exist and have been termed molecular devices.

1.5 Molecular Devices

Molecular devices are sets of interrelated molecules, not necessarily covalently linked, that perform a function when exposed to an external stimulus.[180-185] The first serious proposal of molecular devices came from Richard Feynman in his 1959 lecture to the American Physical Society. In his address, Feynmann challenged the limitations of the top down approach to technology, stating that the miniaturisation of components to increase efficiency and functionality of machines has intrinsic limitations. The title of his address, "There's plenty of room at the bottom", aptly offers a solution - to approach the advance of technology from the bottom-up, that is, through mastering of molecular information.[186]

Molecular devices may be characterised according to the type of function, the nature of the energy input, the readout, the repeatability of the function and the timescale of one complete cycle of the device.[181,182] As molecular devices are a relatively new area in chemistry, it remains convenient to categorise them according to the type of function, which is in many cases based upon the movement of individual components.

1.5.1 Types of Device

Initial investigations into molecular devices[182,187,188] focused on simple motions or functions such as rotary motions,[189,190] shuttling,[183,191-193] tweezing,[194-196] controlled recognition[197] and restriction of motion,[198] as shown in Figure 1.32. The mastering of such simple motions eventually led to the evolution of more complex devices, including shuttle-based molecular elevators,[199] cargo transporters,[200] Boolean logic gates[201], molecular walkers,[202] and sequence-specific peptide synthesisers.[203]

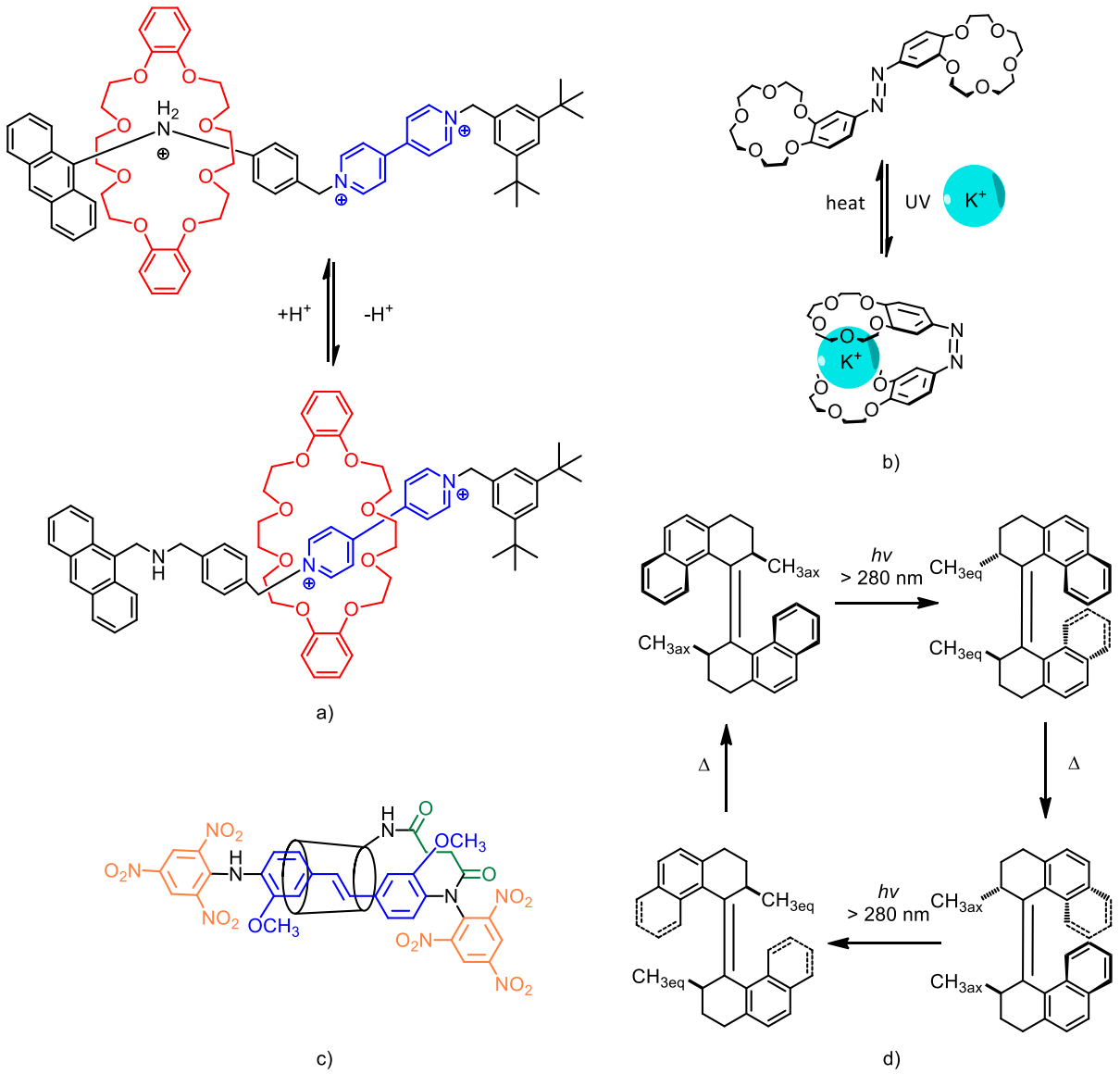

Figure 1.32: A series of molecular devices including a) a molecular shuttle composing a crown-ether based macrocycle that moves along dialkylammonium and bipyridinium recognition sites of an axle depending on the pH,[191] b) a molecular tweezer based upon a crown-ether functionalised azobenzene that is able to bind to potassium ion when photoirradiated,[204] c) a CD-based molecular ratchet tooth and pawl that restricts the motion of the CD due to the presence of a methoxy group[198] and d) a molecular rotor based upon the rotation of aromatic groups around an alkene moiety, regulated by *E* to *Z* photoisomerisation.[189]

Cyclodextrins have routinely been used in the design of molecular devices.[205-207] Easton *et al*. used the shuttling motion of a stilbene-modified α-CD Janus complex to replicate the expansion and contraction motion of a biological muscle,[1,208,209] as shown in Figure 1.33. The stilbene moiety is able to photoisomerise from the *E* to *Z* isomer, changing the position of the CD group on the axle component, causing an overall contraction of the length of the Janus complex. Various other molecular muscles have also been synthesised.[145,183,184,210-215]

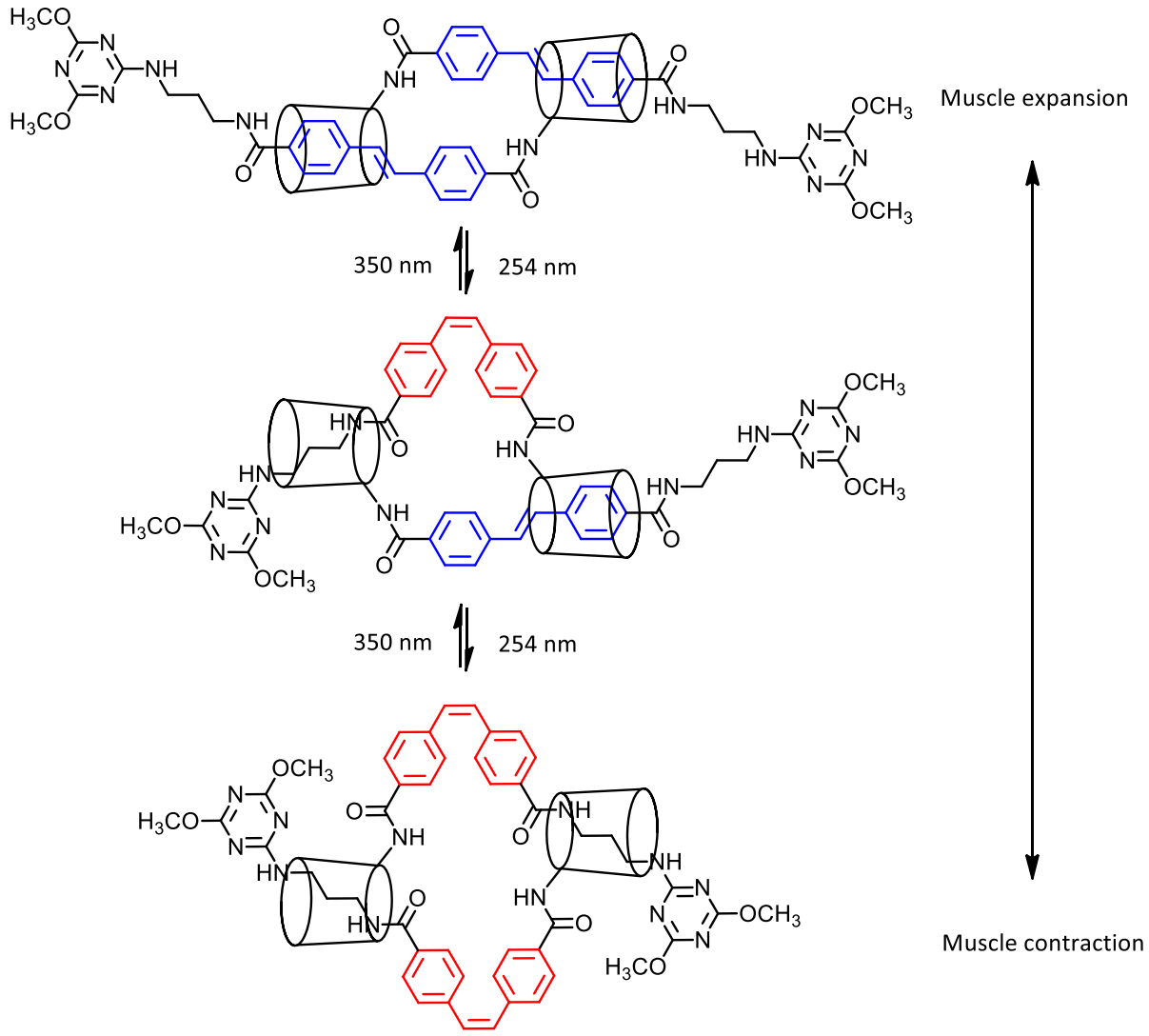

Figure 1.33: Structure of a molecular muscle based on a stilbene-modified α-CD Janus, which expands and contracts upon photoirradiation.[209]

1.5.2 Molecular Devices on Particles and Surfaces in Materials

The evolution of molecular devices has progressed to the functionalisation of devices on surfaces, particles and incorporation within materials. This has proved to be extremely fruitful as molecular motions may be visualised on the macroscopic scale. Leigh, Rudolf, Zerbetto *et al*. demonstrated the macroscopic transport of a liquid using a molecular shuttle.[216] A light-responsive, rotaxane-based molecular shuttle was grafted onto a self-assembled monolayer of 11-mercaptoundecanoic acid on Au(III) and deposited onto glass. A droplet of diiodomethane placed on this surface was shown to laterally move across the surface of the monolayer when photoirradiated. The droplet was also able to oppose gravity by moving up an incline of 12°, as shown in Figure 1.34.

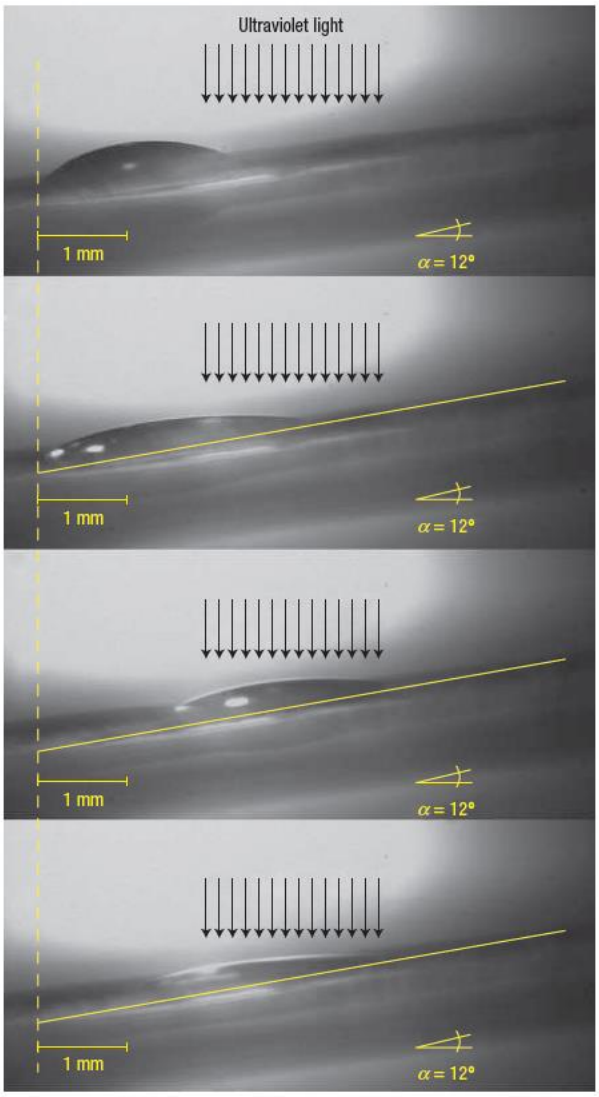

Figure 1.34: A 1.25 μL droplet of diiodomethane moving up a 12° incline of a self-assembled monolayer composed of a light-responsive, rotaxane-based molecular shuttle grafted onto 11-mercaptoundecanoic acid on Au(III), deposited onto glass. The movement of the drop (from top to bottom) is controlled by photoirradiation of the shuttle.

The unique properties of CDs were incorporated into functionalised nanoparticles to create CD-gated smart cargo delivery systems.[217] Stoddart, Zink *et al*. functionalised silica nanoparticles with azobenzene stalks,[218] as shown in Figure 1.35. β-Cyclodextrin threaded onto the *E* isomer of the azobenzene stalks, thereby blocking the pores of the nanoparticle. As β-CD is incapable of threading onto *Z*-azobenzene, the β-CD-gating of the nanoparticle could be moderated by photoisomerisation of the azobenzene moiety. The smart release of cargo by this system was demonstrated using Rhodamine B (RB), which could accommodate within the pores of the nanoparticle. RB could then be trapped or released upon photoirradiation.

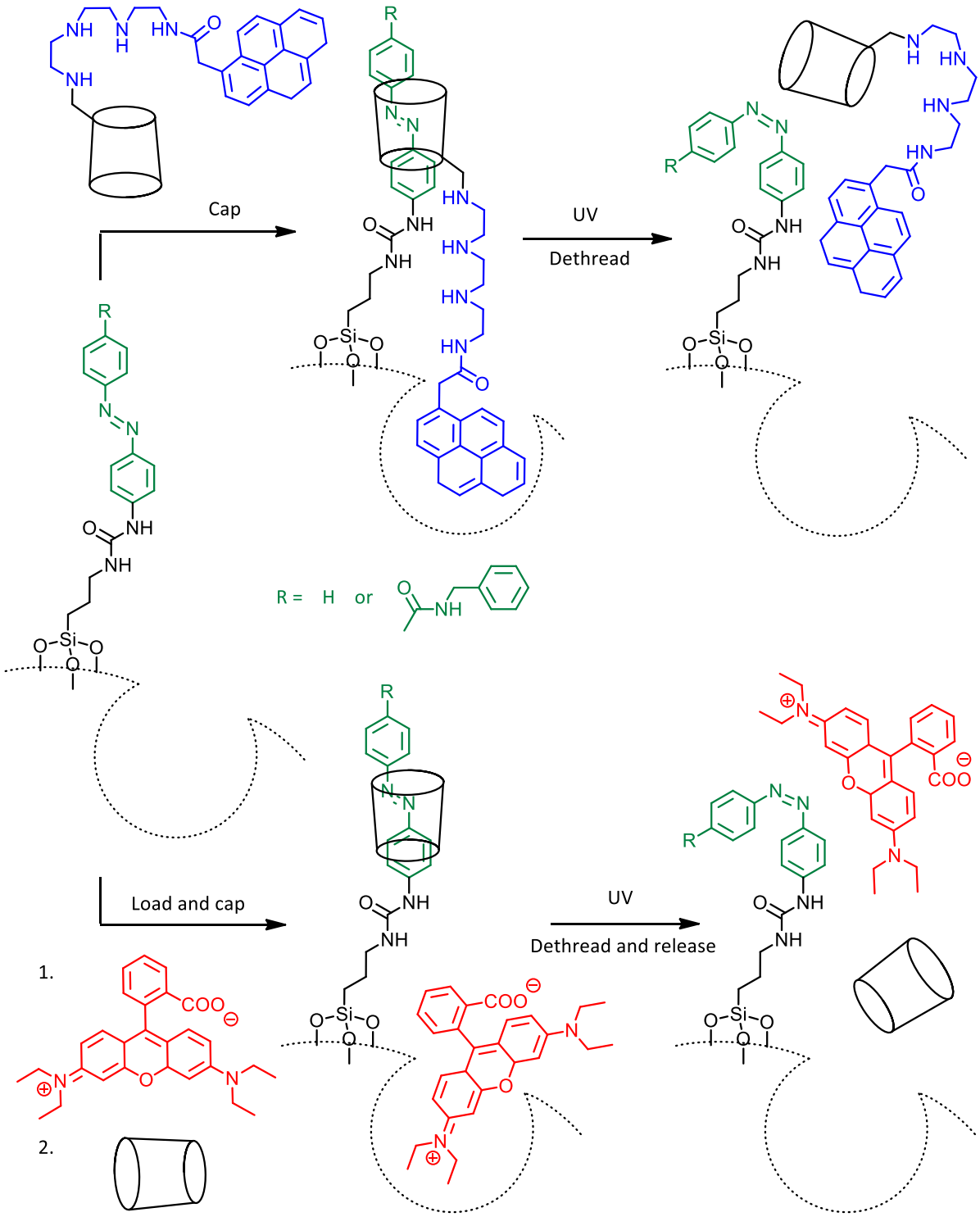

Figure 1.35: Operation of a β-CD-gated cargo delivery system based upon azobenzene-surface-functionalised silica nanoparticles (dashed lines).[218] The top reaction scheme shows the threading and dethreading of modified β-CD and the bottom reaction scheme demonstrates the capture and release of RB, moderated by photoirradiation of the azobenzene moiety, controlling the gating by β-CD.

1.5.3 Barriers to Success

As the field of molecular devices expands and more motions are realised with greater functionalities, new challenges emerge. We now wish to not only revel in the achievement of constructing a molecular device, but also understand the controls of the system in more detail.

The form of energy required to effect the motion is crucial.[181] Chemical energy is the most obvious kind of energy, which includes the input of metals, electrons, acids or bases to drive some kind of reaction. However, as molecular devices need to be reversible and almost infinitely cyclical, a constant supply of chemical reactants is required. These chemical reactants, which can be thought of as fuel, will cause an accumulation of waste products, which if not removed, could compromise the operation of the device.[181,192] Therefore, in many systems, photochemical or photoelectrical energy may be preferred as external stimuli. Photoelectrically driven devices have the advantage of a ready supply of electrodes, which may be the easiest way to connect molecular devices to the macroscopic world, while photochemically driven devices can operate within a small space and in a very short time domain (i.e. through use of lasers).[181,182,188,219] Both stimuli also share an ease in output readings and on-off activation.

Even if the energy input is mastered, molecular devices may not realise their full potential due to fundamental design flaws. Currently, molecular devices are designed to oppose thermal motion; however, nature utilises rather than opposes Brownian motion, allowing substrates to mix very rapidly in spite of highly viscous environments. Additionally, nature necessarily operates far from equilibrium, whereas non-biological chemistry eventually achieves equilibrium.[180] If molecular devices are to find practical applications, issues of energy input, equilibrium and an understanding of thermodynamic and kinetic controls of self-assembly need to be realised to a much greater extent than is presently the case.

1.6 Azobenzene

The research into various aspects of CD chemistry described in this thesis involves azobenzene and its isomers to a substantial extent, and accordingly some aspects of the chemistry of azobenzene are now explored. Azobenzene is a diazene derivative and a common component in supramolecular chemistry.[107,188,218] Azobenzene is able to photoisomerise from the thermodynamically more stable *E* isomer to the *Z* isomer and can thermally reverse isomerise back, as shown in Figure 1.36. As azobenzene exhibits substantial photostability and negligible decomposition, even after multiple photoisomerisation cycles, it remains a popular constituent in a wide variety of photoswitchable molecular devices and materials, enabling the conversion of light to mechanical energy.[220]

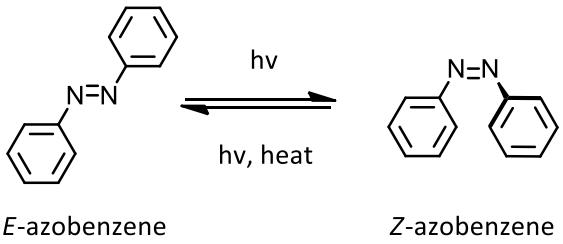

Figure 1.36: Structures of *E*- and *Z*-azobenzene interconverted through photoirradiation and heat.

The *E* isomer of azobenzene exists as a planar structure with C_{2h} symmetry, while the *Z* isomer is non-planar with C_2 symmetry.[221] The UV-vis absorption features of azobenzene are summarised in Table 1.1.[222] The UV-vis spectrum of azobenzene, in either the *E* or *Z* form, consists of two bands, the symmetry allowed $\pi \rightarrow \pi^*$ transition and the symmetry forbidden $n \rightarrow \pi^*$ transition, corresponding to the excitation of azobenzene from the ground state S_0 to excited states S_2 and S_1, respectively. The *Z* isomer has a weaker $\pi \rightarrow \pi^*$ transition at a shorter wavelength, due to the non-planar configuration, but a stronger $n \rightarrow \pi^*$ transition.[223]

Table 1.1: UV-vis absorption features of azobenzene isomers.[222]

Isomer	Transition	λ_{max} (nm)	ε (L mol^{-1} cm^{-1})
E	$\pi \rightarrow \pi^*$	320	~22000
	$n \rightarrow \pi^*$	450	~400
Z	$\pi \rightarrow \pi^*$	250	~11000
	$\pi \rightarrow \pi^*$	270	~5000
	$n \rightarrow \pi^*$	450	~1500

1.6.1 Mechanism of Isomerisation

Much of the utility of azobenzene relates to the isomerisation mechanism which is stimulated by both irradiation and heat, and which has been the subject of intensive research and debate.[224-235] Four mechanisms have been proposed for the isomerisation process,[222] as shown in Figure 1.37. Each mechanism is defined by a unique transition state, which may relax to form either the *E* or *Z* ground state isomer such that the photostationary state often consists of a mixture of isomers.

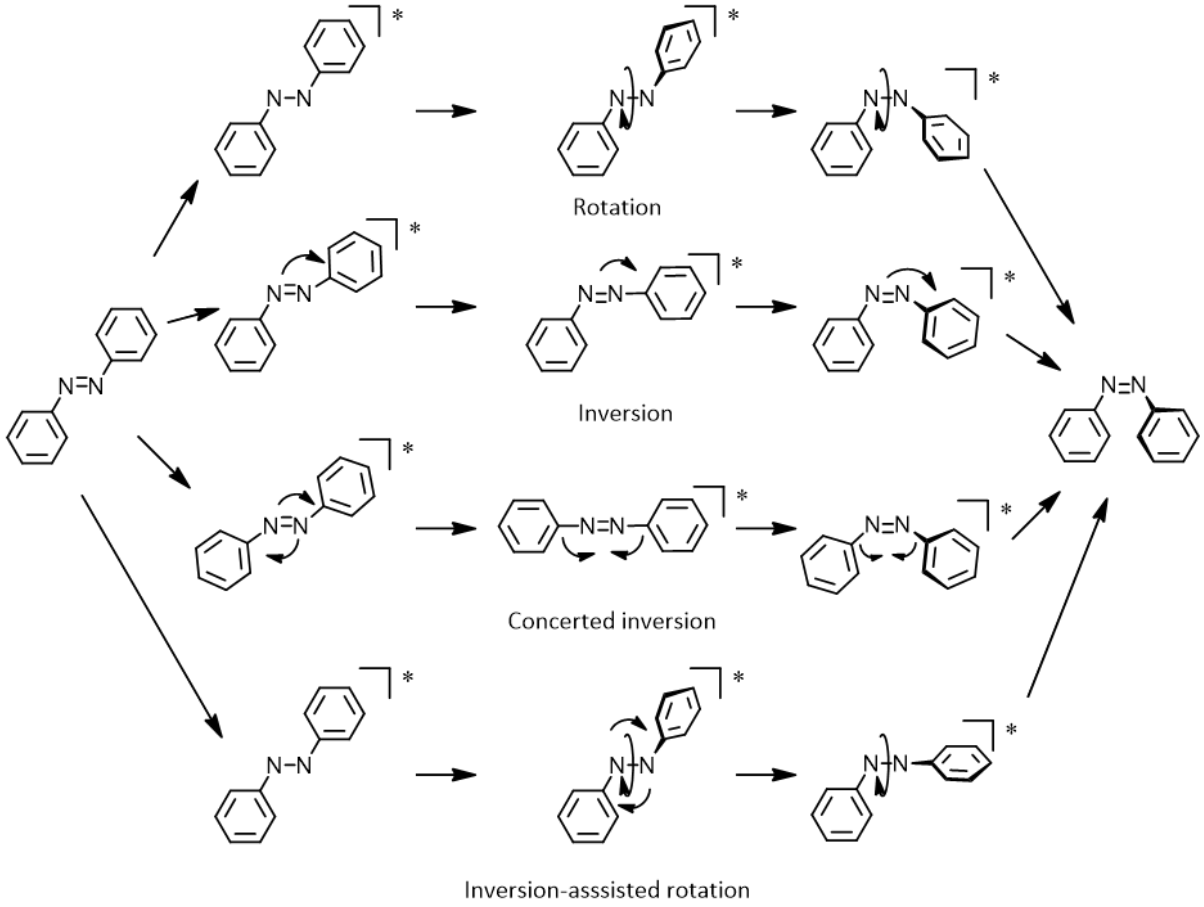

Figure 1.37: Possible mechanisms of photoisomerisation between *E* and *Z*-azobenzene.[222]

The rotation mechanism involves an initial breakage of the N=N bond, followed by free rotation about the N-N bond that alters the C-N-N-C dihedral angle. The inversion mechanism is initiated by one N=N-C angle forming a transition state at 180°, while the concerted inversion mechanism has a transition state arising from both N=N-C angles at linearity. The inversion-assisted rotation mechanism, sometimes known as the hula-twist mechanism, involves changes in both the C-N-N-C dihedral angle (following rupture of the N=N bond) and N-N-C angle. The transition state of the concerted inversion mechanism is non-polar while the other three mechanisms are polar.

Evidence exists for all four mechanisms and consequently a single mechanism cannot fully describe the isomerisation pathway for azobenzene. In reality, the prevalence of operation of a particular mechanism of isomerisation is likely to differ to accommodate various intrinsic and extrinsic factors such as substitution and solvent.[222] However, this has not hindered the manipulation of azobenzene to influence isomerisation quantum yields, rates of isomerisation and the thermodynamic stability of either isomer. As such, azobenzene functionalisation has sort to better understand and invoke control over the photochemical properties of azobenzene.

1.6.2 Perturbations of Isomerisation

As the UV-vis absorption spectra of *E*- and *Z*-azobenzene overlap, irradiation of one isomer will necessarily cause irradiation in the other.[236] While interconversion between the two isomers may be controlled by the wavelength of irradiation, temperature, polarity and solvent, altering these factors gives limited advantages.[222] Therefore, functionalisation of azobenzene has been explored to separate the absorbance range of each isomer to exhibit some degree of control over the thermodynamic stability of the isomers and rates of isomerisation.

The *Z* isomer has been made more thermodynamically stable than the *E* isomer by functionalisation of azobenzene with electron withdrawing and donating groups and sterically bulky groups. Bléger, Brouwer, Hecht *et al*. functionalised azobenzene at the *ortho*-position with fluorine to create near quantitative two-way isomerisation.[220] Fluorine at the *ortho*-position acts to reduce the electron density around the N=N bond, thereby lowering the energy of the n-orbital and hence, separating the energy of the n $\rightarrow \pi^*$ transition between the two isomers. The *Z* isomer was found to have a half-life of ca. 700 days. Similarly, Temps *et al*. formed a covalent bond between the two benzene rings to create a bridged azobenzene.[236] Due to ring strain, the *Z* isomer of the bridged azobenzene was more thermodynamically stable than the *E* isomer.

The rates of photoisomerisation and thermal isomerisation have also been controlled.[226] Jurczaka *et al*. reported that the thermal reverse isomerisation from *Z*- to *E*-azobenzene could be controlled by the addition of an anion such as a spherical halogen (F^-, Br^-) or Y-shaped carboxylate ($CH_3CO_2^-$, $PhCO_2^-$).[237] The anion transfers electron density to the π-system of azobenzene, increasing the repulsion between electron pairs on the N=N bond. Similarly, the addition of a catalyst was investigated by Scaiano *et al*., using gold nanoparticles to catalyse the isomerisation from *Z*- to *E*-azobenzene.[238]

Research into the control of azobenzene isomerisation has also elucidated other structures. While the *E* isomer is often planar, several examples of distorted structures have been reported.[227,236] Tamaoki *et al*. synthesised azobenzenophanes, cyclically methylene-linked azobenzene oligomers. The crystal structure of these oligomers indicated that *E*-azobenzene adopted a distorted structure, out of planarity, due to ring strain of the macrocycle.[239,240] Evidence for the distortion comes from UV-vis spectroscopy experiments that demonstrate a reduced extinction coefficient and a blue-shift in λ_{max} when compared with planar isomers.

While there has been extensive research into understanding and designing azobenzene groups for use as photochemical switches in supramolecular chemistry, our knowledge remains limited. For example, the position of azobenzene modification may be important. Despite the wide-ranging investigations into functionalising azobenzenes, few studies[241-243] have systematically sought to understand the effect of structural isomerisation on the photochemical properties of modified azobenzenes.

1.6.3 Effect of Cyclodextrin

Given the prevalence of azobenzene as a separate entity or as a substituent in many CD studies,[59,155,244] the effect of a CD moiety on azobenzene isomerization is an important consideration. While the many examples of azobenzene in CD chemistry has focused primarily on its utility as a photocontrollable moiety,[215,245] some research has investigated both the influence of azobenzene on CD complexation[246,247] and the effects of CD on azobenzene photochemistry. For example, de Rossi *et al*. discovered that the *Z* to *E* thermal isomerisation of some azo dyes were inhibited when complexed within the β-CD annulus.[248] When considering the continued use of azobenzene in CD chemistry, particularly to affect photochemical change, an understanding of the influence the two compounds exhibit on each other is crucial.

1.7 Research Objectives

Combinations of CDs and azobenzene have consistently featured in supramolecular chemistry owing to their complexation capabilities and photochemistry, respectively. However, our understanding of the factors that drive complexation (such as thermodynamics and kinetics) in CD-azobenzene systems is limited.

To gain further understanding of the fundamental chemistry behind CD-azobenzene systems, we have chosen to study azobenzene-substituted β-CD in oligomeric, polymeric and mechanically interlocked molecule (in the form of a molecular muscle) forms, as shown in Figure 1.38. Three structural isomers of azobenzene-linked β-CD dimers are synthesised.

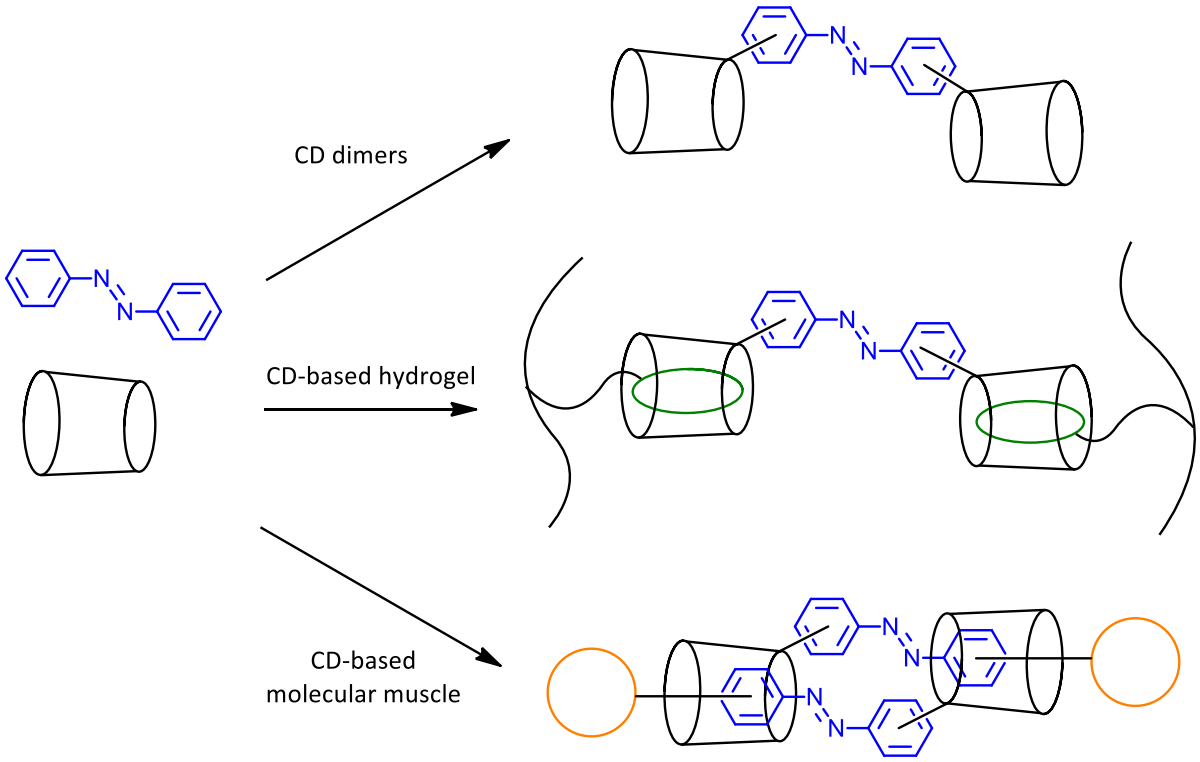

Figure 1.38: Proposed formation of possible oligomers, polymeric hydrogels and molecular devices based on β-CD and azobenzene.

While several similar CD dimers already exist,[59,249-252] there are no studies on the effect of structural isomerisation on the complexation behaviour or photochemistry of these CD-dimers. Thus, the effect of structural isomerisation of the three azobenzene-linked β-CD dimers to form host-guest complexes with a range of guests, and to form cross-links through the complexation of substituents on separate polymer chains in the formation of host-guest linked hydrogel is explored. In addition the synthesis of an azobenzene-modified β-CD molecular muscle through the self-assembly of a heteroditopic monomer is attempted. There are several examples of CD-based molecular muscles, but most have used α-CD[209,215,253] rather than β-CD.

1.7.1 Aims and Sequence of this Research

The aims of this research are to increase our understanding of azobenzene-modified β-CDs. The complexation behaviour and photochemistry of azobenzene-modified β-CD will be studied on the oligomeric, polymeric and mechanically interlocked molecule (MIM) scale.

Chapter 2 describes the attempted synthesis and characterisation of three structural isomers of an azobenzene-linked β-CD dimer. The effect of structural isomerisation on the photochemistry of the dimers will be investigated. The photochemistry of the dimers will be studied by ^{1}H NMR and UV-vis spectroscopy.

Chapter 3 describes the effect of β-CD modification on the host-guest complexation behaviour of the β-CD oligomers. The complexation behaviour, which includes the complexation constants, thermodynamics and kinetics associated with the host-guest complexation with three dye molecules, will be studied by 2D ^{1}H NMR and UV-vis spectroscopy.

Chapter 4 describes the host-guest complexation behaviour of modified β-CD hosts with four porphyrins. The effect of both host and guest modification on the complexation behaviour will be investigated by ^{1}H NMR and UV-vis spectroscopy and molecular modelling.

Chapter 5 describes the formation of host-guest linked hydrogels based on the three azobenzene linked β-CD dimers and four adamantyl- and alkyl-substituted poly(acrylate)s in aqueous solution. The complexation behaviour between the host and guest will be studied by isothermal titration calorimetry and 2D ^{1}H NMR spectroscopy. The formation of the hydrogels and their resultant macroscopic properties will be studied by rheology. The effect of photoisomerisation of the dimers on the rheological properties of the hydrogels will also be investigated.

Chapter 6 describes the attempted synthesis and characterisation of three new molecular muscles based on an azobenzene-modified β-CD heteroditopic monomer. The formation of either a cyclic or acyclic daisy chain is determined by 2D ROESY NMR spectroscopy and mass spectrometry.

1.8 References

(1) Vale, R. D.; Milligan, R. A. *Science* **2000**, *288*, 88.
(2) Lehn, J. M. *Angew. Chem. Int. Ed. Engl.* **1988**, *27*, 89.
(3) Lehn, J. M. *Angew. Chem. Int. Ed. Engl.* **1990**, *29*, 1304.
(4) Gale, P. A.; Steed, J. W. *Supramolecular chemistry: from molecules to nanomaterials*; Wiley, Chichester, West Sussex, **2012**.
(5) Cram, D. J. *Angew. Chem. Int. Ed. Engl.* **1986**, *25*, 1039.
(6) Pedersen, C. J. *J. Am. Chem. Soc.* **1967**, *89*, 2495.
(7) Pedersen, C. J. *Angew. Chem.* **1988**, *27*, 1021.
(8) Cram, D. J.; Cram, J. M. *Science* **1974**, *183*, 803.
(9) Cram, D. J.; Cram, J. M. *Acc. Chem. Res.* **1978**, *11*, 8.
(10) Cram, D. J. *Angew. Chem. Int. Ed. Engl.* **1988**, *27*, 1009.
(11) Saenger, W. R.; Jacob, J.; Gessler, K.; Steiner, T.; Hoffmann, D.; Sanbe, H.; Koizumi, K.; Smith, S. M.; Takaha, T. *Chem. Rev.* **1998**, *98*, 1787.
(12) Saenger, W.; Steiner, T. *Acta Crystallogr. Sect. A* **1998**, *54*, 798.
(13) Biedermann, F.; Nau, W. M.; Schneider, H.-J. *Angew. Chem.* **2014**, *53*, 11158.
(14) Rekharsky, M. V.; Inoue, Y. *Chem. Rev.* **1998**, *98*, 1875.
(15) Inoue, Y.; Hakushi, T.; Liu, Y.; Tong, L. H.; Shen, B. J.; Jin, D. S. *J. Am. Chem. Soc.* **1993**, *115*, 475.
(16) Inoue, Y.; Liu, Y.; Tong, L. H.; Shen, B. J.; Jin, D. S. *J. Am. Chem. Soc.* **1993**, *115*, 10637.
(17) Liu, L.; Guo, Q. X. *J. Inclusion Phenom. Macrocyclic Chem.* **2002**, *42*, 1.
(18) Schneider, H. J.; Hacket, F.; Rudiger, V.; Ikeda, H. *Chem. Rev.* **1998**, *98*, 1755.
(19) Cohen, Y.; Avram, L.; Frish, L. *Angew. Chem.* **2005**, *44*, 520.
(20) Ferrazza, R.; Rossi, B.; Guella, G. *J. Phys. Chem. B* **2014**, *118*, 7147.
(21) Arakawa, R.; Yamaguchi, T.; Takahashi, A.; Fujimoto, T.; Kaneda, T. *J. Am. Soc. Mass. Spectrom.* **2003**, *14*, 1116.
(22) Franski, R.; Gierczyk, B.; Schroeder, G.; Beck, S.; Springer, A.; Linscheid, M. *Carbohydr. Res.* **2005**, *340*, 1567.
(23) Bertaut, E.; Landy, D. *Beilstein J. Org. Chem.* **2014**, *10*, 2630.
(24) Bouchemal, K.; Mazzaferro, S. *Drug Discov. Today* **2012**, *17*, 623.
(25) Wszelaka-Rylik, M.; Gierycz, P. *J. Therm. Anal. Calorim.* **2013**, *111*, 2029.
(26) Barr, L.; Dumanski, P. G.; Easton, C. J.; Harper, J. B.; Lee, K.; Lincoln, S. F.; Meyer, A. G.; Simpson, J. S. *J. Inclusion Phenom. Macrocyclic Chem.* **2004**, *50*, 19.
(27) Barr, L.; Easton, C. J.; Lee, K.; Lincoln, S. F.; Simpson, J. S. *Tetrahedron Lett.* **2002**, *43*, 7797.
(28) Khan, A. R.; Forgo, P.; Stine, K. J.; D'Souza, V. T. *Chem. Rev.* **1998**, *98*, 1977.
(29) Martin, K. A.; Czarnik, A. W. *Tetrahedron Lett.* **1994**, *35*, 6781.
(30) Zaborova, E.; Guitet, M.; Prencipe, G.; Bleriot, Y.; Menand, M.; Sollogoub, M. *Angew. Chem.* **2013**, *52*, 639.
(31) Bistri, O.; Sinay, P.; Barbero, J. J.; Sollogoub, M. *Chem. Eur. J.* **2007**, *13*, 9757.
(32) Bistri, O.; Sinay, P.; Sollogoub, M. *Chem. Commun.* **2006**, 1112.
(33) Guieu, S.; Sollogoub, M. *J. Org. Chem.* **2008**, *73*, 2819.
(34) Wang, B.; Zaborova, E.; Guieu, S.; Petrillo, M.; Guitet, M.; Bleriot, Y.; Menand, M.; Zhang, Y.; Sollogoub, M. *Nature Commun.* **2014**, *5*.
(35) Breslow, R.; Halfon, S.; Zhang, B. L. *Tetrahedron* **1995**, *51*, 377.
(36) Harada, T.; Pham, D. T.; Leung, M. H. M.; Huy, T. N.; Lincoln, S. F.; Easton, C. J.; Kee, T. W. *J. Phys. Chem. B* **2011**, *115*, 1268.
(37) Haskard, C. A.; Easton, C. J.; May, B. L.; Lincoln, S. F. *J. Phys. Chem.* **1996**, *100*, 14457.
(38) Liu, Y.; Chen, Y. *Acc. Chem. Res.* **2006**, *39*, 681.
(39) Easton, C. J.; vanEyk, S. J.; Lincoln, S. F.; May, B. L.; Papageorgiou, J.; Williams, M. L. *Aust. J. Chem.* **1997**, *50*, 9.

(40) Pham, D. T.; Clements, P.; Easton, C. J.; Papageorgiou, J.; Maya, B. L.; Lincoln, S. F. *New J. Chem.* **2008**, *32*, 712.
(41) Menuel, S.; Azaroual, N.; Landy, D.; Six, N.; Hapiot, F.; Monflier, E. *Chem. Eur. J.* **2011**, *17*, 3949.
(42) Venema, F.; Nelissen, H. F. M.; Berthault, P.; Birlirakis, N.; Rowan, A. E.; Feiters, M. C.; Nolte, R. J. M. *Chem. Eur. J.* **1998**, *4*, 2237.
(43) Breslow, R.; Chung, S. *J. Am. Chem. Soc.* **1990**, *112*, 9659.
(44) Tabushi, I.; Kuroda, Y.; Shimokawa, K. *J. Am. Chem. Soc.* **1979**, *101*, 1614.
(45) Kumprecht, L.; Budesinsky, M.; Vondrasek, J.; Vymetal, J.; Cerny, J.; Cisarova, I.; Brynda, J.; Herzig, V.; Koutnik, P.; Zavada, J.; Kraus, T. *J. Org. Chem.* **2009**, *74*, 1082.
(46) Bistri-Aslanoff, O.; Bleriot, Y.; Auzely-Velty, R.; Sollogoub, M. *Org. Biomol. Chem.* **2010**, *8*, 3437.
(47) Dong, D.; Baigl, D.; Cui, Y.; Sinay, P.; Sollogoub, M.; Zhang, Y. *Tetrahedron* **2007**, *63*, 2973.
(48) Krejci, L.; Budesinsky, M.; Cisarova, I.; Kraus, T. *Chem. Commun.* **2009**, 3557.
(49) Bistri, O.; Lecourt, T.; Mallet, J. M.; Sollogoub, M.; Sinay, P. *Chem. Biodivers.* **2004**, *1*, 129.
(50) Michels, J. J.; Huskens, J.; Reinhoudt, D. N. *J. Am. Chem. Soc.* **2002**, *124*, 2056.
(51) Kano, K.; Itoh, Y.; Kitagishi, H.; Hayashi, T.; Hirotat, S. *J. Am. Chem. Soc.* **2008**, *130*, 8006.
(52) Watanabe, K.; Kitagishi, H.; Kano, K. *Angew. Chem.* **2013**, *52*, 6894.
(53) Hanh-Trang, N.; Duc-Truc, P.; Lincoln, S. F.; Wang, J.; Guo, X.; Easton, C. J.; Prud'homme, R. K. *Polym. Chem.* **2013**, *4*, 820.
(54) Kikuchi, T.; Narita, M.; Hamada, F. *Tetrahedron* **2001**, *57*, 9317.
(55) Nguyen, H.-T.; Pham, D.-T.; Easton, C. J.; Lincoln, S. F. *Aust. J. Chem.* **2013**, *66*, 1057.
(56) Sasaki, K.; Nagasaka, M.; Kuroda, Y. *Chem. Commun.* **2001**, 2630.
(57) Lecourt, T.; Bleriot, Y.; Auzely-Velty, R.; Sollogoub, M. *Chem. Commun.* **2010**, *46*, 2238.
(58) Nelissen, H. F. M.; Schut, A. F. J.; Venema, F.; Feiters, M. C.; Nolte, R. J. M. *Chem. Commun.* **2000**, 577.
(59) Kikuchi, T.; Narita, M.; Hamada, F. *J. Inclusion Phenom. Macrocyclic Chem.* **2002**, *44*, 329.
(60) Zhang, J.; Ma, P. X. *Adv. Drug Delivery Rev.* **2013**, *65*, 1215.
(61) Li, J.; Loh, X. J. *Adv. Drug Delivery Rev.* **2008**, *60*, 1000.
(62) van de Manakker, F.; Vermonden, T.; van Nostrum, C. F.; Hennink, W. E. *Biomacromolecules* **2009**, *10*, 3157.
(63) Liu, B.-w.; Zhou, H.; Zhou, S.-t.; Yuan, J.-y. *Eur. Polym. J.* **2015**, *65*, 63.
(64) Schmidt, B. V. K. J.; Hetzer, M.; Ritter, H.; Barner-Kowollik, C. *Prog. Polym. Sci.* **2014**, *39*, 235.
(65) Chen, G.; Jiang, M. *Chem. Soc. Rev.* **2011**, *40*, 2254.
(66) Harada, A. *J. Polym. Sci. A Polym. Chem.* **2006**, *44*, 5113.
(67) Liu, K. L.; Zhang, Z.; Li, J. *Soft Matter* **2011**, *7*, 11290.
(68) Tan, S.; Ladewig, K.; Fu, Q.; Blencowe, A.; Qiao, G. G. *Macromol. Rapid Commun.* **2014**, *35*, 1166.
(69) Concheiro, A.; Alvarez-Lorenzo, C. *Adv. Drug Delivery Rev.* **2013**, *65*, 1188.
(70) Li, J. *NPG Asia Mater.* **2010**, *2*, 112.
(71) Appel, E. A.; del Barrio, J.; Loh, X. J.; Scherman, O. A. *Chem. Soc. Rev.* **2012**, *41*, 6195.
(72) Harada, A.; Takashima, Y.; Nakahata, M. *Acc. Chem. Res.* **2014**, *47*, 2128.
(73) Sangeetha, N. M.; Maitra, U. *Chem. Soc. Rev.* **2005**, *34*, 821.
(74) Wei, Z.; Yang, J. H.; Zhou, J.; Xu, F.; Zrinyi, M.; Dussault, P. H.; Osada, Y.; Chen, Y. M. *Chem. Soc. Rev.* **2014**, *43*, 8114.
(75) Hoare, T. R.; Kohane, D. S. *Polymer* **2008**, *49*, 1993.
(76) Hoffman, A. S. *Adv. Drug Delivery Rev.* **2002**, *54*, 3.
(77) Lee, K. Y.; Mooney, D. J. *Chem. Rev.* **2001**, *101*, 1869.
(78) Pinho, E.; Grootveld, M.; Soares, G.; Henriques, M. *Crit. Rev. Biotechnol.* **2014**, *34*, 328.
(79) Renard, E.; Deratani, A.; Volet, G.; Sebille, B. *Eur. Polym. J.* **1997**, *33*, 49.
(80) Li, J. *Inclusion Polymers* **2009**, *222*, 79.
(81) Huang, F. H.; Gibson, H. W. *Prog. Polym. Sci.* **2005**, *30*, 982.

(82) Harada, A.; Okada, M.; Li, J.; Kamachi, M. *Macromolecules* **1995**, *28*, 8406.
(83) Li, J.; Harada, A.; Kamachi, M. *Polym. J.* **1994**, *26*, 1019.
(84) Zhao, S.-P.; Zhang, L.-M.; Ma, D. *J. Phys. Chem. B* **2006**, *110*, 12225.
(85) Li, J.; Li, X.; Zhou, Z. H.; Ni, X. P.; Leong, K. W. *Macromolecules* **2001**, *34*, 7236.
(86) Li, J.; Ni, X. P.; Leong, K. *Angew. Chem.* **2003**, *42*, 69.
(87) Sabadini, E.; Cosgrove, T. *Langmuir* **2003**, *19*, 9680.
(88) He, L. H.; Huang, J.; Chen, Y. M.; Xu, X. J.; Liu, L. P. *Macromolecules* **2005**, *38*, 3845.
(89) Wei, K.; Li, J.; Chen, G.; Jiang, M. *ACS Macro Lett.* **2013**, *2*, 278.
(90) Huh, K. M.; Ooya, T.; Lee, W. K.; Sasaki, S.; Kwon, I. C.; Jeong, S. Y.; Yui, N. *Macromolecules* **2001**, *34*, 8657.
(91) Huh, K. M.; Cho, Y. W.; Chung, H.; Kwon, I. C.; Jeong, S. Y.; Ooya, T.; Lee, W. K.; Sasaki, S.; Yui, N. *Macromol. Biosci.* **2004**, *4*, 92.
(92) Choi, H. S.; Yamamoto, K.; Ooya, T.; Yui, N. *Chemphyschem* **2005**, *6*, 1081.
(93) Wang, J.; Li, L.; Guo, X.; Zheng, L.; Pham, D.-T.; Lincoln, S. F.; Ngo, H. T.; Clements, P.; May, B. L.; Prud'homme, R. K.; Easton, C. J. *Ind. Eng. Chem. Res.* **2011**, *50*, 7566.
(94) Guo, X. H.; Abdala, A. A.; May, B. L.; Lincoln, S. F.; Khan, S. A.; Prud'homme, R. K. *Macromolecules* **2005**, *38*, 3037.
(95) Li, L.; Guo, X.; Wang, J.; Liu, P.; Prud'homme, R. K.; May, B. L.; Lincoln, S. F. *Macromolecules* **2008**, *41*, 8677.
(96) Guo, X. H.; Wang, J.; Li, L.; Pham, D. T.; Clements, P.; Lincoln, S. F.; May, B. L.; Chen, Q. C.; Zheng, L.; Prud'homme, R. K. *J. Polym. Sci. Part B Polym. Phys.* **2010**, *48*, 1818.
(97) Wang, J.; Duc-Truc, P.; Kee, T. W.; Clafton, S. N.; Guo, X.; Clements, P.; Lincoln, S. F.; Prud'homme, R. K.; Easton, C. J. *Macromolecules* **2011**, *44*, 9782.
(98) Guo, X.; Abdala, A. A.; May, B. L.; Lincoln, S. F.; Khan, S. A.; Prud'homme, R. K. *Polymer* **2006**, *47*, 2976.
(99) Kretschmann, O.; Choi, S. W.; Miyauchi, M.; Tomatsu, I.; Harada, A.; Ritter, H. *Angew. Chem.* **2006**, *45*, 4361.
(100) Bernert, D. B.; Boehm, I.; Isenbuegel, K.; Schoenenberg, L.; Ritter, H. *Polym. Int.* **2012**, *61*, 413.
(101) Koopmans, C.; Ritter, H. *Macromolecules* **2008**, *41*, 7418.
(102) van de Manakker, F.; van der Pot, M.; Vermonden, T.; van Nostrum, C. F.; Hennink, W. E. *Macromolecules* **2008**, *41*, 1766.
(103) van de Manakker, F.; Kroon-Batenburg, L. M. J.; Vermonden, T.; van Nostrum, C. F.; Hennink, W. E. *Soft Matter* **2010**, *6*, 187.
(104) Yingxue, Z.; Xiaodong, F.; Wanbin, Z.; Dan, X.; Jie, K. *J. Polym. Res.* **2014**, *21*, 0359 (10 pp.).
(105) Wang, J.; Xu, Y. S.; Wang, Y. M.; Liu, J. J.; Xu, J.; Li, L.; Nguyen, H. T.; Pham, D. T.; Lincoln, S. F.; Guo, X. H. *RSC Adv.* **2015**, *5*, 46067.
(106) Guo, X. H.; Wang, J.; Li, L.; Pham, D. T.; Clements, P.; Lincoln, S. F.; May, B. L.; Chen, Q. C.; Zheng, L.; Prud'homme, R. K. *Macromol. Rapid Commun.* **2010**, *31*, 300.
(107) Zhao, Y.-L.; Stoddart, J. F. *Langmuir* **2009**, *25*, 8442.
(108) Peng, L.; Zhang, H.; Feng, A.; Huo, M.; Wang, Z.; Hu, J.; Gao, W.; Yuan, J. *Polym. Chem.* **2015**, *6*, 3652.
(109) Tomatsu, I.; Hashidzume, A.; Harada, A. *Macromol. Rapid Commun.* **2006**, *27*, 238.
(110) Joung, Y.-K.; Ooya, T.; Yamaguchi, M.; Yui, N. *Adv. Mat.* **2007**, *19*, 396.
(111) Nakahata, M.; Takashima, Y.; Yamaguchi, H.; Harada, A. *Nature Commun.* **2011**, *2*.
(112) Chen, H.; Ma, X.; Wu, S.; Tian, H. *Angew. Chem.* **2014**, *53*, 14149.
(113) Yasin, A.; Zhou, W.; Yang, H.; Li, H.; Chen, Y.; Zhang, X. *Macromol. Rapid Commun.* **2015**, *36*, 845.
(114) Hashidzume, A.; Zheng, Y. T.; Takashima, Y.; Yamaguchi, H.; Harada, A. *Macromolecules* **2013**, *46*, 1939.
(115) Yamaguchi, H.; Kobayashi, Y.; Kobayashi, R.; Takashima, Y.; Hashidzume, A.; Harada, A. *Nature Commun.* **2012**, *3*.

(116) Chen, B.; Liu, K. L.; Zhang, Z.; Ni, X.; Goh, S. H.; Li, J. *Chem. Commun.* **2012**, *48*, 5638.
(117) Zhang, Z.-X.; Liu, K. L.; Li, J. *Angew. Chem.* **2013**, *52*, 6180.
(118) Liu, J.; Chen, G.; Guo, M.; Jiang, M. *Macromolecules* **2010**, *43*, 8086.
(119) Du, P.; Liu, J.; Chen, G.; Jiang, M. *Langmuir* **2011**, *27*, 9602.
(120) Tamesue, S.; Takashima, Y.; Yamaguchi, H.; Shinkai, S.; Harada, A. *Eur. J. Org. Chem.* **2011**, 2801.
(121) Klink, M.; Ritter, H. *Macromol. Rapid Commun.* **2008**, *29*, 1208.
(122) Ogoshi, T.; Takashima, Y.; Yamaguchi, H.; Harada, A. *J. Am. Chem. Soc.* **2007**, *129*, 4878.
(123) Wang, Z.; Chen, Y. *Macromolecules* **2007**, *40*, 3402.
(124) Himmelein, S.; Lewe, V.; Stuart, M. C. A.; Ravoo, B. J. *Chem. Sci.* **2014**, *5*, 1054.
(125) Ikeda, T.; Ooya, T.; Yui, N. *Macromol. Rapid Commun.* **2000**, *21*, 1257.
(126) Rizzo, C.; D'Anna, F.; Marullo, S.; Vitale, P.; Noto, R. *Eur. J. Org. Chem.* **2014**, *2014*, 1013.
(127) Zhang, J.; Shen, X. *J. Phys. Chem. B* **2013**, *117*, 1451.
(128) Krishnan, R.; Gopidas, K. R. *J. Phys. Chem. Lett.* **2011**, *2*, 2094.
(129) Jiang, L.; Yan, Y.; Huang, J. *Soft Matter* **2011**, *7*, 10417.
(130) Deng, W.; Yamaguchi, H.; Takashima, Y.; Harada, A. *Angew. Chem.* **2007**, *46*, 5144.
(131) Deng, W.; Yamaguchi, H.; Takashima, Y.; Harada, A. *Chem. Asian J.* **2008**, *3*, 687.
(132) Zhang, Q. W.; Qu, D. H.; Wu, J. C.; Ma, X.; Wang, Q. C.; Tian, H. *Langmuir* **2013**, *29*, 5345.
(133) Zhang, Q.; Qu, D.-H.; Ma, X.; Tian, H. *Chem. Commun.* **2013**, *49*, 9800.
(134) Guo, M.; Jiang, M.; Pispas, S.; Yu, W.; Zhou, C. *Macromolecules* **2008**, *41*, 9744.
(135) Kihara, N.; Hinoue, K.; Takata, T. *Macromolecules* **2005**, *38*, 223.
(136) Fleury, G.; Schlatter, G.; Brochon, C.; Hadziioannou, G. *Polymer* **2005**, *46*, 8494.
(137) Sakai, T.; Murayama, H.; Nagano, S.; Takeoka, Y.; Kidowaki, M.; Ito, K.; Seki, T. *Adv. Mat.* **2007**, *19*, 2023.
(138) Okumura, Y.; Ito, K. *Adv. Mat.* **2001**, *13*, 485.
(139) Rodell, C. B.; MacArthur, J. W., Jr.; Dorsey, S. M.; Wade, R. J.; Wang, L. L.; Woo, Y. J.; Burdick, J. A. *Adv. Funct. Mat.* **2015**, *25*, 636.
(140) Zhu, J.-L.; Liu, K. L.; Zhang, Z.; Zhang, X.-Z.; Li, J. *Chem. Commun.* **2011**, *47*, 12849.
(141) Bin Imran, A.; Esaki, K.; Gotoh, H.; Seki, T.; Ito, K.; Sakai, Y.; Takeoka, Y. *Nature Commun.* **2014**, *5*.
(142) Peters, O.; Ritter, H. *Angew. Chem.* **2013**, *52*, 8961.
(143) Nakahata, M.; Takashima, Y.; Harada, A. *Angew. Chem.* **2014**, *53*, 3617.
(144) Nakamura, T.; Takashima, Y.; Hashidzume, A.; Yamaguchi, H.; Harada, A. *Nature Commun.* **2014**, *5*.
(145) Takashima, Y.; Hatanaka, S.; Otsubo, M.; Nakahata, M.; Kakuta, T.; Hashidzume, A.; Yamaguchi, H.; Harada, A. *Nature Commun.* **2012**, *3*, 1270.
(146) Bruns, C. J.; Stoddart, J. F. In *Beauty in Chemistry: Artistry in the Creation of New Molecules*; Fabbrizzi, L., Ed. 2012; Vol. 323, p 19.
(147) Stoddart, J. F. *Chem. Soc. Rev.* **2009**, *38*, 1802.
(148) Nepogodiev, S. A.; Stoddart, J. F. *Chem. Rev.* **1998**, *98*, 1959.
(149) Sakuda, J.; Yasuda, T.; Kato, T. *Isr. J. Chem.* **2012**, *52*, 854.
(150) Collier, C. P.; Mattersteig, G.; Wong, E. W.; Luo, Y.; Beverly, K.; Sampaio, J.; Raymo, F. M.; Stoddart, J. F.; Heath, J. R. *Science* **2000**, *289*, 1172.
(151) Asakawa, M.; Ashton, P. R.; Balzani, V.; Credi, A.; Hamers, C.; Mattersteig, G.; Montalti, M.; Shipway, A. N.; Spencer, N.; Stoddart, J. F.; Tolley, M. S.; Venturi, M.; White, A. J. P.; Williams, D. J. *Angew. Chem.* **1998**, *37*, 333.
(152) Iwamoto, H.; Takizawa, W.; Itoh, K.; Hagiwara, T.; Tayama, E.; Hasegawa, E.; Haino, T. *J. Org. Chem.* **2013**, *78*, 5205.
(153) Ma, X.; Tian, H. *Chem. Soc. Rev.* **2010**, *39*, 70.
(154) Girek, T. *J. Inclusion Phenom. Macrocyclic Chem.* **2012**, *74*, 1.
(155) Dawson, R. E.; Maniam, S.; Lincoln, S. F.; Easton, C. J. *Org. Biomol. Chem.* **2008**, *6*, 1814.

(156) Ogoshi, T.; Aoki, T.; Shiga, R.; Iizuka, R.; Ueda, S.; Demachi, K.; Yamafuji, D.; Kayama, H.; Yamagishi, T.-a. *J. Am. Chem. Soc.* **2012**, *134*, 20322.
(157) Sugino, H.; Kawai, H.; Umehara, T.; Fujiwara, K.; Suzuki, T. *Chem. Eur. J.* **2012**, *18*, 13722.
(158) Aoki, D.; Uchida, S.; Nakazono, K.; Koyama, Y.; Takata, T. *ACS Macro Lett.* **2013**, *2*, 461.
(159) Ma, X. A.; Cao, J. J.; Wang, Q. C.; Tian, H. *Chem. Commun.* **2011**, *47*, 3559.
(160) Wenz, G.; Han, B. H.; Muller, A. *Chem. Rev.* **2006**, *106*, 782.
(161) Li, S.; Weng, G.-H.; Lin, W.; Sun, Z.-B.; Zhou, M.; Zhu, B.; Ye, Y.; Wu, J. *Polym. Chem.* **2014**, *5*, 3994.
(162) Ke, C. F.; Smaldone, R. A.; Kikuchi, T.; Li, H.; Davis, A. P.; Stoddart, J. F. *Angew. Chem.* **2013**, *52*, 381.
(163) Momcilovic, N.; Clark, P. G.; Boydston, A. J.; Grubbs, R. H. *J. Am. Chem. Soc.* **2011**, *133*, 19087.
(164) Avestro, A. J.; Belowich, M. E.; Stoddart, J. F. *Chem. Soc. Rev.* **2012**, *41*, 5881.
(165) Fredy, J. W.; Scelle, J.; Guenet, A.; Morel, E.; de Beaumais, S. A.; Menand, M.; Marvaud, V.; Bonnet, C. S.; Toth, E.; Sollogoub, M.; Vives, G.; Hasenknopf, B. *Chem. Eur. J.* **2014**, *20*, 10915.
(166) Ooya, T.; Yui, N. *Macromol. Chem. Phys.* **1998**, *199*, 2311.
(167) Ooya, T.; Choi, H. S.; Yamashita, A.; Yui, N.; Sugaya, Y.; Kano, A.; Maruyama, A.; Akita, H.; Ito, R.; Kogure, K.; Harashima, H. *J. Am. Chem. Soc.* **2006**, *128*, 3852.
(168) Harada, A.; Li, J.; Kamachi, M. *Nature* **1993**, *364*, 516.
(169) Rotzler, J.; Mayor, M. *Chem. Soc. Rev.* **2013**, *42*, 44.
(170) Cantrill, S. J.; Youn, G. J.; Stoddart, J. F.; Williams, D. J. *J. Org. Chem.* **2001**, *66*, 6857.
(171) Wolf, A.; Moulin, E.; Cid, J.-J.; Goujon, A.; Du, G.; Busseron, E.; Fuks, G.; Giuseppone, N. *Chem. Commun.* **2015**, *51*, 4212.
(172) Bruns, C. J.; Li, J.; Frasconi, M.; Schneebeli, S. T.; Iehl, J.; de Rouville, H.-P. J.; Stupp, S. I.; Voth, G. A.; Stoddart, J. F. *Angew. Chem.* **2014**, *53*, 1953.
(173) Miyauchi, M.; Harada, A. *J. Am. Chem. Soc.* **2004**, *126*, 11418.
(174) Hoshino, T.; Miyauchi, M.; Kawaguchi, Y.; Yamaguchi, H.; Harada, A. *J. Am. Chem. Soc.* **2000**, *122*, 9876.
(175) Lock, J. S.; May, B. L.; Clements, P.; Lincoln, S. F.; Easton, C. J. *Org. Biomol. Chem.* **2004**, *2*, 1381.
(176) Fujimoto, T.; Sakata, Y.; Kaneda, T. *Chem. Lett.* **2000**, 764.
(177) Kanaya, A.; Takashima, Y.; Harada, A. *J. Org. Chem.* **2011**, *76*, 492.
(178) Yamauchi, K.; Takashima, Y.; Hashidzume, A.; Yamaguchi, H.; Harada, A. *J. Am. Chem. Soc.* **2008**, *130*, 5024.
(179) Miyauchi, M.; Kawaguchi, Y.; Harada, A. *J. Inclusion Phenom. Macrocyclic Chem.* **2004**, *50*, 57.
(180) Kay, E. R.; Leigh, D. A.; Zerbetto, F. *Angew. Chem.* **2007**, *46*, 72.
(181) Ballardini, R.; Balzani, V.; Credi, A.; Gandolfi, M. T.; Venturi, M. *Acc. Chem. Res.* **2001**, *34*, 445.
(182) Balzani, V.; Credi, A.; Ferrer, B.; Silvi, S.; Venturi, M. In *Molecular Machines*; Kelly, T. R., Ed. 2005; Vol. 262, p 1.
(183) Collin, J. P.; Dietrich-Buchecker, C.; Gavina, P.; Jimenez-Molero, M. C.; Sauvage, J. P. *Acc. Chem. Res.* **2001**, *34*, 477.
(184) Jimenez-Molero, M. C.; Dietrich-Buchecker, C.; Sauvage, J. P. *Chem. Commun.* **2003**, 1613.
(185) Silvi, S.; Venturi, M.; Credi, A. *Chem. Commun.* **2011**, *47*, 2483.
(186) Leake, M. C. *Philos. Trans. R. Soc. B-Biol. Sci.* **2013**, *368*.
(187) Lucia, U. *Chem. Phys. Lett.* **2013**, *556*, 242.
(188) Balzani, V. *Photochem. Photobiol. Sci.* **2003**, *2*, 459.
(189) Koumura, N.; Zijlstra, R. W. J.; van Delden, R. A.; Harada, N.; Feringa, B. L. *Nature* **1999**, *401*, 152.

(190) Puigmarti-Luis, J.; Saletra, W. J.; Gonzalez, A.; Amabilino, D. B.; Perez-Garcia, L. *Chem. Commun.* **2014**, *50*, 82.
(191) Ashton, P. R.; Ballardini, R.; Balzani, V.; Baxter, I.; Credi, A.; Fyfe, M. C. T.; Gandolfi, M. T.; Gomez-Lopez, M.; Martinez-Diaz, M. V.; Piersanti, A.; Spencer, N.; Stoddart, J. F.; Venturi, M.; White, A. J. P.; Williams, D. J. *J. Am. Chem. Soc.* **1998**, *120*, 11932.
(192) Silvi, S.; Venturi, M.; Credi, A. *J. Mater. Chem.* **2009**, *19*, 2279.
(193) Zhu, L. L.; Yan, H.; Wang, X. J.; Zhao, Y. L. *J. Org. Chem.* **2012**, *77*, 10168.
(194) Leblond, J.; Petitjean, A. *Chemphyschem* **2011**, *12*, 1043.
(195) Hardouin-Lerouge, M.; Hudhomme, P.; Salle, M. *Chem. Soc. Rev.* **2011**, *40*, 30.
(196) Klaerner, F.-G.; Schrader, T. *Acc. Chem. Res.* **2013**, *46*, 967.
(197) Coulston, R. J.; Onagi, H.; Lincoln, S. F.; Easton, C. J. *J. Am. Chem. Soc.* **2006**, *128*, 14750.
(198) Onagi, H.; Blake, C. J.; Easton, C. J.; Lincoln, S. F. *Chem. Eur. J.* **2003**, *9*, 5978.
(199) Badjic, J. D.; Ronconi, C. M.; Stoddart, J. F.; Balzani, V.; Silvi, S.; Credi, A. *J. Am. Chem. Soc.* **2006**, *128*, 1489.
(200) Armaroli, N.; Balzani, V.; Collin, J. P.; Gavina, P.; Sauvage, J. P.; Ventura, B. *J. Am. Chem. Soc.* **1999**, *121*, 4397.
(201) Li, A. F.; Ruan, Y. B.; Jiang, Q. Q.; He, W. B.; Jiang, Y. B. *Chem. Eur. J.* **2010**, *16*, 5794.
(202) von Delius, M.; Leigh, D. A. *Chem. Soc. Rev.* **2011**, *40*, 3656.
(203) De Bo, G.; Kuschel, S.; Leigh, D. A.; Lewandowski, B.; Papmeyer, M.; Ward, J. W. *J. Am. Chem. Soc.* **2014**, *136*, 5811.
(204) Shinkai, S.; Nakaji, T.; Ogawa, T.; Shigematsu, K.; Manabe, O. *J. Am. Chem. Soc.* **1981**, *103*, 111.
(205) Lock, J. S.; May, B. L.; Clements, P.; Lincoln, S. F.; Easton, C. J. *Org. Biomol. Chem.* **2004**, *2*, 337.
(206) Harada, A. *Acc. Chem. Res.* **2001**, *34*, 456.
(207) Sun, T.; Zhang, H. C.; Li, Y. M.; Xin, F. F.; Kong, L.; Hao, A. Y. *Progress in Chemistry* **2010**, *22*, 2156.
(208) Rayment, I.; Holden, H. M.; Whittaker, M.; Yohn, C. B.; Lorenz, M.; Holmes, K. C.; Milligan, R. A. *Science* **1993**, *261*, 58.
(209) Dawson, R. E.; Lincoln, S. F.; Easton, C. J. *Chem. Commun.* **2008**, 3980.
(210) Jimenez-Molero, M. C.; Dietrich-Buchecker, C.; Sauvage, J. P. *Chem. Eur. J.* **2002**, *8*, 1456.
(211) Liu, Y.; Flood, A. H.; Bonvallett, P. A.; Vignon, S. A.; Northrop, B. H.; Tseng, H. R.; Jeppesen, J. O.; Huang, T. J.; Brough, B.; Baller, M.; Magonov, S.; Solares, S. D.; Goddard, W. A.; Ho, C. M.; Stoddart, J. F. *J. Am. Chem. Soc.* **2005**, *127*, 9745.
(212) Niess, F.; Duplan, V.; Sauvage, J. P. *Chem. Lett.* **2014**, *43*, 964.
(213) Bruns, C. J.; Stoddart, J. F. *Acc. Chem. Res.* **2014**, *47*, 2186.
(214) Jimenez, M. C.; Dietrich-Buchecker, C.; Sauvage, J. P. *Angew. Chem.* **2000**, *39*, 3284.
(215) Tsuda, S.; Aso, Y.; Kaneda, T. *Chem. Commun.* **2006**, 3072.
(216) Berna, J.; Leigh, D. A.; Lubomska, M.; Mendoza, S. M.; Perez, E. M.; Rudolf, P.; Teobaldi, G.; Zerbetto, F. *Nature Mater.* **2005**, *4*, 704.
(217) Zhou, S.; Sha, H.; Ke, X.; Liu, B.; Wang, X.; Du, X. *Chem. Commun.* **2015**, *51*, 7203.
(218) Ferris, D. P.; Zhao, Y. L.; Khashab, N. M.; Khatib, H. A.; Stoddart, J. F.; Zink, J. I. *J. Am. Chem. Soc.* **2009**, *131*, 1686.
(219) Balzani, V.; Credi, A.; Venturi, M. *Chem. Soc. Rev.* **2009**, *38*, 1542.
(220) Bleger, D.; Schwarz, J.; Brouwer, A. M.; Hecht, S. *J. Am. Chem. Soc.* **2012**, *134*, 20597.
(221) Traetteberg, M.; Hilmo, I.; Hagen, K. *J. Mol. Struct.* **1977**, *39*, 231.
(222) Bandara, H. M. D.; Burdette, S. C. *Chem. Soc. Rev.* **2012**, *41*, 1809.
(223) Griffith.J *Chem. Soc. Rev.* **1972**, *1*, 481.
(224) Rau, H.; Luddecke, E. *J. Am. Chem. Soc.* **1982**, *104*, 1616.
(225) Quick, M.; Dobryakov, A. L.; Gerecke, M.; Richter, C.; Berndt, F.; Ioffe, I. N.; Granovsky, A. A.; Mahrwald, R.; Ernsting, N. P.; Kovalenko, S. A. *J. Phys. Chem. B* **2014**, *118*, 8756.
(226) Rau, H.; Shen, Y. Q. *J. Photochem. Photobiol., A* **1988**, *42*, 321.

(227) Garcia-Fernandez, P.; Liu, Y.; Bersuker, I. B.; Boggs, J. E. *Phys. Chem. Chem. Phys.* **2011**, *13*, 3502.
(228) Diau, E. W. G. *J. Phys. Chem. A* **2004**, *108*, 950.
(229) Tan, E. M. M.; Amirjalayer, S.; Smolarek, S.; Vdovin, A.; Zerbetto, F.; Buma, W. J. *Nature Commun.* **2015**, *6*, 5860.
(230) Pancur, T.; Renth, F.; Temps, F.; Harbaum, B.; Kruger, A.; Herges, R.; Nather, C. *Phys. Chem. Chem. Phys.* **2005**, *7*, 1985.
(231) Nagele, T.; Hoche, R.; Zinth, W.; Wachtveitl, J. *Chem. Phys. Lett.* **1997**, *272*, 489.
(232) Fujino, T.; Arzhantsev, S. Y.; Tahara, T. *J. Phys. Chem. A* **2001**, *105*, 8123.
(233) Lednev, I. K.; Ye, T. Q.; Matousek, P.; Towrie, M.; Foggi, P.; Neuwahl, F. V. R.; Umapathy, S.; Hester, R. E.; Moore, J. N. *Chem. Phys. Lett.* **1998**, *290*, 68.
(234) Schultz, T.; Quenneville, J.; Levine, B.; Toniolo, A.; Martinez, T. J.; Lochbrunner, S.; Schmitt, M.; Shaffer, J. P.; Zgierski, M. Z.; Stolow, A. *J. Am. Chem. Soc.* **2003**, *125*, 8098.
(235) Conti, I.; Garavelli, M.; Orlandi, G. *J. Am. Chem. Soc.* **2008**, *130*, 5216.
(236) Siewertsen, R.; Neumann, H.; Buchheim-Stehn, B.; Herges, R.; Naether, C.; Renth, F.; Temps, F. *J. Am. Chem. Soc.* **2009**, *131*, 15594.
(237) Dabrowa, K.; Niedbala, P.; Jurczak, J. *Chem. Commun.* **2014**, *50*, 15748.
(238) Hallett-Tapley, G. L.; D'Alfonso, C.; Pacioni, N. L.; McTiernan, C. D.; Gonzalez-Bejar, M.; Lanzalunga, O.; Alarcon, E. I.; Scaiano, J. C. *Chem. Commun.* **2013**, *49*, 10073.
(239) Norikane, Y.; Kitamoto, K.; Tamaoki, N. *J. Org. Chem.* **2003**, *68*, 8291.
(240) Norikane, Y.; Tamaoki, N. *Eur. J. Org. Chem.* **2006**, 1296.
(241) Yang, C.-a.; Xie, H.; Zhong, G.; Zhang, H. *Polymer* **2013**, *54*, 3238.
(242) Rodriguez, M. A.; Braslavsky, S. E. *J. Phys. Chem. A* **1999**, *103*, 6295.
(243) Park, S. K.; Lee, C.; Min, K. C.; Lee, N. S. *Bull. Korean Chem. Soc.* **2005**, *26*, 1170.
(244) Fukushima, M.; Osa, T.; Ueno, A. *J. Chem. Soc., Chem. Commun.* **1991**, 15.
(245) Tamesue, S.; Takashima, Y.; Yamaguchi, H.; Shinkai, S.; Harada, A. *Angew. Chem.* **2010**, *49*, 7461.
(246) Liu, Y.; Zhao, Y. L.; Chen, Y.; Guo, D. S. *Org. Biomol. Chem.* **2005**, *3*, 584.
(247) Rajendiran, N.; Sankaranarayanan, R. K. *Carbohydr. Polym.* **2014**, *106*, 422.
(248) Sanchez, A. M.; deRossi, R. H. *J. Org. Chem.* **1996**, *61*, 3446.
(249) Ma, H. C.; Wang, F.; Li, W. F.; Ma, Y.; Yao, X. Q.; Lu, D. D.; Yang, Y. X.; Zhang, Z.; Lei, Z. Q. *J. Phys. Org. Chem.* **2014**, *27*, 722.
(250) Hamon, F.; Blaszkiewicz, C.; Buchotte, M.; Banaszak-Leonard, E.; Bricout, H.; Tilloy, S.; Monflier, E.; Cezard, C.; Bouteiller, L.; Len, C.; Djedaini-Pilard, F. *Beilstein J. Org. Chem.* **2014**, *10*, 2874.
(251) Casas-Solvas, J. M.; Martos-Maldonado, M. C.; Vargas-Berenguel, A. *Tetrahedron* **2008**, *64*, 10919.
(252) Liu, Y.; Kang, S.; Chen, Y.; Yang, Y. W.; Huskens, J. *J. Inclusion Phenom. Macrocyclic Chem.* **2006**, *56*, 197.
(253) Li, S. J.; Taura, D.; Hashidzume, A.; Harada, A. *Chem. Asian J.* **2010**, *5*, 2281.

CHAPTER 2

Synthesis and Photochemistry of Structural Isomers of Azobenzene-linked β-Cyclodextrin Dimers

2.1 Introduction

Cyclodextrin dimers are common components in supramolecular chemistry as they display enhanced binding affinities for a range of guests and are therefore suitable for applications ranging from drug delivery to catalysis.[1-4] Similarly, azobenzene has been deployed as a photocontrollable moiety in a variety of supramolecular systems including CD supramolecular systems.[5-8] Gaining an understanding of the combined effects of CDs and azobenzene is essential to developing potential practical applications of these systems. To this effect, several researchers have synthesised azobenzene-linked CD dimers which are the subject of the present study.[9,10]

Ueno *et al.* linked two β-CD entities to azobenzene through an ether link and explored the photoisomerisation of the azobenzene moiety from the *E* to Z isomer.[11] A maximum *Z* isomer proportion of 65.8% was achieved upon irradiation with 320 – 380 nm light. The half-life of the *Z* isomer was found to be 54.8 hours in aqueous solution at 298 K. Similarly, Djedaini-Pilard *et al.* amide-coupled azobenzene and two β-CD groups and investigated both the photochemical and host-guest complexation properties.[12] Sequential photoisomerisation cycles showed no fatigue in the system, while host-guest complexation experiments with an EDTA-linked adamantane dimer were performed to characterise the complexation properties of the host azobenzene-linked β-CD dimer.

The limited range of studies on azobenzene-linked CD dimers leave many avenues to be explored, such as the effect of structural isomerisation on the photochemical and complexation properties. In each aforementioned cases,[11,12] β-CD was substituted at the *para*-position of the phenyl ring of azobenzene, however, both *meta*- and *ortho*-positions are also potentially available for substitution.

The effect of structural isomerisation on the photochemistry of azobenzene has, to some degree, been explored[13-15] and may be extended to CD-substituted azobenzene compounds. Woolley *et al.* synthesised several 4,4'-diamidoazobenzenes substituted with various amine groups at the *ortho*-positions.[16] The *ortho*-substituents were found to selectively stabilise the *Z* isomer by comparison with the parent azobenzene. The stabilisation of the *Z* isomer was attributed to a tight packing of *ortho*-substituents to form a local, stabilising, hydrophobic cage around the azo group. Hara *et al.* substituted azobenzene with sterically bulky diethyl groups at the *ortho*- and *meta*-positions.[17] The rate of thermal *Z* to *E* isomerisation for the *ortho*-diethylated azobenzene was 30 times slower than the rate for the *meta*-diethylated azobenzene. The bulky diethyl substituents of the *ortho*-diethylated azobenzene reduces the free volume required for isomerisation.

These appear to be the only reported studies of the effect of structural isomerisation on the photochemistry of azobenzene-linked β-CD dimers. However, it is possible that structural isomers of azobenzene-linked β-CD dimers, where the β-CD group is substituted at either the *ortho*-, *meta*- or *para*- position, possess varying photostationary state (PS) ratios of *E* and *Z* isomers, rates of photoisomerisation and reverse thermal isomerisation, and different complexation properties.

2.1.1 Aims of this study

The aim of this research is to synthesise and characterise three structural isomers of azobenzene-linked β-CD dimers: *bis*(6^{A}-deoxy-β-cyclodextrin-6^{A}-yl)-4,4'-aminocarbonylazobenzene (*p*-β-CD$_2$az), *bis*(6^{A}-deoxy-β-cyclodextrin-6^{A}-yl)-3,3'-aminocarbonylazobenzene (*m*-β-CD$_2$az) and *bis*(6^{A}-deoxy-β-cyclodextrin-6^{A}-yl)-2,2'-aminocarbonylazobenzene (*o*-β-CD$_2$az), in which the β-CD substituent is in the *para*, *meta* or *ortho* position of both phenyl rings of azobenzene as shown in Figure 2.1. The *p*-β-CD$_2$az isomer has previously been synthesised,[12] and the newly synthesized *m*-β-CD$_2$az isomer is reported here. Attempts to prepare the *o*-β-CD$_2$az isomer are described herein but proved unsuccessful, and the reasons for this are discussed. The photochemical properties of the *p*-β-CD$_2$az and *m*-β-CD$_2$az dimers, including PS ratios of *E* and *Z* isomers and rates of reverse thermal isomerisation, are investigated by NMR and UV-vis spectroscopy before and after photoirradiation. The influence of 1-adamantanecarboxylate (ADC) on the isomerisation properties of the *p*-β-CD$_2$az and *m*-β-CD$_2$az dimers is also investigated by NMR spectroscopy.

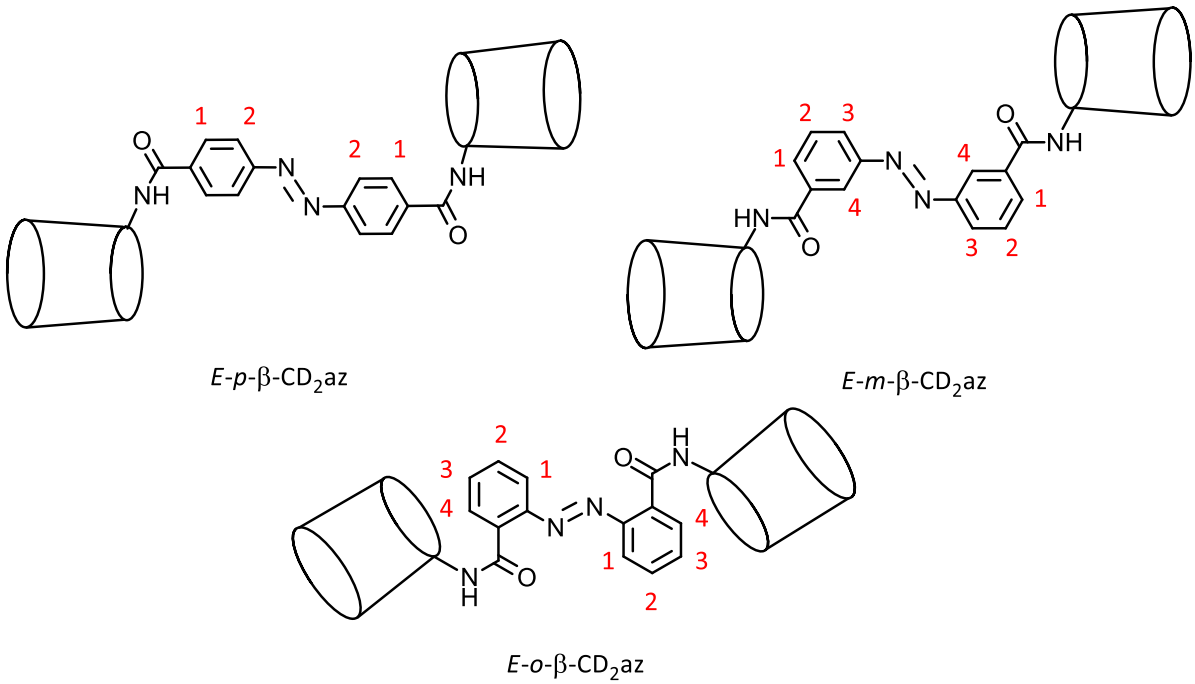

Figure 2.1: Structural isomers of azobenzene-linked β-CD dimers, depicted here as *E* isomers.

2.2 Results and Discussion

2.2.1 Synthesis of β-CD Dimers

The dimers *p*-β-CD_2az and *m*-β-CD_2az were first prepared by synthesising 6^A-amino-6^A-deoxy-β-CD (6β-$CDNH_2$). The synthesis of 6β-$CDNH_2$ required an initial modification of native β-CD. The first step is the reaction of native β-CD with *p*-toluenesulfonyl chloride (TsCl) to form 6^A-O-(4-methylbenzenesulfonyl)-β-CD (6β-CDTs).[18] As TsCl is a mild electrophile, substitution is regioselectively directed towards the C6 OH group of β-CD. The introduction of a tosyl group onto β-CD allowed nucleophilic substitution with ammonia to give 6β-$CDNH_2$.[19] A summary of the synthesis of 6β-$CDNH_2$ is given in Figure 2.2.

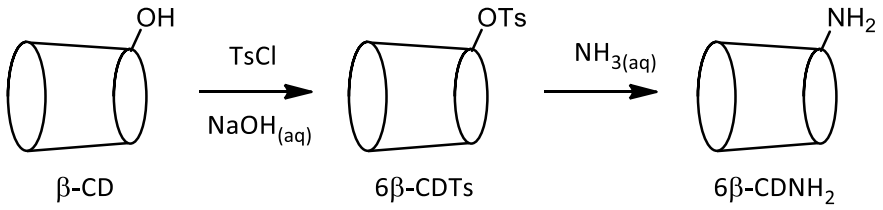

Figure 2.2: The synthesis of 6β-$CDNH_2$.

The modified azobenzene compounds were then synthesised from the parent *para- or meta*-nitrobenzoic acid in a basic solution containing glucose to yield either the *para*- or *meta*-*E*-azobenzene-dicarboxylic acid (*E*-*p*-AzCOOH or *E*-*m*-AzCOOH), respectively, as shown in Figure 2.3.[20-22] The final step in the synthesis of *p*-β-CD_2az and *m*-β-CD_2az involved the coupling of 6β-$CDNH_2$ with *E*-*p*-AzCOOH and *E*-*m*-AzCOOH, respectively, using hydroxybenzotriazole (HoBT) and dicyclohexylcarbodiimide (DCC), which are established amide coupling reagents, as shown in Figure 2.4.[23] Full synthetic details are given in Chapter 7.

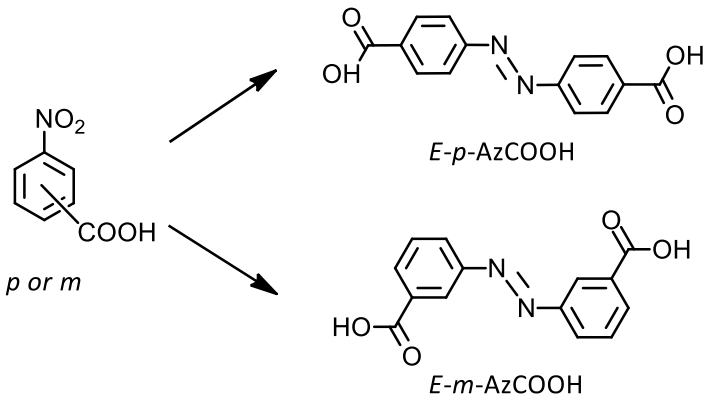

Figure 2.3: The synthesis of modified-azobenzenes.

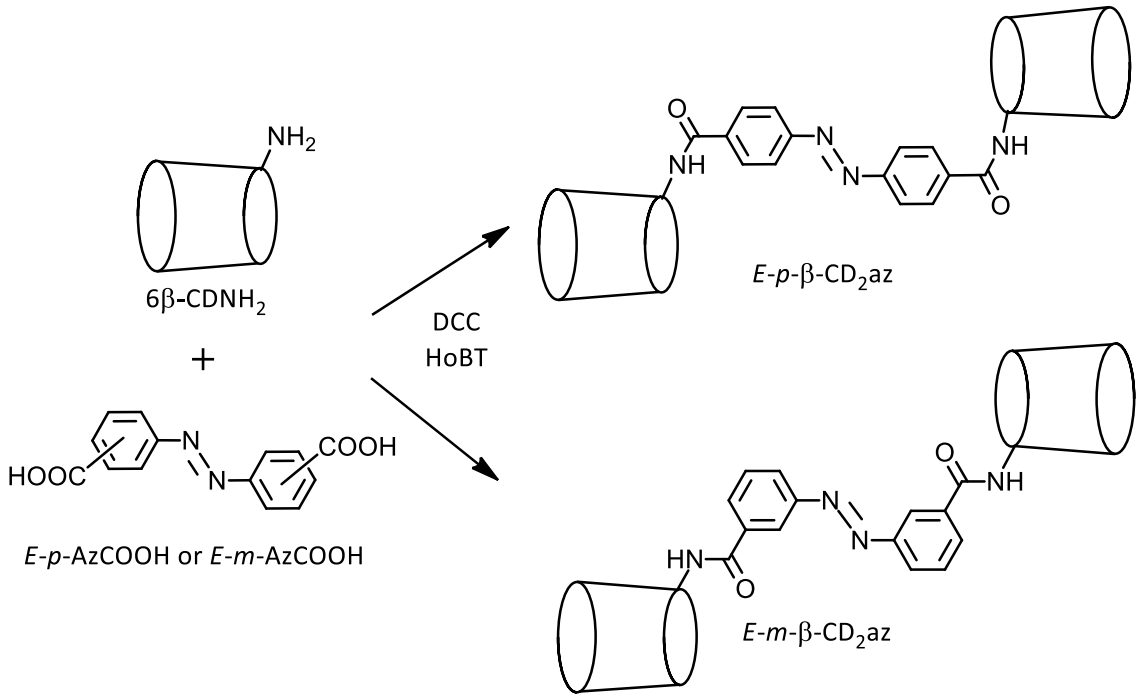

Figure 2.4: The synthesis of *p*-β-CD_2az and *m*-β-CD_2az, depicted here as *E* isomers.

The synthesis of *o*-β-CD_2az was also attempted, following a similar procedure as *p*-β-CD_2az and *m*-β-CD_2az. The synthesis of *ortho*-*E*-azobenzene-dicarboxylic acid (*E*-*o*-AzCOOH) was attempted by the reaction of *ortho*-nitrobenzoic acid in a basic solution containing glucose. An additional nitrophenol group was added to *E*-*o*-AzCOOH to form *bis*(4-nitrophenyl)-*E*-2,2'-dicarboxyazobenzene (*E*-*o*-Aznp), before direct substitution with 6β-$CDNH_2$, as shown in Figure 2.5.

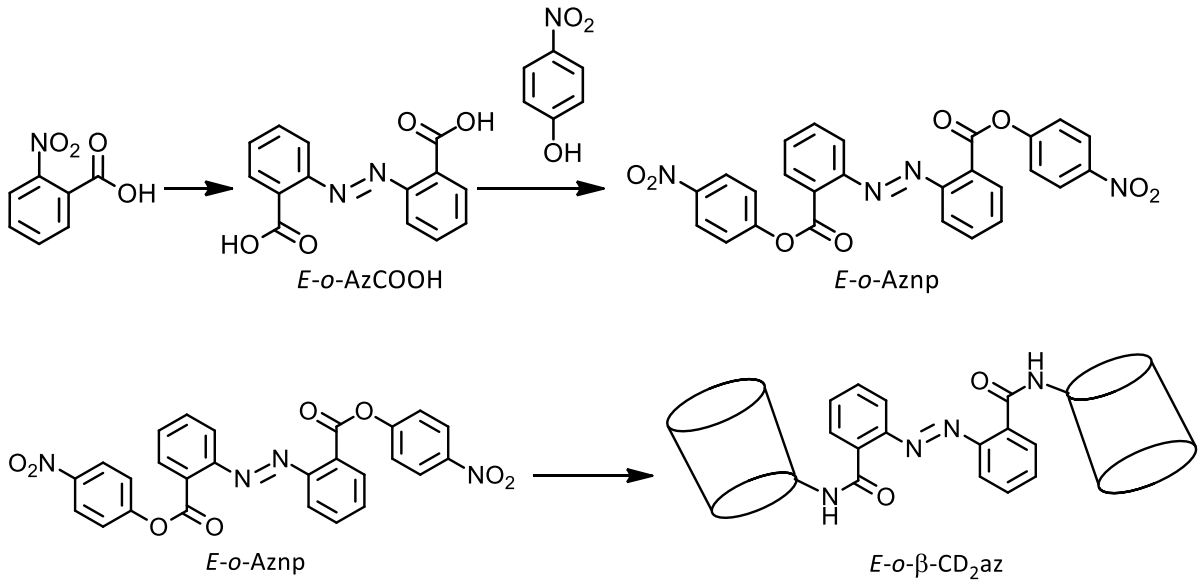

Figure 2.5: The proposed synthesis of *o*-β-CD_2az, depicted here as the *E* isomer.

However, the evaluation of the final compound by ^{1}H NMR spectroscopy and mass spectrometry did not conclusively identify *o*-β-CD_2az as the final product and therefore, further analysis was undertaken. The final product is henceforth referred to as **1**. The ^{1}H NMR spectrum of **1** in D_2O produced resonances consistent with *o*-β-CD_2az. A summary of the resonances is given in Table 2.1.

Table 2.1: Summary of ^{1}H NMR resonances of **1** (2.0×10^{-3} mol dm^{-3}) in D_2O at 298.2 K.

Resonance	Shift (ppm)	Type	Coupling Constant (Hz)	Relative intensity
A	7.47	d	8.1	1
B	7.37	t	7.8	1
C	6.91	d	8.1	1
D	6.86	t	8.1	1
E	5.15 – 5.03	m	-	7
F	4.11 – 3.90	m	-	42

Resonances A – D are consistent with the H1 – H4 protons of azobenzene as they occur within the aromatic region. Resonance E is well-defined as the H1 proton of β-CD, while resonance F is consistent with the H2 – H6 resonances of β-CD. The relative intensity of the resonances could correspond to an azobenzene-linked β-CD dimer. However, the mass spectrum did not yield the expected parent ion corresponding to $[M + H]^+$ or $[M + Na]^+$ of *o*-β-CD_2az. As *o*-β-CD_2az was expected to be sterically strained, it seemed possible that fragmentation may occur. However, further experiments were needed to confirm the structure of **1**.

Crystals of **1** were grown from an aqueous solution by vapour diffusion with ethanol. X-ray diffraction data were collected at 150(2) K with Mo Kα radiation (λ = 0.7107 Å) at 100(2) K on the MX-1 beamline of the Australian Synchrotron (λ = 0.7107 Å).[24] Data sets were corrected for absorption using a multi-scan method, and structures were solved by direct methods using SHELXS-2013, and refined by full-matrix least squares on F^2 by SHELXL-2014, interfaced through the program X-Seed.[25,26] X-ray diffraction experiments were performed by Dr Campbell Coghlan. A summary of the crystallographic data is shown in Table 2.2 and the calculated structure of **1** is given in Figure 2.6.

Table 2.2: Crystallographic data of **1**.

Formula		$C_{49}H_{76}N_2O_{35}$
Formula Weight (g mol^{-1})		1253.12
Space Group		C 2 2 2_1
Cell Constants	*a* (Å)	24.121(5)
	b (Å)	19.093(4)
	c (Å)	33.573(7)
Cell Angle	*a* (°)	90
	b (°)	90
	c (°)	90
Cell Volume (Å^3)		15461.8
Number of reflections		34285
Number of observations		135969
Number of parameters		776
R value (%)		8.99
Max. shift (esd)		0034
Max. residual electron density (e Å^{-3})	positive	0.464
	negative	-0.576

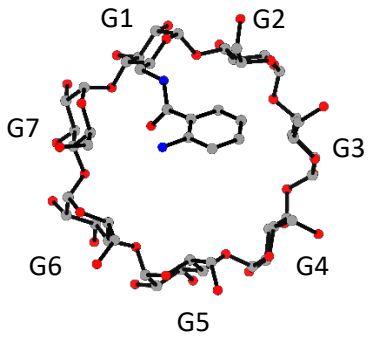

Figure 2.6: Structure of **1**, with each glucose unit (G1 – G7) of β-CD labelled. The carbon, oxygen and nitrogen atoms are shown in grey, red and blue, respectively.

The crystal structure of **1** clearly shows that the synthesis of *o*-β-CD_2az was not successful. β-Cyclodextrin was modified with an aminophenyl substituent rather than azobenzene to form (6^A-deoxy-β-cyclodextrin-6^A-yl)-2-aminocarbonyl-aminobenzene (β-CDab). The synthesis of β-CDab instead of *o*-β-CD_2az occurred as the initial preparation of *E*-*o*-AzCOOH was not successful. This reaction initially requires the reduction of the nitro group of nitrobenzoic acid to an amine, followed by oxidation of the amine to form the azo bond with an adjacent molecule.[22] However, while the reduction appears to have been successful, the subsequent oxidation did not form the azo bond, possibly due to steric hindrance of the *ortho*-carboxylic acid groups. Therefore, upon nitrophenol modification and substitution with 6β-$CDNH_2$, the final compound that formed was β-CDab. This

structure matches the NMR results, with resonances A, B, C and D corresponding to the H1, H2, H4 and H3 protons of the aminophenyl group, respectively. The structure also matches the mass spectrum results, which showed a parent ion at 1275.22 m/z, corresponding to the $[M + Na]^+$ ion. The synthesis of β-CDab is given in Figure 2.7. Full synthetic details are given in Chapter 7.

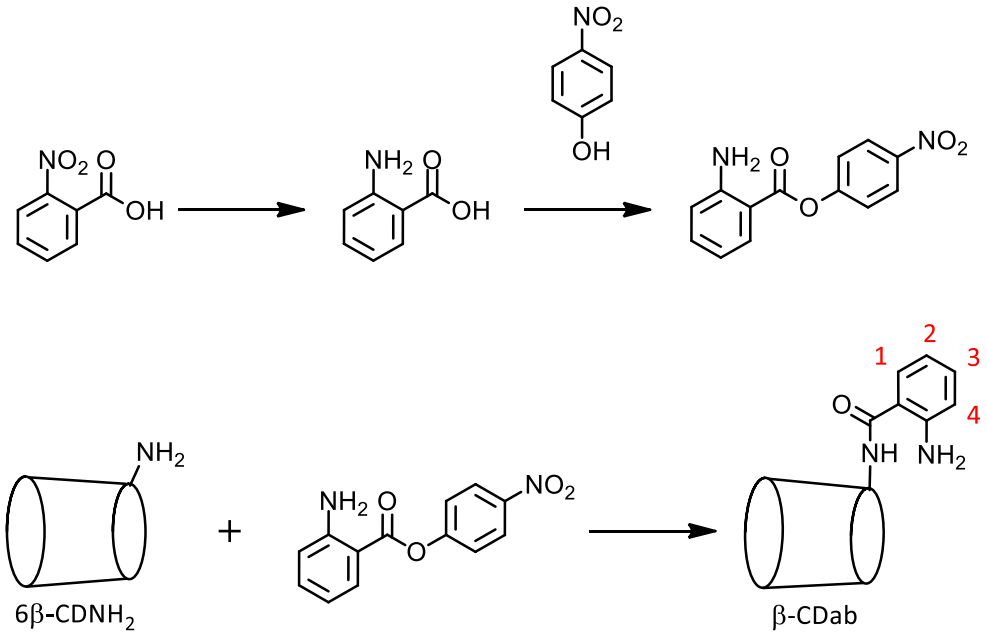

Figure 2.7: The synthesis of β-CDab.

2.2.1.1 Crystal structure of β-CDab

The crystal structure of β-CDab was further analysed. The modification of β-CD with the aminophenyl substituent moderately distorts the β-CD structure. The O4 atoms of each glucose unit are coplanar. The average distance between O4 atoms is 4.370 Å, while the average distance between each O4 atom and the centre of the β-CD group is 5.035 Å. As native β-CD is characterised by O4 to O4' distances of 4.3 Å and O4 to centre distances of 5.0 Å,[27] the β-CD group of β-CDab has retained some its approximate heptagonal symmetry. All measured distances between the O4 atoms and the distances between O4 atoms and the centre of β-CD are given in Table 2.10 and Table 2.11, respectively, in 2.5 Appendix.

However, there are some differences in the tilt angle, which is defined as the angle between the plane through all seven O4 atoms and the plane through C1, C4, O4 and O4' atoms of each glucose unit. There is significant variation in the tilt angles of β-CDab, ranging from 8.06° – 12.80°, with an average of 9.21°. All tilt angles are given in Table 2.12 in 2.5 Appendix. The average tilt angle of native β-CD is 14°, thus the reduced tilt angle results in a reduced inclination of each glucose unit of β-CDab. This reduced inclination decreases the distance between the secondary hydroxyl groups, increasing the strength of hydrogen bond interactions.[28]

The crystal packing arrangement of β-CDab was also analysed. Generally, CD compounds form three main types of packing arrangements: channel-, cage- and layer-type.[27,29] Channel-type packing structures comprise CD groups stacked to form infinite columns, held together by hydrogen bonding of adjacent hydroxyl groups, as shown in Figure 2.8a,b. As the CD groups of adjacent molecules may stack with both primary or secondary faces interacting or with one primary and one secondary face interacting, the structures are generally classified as either head-to-head or head-to-tail, respectively.

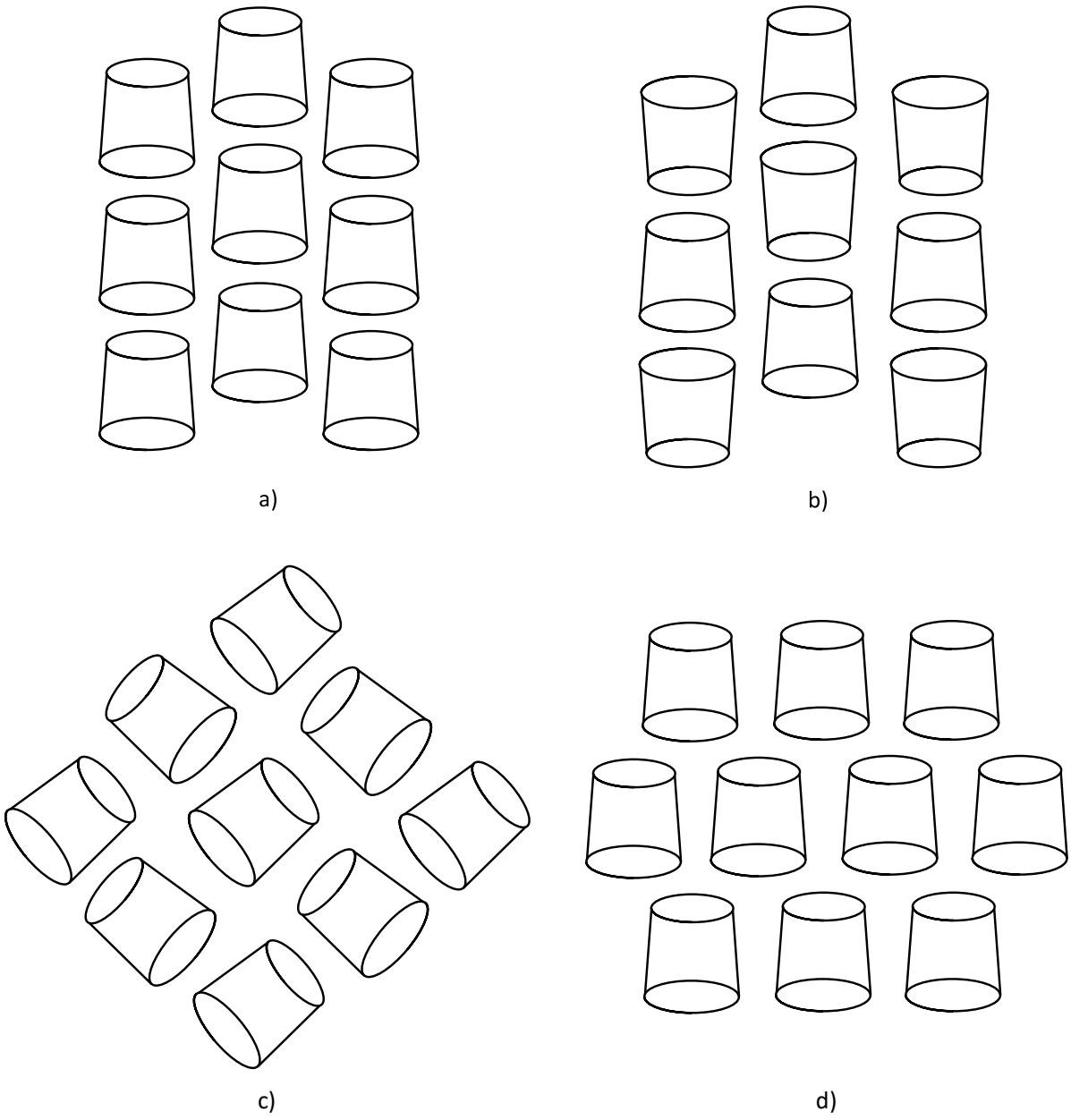

Figure 2.8: Various crystal packing arrangements of CD including a) head-to-tail channel-type packing, b) head-to-head channel-type packing, c) cage-type packing and d) layer-type packing.

Cage-type packing arrangements consist of CD molecules packed crosswise such that the side of one CD molecule is interacting with either the primary or secondary face of an adjacent CD molecule, as shown in Figure 2.8c. The cavity of each CD molecule is blocked, hence the term cage. The layer-type packing arrangement is similar to the cage-type as the CD cavities are blocked by neighbouring CD molecules. However, the CD molecules in the layer-type arrangement pack side by side and adjacent layers are displaced by approximately half a CD width such that the arrangement resembles a brick wall, as shown in Figure 2.8d.

The crystal structure of β-CDab shows that the aminophenyl substituent of one β-CDab interacts with an adjacent aminophenyl substituent to form a dimer that resembles a Janus form, as shown in Figure 2.9. The two substituents are parallel with a slight displacement, and the distance between the centroids of these two aminophenyl substituents is 3.71 Å, indicating π–π stacking.[30]

Further one dimensional packing occurs between adjacent β-CDab dimers. The hydroxyl groups on the secondary face of β-CD on one dimer interact with the hydroxyl groups of β-CD on an adjacent dimer, forming a head-to-head channel-type packing arrangement, as shown in Figure 2.10. The distances between the O2 and O3 atoms of adjacent β-CD groups are given in Table 2.13 in 2.5 Appendix. The O2/O3 to O2'/O3' distances are between 2.75 – 3.12 Å, with an average distance of 2.98 Å, consistent with hydrogen bonding.[31] Therefore, the packing of β-CDab within a crystal structure is held together by π–π stacking of adjacent aminophenyl substituents and hydrogen bonding interactions between adjacent secondary hydroxyl groups of β-CD to form a Janus form, head-to-head, channel-type packing arrangement.

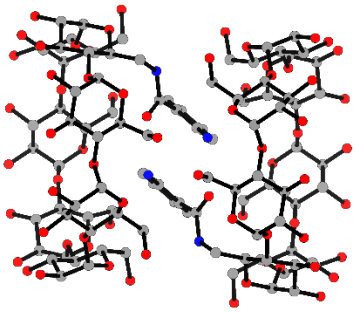

Figure 2.9: One dimensional packing arrangement of two β-CDab molecules. The carbon, oxygen and nitrogen atoms are shown in grey, red and blue, respectively.

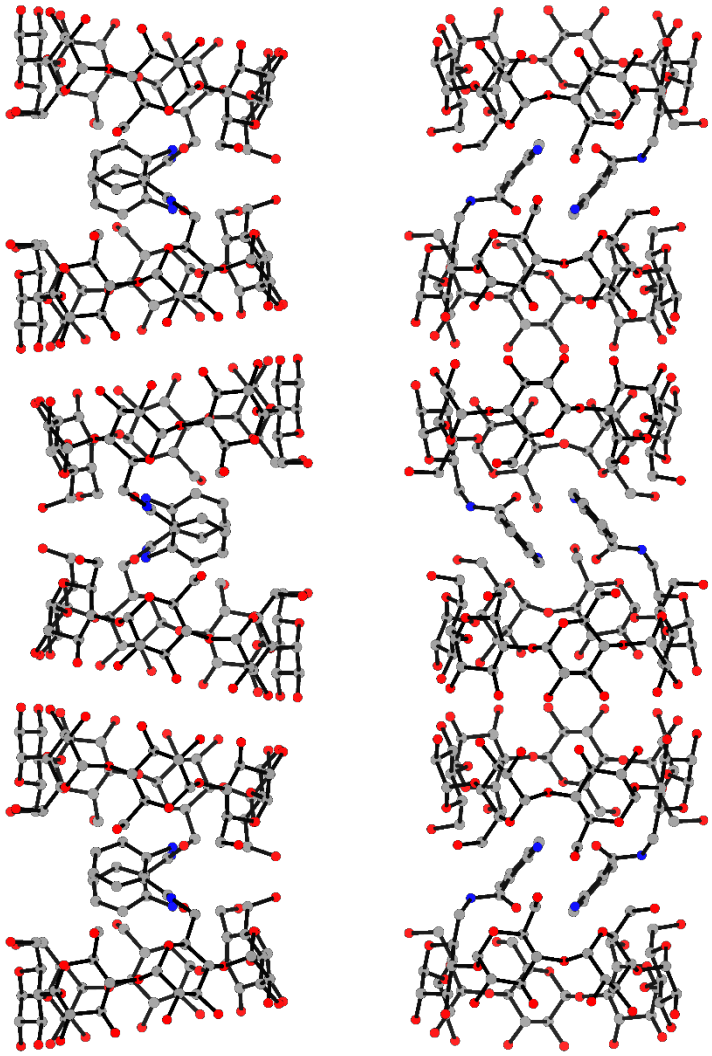

Figure 2.10: One dimensional channel-type packing arrangement of β-CDab. Two views are shown, differing by a 90° rotation. The carbon, oxygen and nitrogen atoms are shown in grey, red and blue, respectively.

The crystal packing arrangement of β-CDab is very different to most other mono-substituted β-CD compounds. Harata *et al.* synthesised a phenylethyl-substituted β-CD compound and determined the crystal structure.[28] The compound formed a head-to-tail, channel-type crystal packing arrangement. However, unlike β-CDab, the phenylethyl substituent of one molecule was included in the β-CD cavity of an adjacent molecule, thus the channel structure resembled an acyclic daisy chain. This acyclic daisy chain-style, head-to-tail, channel-type crystal packing arrangement is common amongst mono-substituted β-CD compounds.[32-35]

There are some examples of Janus form, head-to-head, channel-type crystal packing arrangements of mono-modified β-CD compounds. One of the earliest reports of Janus form packing was by Lichtenthaler *et al.*, who synthesised an imidazolylthiol-substituted β-CD compound.[36] The repeating

unit of the crystal structure was a head-to-head dimer consisting of imidazolyl substituents mutually residing over, yet not penetrating, the cavity of both β-CD groups. This packing mode was labelled 'Yin-Yang'. Similarly, Fan *et al.* synthesised a phenol-substituted β-CD compound and determined that the crystal packing arrangement was based upon a head-to-head dimer.[37] However, unlike the crystal structure of the imidazolythiol-substituted β-CD, the two phenol substituents fully penetrate the cavity of the adjacent β-CD group. A similar packing arrangement was described by Guo *et al.*[38] While the crystal packing arrangement of β-CDab is similar to these other Janus form crystal structures, the stabilisation of the Janus form by π-π stacking of the aminophenyl substituents appears to be unique.

The differences in the crystal packing arrangements are likely due to the nature of the substituent, in particular the position of substitution, length, linker atoms and suitability to complex within a CD cavity. Minor changes to the nature of the substituent can dramatically alter the crystal packing.[27,37] To identify the preference for β-CDab to arrange into a Janus form, the crystal packing structure of β-CDab was compared to another aminophenyl-substituted β-CD compound. Fan *et al.* modified β-CD with a *para*-substituted aminophenyl group (*p*-β-CDab).[37] The substituent was attached to the C6 position of β-CD via an ester link. Unlike β-CDab, *p*-β-CDab formed an acyclic daisy chain-style, head-to-tail, channel-type crystal packing arrangement.

Both β-CDab and *p*-β-CDab have rigid amide and ester links, respectively, connecting the aminophenyl substituents to β-CD. Therefore, the major difference is the position of the amino group on the phenyl ring. Substitution of the phenyl ring with an amine group at the *para* position does not significantly alter the width of the phenyl group and therefore, *para*-aminophenyl will have a similar size profile to the cavity of β-CD, allowing daisy chain-style packing. However, substitution of the phenyl ring at the *ortho* position will alter both the size profile and hydrophobicity of the phenyl group and thus, the penetration of the *ortho*-aminophenyl substituent into an adjacent β-CD cavity is no longer favoured. Hence, β-CDab forms a Janus form packing arrangement, stabilised by π-π stacking of the aminophenyl substituents.

2.2.2 Characterisation of Photochemical Properties of the *p*-βCD$_2$az and *m*-βCD$_2$az Dimers

In principle, the azobenzene moiety in *p*-β-CD$_2$az and *m*-β-CD$_2$az may undergo photoisomerisation from the *E* to *Z* isomer by irradiation with UV light and photoisomerisation from the *Z* to *E* isomer by irradiation with visible light. Azobenzene may also undergo reverse thermal isomerisation in the dark from the *Z* to the *E* isomer.[5] The isomerisation equilibria for *p*-β-CD$_2$az and *m*-β-CD$_2$az are shown in Figure 2.11.

The PS ratios of *p*-β-CD$_2$az and *m*-β-CD$_2$az before and after irradiation with UV and visible light were characterised by UV-vis and ^{1}H NMR spectroscopy. Irradiation wavelengths of 300 – 355 nm and >400 nm were chosen for this study. As β-CDab does not possess an azo bond, it was not considered for isomerisation studies.

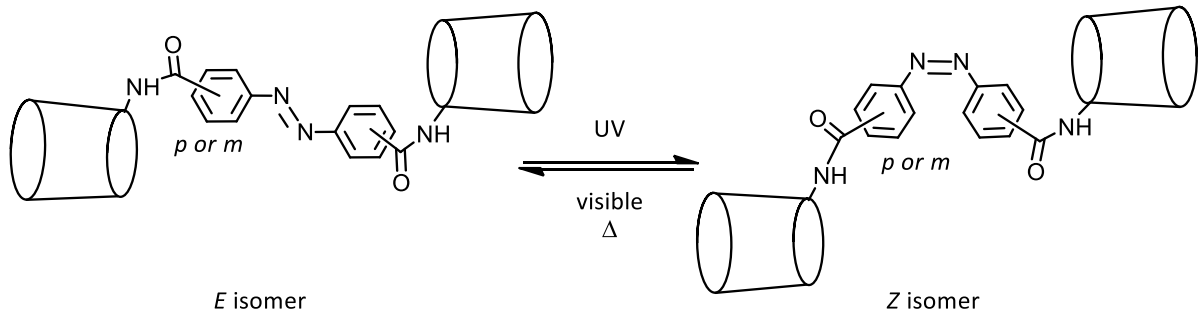

Figure 2.11: Photoisomerisation and reverse thermal isomerisation between the *E* and *Z* isomers of *p*-β-CD$_2$az and *m*-β-CD$_2$az.

2.2.2.1 UV-vis spectroscopy of the *p*-β-CD$_2$az and *m*-β-CD$_2$az Dimers

The photoisomerisation of *p*-βCD$_2$az and *m*-βCD$_2$az was monitored by UV-vis absorption spectroscopy. The two dimers were prepared in aqueous phosphate buffer (pH 7.0, *I* = 0.01 mol dm^{-3}) at 298.2 K and irradiated first at 300 – 355 nm and then >400 nm using a 500 W Xe lamp equipped with cut-off filters. The samples were irradiated and the spectra were recorded at intervals until no further change in absorption was detected. The UV-vis spectra of *p*-β-CD$_2$az and *m*-β-CD$_2$az before irradiation were compared against that of potassium *E*-4,4'-azobenzene-dicarboxylate (K$_2$.*E*-*p*-Az(COO)$_2$), as shown in Figure 2.12. A summary of the maximum wavelengths, λ_{max}, and extinction coefficients, ε_{max}, is given in Table 2.3.

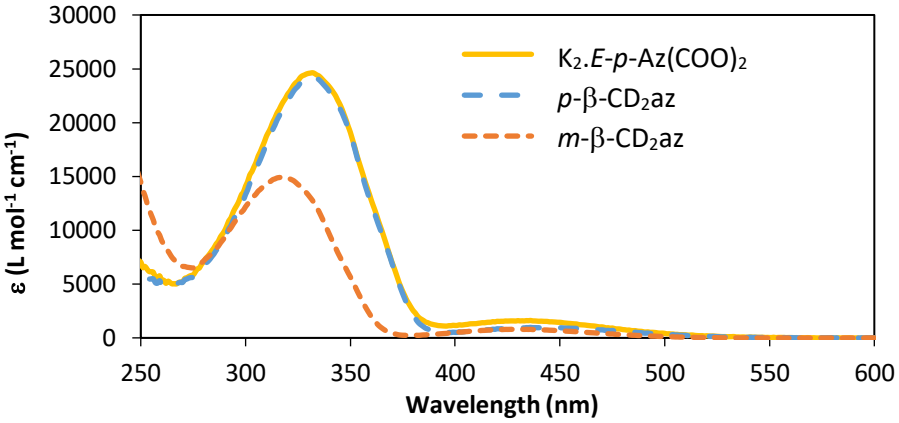

Figure 2.12: UV-vis absorption spectra of *p*-β-CD_2az, *m*-β-CD_2az, and K_2.*E*-*p*-Az$(COO)_2$ in aqueous phosphate buffer (pH 7.0, *I* = 0.01 mol dm^{-3}) at 298.2 K prior to irradiation.

Table 2.3: Maximum wavelengths, λ_{max}, and extinction coefficients, ε_{max}, of *p*-β-CD_2az, *m*-β-CD_2az and K_2.*E*-*p*-Az$(COO)_2$ in aqueous phosphate buffer (pH 7.0, *I* = 0.01 mol dm^{-3}) at 298.2 K.

Species	λ_{max1} (nm)	ε_{max1} (L mol^{-1} cm^{-1})	λ_{max2} (nm)	ε_{max2} (L mol^{-1} cm^{-1})
K_2.*E*-*p*-Az$(COO)_2$	332	24600	436	1616
p-β-CD_2az	332	24200	436	970
m-β-CD_2az	318	14900	430	800

The UV-vis absorption spectra of *p*-β-CD_2az and *m*-β-CD_2az at the PS shows absorption in the UV (λ_{max1} and ε_{max1}) and visible (λ_{max2} and ε_{max2}) regions corresponding to the π-π* transition and *n*-π* transition, respectively, similar to the known photochemical properties of unsubstituted azobenzene.[5] The spectrum of *p*-β-CD_2az closely resembles that of K_2.*E*-*p*-Az$(COO)_2$, with both species exhibiting a λ_{max1} of 332 nm and ε_{max1} values of 24200 and 24600 L mol^{-1} cm^{-1}, respectively. As K_2.*E*-*p*-Az$(COO)_2$ is likely to exist predominantly as a planar *E* isomer,[5] the similar UV-vis absorption characteristics suggest that *p*-β-CD_2az also exists predominantly as the *E* isomer. Interestingly, while the λ_{max2} wavelengths between *p*-βCD_2az and K_2.*E*-*p*-Az$(COO)_2$ are identical, the ε_{max2} of *p*-β-CD_2az is about half that of *E*-*p*-Az$(COOK)_2$, consistent with the substitution of β-CD groups onto azobenzene at the *para* positions diminishing the intensity of the *n*-π* transition.

The spectrum of *m*-β-CD_2az has a blue-shifted λ_{max1}, by comparison with that of *p*-β-CD_2az, of 318 nm, with a diminished ε_{max1} of 14900 L mol^{-1} cm^{-1}. As *Z*-azobenzene exhibits a blue shifted λ_{max1} and reduced ε_{max1} by comparison with that of *E*-azobenzene,[5] the absorption properties of *m*-β-CD_2az suggest that the PS state consists of some proportion of the *Z* isomer. As *p*-β-CD_2az appears to exist predominantly as the *E* isomer and *m*-β-CD_2az exists in some proportion as the *Z* isomer, we may expect the UV-vis spectrum of *m*-β-CD_2az to show a larger ε_{max2} value, concordant with most of the observed *Z* isomers of azobenzene.[5] However, the ε_{max2} of *m*-β-CD_2az is less than the ε_{max2} value of *p*-

β-CD_2az, again indicating that the substitution of azobenzene with β-CD decreases the intensity of the *n*-π* transition.

The PS ratios of the *E* and *Z* isomers of each dimer were investigated by monitoring changes in the UV-vis absorption spectrum upon irradiation with UV and visible light, which is likely to induce *E* to *Z* and *Z* to *E* isomerisation, respectively. The changes in UV-vis spectra upon irradiation of *p*-β-CD_2az and *m*-β-CD_2az are shown in Figure 2.13 – Figure 2.16.

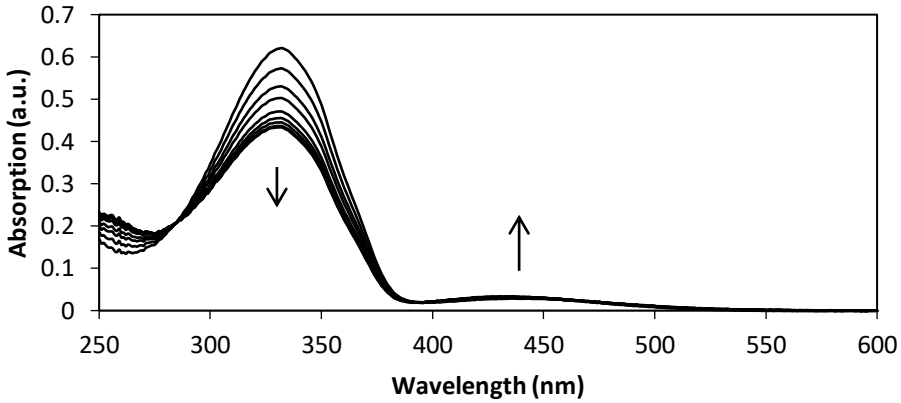

Figure 2.13: UV-vis absorption spectra of *p*-β-CD_2az (2.5×10^{-5} mol dm^{-3}) in aqueous phosphate buffer (pH 7.0, I = 0.10 mol dm^{-3}) at 298.2 K, irradiated with 300 – 355 nm light over 20 minutes. The arrows indicate the direction of the UV-vis absorption change with time.

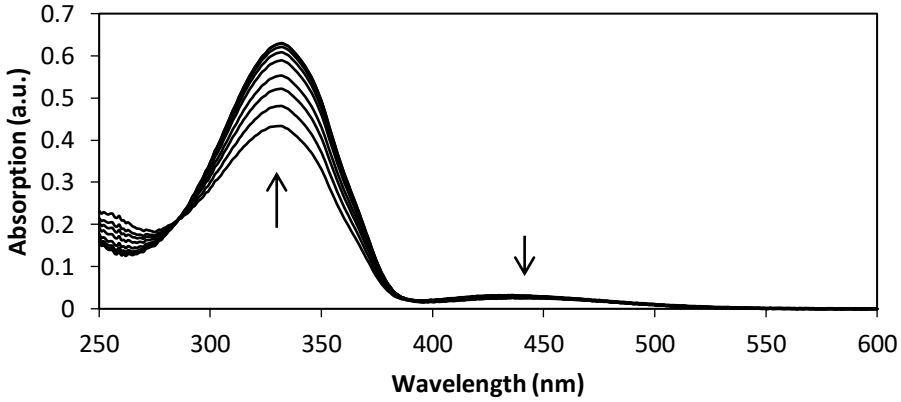

Figure 2.14: UV-vis absorption spectra of an initially UV irradiated (300 – 355 nm) sample of *p*-β-CD_2az (2.5×10^{-5} mol dm^{-3}) in aqueous phosphate buffer (pH 7.0, I = 0.10 mol dm^{-3}) at 298.2 K, irradiated with visible light (>400 nm) over 20 minutes. The arrows indicate the direction of the UV-vis absorption change with time.

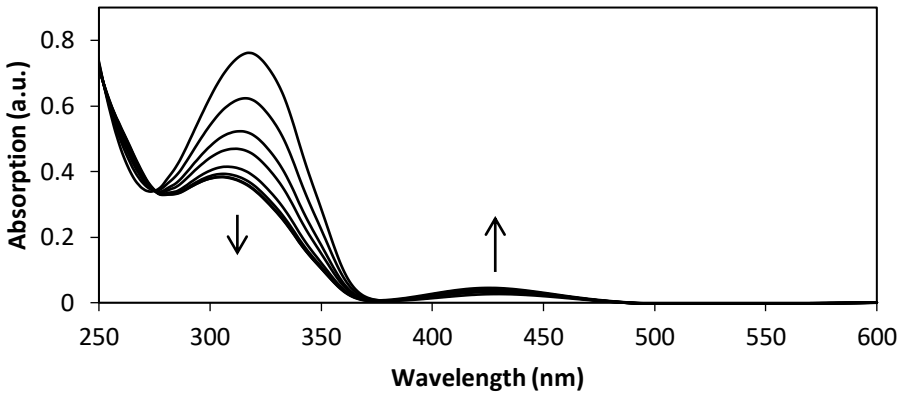

Figure 2.15: UV-vis absorption spectra of *m*-β-CD_2az (5.0×10^{-5} mol dm^{-3}) in aqueous phosphate buffer (pH 7.0, *I* = 0.10 mol dm^{-3}) at 298.2 K, irradiated with 300 – 355 nm light over 15 minutes. The arrows indicate the direction of the UV-vis absorption change with time.

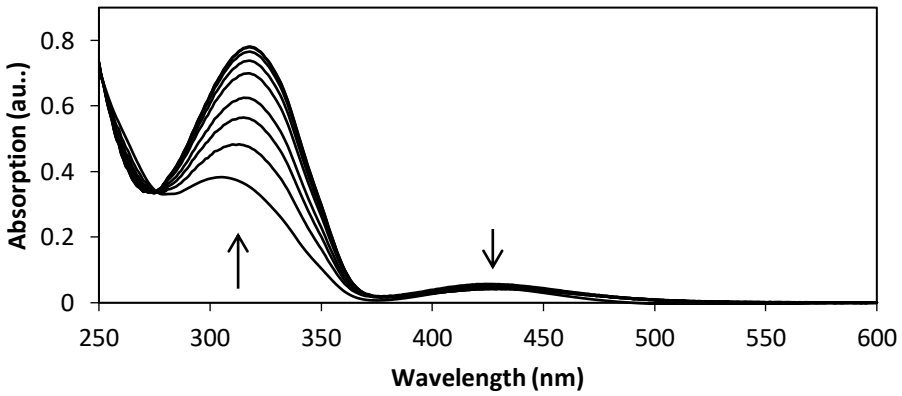

Figure 2.16: UV-vis absorption spectra of an initially UV irradiated (300 – 355 nm) sample of *m*-β-CD_2az (5.0×10^{-5} mol dm^{-3}) in aqueous phosphate buffer (pH 7.0, *I* = 0.10 mol dm^{-3}) at 298.2 K, irradiated with visible light (>400 nm) over 20 minutes. The arrows indicate the direction of the UV-vis absorption change with time.

The change in the UV-vis absorption spectra of *p*-β-CD_2az and *m*-β-CD_2az upon irradiation with 300 – 355 nm or >400 nm light is similar to that expected from unmodified azobenzene.[5] Irradiation with 300 – 355 nm light leads to a decrease in absorption in the π-π* region and an increase in absorption in the *n*-π* region, while irradiation with >400 nm shows the opposite trend, suggesting isomerisation from *E* to *Z* isomer and *Z* to *E* isomer, respectively. The decrease in absorbance upon irradiation with 300 – 355 nm light is also accompanied by a blue shift in λ_{max1} of 2 nm and 8 nm for *p*-β-CD_2az and *m*-β-CD_2az, respectively, consistent with photoisomerisation to the *Z* isomer.

2.2.2.2 ^{1}H NMR spectroscopy of the *p*-β-CD_2az and *m*-β-CD_2az Dimers

The PS of *p*-β-CD_2az and *m*-β-CD_2az (2.0×10^{-3} mol dm^{-3}) before and after irradiation were studied by ^{1}H NMR spectroscopy in D_2O phosphate buffer (pD 7.0, I = 0.10 mol dm^{-3}) at 298.2 K. The spectrum of each dimer was taken before and immediately after irradiation at 300 – 355 nm to investigate the *E* to *Z* isomerisation process. As azobenzene is known to exhibit reverse thermal isomerisation from *Z* to *E* isomer,[5] spectra were also recorded 24 hours after irradiation at 300 – 355 nm. The spectrum of each dimer was also recorded following irradiation with 300 – 355 nm and then >400 nm, to investigate the *Z* to *E* photoisomerisation. A 500 W Xe lamp with cut-off filters was used for the irradiations. The ^{1}H NMR spectra of *p*-β-CD_2az and *m*-β-CD_2az before and after irradiation are shown in Figure 2.17 and Figure 2.18, respectively and a summary of resonances in the aromatic region is given in Table 2.4.

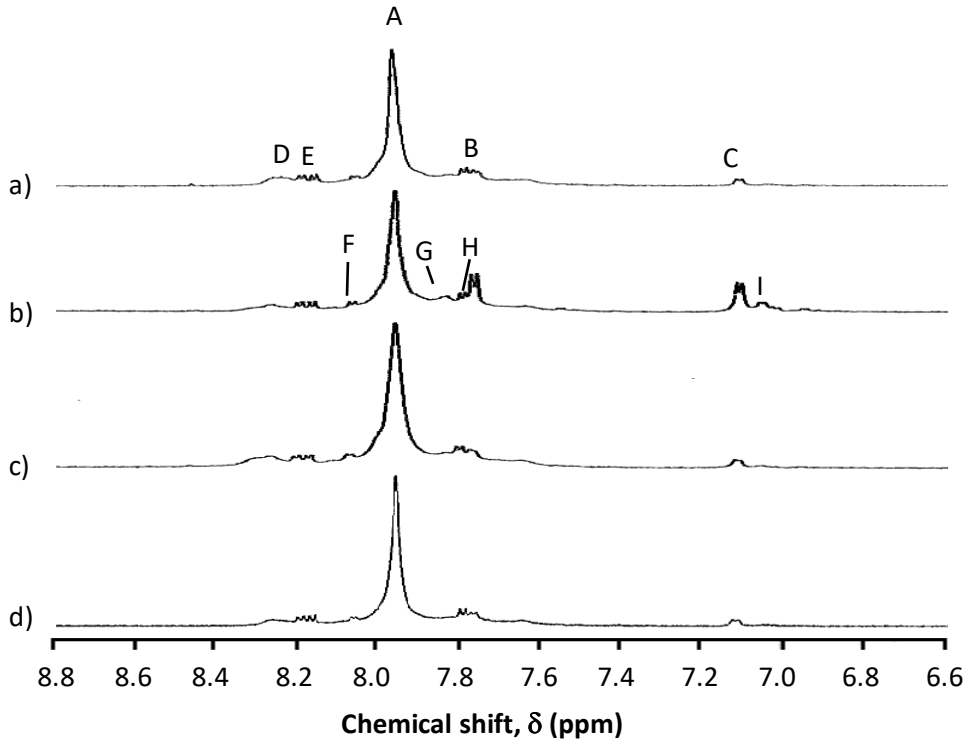

Figure 2.17: ^{1}H NMR spectra of *p*-β-CD_2az (2.0×10^{-3} mol dm^{-3}) prepared in D_2O phosphate buffer (pD 7.0, I = 0.10 mol dm^{-3}) at 298.2 K (a) prior to irradiation, (b) irradiated with UV light (300 – 355 nm), (c) 24 hours after irradiation with UV light and (d) irradiated with visible light (>400 nm).

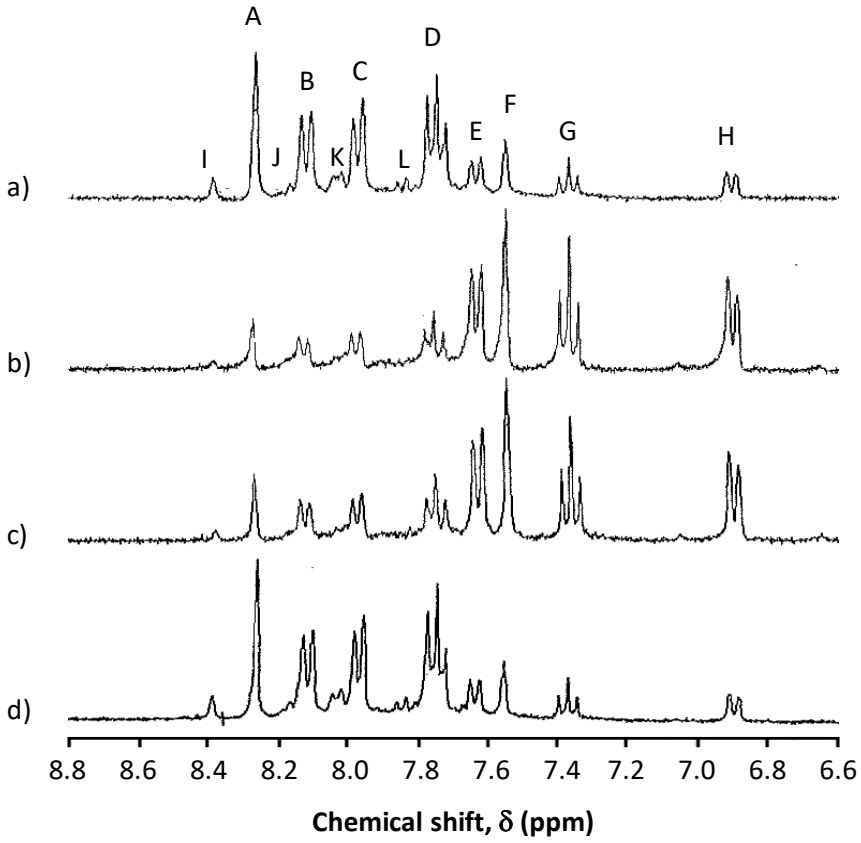

Figure 2.18: ^{1}H NMR spectra of *m*-β-CD_2az (2.0×10^{-3} mol dm^{-3}) prepared in D_2O phosphate buffer (pD 7.0, *I* = 0.10 mol dm^{-3}) at 298.2 K (a) prior to irradiation, (b) irradiated with UV light (300 – 355 nm), (c) 24 hours after irradiation with UV light and (d) irradiated with visible light (>400 nm).

Table 2.4: Summary of ^{1}H NMR resonances in the aromatic region for *p*-β-CD_2az and *m*-β-CD_2az (2.0×10^{-3} mol dm^{-3}) in D_2O phosphate buffer (pD 7.0, *I* = 0.10 mol dm^{-3}) at 298.2 K. The type of resonance is not specified for low intensity peaks as the assignment is ambiguous.

	***p*-β-CD_2az**			***m*-β-CD_2az**		
Resonance	**Shift (ppm)**	**Type**	**Coupling Constant (Hz)**	**Shift (ppm)**	**Type**	**Coupling Constant (Hz)**
A	7.96	s	-	8.27	s	-
B	7.78	m	-	8.12	d	8.1
C	7.09	m	-	7.97	d	7.8
D	8.27	br	-	7.75	t	8.1
E	8.19	-	-	7.64	d	7.8
F	8.06	-	-	7.55	s	-
G	7.82	-	-	7.37	t	7.8
H	7.69	-	-	6.90	d	7.5
I	7.06	-	-	8.39	s	-
J	-	-	-	8.18	-	-
K	-	-	-	8.02	-	-
L	-	-	-	7.83	-	-

The resonances in each ^{1}H NMR spectrum were assigned to either the *E* or *Z* isomer based upon the chemical shifts, multiplicity, change in intensity upon irradiation and likely PS under ambient conditions, as derived from the UV-vis absorption experiments. The aromatic resonances corresponding to unsubstituted *E*-azobenzene range from 7.1 ppm to 8.0 ppm, while the aromatic resonances corresponding to *Z*-azobenzene range from 6.7 ppm to 6.8 ppm.[39] This trend generally holds for a variety of substituted azobenzenes, with *E*-azobenzene resonances downfield from *Z*-azobenzene resonances,[39,40] due to the enhanced electron density arising from the extended conjugation of the planar *E* isomer.

The ^{1}H NMR spectrum of *p*-β-CD_2az under ambient conditions (Figure 2.17a) shows a large singlet, A, at 8.19 ppm, which represents the *E*-azobenzene H1 and H2 protons. While we may have expected to observe an AB system, sometimes called an AB quartet, comprising a set of two doublets in the NMR spectrum,[41] the *J* value and chemical shift differences appears to have tended towards 0 such that the two sets of protons are magnetically equivalent.

The resonances labelled B and C in the *p*-β-CD_2az NMR spectrum increase in intensity upon irradiation with UV light and diminish in intensity upon irradiation with visible light and therefore correspond to *Z*-azobenzene H1 and H2 protons, respectively. Interestingly, while resonance A forms a singlet, resonances B and C form a distinct AB system, especially noticeable after irradiation with UV light. There is a large difference in the chemical shifts between C and D of 0.69 ppm, which may be due to an interaction of H2 protons on adjacent phenyl groups of azobenzene, rendering them inequivalent, as shown in Figure 2.19.

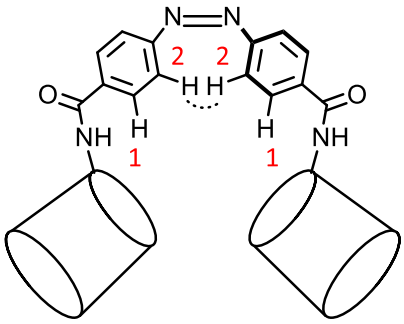

Figure 2.19: Possible interaction between H2 protons of *p*-β-CD_2az on adjacent phenyl groups, as shown by a dotted curve.

The *p*-β-CD_2az NMR spectrum also shows low intensity resonances labelled D – I. These resonances were initially thought to be impurities and therefore, the compound was recrystallised. However, the same NMR spectrum was produced. These low intensity resonances are also present in the *p*-β-CD_2az NMR spectrum reported by Djedaini-Pillard *et al.*[12] and therefore, are not expected to be impurities.

As some of the resonances change in intensity upon irradiation, namely H and I, the resonances may represent intermediate structures. Due to the low intensity, the multiplicities were difficult to define. However, it appears that resonance E is an AB system, resonances F and G form an AB system and resonances H and I form an AB system. Correspondingly, resonance D may also represent a broadened AB system. These AB systems are likely to refer to the H1 and H2 protons of *p*-β-CD_2az, arising from different isomerisation intermediates.

Azobenzene, and hence *p*-β-CD_2az, may undergo isomerisation by four possible mechanisms,[5] giving rise to four possible intermediates, as shown in Figure 2.20. The structure of each intermediate would correspond to different ^{1}H NMR spectra, based upon the relationship between the two phenyl groups of azobenzene. The intermediates arising from the rotation, inversion and inversion-assisted rotation mechanisms would lead to two AB systems each. However, we may expect the intermediates arising from the rotation and inversion-assisted rotation mechanisms to have a similar structure as both mechanisms involve the rotation of one phenyl group relative to the other. The intermediate corresponding to the concerted inversion mechanism would lead to a single AB system as the two phenyl groups are equivalent.

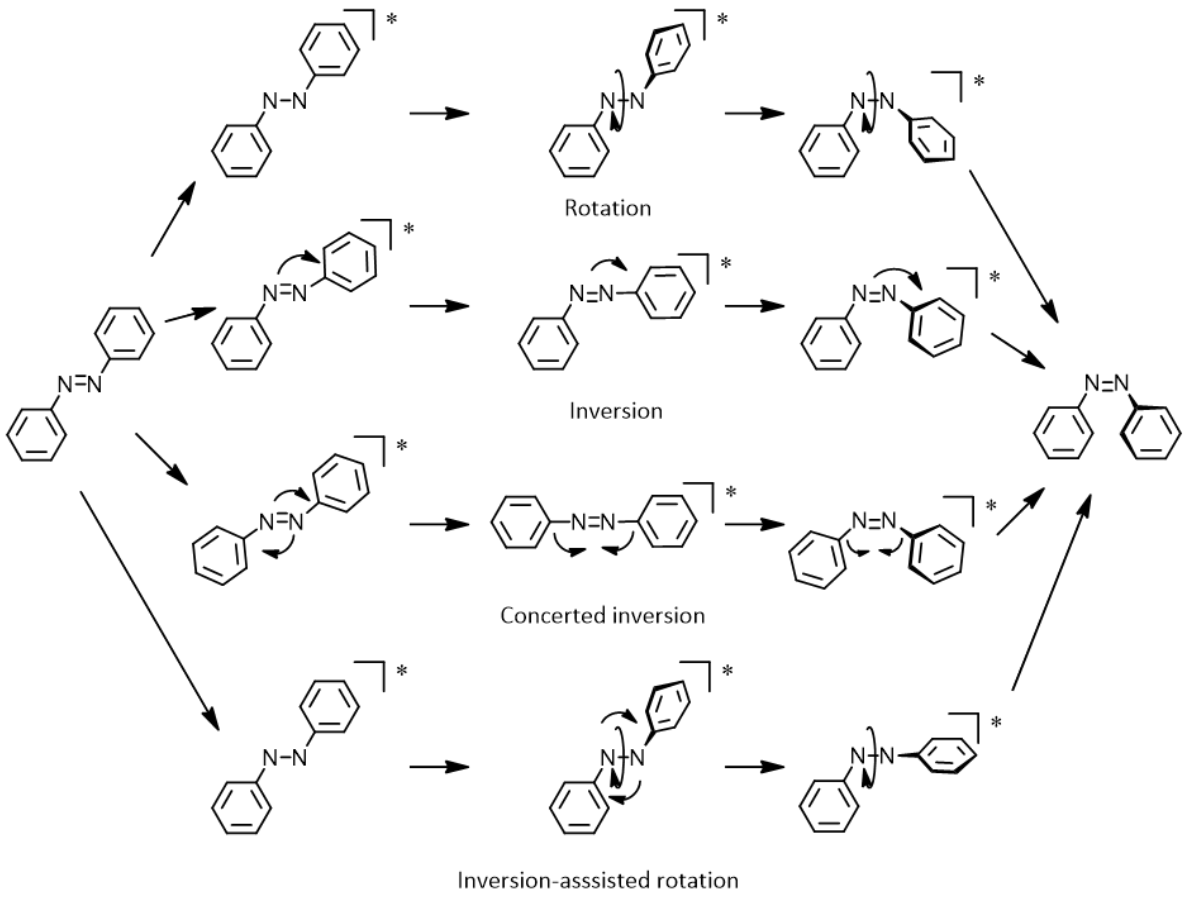

Figure 2.20: Possible mechanisms of photoisomerisation between *E* and *Z*-azobenzene.[5]

As the *p*-β-CD_2az NMR spectrum indicates at least three AB systems from resonances D – I, more than one isomerisation intermediate is present. As resonance D is broadened, the intermediate may reflect a structure whereby the two β-CD groups experience significant movement. As resonances D – G are closest to resonance A, the corresponding intermediate is likely to have a similar structure to the *E* isomer, indicative of either the rotation or inversion-assisted rotation mechanism. Conversely, resonances H and I are closest to resonances B and C, and therefore, the corresponding intermediate is likely to have a structure similar to the *Z* isomer, indicative of the inversion or concerted inversion mechanism. The existence of more than one isomerisation mechanism is possible as *p*-β-CD_2az undergoes *E* to *Z* photoisomerisation, *Z* to *E* photoisomerisation and *Z* to *E* thermal isomerisation. As the intensities of resonances D – I are low by comparison with resonances A – C (approximately 5%), they were not further considered in the determination of the PS ratio of *p*-β-CD_2az.

The ^{1}H NMR spectrum of *m*-β-CD_2az under ambient conditions (Figure 2.18a) shows 8 significant resonances in the aromatic region, representing both *E*- and *Z*-azobenzene protons, consistent with the UV-vis spectra. The four resonances labelled A, B, C and D represent the *E*-azobenzene H4, H1, H3 and H2 protons, respectively, as the intensity of the resonances decrease upon irradiation with UV light. Therefore, the resonances labelled E, F, G and H represent the *Z*-azobenzene H4, H1, H3 and H2 protons, respectively, which conversely increase in intensity upon irradiation with UV light. The chemical shifts of the assigned *E*- and *Z*-azobenzene protons of *m*-β-CD_2az are also aligned with the known chemical shifts of other *E*- and *Z*-azobenzene compound.[39] The *E*-azobenzene protons of *m*-β-CD_2az are between 7.75 ppm and 8.27 ppm, downfield from the *Z*-azobenzene protons of *m*-β-CD_2az between 6.90 ppm and 7.64 ppm.

The *m*-β-CD_2az NMR spectrum also shows several minor, yet significant, resonances labelled I – L. As resonances I, J, K and L, are shoulder resonances of A, B, C and D, they likely correspond to the H4, H1, H3 and H2 protons, respectively. While the intensity of these resonances change upon irradiation, they do not represent *Z*-azobenzene protons as their resonances are downfield of resonances E – H and in the range of the *E*-azobenzene protons. Therefore, they are likely to represent an intermediate with a structure similar to the *E* isomer, indicative of the rotation or inversion-assisted rotation mechanism. The intermediate, which may be denoted as *E'Z'*-*m*-β-CD_2az, comprises approximately 12% of the total isomer population. As the population of the *E* isomer, *Z* isomer and intermediate of *m*-β-CD_2az can be determined, the change in the Gibbs Free Energy (ΔG) between the species can be derived, as shown in Table 2.5. Full details describing the equilibrium between each species and calculation of ΔG are found in 2.5 Appendix.

Table 2.5: The change in Gibbs Free Energy (ΔG) for the equilibrium between the *E* isomer, *Z* isomer and intermediate of *m*-β-CD_2az.

Isomerisation	ΔG (kJ mol^{-1})
E-*m*-β-CD_2az to *Z*-*m*-β-CD_2az	2.84 ± 0.24
E-*m*-β-CD_2az to *E'Z'*-*m*-β-CD_2az	3.40 ± 0.24
E'Z'-*m*-β-CD_2az to *Z*-*m*-β-CD_2az	-0.55 ± 0.24

Intermediate structures between the *E* and *Z* isomers of azobenzene compounds are generally not reported. However, the modification of azobenzene with β-CD appears to stabilise the intermediates in the *p*-β-CD_2az and *m*-β-CD_2az systems. This stabilisation may be present due to hydrogen bonding between adjacent β-CD groups or interactions between the β-CD groups and the azobenzene linker.[42-44] In the case of *p*-β-CD_2az, the latter explanation may be more likely due to the greater distance between the β-CD groups.

Given the assignment of each resonance in the ^{1}H NMR spectra of both dimers, the resonances corresponding to the *E*- and *Z*-azobenzene protons were integrated to determine the relative proportions present before and after each irradiation experiment. A summary of the PS ratios of *p*-β-CD_2az and *m*-β-CD_2az is given in Table 2.6.

Table 2.6: Proportion of *E* and *Z* isomers of *p*-β-CD_2az and *m*-β-CD_2az before and after irradiation at UV (300 – 355 nm) and visible (>400 nm) light, as determined by ^{1}H NMR spectroscopy.

	Before Irradiation		Immediately after UV irradiation		24hrs after UV irradiation		Immediately after vis irradiation	
Dimer	% *E*	% *Z*	% *E*	% *Z*	% *E*	% *Z*	% *E*	% *Z*
p-β-CD_2az	95	<5	80	20	95	<5	95	<5
m-β-CD_2az	76	24	39	61	39	61	76	24

The PS ratios of the *E* and *Z* isomers of *p*-β-CD_2az and *m*-β-CD_2az before and after irradiation are significantly different. Under ambient conditions, the proportion of the *E* and *Z* isomers of *p*-β-CD_2az and *m*-β-CD_2az were 95% and 5%, and 78% and 22%, respectively. This result is consistent with the deductions made from their respective UV-vis spectra. The UV-vis spectrum of *p*-β-CD_2az is similar to K_2.*E*-*p*-Az$(COO)_2$, indicating a PS consisting primarily of the *E* isomer, while the UV-vis spectrum of *m*-β-CD_2az shows a blue shift in λ_{max1} and reduced ε_{max1}, consistent with *m*-β-CD_2az existing as a mixture of *E* and *Z* isomers.

The PS ratios of *p*-β-CD_2az and *m*-β-CD_2az after irradiation at 300 – 355 nm are noticeably different. Immediately after irradiation at 355 nm, the proportion of both *Z*-*p*-β-CD_2az and *Z*-*m*-β-CD_2az increased. However, 24 hours after irradiation, the ratio of *E* and *Z* isomers of *p*-β-CD_2az reverted

back to the initial ratio under ambient conditions, while the ratio of *E* and *Z* isomers of *m*-β-CD_2az remained unchanged. This indicates that *m*-β-CD_2az does not undergo reverse thermal isomerisation during the investigated timescale and that *Z*-*m*-β-CD_2az possesses greater stability than *Z*-*p*-β-CD_2az.

The PS ratios of *p*-β-CD_2az and *m*-β-CD_2az after irradiation at >400 nm light are similar. The two samples were irradiated with >400 nm immediately after irradiation with 355 nm, to determine the PS ratios after *Z* to *E* photoisomerisation. Both *p*-β-CD_2az and *m*-β-CD_2az exhibited *Z* to *E* isomerisation when irradiated with >400 nm, reforming the PS ratio under ambient conditions.

2.2.2.3 Summary and Discussion of Photochemical Properties of the *p*-β-CD_2az and *m*-β-CD_2az Dimers

From the photoisomerisation experiments using UV-vis and ^{1}H NMR spectroscopy, structural isomerisation has a clear influence on the stability of the *E* and *Z* isomers and hence the photoisomerisation properties of *p*-β-CD_2az and *m*-β-CD_2az. The differences are summarised in Table 2.7.

Table 2.7: Summary of photochemical properties of azobenzene, *p*-β-CD_2az and *m*-β-CD_2az.

Compound	Photoisomerisation *E* to *Z* and *Z* to *E*	Thermal isomerisation *Z* to *E*	PS ratio before irradiation
azobenzene[5]	Yes	Yes	100% *E* isomer
p-β-CD_2az	Yes	Yes	~95% *E* isomer
m-β-CD_2az	Yes	No	Mix of *E* and *Z* isomers

The differences in the photochemical properties between *p*-β-CD_2az and *m*-β-CD_2az are likely to result from the proximity between the two β-CD groups in each dimer. One of the major differences is the prevalence of the *Z* isomer of *m*-β-CD_2az under ambient conditions. In principle, the stability of the *Z* isomer of *m*-β-CD_2az may arise due to the β-CD groups of *m*-β-CD_2az experiencing some steric interference. This may cause the phenyl rings of azobenzene to distort from planarity to accommodate the additional bulk, thus adopting the *Z* isomer configuration. This has previously been established by Rau and Yu-Quan and Forber *et al.,* who substituted azobenzene with alkyl groups at the *ortho* position, effectively increasing the steric strain around the azo bond.[15,45] In both cases, the phenyl rings of azobenzene distorted to minimise interactions between the bulky *ortho*-substituents and the lone pair of electrons on the nitrogen atom, while the N-N-C angle also opened up, corresponding to a blue shift and reduced intensity of the π-π* transition. In some situations, photoisomerisation was not observed. While these studies did suggest a diminished proportion of the *Z* isomer, Bunce *et al.* also synthesised a series of highly hindered alkyl-substituted azobenzenes with isolable and stable *Z* isomers.[46]

In the case of *m*-β-CD_2az, a stable *Z* isomer may form not only from the tendency for the azobenzene moiety to distort from planarity to accommodate the bulky β-CD groups, but also due to the attractive hydrogen bonding interactions between adjacent β-CD groups.[42-44] Stabilisation of the *Z* isomer of azobenzene through non-covalent interactions has previously been reported by Haworth and Chambers through modification of azobenzene with a peptide chain.[47] The *Z* isomer was stabilised due to hydrophobic interactions between the peptide chain and phenyl groups of azobenzene. Meyers-Almes *et al.* similarly used interactions with a protein surface to stabilise the *Z* isomer of azobenzene.[48]

While the interaction between β-CD groups of *m*-β-CD_2az is sufficient to explain the stability of the *Z* isomer, other factors may be considered. Azobenzene may act as a guest to complex within the β-CD cavity. Niino *et al.* previously stabilised a *Z*-azobenzene derivative via complexation with β-CD.[49] In the case of *m*-β-CD_2az, one of the β-CD groups may partially encapsulate or interact with one of the phenyl groups of azobenzene.[50] However, if this were the case, we may expect that the hydrogen atoms of each phenyl ring to be magnetically inequivalent and differentiable via NMR spectroscopy.

As the stability of the *Z* isomer of *m*-β-CD_2az is likely to have several origins, so too may the lack of observable *Z* to *E* thermal isomerisation. For example, due to the significant steric bulk of the β-CD groups surrounding the azobenzene moiety, the lack of thermal isomerisation of *Z*-*m*-β-CD_2az may be due to a lack of free volume within the system, which would be required for the rotation or inversion of one of the phenyl groups of azobenzene during isomerisation.[17] The inherent stability of the *Z* isomer may also prevent thermal isomerisation. Such a phenomenon has already been observed by Tamaoki *et al.*[40] Macrocyclic azobenzene dimers (azobenzenophanes) were synthesised with a thermodynamically stable *Z*-*Z* isomer, which also exhibited thermal isomerisation from the *E*-*E* to the *Z*-*Z* isomer. The thermodynamic stability of the *Z*-*Z* isomer was attributed to the strained geometry of the azobenzenophanes to disfavor the *E*-*E* isomer.

In the case of *p*-β-CD_2az, the lower proportion of the *Z* isomer under ambient conditions arises due to a longer distance between the two β-CD groups. The longer distance appears to relieve the steric interaction between the two β-CD groups, resulting in photochemical properties that are more aligned with unmodified azobenzene. Reverse thermal isomerisation is observed as the phenyl groups may move independently of the *para*-substituted β-CD groups.

The results of this study indicate that the distance between the two β-CD groups of an azobenzene-linked β-CD dimer greatly influences the photochemical properties. As the distance between the two β-CD groups decreases, the distortion of the phenyl rings of the azobenzene moiety increases, while

the attractive force between adjacent β-CD groups increases. These two interactions contribute to the stabilization of the *Z* isomer. Additionally, a shorter distance between the two β-CD groups decreases the free volume available for rotation or inversion of the phenyl groups of azobenzene, which is required for isomerisation, resulting in diminished thermal isomerisation pathways from the *E* to the *Z* isomer.

The differences in the PS ratios and isomerisation of the two dimers are noteworthy. While there have been several studies combining the host properties of CDs with the photochemical utilities of azobenzene,[6,9-12,51-53] there has been little investigation into the influence of CD on the photochemical properties of azobenzene.[54]

2.2.3 Effect of guest complexation on the isomerisation properties of the *p*-β-CD$_2$az and *m*-β-CD$_2$az Dimers

The effect of guest complexation on the isomerisation properties of *p*-β-CD$_2$az and *m*-β-CD$_2$az was studied by NMR spectroscopy. 1-Adamantanecarboxylate (ADC) (generated by the deprotonation of 1-adamantanecarboxylic acid in D_2O phosphate buffer at pD 7.0) as shown in Figure 2.21, was chosen as the guest to influence the isomerisation. ADC is known to form a strong complex with β-CD, characterised by a host-guest equilibrium constant, *K*, of 1400 dm mol^{-1}.[55] The potential effect of ADC on the isomerisation properties of the dimers was attributed to the presence of the carboxylate group, which may disrupt any favourable interactions between the β-CD groups of each dimer.

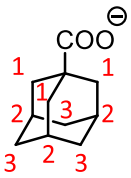

Figure 2.21: Structure of ADC.

2.2.3.1 2D ^{1}H ROESY NMR spectroscopy

The complexation behaviour of *p*-β-CD_2az and *m*-β-CD_2az with ADC was studied by 2D ^{1}H ROESY NMR spectroscopy. Solutions of each dimer (5.0×10^{-3} mol dm^{-3}) and ADC (1.0×10^{-2} mol dm^{-3}) combination were prepared in D_2O phosphate buffer (pD 7.0, I = 0.10 mol dm^{-3}) at 298.2 K. The concentration of ADC was double that of the dimer to account for the presence of two β-CD groups per dimer such that the mole ratio of β-CD groups to ADC was 1:1. The 2D ^{1}H ROESY NMR spectra for the complexation of ADC by *p*-β-CD_2az and *m*-β-CD_2az are given in Figure 2.22 and Figure 2.23, respectively.

2D ^{1}H ROESY NMR spectroscopy was used to determine the presence of a dimer·ADC complex. A nuclear Overhauser enhancement (NOE) cross-peak between interior protons of β-CD (H3, H5 and H6) and protons of ADC will be observed if β-CD groups of the dimer and ADC are within 4 Å of each other, indicating that ADC has been incorporated within the β-CD cavity to form a complex.[56] The interior protons of native β-CD are readily distinguished as native β-CD is homochiral. However, the modification of β-CD or the complexation of a guest by native β-CD causes a loss of homochirality and hence, proton resonances in an NMR spectrum may display significant broadening or overlap. Therefore, cross-peaks occurring between the H2 – H6 protons of a modified β-CD compound and protons of a guest are generally considered to indicate complexation.[56]

The 2D ^{1}H ROESY NMR spectra for the complexation of ADC by either dimer show similar results, with cross-peaks arising between the H1 – H3 resonances of ADC and the H2 – H6 resonances of β-CD in either dimer. Therefore, ADC forms a complex with *p*-β-CD_2az and *m*-β-CD_2az. However, the spectra do not indicate the point of ADC entry into either the primary or secondary face of β-CD. The spectra also do not suggest the location of the carboxylate group of ADC, which is thought to influence the isomerisation properties.

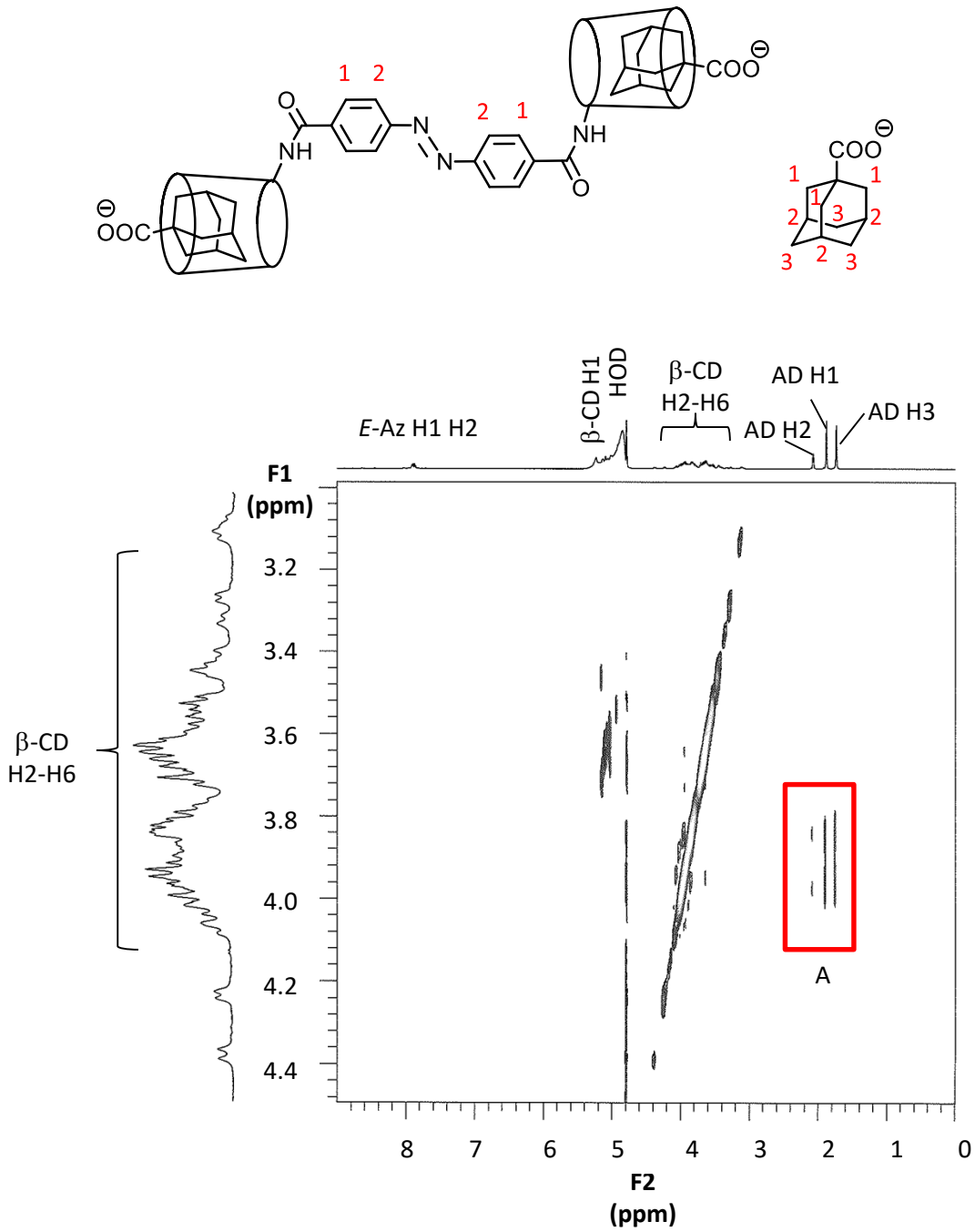

Figure 2.22: 2D ^{1}H ROESY NMR spectrum of *p*-β-CD_2az (5.0×10^{-3} mol dm^{-3}) and ADC (1.0×10^{-2} mol dm^{-3}) prepared in D_2O phosphate buffer (pD 7.0, *I* = 0.10 mol dm^{-3}) at 298.2 K. Rectangle A highlights cross-peaks arising from NOE interactions between the annular protons of β-CD and protons of ADC. A possible structure is shown above, as well as an annotated structure of ADC.

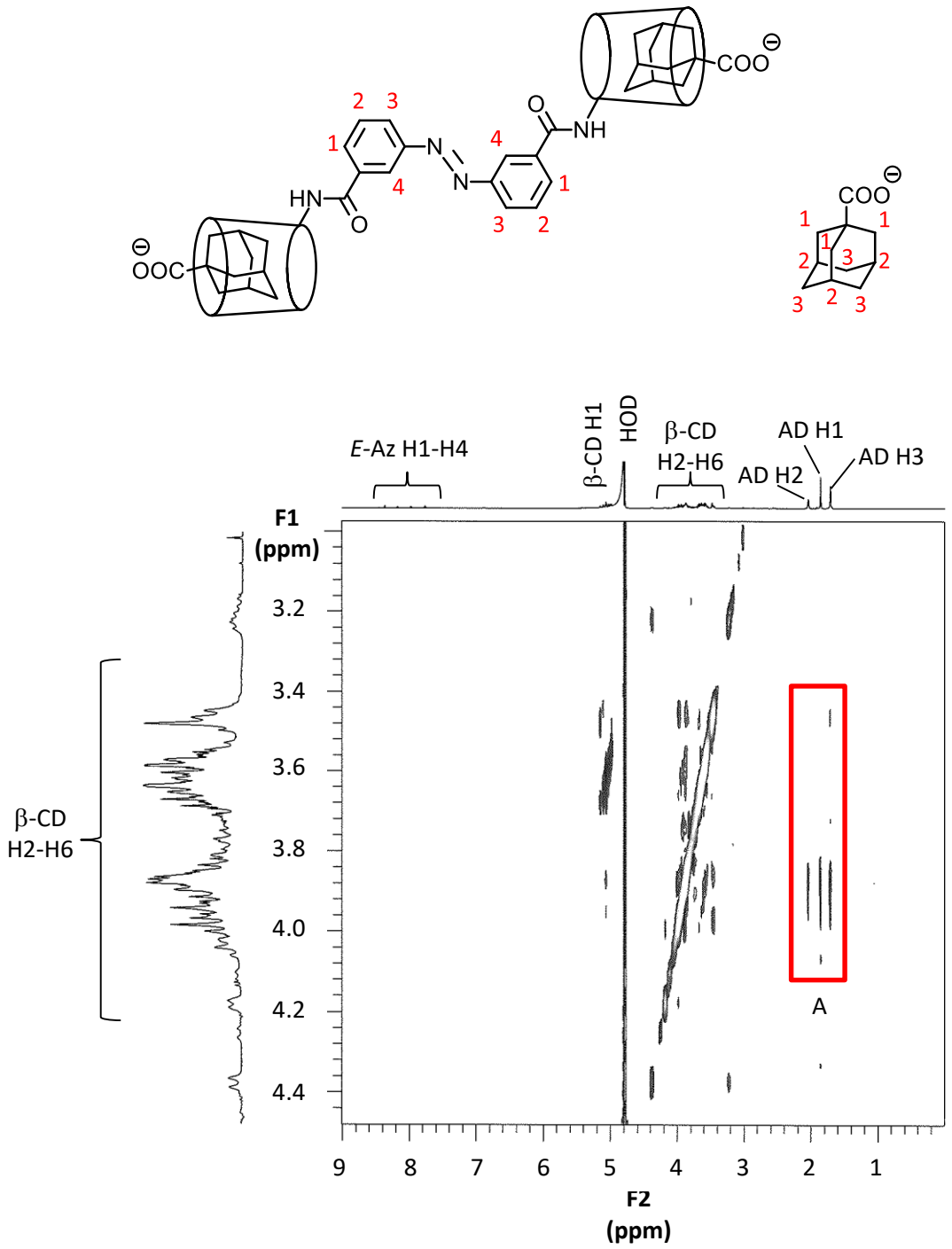

Figure 2.23: 2D ^{1}H ROESY NMR spectrum of *m*-β-CD_2az (5.0×10^{-3} mol dm^{-3}) and ADC (1.0×10^{-2} mol dm^{-3}) prepared in D_2O phosphate buffer (pD 7.0, I = 0.10 mol dm^{-3}) at 298.2 K. Rectangle A highlights cross-peaks arising from NOE interactions between the annular protons of β-CD and protons of ADC. A possible structure is shown above, as well as an annotated structure of ADC.

2.2.3.2 ^{1}H NMR spectroscopy

The PS ratios of the *E* and *Z* isomers of *p*-β-CD_2az and *m*-β-CD_2az complexed with ADC before and after irradiation were determined by ^{1}H NMR spectroscopy. Each combination of dimer (5.0×10^{-3} mol dm^{-3}) and ADC (1.0×10^{-2} mol dm^{-3}) was prepared in D_2O phosphate buffer (pH 7.0, *I* = 0.01 mol dm^{-3}) at 298.2 K. The spectrum of each combination was taken before, immediately after and 24 hours after irradiation at 300 – 355 nm. Spectra were also recorded following irradiation with 300 – 355 nm and then >400 nm. Irradiation was achieved using a 500 W Xe lamp with cut-off filters. The ^{1}H NMR spectra of the *p*-β-CD_2az·ADC and *m*-β-CD_2az·ADC systems are shown in Figure 2.24 and Figure 2.25 respectively. A summary of the ^{1}H NMR aromatic resonances is given in Table 2.8.

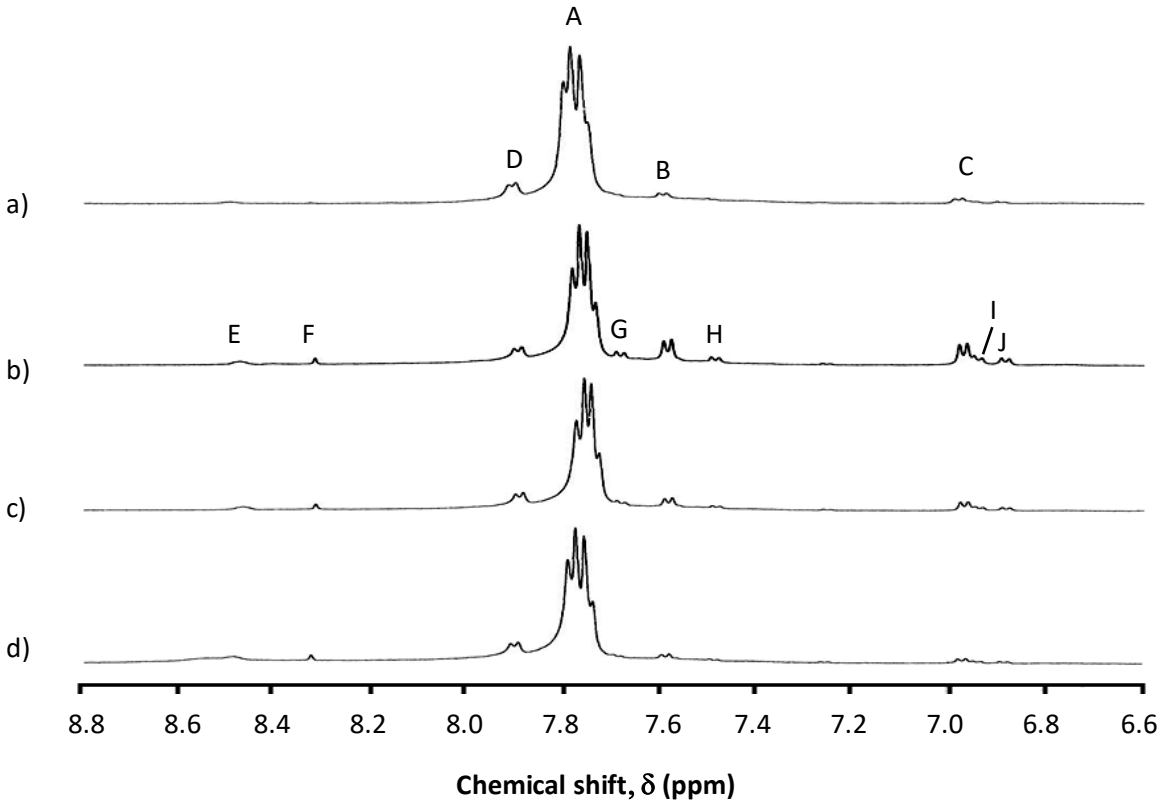

Figure 2.24: ^{1}H NMR spectra of *p*-β-CD_2az (5.0×10^{-3} mol dm^{-3}) and ADC (1.0×10^{-2} mol dm^{-3}) prepared in D_2O phosphate buffer (pD 7.0, *I* = 0.10 mol dm^{-3}) at 298.2 K (a) prior to irradiation, (b) irradiated with UV light (300 – 355 nm), (c) 24 hours after irradiation with UV light and (d) irradiated with visible light (>400 nm).

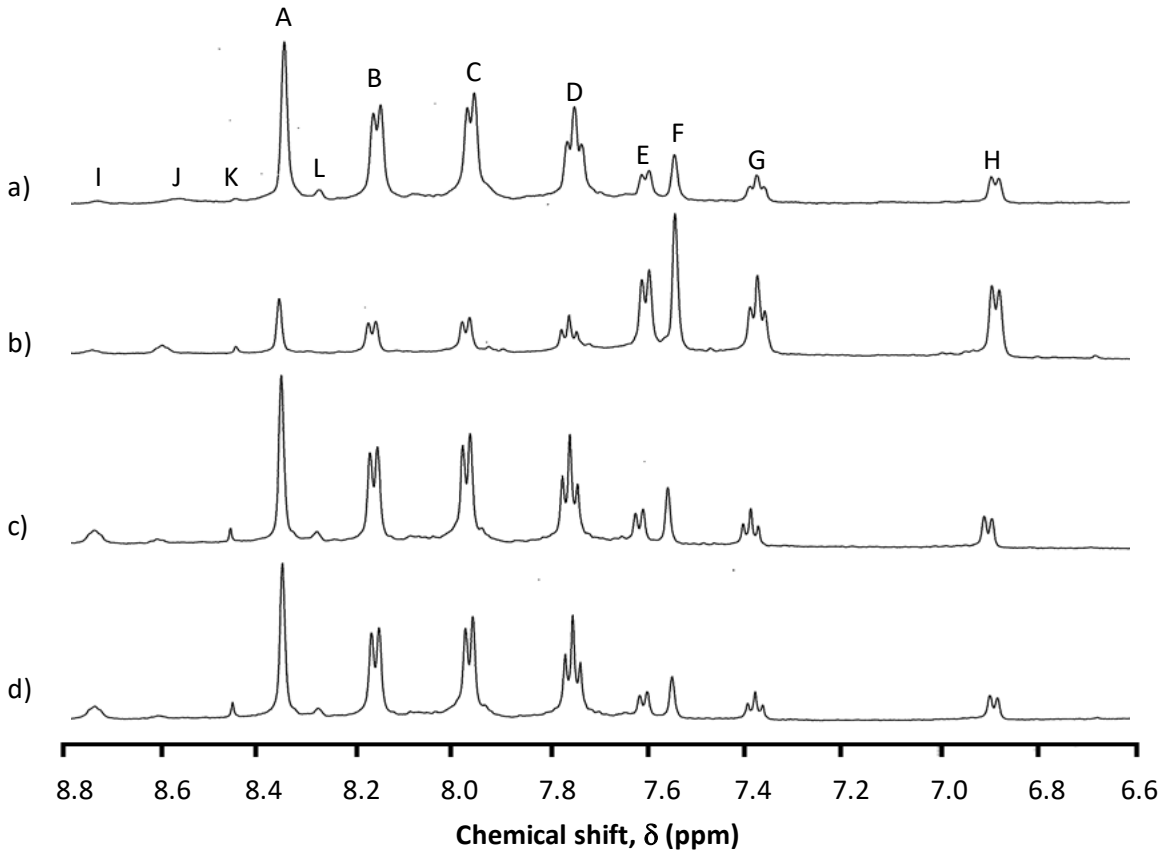

Figure 2.25: ^{1}H NMR spectra of *m*-β-CD_2az (5.0×10^{-3} mol dm^{-3}) and ADC (1.0×10^{-2} mol dm^{-3}) prepared in D_2O phosphate buffer (pD 7.0, *I* = 0.10 mol dm^{-3}) at 298.2 K (a) prior to irradiation, (b) irradiated with UV light (300 – 355 nm), (c) 24 hours after irradiation with UV light and (d) irradiated with visible light (>400 nm).

Table 2.8: Summary of the ^{1}H NMR resonances in the aromatic region for *p*-β-CD_2az·ADC and *m*-β-CD_2az·ADC in D_2O phosphate buffer (pD 7.0, *I* = 0.10 mol dm^{-3}) at 298.2 K. The type of resonance is not specified for low intensity peaks as the assignment is ambiguous.

	***p*-β-CD_2az·ADC**			***m*-β-CD_2az·ADC**		
Resonance	**Shift (ppm)**	**Type**	**Coupling Constant (Hz)**	**Shift (ppm)**	**Type**	**Coupling Constant (Hz)**
A	7.81	m	-	8.37	s	-
B	7.59	d	9.7	8.18	d	9.2
C	6.95	d	9.7	7.99	d	8.7
D	7.90	d	9.7	7.78	t	9.7
E	8.49	br	-	7.63	d	9.0
F	8.33	s	-	7.57	s	-
G	7.69	d	9.7	7.40	t	9.0
H	7.49	d	9.7	6.91	d	9.5
I	6.93	d	9.7	8.75	-	-
J	6.88	d	9.7	8.55	-	-
K	-	-	-	8.48	-	-
L	-	-	-	8.30	-	-

The resonances in each ^{1}H NMR spectra were assigned to either the *E* or *Z* isomer, based upon the chemical shifts, multiplicity and change in intensity upon irradiation. The assignment of the azobenzene resonances of both dimer·ADC systems are analogous to the dimers in the absence of ADC.

Resonances A, B, C and D of the *p*-β-CD_2az·ADC H^1 NMR spectrum shift upfield by 0.15 ppm, 0.19 ppm, 0.14 ppm and 0.29 ppm, respectively, by comparison with the analogous resonances of *p*-β-CD_2az alone. The resonances labelled A in the *p*-β-CD_2az·ADC system correspond to the *E*-azobenzene H1 and H2 protons, while minor resonances labelled B and C correspond to the *Z*-azobenzene H1 and H2 protons, respectively.

Resonance A of the *p*-β-CD_2az·ADC system differs in multiplicity to the analogous resonance of *p*-β-CD_2az alone. While resonance A appears as a singlet in the NMR spectrum of *p*-β-CD_2az alone, the expected AB system is exposed in the *p*-β-CD_2az·ADC system. The addition of ADC may cause a distortion of the electron density to magnetically differentiate the two protons of the phenyl rings. It is noted that while different concentrations of *p*-β-CD_2az were used for the H^1 NMR studies of *p*-β-CD_2az alone and with ADC, this did not influence the multiplicity of resonance A.

Similar to the ^{1}H NMR spectrum of *p*-β-CD_2az alone, the spectrum of the *p*-β-CD_2az·ADC system shows minor resonances labelled D – J, likely representing isomerisation intermediates. Resonance D is a doublet, although it may be part of an AB system which is partially obscured by resonance A. Resonances G and H appear to form an AB system, as do resonances I and J. Resonances E and F may also represent an intermediate.

Resonances G – I only appear after UV irradiation and represent an intermediate arising from *E* to *Z* photoisomerisation. As the resonances are close to resonances B and C, their corresponding structure resembles the *Z* isomer, indicative of the inversion or concerted inversion mechanism. Conversely, resonances D – F are downfield of G – I and therefore, their structures are likely to resemble the *E* isomer, indicative of the rotation or inversion-assisted rotation mechanism. As the intensities of resonances D – J are low by comparison with resonances A – C (approximately 5%), they were not considered in the further considered in the determination of the PS ratios.

The main resonances of the *m*-β-CD_2az·ADC system, A – H, experience a downfield shift between 0.01 – 0.10 ppm by comparison with the analogous resonances of *m*-β-CD_2az alone. The resonances labelled A, B, C and D in the *m*-β-CD_2az·ADC system represent the *E*-azobenzene H4, H1, H3 and H2 protons while the resonances labelled E, F, G and H represent the *Z*-azobenzene H4, H1, H3 and H2 protons. As with *m*-β-CD_2az alone, there are some minor resonances downfield of the *E*-azobenzene

resonances, which are labelled I – L. While the intensity of these resonances change upon irradiation, they do not represent *Z*-azobenzene protons as their resonances are downfield of resonances E – H and in the range of the *E*-azobenzene protons. Therefore, they are likely to represent an intermediate with a structure similar to *E*-azobenzene, indicative of the rotation and inversion-assisted rotation mechanisms. As the intensities of resonances I – L are low by comparison with the resonances A – H (less than 5%), they were not considered in the determination of the PS ratio of *m*-β-CD_2az·ADC.

A summary of the proportion of *E* and *Z* isomers is given in Table 2.9. A comparison of the proportion of *E* isomers of *p*-β-CD_2az, *p*-β-CD_2az·ADC, *m*-β-CD_2az and *m*-β-CD_2az·ADC is given in Figure 2.26.

Table 2.9: Proportion of *E* and *Z* isomers of *p*-β-CD_2az and *m*-β-CD_2az complexed with ADC before and after irradiation with UV (300 – 355 nm) and visible (>400 nm) light, as determined by ^{1}H NMR spectroscopy.

	Before Irradiation		**Immediately after UV irradiation**		**24hrs after UV irradiation**		**Immediately after vis irradiation**	
System	*% E*	*% Z*	*% E*	*% Z*	*% E*	*% Z*	*% E*	*% Z*
p-β-CD_2az·ADC	95	<5	80	20	90	10	95	<5
m-β-CD_2az·ADC	78	22	35	65	77	23	78	22

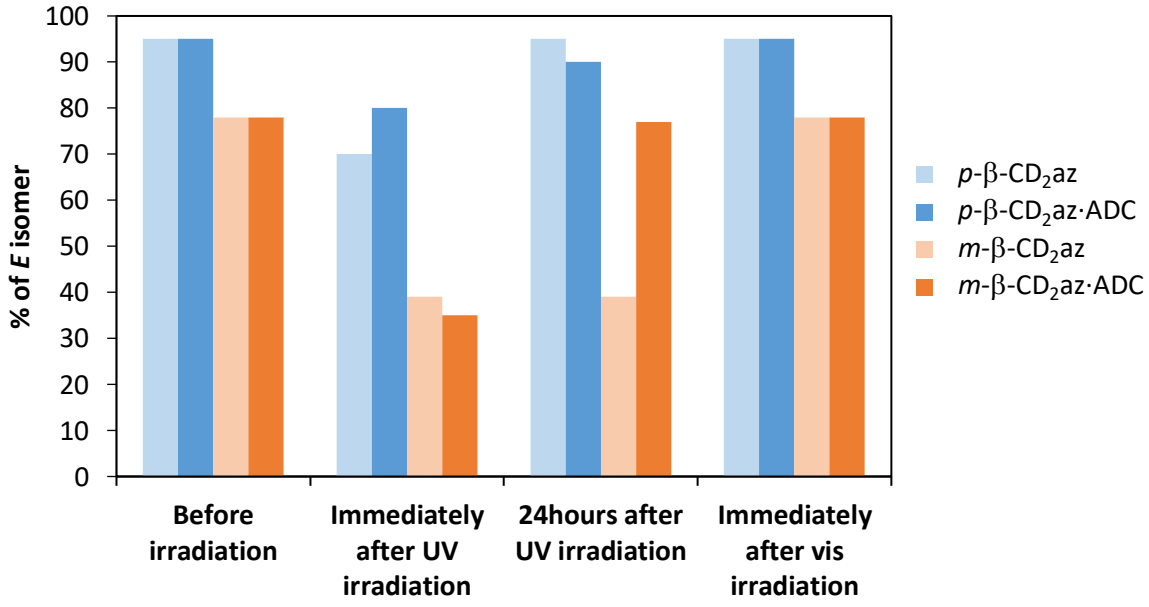

Figure 2.26: Proportion of *E* isomers of *p*-β-CD_2az and *m*-β-CD_2az alone and in combination with ADC before and after irradiation with UV (300 – 355 nm) and visible (>400 nm) light, as determined by ^{1}H NMR spectroscopy.

The initial PS ratios of either dimer·ADC system are largely unchanged by comparison with the dimers alone. However, there are differences in the proportion of *E* and *Z* isomers of *p*-β-CD_2az and *m*-β-CD_2az upon irradiation with UV light. The proportion of the *Z* isomer in the *p*-β-CD_2az·ADC system remains unchanged at 20% by comparison with *p*-β-CD_2az alone. Similarly, the proportion of the *Z* isomer in the *m*-β-CD_2az·ADC system is 65%, an increase from 61% from *m*-β-CD_2az alone. However, this difference is not significant due to the error in NMR integration. Similarly, ADC does not affect the *E* to Z photoisomerisation, with no discernible differences in the PS ratios after irradiation with visible light between the complexed and uncomplexed dimers.

However, a significant difference in the reverse thermal isomerisation was observed between the complexed and uncomplexed *m*-β-CD_2az systems. In the absence of ADC complexation, *m*-β-CD_2az does not exhibit reverse thermal isomerisation after 24 hours. However, upon complexation with ADC, reverse thermal isomerisation is observed. The ratio of *E* and *Z* isomers of the *m*-β-CD_2az·ADC system 24 hours after irradiation with UV is the same as the initial ratio under ambient conditions. Therefore, ADC acts as a catalyst to increase the rate of reverse thermal isomerisation of *m*-β-CD_2az. An analogous effect for the *p*-β-CD_2az·ADC system was not observed.

Several explanations may explain the role of ADC as a catalyst for the reverse thermal isomerisation. As the ratio of ADC to *m*-β-CD_2az was set at 2:1, there was one ADC per β-CD group. Therefore, given the strong affinity of ADC to the β-CD cavity,[55] we may expect both β-CD groups of *m*-β-CD_2az to be occupied by ADC. Upon irradiation of the *m*-β-CD_2az·ADC system, a substantial proportion of the *Z* isomer forms, resulting in two β-CD groups of *m*-βCD_2az in close proximity. As the *Z* isomer of *m*-βCD_2az is thought to possess some stability due to favourable hydrogen bonding interactions between the adjacent β-CD groups or favourable interactions between β-CD and azobenzene, ADC may act to destabilise these interactions. This destabilisation may arise from either the repulsive interactions of the carboxylate groups of adjacently complexed ADC groups or unfavourable steric interactions, depending on the mode of ADC entry.

Another explanation involves the possibility of the carboxylate groups of the complexed ADC transferring some electron density to the π system of azobenzene, increasing the repulsion between the two nitrogen atoms of azobenzene. This situation has previously been established by Jurczak *et al.*[57] Anions were bound to a urea-modified azobenzene, and were demonstrated to catalyse the rate of reverse thermal isomerisation. Anions that were strongly basic produced the greatest catalytic affect and also induced a large red shift in the π-π* bands of the urea-modified azobenzene. This is likely to suggest that the anion transfers electrons to the π system of azobenzene, potentially creating an extended, conjugated π system.

Given the limited data obtained for the catalytic effect of ADC on the reverse thermal isomerisation of *m*-β-CD_2az, it remains unwise to draw too many conclusions regarding the mode of action, as well as the lack of influence on the photochemical properties of *p*-β-CD_2az. However, we may conclude from this study that the catalytic effect of ADC does not completely diminish the inherent stability of the *Z* isomer as the PS ratio of the *m*-β-CD_2az under ambient conditions does not change upon complexation with ADC.

2.3 Conclusion

Two structural isomers of azobenzene-linked β-CD dimers have been synthesised, differing by the position of the β-CD groups towards the azobenzene group, either *para* or *meta*, corresponding to *p*-β-CD_2az and *m*-β-CD_2az, respectively. The PS ratio of the *E* and *Z* isomers and the photoisomerisation properties of each dimer were determined by UV-vis and ^{1}H NMR spectroscopy.

The PS ratio and photoisomerisation properties of *p*-β-CD_2az closely resembles unmodified azobenzene. Under ambient conditions, *p*-β-CD_2az exists predominantly as the *E* isomer, however, irradiation with UV light causes photoisomerisation from the *E* to *Z* isomer. Reverse thermal and photoisomerisation from the *Z* to the *E* isomer is also observed. Conversely, the photoisomerisation properties of *m*-β-CD_2az differ markedly from *p*-β-CD_2az. A mixture of *E* and Z isomers, as well as a stable intermediate structure, are observed for *m*-β-CD_2az under ambient conditions and while photoisomerisation from *E* to *Z* and *Z* to *E* isomers is possible, reverse thermal isomerisation was not observed during the investigated 24-hour period. The differences are likely due to the distance between the two β-CD groups in either dimer. A shorter distance between the two β-CD groups causes the phenyl groups of azobenzene to distort from planarity, thereby adopting a *Z* configuration. Simultaneously, attractive forces between the β-CD groups may help to stabilise the *Z* isomer.

The influence of ADC on the photoisomerisation of *p*-β-CD_2az and *m*-β-CD_2az was also investigated. ADC appears to act as a catalyst to increase the rate of thermal reverse isomerisation of *m*-β-CD_2az. The carboxylate groups of ADC may repel, causing this observed rate increase. There was no influence of ADC on the photoisomerisation of *p*-β-CD_2az during the investigated time scale.

An aminophenyl-modified β-CD compound, β-CDab, was also synthesised and the crystal structure determined. In contrast to many mono-modified β-CD compounds, β-CDab self-assembles to a Janus form, head-to-head, channel-type crystal packing arrangement. The Janus form is held together by π-π stacking of the aminophenyl substituents while the overall channel structure is maintained by hydrogen bonding between adjacent β-CD groups.

This research highlights the importance of structural isomerisation in the design of CD oligomers. Simple variations in the structure of CD oligomers can dramatically influence their properties.

2.4 References

(1) Del Valle, E. M. M. *Process Biochem.* **2004**, *39*, 1033.
(2) Guo, X. H.; Wang, J.; Li, L.; Chen, Q. C.; Zheng, L.; Pham, D. T.; Lincoln, S. F.; May, B. L.; Prud'homme, R. K.; Easton, C. J. *AlChE J.* **2010**, *56*, 3021.
(3) Harada, T.; Pham, D. T.; Leung, M. H. M.; Huy, T. N.; Lincoln, S. F.; Easton, C. J.; Kee, T. W. *J. Phys. Chem. B* **2011**, *115*, 1268.
(4) Harada, T.; Giorgio, L.; Harris, T. J.; Pham, D. T.; Ngo, H. T.; Need, E. F.; Coventry, B. J.; Lincoln, S. F.; Easton, C. J.; Buchanan, G.; Kee, T. W. *Mol. Pharm.* **2013**, *10*, 4481.
(5) Bandara, H. M. D.; Burdette, S. C. *Chem. Soc. Rev.* **2012**, *41*, 1809.
(6) Tamesue, S.; Takashima, Y.; Yamaguchi, H.; Shinkai, S.; Harada, A. *Angew. Chem.* **2010**, *49*, 7461.
(7) Nachtigall, O.; Koerdel, C.; Urner, L. H.; Haag, R. *Angew. Chem.* **2014**, *53*, 9669.
(8) Takashima, Y.; Hatanaka, S.; Otsubo, M.; Nakahata, M.; Kakuta, T.; Hashidzume, A.; Yamaguchi, H.; Harada, A. *Nature Commun.* **2012**, *3*, 1270.
(9) Casas-Solvas, J. M.; Martos-Maldonado, M. C.; Vargas-Berenguel, A. *Tetrahedron* **2008**, *64*, 10919.
(10) Liu, Y.; Kang, S.; Chen, Y.; Yang, Y. W.; Huskens, J. *J. Inclusion Phenom. Macrocyclic Chem.* **2006**, *56*, 197.
(11) Aoyagi, T.; Ueno, A.; Fukushima, M.; Osa, T. *Macromol. Rapid Commun.* **1998**, *19*, 103.
(12) Hamon, F.; Blaszkiewicz, C.; Buchotte, M.; Banaszak-Leonard, E.; Bricout, H.; Tilloy, S.; Monflier, E.; Cezard, C.; Bouteiller, L.; Len, C.; Djedaini-Pilard, F. *Beilstein J. Org. Chem.* **2014**, *10*, 2874.
(13) Yang, C.-a.; Xie, H.; Zhong, G.; Zhang, H. *Polymer* **2013**, *54*, 3238.
(14) Rodriguez, M. A.; Braslavsky, S. E. *J. Phys. Chem. A* **1999**, *103*, 6295.
(15) Rau, H.; Shen, Y. Q. *J. Photochem. Photobiol., A* **1988**, *42*, 321.
(16) Sadovski, O.; Beharry, A. A.; Zhang, F.; Woolley, G. A. *Angew. Chem.* **2009**, *48*, 1484.
(17) Han, M.; Ishikawa, D.; Honda, T.; Ito, E.; Hara, M. *Chem. Commun.* **2010**, *46*, 3598.
(18) Brady, B.; Lynam, N.; O'Sullivan, T.; Ahern, C.; Darcy, R. *Org. Synth.* **2000**, *77*, 220.
(19) Brown, S. E.; Coates, J. H.; Coghlan, D. R.; Easton, C. J.; Vaneyk, S. J.; Janowski, W.; Lepore, A.; Lincoln, S. F.; Luo, Y.; May, B. L.; Schiesser, D. S.; Wang, P.; Williams, M. L. *Aust. J. Chem.* **1993**, *46*, 953.
(20) Ameerunisha, S.; Zacharias, P. S. *J. Chem. Soc., Perkin Trans. 2* **1995**, 1679.
(21) Hamon, F.; Djedaini-Pilard, F.; Barbot, F.; Len, C. *Tetrahedron* **2009**, *65*, 10105.
(22) Merino, E. *Chem. Soc. Rev.* **2011**, *40*, 3835.
(23) Valeur, E.; Bradley, M. *Chem. Soc. Rev.* **2009**, *38*, 606.
(24) McPhillips, T. M.; McPhillips, S. E.; Chiu, H. J.; Cohen, A. E.; Deacon, A. M.; Ellis, P. J.; Garman, E.; Gonzalez, A.; Sauter, N. K.; Phizackerley, R. P.; Soltis, S. M.; Kuhn, P. *J. Synchrotron Radiat.* **2002**, *9*, 401.
(25) Sheldrick, G. M. *Acta Crystallogr. Sect. C: Cryst. Struct. Commun.* **2015**, *71*, 3.
(26) Sheldrick, G. M. *Acta Crystallogr. Sect. A* **2008**, *64*, 112.
(27) Harata, K. *Chem. Rev.* **1998**, *98*, 1803.
(28) Harata, K.; Takenaka, Y.; Yoshida, N. *J. Chem. Soc., Perkin Trans. 2* **2001**, 1667.
(29) Saenger, W. *J. Inclusion Phenom.*, *2*, 445.
(30) Janiak, C. *J. Chem. Soc., Dalton Trans.* **2000**, 3885.
(31) Connors, K. A. *Chem. Rev.* **1997**, *97*, 1325.
(32) Fan, Z.; Jing, Z. L.; Diao, C. H. *Carbohydr. Res.* **2005**, *340*, 513.
(33) Kamitori, S.; Hirotsu, K.; Higuchi, T.; Fujita, K.; Yamamura, H.; Imoto, T.; Tabushi, I. *J. Chem. Soc., Perkin Trans. 2* **1987**, 7.
(34) Fan, Z.; Guo, M.-J.; Diao, C.-H.; Jing, Z.-L.; Chen, X.; Wang, M. *Solid State Sci.* **2010**, *12*, 834.
(35) Eliadou, K.; Giastas, P.; Yannakopoulou, K.; Mavridis, I. M. *J. Org. Chem.* **2003**, *68*, 8550.

(36) Lindner, H. J.; Yuan, D. Q.; Fujita, K.; Kubo, K.; Lichtenthaler, F. W. *Chem. Commun.* **2003**, 1730.
(37) Fan, Z.; Guo, M.; Dong, B.; Diao, C.; Jing, Z.; Chen, X. *Sci. China Chem.* **2010**, *53*, 1089.
(38) Xu, Z.; Chen, X.; Liu, J.; Yan, D.-Q.; Diao, C.-H.; Guo, M.-J.; Fan, Z. *Carbohydr. Res.* **2014**, *393*, 32.
(39) Tait, K. M.; Parkinson, J. A.; Bates, S. P.; Ebenezer, W. J.; Jones, A. C. *J. Photochem. Photobiol., A* **2003**, *154*, 179.
(40) Norikane, Y.; Katoh, R.; Tamaoki, N. *Chem. Commun.* **2008**, 1898.
(41) Leonard, M. *Intermediate Organic Chemistry*; Lulu Enterprises Inc., United States, **2014**.
(42) Travelet, C.; Schlatter, G.; Hebraud, P.; Brochon, C.; Lapp, A.; Anokhin, D. V.; Ivanov, D. A.; Gaillard, C.; Hadziioannou, G. *Soft Matter* **2008**, *4*, 1855.
(43) Liu, K. L.; Zhang, Z.; Li, J. *Soft Matter* **2011**, *7*, 11290.
(44) Li, J.; Loh, X. J. *Adv. Drug Delivery Rev.* **2008**, *60*, 1000.
(45) Forber, C. L.; Kelusky, E. C.; Bunce, N. J.; Zerner, M. C. *J. Am. Chem. Soc.* **1985**, *107*, 5884.
(46) Bunce, N. J.; Ferguson, G.; Forber, C. L.; Stachnyk, G. J. *J. Org. Chem.* **1987**, *52*, 394.
(47) Chambers, E. J.; Haworth, I. S. *J. Chem. Soc., Chem. Commun.* **1994**, 1631.
(48) Korbus, M.; Backe, S.; Meyer-Almes, F.-J. *J. Mol. Recognit.* **2015**, *28*, 201.
(49) Niino, H.; Yabe, A.; Ouchi, A.; Tanaka, M.; Kawabata, Y.; Tamura, S.; Miyasaka, T.; Tagaki, W.; Nakahara, H.; Fukuda, K. *Chem. Lett.* **1988**, 1227.
(50) Menuel, S.; Azaroual, N.; Landy, D.; Six, N.; Hapiot, F.; Monflier, E. *Chem. Eur. J.* **2011**, *17*, 3949.
(51) Liu, Y.; Zhao, Y. L.; Chen, Y.; Guo, D. S. *Org. Biomol. Chem.* **2005**, *3*, 584.
(52) Rajendiran, N.; Sankaranarayanan, R. K. *Carbohydr. Polym.* **2014**, *106*, 422.
(53) Tsuda, S.; Aso, Y.; Kaneda, T. *Chem. Commun.* **2006**, 3072.
(54) Sanchez, A. M.; deRossi, R. H. *J. Org. Chem.* **1996**, *61*, 3446.
(55) Tosner, Z.; Aski, S. N.; Kowalewski, J. *J. Inclusion Phenom. Macrocyclic Chem.* **2006**, *55*, 59.
(56) Schneider, H. J.; Hacket, F.; Rudiger, V.; Ikeda, H. *Chem. Rev.* **1998**, *98*, 1755.
(57) Dabrowa, K.; Niedbala, P.; Jurczak, J. *Chem. Commun.* **2014**, *50*, 15748.

2.5 Appendix

Crystallographic data of β-CDab

Table 2.10: Distances between O4 atoms of adjacent glucose units of β-CDab.

G_n O4···G_{n-1} O4	Distance (Å)
G7···G6	4.332
G6···G5	4.425
G5···G4	4.325
G4···G3	4.387
G3···G2	4.332
G2···G1	4.429
G1···G7	4.358

Table 2.11: Distance between O4 atoms of each glucose unit with the centre of β-CDab.

Glucose unit	Distance (Å)
G1	4.974
G2	5.049
G3	5.093
G4	4.994
G5	4.974
G6	5.122
G7	5.040

Table 2.12: The tilt angle, which is defined as the angle between the plane through each O4 atom and the plane through C1, C4, O4 and O4' of each glucose unit of β-CDab.

Glucose Unit	Tilt Angle (°)
G1	9.19
G2	6.26
G3	10.5
G4	8.06
G5	12.8
G6	8.62
G7	8.98

Table 2.13: Distances between oxygen atoms of adjacent β-CD groups of β-CDab.

Atom of β-CD 1	Atom of β-CD 2	Distance (Å)
G1 O2	G1′ O2	3.124(6)
G1 O2	G7′ O3	3.090(6)
G1 O3	G7′ O3	2.800(5)
G1 O3	G7′ O2	3.008(5)
G2 O2	G7′ O2	2.994(5)
G2 O2	G6′ O3	3.128(6)
G2 O3	G6′ O3	2.848(6)
G2 O3	G6′ O2	3.057(6)
G3 O2	G6′ O2	3.011(6)
G3 O2	G5′ O3	3.018(6)
G3 O3	G5′ O3	2.752(5)
G3 O3	G5′ O2	2.982(5)
G4 O2	G5′ O2	2.968(5)
G4 O2	G4′ 03	3.128(6)
G4 O3	G4′ O3	2.824(6)
G4 O3'	G4′ O2	3.128(6)
G5 O2	G4′ O2	2.968(5)
G5 O2	G3′ O3	2.982(5)
G5 O3	G3′ O3	2.752(5)
G5 O3	G3′ O2	3.018(6)
G6 O2	G3′ O2	3.011(6)
G6 O2	G2′ O3	3.057(6)
G6 O3	G2′ O3	2.848(6)
G6 O3	G2′ O2	3.128(6)
G7 O2	G2′ O2	2.994(5)
G7 O3	G1′ O3	2.800(5)
G7 O2	G1′ O3	3.008(5)
G7 O3	G1′ O2	3.090(6)

Intermediate species of *m*-β-CD_2az

The ^{1}H NMR spectrum of *m*-β-CD_2az indicates the presence of an intermediate, as evidenced by resonances I – L in Figure 2.18. Given that the proportion of each species can be derived from the ^{1}H NMR spectrum, the change in Gibbs Free Energy (ΔG) between each species may be determined.

The equilibrium between *E*-*m*-β-CD_2az and Z-*m*-β-CD_2az is described by Equation 2.1

$$E\text{-}m\text{-}\beta\text{-}CD_2az \underset{}{\overset{K_{E\text{-}Z}}{\rightleftharpoons}} Z\text{-}m\text{-}\beta\text{-}CD_2az \qquad (2.1)$$

The equation for the equilibrium constant, $K_{E\text{-}Z}$, is given by Equation 2.2.

$$K_{E-Z} = \frac{Z\text{-}m\text{-}\beta\text{-}CD_2az}{E\text{-}m\text{-}\beta\text{-}CD_2az} \qquad (2.2)$$

The equation for the $\Delta G_{E\text{-}Z}$ describing the *E* to *Z* isomerisation is given by Equation 2.3.

$$\Delta G_{E-Z} = -RTlnK_{E-Z} \qquad (2.3)$$

As the proportion of each isomer can be determined from the ^{1}H NMR spectrum, the relative concentrations of *E*-*m*-β-CD_2az and *Z*-*m*-β-CD_2az can be used to derived $K_{E\text{-}Z}$ from Equation 2.2. The $\Delta G_{E\text{-}Z}$ value can then be determined using Equation 2.3. Similar equilibrium constant and ΔG expressions may be constructed for the isomerisation between *E*-*m*-β-CD_2az, *Z*-*m*-β-CD_2az and *E'Z'*-*m*-β-CD_2az. A reaction coordinate diagram describing the change in ΔG of these isomerisation pathways is shown in Figure 2.27. An analogous diagram was not constructed for the *p*-β-CD_2az system due to an overlap of resonances corresponding to *E'Z'*-*p*-β-CD_2az.

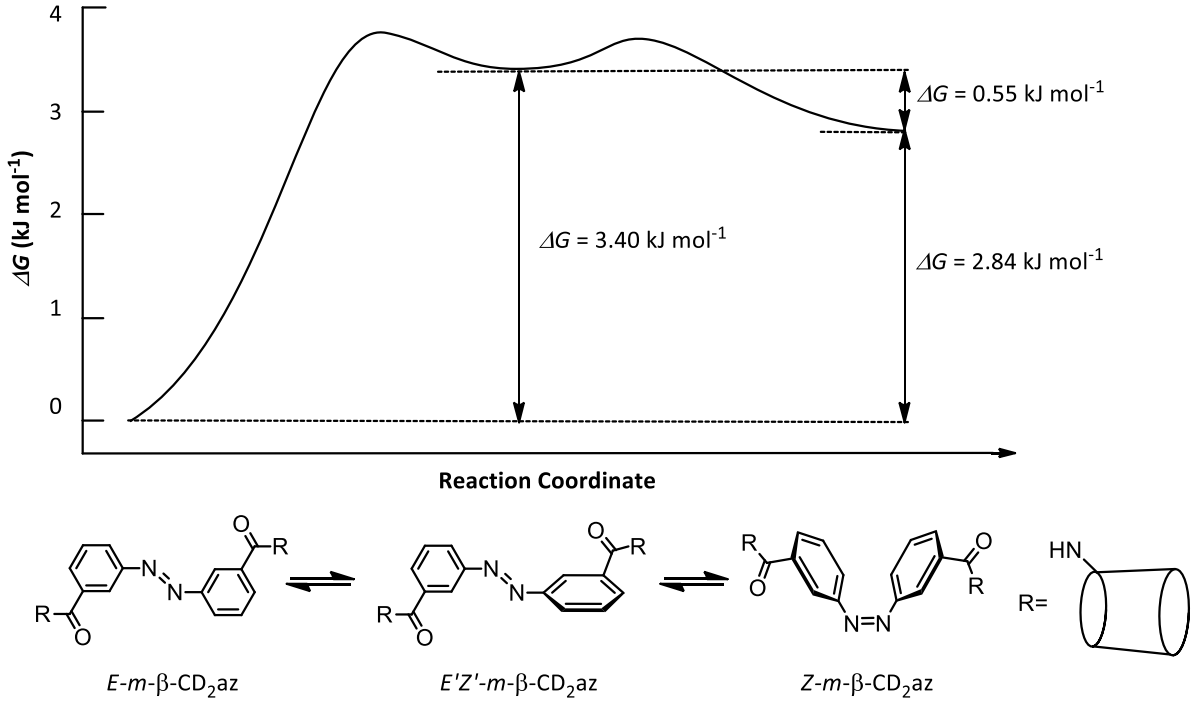

Figure 2.27: Reaction coordinate diagram describing the change in ΔG for the *E* and *Z* isomers of *m*-β-CD_2az as well as an intermediate, *E'Z'-m*-β-CD_2az. Values of ΔG were determined from isomer proportions derived from ^{1}H NMR spectroscopy. The structure given in the figure are for illustrative purposes only and, due to the unknown photoisomerisation mechanism, do not necessarily representat of the true structures.

This page is intentionally left blank

CHAPTER 3

Host-Guest Chemistry of Modified β-Cyclodextrin Oligomers

3.1 Introduction

3.1.1 Organic Dyes

Cyclodextrin oligomers often have increased complexation capabilities by comparison with unmodified, native CDs.[1-3] As a result, the complexation properties of native CDs and CD oligomers are routinely compared by conducting complexation studies with a range of guests.[4-6] Organic dye molecules are frequently used as guests as their commercial availability and photophysical properties offer economical and simple experimentation possibilities.[7-11] Various complexation features are derived from such experiments including the stoichiometry, equilibrium constant (*K*), enthalpy change (ΔH), entropy change (ΔS) and Gibbs free energy change (ΔG) of host-guest complexation.[12-17] In this research, three dyes are chosen for study: Crystal Violet (CV^+), Rhodamine B (RB) and Ethyl Orange (EO^-) which are cationic, zwitterionic and anionic, respectively, and differ significantly structurally, and might be expected to exhibit significant variations in complexation characteristics and thereby provide insight into the complexation process.

3.1.1.1 Crystal Violet

Crystal Violet, *tris*(4-(dimethylamino)phenyl)methylium chloride, also known as gentian violet, is a cationic triphenylmethane dye.[18] The spectroscopic features of CV^+ have been under consistent debate over the last 60 years.[18] The UV-vis absorption spectrum of CV^+ shows two absorption maxima and multiple explanations were initially proposed to explain their origin. The two maxima have been interpreted as arising from the resolution of vibronic structures,[19] the existence of two excited states[20] and the existence of two isomers.[21]

Recently, Maruyama *et al.* used femtosecond probe pump measurements of CV^+ in various solvents to confirm the existence of two ground state isomers.[22] X-ray diffraction studies of single crystals of triphenylmethane perchlorate unveiled a planar structure as one of the ground state isomers and therefore, a similar structure was proposed for CV^+.[23] However, as no other isomer was detected in the solid state, solvent effects of alcohols were considered, leading to the proposal of the pyramidal isomer. The pyramidal isomer is proposed to exist in certain solvents such as water, methanol, ethanol, *n*-propanol and *n*-butanol.[22] The planar (also known as propeller) and pyramidal isomers of CV^+ occur in equilibrium and interconvert depending on the interaction of a solvent molecule with the central carbon atom. Thus, the central carbon atom may be attracted by and pulled towards a solvent molecule, forming the pyramidal isomer, while in the absence of this attraction CV^+ assumes a planar stereochemistry as shown in Figure 3.1.

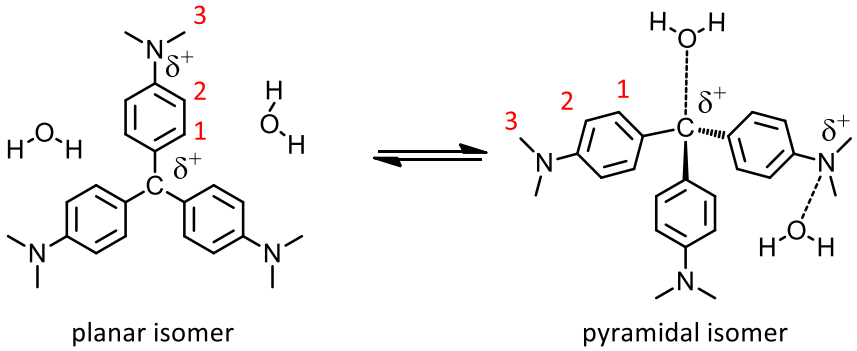

Figure 3.1: Structures of the planar and pyramidal isomers of CV^+ in aqueous solvent.

As the isomerisation of CV^+ occurs due to solvent effects, the planar and pyramidal isomers of CV^+ are sometimes referred to as solvation isomers.[22] The UV-vis absorption spectrum of CV^+ shows two absorption maxima at 590 nm and 557 nm, corresponding to the pyramidal and planar isomers, respectively.[24] Both isomers may be complexed by β-CD.[24]

3.1.1.2 Rhodamine B

Rhodamine B, [9-(2-carboxyphenyl)-6-(diethylamine) xanthen-3-ylidene]-diethylamine, is a xanthene dye, as shown in Figure 3.2. In aqueous solution and at near neutral pH, RB exists predominantly as a zwitterion, in large part due to hydrogen bonding with the solvent media.[25,26]

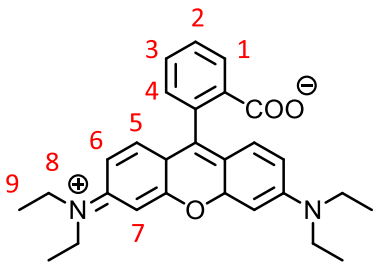

Figure 3.2: Structure of RB as a zwitterion.

3.1.1.3 Ethyl Orange

Ethyl orange, 4-(4-diethylaminophenylazo)benzenesulfonate, is an anionic, azo dye, as shown in Figure 3.3.[27,28] EO^- is analogous to another common azo dye, methyl orange (MO^-), which possesses a dimethylamino group rather than a diethylamino group. Few complexation studies of the complexation of EO^- by CDs have been reported,[29] while more have been reported for MO^-.[30-33] However, complexation studies using EO^- as a guest allow for simpler analysis as MO^- has a propensity to aggregate in solution.[34,35]

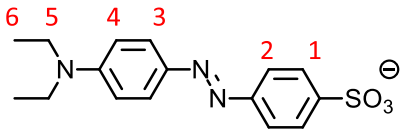

Figure 3.3: Structure of EO^-.

3.1.2 Dimerisation of CV^+, RB and EO^-

Organic dyes sometimes aggregate in solution to form dimers and occasionally trimers and tetramers.[25,36-38] Aggregation is influenced by the concentration of the dye, solvent, pH and temperature. The presence of dye aggregates may be detected by UV-vis spectroscopy as aggregation causes a shift in the λ_{max}, a change in ε_{max} and sometimes the appearance of shoulder peaks in the UV-vis spectra by comparison with that of the monomeric form.[37] The UV-vis absorption features of monomeric CV^+, RB and EO^- are given in Table 3.1.[7,28,36,39]

Table 3.1: Summary of absorption characteristics of monomeric dyes.

Dye	λ_{max} (nm)	10^{-4} ε (mol dm^{-3} cm^{-1})	pH	Solvent system	Reference
CV^+	591	9.8	-	aqueous	36
	590	9.60	7.4	aqueous buffer	7
RB	555	10.5	6.4	aqueous	39
	554	9.62	7.4	aqueous buffer	7
EO^-	472	2.47	-	aqueous	28

The equilibrium expression and equilibrium constants (K_D) for the dimerisation of dyes are given in Equation 3.1 and Table 3.2, respectively.[25,36,39,40] Both CV^+ and RB are known to dimerise in aqueous solution, while limited to no aggregation is expected for EO^-. Given the relatively low dimerisation constants for CV^+ and RB, the dimeric forms exist in negligible amounts under the experimental conditions common in complexation studies.

$$2\ \text{dye} \overset{K_D}{\rightleftharpoons} (\text{dye})_2 \qquad (3.1)$$

Table 3.2: Equilibrium constants, K_D, and the associated experimental conditions for the dimerisation of CV^+, RB and EO^-.

Dye	10^{-3} K_D (dm^3 mol^{-1})	T (K)	pH	Solvent system	Method	Reference
CV^+	0.6 ± 0.1	293	-	aqueous	UV-vis spectroscopy	36
RB	1.8 ± 1.0	298	6.4	aqueous NaCl	Temperature-jump spectrophotometry	39
	1.30 ± 0.26	298	7.2	aqueous	Fluorescence spectrophotometry	25
EO^-	no aggregation	-	-	-	-	40

3.1.3 Complexation of CV^+, RB and EO^- by β-CD

Cyclodextrins are able to form complexes with CV^+, RB and EO^- in aqueous solution. A complex described by a 1:1 stoichiometry between the host and guest may be characterised by the equilibrium constant, K_{11}. The equilibrium expression and summary of complexation constants for the 1:1 complexation between native β-CD and the dyes are given in Equation 3.2 and Table 3.3, respectively.[7,24,29,39]

$$\beta\text{-CD} + \text{dye} \underset{}{\overset{K_{11}}{\rightleftharpoons}} \beta\text{-CD}\cdot\text{dye} \qquad (3.2)$$

Table 3.3: Equilibrium constants, K_{11}, for the 1:1 host-guest complexation between β-CD and the guest dye compounds. Errors were not specified in the reference for the EO^- system.

Guest	10^{-3} K_{11} (dm^3 mol^{-1})	T (K)	pH	Solvent system	Method	Reference
CV^+	4680 ± 40	298	7.0	aqueous buffer	UV-vis spectroscopy	7
	820 – 4300	298	-	aqueous	UV-vis spectroscopy	24
RB	3960 ± 60	298	7.0	aqueous buffer	UV-vis spectroscopy	7
	5900 ± 2300	298	6.4	aqueous	Temperature-jump spectrophotometry	39
EO^-	9030	298	10.6	aqueous buffer	Fluorescence spectroscopy	29

3.1.4 Aims of this study

The aim of this research is to investigate the effect of β-CD modification on the host complexation properties of modified β-CD. This will be achieved by investigating the complexation properties of native β-CD, the mono-modified β-CDab and the β-CD dimer *E*-*p*-β-CD_2az, as shown in Figure 3.4. Cationic CV^+, zwitterionic RB and anionic EO^- will be used as guest molecules. The host-guest complexes will be studied by 2D ^{1}H NMR spectroscopy and UV-vis spectroscopy. Complexation studies with *E/Z*-*m*-β-CD_2az were not included due to the presence of both the *E* and *Z* isomer.

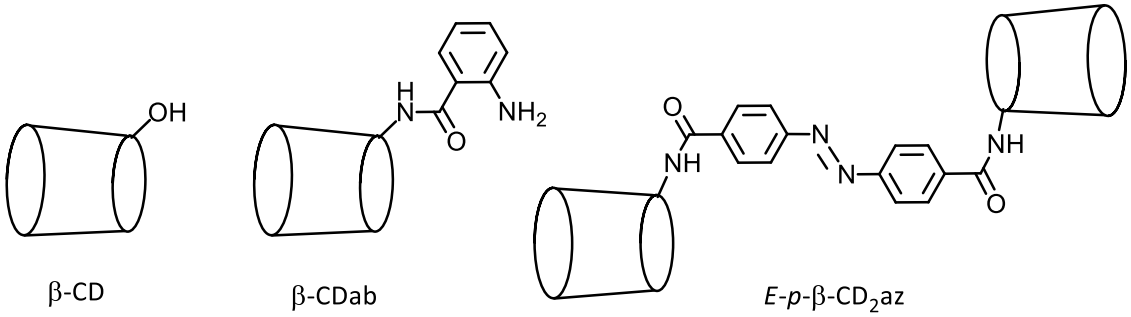

Figure 3.4: Structure of β-CD, β-CDab and *E*-*p*-β-CD_2az.

3.2 Results and Discussion

3.2.1 Complexation of CV^+, RB and EO^- by β-CD, *E*-*p*-βCD_2az and β-CDab

The complexation properties of native β-CD, *E*-*p*-β-CD_2az and β-CDab were examined by performing complexation studies with CV^+, RB and EO^- as guest molecules. 2D ^{1}H ROESY NMR spectroscopy was used to determine the qualitative complexation behavior, while UV-vis spectroscopy was used to quantitatively determine the complexation constants and thermodynamic parameters which govern complexation.

3.2.1.1 Qualitative Investigation of Complexation by 2D ^{1}H ROESY NMR Spectroscopy

The complexation behaviour of native β-CD, *E*-*p*-β-CD_2az and β-CDab with either CV^+, RB or EO^- was examined by 2D ^{1}H NMR spectroscopy. Solutions of each host and guest combination were prepared in D_2O phosphate buffer (pD 7.0, I = 0.10 mol dm^{-3}) at 298.2 K. The 2D ^{1}H ROESY NMR spectra for all host-dye combinations are given in Figure 3.5 – Figure 3.13. Cross-peaks between the H2 – H6 protons of β-CD and the protons of the guest indicate complexation.[7,41]

The complexation behavior of CV^+ with either native β-CD, *E*-*p*-β-CD_2az or β-CDab show similar results. The complexation of CV^+ by native β-CD produces distinct cross-peaks between the H1 – H3 resonances of CV^+ and the H3, H5 and H6 resonances of β-CD. Similarly, the complexation of CV^+ by *E*-*p*-β-CD_2az and β-CDab produces cross-peaks between the H1 – H3 resonances of CV^+ and the H2 – H6 resonances of β-CD in either host. Therefore, CV^+ forms a complex with all three hosts characterised by penetration of the methyl and phenyl groups of CV^+ into the β-CD cavity.

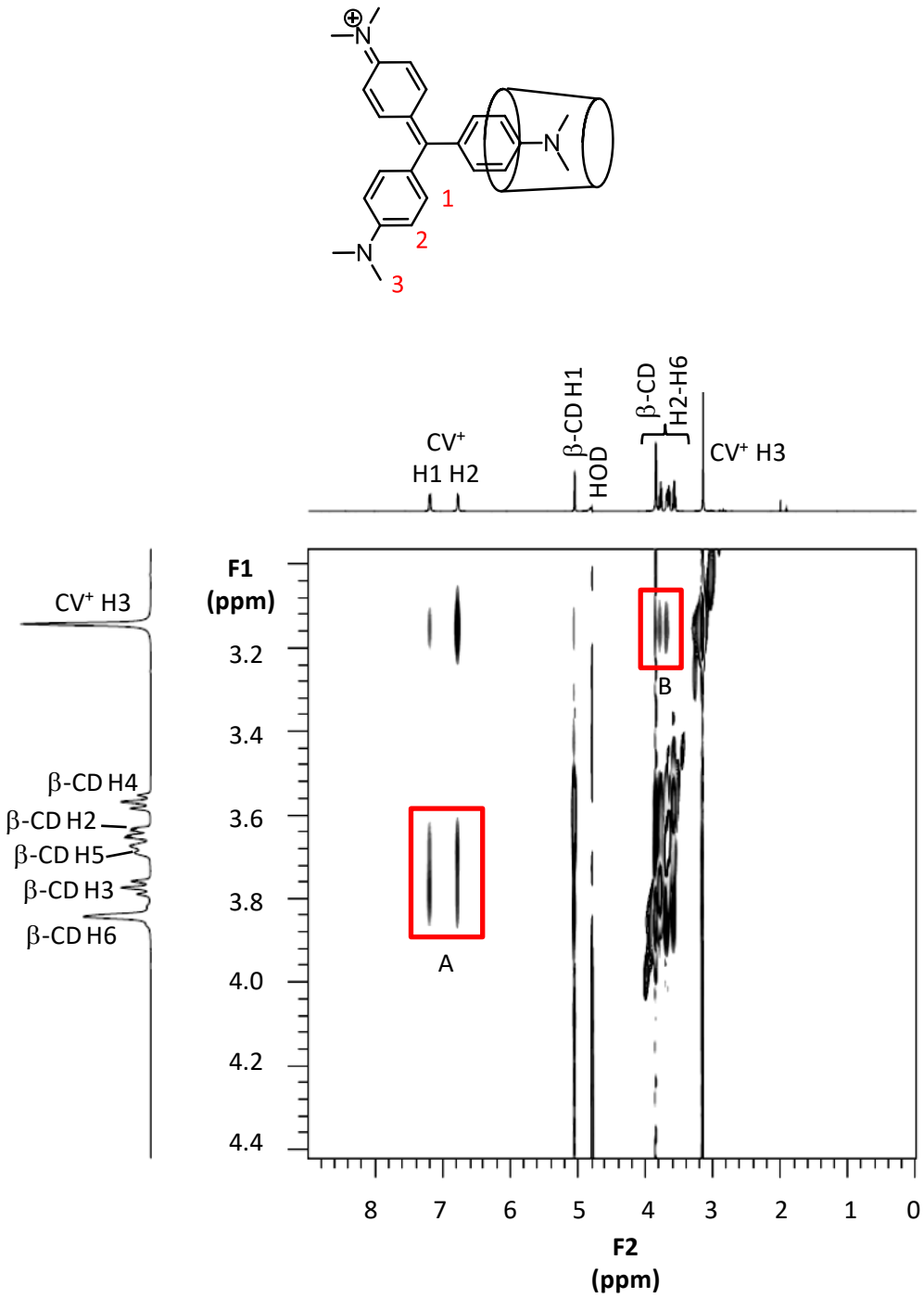

Figure 3.5: 2D ^{1}H ROESY NMR spectrum of β-CD (5.0×10^{-3} mol dm^{-3}) and CV^{+} (5.0×10^{-3} mol dm^{-3}) prepared in D_2O phosphate buffer (pD 7.0, I = 0.10 mol dm^{-3}) at 298.2 K. Rectangles A and B highlight cross-peaks arising from NOE interactions between the annular protons of β-CD and the protons of CV^{+}. A possible dominant structure depicting a 1:1 monotopic complex is shown above.

.

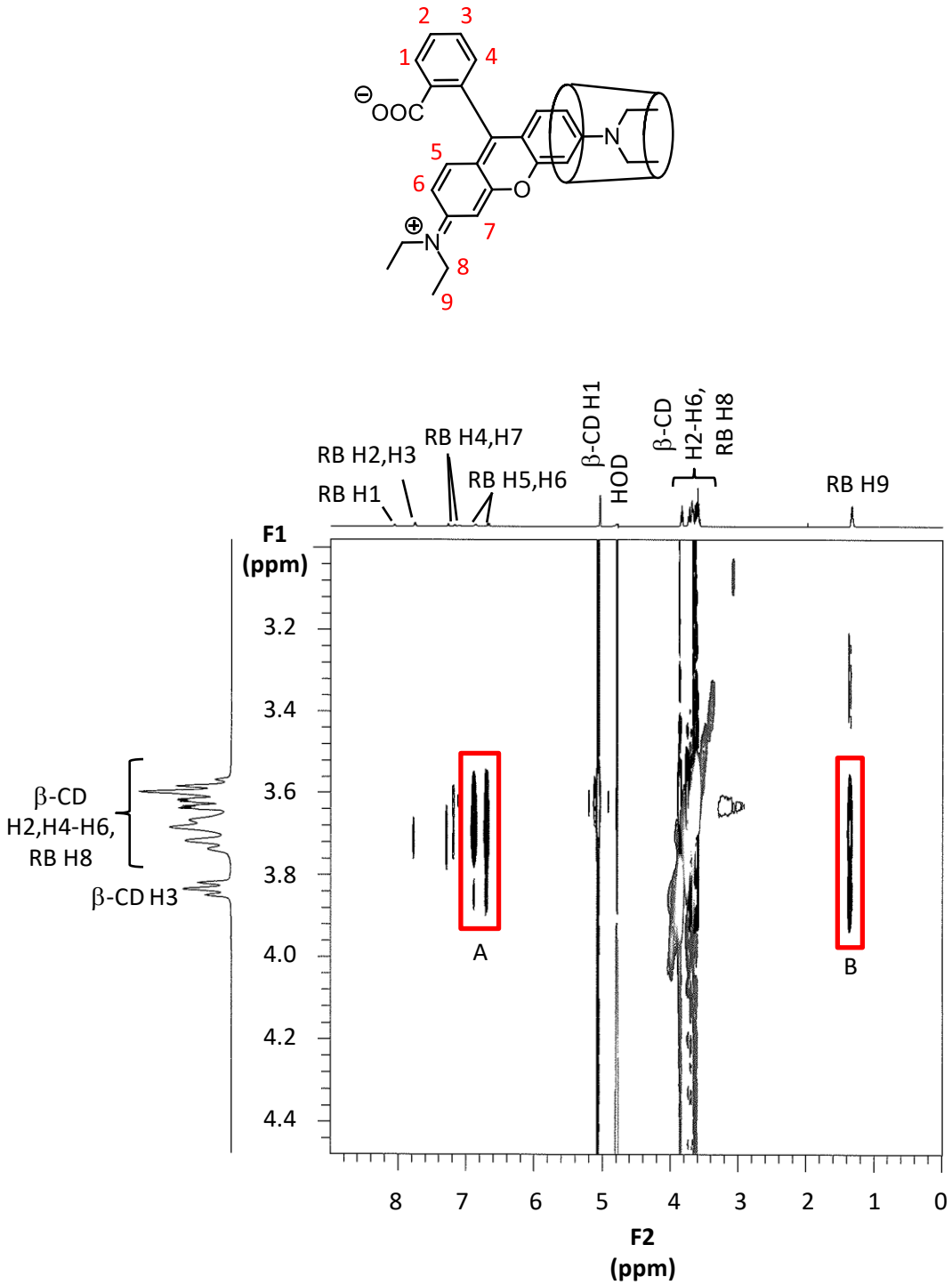

Figure 3.6: 2D ^{1}H ROESY NMR spectrum of β-CD (5.0×10^{-3} mol dm^{-3}) and RB (5.0×10^{-3} mol dm^{-3}) prepared in D_2O phosphate buffer (pD 7.0, I = 0.10 mol dm^{-3}) at 298.2 K. Rectangles A and B highlight cross-peaks arising from NOE interactions between the annular protons of β-CD and the protons of RB. A possible dominant structure depicting a 1:1 monotopic complex is shown above.

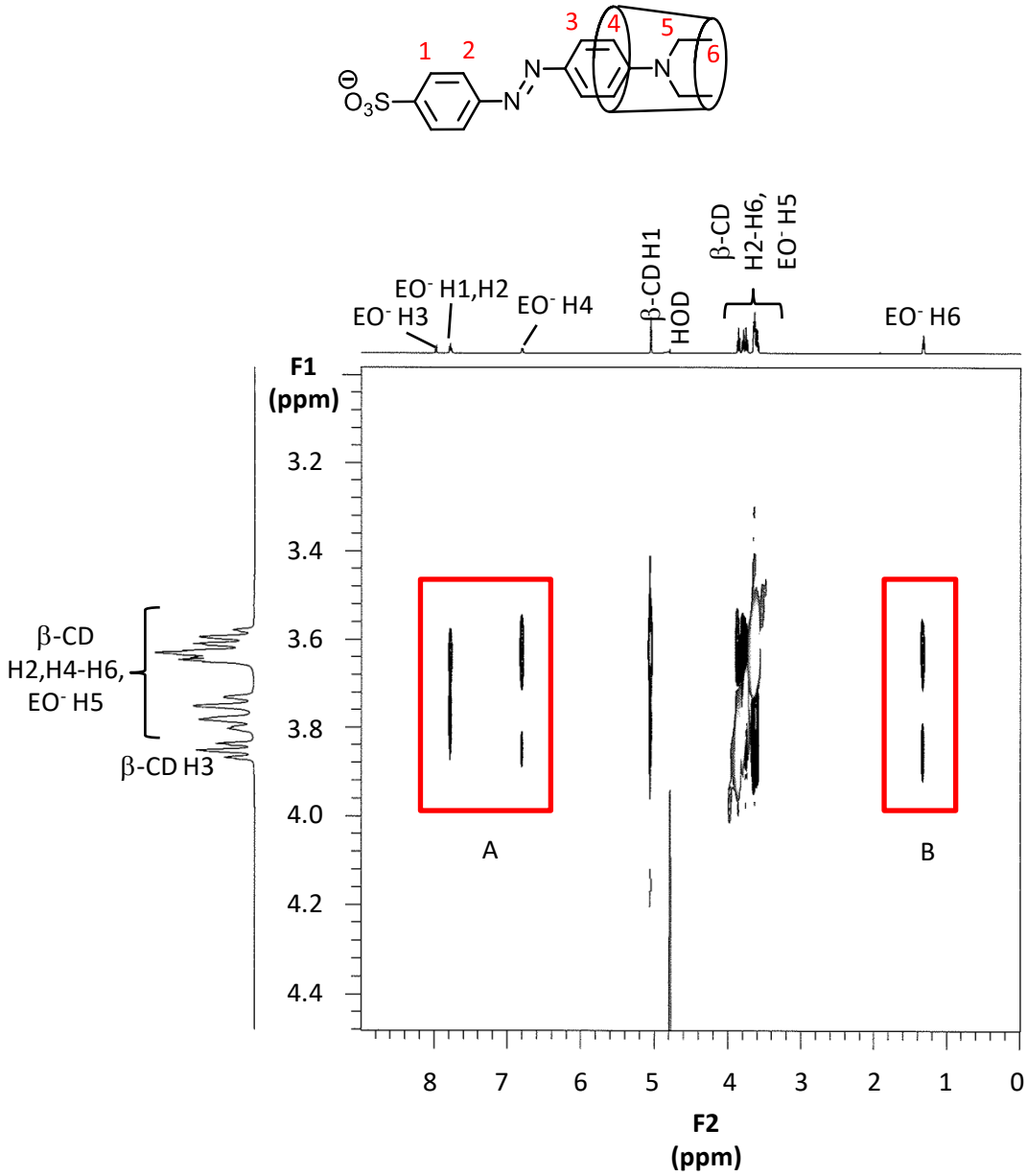

Figure 3.7: 2D ^{1}H ROESY NMR spectrum of β-CD (5.0×10^{-3} mol dm^{-3}) and EO^{-} (5.0×10^{-3} mol dm^{-3}) prepared in D_2O phosphate buffer (pD 7.0, I = 0.10 mol dm^{-3}) at 298.2 K. Rectangles A and B highlight cross-peaks arising from NOE interactions between the annular protons of β-CD and the protons of EO^{-}. A possible dominant 1:1 monotopic complex structure is shown above.

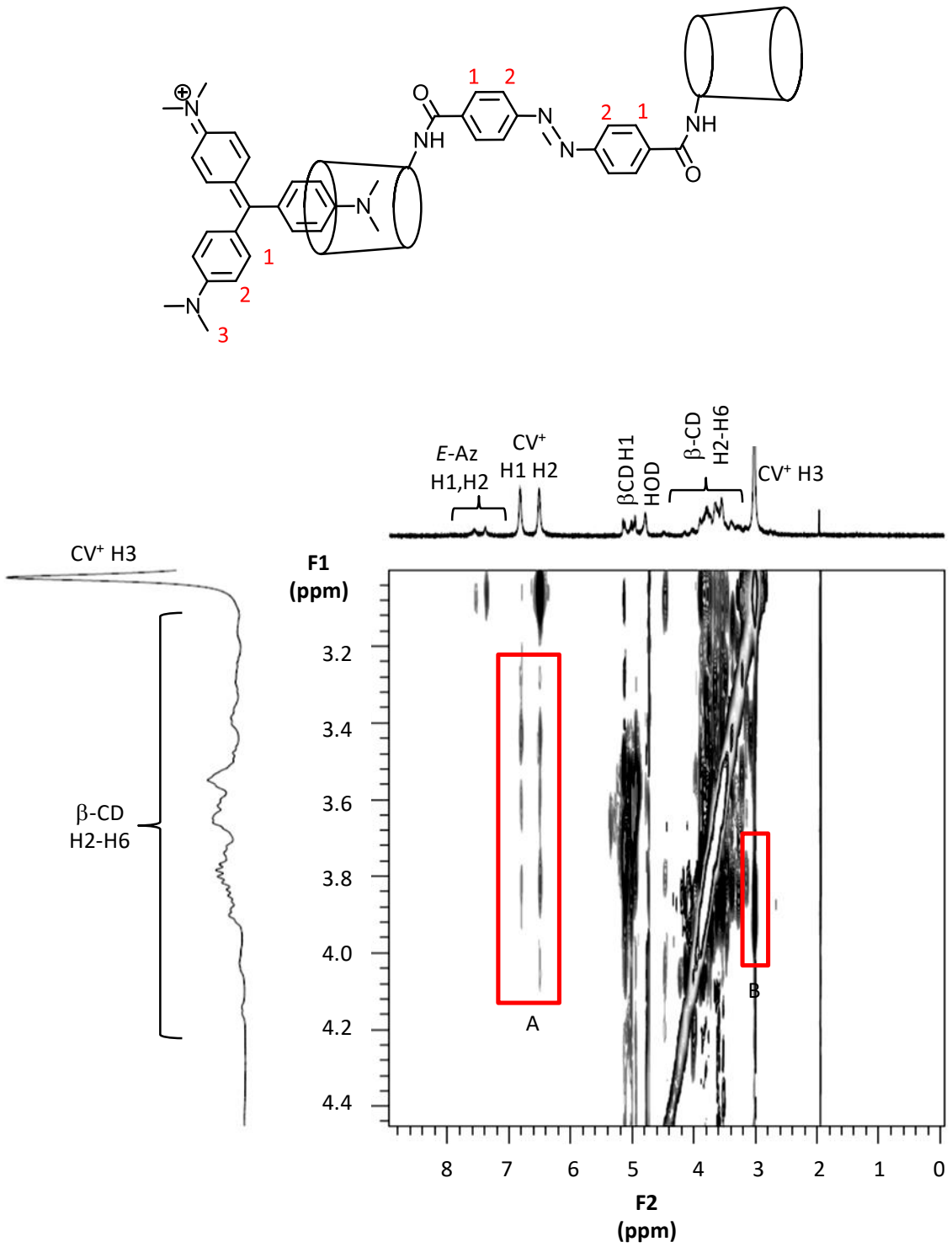

Figure 3.8: 2D ^{1}H ROESY NMR spectrum of *E*-*p*-β-CD_2az (5.0×10^{-3} mol dm^{-3}) and CV^+ (5.0×10^{-3} mol dm^{-3}) prepared in D_2O phosphate buffer (pD 7.0, I = 0.10 mol dm^{-3}) at 298.2 K. Rectangles A and B highlight cross-peaks arising from NOE interactions between the annular protons of β-CD and the protons of CV^+. A possible structure depicting a 1:1 monotopic complex is shown above. A possible 1:1 ditopic complex structure is shown in Figure 3.14.

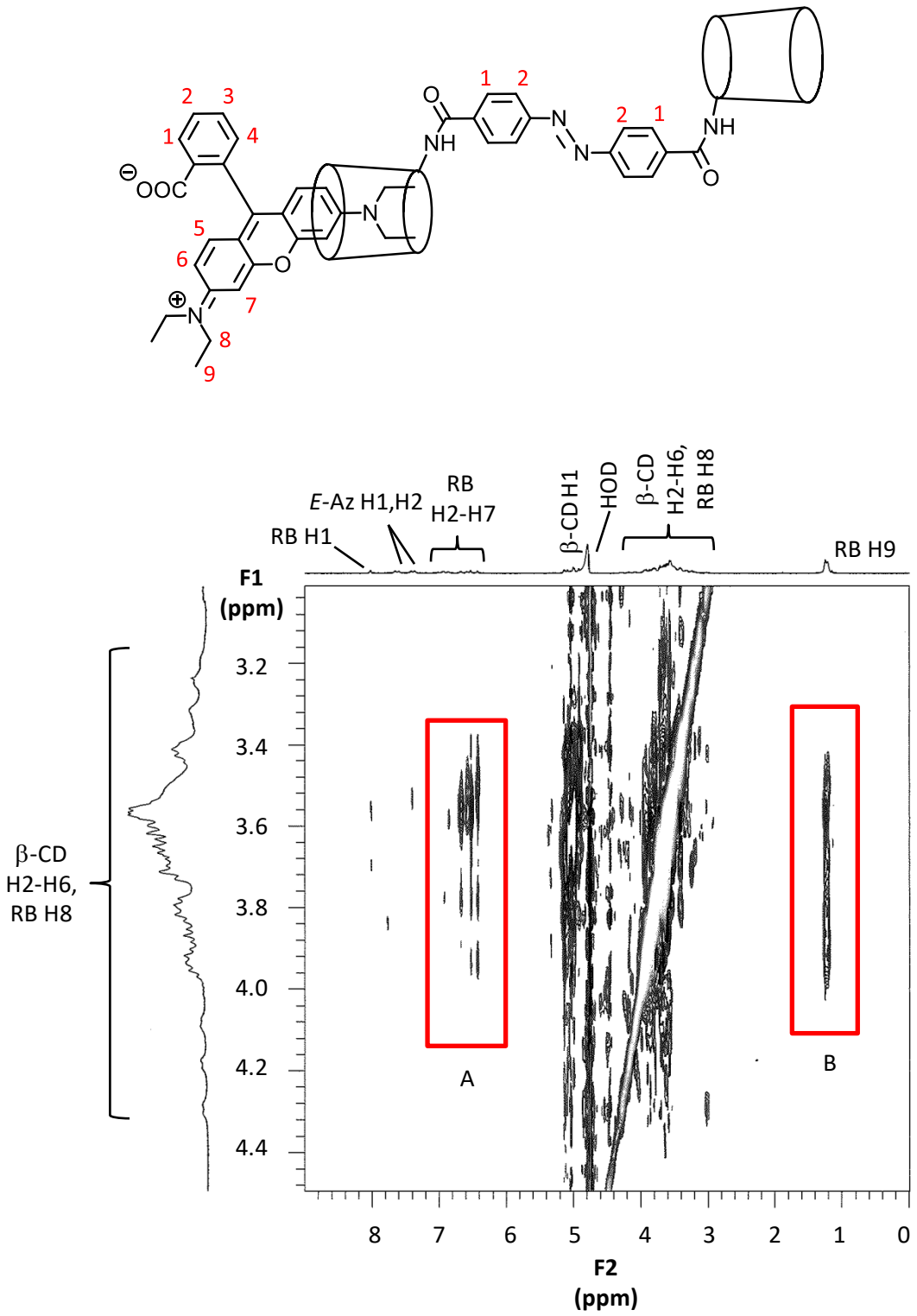

Figure 3.9: 2D ^{1}H ROESY NMR spectrum of *E*-*p*-β-CD_2az (5.0×10^{-3} mol dm^{-3}) and RB (5.0×10^{-3} mol dm^{-3}) prepared in D_2O phosphate buffer (pD 7.0, I = 0.10 mol dm^{-3}) at 298.2 K. Rectangles A and B highlight cross-peaks arising from NOE interactions between the annular protons of β-CD and the protons of RB. A possible structure depicting a 1:1 monotopic complex is shown above.

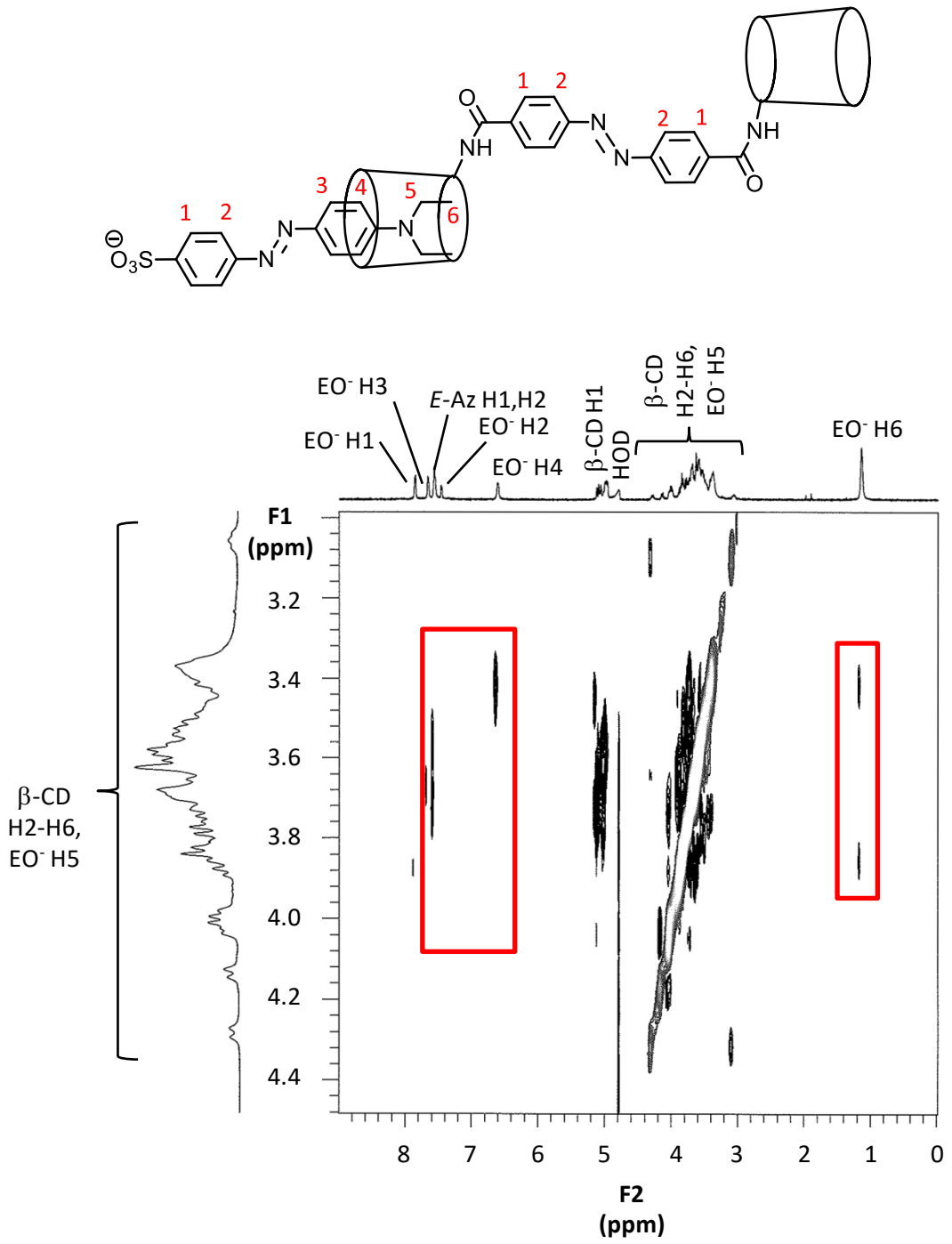

Figure 3.10: 2D ^{1}H ROESY NMR spectrum of *E*-*p*-β-CD_2az (5.0×10^{-3} mol dm^{-3}) and EO^- (5.0×10^{-3} mol dm^{-3}) prepared in D_2O phosphate buffer (pD 7.0, *I* = 0.10 mol dm^{-3}) at 298.2 K. Rectangles A and B highlight cross-peaks arising from NOE interactions between the annular protons of β-CD and the protons of EO^-. A possible structure depicting a 1:1 monotopic complex is shown above.

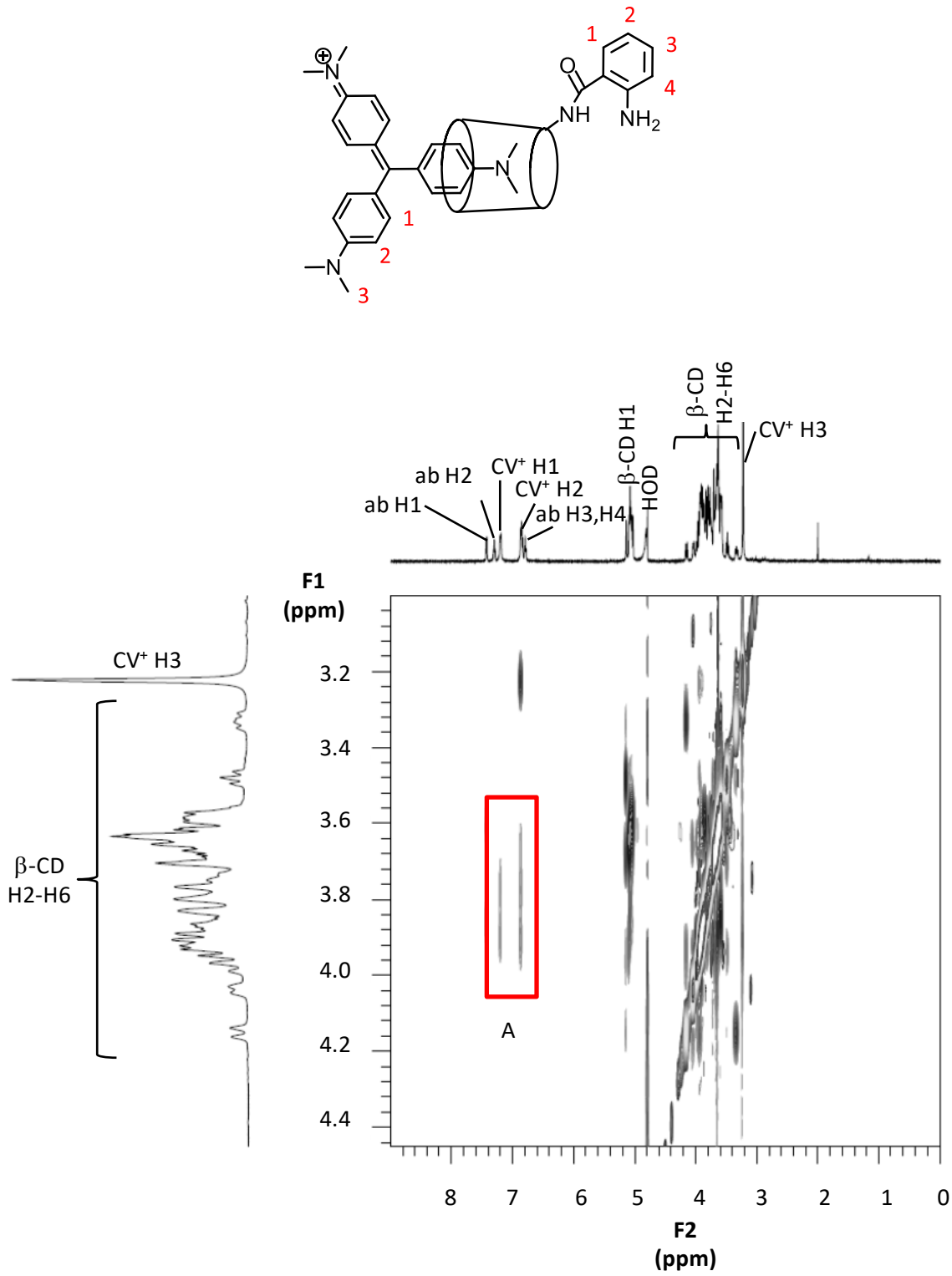

Figure 3.11: 2D ^{1}H ROESY NMR spectrum of β-CDab (1.0×10^{-2} mol dm^{-3}) and CV^{+} (5.0×10^{-3} mol dm^{-3}) prepared in D_2O phosphate buffer (pD 7.0, I = 0.10 mol dm^{-3}) at 298.2 K. Rectangle A highlights cross-peaks arising from NOE interactions between the annular protons of β-CD and the protons of CV^{+}. A possible structure depicting a 1:1 monotopic complex is shown above. The abbreviation 'ab' refers to the aminophenyl substituent of β-CDab.

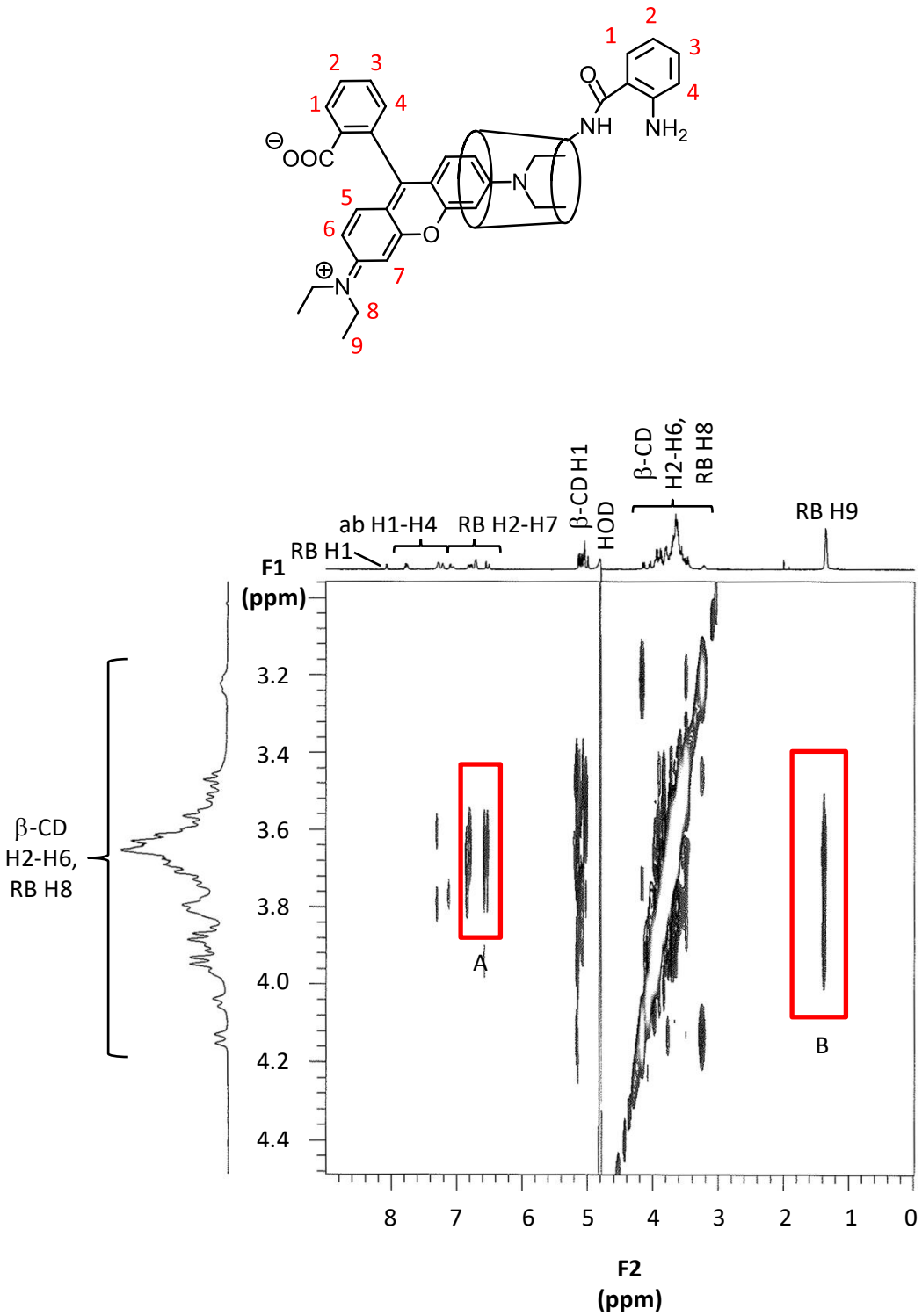

Figure 3.12: 2D ^{1}H ROESY NMR spectrum of β-CDab (1.0×10^{-2} mol dm^{-3}) and RB (5.0×10^{-3} mol dm^{-3}) prepared in D_2O phosphate buffer (pD 7.0, I = 0.10 mol dm^{-3}) at 298.2 K. Rectangles A and B highlight cross-peaks arising from NOE interactions between the annular protons of β-CD and the protons of RB. A possible structure depicting a 1:1 monotopic complex is shown above. The abbreviation 'ab' refers to the aminophenyl substituent of β-CDab.

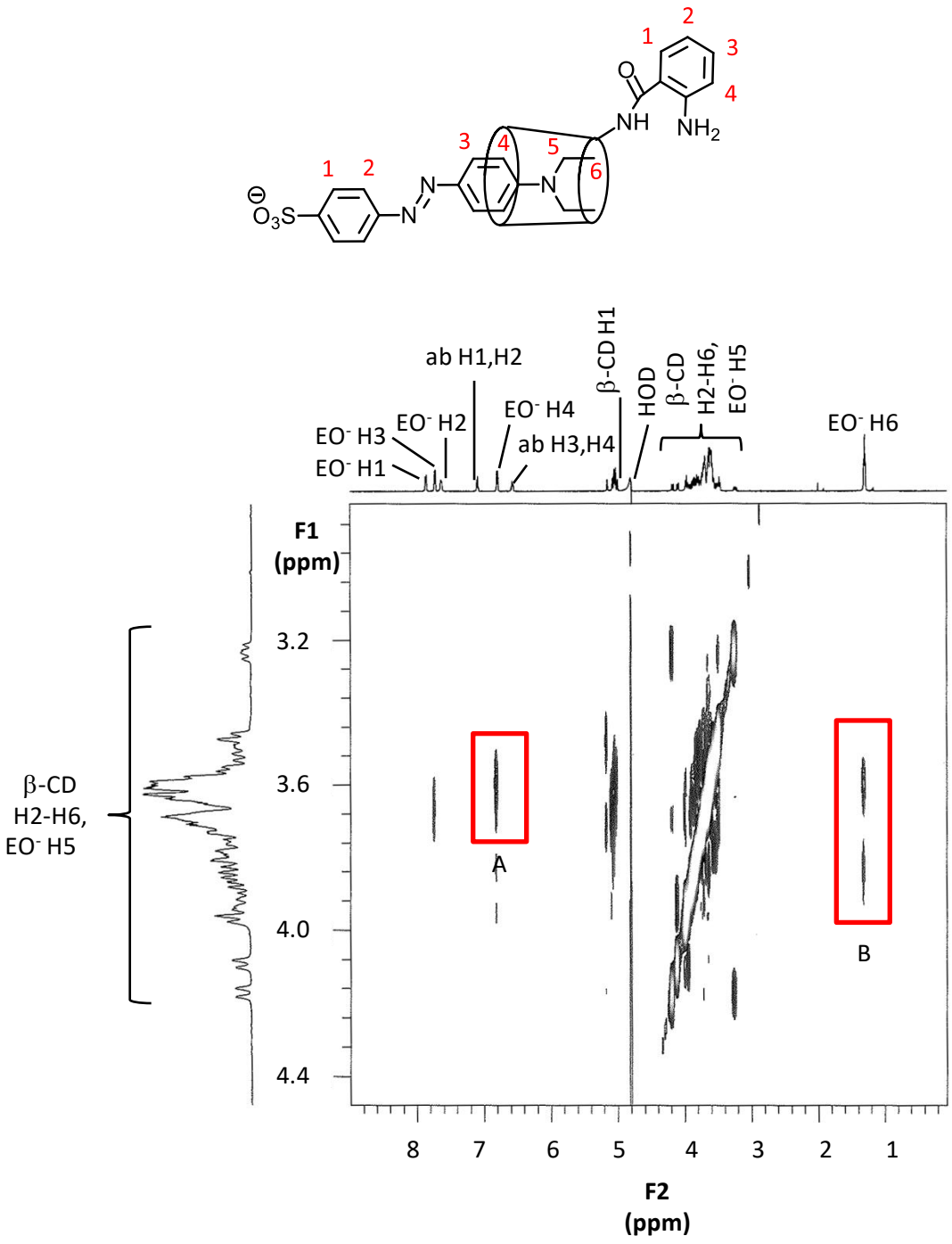

Figure 3.13: 2D ^{1}H ROESY NMR spectrum of β-CDab ($1.0 \times 10^{-@}$ mol dm^{-3}) and EO^- (5.0×10^{-3} mol dm^{-3}) prepared in D_2O phosphate buffer (pD 7.0, I = 0.10 mol dm^{-3}) at 298.2 K. Rectangles A and B highlight cross-peaks arising from NOE interactions between the annular protons of β-CD and the protons of EO^-. A possible structure depicting a 1:1 monotopic complex is shown above. The abbreviation 'ab' refers to the aminophenyl substituent of β-CDab.

While the proton resonances of CV^+ are readily distinguished in the NMR spectra, the proton resonances of RB overlap and shift upon complexation with native β-CD. Therefore, there is some ambiguity in the assignment of the H2 – H8 resonances of RB. Nevertheless, there is certainty in the identification of a complex.

The complexation of RB by native β-CD produces distinct cross-peaks between the H5, H6 and H9 resonances of RB and H2 – H6 resonances of β-CD. The complexation of RB by *E*-*p*-β-CD_2az and β-CDab produces cross-peaks between the H2 – H7 and H9 resonances of RB and the H2 – H6 resonances of the β-CD groups. As there are no cross-peaks apparent between the H1 resonances of RB, it appears that all three β-CD hosts dominantly complex RB via the diethylamino group.

As with CV^+, the proton resonances of EO^- are readily distinguished, although the H5 resonance of EO^- overlaps with the H2 – H6 resonances of β-CD. The complexation of EO^- by native β-CD produces clear cross-peaks between the H1, H2, H4 and H6 resonances of EO^- with the H2 – H6 resonances of β-CD. This indicates that β-CD can either form a 2:1 β-CD_2·EO^- complex or that a 1:1 complex is forming where β-CD shuttles between the alkyl and phenyl groups of EO^-.

The complexation of EO^- by *E*-*p*-β-CD_2az and β-CDab produces cross-peaks only between the H4 and H6 resonances of EO^- and the H2 – H6 resonances of the β-CD groups. This indicates that EO^- is dominantly entering the β-CD cavity via the alkyl end rather than the sulfonate end to minimise the interaction between the charged sulfonate group and hydrophobic β-CD cavity.

While 2D ^{1}H NMR spectroscopy can determine the existence of a complex, the stoichiometry and orientation of the host and guest is unknown. The structures given in Figure 3.5 – Figure 3.13 depict monotopic 1:1 host:guest complexes. However, in principle, 1:1 and 2:1 host:guest complexes may form, characterised by either monotopic or ditopic complexation. Ditopic complexation by a single host is also referred to as cooperative complexation, whereby two β-CD groups of a single β-CD oligomer complex two sites of a single guest.[3] Additionally, the guest may enter the CD cavity via the primary face or secondary face. The preference for primary or secondary face complexation is usually determined by NMR spectroscopy by considering the shifts in proton resonances of β-CD before and after complexation. A shift of the H2 and H3 resonances usually indicates primary face preference while a shift in H5 and H6 resonances indicates secondary face preference. However, given that the H2 – H6 resonances of β-CD are multiplied and superimposed in the spectra of β-CDab and *E*-p-β-CD_2az, the facial preference for complexation is not readily deduced from the NMR spectra.

Figure 3.14 depicts the possible host:guest complex structures of various stoichiometries and orientations, using CV^+ as the guest and either native β-CD or *E*-*p*-βCD_2az as the host. The stoichiometry, preference for a particular orientation and stability of a complex was further characterised by UV-vis spectroscopy as described in 3.2.1.2.

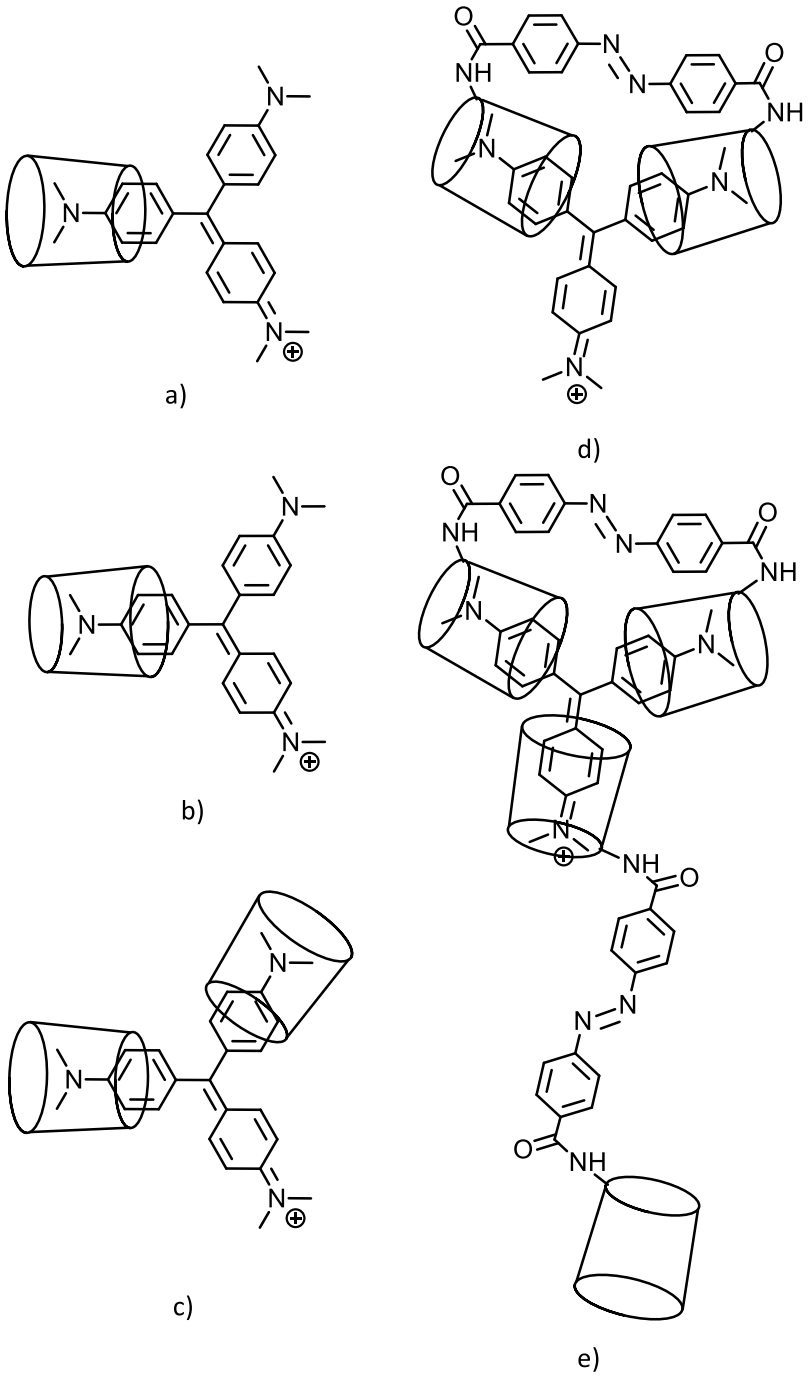

Figure 3.14: Host-guest complexes of various structures and orientations, including a) 1:1 β-CD·CV^+ monotopic complexation through the primary face, b) 1:1 β-CD·CV^+ monotopic complexation through the secondary face, c) 2:1 β-CD_2·CV^+ monotopic complexation through the primary faces, d) 1:1 *E*-*p*-β-CD_2az·CV^+ ditopic complexation through the secondary faces and e) 2:1 (*E*-*p*-β-CD_2az)$_2$·CV^+ showing monotopic and ditopic complexation through the secondary faces.

3.2.1.2 Quantitative Investigation of Complexation by UV-vis spectroscopy

The complexation constants and thermodynamic parameters for the complexation between native β-CD, *E*-*p*-β-CD_2az and β-CDab with CV^+, RB and EO^- were determined by UV-vis spectroscopy. The equilibrium expression for 1:1 complexation between each host and dye is given by Equation 3.3,

$$\text{host + dye} \overset{K_{11}}{\rightleftharpoons} \text{host·dye} \tag{3.3}$$

where the host is either native β-CD, *E*-*p*-β-CD_2az or β-CDab and the dye is either CV^+, RB or EO^-. The equation for the complexation constant, K_{11}, is given by Equation 3.4,

$$K_{11} = \frac{[host \cdot dye]}{[host][dye]} \tag{3.4}$$

The equilibrium expression for the 2:1 complexation of a second host to the existing host·dye complex is given by Equation 3.5,

$$\text{host + host·dye} \overset{K_{21}}{\rightleftharpoons} \text{host}_2\text{·dye} \tag{3.5}$$

The equation for the complexation constant, K_{21}, is given by Equation 3.6,

$$K_{21} = \frac{[host_2 \cdot dye]}{[host][host \cdot dye]} \tag{3.6}$$

The change in Gibbs free energy (ΔG_{11}) for the first equilibrium describing a 1:1 host·dye complex is given by Equation 3.7,

$$\Delta G_{11} = -RTlnK_{11} \tag{3.7}$$

where *R* is the ideal gas constant and *T* is the temperature. ΔG_{11} is also given by Equation 3.8,

$$\Delta G_{11} = \Delta H_{11} - T\Delta S_{11} \tag{3.8}$$

where ΔH_{11} and ΔS_{11} are the changes in enthalpy and entropy for the formation of a 1:1 host·dye complex, respectively. Combining Equations 3.7 and 3.8 leads to Equation 3.9,

$$lnK_{11} = -\frac{\Delta H_{11}}{RT} + \frac{\Delta S_{11}}{R} \tag{3.9}$$

Equation 3.9 is known as the van't Hoff equation and a plot of lnK_{11} versus $1/T$ is known as the van't Hoff plot, where the slope and intercept represent $-\Delta H_{11}/R$ and $\Delta S_{11}/R$, respectively.

In order to calculate the complexation constants and thermodynamic parameters of complexation, the concentrations of the host, dye and host·dye complex in solution must be known, and may be determined by UV-vis spectroscopy.[7,42-44] The total concentration of each species at equilibrium is equal to the initial concentrations of the host and dye, as given by Equations 3.10 and 3.11, respectively.

$$[host]_0 = [host \cdot dye] + [host] \tag{3.10}$$

$$[dye]_0 = [host \cdot dye] + [dye] \tag{3.11}$$

The observed absorbance of the system, A_{obs}, is given by Equation 3.12,

$$A_{obs} = A_{host} + A_{dye} + A_{host \cdot dye} \tag{3.12}$$

Each absorbance term may be expressed in terms of Beer's Law, given by Equation 3.13,

$$A = \varepsilon lc \tag{3.13}$$

where ε is the molar extinction coefficient and *l* is the path length of the cell. Beer's Law, Equation 3.10 and Equation 3.11 may be substituted into Equation 3.12 to give Equation 3.14,

$$\begin{aligned} A_{obs} = \varepsilon_{host}.l.([host]_0 - [host \cdot dye]) + \varepsilon_{dye}.l.([dye]_0 - [host \cdot dye]) \\ + \varepsilon_{host.dye}.l.[host \cdot dye] \end{aligned} \tag{3.14}$$

Equations 3.10, 3.11 and 3.14 may be used to fit a series of UV-vis absorption spectra describing the equilibria consisting of the host, dye and host·dye complex to yield the concentration of each species and hence, the complexation constants. The determination of complexation constants at varying temperatures may then be used to determine the thermodynamic parameters using Equations 3.7 – Equation 3.9 for 1:1 complexes.

The experimental concentrations chosen for these studies were sufficiently low such that the dimerisation of CV^+ or RB did not significantly influence the results. Given that the dimerisation constants of CV^+ and RB are 0.60×10^3 mol dm^{-3} and 1.80×10^3 mol dm^{-3},[36,39] the proportion of dimers in each study was approximately 0.48% and 1.4%, respectively. Therefore, the presence of such small amounts of these dimers is not expected to significantly influence the complexation studies.

The equilibria in which native β-CD, *E-p*-β-CD_2az and β-CDab complex CV^+, RB and EO were characterised by UV-vis spectroscopy in aqueous phosphate buffer (pH 7.0, I = 0.10 mol dm^{-3}) at 308.2 K, 298.2 K, 288.2 K and 278.2 K, following methods reported by Lincoln *et al.*[7,42,43] The absorbance of the dye (varying concentration of a 2 cm^3 solution) was determined against a reference solution (2 cm^3 solution containing aqueous phosphate buffer) in 1 cm matched quartz cells. The solutions were thermostatted at the required temperature for 15 minutes, while stirring, before the absorbance was recorded. The absorbance was recorded at 1 nm intervals using a Cary 5000 UV-vis spectrophotometer. The change in the UV-vis spectrum of the dye solution was monitored as aliquots (5 mm^3) of the host solution were sequentially titrated into the dye and reference cells. The resultant UV-vis absorption spectra were analysed using the non-linear least squares fitting program *HypSpec*,[45] to derive complexation constants for a 1:1 host·dye complex. The UV-vis spectra were fitted over a wavelength range in which significant change in the dye solution absorption occurred upon addition of the host solution. The fitting of the experimental data yielded the complexation constants for the input equilibria, the derived molar absorbances of free and complexed dye and, using the simulation software *HySS*,[46] the speciation of the free and complexed dye with increasing host concentration. Complexation studies between β-CD and CV^+ and RB were performed by Trang Nguyen.[7]

Features of the UV-vis absorption spectra of all host-guest systems were analysed to determine the correct host:guest model to use for fitting. The presence of an isobestic point in the experimental molar absorbances of the dye upon addition of a host is indicative of a 1:1 complex. The molar absorbances of the dye in each host-guest system are shown in Figure 3.15 – Figure 3.17.

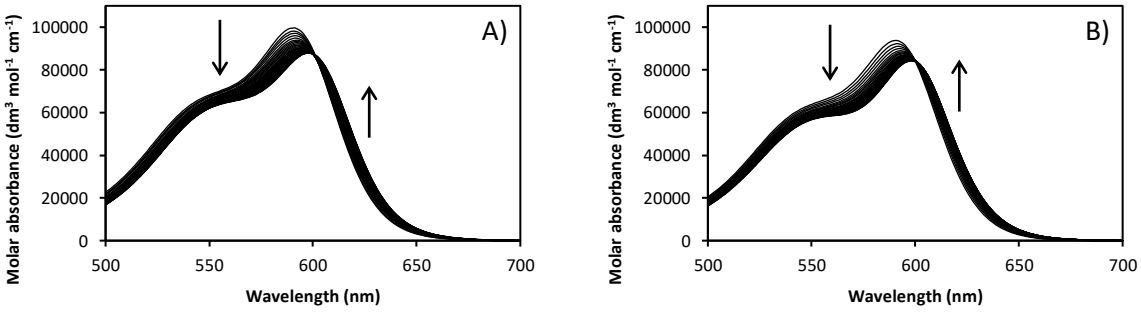

Figure 3.15: UV-vis molar absorbances of CV^+ (initial concentration 8.0 × 10^{-6} mol dm^{-3}) with increasing concentrations of A) *E-p*-β-CD_2az (0 – 9.1 × 10^{-5} mol dm^{-3}) and B) β-CDab (0 – 7.3 × 10^{-4} mol dm^{-3}) in aqueous phosphate buffer (pH 7.0 and I = 0.10 mol dm^{-3}) at 298.2 K. The arrows indicate the direction of change.

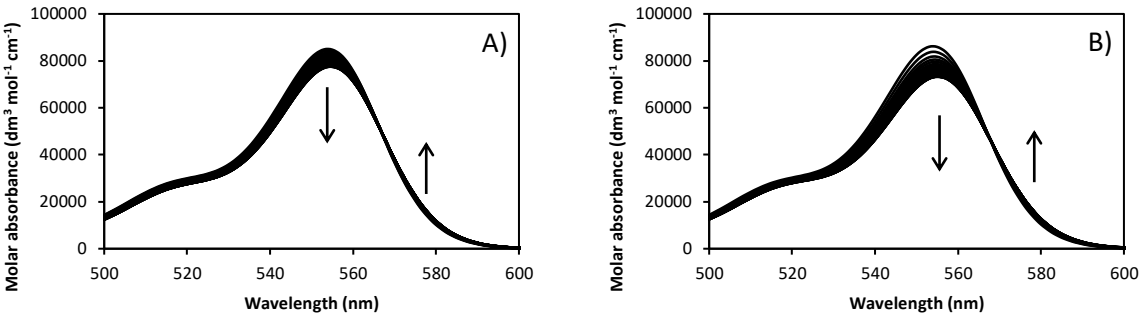

Figure 3.16: UV-vis molar absorbances of RB (initial concentration 8.0×10^{-6} mol dm^{-3}) with increasing concentrations of A) *E*-*p*-β-CD$_2$az (0 – 2.4×10^{-4} mol dm^{-3}) and B) β-CDab (0 – 1.1×10^{-3} mol dm^{-3}) in aqueous phosphate buffer (pH 7.0 and I = 0.10 mol dm^{-3}) at 298.2 K. The arrows indicate the direction of change.

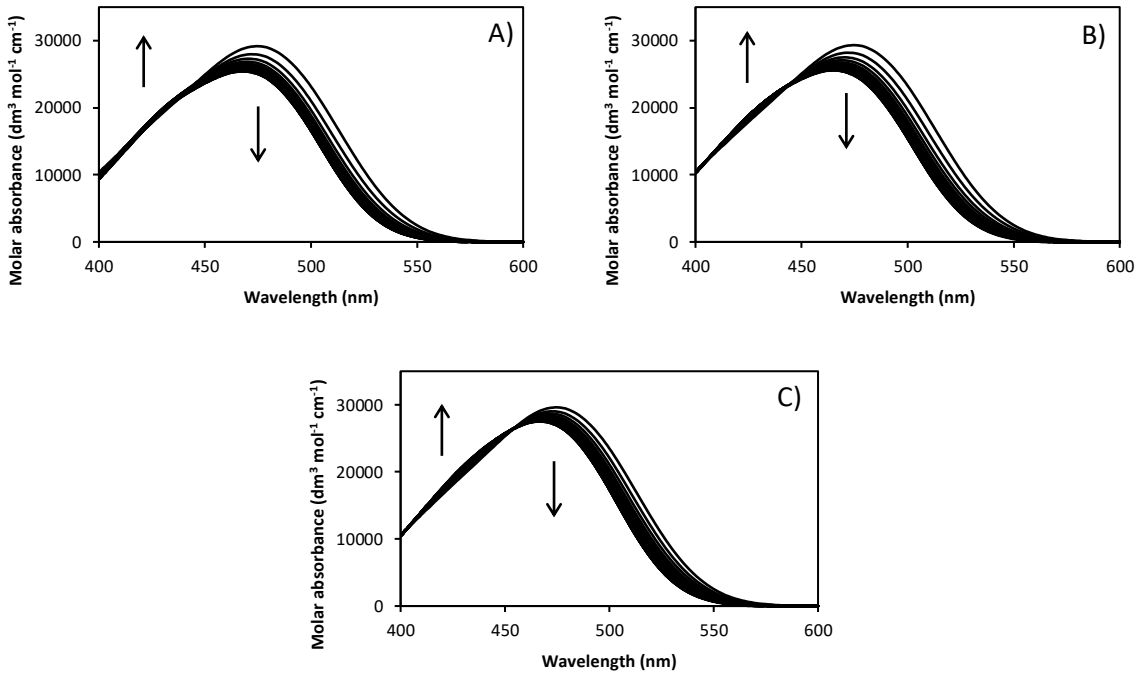

Figure 3.17: UV-vis molar asorbances of EO$^-$ (initial concentration 2.0×10^{-5} mol dm^{-3}) with increasing concentrations of A) *E*-*p*-β-CD$_2$az (0 – 6.4×10^{-4} mol dm^{-3}), B) β-CDab (0 – 8.0×10^{-4} mol dm^{-3}) and C) β-CD (0 – 9.6×10^{-4} mol dm^{-3}) in aqueous phosphate buffer (pH 7.0 and I = 0.10 mol dm^{-3}) at 298.2 K. The arrows indicate the direction of change.

The UV-vis spectra of CV$^+$ shows a decrease in absorbance at the λ_{max} at 590 nm upon addition of both *E*-*p*-β-CD$_2$az and β-CDab. There is also a red shift in the λ_{max} upon increasing host:CV$^+$ ratio. The decrease in molar absorbance and shift in λ_{max} are both indicative of CV$^+$ entering a new chemical environment, which is likely to be the annulus of β-CD. An isobestic point is observed in both systems at approximately 603 nm. Therefore, the complexation of CV$^+$ by *E*-*p*-β-CD$_2$az and β-CDab is likely to be dominated by a 1:1 complex. It should be noted that there is a slight variation in molar absorbance of CV$^+$ alone between the *E*-*p*-β-CD$_2$az and β-CDab host systems. This may occur as CV$^+$

adsorbs onto glass surfaces, which can cause slight changes in the concentration.[36]

The UV-vis spectra of RB shows a decrease in the absorbance at the λ_{max} at 554 nm, upon addition of both *E*-*p*-β-CD_2az and β-CDab. A red shift in the λ_{max} is also observed with increasing host:RB ratio. As the shift is only 2 nm, it is difficult to identify the existence of an isobestic point.

The UV-vis spectra of EO^- shows a decrease in the absorbance at the λ_{max} at 474 nm, upon addition of *E*-*p*-β-CD_2az, β-CDab and β-CD. Unlike the CV^+ and RB systems, there is a slight blue shift in the λ_{max} upon increasing host:EO^- ratio. The isobestic point is not as clear as in the CV^+ systems, but appears to occur at approximately 445 nm for the *E*-*p*-β-CD_2az/EO^- and β-CDab/EO^- systems, and 454 nm for the β-CD/EO^- system.

An algorithm for the formation of 1:1 host-guest complexes, Equation 3.3, was best-fitted to the variation of the UV-vis spectra of the *E*-*p*-β-CD_2az/CV^+ and β-CDab/CV^+ host-guest systems, and the experimental and derived molar absorbances of each system at 298.2 K are shown in Figure 3.18A and B. It is clearly seen that the fit for the *E*-*p*-β-CD_2az/CV^+ system is poor and consistent with the presence of another host-guest complex instead of, or in addition to, a 1:1 complex, while the fit for the β-CDab/CV^+ system is good and consistent with the dominant formation of the β-CDab·CV^+ host·guest complex.

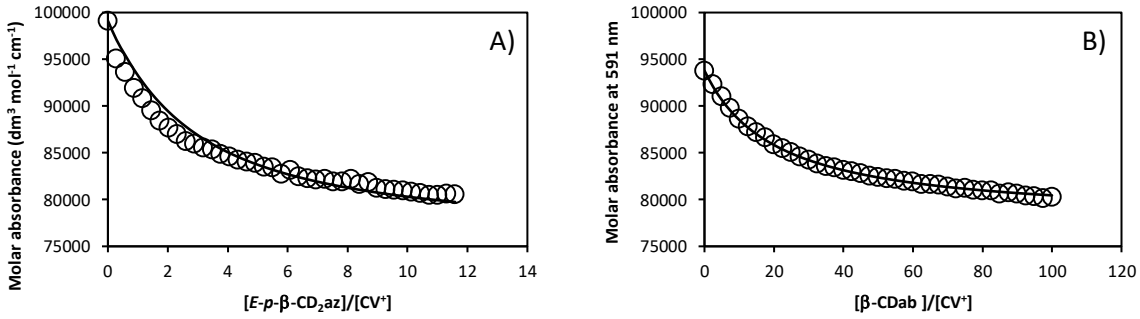

Figure 3.18: UV-vis absorbance data of CV^+ (initial concentration 8.0×10^{-6} mol dm^{-3}) with increasing concentrations of A) *E*-*p*-β-CD_2az (0 – 9.1×10^{-5} mol dm^{-3}) and B) β-CDab (0 – 7.3×10^{-4} mol dm^{-3}) in aqueous phosphate buffer (pH 7.0 and I = 0.10 mol dm^{-3}) at 298.2K showing the experimental (circles) and best fit (line) molar absorbances at 591 nm (fitted at 1 nm intervals over the range 550 – 620 nm) for a 1:1 complex.

It was found that an algorithm for the sequential formation 1:1 and 2:1 host-guest complexes, Equation 3.3 and Equation 3.5, best-fitted the variation of the UV-vis spectrum of the *E*-*p*-β-CD_2az/CV^+ system, and the experimental and derived molar absorbances at 298.2 K are shown in Figure 3.19.

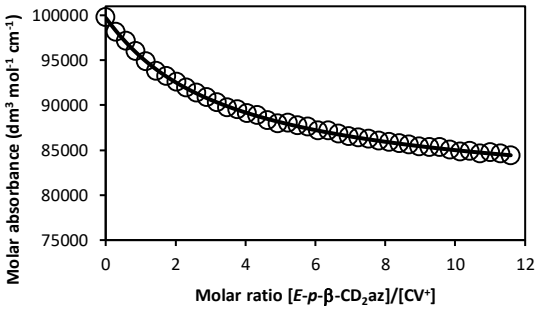

Figure 3.19: UV-vis absorbance data of CV^+ (initial concentration 8.0×10^{-6} mol dm^{-3}) with increasing concentrations of *E*-*p*-β-CD_2az (0 – 9.1×10^{-5} mol dm^{-3}) in aqueous phosphate buffer (pH 7.0 and I = 0.10 mol dm^{-3}) at 298.2 K, showing the experimental (circles) and best fit (line) molar absorbances at 591 nm (fitted at 1 nm intervals over the range 550 – 620 nm) for 1:1 and 2:1 complexes.

The derived K_{11} and K_{21} for the *E*-*p*-β-CD_2az·CV^+ and (*E*-*p*-β-CD_2az)$_2$·CV^+ host guest complexes, and the K_{11} for the β-CDab·CV^+ at 298.2K and also at 278.2 K, 288.2 K and 308.2 K appear in Table 3.4 together with analogous data for β-CD·CV^+ and (β-CD)$_2$·CV^+ from the literature.[7] The complete data sets appear in 3.5 Appendix for: *E*-*p*-β-CD_2az/CV^+ (Figure 3.27 and Figure 3.28 with fitting for sequential formation of *E*-*p*-β-CD_2az·CV^+ and (*E*-*p*-β-CD_2az)$_2$·CV^+ host guest complexes), *E*-*p*-β-CD_2az/CV^+ (Figure 3.41 and Figure 3.42 with unsatisfactory fitting for the *E*-*p*-β-CD_2az·CV^+ host guest complex alone), and for β-CDab/CV^+ (Figure 3.29 and Figure 3.30 with fitting for the β-CDab·CV^+ host guest complex alone).

An algorithm for the formation of 1:1 host-guest complexes, Equation 3.3, fitted well to the absorbance changes for the *E*-*p*-β-CD_2az/RB and β-CDab/RB systems as seen in Figure 3.20.

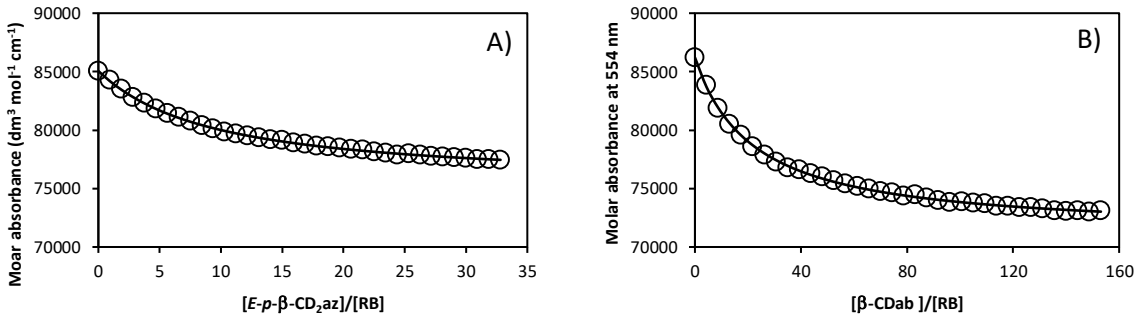

Figure 3.20: UV-vis absorbance data of RB (initial concentration 8.0×10^{-6} mol dm^{-3}) with increasing concentrations of A) *E*-*p*-β-CD_2az (0 – 2.4×10^{-4} mol dm^{-3}) and B) β-CDab (0 – 1.1×10^{-3} mol dm^{-3}) in aqueous phosphate buffer (pH 7.0 and I = 0.10 mol dm^{-3}) at 298.2 K, showing the experimental (circles) and best fit (line) molar absorbances at 554 nm (fitted at 1 nm intervals over the range 520 – 570 nm) for a 1:1 complex.

The complete data sets appear in 3.5 Appendix for: *E*-*p*-β-CD_2az/RB (Figure 3.31 and Figure 3.32 with fitting for the formation of the *E*-*p*-β-CD_2az·RB host-guest complex alone), and for β-CDab/RB (Figure 3.33 and Figure 3.34 with fitting for the β-CDab·RB host-guest complex alone). The derived K_{11} for *E*-*p*-β-CD_2az·RB, β-CDab·RB at 298.2 K and also at 278.2 K, 288.2 K and 308.2 K appear in Table 3.5 together with analogous data for β-CD·RB from the literature.[7]

An algorithm for the formation of 1:1 host-guest complexes, Equation 3.3, fitted well to the absorbance changes for the *E*-*p*-β-CD_2az/EO^-, β-CDab/EO^- and β-CD/EO^- systems as seen in Figure 3.21.

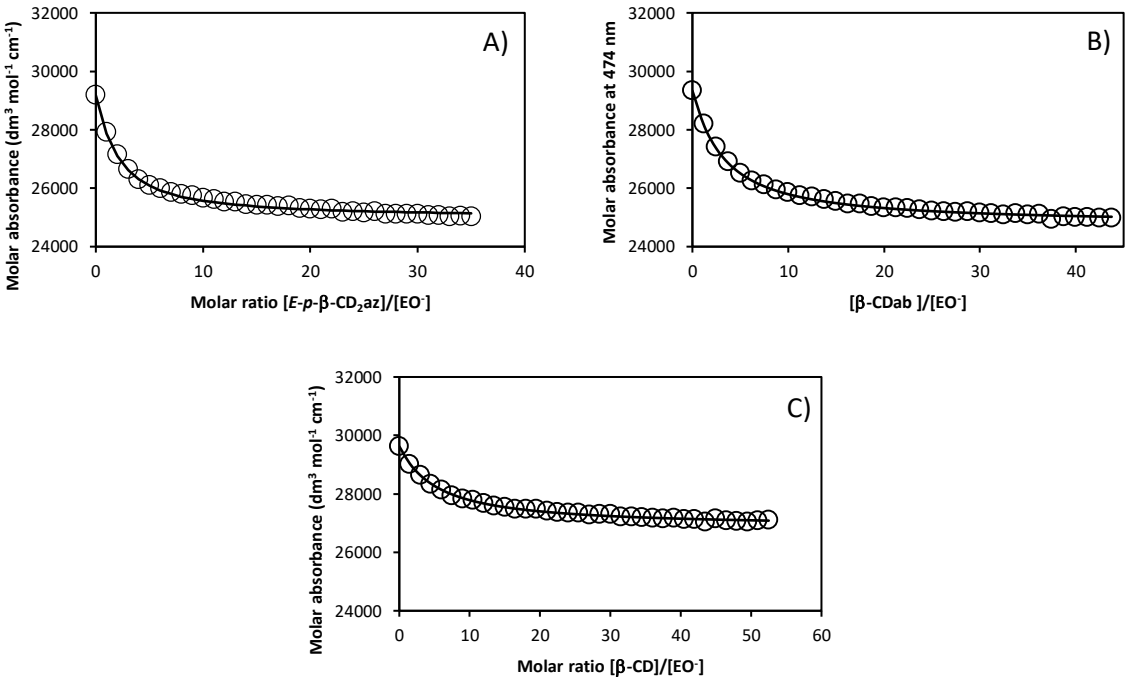

Figure 3.21: UV-vis absorbance data of EO^- (initial concentration 2.0×10^{-5} mol dm^{-3}) with increasing concentrations of A) *E*-*p*-β-CD_2az (0 – 6.4×10^{-4} mol dm^{-3}), B) β-CDab (0 – 8.0×10^{-4} mol dm^{-3}) and C) β-CD (0 – 9.6×10^{-4} mol dm^{-3}) in aqueous phosphate buffer (pH 7.0 and I = 0.10 mol dm^{-3}) at 298.2 K showing the experimental (circles) and best fit (line) molar absorbances at 474 nm (fitted at 1 nm intervals over the range 425 – 520 nm) for a 1:1 complex.

The complete data sets appear in 3.5 Appendix for: *E*-*p*-β-CD_2az/EO^- (Figure 3.35 and Figure 3.36 with fitting for the formation of the *E*-*p*-β-CD_2az·PB host-guest complex alone), for β-CDab/EO^- (Figure 3.37 and Figure 3.38 with fitting for the β-CDab·PB host-guest complex alone), and for β-CD/EO^- (Figure 3.39 and Figure 3.40 with fitting for the β-CD·EO^- host-guest complex alone). The derived K_{11} for *E*-*p*-β-CD_2az·EO^-, β-CDab·EO^- and β-CD·EO^- at 298.2 K and also at 278.2 K, 288.2 K and 308.2 K appear in Table 3.6.

The complexation constants for the 1:1 host.guest complex, K_{11}, determined at 278.2 K, 288.2 K, 298.2 K and 308.2 K were used to construct van't Hoff plots and derive ΔG_{11}, ΔH_{11} and ΔS_{11} of complexation. The van't Hoff plots for the complexation of CV^+, RB and EO^- by the hosts are shown in Figure 3.22, Figure 3.23 and Figure 3.24, respectively. An algorithm for the van't Hoff equation was best-fitted to the K_{11} data using the *GraphPad Prism* protocol.[47] Given the higher error estimates associated with the determination of K_{21} by comparison with those for K_{11}, analogous van't Hoff plots characterising 2:1 host$_2$·dye systems were not constructed. A summary and discussion of the complexation constants and thermodynamic parameters for the complexation of CV^+, RB and EO^- by native β-CD, *E*-*p*-β-CD$_2$az and β-CDab are given in Section 3.2.1.2.1 – Section 3.2.1.2.3.

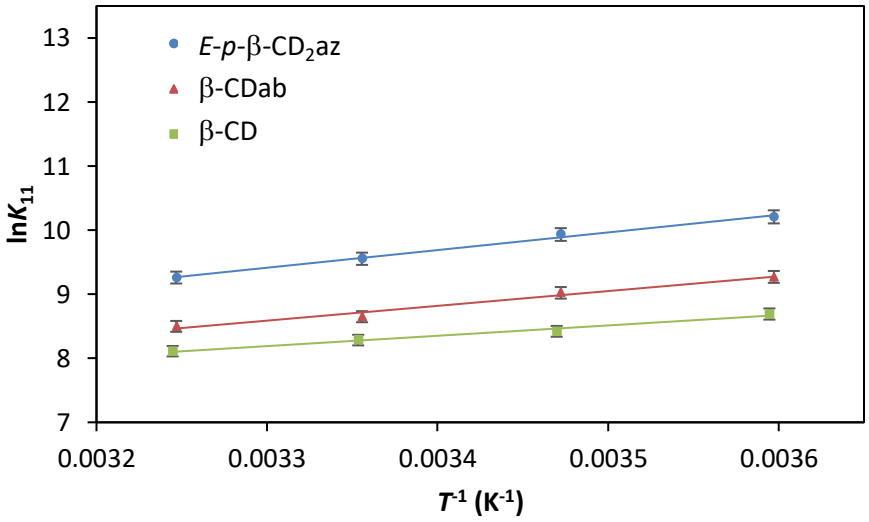

Figure 3.22: Plots of lnK_{11}, as determined by UV-vis spectroscopy at various temperatures, against T^{-1} for the β-CD·CV^+ complex (R^2 = 0.9982), the *E*-*p*-β-CD$_2$az·CV^+ complex (R^2 = 0.9974) and the β-CDab·CV^+ complex (R^2 = 0.9898). The icons represent the experimental data and the solid lines represent the best fit of the van't Hoff equation to the K_{11} data derived using the *GraphPad Prism* protocol.[47] The R^2 values refer to the fit of Equation 3.9 to the K_{11} data. The error bars represent the fitting errors.

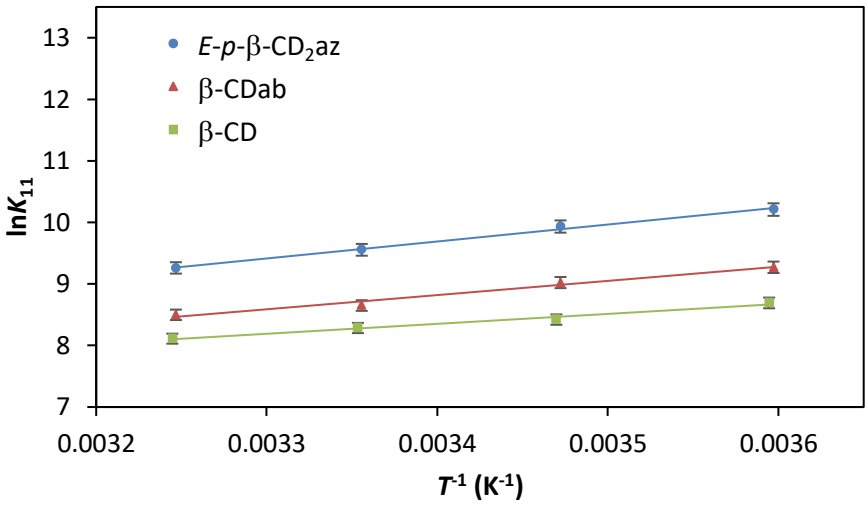

Figure 3.23: Plots of lnK_{11}, as determined by UV-vis spectroscopy at various temperatures, against T^{-1} for the β-CD·RB complex (R^2 = 0.9849), the *E*-*p*-β-CD_2az·RB complex (R^2 = 0.9937) and the β-CDab·RB complex (R^2 = 0.9809). The icons represent the experimental data and the solid lines represent the best fit of the van't Hoff equation to the K_{11} data derived using the *GraphPad Prism* protocol.[47] The R^2 values refer to the fit of Equation 3.9 to the K_{11} data. The error bars represent the fitting errors.

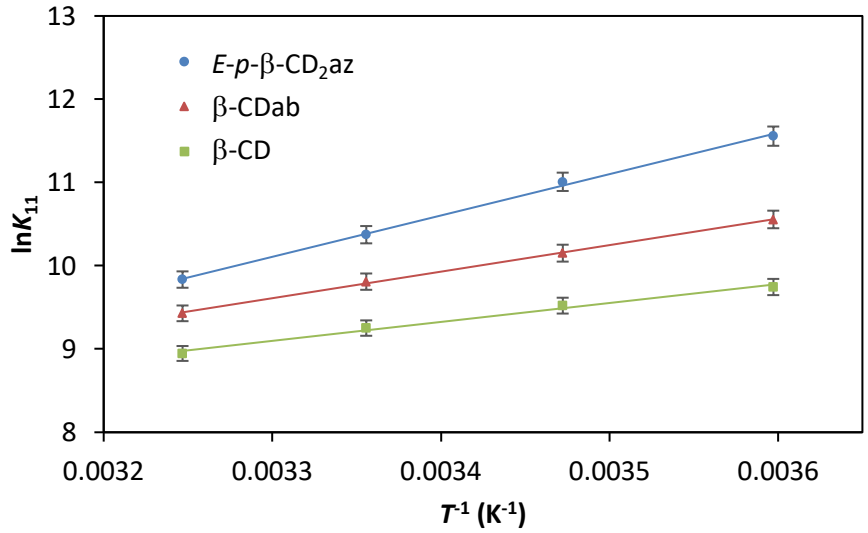

Figure 3.24: Plots of lnK_{11}, as determined by UV-vis spectroscopy at various temperatures, against T^{-1} for formation of the β-CD·EO^- complex (R^2 = 0.9902), the *E*-*p*-β-CD_2az·EO^- complex (R^2 = 0.9982 and the β-CDab·EO^- complex (R^2 = 0.9991). The icons represent the experimental data and the solid lines represent the best fit of the van't Hoff equation to the K_{11} data derived using the *GraphPad Prism* protocol.[47] The R^2 values refer to the fit of Equation 3.9 to the K_{11} data. The error bars represent the fitting errors.

3.2.1.2.1 Complexation of CV^+ by β-CD, *E*-*p*-β-CD_2az and β-CDab

The complexation constants and thermodynamic parameters for the complexation of CV^+ by native β-CD, *E*-*p*-β-CD_2az and β-CDab are presented in Table 3.4. The K_{11} derived for the complexation of CV^+ by *E*-*p*-β-CD_2az at 298.2K is approximately thirty-six times larger than the K_{11} derived for CV^+ complexation by native β-CD, consistent with cooperative ditopic complexation of CV^+ by both β-CD groups of *E*-*p*-β-CD_2az.[1,9] Such complexation is possible as CV^+ has three equivalent 4-(dimethylamino)phenyl groups, two of which may complex with two β-CD groups. The cooperative complexation is also consistent with the thermodynamic parameters, which shows the ΔH_{11} for the *E*-*p*-β-CD_2az·CV^+ complex to be six times more negative than the ΔH_{11} for the β-CD·CV^+ complex. The negative $T\Delta S_{11}$ for the *E*-*p*-β-CD_2az·CV^+ complex is consistent with the entropic gain arising from the expulsion of water molecules from the β-CD cavity upon complexation being greater than the entropic loss from the formation of a ditopic complex. There is, however, a slight uncertainty in the data for the *E*-*p*-β-CD_2az·CV^+ complex as up to 5% of *p*-βCD_2az may exist as the *Z* isomer. This is also the case for the complexation studies with RB and EO^-.

Table 3.4: Complexation constants and thermodynamic parameters for the complexation of CV^+ by native β-CD, *E*-*p*-β-CD_2az and β-CDab in aqueous phosphate buffer (pH 7.0 and I = 0.10 mol dm^{-3}) at varying temperatures.

Host	T (K)	10^{-3} K_{11}[a] (dm mol^{-1})	10^{-3} K_{21}[a] (dm mol^{-1})	ΔG_{11}[b] (kJ mol^{-1})	ΔH_{11}[c] (kJ mol^{-1})	$T\Delta S_{11}$[d] (kJ mol^{-1})
E-*p*-β-CD_2az	308.2	62.3 ± 0.3	9.04 ± 0.04	-28.3 ± 0.1	-65.7 ± 2.4	-37.2 ± 1.3
	298.2	171 ± 1	17.7 ± 0.1	-29.9 ± 0.1	-65.7± 2.4	-36.0 ± 1.3
	288.2	372 ± 1	20.9 ± 0.1	-30.7 ± 0.1	-65.7± 2.4	-34.7 ± 1.2
	278.2	1130 ± 10	23.2 ± 0.1	-32.2 ± 0.1	-65.7± 2.4	-33.5 ± 1.2
β-CDab	308.2	4.70 ± 0.01	-	-21.7 ± 0.1	-18.6 ± 1.3	3.08 ± 0.22
	298.2	6.20 ± 0.01	-	-21.6 ± 0.1	-18.6 ± 1.3	2.98 ± 0.21
	288.2	8.31 ± 0.01	-	-21.6 ± 0.1	-18.6 ± 1.3	2.88 ± 0.21
	278.2	10.2 ± 0.1	-	-21.3 ± 0.1	-18.6 ± 1.3	2.78 ± 0.20
β-CD[7]	308.2	4.07 ± 0.04	0.13 ± 0.01	-21.3 ± 0.1	-11.7 ± 0.6	9.6 ± 0.7
	298.2	4.68 ± 0.07	0.21 ± 0.02	-21.0 ± 0.1	-11.7 ± 0.6	9.3 ± 0.7
	288.2	5.62 ± 0.06	0.22 ± 0.02	-20.7 ± 0.1	-11.7 ± 0.6	9.0 ± 0.7
	278.2	6.61 ± 0.08	0.35 ± 0.03	-20.4 ± 0.1	-11.7 ± 0.6	8.7 ± 0.7

[a] Errors calculated from UV-vis titration data using *HypSpec* fitting program, and rounded up to the last significant figure. [b] Errors calculated using the errors of K_{11} and the equation $\Delta G_{11} = -RT\ln K_{11}$, and rounded up to the last significant figure. [c] Errors calculated from the van't Hoff plot using *GraphPad Prism* software.[47] [d] Errors calculated from the sum of the relative errors in ΔG_{11} and ΔH_{11} shown are those derived from vant' Hoff plots of $\ln K_{11}$ against $1/T$. The errors do not take into account experimental estimated to be ≤ 5% for K_{11}.and ≤ 10% for K_{21}.

In the β-CDab·CV^+ complex, only one of the 4-(dimethylamino)phenyl groups of CV^+ is complexed and is characterised by K_{11}. A similar situation prevails in the native β-CD·CV^+ complex and its K_{11} is similar to that for β-CDab·CV^+. In both cases, ΔH_{11} is much less than that for *E*-*p*-βCD_2az·CV^+ and $T\Delta S_{11}$ is positive whereas that for *E*-*p*-βCD_2az·CV^+ is substantially negative. The greater ΔH_{11} for *E*-*p*-β-CD_2az·CV^+ is anticipated for the ditopic complexation of CV^+ and consequent strong complexing interaction. As noted above, the strongly negative $T\Delta S_{11}$ for the *E*-*p*-β-CD_2az·CV^+ complex indicates that the entropic gain arising from the expulsion of water from the β-CD cavity upon complexation is greater than the entropic loss from the formation of a ditopic complex, whereas the positive $T\Delta S_{11}$ for the β-CD·CV^+ and β-CDab·CV^+ complexes indicates that the entropic gain arising from the expulsion of water from the β-CD cavity upon complexation in both cases offsets the entropic loss from the formation of a complex. The more negative ΔH_{11} and less positive $T\Delta S_{11}$ for β-CDab·CV^+, by comparison with those for β-CD·CV^+, may arise from additional stabilisation and a decreased entropy arising from stabilising interactions between the aminophenyl substituent of β-CDab and the non-complexed phenyl groups of CV^+ in β-CDab·CV^+. These interactions are absent in the β-CD·CV^+ complex, which is characterised by a less negative ΔH_{11} and a more positive $T\Delta S_{11}$.

Two 2:1 complexes characterised by K_{21} were also detected: (*E*-*p*-β-CD_2az)$_2$·CV^+ and β-CD_2·CV^+. The magnitudes of K_{21} for both complexes are significantly less than their respective K_{11} values. This decreased stability is expected as the probability of a favourable collision leading to reaction is decreased as two and one of the dimethylaminophenyl groups of CV^+ are already complexed in the *E*-*p*-β-CD_2az·CV^+ and β-CD·CV^+ precursor complexes, respectively. In (*E*-*p*-β-CD_2az)$_2$·CV^+, the second complexing *E*-*p*-β-CD_2az is monotopic, which might be expected to lessen the stability of its complex by comparison with that of the ditopic complexing of the first *E*-*p*-β-CD_2az.

The magnitude of the K_{21} for the *E*-*p*-β-CD_2az·CV^+ complex is 10% of the magnitude of the K_{11} at 298.2 K. Therefore, there is a larger proportion of the 2:1 complex in the *E*-*p*-β-CD_2az·CV^+ complex by comparison with the β-CD·CV^+ complex. This may arise due to the enhanced probability of collision for the *E*-*p*-β-CD_2az dimer and β-CD dimers generally by comparison with that of a β-CD monomer.

A K_{21} value could not be derived for the β-CDab system. The lack of K_{21} is likely due to the experimental conditions. In the case of the β-CD·CV^+ complex, the magnitude of the K_{21} value is only 4.4% of the K_{11} value at 298.2 K, indicating a negligible proportion of the 2:1 species. Therefore, the lack of K_{21} equilibrium in the β-CDab·CV^+ complex does not necessarily imply that no 2:1 complex forms, rather, similar to the β-CD/CV^+ system, the proportion of the 2:1 complex by comparison with the 1:1 complex may be negligible and not characterised under these experimental conditions.

3.2.1.2.2 Complexation of RB by β-CD, *E-p*-β-CD_2az and β-CDab

A summary of the complexation constants and thermodynamic parameters for the complexation of RB by native β-CD, *E-p*-β-CD_2az and β-CDab is given in Table 3.5.

Table 3.5: Complexation constants and thermodynamic parameters for the complexation of RB by native β-CD, *E-p*-β-CD_2az and β-CDab in aqueous phosphate buffer (pH 7.0 and I = 0.10 mol dm^{-3}) at varying temperatures.

Host	T (K)	10^{-3} K_{11}[a] ($dm\ mol^{-1}$)	10^{-3} K_{21}[a] ($dm\ mol^{-1}$)	ΔG_{11}[b] ($kJ\ mol^{-1}$)	ΔH_{11}[c] ($kJ\ mol^{-1}$)	$T\Delta S_{11}$[d] ($kJ\ mol^{-1}$)
E-p-β-CD_2az	308.2	10.5 ± 0.1	-	-23.7 ± 0.1	-22.9 ± 1.3	0.807 ± 0.045
	298.2	14.1 ± 0.1	-	-23.7 ± 0.1	-22.9 ± 1.3	0.780 ± 0.044
	288.2	20.6 ± 0.1	-	-23.8 ± 0.1	-22.9 ± 1.3	0.754 ± 0.042
	278.2	27.1 ± 0.1	-	-23.6 ± 0.1	-22.9 ± 1.3	0.728 ± 0.041
β-CDab	308.2	4.91 ± 0.01	-	-21.7 ± 0.1	-19.2 ± 1.9	2.47 ± 0.24
	298.2	5.71 ± 0.01	-	-21.6 ± 0.1	-19.2 ± 1.9	2.39 ± 0.24
	288.2	8.28 ± 0.01	-	-21.5 ± 0.1	-19.2 ± 1.9	2.31 ± 0.23
	278.2	10.6 ± 0.1	-	-21.4 ± 0.1	-19.2 ± 1.9	2.23 ± 0.22
β-CD[7]	308.2	3.33 ± 0.04	-	-20.8 ± 0.1	-13.5 ± 0.7	7.3 ± 0.6
	298.2	3.96 ± 0.06	-	-20.6 ± 0.1	-13.5 ± 0.7	7.1 ± 0.6
	288.2	4.54 ± 0.05	-	-20.3 ± 0.1	-13.5 ± 0.7	6.8 ± 0.6
	278.2	5.95 ± 0.08	-	-20.1 ± 0.1	-13.5 ± 0.7	6.6 ± 0.6

[a] Errors calculated from UV-vis titration data using *HypSpec* fitting program, and rounded up to the last significant figure. [b] Errors calculated using the errors of K_{11} and the equation $\Delta G_{11} = -RT\ln K_{11}$, and rounded up to the last significant figure. [c] Errors calculated from the van't Hoff plot using *GraphPad Prism* software.[47] [d] Errors calculated from the sum of the relative errors in ΔG_{11} and ΔH_{11} shown are those derived from vant' Hoff plots of $\ln K_{11}$ against $1/T$. The errors do not take into account experimental estimated to be ≤ 5% for K_{11}.

The K_{11} derived from the complexation of RB by *E-p*-β-CD_2az at 298.2 K is approximately 3.6 times larger than the complexation by native β-CD. This difference is smaller than the analogous CV^+ systems which indicates that *E-p*-β-CD_2az experiences diminished cooperative complexation with RB. The larger K_{11} may instead be due to the enhanced probability of a productive collision for the *E-p*-β-CD_2az dimer rather than for β-CD monomers. The diminished cooperative complexation of *E-p*-βCD_2az is also reflected in the thermodynamic parameters, which shows that the ΔH_{11} and $T\Delta S_{11}$ values at 298.2 K are more positive than the analogous values for the *E-p*-β-CD_2az·CV^+ complex. Additionally, the positive $T\Delta S_{11}$ for the *E-p*-β-CD_2az·RB complex indicates that the entropic gain arising from the expulsion of water molecules from the β-CD cavity upon complexation offsets the entropic loss from the formation of a complex.

The diminished cooperative complexation observed in the *E*-*p*-β-CD_2az·RB complex may be explained in terms of the RB structure. In principle, *E*-*p*-β-CD_2az may complex three possible sites of RB: the carboxyphenyl group and either of the two diethylamino groups. From the 2D ^{1}H ROESY NMR spectrum, only the diethylamino groups are suitable for complexation The complexation of one diethylamino group may cause a more localised positive charge on the adjacent diethylamino group, thereby diminishing the strength of a cooperative complex.

The rationalisation for the diminished cooperative complexation observed in the *E*-*p*-β-CD_2az·RB complex may also be applied to explain the absence of K_{21} equilibria in any of the systems. The localised positive charge on one diethylamino group as well as the carboxylate substituent on the carboxyphenyl group of RB do not facilitate the addition of a second host to an existing 1:1 complex. Therefore, although RB possesses three possible sites for complexation, only one diethylamino group is suitable.

The derived complexation and thermodynamic data of the β-CDab·RB and native β-CD·RB complexes are similar to those of the CV^+ systems. The magnitude of the K_{11} values are similar and both hosts complex monotopically to RB. Similar to the CV^+ systems, the ΔH_{11} and $T\Delta S_{11}$ of the β-CDab·RB complex are more negative than in the β-CD·RB complex. Once again, the aminophenyl substituent of β-CDab may display an attractive interaction with the non-complexed aromatic rings of RB, leading to favourable enthalpy change, yet correspondingly unfavourable entropy change. Therefore, the modification of native β-CD with an aminophenyl substituent does not significantly influence the stability of a complex, but may alter the thermodynamic controls, similar to the deductions made for the CV^+ studies.

3.2.1.2.3 Complexation of EO^- by β-CD, *E-p*-β-CD_2az and β-CDab

A summary of the complexation constants and thermodynamic parameters for the complexation of EO^- by native β-CD, *E-p*-β-CD_2az and β-CDab is given in Table 3.6.

Table 3.6: Complexation constants and thermodynamic parameters for the complexation of EO^- by native β-CD, *E-p*-β-CD_2az and β-CDab in aqueous phosphate buffer (pH 7.0 and I = 0.10 mol dm^{-3}) at varying temperatures.

Host	T (K)	10^{-3} K_{11}[a] (dm mol^{-1})	10^{-3} K_{21}[a] (dm mol^{-1})	ΔG_{11}[b] (kJ mol^{-1})	ΔH_{11}[c] (kJ mol^{-1})	$T\Delta S_{11}$[d] (kJ mol^{-1})
E-p-β-CD_2az	308.2	18.6 ± 0.1	-	-25.2 ± 0.1	-41.3 ± 1.3	-16.1 ± 0.5
	298.2	32.0 ± 0.1	-	-25.7 ± 0.1	-41.3 ± 1.3	-15.6 ± 0.5
	288.2	60.4 ± 0.1	-	-26.4 ± 0.1	-41.3 ± 1.3	-15.1 ± 0.5
	278.2	104 ± 1	-	-26.7 ± 0.1	-41.3 ± 1.3	-14.6 ± 0.4
β-CDab	308.2	12.4 ± 0.1	-	-24.1 ± 0.1	-26.5 ± 0.5	-2.37 ± 0.05
	298.2	18.2 ± 0.1	-	-24.3 ± 0.1	-26.5 ± 0.5	-2.29 ± 0.05
	288.2	25.6 ± 0.1	-	-24.3 ± 0.1	-26.5 ± 0.5	-2.22 ± 0.05
	278.2	38.4 ± 0.1	-	-24.4 ± 0.1	-26.5 ± 0.5	-2.14 ± 0.05
β-CD	308.2	7.68 ± 0.01	-	-22.9 ± 0.1	-18.9 ± 1.3	4.05 ± 0.28
	298.2	10.4 ± 0.1	-	-22.9 ± 0.1	-18.9 ± 1.3	3.92 ± 0.27
	288.2	13.6 ± 0.1	-	-22.8 ± 0.1	-18.9 ± 1.3	3.78 ± 0.26
	278.2	17.1 ± 0.1	-	-22.5 ± 0.1	-18.9 ± 1.3	3.65 ± 0.25

[a] Errors calculated from UV-vis titration data using *HypSpec* fitting program, and rounded up to the last significant figure. [b] Errors calculated using the errors of K_{11} and the equation $\Delta G_{11} = -RT\ln K_{11}$, and rounded up to the last significant figure. [c] Errors calculated from the van't Hoff plot using *GraphPad Prism* software.[47] [d] Errors calculated from the sum of the relative errors in ΔG_{11} and ΔH_{11} shown are those derived from vant' Hoff plots of $\ln K_{11}$ against $1/T$. The errors do not take into account experimental estimated to be ≤ 5% for K_{11} and ≤ 10% for K_{21}.

The complexation of EO^- by the three hosts follows a similar trend to the RB systems. The K_{11} of the *E-p*-β-CD_2az·EO^- complex is only 3.1 times larger than the K_{11} of the β-CD·EO^- complex at 298.2 K. As the ΔH_{11} of the *E-p*-β-CD_2az·EO^- complex is more than twice as negative as the ΔH_{11} for the β-CD·EO^- complex and the $T\Delta S_{11}$ is negative, some cooperative complexation may exist in the *E-p*-β-CD_2az·EO^- complex but is diminished by comparison with the *E-p*-β-CD_2az CV^+ complex. Therefore, the larger K_{11} value of the *E-p*-β-CD_2az·EO^- complex may also be substantially due to the greater probability of collision for a β-CD dimer.

The structure of EO^- may be responsible for the diminished cooperative complexation by comparison with that of tritopic CV^+ as it is a charged ditopic dye. A cooperative complex would force one of the β-CD groups of *E-p*-β-CD_2az to complex the alkyl end of EO^-, while the other complexes the charged sulfonate end of EO^-. As the latter is likely to be less favourable, cooperative complexation is diminished and the β-CD groups of *E-p*-β-CD_2az dominantly complex the alkyl end of EO^-, consistent with the 2D ^{1}H ROESY NMR data. The structure of EO^- may also account for the lack of K_{21} in any

system as the sulfonate end of EO^- is too hydrophilic for significant complexation of a second β-CD entity.

Interestingly, K_{11} for the *E*-*p*-β-CD_2az·EO^- complex is twice as large as the *E*-*p*-βCD_2az·RB complex at 298.2 K, while the ΔH_{11} value for the *E*-*p*-β-CD_2az·EO^- complex is negative and almost twice as large in magnitude as that for the complex *E*-*p*-β-CD_2az·RB. Therefore, while both systems experience diminished cooperative complexation, there are some interactions probably occurring in the *E*-*p*-β-CD_2az·EO^- complex that are absent in the *E*-*p*-β-CD_2az·RB complex. As both *E*-*p*-β-CD_2az and EO^- possess azobenzene groups, there may be some favourable π-π stacking interactions to increase the enthalpic stability. However, this may impart unfavourable steric interactions between the non-complexed β-CD group of *E*-*p*-β-CD_2az and the sulfonate end of EO^- and lead to the substantial negative $T\Delta S_{11}$ value.

The influence of the sulfonate group of EO^- may also extend to the β-CD·EO^- system. The 2D ^{1}H ROESY NMR spectrum showed NOE cross-peaks between the H1, H2, H4 and H6 resonances of EO^- and the H2 – H6 resonances of β-CD. While this could suggest that a 2:1 β-CD_2·EO^- complex is forming, the lack of any evidence found for a 2:1 complex in the UV-vis is consistent with a single β-CD host shuttling between the alkyl group and phenyl groups of EO^-. This may also explain the larger K_{11} for the β-CD·EO^- system by comparison with those for the β-CD·CV^+ or β-CD·RB complexes.

The complexation of β-CDab with EO^- shows a similar trend to the CV^+ and RB systems. The K_{11} for the β-CDab·EO^- complex is similar to that of the β-CD·EO^- complex, while the ΔH_{11} and $T\Delta S_{11}$ are both more negative. Therefore, the modification of β-CD with an aminophenyl substituent does not significantly alter the stability of a complex, however, extra attractive interactions between the aminophenyl substituent of β-CDab and the non-complexed aromatic rings of EO^- may facilitate different thermodynamic controls as discussed earlier. As the β-CDab·EO^- complex is characterised by a larger K_{11} and more negative ΔH_{11} than the those of the β-CDab·CV^+ and β-CDab·RB complexes, there may be more direct overlap between the aminophenyl subsituent of β-CDab and the non-complexed aromatic rings of EO^-, by comparison with similar interactions in the other two systems.

3.2.1.3 Enthalpy-entropy linear relationship

The thermodynamic parameters for each of the host-guest systems studied may be further compared to other CD-guest systems in the literature. This consideration is important due to the enthalpy-entropy compensation effect, which is a phenomenon expected in most CD·guest systems.[14-16,48] The enthalpy-entropy compensation effect is observed when a plot of the ΔH and $T\Delta S$ values for a series of CD-based host-guest complexes yields a linear relationship.

This compensatory relationship between enthalpy and entropy suggests that both thermodynamic terms are influenced by each other such that during the complexation of a guest by a CD host, a favourable enthalpy change is compensated for by an unfavourable entropy change, and *vice versa*.

There are multiple possible origins of this compensatory effect of either enthalpy or entropy. For example, the formation of a complex is enthalpically favoured due to the hydrophobic effect, where hydrophobic portions of the guest interact with the hydrophobic cavity of β-CD. However, this favourable enthalpy change is compensated by an unfavourable entropy change, which arises from the formation of a single complex from two species. Various other favourable and unfavourable thermodynamic factors occur during complexation and no single explanation can satisfactorily describe the enthalpy-entropy compensation effect.[4,16,49]

The relationship between the change in enthalpy and entropy is shown by Equation 3.15,

$$T\Delta S_{11} = \alpha\Delta H_{11} + T\Delta S_{11,0} \quad (3.15)$$

where $T\Delta S_{11}$ and ΔH_{11} are experimental data; α is the slope of a plot of $T\Delta S_{11}$ against ΔH_{11} and $T\Delta S_{11,0}$ and is obtained when $\Delta H_{11} = 0$ ($\Delta H_{11,0}$) at the zero intercept. The size of α indicates the extent to which changes in complex stability (proportional to ΔG_{11}) occur through enthalpic stabilisation, $\Delta\Delta H_{11}$, caused by variation of the identity of the host are cancelled through entropic loss, $\Delta\Delta S_{11}$, as shown in Equation 3.16,

$$\Delta G_{11} = (1 - \alpha)\Delta\Delta H_{11} \quad (3.16)$$

such that only $(1 - \alpha)$ of the enthalpic increase can add to the host-guest complex stabilisation. Thus, $T\Delta S_{11,0}$ is the inherent host-guest complex stability, $\Delta G_{11,0}$, when $\Delta H_{11} = 0$ ($\Delta H_{11,0}$). (It should be noted that Equation 3.16 does not represent a necessary relationship, but is one observed for a variety of equilibria involving CDs.)

The enthalpy-entropy linear relationship for 1:1 host·dye complexes of β-CD, *E*-*p*-β-CD_2az and β-CDab with CV^+, RB and EO^- is shown in Figure 3.25. The entropy and enthalpy of complexation for the systems in this study were also compared against literature values,[16] as shown in Figure 3.26.

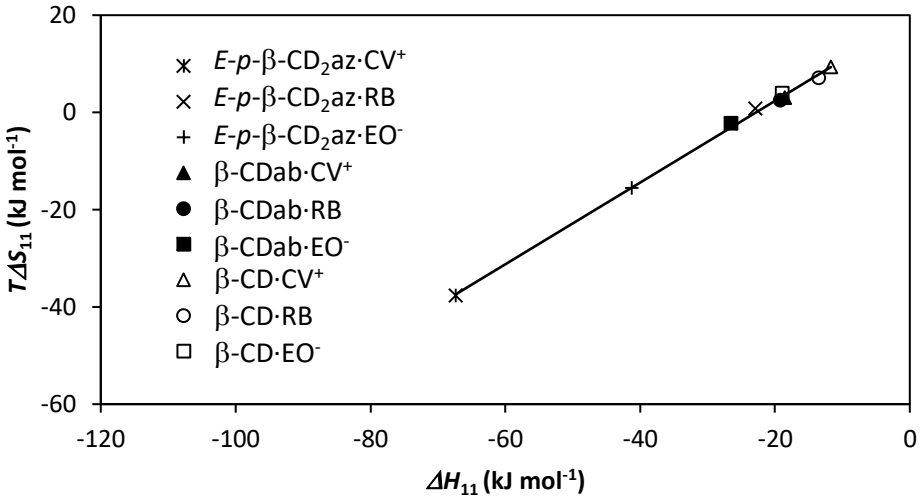

Figure 3.25: Linear relationship between ΔH_{11} and $T\Delta S_{11}$ for the 1:1 complexation of native β-CD, *E*-*p*-β-CD$_2$az and β-CDab with CV$^+$, RB and EO$^-$ in aqueous phosphate buffer (pH 7.0 and I = 0.10 mol dm^{-3}) at 298.2 K (R^2 = 0.9982). The icons represent the experimental data and the solid lines represent the best fit of Equations 3.15 to the thermodynamic parameters, derived using the *Graphpad Prism* protocol.[47]

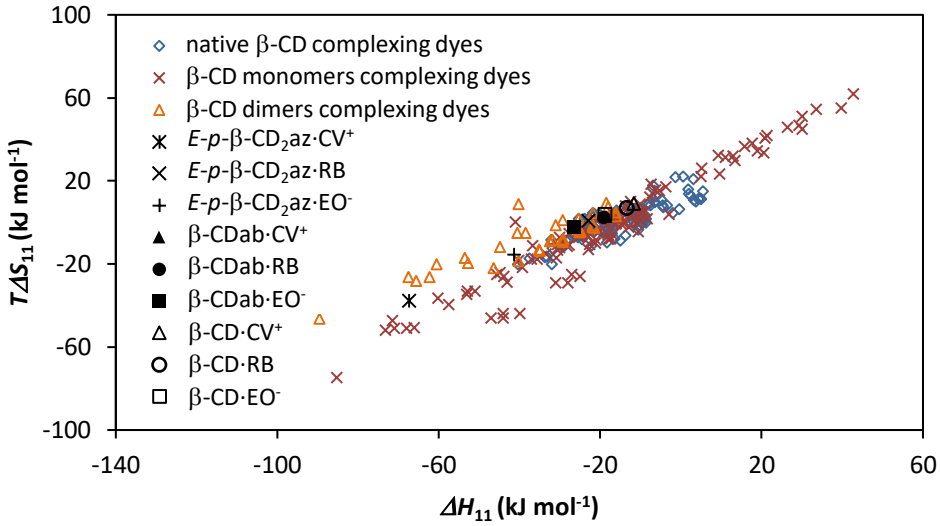

Figure 3.26: Linear relationship between ΔH_{11} and $T\Delta S_{11}$ for the 1:1 complexation of various dyes by native and modified β-CDs at 298 K obtained from the literature.[7,16,48]

The linear relationship between the ΔH_{11} and $T\Delta S_{11}$ for the 1:1 complexation of native β-CD, *E*-*p*-β-CD_2az and β-CDab with CV^+, RB and EO^- gives a $T\Delta S_0$ value of 20.5 kJ mol^{-1}, indicating that in the absence of any enthalpic change, the nine systems studied are entropically stabilised. This entropic stabilisation is likely to arise largely from the expulsion of water molecules from the β-CD cavity upon dye complexation.[14,50]

The α value for the nine systems studied is 0.84 a.u., indicating that approximately 84% of the $\Delta\Delta H_{11}$ is compensated by the $\Delta\Delta S_{11}$. This value is slightly greater than for β-CD alone, which has an α value of 0.8 a.u.[16] The similarity suggests that most of the thermodynamic parameters that govern the complexation of β-CD, *E*-*p*-β-CD_2az and β-CDab with CV^+, RB and EO^- may be explained dominantly by the properties of β-CD itself, and only a small fraction of the thermodynamic parameters are influenced by the modification of β-CD, the differences in the dyes or the experimental conditions. This is also evident in Figure 3.26, which shows that the ΔH_{11} and $T\Delta S_{11}$ values of the systems in this study are well within the range of the literature CD-guest systems.

3.3 Conclusion

The effect of β-CD modification on the host complexation properties of various β-CD compounds were determined. The complexation of native β-CD, *E*-*p*-β-CD_2az and β-CDab with CV^+, RB and EO^- was studied by 2D ^{1}H ROESY NMR spectroscopy and UV-vis spectroscopy. The complexation constants, K_{11} and K_{21} (where possible), and the thermodynamic parameters governing 1:1 complexation, ΔG_{11}, ΔH_{11} and ΔS_{11}, were derived for each system.

The 2D ^{1}H ROESY NMR data indicated that the hosts complex each guest at a similar position. However, the UV-vis studies indicated that the stoichiometry and strength of complexation were different for each system, which is a result of both β-CD modification and differences between the dyes. In general, the complexation of the dyes by β-CDab and β-CD were similar, indicating that the modification of β-CD with an aminophenyl group does little to affect the strength of a complex, although the thermodynamic controls may be influenced. The complexation of the dyes with *E*-*p*-β-CD_2az were generally stronger. The two β-CD groups of *E*-*p*-βCD_2az allowed for the cooperative complexation of the dyes. However, cooperative complexation was diminished with RB and EO^- due to the structure of the dyes.

The thermodynamic parameters governing complexation showed some differences. A larger K_{11} generally results in a more negative ΔH_{11}. However, the enthalpy-entropy linear relationship that is observed for the nine systems studied indicates that the thermodynamic parameters are determined largely by the properties of β-CD alone and that modification of β-CD with an aminophenyl substituent or the formation of an azobenzene-linked β-CD dimer plays a minor role.

This research contributes to the overall understanding of factors that influence β-CD and modified β-CD complexation properties. The results, when analysed within the larger scope of CD complexation studies, should help to inform the design of future CD systems.

3.4 References

(1) Liu, Y.; Chen, Y. *Acc. Chem. Res.* **2006**, *39*, 681.
(2) Breslow, R.; Halfon, S.; Zhang, B. L. *Tetrahedron* **1995**, *51*, 377.
(3) Breslow, R.; Greenspoon, N.; Guo, T.; Zarzycki, R. *J. Am. Chem. Soc.* **1989**, *111*, 8296.
(4) Cramer, F.; Saenger, W.; Spatz, H. C. *J. Am. Chem. Soc.* **1967**, *89*, 14.
(5) Eftink, M. R.; Andy, M. L.; Bystrom, K.; Perlmutter, H. D.; Kristol, D. S. *J. Am. Chem. Soc.* **1989**, *111*, 6765.
(6) Breslow, R.; Chung, S. *J. Am. Chem. Soc.* **1990**, *112*, 9659.
(7) Nguyen, H. T.; Pham, D. T.; Easton, C. J.; Lincoln, S. F. *Aust. J. Chem.* **2013**, *66*, 1057.
(8) Saudan, C.; Dunand, F. A.; Abou-Hamdan, A.; Bugnon, P.; Lye, P. G.; Lincoln, S. F.; Merbach, A. E. *J. Am. Chem. Soc.* **2001**, *123*, 10290.
(9) Haskard, C. A.; Easton, C. J.; May, B. L.; Lincoln, S. F. *J. Phys. Chem.* **1996**, *100*, 14457.
(10) Schiller, R. L.; Lincoln, S. F.; Coates, J. H. *J. Chem. Soc. Faraday Trans. I* **1987**, *83*, 3237.
(11) Schiller, R. L.; Coates, J. H.; Lincoln, S. F. *J. Chem. Soc. Faraday Trans. I* **1984**, *80*, 1257.
(12) Hocquelet, C.; Jankowski, C. K.; Pelletier, A. L.; Tabet, J.-C.; Lamouroux, C.; Berthault, P. *J. Inclusion Phenom. Macrocyclic Chem.* **2011**, *69*, 75.
(13) Connors, K. A. *Chem. Rev.* **1997**, *97*, 1325.
(14) Inoue, Y.; Hakushi, T.; Liu, Y.; Tong, L. H.; Shen, B. J.; Jin, D. S. *J. Am. Chem. Soc.* **1993**, *115*, 475.
(15) Inoue, Y.; Liu, Y.; Tong, L. H.; Shen, B. J.; Jin, D. S. *J. Am. Chem. Soc.* **1993**, *115*, 10637.
(16) Rekharsky, M. V.; Inoue, Y. *Chem. Rev.* **1998**, *98*, 1875.
(17) Stilbs, R. R. J. C. P. *J. Inclusion Phenom.* **1983**, *1*, 159.
(18) Duxbury, D. F. *Chem. Rev.* **1993**, *93*, 381.
(19) Angeloni, L.; Smulevich, G.; Marzocchi, M. P. *J. Mol. Struct.* **1980**, *61*, 331.
(20) Lueck, H. B.; McHale, J. L.; Edwards, W. D. *J. Am. Chem. Soc.* **1992**, *114*, 2342.
(21) Lewis, G. N.; Magel, T. T.; Lipkin, D. *J. Am. Chem. Soc.* **1942**, *64*, 1774.
(22) Maruyama, Y.; Ishikawa, M.; Satozono, H. *J. Am. Chem. Soc.* **1996**, *118*, 6257.
(23) Gomesdem.Ah; Macgilla.Ch; Eriks, K. *Acta Crystallogr.* **1965**, *18*, 437.
(24) Garcia-Rio, L.; Godoy, A.; Leis, J. R. *Chem. Phys. Lett.* **2005**, *401*, 302.
(25) Gal, M. E.; Kelly, G. R.; Kurucsev, T. *J. Chem. Soc., Perkin Trans. 2* **1973**, 395.
(26) Hinckley, D. A.; Seybold, P. G.; Borris, D. P. *Spectrochim. Acta Mol. Biomol. Spectrosc.* **1986**, *42*, 747.
(27) Merino, E. *Chem. Soc. Rev.* **2011**, *40*, 3835.
(28) Ding, Z. F.; Reymond, F.; Baumgartner, P.; Fermin, D. J.; Brevet, P. F.; Carrupt, P. A.; Girault, H. H. *Electrochim. Acta* **1998**, *44*, 3.
(29) Fujita, K.; Ejima, S.; Imoto, T. *J. Chem. Soc., Chem. Commun.* **1984**, 1277.
(30) Connors, K. A.; Mulski, M. J.; Paulson, A. *J. Org. Chem.* **1992**, *57*, 1794.
(31) Clarke, R. J.; Coates, J. H.; Lincoln, S. F. *Carbohydr. Res.* **1984**, *127*, 181.
(32) Harata, K. *Bull. Chem. Soc. Jpn.* **1976**, *49*, 1493.
(33) Tawarah, K. M.; Abushamleh, H. M. *J. Inclusion Phenom. Mol. Recognit. Chem.* **1991**, *11*, 29.
(34) de Oliveira, H. P.; Oliveira, E. G. L.; de Melo, C. P. *J. Colloid Interface Sci.* **2006**, *303*, 444.
(35) Devijlder, M. *J. Chem. Soc. Faraday Trans. I* **1981**, *77*, 129.
(36) Stork, W. H. J.; Lippits, G. J. M.; Mandel, M. *J. Phys. Chem.* **1972**, *76*, 1772.
(37) Chambers, R. W.; Kajiwara, T.; Kearns, D. R. *J. Phys. Chem.* **1974**, *78*, 380.
(38) Suzuki, K.; Tsuchiya, M. *Bull. Chem. Soc. Jpn.* **1971**, *44*, 967.
(39) Lincoln, S. F.; Coates, J. H.; Schiller, R. L. *J. Inclusion Phenom.* **1987**, *5*, 709.
(40) Karukstis, K. K.; Perelman, L. A.; Wong, W. K. *Langmuir* **2002**, *18*, 10363.
(41) Schneider, H. J.; Hacket, F.; Rudiger, V.; Ikeda, H. *Chem. Rev.* **1998**, *98*, 1755.
(42) Harada, T.; Pham, D. T.; Leung, M. H. M.; Huy, T. N.; Lincoln, S. F.; Easton, C. J.; Kee, T. W. *J. Phys. Chem. B* **2011**, *115*, 1268.

(43) Wang, J.; Duc-Truc, P.; Kee, T. W.; Clafton, S. N.; Guo, X.; Clements, P.; Lincoln, S. F.; Prud'homme, R. K.; Easton, C. J. *Macromolecules* **2011**, *44*, 9782.
(44) Thordarson, P. *Chem. Soc. Rev.* **2011**, *40*, 1305.
(45) Gans, P.; Sabatini, A.; Vacca, A. *Talanta* **1996**, *43*, 1739.
(46) Alderighi, L.; Gans, P.; Ienco, A.; Peters, D.; Sabatini, A.; Vacca, A. *Coord. Chem. Rev.* **1999**, *184*, 311.
(47) Motulsky, H. J.; Christopoulos, A. *Fitting models to biological data using linear and nonlinear regression: A practical guide to curve fitting*; GraphPad Prism Software Inc., San Diego, CA, **2003**.
(48) Zhang, B. L.; Breslow, R. *J. Am. Chem. Soc.* **1993**, *115*, 9353.
(49) Liu, L.; Guo, Q. X. *J. Inclusion Phenom. Macrocyclic Chem.* **2002**, *42*, 1.
(50) Liu, Y.; Han, B. H.; Li, B.; Zhang, Y. M.; Zhao, P.; Chen, Y. T.; Wada, T.; Inoue, Y. *J. Org. Chem.* **1998**, *63*, 1444.

3.5 Appendix

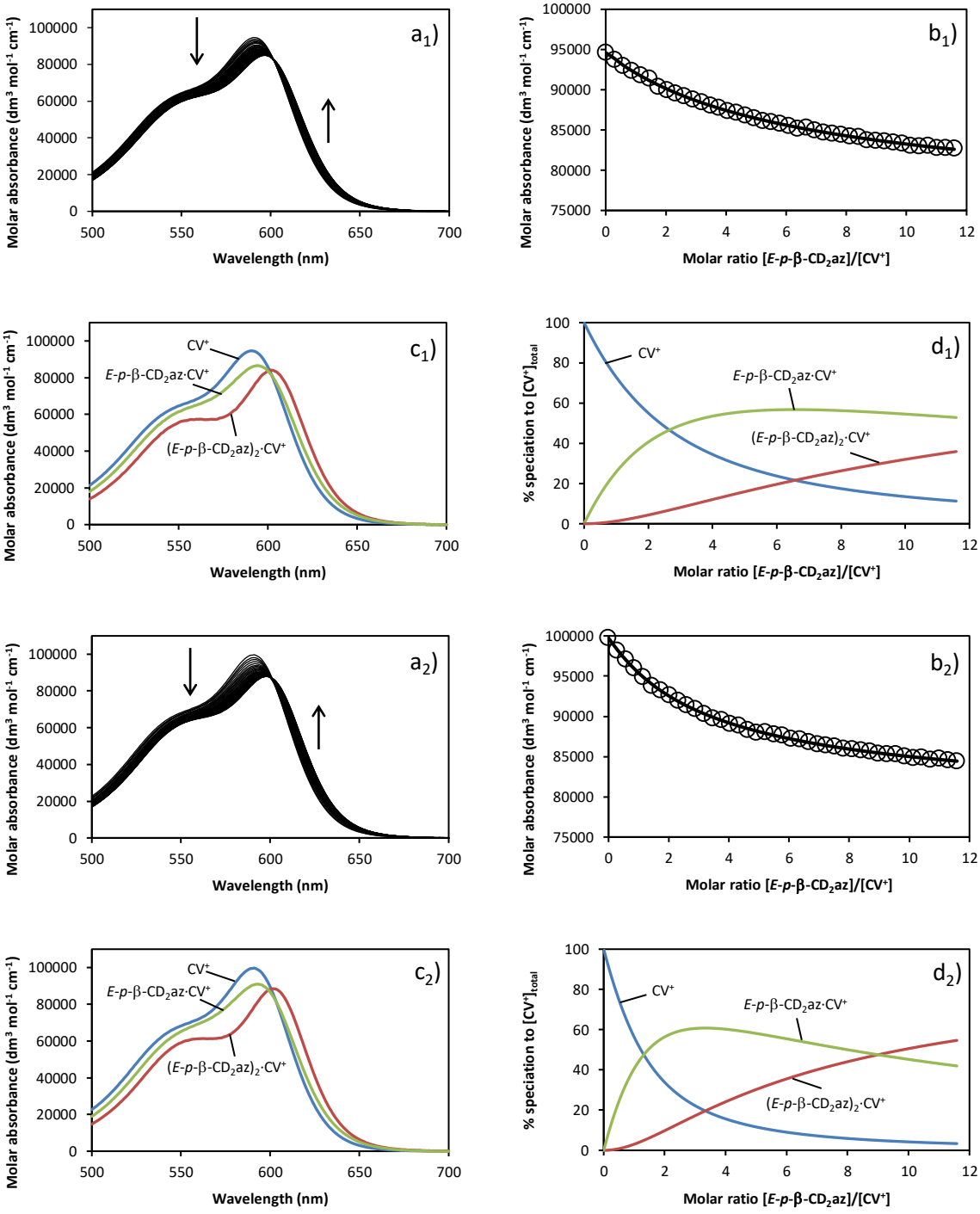

Figure 3.27: UV-vis absorbance data of CV^+ (initial concentration 8.0×10^{-6} mol dm^{-3}) with increasing concentrations of *E*-*p*-β-CD_2az (0 – 9.1×10^{-5} mol dm^{-3}) in aqueous phosphate buffer (pH 7.0 and I = 0.10 mol dm^{-3}) showing a) the molar absorption spectrum, the arrows indicating the direction of change, b) the experimental (circles) and best fit (line) molar absorbances at 591 nm (fitted at 1 nm intervals over the range 550 – 620 nm) for 1:1 and 2:1 complexes, c) the calculated molar absorbances, and d) the calculated speciation of free and complexed CV^+. The concentration of *E*-*p*-β-CD_2az was 0.93 mmol dm^{-3}, titrating with 5 mm^3 aliquots to a 2 cm^3 solution of CV^+ in a 1 cm path length cell. Note: a_1-d_1 and a_2-d_2 refer to 308.2 K and 298.2 K, respectively.

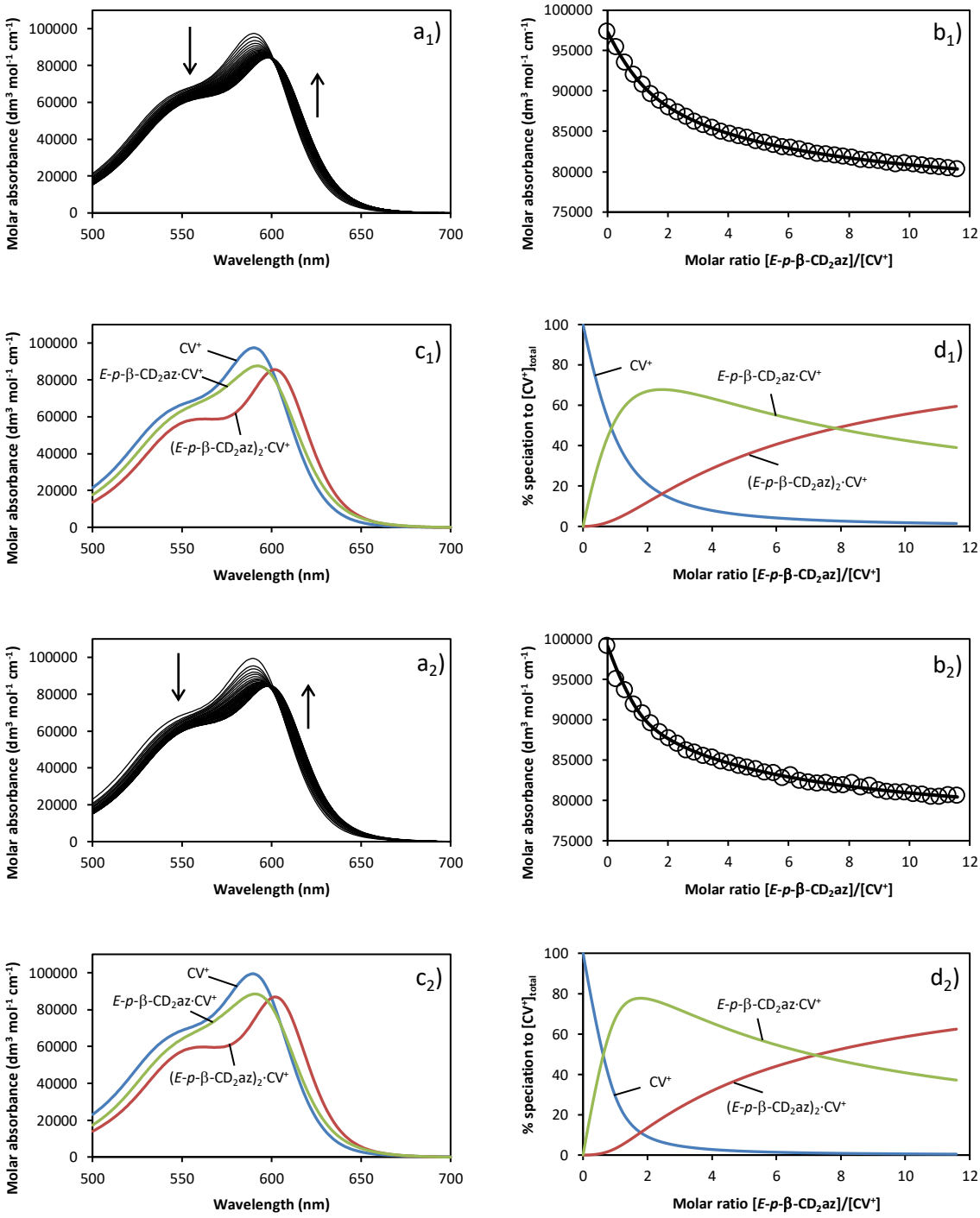

Figure 3.28: UV-vis absorbance data of CV^+ (initial concentration 8.0×10^{-6} mol dm^{-3}) with increasing concentrations of *E*-*p*-β-CD_2az (0 – 9.1×10^{-5} mol dm^{-3}) in aqueous phosphate buffer (pH 7.0 and I = 0.10 mol dm^{-3}) showing a) the molar absorption spectrum, the arrows indicating the direction of change, b) the experimental (circles) and best fit (line) molar absorbances at 591 nm (fitted at 1 nm intervals over the range 550 – 620 nm) for 1:1 and 2:1 complexes, c) the calculated molar absorbances, and d) the calculated speciation of free and complexed CV^+. The concentration of *E*-*p*-β-CD_2az was 0.93 mmol dm^{-3}, titrating with 5 mm^3 aliquots to a 2 cm^3 solution of CV^+ in a 1 cm path length cell. Note: a_1-d_1 and a_2-d_2 refer to 288.2 K and 278.2 K, respectively.

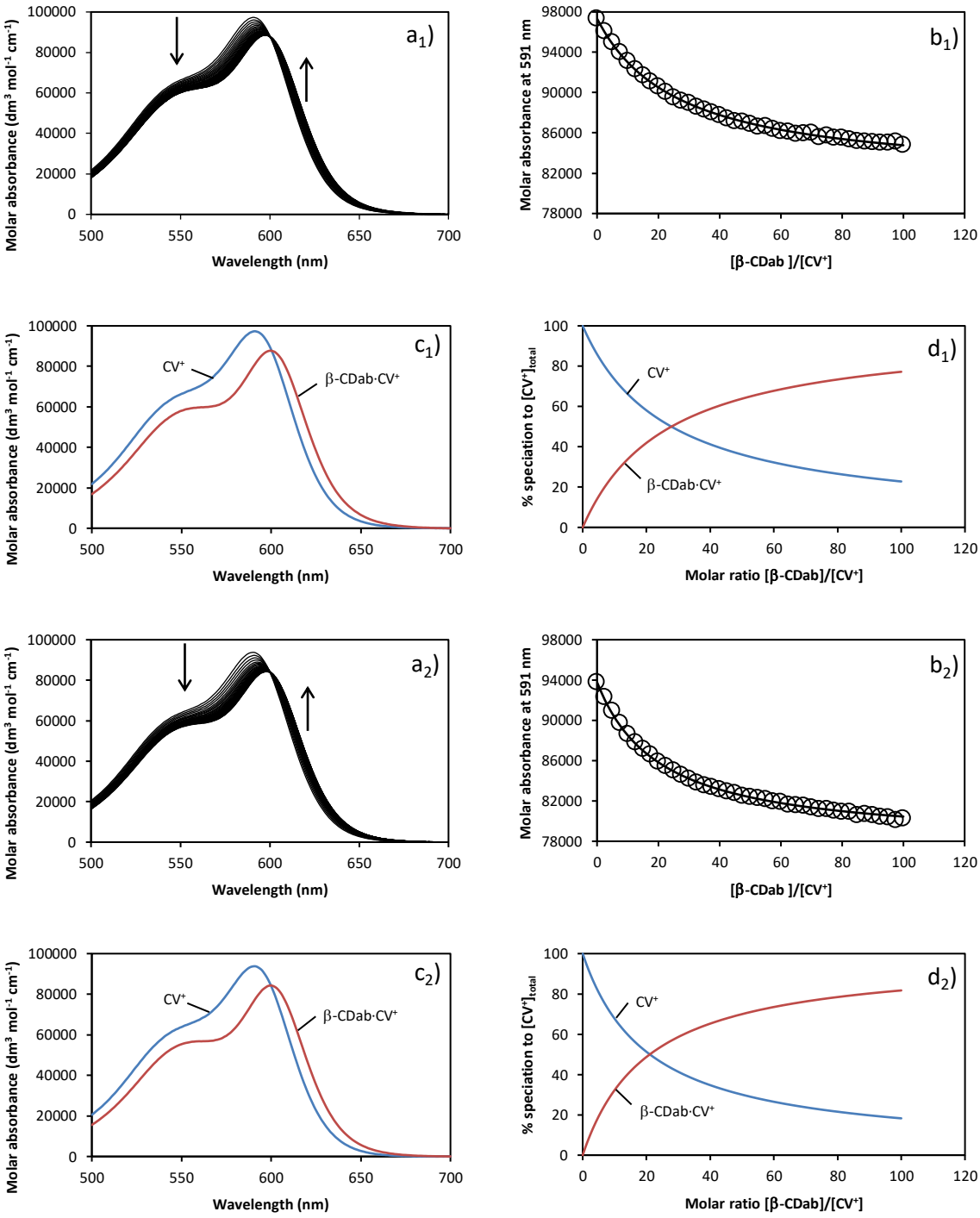

Figure 3.29: UV-vis absorbance data of CV^+ (initial concentration 8.0×10^{-6} mol dm^{-3}) with increasing concentrations of β-CDab (0 – 7.3×10^{-4} mol dm^{-3}) in aqueous phosphate buffer (pH 7.0 and I = 0.10 mol dm^{-3}) showing a) the molar absorption spectrum, the arrows indicating the direction of change, b) the experimental (circles) and best fit (line) molar absorbances at 591 nm (fitted at 1 nm intervals over the range 550 – 620 nm) for a 1:1 complex, c) the calculated molar absorbances, and d) the calculated speciation of free and complexed CV^+. The concentration of β-CDab was 0.008 mol dm^{-3}, titrating with 5 mm^3 aliquots to a 2 cm^3 solution of CV^+ in a 1 cm path length cell. Note: a_1-d_1 and a_2-d_2 refer to 308.2 K and 298.2 K, respectively.

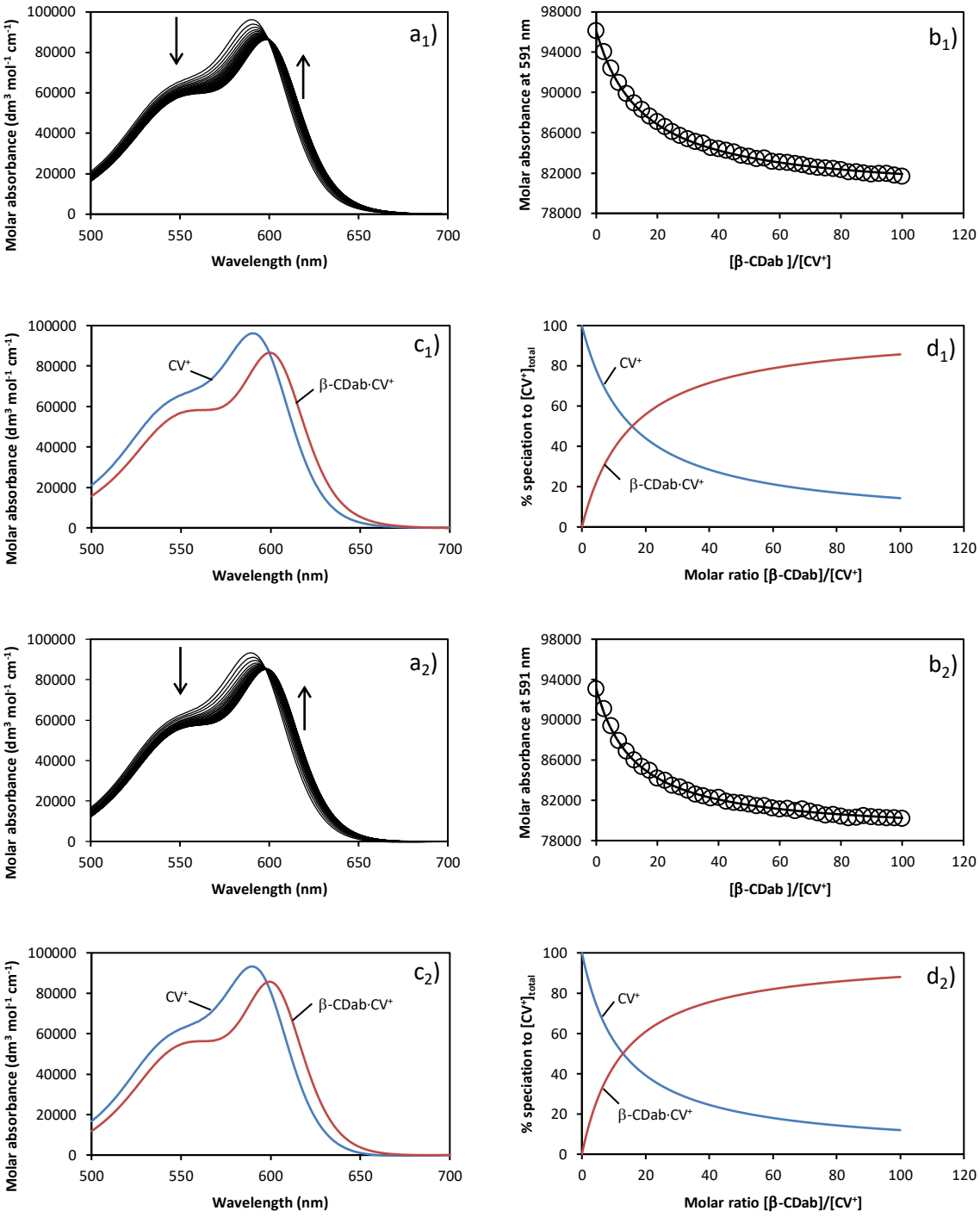

Figure 3.30: UV-vis absorbance data of CV^+ (initial concentration 8.0×10^{-6} mol dm^{-3}) with increasing concentrations of β-CDab ($0 - 7.3 \times 10^{-4}$ mol dm^{-3}) in aqueous phosphate buffer (pH 7.0 and I = 0.10 mol dm^{-3}) showing a) the molar absorption spectrum, the arrows indicating the direction of change, b) the experimental (circles) and best fit (line) molar absorbances at 591 nm (fitted at 1 nm intervals over the range 550 – 620 nm) for a 1:1 complex, c) the calculated molar absorbances, and d) the calculated speciation of free and complexed CV^+. The concentration of β-CDab was 0.008 mol dm^{-3}, titrating with 5 mm^3 aliquots to a 2 cm^3 solution of CV^+ in a 1 cm path length cell. Note: a_1-d_1 and a_2-d_2 refer to 288.2 K and 278.2 K, respectively.

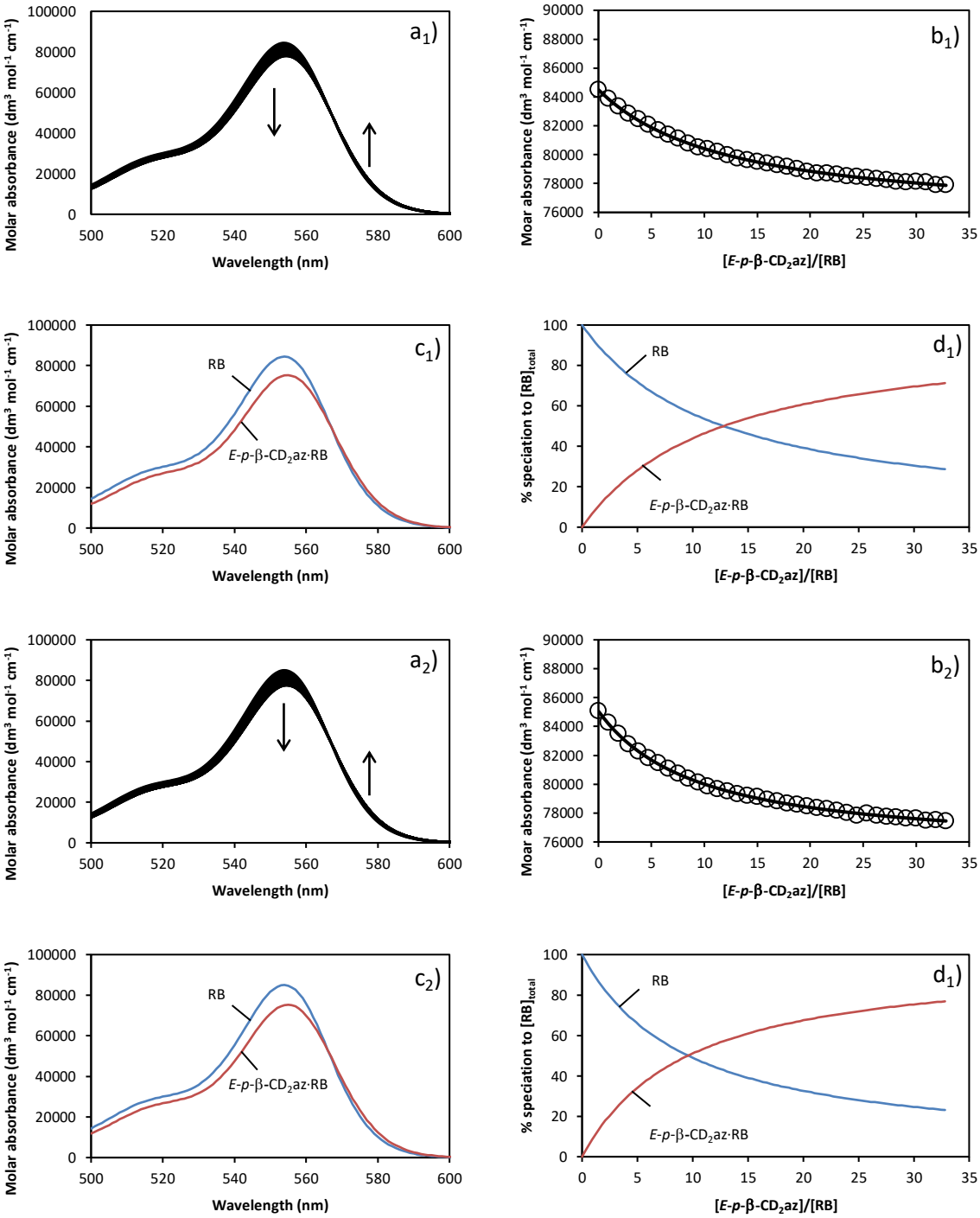

Figure 3.31: UV-vis absorbance data of RB (initial concentration 8.0×10^{-6} mol dm^{-3}) with increasing concentrations of *E*-*p*-β-CD_2az ($0 - 2.4 \times 10^{-4}$ mol dm^{-3}) in aqueous phosphate buffer (pH 7.0 and I = 0.10 mol dm^{-3}) showing a) the molar absorption spectrum, the arrows indicating the direction of change, b) the experimental (circles) and best fit (line) molar absorbances at 554 nm (fitted at 1 nm intervals over the range 520 – 570 nm) for a 1:1 complex, c) the calculated molar absorbances, and d) the calculated speciation of free and complexed RB. The concentration of *E*-*p*-β-CD_2az was 0.003 mol dm^{-3}, titrating with 5 mm^3 aliquots to a 2 cm^3 solution of RB in a 1 cm path length cell. Note: a_1-d_1 and a_2-d_2 refer to 308.2 K and 298.2 K, respectively.

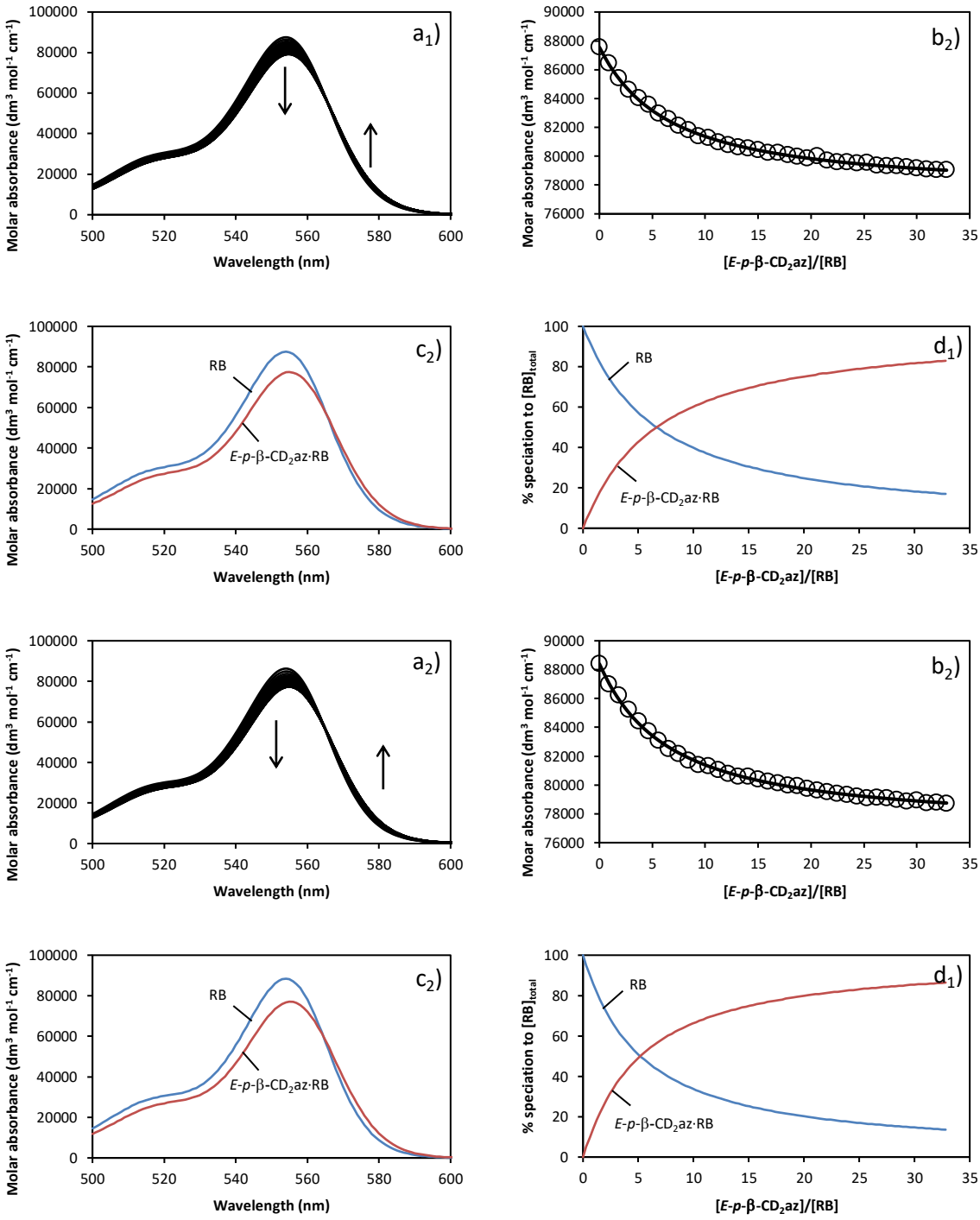

Figure 3.32: UV-vis absorbance data of RB (initial concentration 8.0×10^{-6} mol dm^{-3}) with increasing concentrations of *E*-*p*-β-CD_2az (0 – 2.4×10^{-4} mol dm^{-3}) in aqueous phosphate buffer (pH 7.0 and I = 0.10 mol dm^{-3}) showing a) the molar absorption spectrum, the arrows indicating the direction of change, b) the experimental (circles) and best fit (line) molar absorbances at 554 nm (fitted at 1 nm intervals over the range 520 – 570 nm) for a 1:1 complex, c) the calculated molar absorbances, and d) the calculated speciation of free and complexed RB. The concentration of *E*-*p*-β-CD_2az was 0.003 mol dm^{-3}, titrating with 5 mm^3 aliquots to a 2 cm^3 solution of RB in a 1 cm path length cell. Note: a_1-d_1 and a_2-d_2 refer to 288.2 K and 278.2 K, respectively.

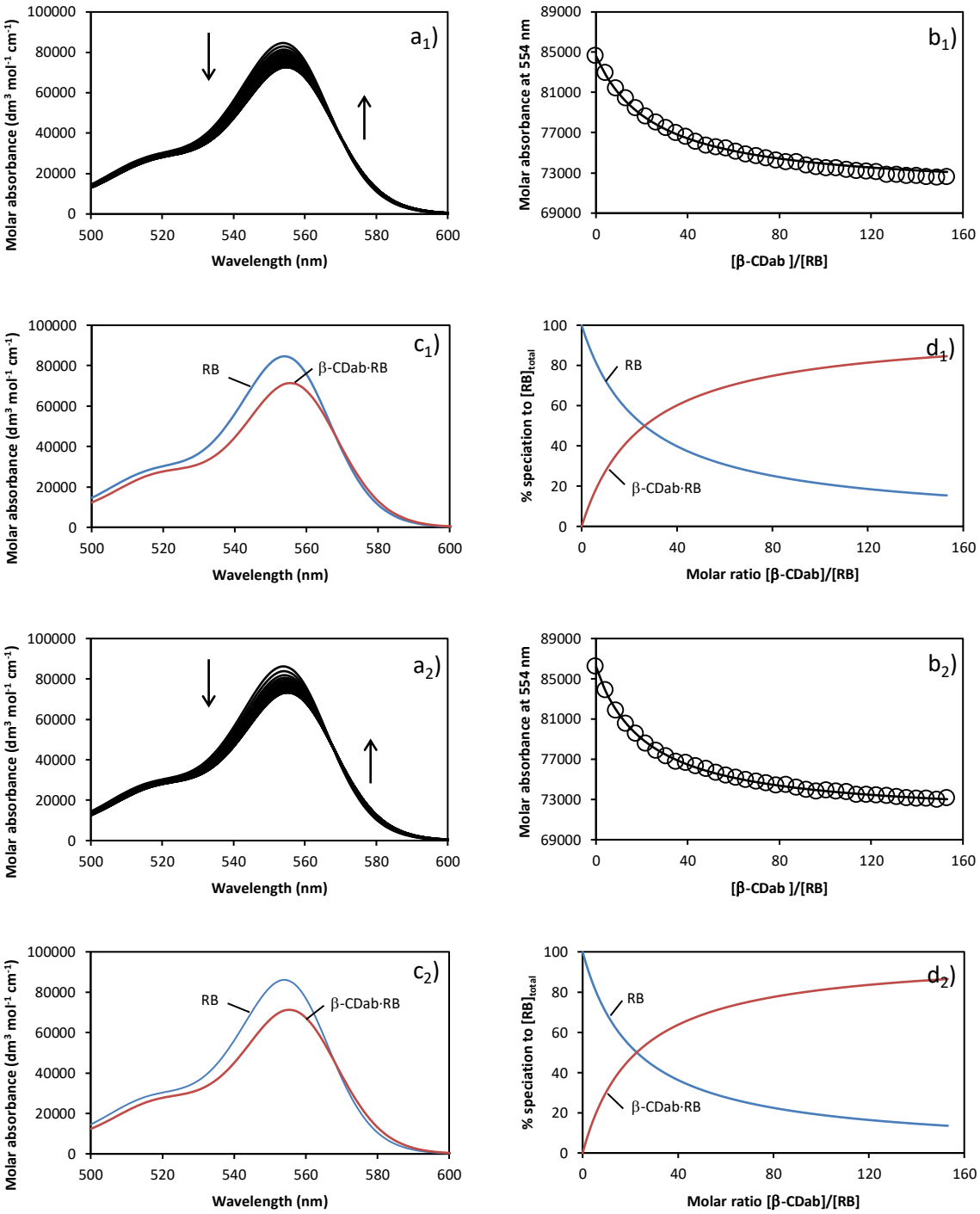

Figure 3.33: UV-vis absorbance data of RB (initial concentration 8.0×10^{-6} mol dm^{-3}) with increasing concentrations of β-CDab ($0 – 1.1 \times 10^{-3}$ mol dm^{-3}) in aqueous phosphate buffer (pH 7.0 and I = 0.10 mol dm^{-3}) showing a) the molar absorption spectrum, the arrows indicating the direction of change, b) the experimental (circles) and best fit (line) molar absorbances at 554 nm (fitted at 1 nm intervals over the range 520 – 570 nm) for a 1:1 complex, c) the calculated molar absorbances, and d) the calculated speciation of free and complexed RB. The concentration of β-CDab was 0.014 mol dm^{-3}, titrating with 5 mm^3 aliquots to a 2 cm^3 solution of RB in a 1 cm path length cell. Note: a_1-d_1 and a_2-d_2 refer to 308.2 K and 298.2 K, respectively.

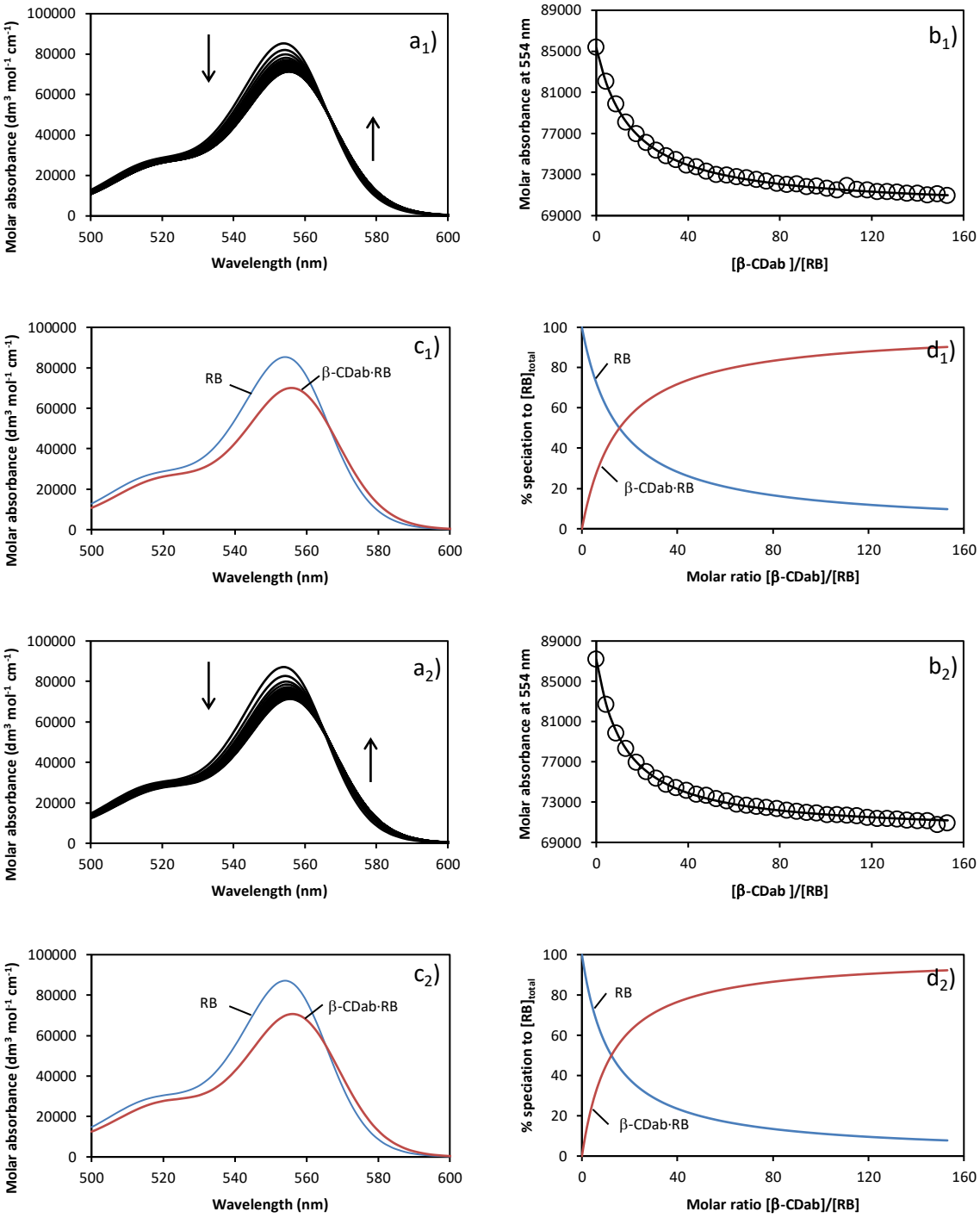

Figure 3.34: UV-vis absorbance data of RB (initial concentration 8.0×10^{-6} mol dm^{-3}) with increasing concentrations of β-CDab ($0 - 1.1 \times 10^{-3}$ mol dm^{-3}) in aqueous phosphate buffer (pH 7.0 and I = 0.10 mol dm^{-3}) showing a) the molar absorption spectrum, the arrows indicating the direction of change, b) the experimental (circles) and best fit (line) molar absorbances at 554 nm (fitted at 1 nm intervals over the range 520 – 570 nm) for a 1:1 complex, c) the calculated molar absorbances, and d) the calculated speciation of free and complexed RB. The concentration of β-CDab was 0.014 mol dm^{-3}, titrating with 5 mm^3 aliquots to a 2 cm^3 solution of RB in a 1 cm path length cell. Note: a_1-d_1 and a_2-d_2 refer to 288.2 K and 278.2 K, respectively.

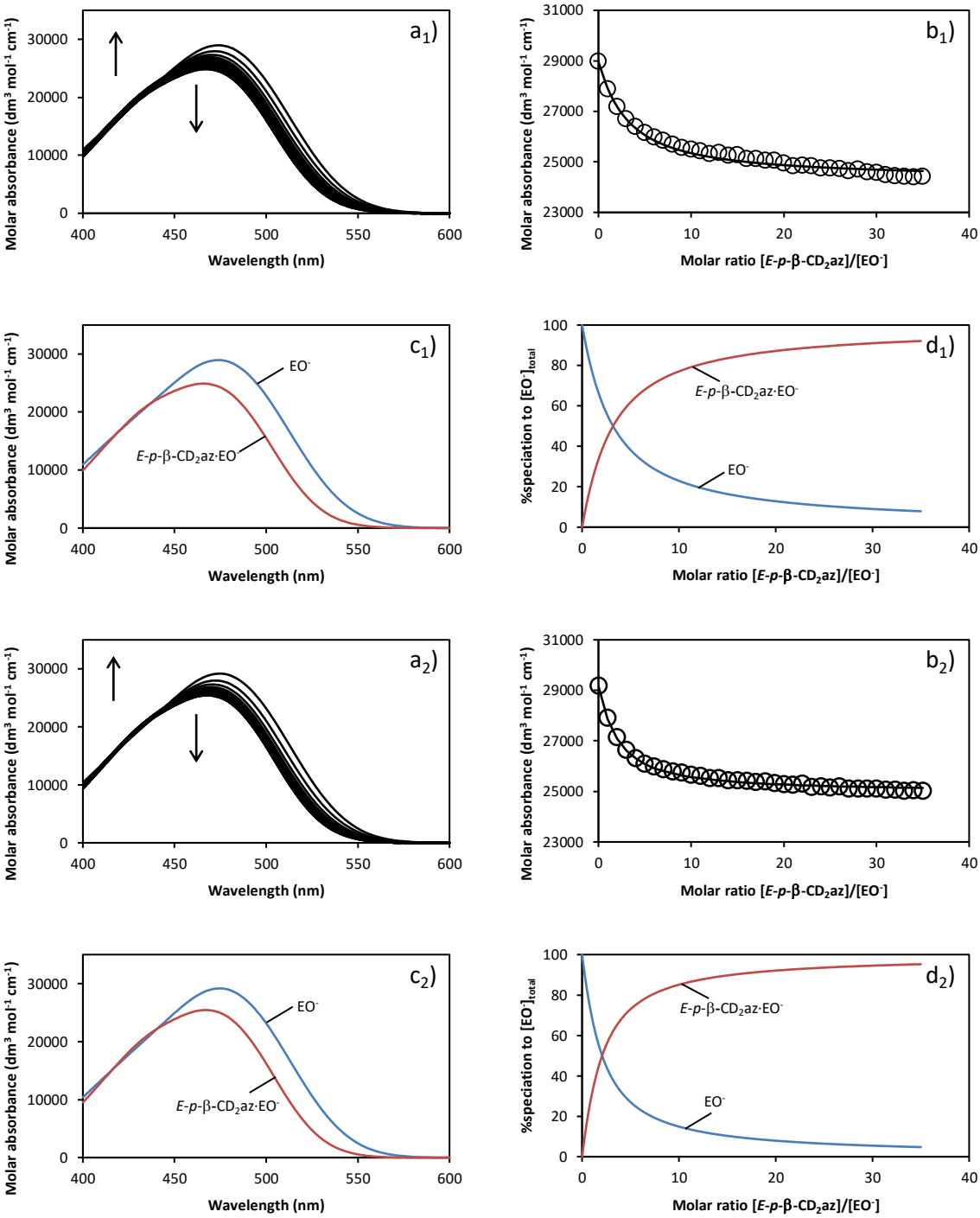

Figure 3.35: UV-vis absorbance data of EO^- (initial concentration 2.0×10^{-5} mol dm^{-3}) with increasing concentrations of *E*-*p*-β-CD_2az ($0 - 6.4 \times 10^{-4}$ mol dm^{-3}) in aqueous phosphate buffer (pH 7.0 and I = 0.10 mol dm^{-3}) showing a) the molar absorption spectrum, the arrows indicating the direction of change, b) the experimental (circles) and best fit (line) molar absorbances at 474 nm (fitted at 1 nm intervals over the range 425 – 520 nm) for a 1:1 complex, c) the calculated molar absorbances, and d) the calculated speciation of free and complexed EO^-. The concentration of *E*-*p*-β-CD_2az was 0.008 mol dm^{-3}, titrating with 5 mm^3 aliquots to a 2 cm^3 solution of EO^- in a 1 cm path length cell. Note: a_1-d_1 and a_2-d_2 refer to 308.2 K and 298.2 K, respectively.

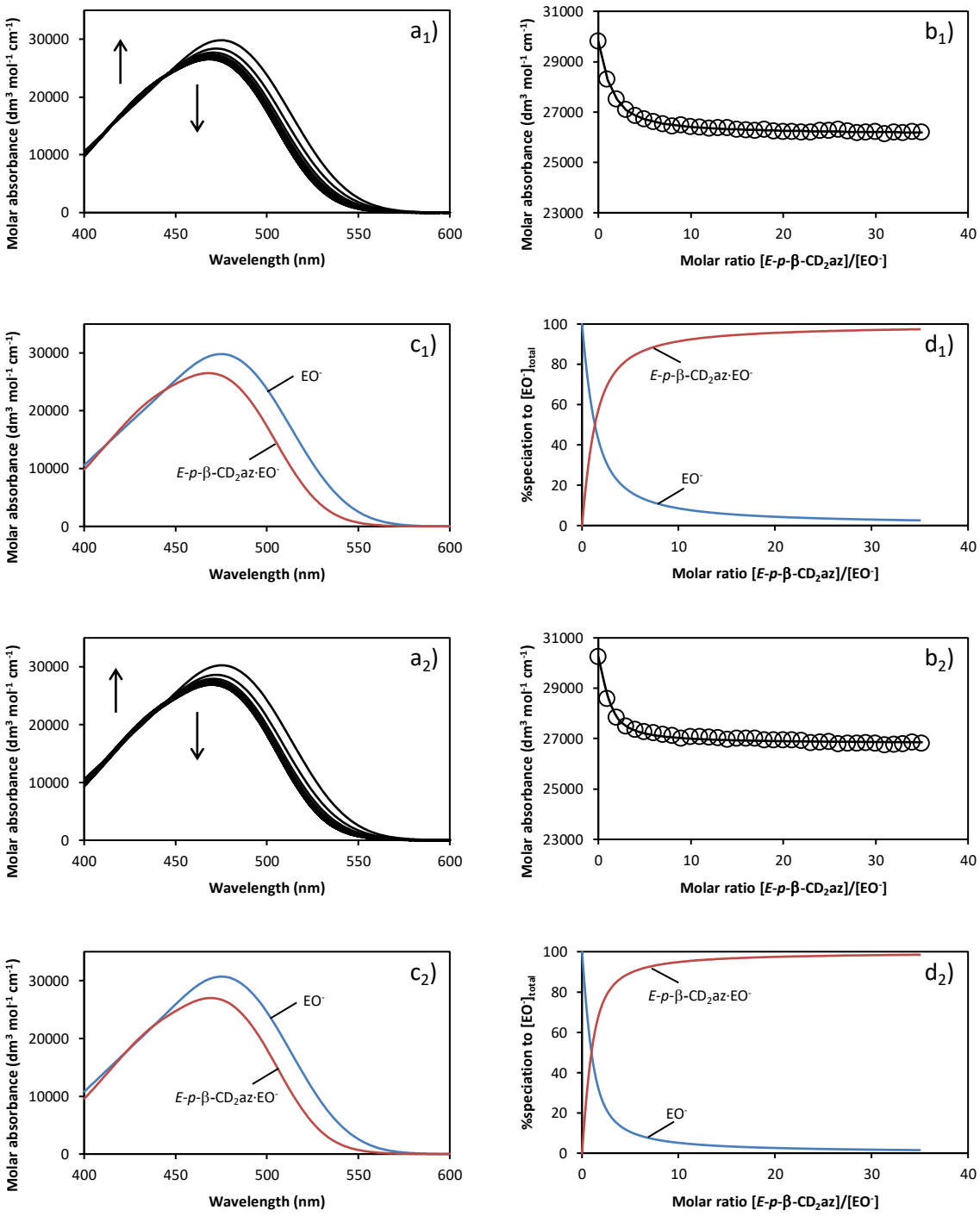

Figure 3.36: UV-vis absorbance data of EO^- (initial concentration 2.0×10^{-5} mol dm^{-3}) with increasing concentrations of *E-p*-β-CD_2az ($0 - 6.4 \times 10^{-4}$ mol dm^{-3}) in aqueous phosphate buffer (pH 7.0 and I = 0.10 mol dm^{-3}) showing a) the molar absorption spectrum, the arrows indicating the direction of change, b) the experimental (circles) and best fit (line) molar absorbances at 474 nm (fitted at 1 nm intervals over the range 425 – 520 nm) for a 1:1 complex, c) the calculated molar absorbances, and d) the calculated speciation of free and complexed EO^-. The concentration of *E-p*-β-CD_2az was 0.008 mol dm^{-3}, titrating with 5 mm^3 aliquots to a 2 cm^3 solution of EO^- in a 1 cm path length cell. Note: a_1-d_1 and a_2-d_2 refer to 288.2 K and 278.2 K, respectively.

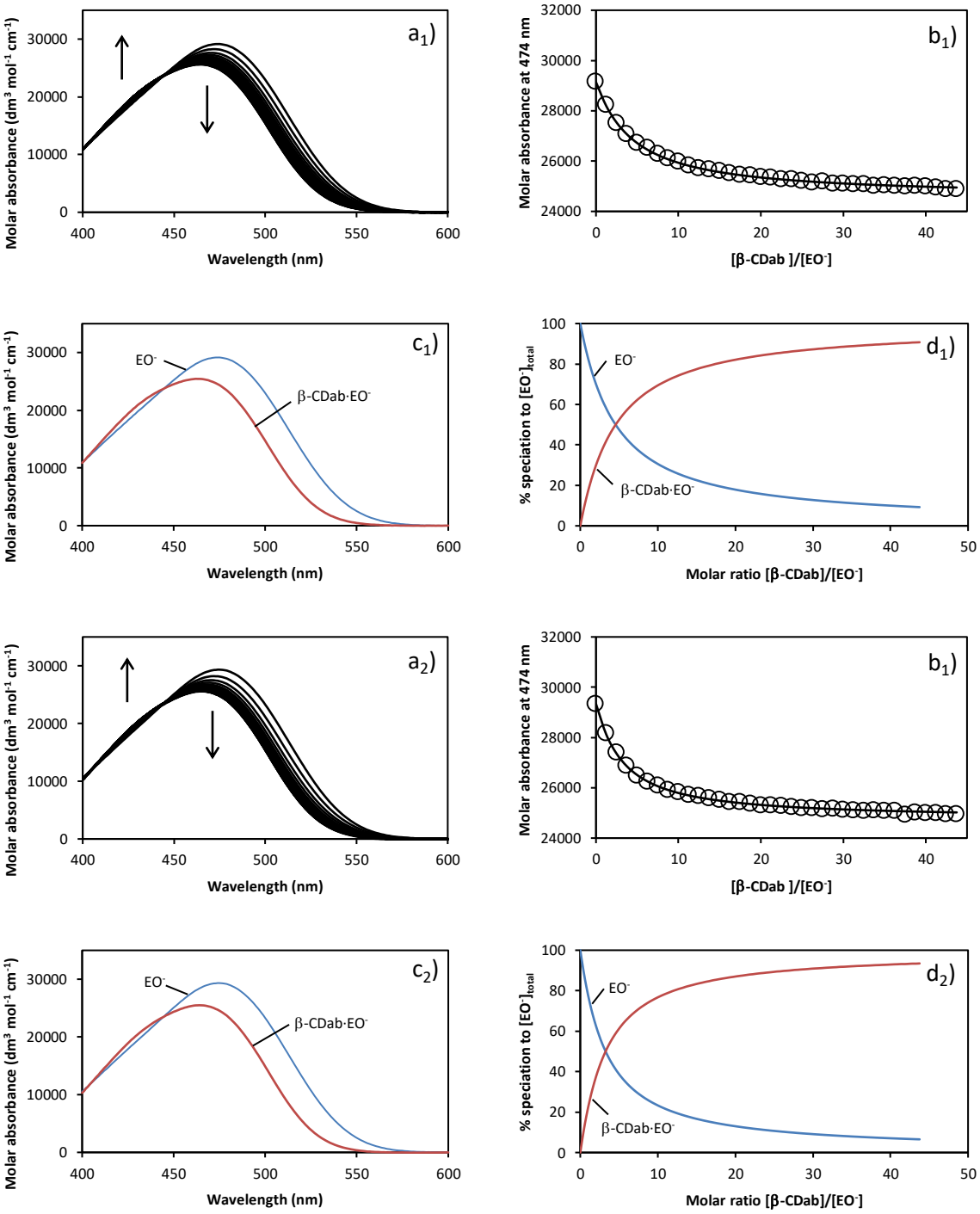

Figure 3.37: UV-vis absorbance data of EO^- (initial concentration 2.0×10^{-5} mol dm^{-3}) with increasing concentrations of β-CDab ($0 – 8.0 \times 10^{-4}$ mol dm^{-3}) in aqueous phosphate buffer (pH 7.0 and I = 0.10 mol dm^{-3}) showing a) the molar absorption spectrum, the arrows indicating the direction of change, b) the experimental (circles) and best fit (line) molar absorbances at 474 nm (fitted at 1 nm intervals over the range 425 – 520 nm) for a 1:1 complex, c) the calculated molar absorbances, and d) the calculated speciation of free and complexed EO^-. The concentration of β-CDab was 0.01 mol dm^{-3}, titrating with 5 mm^3 aliquots to a 2 cm^3 solution of EO^- in a 1 cm path length cell. Note: a_1-d_1 and a_2-d_2 refer to 308.2 K and 298.2 K, respectively.

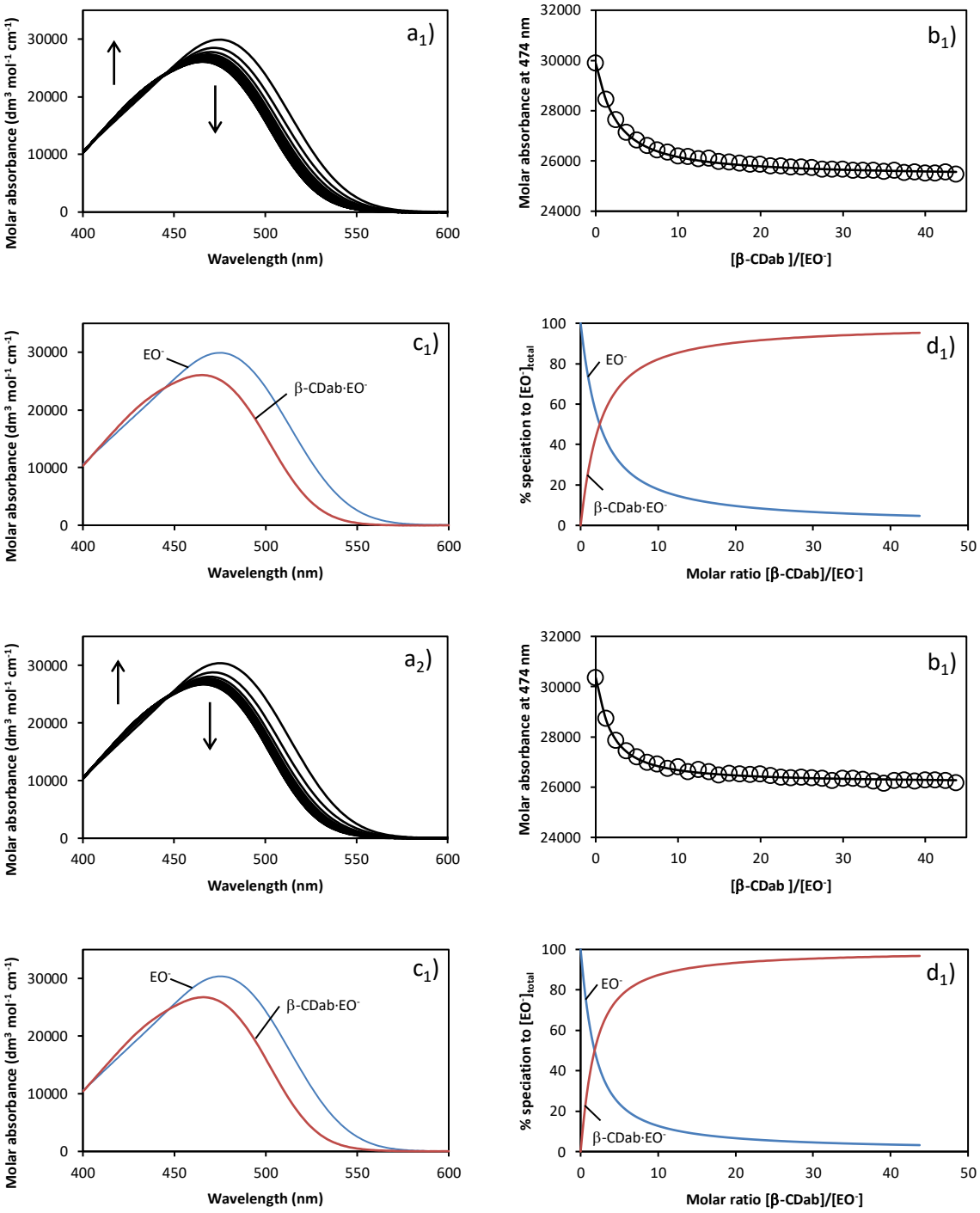

Figure 3.38: UV-vis absorbance data of EO^- (initial concentration 2.0×10^{-5} mol dm^{-3}) with increasing concentrations of β-CDab ($0 – 8.0 \times 10^{-4}$ mol dm^{-3}) in aqueous phosphate buffer (pH 7.0 and I = 0.10 mol dm^{-3}) showing a) the molar absorption spectrum, the arrows indicating the direction of change, b) the experimental (circles) and best fit (line) molar absorbances at 474 nm (fitted at 1 nm intervals over the range 425 – 520 nm) for a 1:1 complex, c) the calculated molar absorbances, and d) the calculated speciation of free and complexed EO^-. The concentration of β-CDab was 0.01 mol dm^{-3}, titrating with 5 mm^3 aliquots to a 2 cm^3 solution of EO^- in a 1 cm path length cell. Note: a_1-d_1 and a_2-d_2 refer to 288.2 K and 278.2 K, respectively.

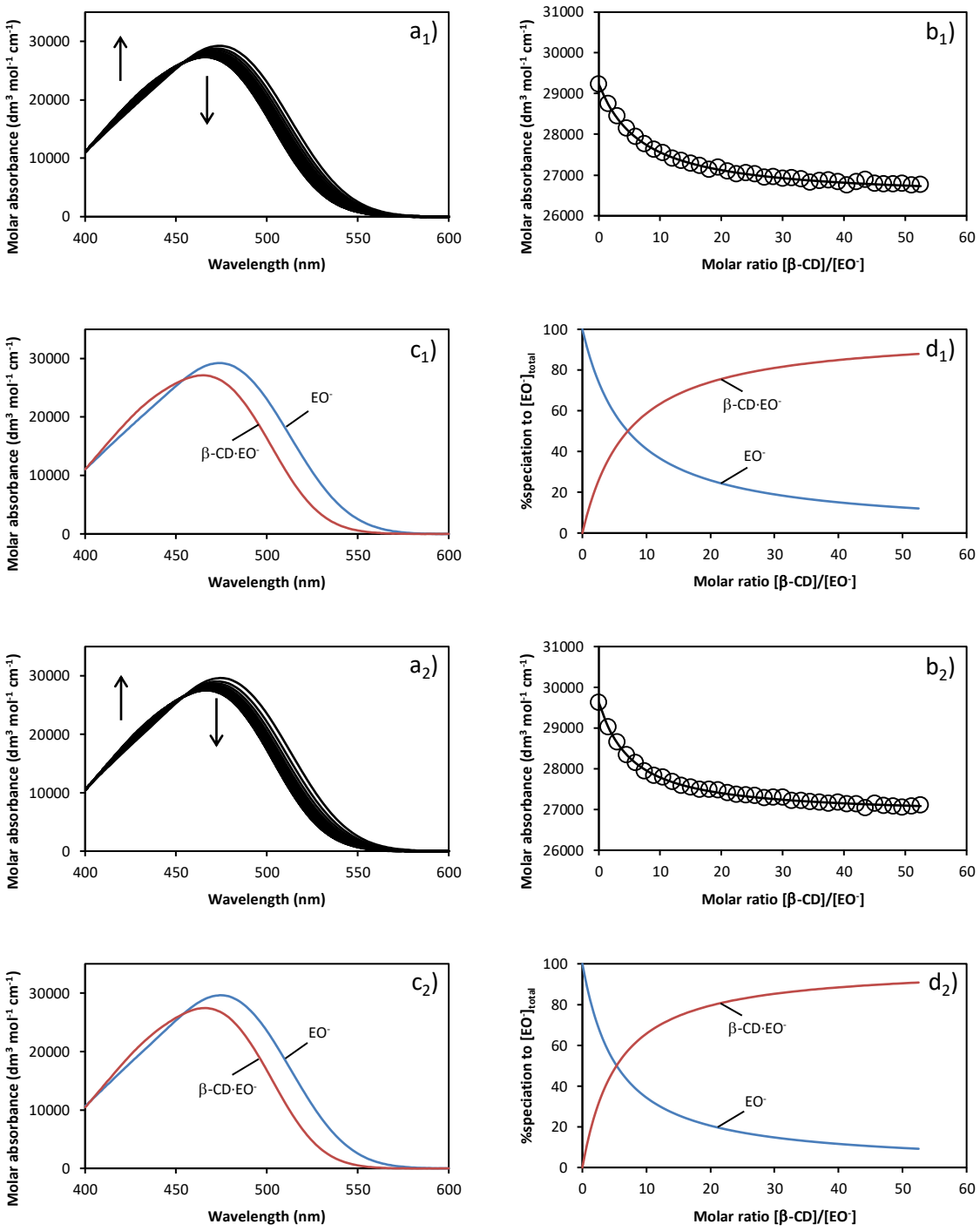

Figure 3.39: UV-vis absorbance data of EO^- (initial concentration 2.0×10^{-5} mol dm^{-3}) with increasing concentrations of β-CD ($0 - 9.6 \times 10^{-4}$ mol dm^{-3}) in aqueous phosphate buffer (pH 7.0 and I = 0.10 mol dm^{-3}) showing a) the molar absorption spectrum, the arrows indicating the direction of change, b) the experimental (circles) and best fit (line) molar absorbances at 474 nm (fitted at 1 nm intervals over the range 425 – 520 nm) for a 1:1 complex, c) the calculated molar absorbances, and d) the calculated speciation of free and complexed EO^-. The concentration of β-CD was 0.012 mol dm^{-3}, titrating with 5 mm^3 aliquots to a 2 cm^3 solution of EO^- in a 1 cm path length cell. Note: a_1-d_1 and a2-d_2 refer to 308.2 K and 298.2 K, respectively.

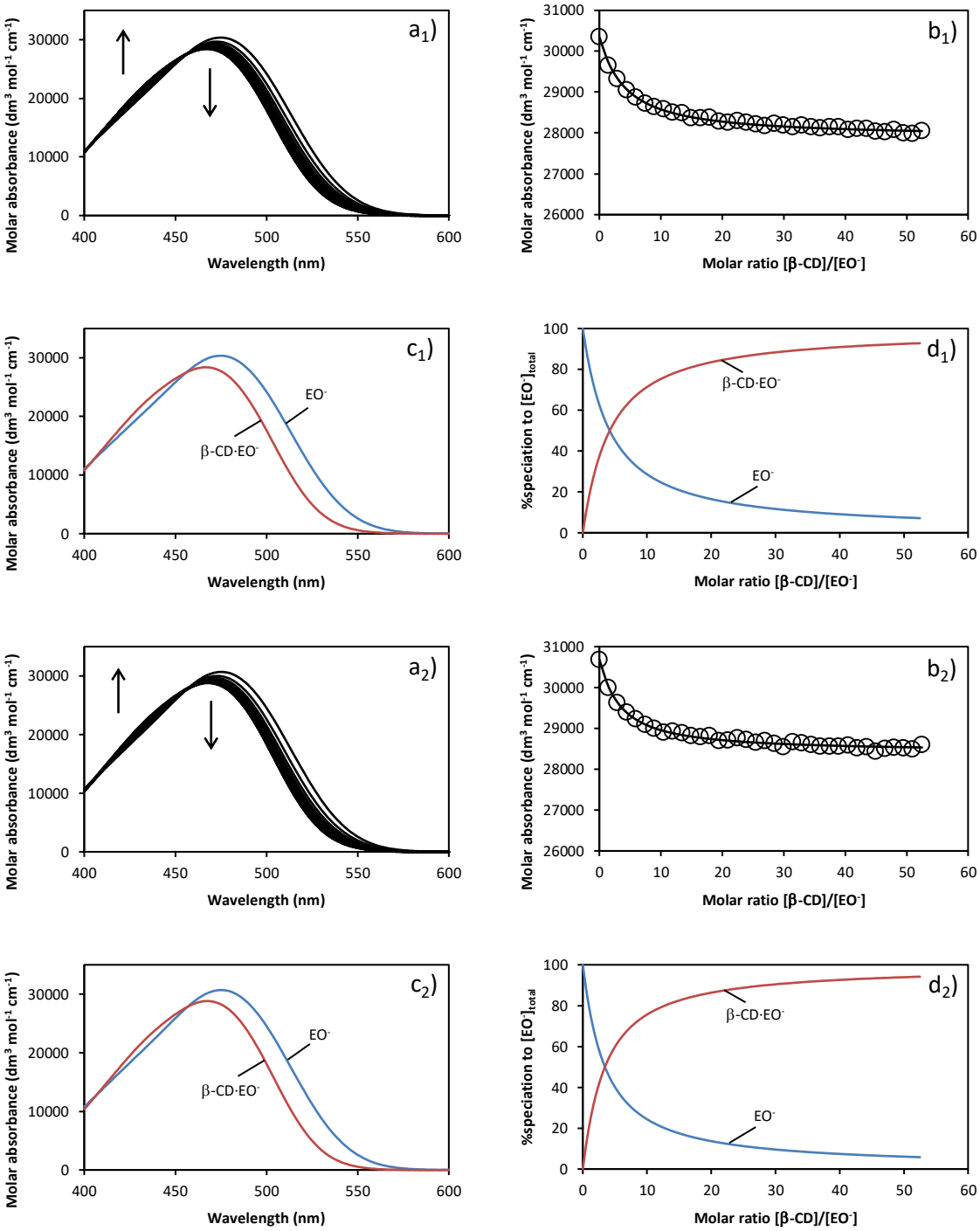

Figure 3.40: UV-vis absorbance data of EO^- (initial concentration 2.0×10^{-5} mol dm^{-3}) with increasing concentrations of β-CD ($0 - 9.6 \times 10^{-4}$ mol dm^{-3}) in aqueous phosphate buffer (pH 7.0 and I = 0.10 mol dm^{-3}) showing a) the molar absorption spectrum, the arrows indicating the direction of change, b) the experimental (circles) and best fit (line) molar absorbances at 474 nm (fitted at 1 nm intervals over the range 425 – 520 nm) for a 1:1 complex, c) the calculated molar absorbances, and d) the calculated speciation of free and complexed EO^-. The concentration of β-CD was 0.012 mol dm^{-3}, titrating with 5 mm^3 aliquots to a 2 cm^3 solution of EO^- in a 1 cm path length cell. Note: a_1-d_1 and a_2-d_2 refer to 288.2 K and 278.2 K, respectively.

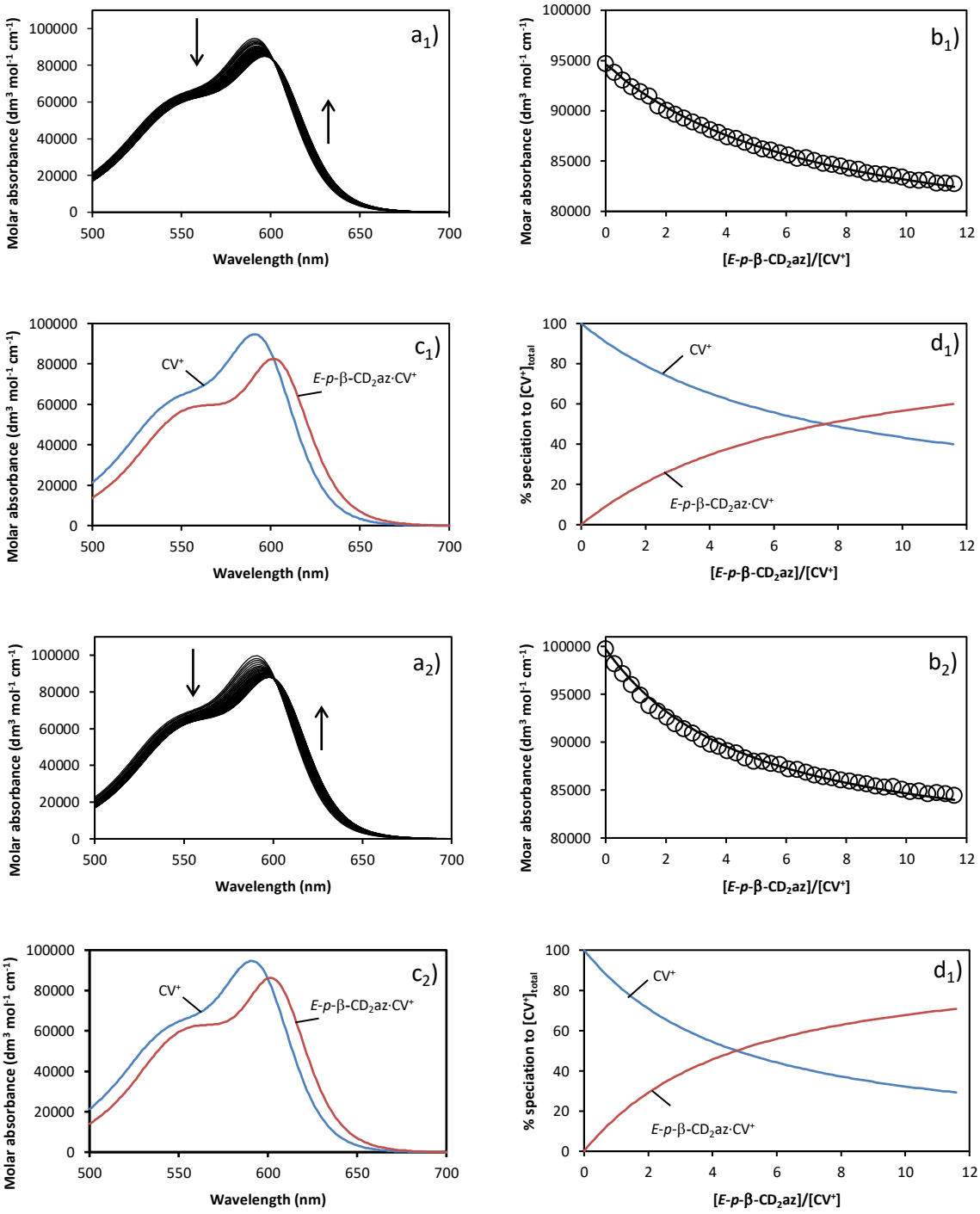

Figure 3.41: UV-vis absorbance data of CV^+ (initial concentration 8.0×10^{-6} mol dm^{-3}) with increasing concentrations of *E*-*p*-β-CD_2az (0 – 9.1×10^{-5} mol dm^{-3}) in aqueous phosphate buffer (pH 7.0 and I = 0.10 mol dm^{-3}) showing a) the molar absorption spectrum, the arrows indicating the direction of change, b) the experimental (circles) and best fit (line) molar absorbances at 591 nm (fitted at 1 nm intervals over the range 550 – 620 nm) for a 1:1 complex, c) the calculated molar absorbances, and d) the calculated speciation of free and complexed CV^+. The concentration of *E*-*p*-β-CD_2az was 0.93 mmol dm^{-3}, titrating with 5 mm^3 aliquots to a 2 cm^3 solution of CV^+ in a 1 cm path length cell. Note: a_1-d_1 and a_2-d_2 refer to 308.2 K and 298.2 K, respectively.

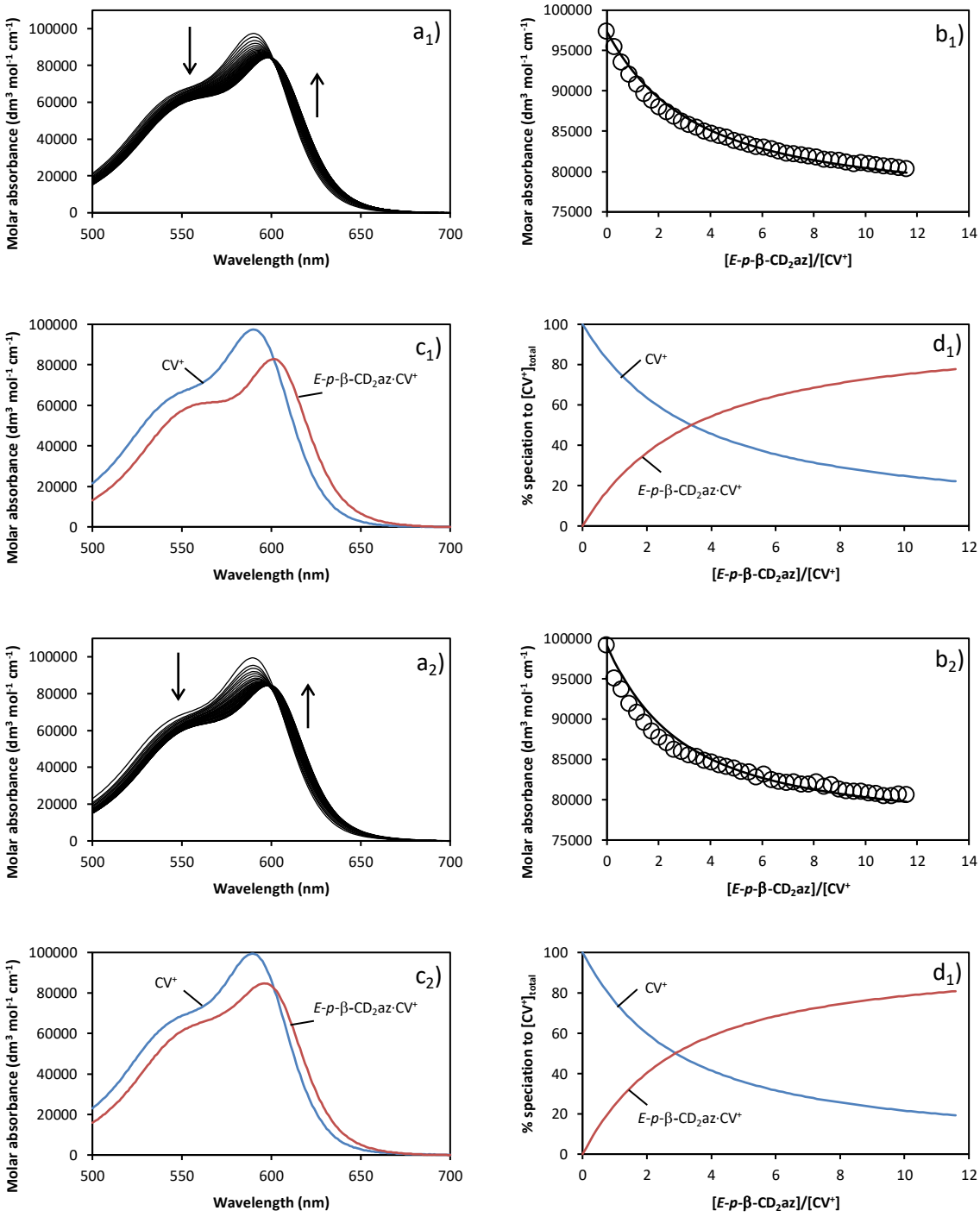

Figure 3.42: UV-vis absorbance data of CV^+ (initial concentration 8.0×10^{-6} mol dm^{-3}) with increasing concentrations of *E*-*p*-β-CD_2az (0 – 9.1×10^{-5} mol dm^{-3}) in aqueous phosphate buffer (pH 7.0 and I = 0.10 mol dm^{-3}) showing a) the molar absorption spectrum, the arrows indicating the direction of change, b) the experimental (circles) and best fit (line) molar absorbances at 591 nm (fitted at 1 nm intervals over the range 550 – 620 nm) for a 1:1 complex, c) the calculated molar absorbances, and d) the calculated speciation of free and complexed CV^+. The concentration of *E*-*p*-β-CD_2az was 0.93 mmol dm^{-3}, titrating with 5 mm^3 aliquots to a 2 cm^3 solution of CV^+ in a 1 cm path length cell. Note: a_1-d_1 and a_2-d_2 refer to 288.2 K and 278.2 K, respectively.

CHAPTER 4

Complexation of Porphyrins by β-Cyclodextrin Oligomers

4.1 Introduction

4.1.1 Porphyrins

Porphyrins are a class of naturally occurring macrocycles characterised by four pyrrole units connected through methine bridges.[1] The highly conjugated structure of porphyrins result in significant light absorption properties, with strong absorption at ~400 nm (Soret Band region) and in the 600 – 800 nm range (Q band region).[2,3] These light harvesting capabilities, along with low biological toxicity, have resulted in the exploration of porphyrins as photosensitisers for a vast range of applications including photodynamic therapy (PDT).[3-6]

Photodynamic therapy is a technique used to treat some cancers and diseases *in situ*, by the production of cytotoxic singlet oxygen, as catalysed by a photosensitiser.[7] In order for porphyrins to act as photosensitisers, they must, among other requirements, possess high absorption in the IR region (Q bands) and high stability under physiological conditions.[3]

The properties of a porphyrin may be altered by functionalising the tetrapyrrole core. The addition of charged phenyl groups are of particular interest as they lead to enhanced water solubility and hence, application in biological media.[8] In this research, four porphyrins are chosen for study: *meso*-tetra(4-sulfonatophenyl)porphine (TSPP), *meso*-tetra(4-carboxyphenyl)porphine (TCPP), meso-tetra(4-*N*,*N*,*N*-trimethylanilinium)porphine (TMAP) and *meso*-tetra(*N*-methyl-4-pyridyl)porphine (TMPyP). These porphyrins are commercially available and differ by the functional group attached to the tetrapyrrole core. Additionally, two porphyrins are anionic (TSPP and TCPP) and two are cationic (TMAP and TMPyP). The four porphyrins are depicted in Figure 4.1 and, as is common practice, the number of NH protons and total charge of the porphyrin are specified. The main absorption characteristics of the four porphyrins at the Soret band are summarised in Table 4.1.[8-16]

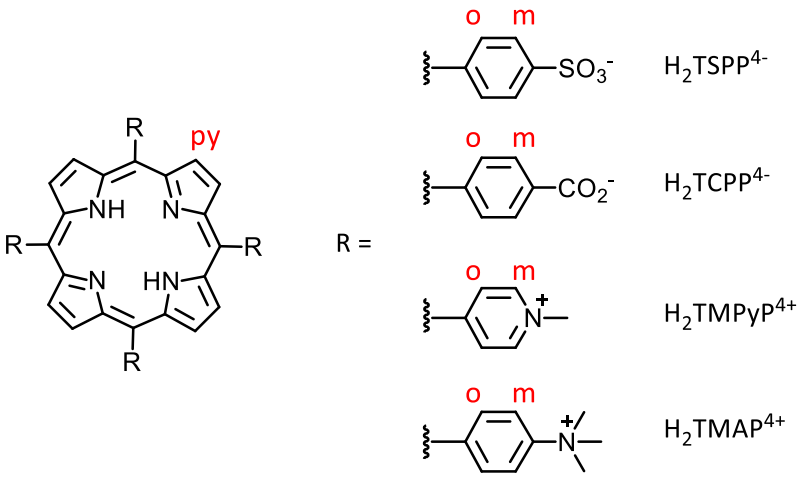

Figure 4.1: The structure of TSPP, TCPP, TMAP and TMPyP as diacids. The total number of amine and imine protons, as well as the total charge of each porphyrin are specified in the abbreviations.

Table 4.1: UV-vis absorption characteristics for TSPP, TCPP, TMAP and TMPyP. The total number of amine and imine protons as well as the total charge of each porphyrin have been specified based upon the pH.

Porphyrin	λ_{max} (nm)	10^{-3} ε (mol dm^{-3} cm^{-1})	pH	Solvent system	Reference
H_3TSPP^{3-}	412	530	5	aqueous	8
/H_2TSPP^{4-}	413	214	-	aqueous	9
H_3TCPP^{3-}	419	339	-	DMF	8
/H_2TCPP^{4-}	415	386	7.5	aqueous buffer	10
H_2TMAP^{4+}	412	416	-	aqueous	11
	412	242	7.4	aqueous buffer	12
	412	178	-	aqueous	13
H_2TMPyP^{4+}	424	226	5	aqueous	8
	425	226	6.8	aqueous buffer	14
	422	220	-	aqueous	15
	422	210	7	aqueous buffer	16

4.1.2 Porphyrin Speciation

Porphyrins may exist as either a free base, mono-acid or di-acid, as shown in Figure 4.2, depending on the protonation of the two imine groups.[17] The stepwise deprotonations from the di-acid to the mono-acid and from the mono-acid to the free base are characterised by the acid dissociation constants pK_{a1} and pK_{a2}, respectively. The pK_a values for TSPP, TCPP, TMAP and TMPyP are given in Table 4.2.[17,18,19]

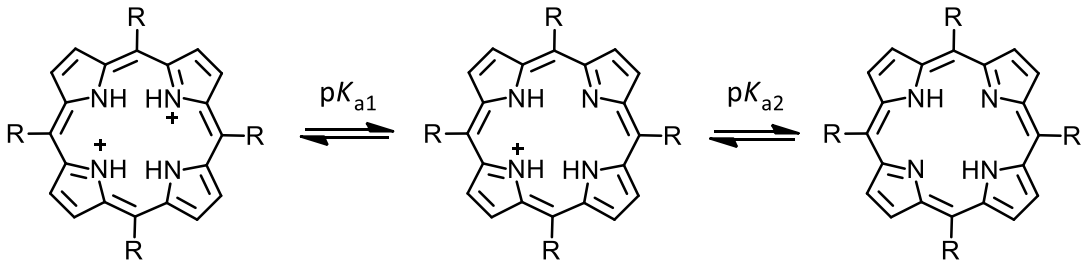

Figure 4.2: The equilibrium between the diacid, monoacid and free base forms of substituted porphyrins.

Table 4.2: Acid dissociation constants, pK_a, for TSPP, TCPP, TMAP and TMPyP.

Porphyrin	pK_{a1}	pK_{a2}	T (K)	Solvent	Reference
TSPP	4.85	4.91	298	aqueous 0.1 M $NaClO_4$	18
TCPP	6.0	6.6	298	aqueous NaCl	17
TMAP	2.3	3.6	298	aqueous NaCl	17
TMPyP	<1	1.4	299	aqueous 0.2 M $NaNO_3$	19

At pH 7, TSPP, TMAP and TMPyP exist predominantly as free bases (H_2TSPP^{4-}, H_2TMAP^{4+} and H_2TMPyP^{4+}, respectively) owing to relatively low pK_{a1} and pK_{a2} values. However, the relatively higher pK_{a1} and pK_{a2} values of TCPP result in a significant portion of the mono-acid present at pH 7. In an aqueous phosphate buffer solution (pH 7.0, I = 0.10 mol dm^{-3}), TCPP exists as 3% H_4TCPP^{2-}, 27% H_3TCPP^{3-} and 70% H_2TCPP^{4-}.[20]

4.1.3 Aggregation of Porphyrins

Water-soluble porphyrins have been known to form aggregates in solutions, which may hamper their utility in biological applications.[10] The formation of porphyrin dimers may be characterised by an equilibrium (or dimerisation) constant, K_D, as shown in Equation 4.1. The aggregation of porphyrins is dependent upon various factors including the porphyrin concentration, substituents, pK_a, acidity of the solution and presence of salts. The equilibrium constants for the dimerisation of H_2TSPP^{4-}, H_3TCPP^{3-}/H_2TCPP^{4-}, H_2TMAP^{4+} and H_2TMPyP^{4+} are given in Table 4.3.[10,17,20-23,24]

$$2\text{porphyrin} \underset{}{\overset{K_D}{\rightleftharpoons}} \text{porphyrin}_2 \qquad (4.1)$$

Table 4.3: Equilibrium constants, K_D, and the associated experimental conditions for the dimerisation of various porphyrins.

Porphyrin	10^{-4} K_D (dm^3 mol^{-1})	T (K)	pH	Solvent	Method	Reference
H_2TSPP^{4-}	9.60 ± 0.96	293	7	aqueous buffer	Temperature-Jump Spectrophotometry	21
	3.48 ± 0.26	298	7.4	aqueous buffer	Fluorescence Spectroscopy	22
	1.54 ± 0.13	298.2	7	aqueous buffer	UV-vis and NMR spectroscopy	23
H_3TCPP^{3-} /H_2TCPP^{4-}	4.55	298	7.5	aqueous buffer	UV-vis spectroscopy	10
	3.59 ± 0.18	298.2	7	aqueous buffer	UV-vis spectroscopy	20
H_2TMAP^{4+}	no aggregation[a]	298	-	aqueous	UV-vis spectroscopy	24
H_3TMAP^{5+}/ H_2TMAP^{4+}	no aggregation[b]	298	3.1-13	aqueous	UV-vis spectroscopy	17
H_4TMPyP^{6+}	no aggregation[c]	298	0	aqueous	UV-vis and Temperature Jump	10
H_2TMPyP^{4+}	no aggregation[c]	298	7.2	aqueous	UV-vis and Temperature Jump	10
	no aggregation[d]	292 - 333	-	aqueous	UV-vis spectroscopy	22

[a] up to 2.0 × 10^{-4} mol dm^{-3}

[b] at 5.0 × 10^{-6} mol dm^{-3}

[c] up to 6.0 × 10^{-5} mol dm^{-3}

[d] up to 1.0 × 10^{-4} mol dm^{-3}

The two anionic porphyrins have a greater tendency to aggregate than the cationic porphyrins. In principle, two main forms of aggregation are possible: H-aggregates and J-aggregates, as shown in Figure 4.3. H-Aggregates are typified by a complete face-to-face interaction of the tetrapyrrole core of two or more porphyrins while J-aggregates exhibit edge-to-edge interactions as the porphyrins are slightly displaced.[17]

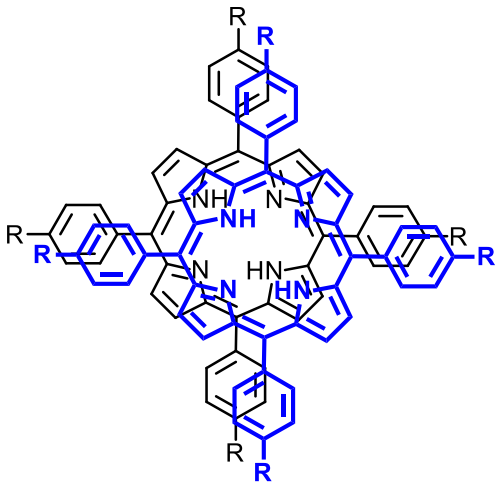

H-Aggregates

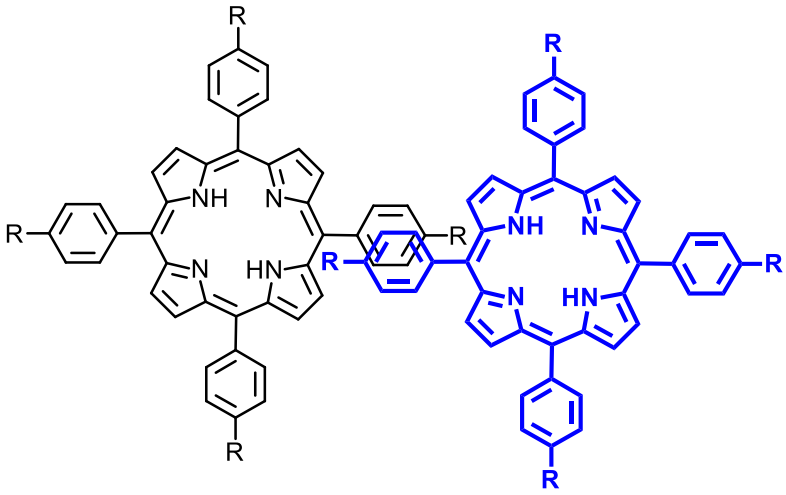

J-Aggregates

Figure 4.3: Proposed structure of H- and J-aggregates of porphyrins.[17]

Various explanations have been proposed to explain the differences in aggregation between anionic and cationic porphyrins. The aggregation of anionic porphyrins has generally been described as occurring due to the lipophilic attraction of adjacent porphyrin centres. The negative charges on the sulfonate and carbonate groups of H_2TSPP^{4-} and H_3TCPP^{3-}/H_2TCPP^{4-}, respectively, are shielded by the positive counterions, thereby reducing electrostatic repulsion and increasing lipophilic attraction.[22] However, given that cationic porphyrins also possess counterions, other factors also influence the aggregation.

Pasternack *et al.* proposed that cationic porphyrins tend not to aggregate as the positive periphery of the porphyrin causes a more even delocalisation of the π-electron cloud, thus resulting in enhanced electrostatic repulsion. However, the negative periphery of anionic porphyrins causes a more localised electron density at the centre of the porphyrin, which increases basicity and facilitates greater van der Waal's interactions.[10] Kano *et al.* meanwhile proposed that the positive charges on the periphery of cationic porphyrins are delocalised on the porphine ring system, which inhibits aggregation.[25]

Aside from electronic effects, Kano *et al.* have demonstrated that hydrophobic alkyl substituents on the periphery of a porphyrin may also facilitate aggregation and hence, structural effects influence porphyrin aggregation.[26] Additionally, higher salt concentrations may favour porphyrin aggregation as the built-up charge that occurs upon porphyrin aggregation is partially shielded by the presence of a salt.[27] Clearly, multiple factors influence porphyrin aggregation and more research is needed to fully understand these systems.

4.1.4 Complexation with Cyclodextrins

The use of porphyrins in applications including PDT may be aided by complexation with CDs. Cyclodextrins may be used to slow thermal or oxidative degradation of porphyrins, disperse porphyrin aggregates, enhance solubility and increase the production of singlet oxygen.[28-30]

The complexation of the four porphyrins by native CD and CD derivatives may be characterised by a complexation constant, K_{11}, as shown in Equation 4.2.

$$\text{host} + \text{porphyrin} \underset{}{\overset{K_{11}}{\rightleftharpoons}} \text{host}\cdot\text{porphyrin} \qquad (4.2)$$

Given the likelihood of CD complexing via the hydrophobic phenyl groups of the porphyrin, multiple host:guest stoichiometries may exist. Various studies have derived complexation constants for H_2TSPP^{4-} and $H_3TCPP^{3-}/H_2TCPP^{4-}$ with native β-CD, as summarised in Table 4.4.[31-34] There have been some studies confirming the complexation of H_2TMAP^{4+} and H_2TMPyP^{4+} by β-CD,[15,35,36] but none have reliably derived a K_{11} value.

Table 4.4: Equilibrium constants, K_{11}, for the 1:1 host:guest complexation between β-CD and either H_2TSPP^{4-} and $H_3TCPP^{3-}/H_2TCPP^{4-}$.

Guest	10^{-3} K_{11} (dm^3 mol^{-1})	T (K)	pH	Solvent system	Method	Reference
H_2TSPP^{4-}	1.40 ± 0.14	298	7	aqueous buffer	Fluorescence	31
	31.0 ± 4.0	298	-	aqueous	Isothermal titration calorimetry	32
	5.60	298	7	aqueous buffer	UV-vis	33
	17.0 ± 3.0	298	-	aqueous	UV-vis	34
$H_3TCPP^{3-}/H_2TCPP^{4-}$	1.70 ± 0.17	-	7	aqueous buffer	Fluorescence	31

4.1.5 Aims of this study

The aims of this research are to investigate the complexation of TSPP, TCPP, TMAP and TMPyP by native β-CD and β-CDab, as shown in Figure 4.4. The azobenzene-linked β-CD dimers from Chapter 2 were not chosen for complexation studies due to a substantial proportion of the *Z* isomer existing under ambient conditions. This study will elucidate the effect of porphyrin substituents on the complexation capabilities of native β-CD and β-CDab. Simultaneously, this study will determine the potential of β-CDab to stabilise porphyrins for use in biological applications.

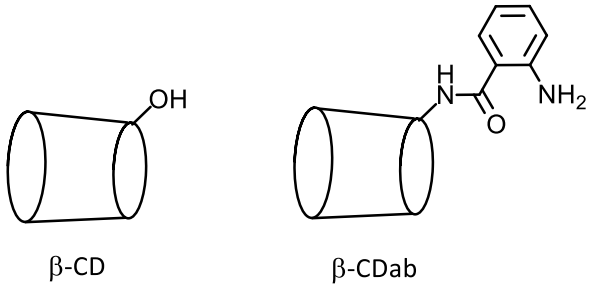

Figure 4.4: Structure of β-CD and β-CDab.

As the experiments in this study will be performed in aqueous phosphate buffer solution (pH 7.0, I = 0.10 mol dm^{-3}), TSPP, TMAP and TMPyP will exist predominantly as the free bases: H_2TSPP^{4-}, H_2TMAP^{4+} and H_2TMPyP^{4+}, respectively. However, TCPP will exist as 3% H_4TCPP^{2-}, 27% $H_3TCPP^{3-}$and 70% H_2TCPP^{4-}.[20] As the proportion of H_4TCPP^{2-} is small, the TCPP species in this study will be referred to as $H_3TCPP^{3-}/H_2TCPP^{4-}$.

The host-guest complexes will be qualitatively characterised using 1D and 2D ^{1}H NMR spectroscopy and quantitatively characterised using UV-vis spectroscopy to determine the equilibrium constants and thermodynamic parameters of complexation. Simple gas-phase molecular modelling studies will also be undertaken to investigate the geometry of the complexes formed.

This research aims to gain a systematic understanding of the factors that influence the complexation of porphyrins and the influence of modifications of the β-CD host. This will ultimately lead to more targeted research into the use of porphyrins and β-CD for biological applications.

4.2 Results and Discussion

4.2.1 Complexation of H_2TSPP^{4-}, $H_3TCPP^{3-}/H_2TCPP^{4-}$, H_2TMAP^{4+} and H_2TMPyP^{4+} by β-CD and β-CDab

The complexation of H_2TSPP^{4-}, $H_3TCPP^{3-}/H_2TCPP^{4-}$, H_2TMAP^{4+} and H_2TMPyP^{4+} by native β-CD and β-CDab was studied by NMR and UV-vis spectroscopy. 1D and 2D ^{1}H NMR spectroscopy were used to determine the qualitative complexation behaviour, while UV-vis spectroscopy was used to quantitatively describe the complexation constants and thermodynamic parameters which govern complexation.

4.2.1.1 Qualitative Investigation of Complexation by 1D ^{1}H NMR Spectroscopy

The complexation behaviour of H_2TSPP^{4-}, $H_3TCPP^{3-}/H_2TCPP^{4-}$, H_2TMAP^{4+} and H_2TMPyP^{4+} with either native β-CD or β-CDab was studied by 1D ^{1}H NMR spectroscopy. Solutions of each host (β-CD or β-CDab), porphyrin (H_2TSPP^{4-}, $H_3TCPP^{3-}/H_2TCPP^{4-}$, H_2TMAP^{4+} or H_2TMPyP^{4+}) and host-porphyrin combination were prepared in D_2O phosphate buffer (pD 7.0, I = 0.10 mol dm^{-3}) at 298.2 K.

Due to the relatively high concentrations used in the ^{1}H NMR studies (by comparison with those of the UV-vis studies discussed later), aggregation is expected for H_2TSPP^{4-} and $H_3TCPP^{3-}/H_2TCPP^{4-}$. The concentration of H_2TSPP^{4-} and $H_3TCPP^{3-}/H_2TCPP^{4-}$ used in the NMR studies is 4.8×10^{-3} mol dm^{-3}. Assuming a K_D of 1.54×10^4 dm^3 mol^{-1} and 3.59×10^4 dm^3 mol^{-1} for H_2TSPP^{4-} and H_3TCPP^{3-}/H_2TCPP^4,[20,23] respectively, both porphyrins exists primarily as a dimer (98% and 99%, respectively). Conversely, either H_2TMAP^{4+} or H_2TMPyP^{4+} is not expected to aggregate significantly and therefore exist predominantly as a monomer. While H_2TSPP^{4-} and $H_3TCPP^{3-}/H_2TCPP^{4-}$ appear primarily as aggregates, the addition of a β-CD host can disperse aggregates due to the formation of a complex.[37] Therefore, ^{1}H NMR spectroscopy is a sensitive technique through which to compare the complexation properties of the four porphyrins by the β-CD and β-CDab hosts.

The host-porphyrin complexes may adopt various stoichiometries and orientations. As each porphyrin possesses four possible complexation sites, up to four β-CD groups may complex. However, due to the entropic loss associated with the sequential addition of hosts, only 1:1 and 2:1 host:porphyrin complexes are expected. In the case of 2:1 complexes, the second β-CD group may complex either *anti* or *syn* to the adjacent β-CD. Additionally, each β-CD may complex through the primary or secondary face. Figure 4.5 depicts 1:1 host·porphyrin complexes through the primary and secondary face as well as 2:1 host$_2$·porphyrin complexes with *anti*- and *syn*-conformations. The complexes are exemplified using native β-CD as the host and H_2TSPP^{4-} as the porphyrin.

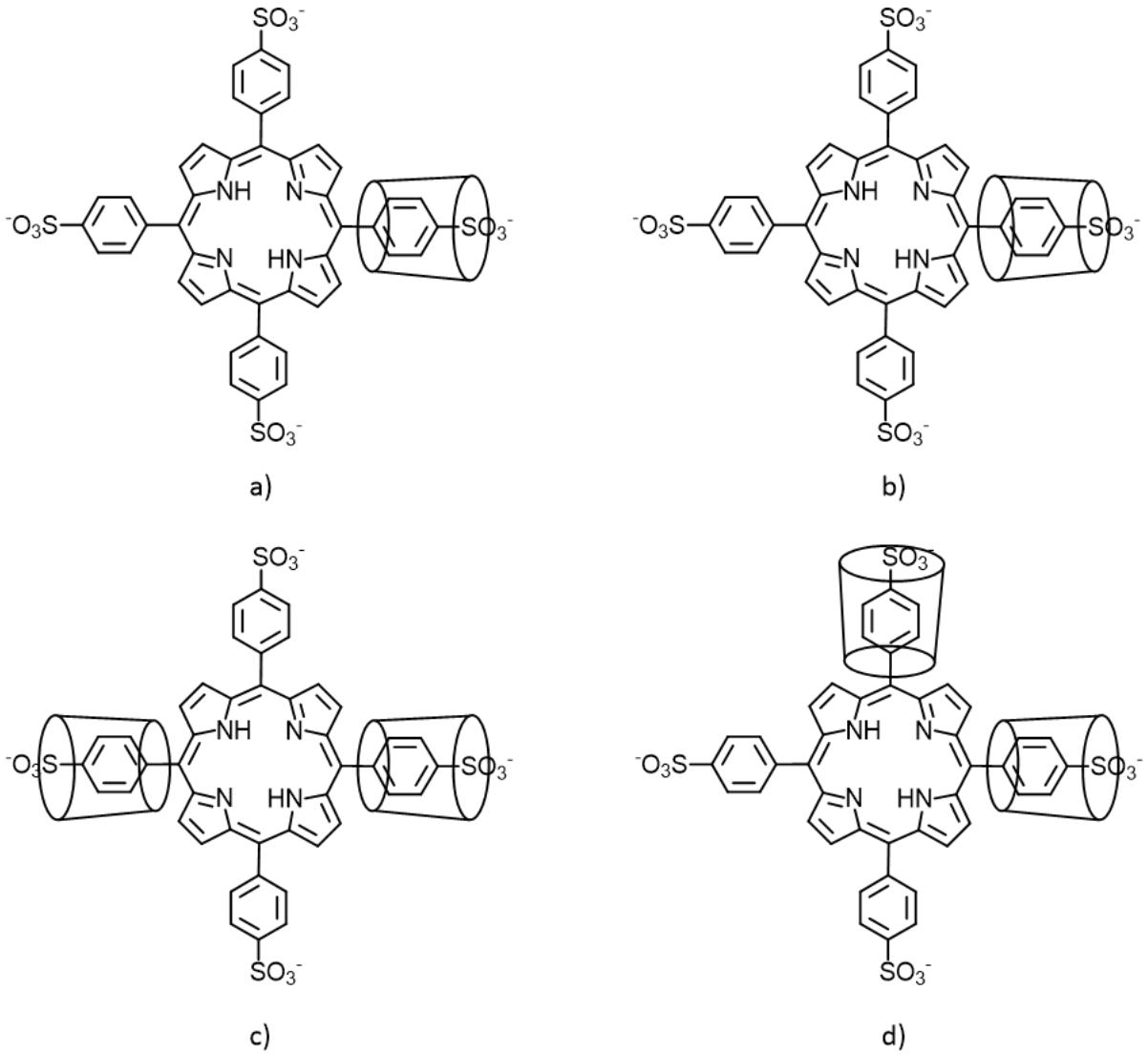

Figure 4.5: Host:porphyrin complexes of various stoichiometries and orientations including a) 1:1 β-CD·H_2TSPP^{4-} complex through the primary face, b) 1:1 β-CD·H_2TSPP^{4-} through the secondary face, c) 2:1 β-CD_2·H_2TSPP^{4-} *anti*-conformation complex through the primary face and d) 2:1 β-CD_2·H_2TSPP^{4-} *syn*-conformation complex through the primary face.

The incorporation of a porphyrin into a β-CD cavity results in new chemical environments for both the porphyrin and interior protons of β-CD. Therefore, a difference in the chemical shifts of the proton resonances of the compounds alone and in combination indicates that complexation has occurred.[38] Preferential entry of the guest through either the primary or secondary face of β-CD may be detected based upon the chemical shift changes of the H2 – H6 protons of β-CD. The H2 and H3 protons of β-CD surround the primary face while the H5 and H6 protons frame the secondary face. However, the stoichiometry of the complexes cannot be determined from a single experiment; this requires a determination of the variation of the chemical shift changes with solution concentration and composition.

4.2.1.1.1 ^{1}H NMR spectroscopic study of the complexation of H_2TSPP^{4-}, H_3TCPP^{3-}/H_2TCPP^{4-}, H_2TMAP^{4+} and H_2TMPyP^{4+} by β-CD

The ^{1}H NMR spectra of the porphyrins, β-CD and their mixtures are shown in Figure 4.6 – Figure 4.9. The porphyrin proton resonances are annotated according to the proton labelling in Figure 4.1, and those of β-CD according to the labelling used in previous chapters. The chemical shifts of the ^{1}H resonances are collected in Table 4.5 – Table 4.8.

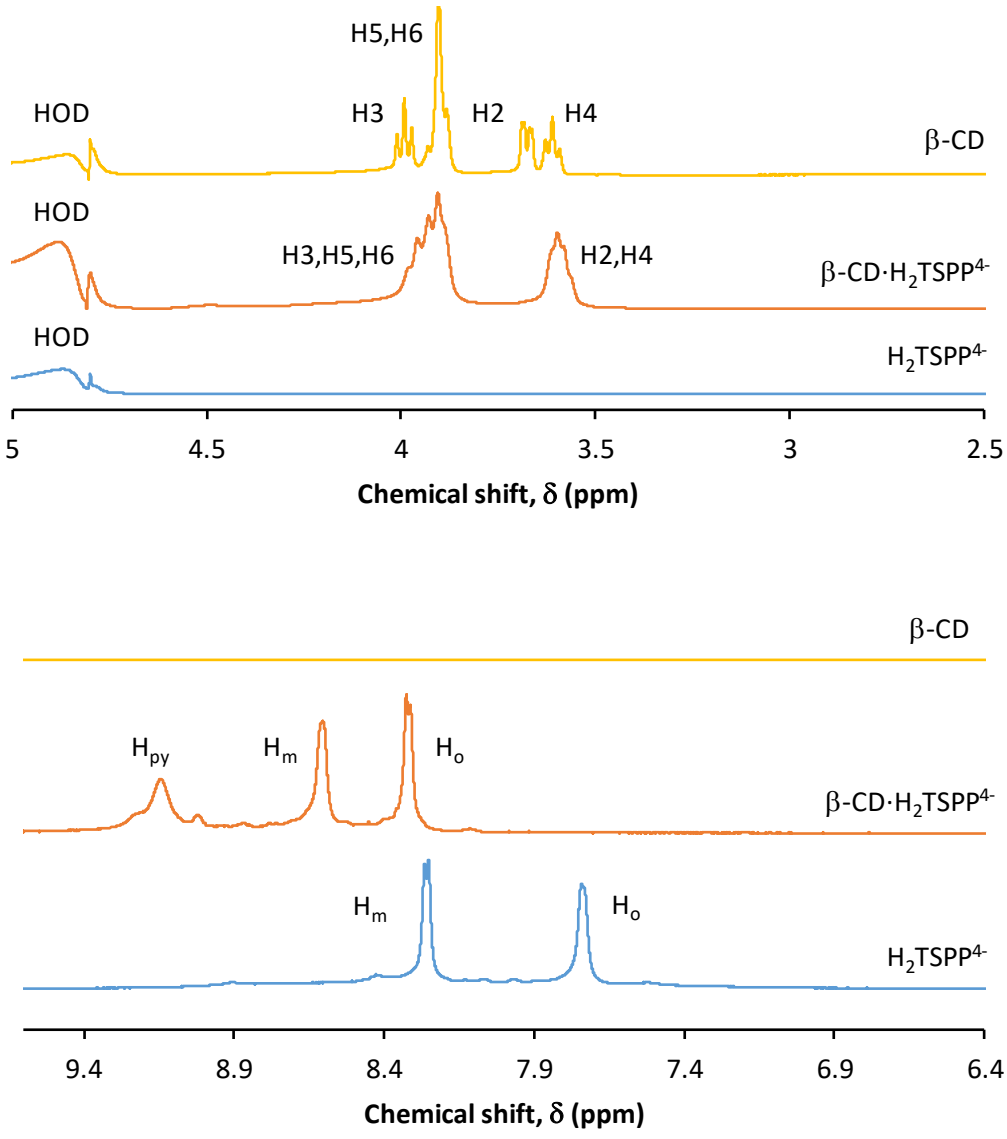

Figure 4.6: ^{1}H NMR spectra of H_2TSPP^{4-} (4.8×10^{-3} mol dm^{-3}), β-CD (4.8×10^{-3} mol dm^{-3}) and H_2TSPP^{4-} (4.8×10^{-3} mol dm^{-3}) with one molar equivalent of β-CD in D_2O phosphate buffer (pD 7.0, I = 0.10 mol dm^{-3}) at 298.2 K.

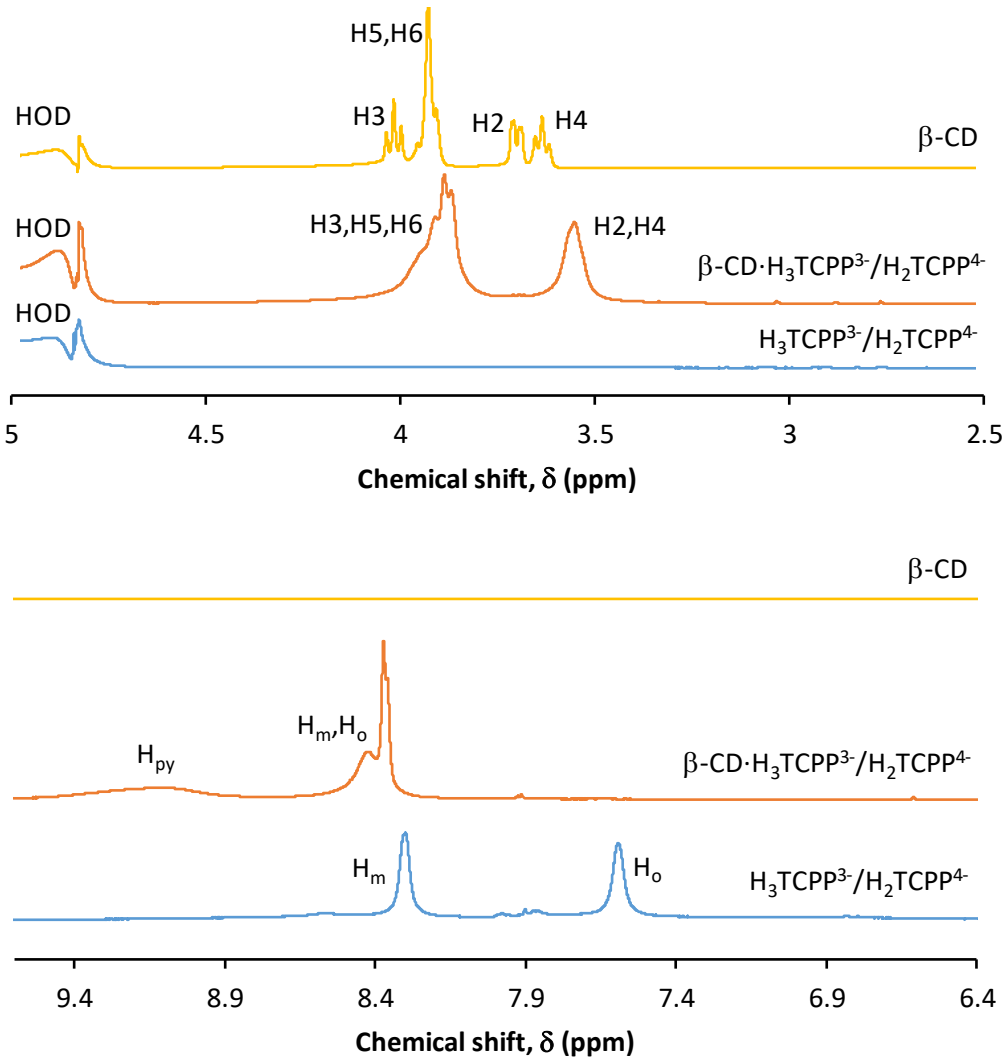

Figure 4.7: ^{1}H NMR spectra of $H_3TCPP^{3-}/H_2TCPP^{4-}$ (4.8×10^{-3} mol dm^{-3}), β-CD (4.8×10^{-3} mol dm^{-3}) and $H_3TCPP^{3-}/H_2TCPP^{4-}$($4.8 \times 10^{-3}$ mol dm^{-3}) with one molar equivalent of β-CD in D_2O phosphate buffer (pD 7.0, I = 0.10 mol dm^{-3}) at 298.2 K.

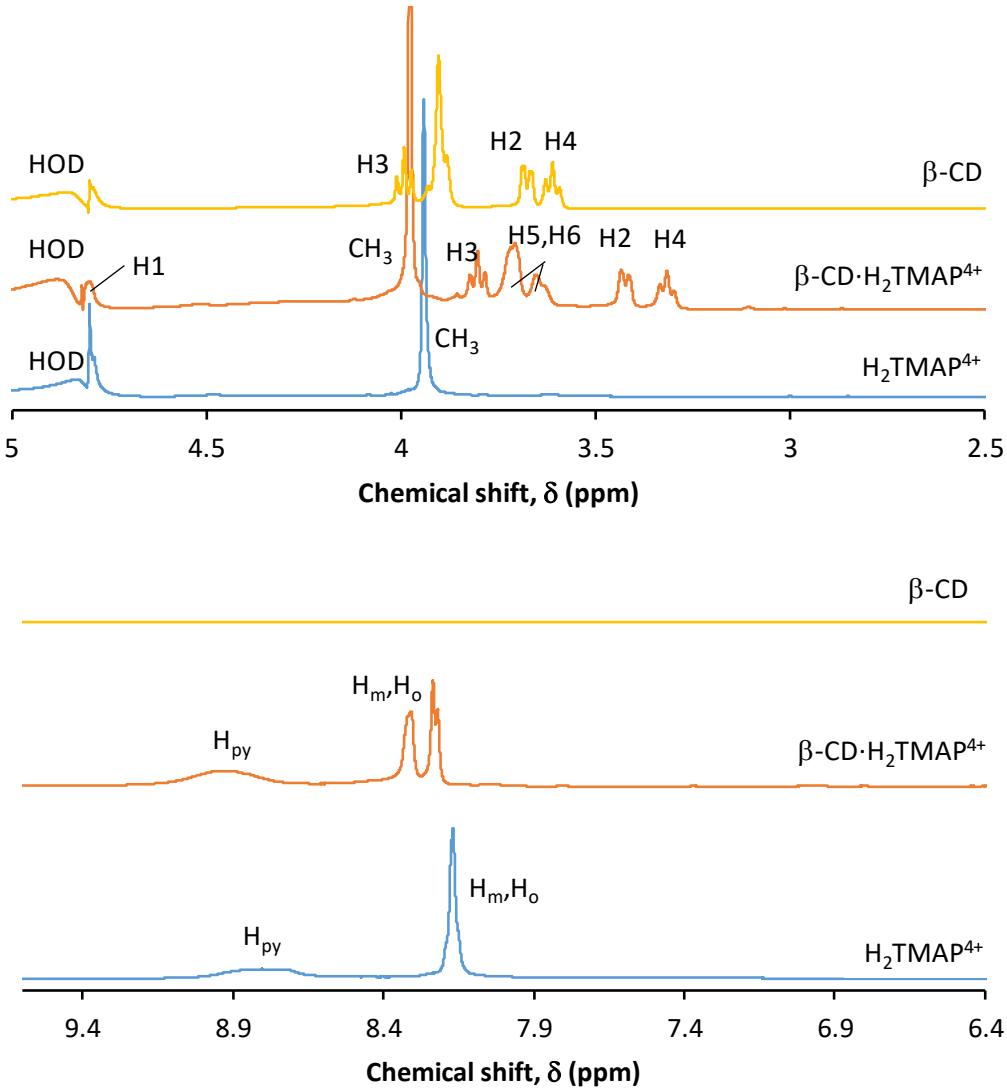

Figure 4.8: ^{1}H NMR spectra of H_2TMAP^{4+} (4.8×10^{-3} mol dm^{-3}), β-CD (4.8×10^{-3} mol dm^{-3}) and H_2TMAP^{4+} (4.8×10^{-3} mol dm^{-3}) with one molar equivalent of β-CD in D_2O phosphate buffer (pD 7.0, I = 0.10 mol dm^{-3}) at 298.2 K.

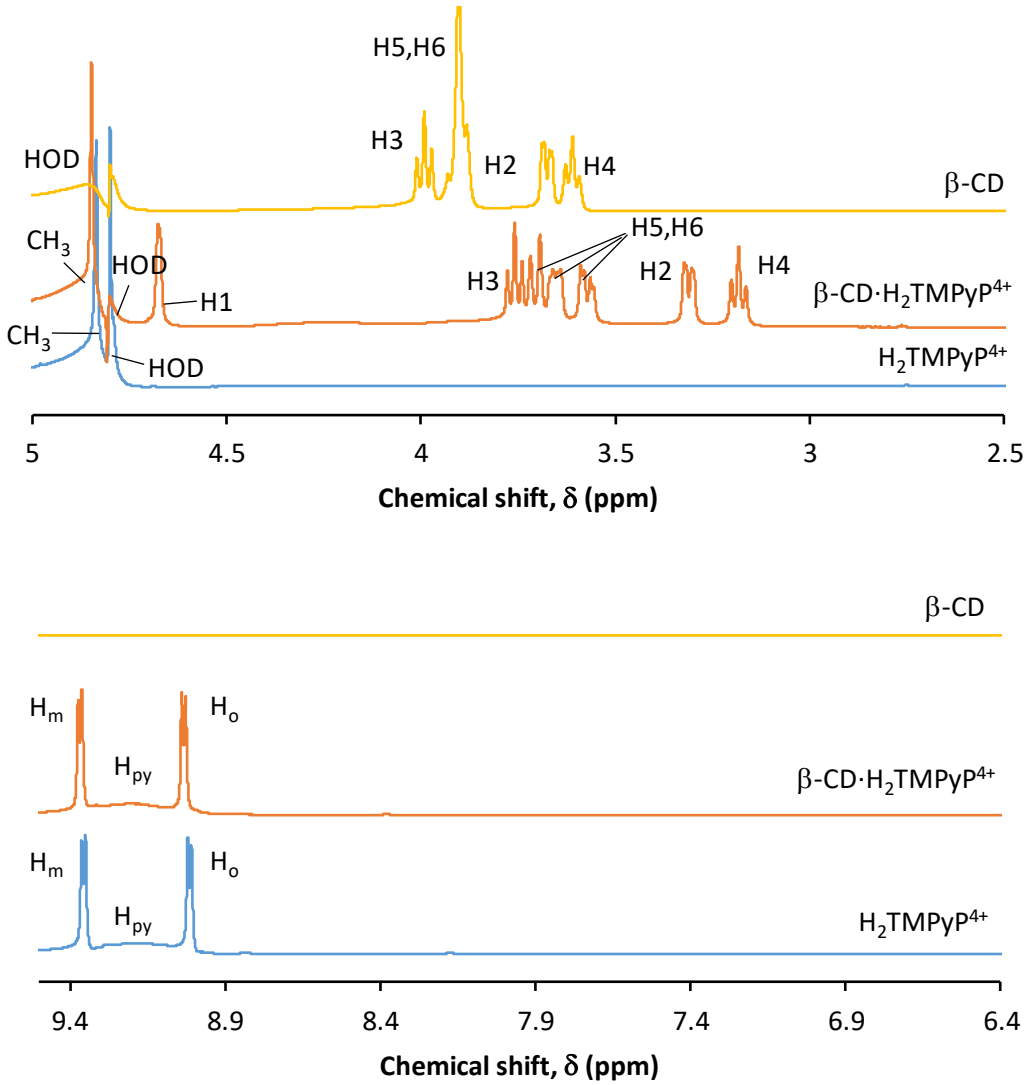

Figure 4.9: ^{1}H NMR spectra of H_2TMPyP^{4+} (4.8×10^{-3} mol dm^{-3}), β-CD (4.8×10^{-3} mol dm^{-3}) and H_2TMPyP^{4+} (4.8×10^{-3} mol dm^{-3}) with one molar equivalent of β-CD in D_2O phosphate buffer (pD 7.0, I = 0.10 mol dm^{-3}) at 298.2 K.

Table 4.5: Summary of ^{1}H NMR resonances for β-CD, H_2TSPP^{4-} and β-CD·H_2TSPP^{4-} in D_2O phosphate buffer (pD 7.0, I = 0.10 mol dm^{-3}) at 298.2 K.

		β-CD	**H_2TSPP^{4-}**	**β-CD·H_2TSPP^{4-}**
Porphyrin	**H_m**	-	8.26 (d, J = 6.55 Hz)	8.60 (s)
	H_o	-	7.74 (s)	8.31 (d, J = 7.6 Hz)
	H_{py}	-	broadened	9.14 (br s)
β-CD	**H1**	5.09 (s)	-	5.05 (br m)
	H2	3.68 (d, J = 10.2 Hz)	-	3.59 (br m)
	H3	3.99 (t, J = 9.3 Hz)	-	3.91 (br m)
	H4	3.61(t, J = 8.6 Hz)	-	3.59 (br m)
	H5	3.8 – 3.9 (br m)	-	3.91 (br m)

Table 4.6: Summary of ^{1}H NMR resonances for β-CD, H_3TCPP^{3-}/H_2TCPP^{4-} and β-CD·H_3TCPP^{3-}/H_2TCPP^{4-} in D_2O phosphate buffer (pD 7.0, I = 0.10 mol dm^{-3}) at 298.2 K.

		β-CD	**H_3TCPP^{3-}/H_2TCPP^{4-}**	**β-CD·H_3TCPP^{3-}/H_2TCPP^{4-}**
Porphyrin	**H_m**	-	8.30 (s)	8.42 (br s), 8.37 (s)
	H_o	-	7.59 (s)	
	H_{py}	-	broadened	9.13 (br s)
β-CD	**H1**	5.09 (s)	-	5.01 (br m)
	H2	3.68 (d, J = 10.2 Hz)	-	3.53 (br s)
	H3	3.99 (t, J = 9.3 Hz)	-	3.86 (br m)
	H4	3.61(t, J = 8.6 Hz)	-	3.53 (br s)
	H5	3.8 – 3.9 (br m)	-	3.86 (br m)

Table 4.7: Summary of ^{1}H NMR resonances for β-CD, H_2TMAP^{4+} and β-CD·H_2TMAP^{4+} in D_2O phosphate buffer (pD 7.0, *I* = 0.10 mol dm^{-3}) at 298.2 K.

		β-CD	H_2TMAP^{4+}	β-CD·H_2TMAP^{4+}
Porphyrin	**CH_3**	-	3.95 (s)	3.96 (s)
	H_m	-	8.18 (s)	8.29 (s), 8.21 (d, J = 8.2 Hz)
	H_o	-		
	H_{py}	-	8.84 (br s)	8.91 (br s)
β-CD	**H1**	5.09 (s)	-	4.79 (s)
	H2	3.68 (d, J = 10.2 Hz)	-	3.46 (d, J = 10.0 Hz)
	H3	3.99 (t, J = 9.3 Hz)	-	3.78 (t, J = 9.5 Hz)
	H4	3.61(t, J = 8.6 Hz)	-	3.30 (t, J = 8.4 Hz)
	H5	3.8 – 3.9 (br m)	-	3.62 (m)
	H6		-	3.69 (m)

Table 4.8: Summary of ^{1}H NMR resonances for β-CD, H_2TMPyP^{4+} and β-CD·H_2TMPyP^{4+} in D_2O phosphate buffer (pD 7.0, *I* = 0.10 mol dm^{-3}) at 298.2 K.

		β-CD	H_2TMPyP^{4+}	β-CD·H_2TMPyP^{4+}
Porphyrin	**CH_3**	-	4.76 (s)	4.84 (s)
	H_m	-	9.32 (d, J = 5.7 Hz)	9.32 (d, J = 6.7 Hz)
	H_o	-	8.98 (d, J = 6.7 Hz)	8.99 (d, J = 5.8 Hz)
	H_{py}	-	9.14 (br s)	9.16 (br s)
β-CD	**H1**	5.09 (s)	-	4.84 (s)
	H2	3.68 (d, J = 10.2 Hz)	-	3.31 (d, J = 9.0 Hz)
	H3	3.99 (t, J = 9.3 Hz)	-	3.76 (t, J = 9.2Hz)
	H4	3.61(t, J = 8.6 Hz)	-	3.18 (t, J = 8.3 Hz)
	H5	3.8 – 3.9 (br m)	-	3.5 – 3.9 (br m)
	H6		-	

The ^{1}H NMR spectrum of H_2TSPP^{4-} alone (Figure 4.6) shows two resonances corresponding to the H_m and H_o protons. The H_{py} resonance appears to have broadened into the baseline as a result of the slow to intermediate (NMR time scale) tautomerism of the H_2TSPP^{4-} imine protons.[9,23,39] Upon complexation with β-CD, the H_m and H_o resonances shift downfield by 0.34 ppm and 0.57 ppm, respectively, indicating complexation of the *p*-sulfonatophenyl groups into the β-CD annulus.

The complexation of H_2TSPP^{4-} by β-CD is also likely to result in a disruption of H_2TSPP^{4-} aggregation. The diameters of the primary and secondary face of β-CD are 600 pm and 650 pm, respectively, while the width of a phenyl ring is ~470 pm.[40] Therefore, it appears that only one phenyl ring is able to reside in the cavity of β-CD which requires a disruption of porphyrin aggregates.[16] However, the

complete dissociation of the aggregate is likely to depend on the type of aggregate: H- or J-aggregate. The complexation of a porphyrin with a single β-CD host may allow porphyrins to remain as J-aggregates as the edge of the porphyrins may still interact. However, the entropic loss associated with a three-component (two porphyrins and one β-CD host) complex may disfavor the retention of J-aggregates.

The H_{py} resonance of H_2TSPP^{4-} becomes more apparent upon complexation with β-CD, indicating that the rate of tautomerism of H_2TSPP^{4-} either increases to the fast exchange limit or slows substantially upon dissociation of the porphyrin aggregate upon complexation: possibilities which are not distinguished between on the basis of these data. The H2 resonance of β-CD shifts upfield by 0.08 ppm upon complexation with H_2TSPP^{4-}, becoming superimposed with the H4 resonance. Similarly, the H3 resonance of β-CD shifts upon complexation with H_2TSPP^{4-}, superimposing with the H5 and H6 resonances. This is consistent with β-CD complexing the *p*-sulfonatophenyl groups of H_2TSPP^{4-} through the secondary face. Such a configuration probably allows significant hydration of the sulfonate group of H_2TSPP^{4-} as it largely resides outside the β-CD cavity. This preferential complexation of H_2TSPP^{4-} by the secondary face has previously been established by Ribo *et al.* and may be due to the larger opening of the secondary face.[37]

The secondary face preference may also be explained by electronic effects. As there is an imbalance in the number of hydroxyl groups on either face of β-CD, a dipole moment with its negative end at the centre of the secondary face and its positive pole at the centre of the primary face exists. Inoue *et al.* previously established that the dipole-dipole interaction between α-CD and either benzoic acid, *p*-nitrophenol or *p*-hydroxybenzoic acid significantly influenced the final host-guest orientation. Complexes were formed which favoured the antiparallel alignment of dipole moments of the host and the guest.[41] Therefore, as H_2TSPP^{4-} contains permanent negative charges on the sulfonate groups, complexation through the secondary face tends to be preferred to oppositely align the dipole moments of the porphyrin and β-CD.

The complexation of $H_3TCPP^{3-}/H_2TCPP^{4-}$ by β-CD (Figure 4.7) shows similar results to the β-CD/H_2TSPP^{4-} system, with an upfield shift of the H2 and H3 resonances of β-CD of 0.15 ppm and 0.13 ppm, respectively, upon complexation with $H_3TCPP^{3-}/H_2TCPP^{4-}$. The H_m and H_o resonances of $H_3TCPP^{3-}/H_2TCPP^{4-}$ are superimposed upon complexation with β-CD and are difficult to definitively assign. However, the H_m and H_o resonances of $H_3TCPP^{3-}/H_2TCPP^{4-}$ shift upfield by at least 0.07 ppm and 0.78 ppm upon complexation with β-CD, respectively.

The ^{1}H NMR spectrum in Figure 4.7 indicates that $H_3TCPP^{3-}/H_2TCPP^{4-}$ is complexing through the secondary face of β-CD. As the H_o resonance of $H_3TCPP^{3-}/H_2TCPP^{4-}$ undergoes a much greater upfield shift than the H_m resonance, the *p*-carbonatophenyl groups of $H_3TCPP^{3-}/H_2TCPP^{4-}$ may penetrate the β-CD cavity more deeply than does H_2TSPP^{4-} in the analogous β-CD·H_2TSPP^{4-} complex. As with the *p*-sulfonatophenyl group of H_2TSPP^{4-}, the *p*-carbonatophenyl groups of $H_3TCPP^{3-}/H_2TCPP^{4-}$ possess permanent negative charges. Therefore, the complexation of $H_3TCPP^{3-}/H_2TCPP^{4-}$ by β-CD is probably dominated by a secondary face entry as this favours the antiparallel arrangement of dipole moments of both host and guest. The ^{1}H NMR spectrum also shows that the H_{py} resonance of $H_3TCPP^{3-}/H_2TCPP^{4-}$ becomes apparent upon complexation with β-CD. Therefore, as for H_2TSPP^{4-}, β-CD either increases the rate of tautomerism of $H_3TCPP^{3-}/H_2TCPP^{4-}$ to the fast exchange limit or slows it substantially upon dissociation of the porphyrin aggregate when complexation occurs. Such complexation is also likely to greatly disrupt $H_3TCPP^{3-}/H_2TCPP^{4-}$ aggregation.

The H_m and H_o resonances of H_2TMAP^{4+} alone in the ^{1}H NMR spectrum shown in Figure 4.8 are superimposed but become magnetically inequivalent upon complexation by β-CD. There is some ambiguity in the assignment of the H_m and H_o resonances of complexed H_2TMAP^{4+}, however, one of these resonances shifts downfield by 0.03 ppm, while the other shifts downfield by 0.11 ppm. The CH_3 resonances of H_2TMAP^{4+} shows a slight upfield shift of 0.01 ppm upon complexation by β-CD. The greater shifts shown by the H_m and H_o resonances by comparison with that of the CH_3 resonances is consistent with dominant β-CD placement over the phenyl groups of H_2TMAP^{4+} in the complex.

The H2 – H6 resonances of β-CD shift upfield by 0.21 – 0.31 ppm upon complexation with H_2TMAP^{4+}, indicating that neither the primary or secondary face of β-CD is preferred during complexation consistent with complexation occurring through the primary and secondary faces of β-CD to similar extents. As with the anionic porphyrins, the cationic porphyrins may prefer to enter through the secondary face of β-CD due to the larger opening. However, as H_2TMAP^{4+} consists of permanent positive charges at the anilinium group, entry through the primary face would favor the antiparallel alignment of the dipole moments of H_2TMAP^{4+} and β-CD. Therefore, as the primary face and secondary face of β-CD are contrastingly favoured, no preference is observed, resulting in a mixture of these geometries.

The complexation of H_2TMPyP^{4+} by β-CD shows upfield shifts of the H2 – H6 protons of β-CD in the ^{1}H NMR spectrum shown in Figure 4.9, in a similar manner to the β-CD/H_2TMAP^{4+} system. The H2, H3 and H4 resonances of β-CD shift upfield by 0.37 ppm, 0.23 ppm and 0.43 ppm, respectively, while the H5 and H6 resonances shift upfield and are magnetically differentiated upon complexation with

H_2TMPyP^{4+}. However, the H_m, H_o and CH_3 resonances of H_2TMPyP^{4+} do not significantly shift upon complexation. The shifts in resonances closesly matches those reported by Mosinger *et al.*, who attributed the NMR pattern as resulting from non-covalent interactions between the porphyrin and internal and external surfaces of β-CD.[15] However, the lack of significant shift in the porphyrin resonances is also likely to indicate weak internal complexation.

Weak stability for the β-CD·H_2TMPyP^{4+} complex is due to the delocalisation of the positive charge of H_2TMPyP^{4+} onto the pyridine ring. As a result, complexation within the β-CD annulus may be hindered by repulsion between the positive end of the β-CD dipole moment at the primary face of the annulus and the positively charged pyridines of H_2TMPyP^{4+}.[34] Additionally, complexation via the methyl group of H_2TMPyP^{4+} would be weak due to a size mis-match between the methyl group and internal cavity of β-CD. To some extent this may be compensated for by weak interactions between H_2TMPyP^{4+} and the external surface of β-CD. However, this does not completely exclude the possibility of limited internal complexation which contributes to only minor changes in the ^1H NMR spectrum of both the porphyin and β-CD.

4.2.1.1.2 ^{1}H NMR spectroscopic study of the complexation of H_2TSPP^{4-}, H_3TCPP^{3-}/H_2TCPP^{4-}, H_2TMAP^{4+} and H_2TMPyP^{4+} by β-CDab

The ^{1}H NMR spectra of the porphyrins, β-CDab and their mixtures are shown in Figure 4.10 – Figure 4.13. The porphyrin proton resonances are annotated according to the proton labelling in Figure 4.1, and those of β-CDab according to the labelling used in previous chapters. The chemical shifts of the ^{1}H resonances are collected in Table 4.9 – Table 4.12.

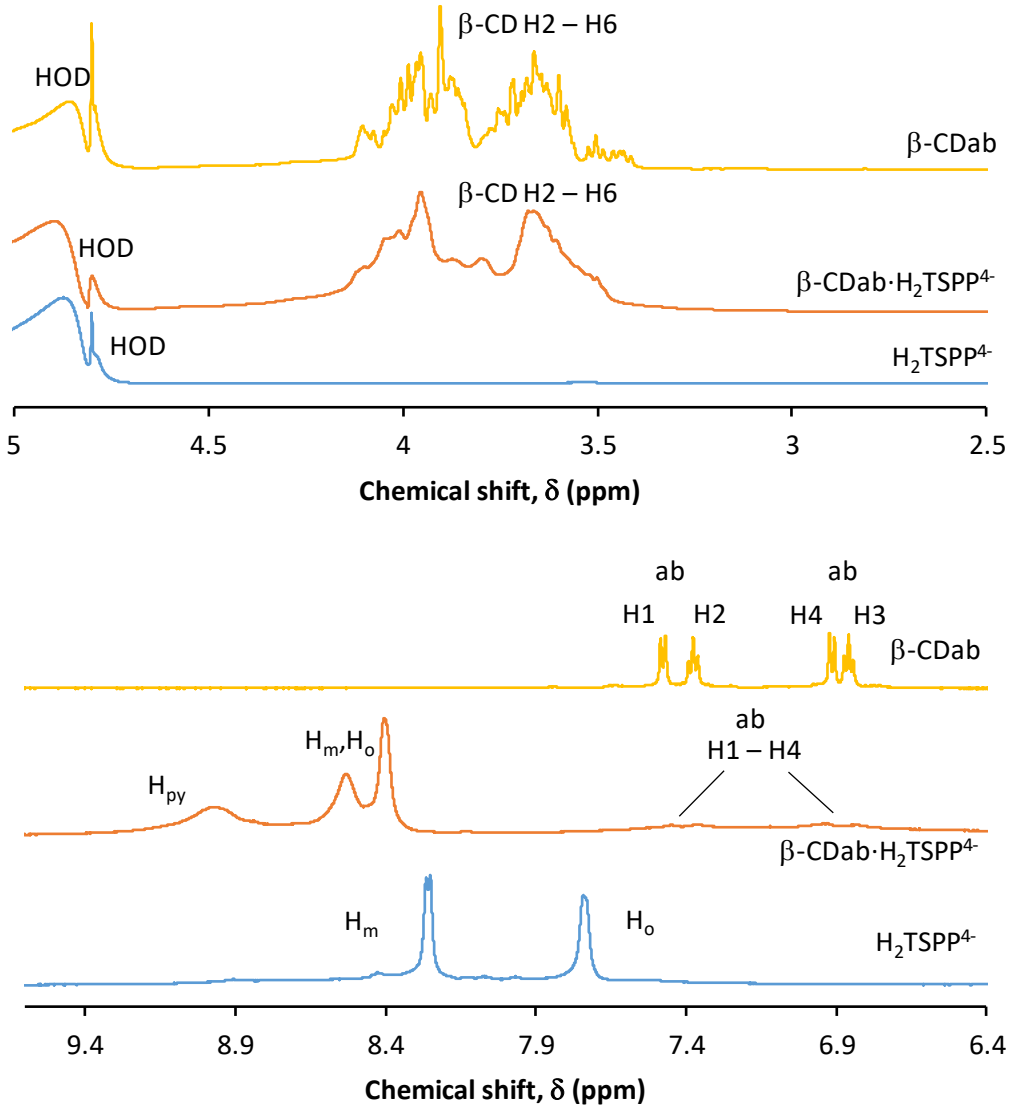

Figure 4.10: ^{1}H NMR spectra of H_2TSPP^{4-} (4.8×10^{-3} mol dm^{-3}), β-CDab (9.6×10^{-3} mol dm^{-3}) and H_2TSPP^{4-} (4.8×10^{-3} mol dm^{-3}) with one molar equivalent of β-CDab in D_2O phosphate buffer (pD 7.0, I = 0.10 mol dm^{-3}) at 298.2 K.

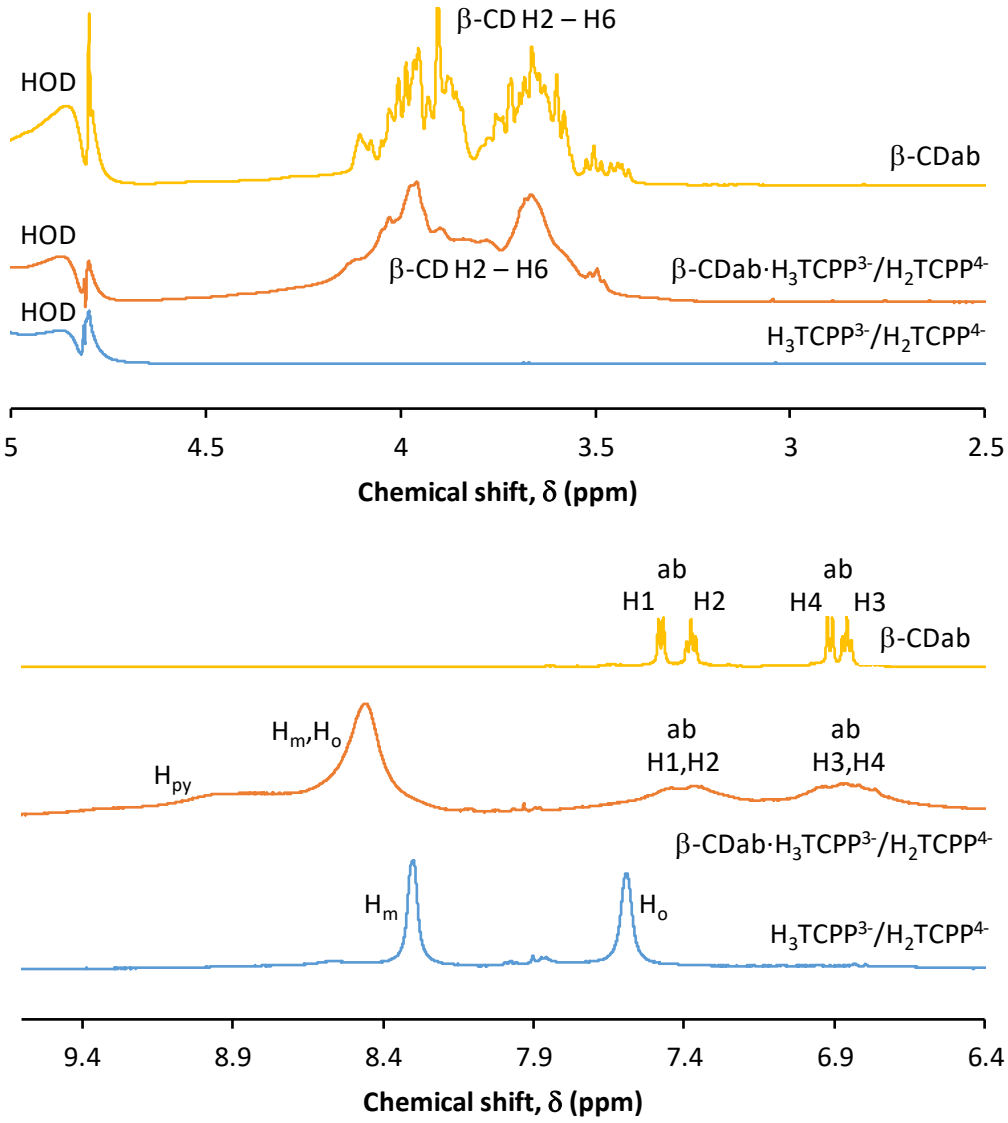

Figure 4.11: ^{1}H NMR spectra of $H_3TCPP^{3-}/H_2TCPP^{4-}$ (4.8×10^{-3} mol dm^{-3}), β-CDab (9.6×10^{-3} mol dm^{-3}) and $H_3TCPP^{3-}/H_2TCPP^{4-}$ (4.8×10^{-3} mol dm^{-3}) with one molar equivalent of β-CDab in D_2O phosphate buffer (pD 7.0, I = 0.10 mol dm^{-3}) at 298.2 K.

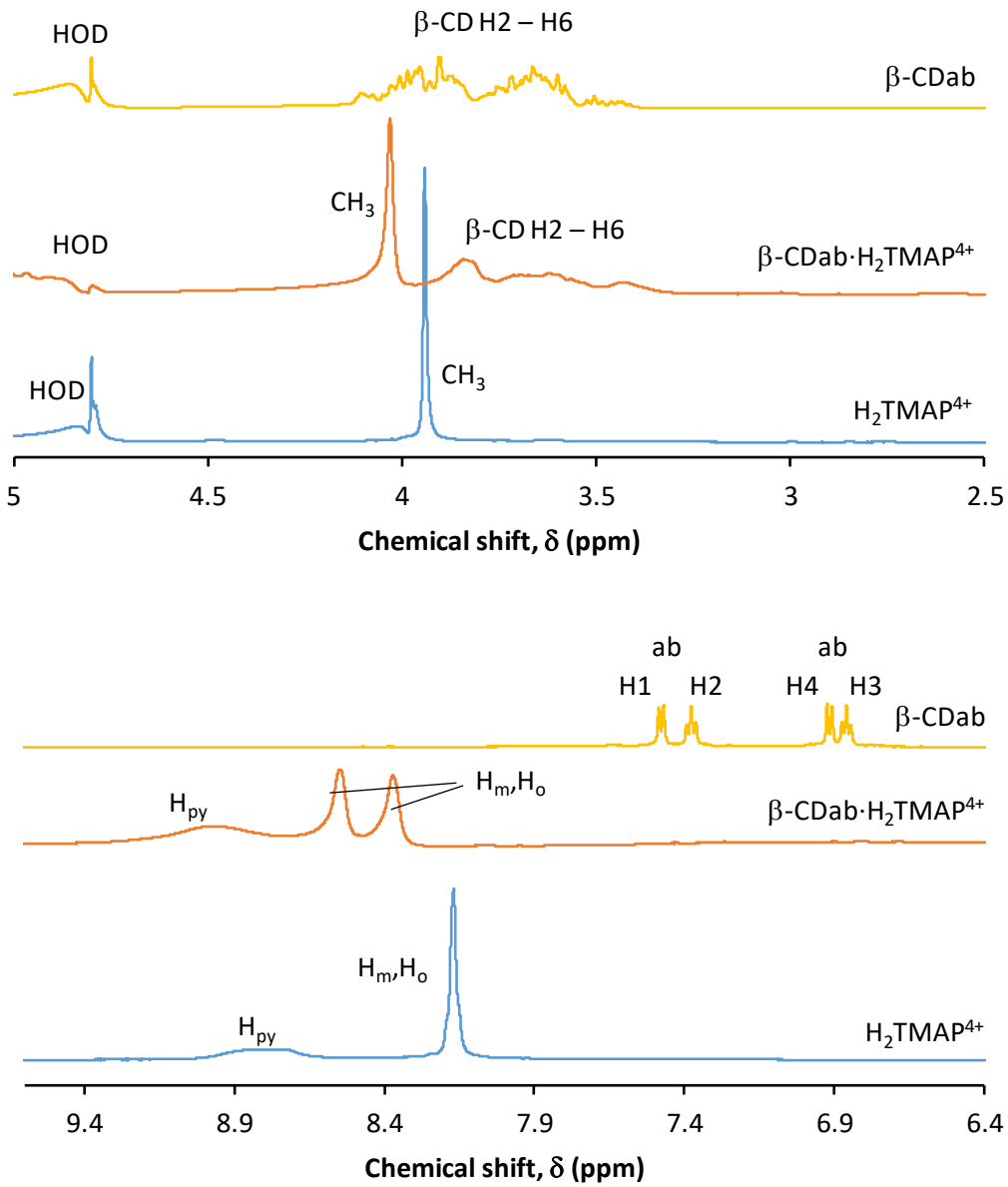

Figure 4.12: ^{1}H NMR spectra of H_2TMAP^{4+} (4.8×10^{-3} mol dm^{-3}), β-CDab (9.6×10^{-3} mol dm^{-3}) and H_2TMAP^{4+} (4.8×10^{-3} mol dm^{-3}) with one molar equivalent of β-CDab in D_2O phosphate buffer (pD 7.0, I = 0.10 mol dm^{-3}) at 298.2 K.

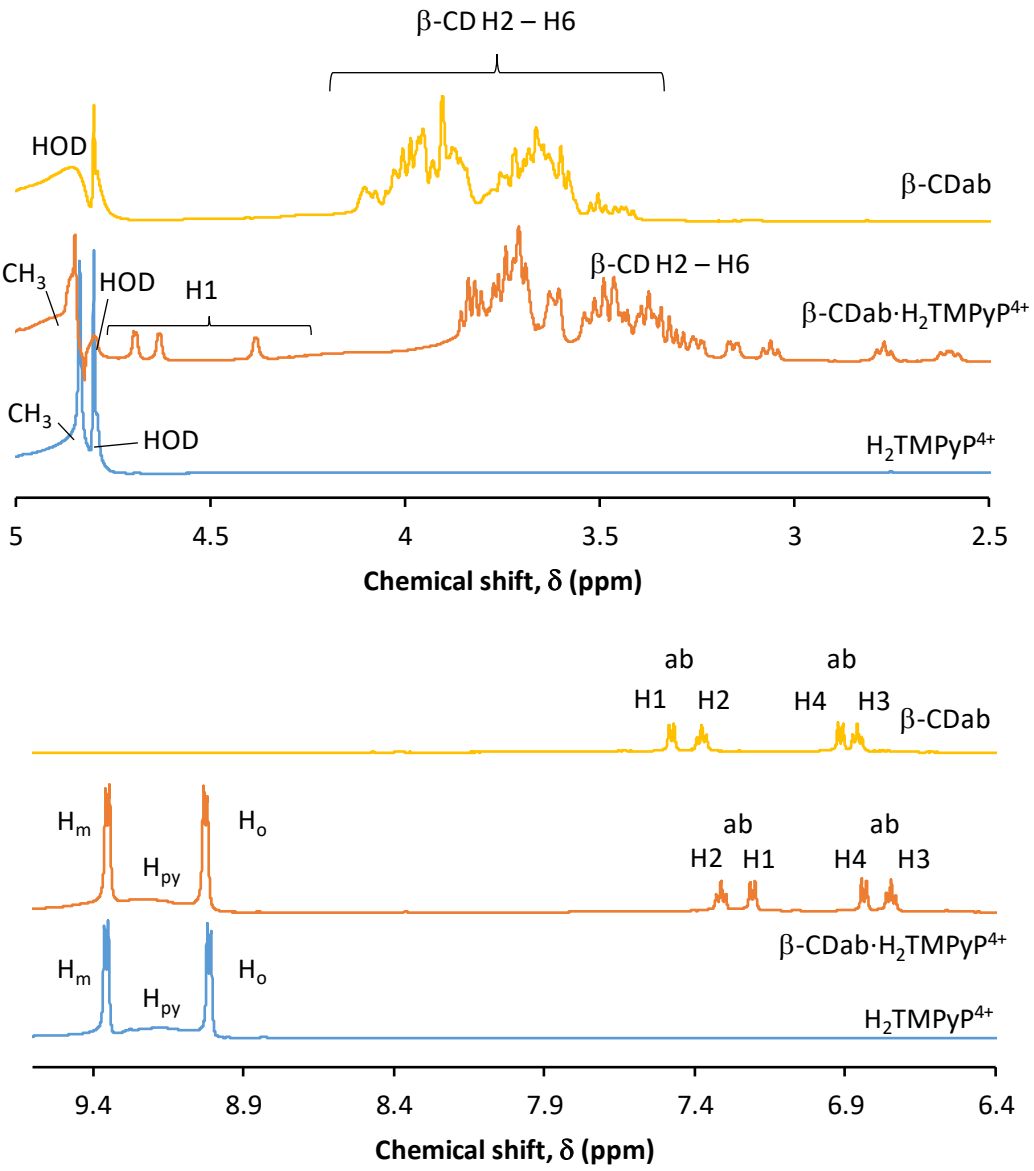

Figure 4.13: ^{1}H NMR spectra of H_2TMPyP^{4+} (4.8×10^{-3} mol dm^{-3}), β-CDab (9.6×10^{-3} mol dm^{-3}) and H_2TMPyP^{4+} (4.8×10^{-3} mol dm^{-3}) with one molar equivalent of β-CDab in D_2O phosphate buffer (pD 7.0, I = 0.10 mol dm^{-3}) at 298.2 K.

Table 4.9: Summary of ^{1}H NMR resonances for β-CDab, H_2TSPP^{4-} and β-CDab·H_2TSPP^{4-} in D_2O phosphate buffer (pD 7.0, *I* = 0.10 mol dm^{-3}) at 298.2 K.

		β-CDab	**H_2TSPP^{4-}**	**β-CDab·H_2TSPP^{4-}**
Porphyrin	**H_m**	-	8.26 (d, J = 6.55 Hz)	8.41 (s), 8.54 (s)
	H_o	-	7.74 (s)	
	H_{py}	-	broadened	8.96 (br s)
Aminophenyl group	**H1**	7.48 (d, J = 7.6 Hz)	-	6.2 – 8.1 (br m)
	H2	7.38 (t, J = 7.7 Hz)	-	
	H3	6.86 (t, J = 7.2 Hz)	-	
	H4	6.92 (d, J = 8.6 Hz)	-	
β-CD group	**H1**	5.09 (s)	-	5.06 (br m)
	H2	3.3 - 4.3 (br m)	-	3.2 - 4.7 (br m)
	H3		-	
	H4		-	
	H5		-	
	H6		-	

Table 4.10: Summary of ^{1}H NMR resonances for β-CDab, H_3TCPP^{3-}/H_2TCPP^{4-} and β-CDab·H_3TCPP^{3-}/H_2TCPP^{4-}in D_2O phosphate buffer (pD 7.0, *I* = 0.10 mol dm^{-3}) at 298.2 K.

		β-CDab	**H_3TCPP^{3-}/H_2TCPP^{4-}**	**β-CDab·H_3TCPP^{3-}/H_2TCPP^{4-}**
Porphyrin	**H_m**	-	8.30 (s)	8.46 (s)
	H_o	-	7.59 (s)	
	H_{py}	-	broadened	8.83 (br s)
Aminophenyl group	**H1**	7.48 (d, J = 7.6 Hz)	-	7.1 - 7.8 (br s)
	H2	7.38 (t, J = 7.7 Hz)	-	
	H3	6.86 (t, J = 7.2 Hz)	-	6.2 - 7.1 (br s)
	H4	6.92 (d, J = 8.6 Hz)	-	
β-CD group	**H1**	5.09 (s)	-	5.07 (br m)
	H2	3.3 - 4.3 (br m)	-	3.0 - 4.6 (br m)
	H3		-	
	H4		-	
	H5		-	
	H6		-	

Table 4.11: Summary of ^{1}H NMR resonances for β-CDab, H_2TMAP^{4+} and β-CDab·H_2TMAP^{4+} in D_2O phosphate buffer (pD 7.0, I = 0.10 mol dm^{-3}) at 298.2 K.

		β-CDab	**H_2TMAP^{4+}**	**β-CDab·H_2TMAP^{4+}**
Porphyrin	**CH_3**	-	3.95 (s)	4.03 (s)
	H_m	-	8.18 (s)	8.32 (s), 8.53 (s)
	H_o	-		
	H_{py}	-	8.84 (br s)	8.98 (br s)
Aminophenyl group	**H1**	7.48 (d, J = 7.6 Hz)	-	6.3 – 8.0
	H2	7.38 (t, J = 7.7 Hz)	-	
	H3	6.86 (t, J = 7.2 Hz)	-	
	H4	6.92 (d, J = 8.6 Hz)	-	
β-CD group	**H1**	5.09 (s)	-	5.02 (br m)
	H2	3.3 - 4.3 (br m)	-	3.2 - 4.7 (br m)
	H3		-	
	H4		-	
	H5		-	
	H6		-	

Table 4.12: Summary of ^{1}H NMR resonances for β-CDab, H_2TMPyP^{4+} and β-CDab·H_2TMPyP^{4+} in D_2O phosphate buffer (pD 7.0, I = 0.10 mol dm^{-3}) at 298.2 K.

		β-CDab	**H_2TMPyP^{4+}**	**β-CDab·H_2TMPyP^{4+}**
Porphyrin	**CH_3**	-	4.76 (s)	4.85 (s)
	H_m	-	9.32 (d, J = 5.7 Hz)	9.30 (d, J = 6.0 Hz)
	H_o	-	8.98 (d, J = 6.7 Hz)	8.98 (d, J = 6.1 Hz)
	H_{py}	-	9.14 (br s)	9.16 (br s)
Aminophenyl group	**H1**	7.48 (d, J = 7.6 Hz)	-	7.26 (t, J = 8.05 Hz)
	H2	7.38 (t, J = 7.7 Hz)	-	7.16 (d, J = 8.05 Hz)
	H3	6.86 (t, J = 7.2 Hz)	-	6.70 (t, J = 7.6 Hz)
	H4	6.92 (d, J = 8.6 Hz)	-	6.79 (d, J = 8.45 Hz)
β-CD group	**H1**	5.09 (s)	-	4.65 (d, J = 2.8 Hz), 4.58 (d, J = 2.8 Hz), 4.33 (d, J = 3.0 Hz)
	H2	3.3 - 4.3 (br m)	-	2.5 - 4.2 (br m)
	H3		-	
	H4		-	
	H5		-	
	H6		-	

The geometry of the complexes formed between all four porphyrins and β-CDab cannot be understood in terms of β-CD facial preferences. The H2 – H6 protons of the β-CD group show significant overlap due to the substiution of β-CD with an aminophenyl substituent as seen in Figure 4.10 – Figure 4.13. However, changes in the porphyrin resonances upon complexation with β-CDab are still apparent, indicating that all four porphyrins may form complexes with β-CDab, as discussed below. Additionally, the H1 – H4 aminophenyl resonances of β-CDab broaden upon complexation with all porphyrins except H_2TMPyP^{4+}.

The broadened aminophenyl resonances of β-CDab (Figure 4.10 – Figure 4.13) may infer some interaction between the aminophenyl substituents and the phenyl or pyrrole groups of the porphyrins. These interactions may be in the form of π-π interactions, which would stabilise the complex. The absence of such an interaction in the β-CDab·H_2TMPyP^{4+} complex may further suggest weak complexation.

The H_m and H_o resonances of H_2TSPP^{4-} shift downfield upon complexation with β-CDab as seen in Figure 4.10. The assignment of the H_m and H_o resonances in the β-CDab/H_2TSPP^{4-} spectrum is unclear, however, the shift is between 0.15 – 0.80 ppm. Additionally, the H_{py} resonance becomes apparent in the β-CDab/H_2TSPP^{4-} spectrum (Figure 4.10), indicating that β-CDab increases the rate of tautomerism to the fast exchange limit or slows it substantially upon dissociation of the porphyrin aggregate. This is also observed for the β-CDab/H_3TCPP^{3-}/H_2TCPP^{4-} system (Figure 4.11) consistent with both anionic porphyrins complexing through the phenyl groups.

The H_m and H_o resonances of H_2TMAP^{4+} change from an undifferentiated singlet to two distinct singlets upon complexation with β-CDab, shifting by between 0.14 – 0.35 ppm, while the CH_3 resonances shifts downfield by 0.08 ppm as seen in Figure 4.12. This indicates that complexation occurs dominantly through the phenyl groups of H_2TMAP^{4+} although complexation through the methyl groups is also possible. Interestingly, the shift in the CH_3 resonances of H_2TMAP^{4+} in the β-CDab/H_2TMAP^{4+} system is much greater than in the β-CD/H_2TMAP^{4+} system (Figure 4.8). Therefore, the aminophenyl substituent of β-CDab may form π-π interactions with the phenyl groups of H_2TMAP^{4+}, thereby enhancing the stability of a β-CDab·H_2TMAP^{4+} complex.

The H_m, H_o and CH_3 resonances of H_2TMPyP^{4+} do not show a significant change in chemical shift in the presence of β-CDab as seen in Figure 4.13. However, the H1 resonances of β-CDab appear as three distinct resonances resonances with chemical shifts between 4.33 – 4.65 ppm in the presence H_2TMPyP^{4+}, consistent with complex formation. The overall ^{1}H NMR pattern of the β-CDab/H_2TMPyP^{4+} system is analogous to that of the β-CD/H_2TMPyP^{4+} system, suggesting a weakly formed β-CDab·H_2TMPyP^{4+} complex.

4.2.1.2 Qualitative Investigation of Complexation by 2D ^{1}H ROESY NMR Spectroscopy

The complexation behaviour of H_2TSPP^{4-}, H_3TCPP^{3-}/H_2TCPP^{4-}, H_2TMAP^{4+} and H_2TMPyP^{4+} with either native β-CD or β-CDab was studied by 2D ^{1}H ROESY NMR spectroscopy. Solutions of each host-guest combination were prepared in D_2O phosphate buffer (pD 7.0, I = 0.10 mol dm^{-3}) at 298.2 K. The 2D ^{1}H ROESY NMR spectra for all host-porphyrin combinations are given in Figure 4.14 – Figure 4.21.

The 2D ^{1}H ROESY NMR spectra of the host/porphyrin systems closely reflect the 1D ^{1}H NMR spectra. The β-CD/H_2TSPP^{4-} spectrum produces cross-peaks between the H3, H5 and H6 resonances of β-CD and the H_{py}, H_m and H_o resonances of H_2TSPP^{4-}, indicating complexation (Figure 4.14). As the H5 and H6 protons are on the secondary face of β-CD, the complexation is likely favoured by the encapsulation of the porphyrin by the secondary face of β-CD, due to the wider opening and anti-parallel arrangement of dipole moments of β-CD and H_2TSPP^{4-}, consistent with the 1D NMR data. Similar results were obtained for the β-CD/H_3TCPP^{3-}/H_2TCPP^{4-} system (Figure 4.15).

The complexation of H_2TSPP^{4-} and H_3TCPP^{3-}/H_2TCPP^{4-} by β-CDab shows similar results, with cross-peaks arising between the H_m and H_o protons of the porphyrin and the H2 – H6 protons of β-CDab (Figure 4.18 – Figure 4.19). As the H2 – H6 protons of the β-CDab are all overlapped, no primary or secondary face complexation preference can be determined.

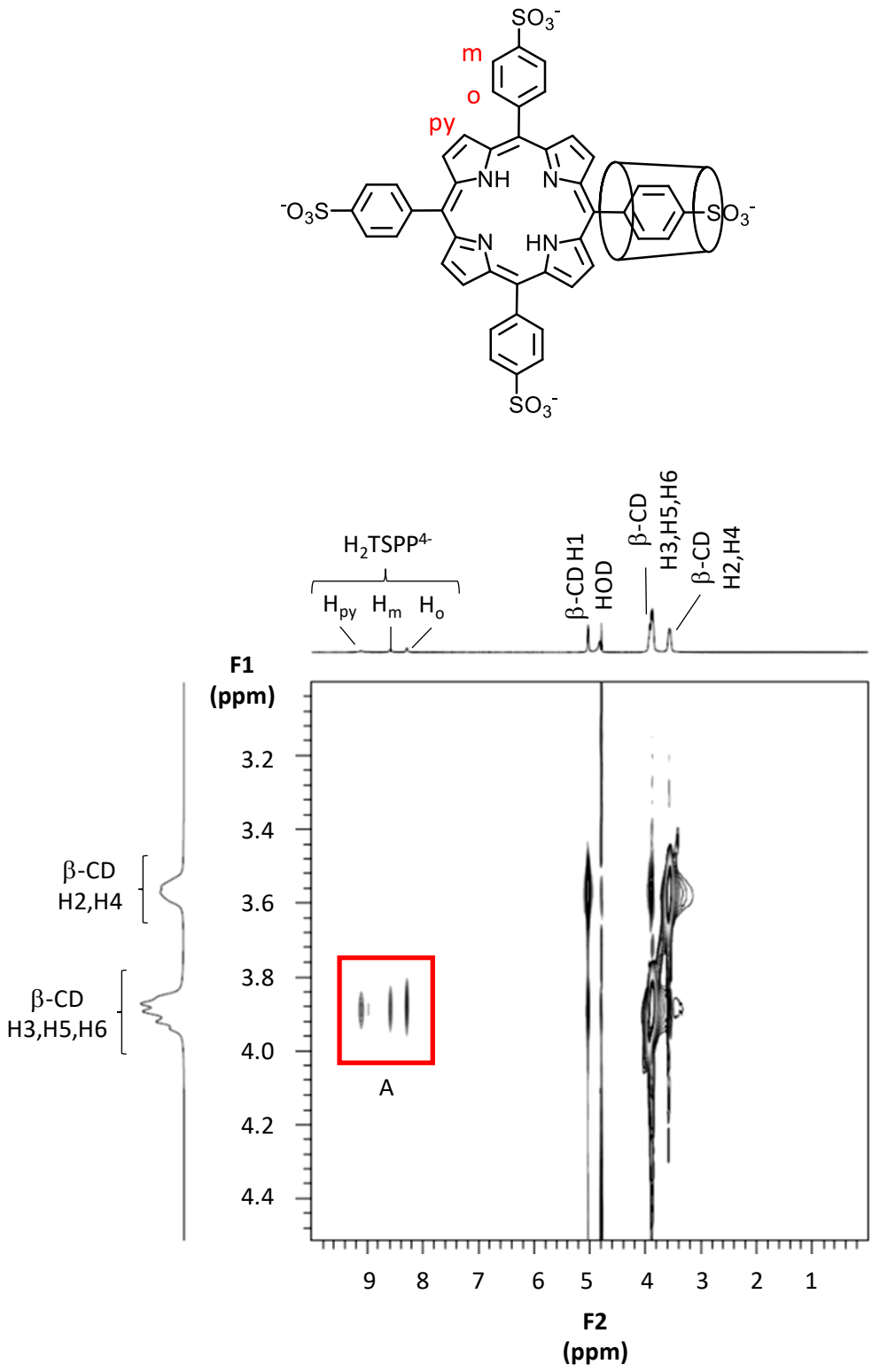

Figure 4.14: 2D ^{1}H ROESY NMR spectrum of β-CD (4.9×10^{-3} mol dm^{-3}) and H_2TSPP^{4-} (4.9×10^{-3} mol dm^{-3}) prepared in D_2O phosphate buffer (pD 7.0, I = 0.10 mol dm^{-3}) at 298.2 K. Rectangle A highlights cross-peaks arising from NOE interactions of the annular protons of β-CD with protons of H_2TSPP^{4-}. A possible dominant structure depicting a 1:1 complex is shown above.

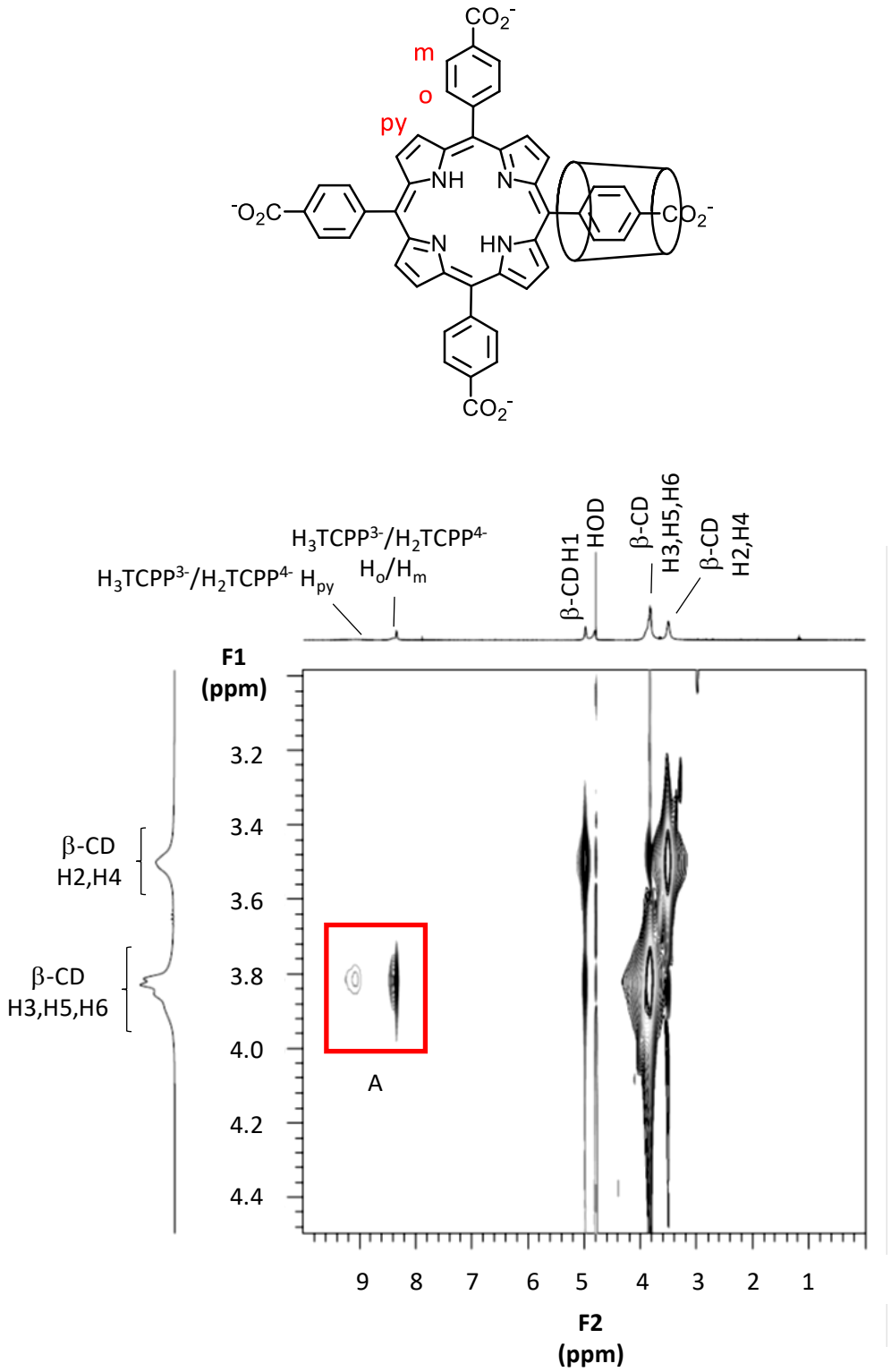

Figure 4.15: 2D ^{1}H ROESY NMR spectrum of β-CD (4.9×10^{-3} mol dm^{-3}) and $H_3TCPP^{3-}/H_2TCPP^{4-}$ (4.9×10^{-3} mol dm^{-3}) prepared in D_2O phosphate buffer (pD 7.0, I = 0.10 mol dm^{-3}) at 298.2 K. Rectangle A highlights cross-peaks arising from NOE interactions of the annular protons of β-CD with protons of $H_3TCPP^{3-}/H_2TCPP^{4-}$. A possible dominant structure depicting a 1:1 complex is shown above.

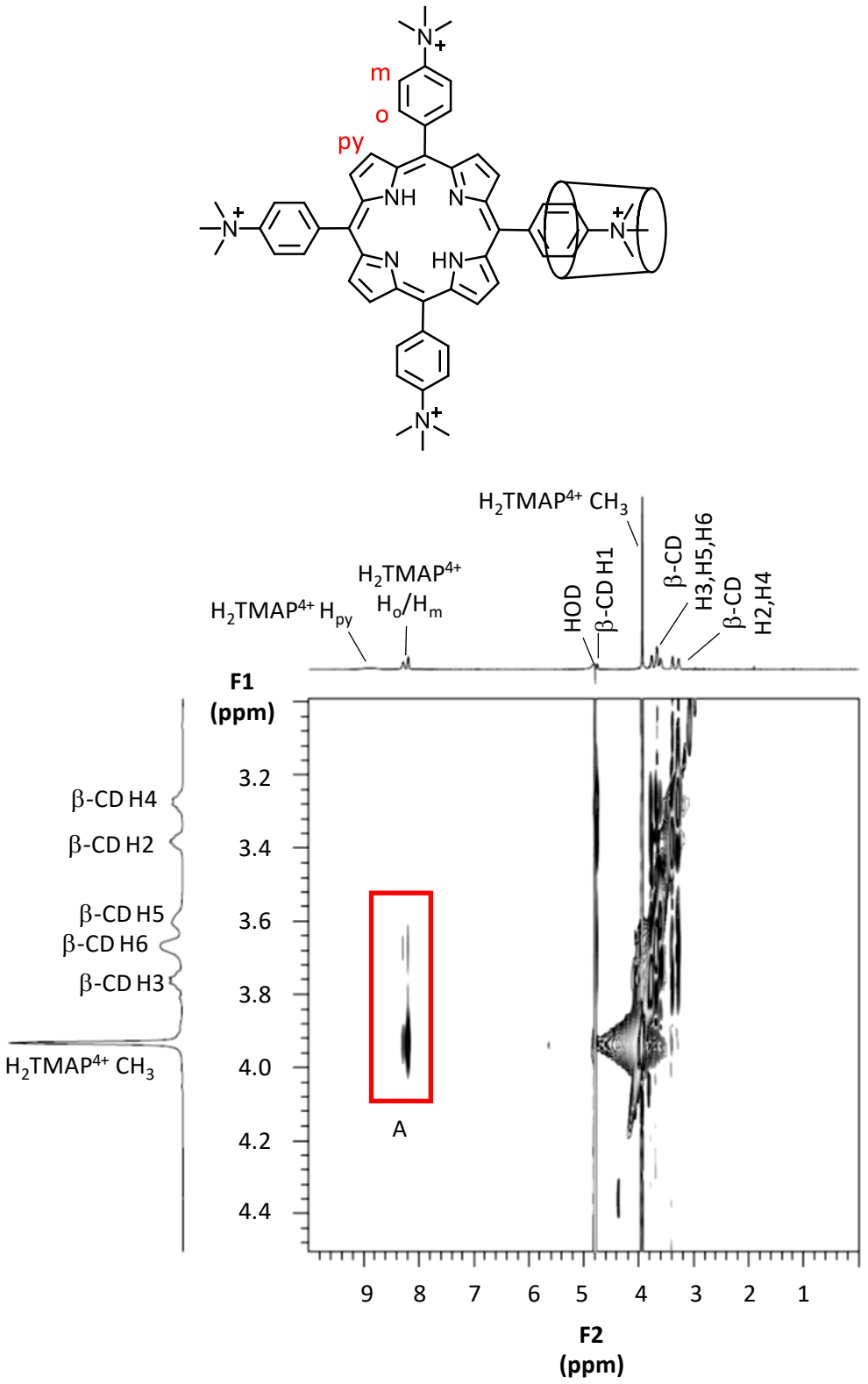

Figure 4.16: 2D ^{1}H ROESY NMR spectrum of β-CD (4.9×10^{-3} mol dm^{-3}) and H_2TMAP^{4+} (4.9×10^{-3} mol dm^{-3}) prepared in D_2O phosphate buffer (pD 7.0, I = 0.10 mol dm^{-3}) at 298.2 K. Rectangle A highlights cross-peaks arising from NOE interactions of the annular protons of β-CD with protons of H_2TMAP^{4+}. A possible dominant structure depicting 1:1 complex is shown above.

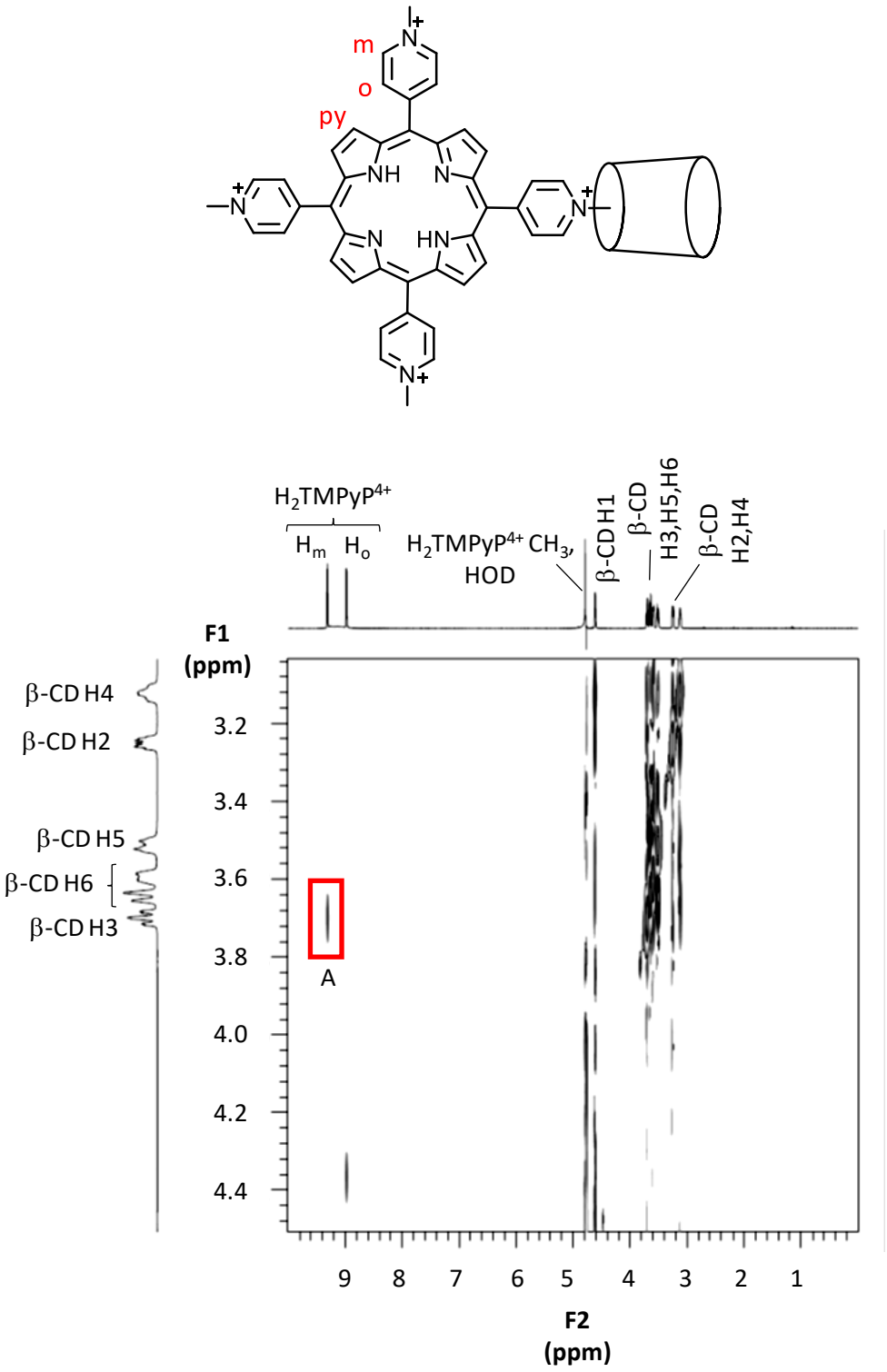

Figure 4.17: 2D ^{1}H ROESY NMR spectrum of β-CD (4.9×10^{-3} mol dm^{-3}) and H_2TMPyP^{4+} (4.9×10^{-3} mol dm^{-3}) prepared in D_2O phosphate buffer (pD 7.0, I = 0.10 mol dm^{-3}) at 298.2 K. Rectangle A highlights cross-peaks arising from NOE interactions of the annular protons of β-CD with protons of H_2TMPyP^{4+}. A possible dominant structure depicting a 1:1 complex is shown above.

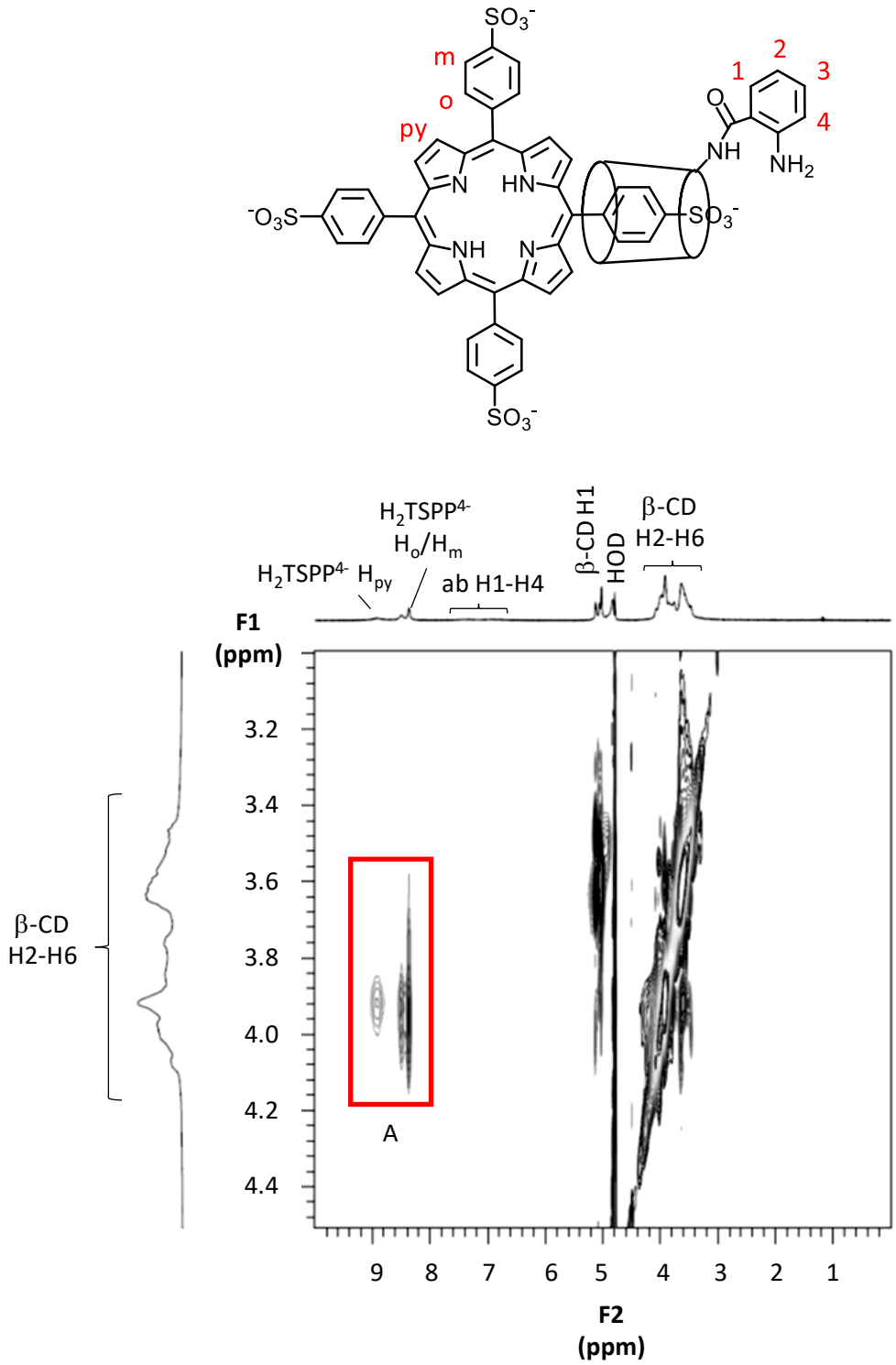

Figure 4.18: 2D ^{1}H ROESY NMR spectrum of β-CDab (6.4×10^{-3} mol dm^{-3}) and H_2TSPP^{4-} (3.2×10^{-3} mol dm^{-3}) prepared in D_2O phosphate buffer (pD 7.0, I = 0.10 mol dm^{-3}) at 298.2 K. Rectangle A highlights cross-peaks arising from NOE interactions of the annular protons of β-CD with protons of H_2TSPP^{4-}. A possible dominant structure depicting a 1:1 complex is shown above. The abbreviation 'ab' refers to the aminophenyl substituent of β-CDab.

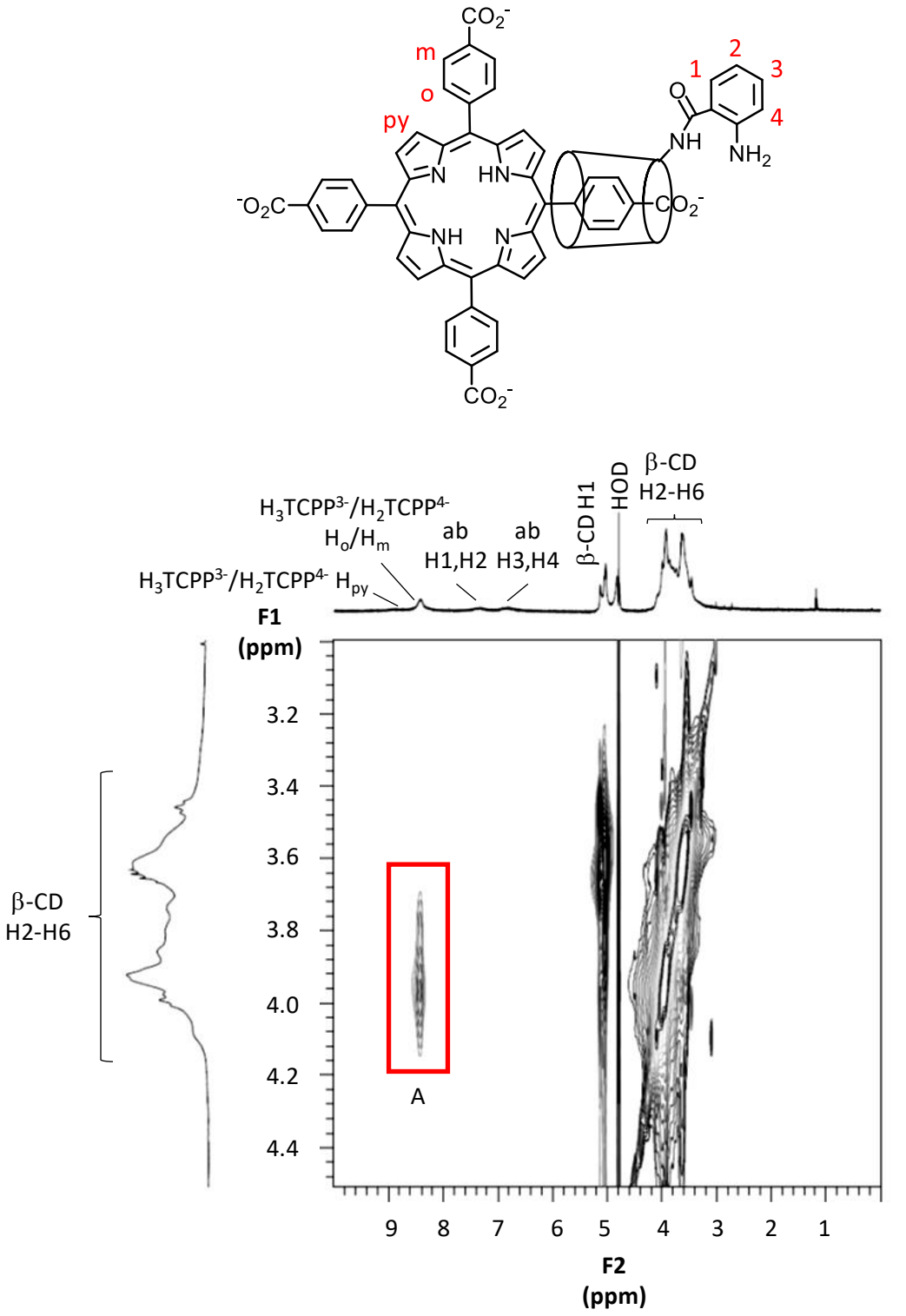

Figure 4.19: 2D ^{1}H ROESY NMR spectrum of β-CDab (6.4×10^{-3} mol dm^{-3}) and $H_3TCPP^{3-}/H_2TCPP^{4-}$ (3.2×10^{-3} mol dm^{-3}) prepared in D_2O phosphate buffer (pD 7.0, I = 0.10 mol dm^{-3}) at 298.2 K. Rectangle A highlights cross-peaks arising from NOE interactions of the annular protons of β-CD with protons of $H_3TCPP^{3-}/H_2TCPP^{4-}$. A possible dominant structure depicting a 1:1 complex is shown above. The abbreviation 'ab' refers to the aminophenyl substituent of β-CDab.

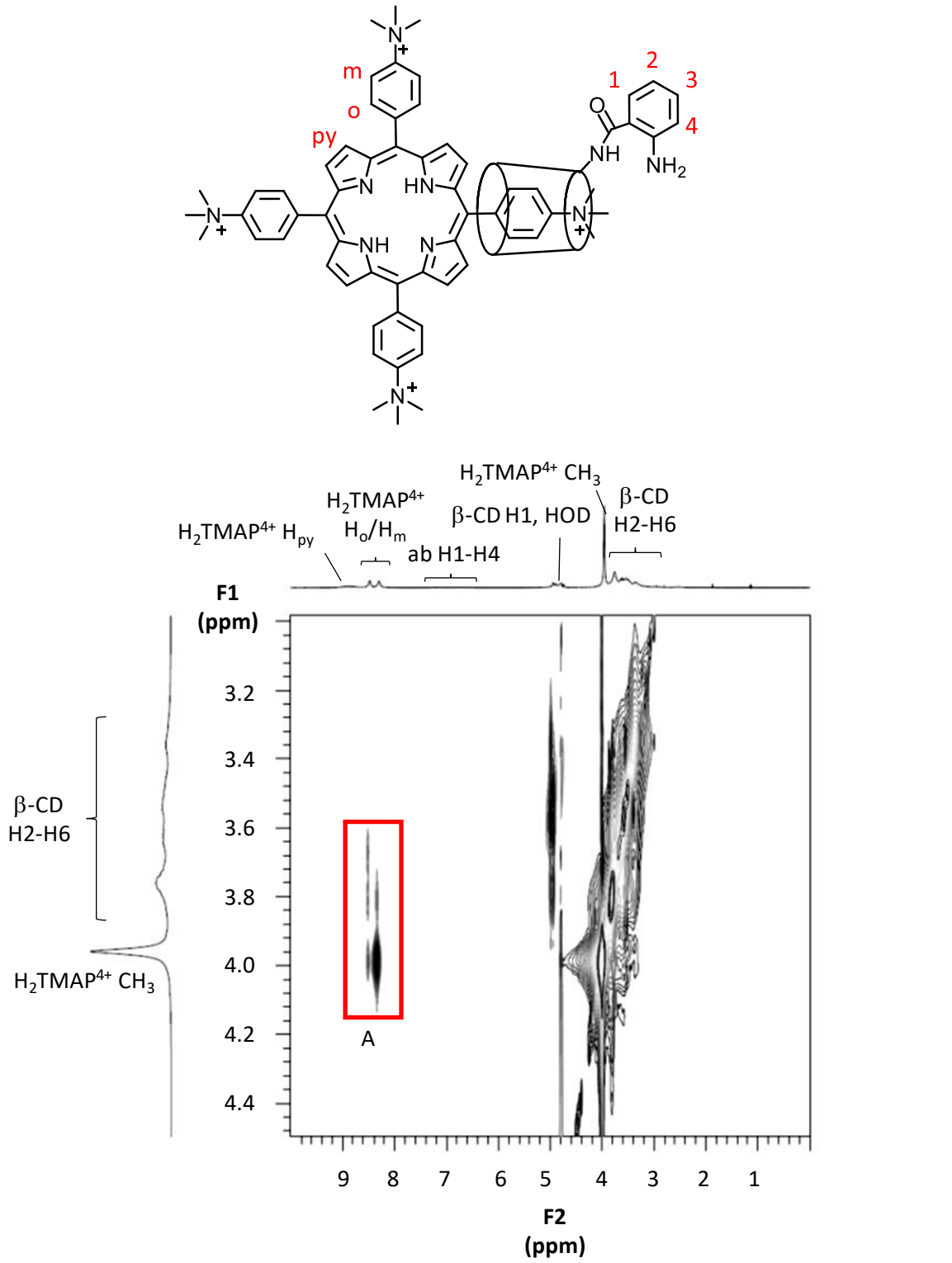

Figure 4.20: 2D ^{1}H ROESY NMR spectrum of β-CDab (6.4×10^{-3} mol dm^{-3}) and H_2TMAP^{4+} (3.2×10^{-3} mol dm^{-3}) prepared in D_2O phosphate buffer (pD 7.0, I = 0.10 mol dm^{-3}) at 298.2 K. Rectangle A highlights cross-peaks arising from NOE interactions of the annular protons of β-CD with protons of H_2TMAP^{4+}. A possible dominant structure depicting a 1:1 complex is shown above. The abbreviation 'ab' refers to the aminophenyl substituent of β-CDab.

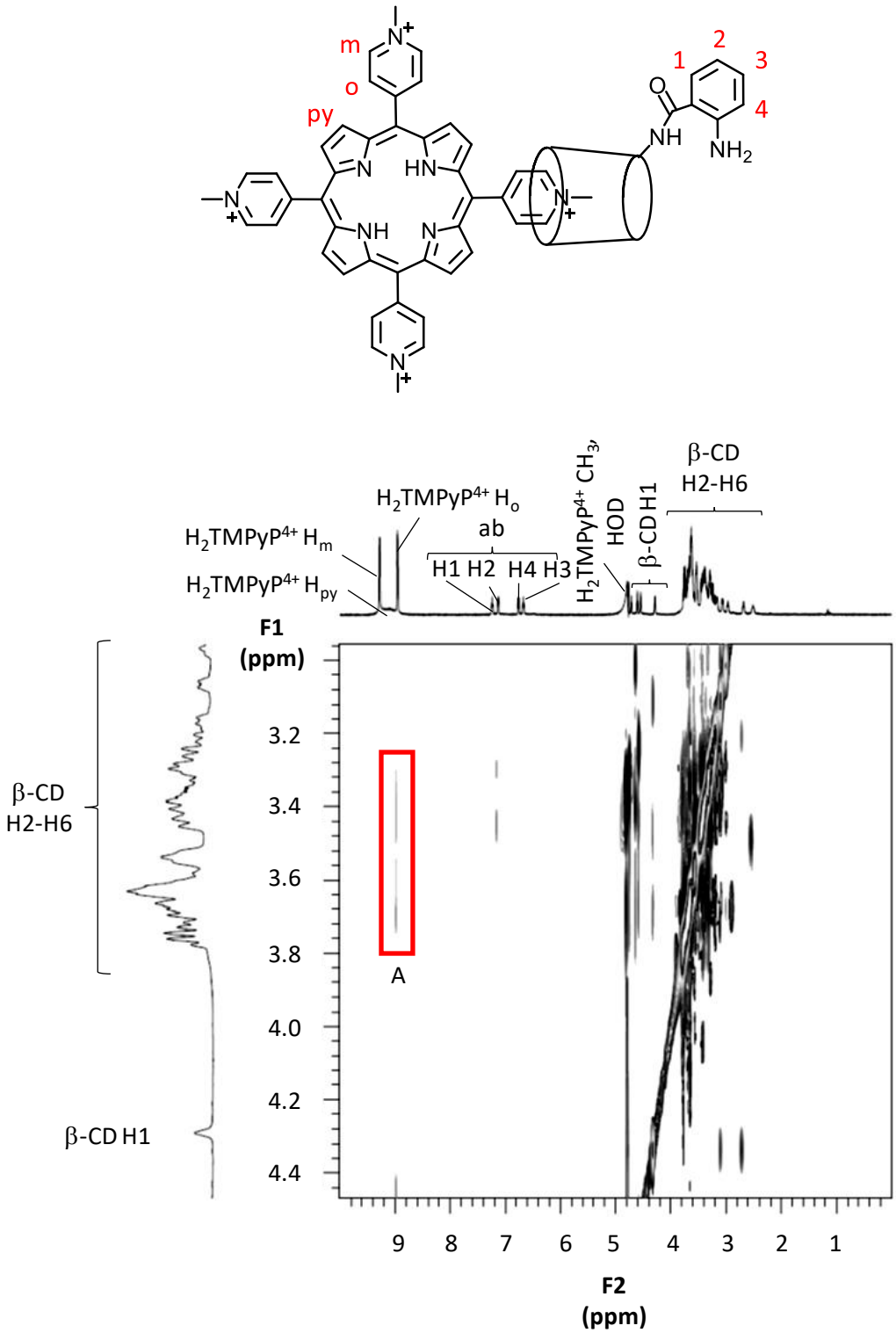

Figure 4.21: 2D ^{1}H ROESY NMR spectrum of β-CDab (6.4×10^{-3} mol dm^{-3}) and H_2TMPyP^{4+} (3.2×10^{-3} mol dm^{-3}) prepared in D_2O phosphate buffer (pD 7.0, I = 0.10 mol dm^{-3}) at 298.2 K. Rectangle A highlights cross-peaks arising from NOE interactions of the annular protons of β-CD with protons of H_2TMPyP^{4+}. A possible dominant structure depicting a 1:1 complex is shown above. The abbreviation 'ab' refers to the aminophenyl substituent of β-CDab.

The β-CD/H_2TMAP^{4+} spectrum produces minor cross-peaks between the H5 and H6 protons of β-CD and the H_m and H_o protons of H_2TMAP^{4+}, indicating complexation is possible, yet likely to be weak (Figure 4.16). As the 1D NMR spectrum produced an upfield shift of the CH_3 protons of H_2TMAP^{4+} upon complexation with β-CD, we may also expect to observe cross-peaks between these protons and the protons of β-CD. However, such cross-peaks are difficult to assign on the 2D ^{1}H ROESY NMR spectrum due to the small chemical shift difference between the CH_3 protons of H_2TMAP^{4+} and the H2 – H6 protons of β-CD. Nevertheless, the 1D and 2D NMR spectra of the β-CD/H_2TMAP^{4+} system are consistent with complex formation. The β-CDab/H_2TMAP^{4+} spectrum (Figure 4.20) showed similar results, with clear cross-peaks between the H_m and H_o protons of H_2TMAP^{4+} and the H2 – H6 protons of β-CDab.

The β-CD/H_2TMPyP^{4+} spectrum (Figure 4.17) produces minor cross-peaks arising between the H_m and CH_3 protons of H_2TMPyP^{4+} and the H2 – H6 protons of β-CD. However, cross-peaks arising from interactions with the CH_3 protons cannot be reliably assigned. As the 1D NMR spectrum did not show any change in the shifts of the H_2TMPyP^{4+} resonances and the 2D NMR shows only minor cross-peaks, the complexation is likely to be weak.

The β-CDab/H_2TMPyP^{4+} spectrum (Figure 4.21) produces minor cross-peaks between the H_{py} protons of H_2TMPyP^{4+} and the H2 – H6 protons of β-CDab. However, similar to the β-CD/H_2TMPyP^{4+} system, the cross-peaks arising from interactions with the CH_3 protons cannot be reliably assigned. Cross-peaks arising from the H_{py} protons of H_2TMPyP^{4+} but not the H_m or H_o protons may indicate some weak association.

In summary, the 1D and 2D NMR studies for the complexation of the four porphyrins by either β-CD or β-CDab show significant differences. The nature and location of the charge of the porphyrin are likely to strongly influence complexation. The two anionic porphyrins, H_2TSPP^{4-} and H_3TCPP^{3-} /H_2TCPP^{4-}, form a complex through penetration of the phenyl groups through the secondary face of β-CD, oppositely aligning the dipole moments of either species. Such an arrangement also results in the charged sulfonate and carbonate groups protruding into the bulk water and a disruption of porphyrin aggregates. The two cationic porphyrins, H_2TMAP^{4+} and H_2TMPyP^{4+}, showed no facial preference upon complexation by β-CD. Additionally, H_2TMAP^{4+} is likely to complex through both the phenyl and methyl groups, while H_2TMPyP^{4+} is likely to complex only weakly through the methyl groups. These results appear to correlate with those reported by Kano *et al.*, which suggested that cationic porphryins do not form strong complexes with CDs.[34] However, the stability of these complexes need to be analysed to further ascertain the validity of this statement.

4.2.1.3 Quantitative Investigation of Complexation by UV-vis spectroscopy

The complexation constants and thermodynamic parameters for the complexation of H_2TSPP^{4-}, $H_3TCPP^{3-}/H_2TCPP^{4-}$, H_2TMAP^{4+} and H_2TMPyP^{4+} by β-CD and β-CDab may in principle be determined by UV-vis spectroscopy. In practice this only proved possible for β-CD complexation of H_2TSPP^{4-} and $H_3TCPP^{3-}/H_2TCPP^{4-}$, and for β-CDab complexation of H_2TSPP^{4-}, $H_3TCPP^{3-}/H_2TCPP^{4-}$ and H_2TMAP^{4+} as is discussed below. The equilibrium expression for the 1:1 complexation of the host and porphyrin is given by Equation 4.3,

$$\text{host} + \text{porphyrin} \overset{K_{11}}{\rightleftharpoons} \text{host}\cdot\text{porphyrin} \tag{4.3}$$

where the host is either β-CD or β-CDab and the porphyrin is either H_2TSPP^{4-}, $H_3TCPP^{3-}/H_2TCPP^{4-}$, H_2TMAP^{4+} or H_2TMPyP^{4+}. The equation for the complexation constant, K_{11}, is given by Equation 4.4,

$$K_{11} = \frac{[host \cdot porphyrin]}{[host][porphyrin]} \tag{4.4}$$

The equilibrium expression for the 2:1 complexation of a second host to the existing host·porphyrin complex is given by Equation 4.5,

$$\text{host}\cdot\text{porphyrin} + \text{host} \overset{K_{21}}{\rightleftharpoons} \text{host}_2\cdot\text{porphyrin} \tag{4.5}$$

The equation for the complexation constant, K_{21}, is given by Equation 4.6,

$$K_{21} = \frac{[host_2 \cdot porphyrin]}{[host][host \cdot porphyrin]} \tag{4.6}$$

The change in Gibbs free energy for the first equilibrium describing a 1:1 host·porphyrin complex is given by Equation 4.7,

$$\Delta G_{11} = -RTlnK_{11} \tag{4.7}$$

where R is the ideal gas constant and T is the temperature. ΔG_{11} is also given by Equation 4.8,

$$\Delta G_{11} = \Delta H_{11} - T\Delta S_{11} \tag{4.8}$$

where ΔH_{11} and ΔS_{11} are the change in enthalpy and entropy for the formation of a 1:1 host·porphyrin complex, respectively. Combining Equation 4.7 and Equation 4.8 leads to the van't Hoff equation, given in Equation 4.9.

$$lnK_{11} = -\frac{\Delta H_{11}}{RT} + \frac{\Delta S_{11}}{R} \quad (4.9)$$

The complexation constants and thermodynamic parameters of complexation may be derived through titrations using UV-vis spectroscopy as the detection system. Detailed experimental procedures for the determination of complexation constants and thermodynamic parameters follow methods reported by Lincoln *et al.*[42-44] and have been previously outlined in Chapter 3.

The complexation constants and thermodynamic parameters for the complexation of the porphyrins by native β-CD and β-CDab were determined by UV-vis spectroscopy in aqueous phosphate buffer (pH 7.0, I = 0.10 mol dm^{-3}) at 308.2 K, 298.2 K, 288.2 K and 278.2 K. The effect of dimerisation was considered for each porphyrin.

Dimerisation presented a significant issue for the systems involving H_3TCPP^{3-}/H_2TCPP^{4-}. The K_D values for H_3TCPP^{3-}/H_2TCPP^{4-} in aqueous phosphate buffer (pH 7.0, I = 0.10 mol dm^{-3}) at 308.2 K, 298.2 K, 288.2 K and 278.2 K are 2.01 × 10^4 dm^{-3} mol^{-1}, 3.59 × 10^4 dm^{-3} mol^{-1}, 5.72 × 10^4 dm^{-3} mol^{-1} and 8.34 × 10^4 dm^{-3} mol^{-1}, corresponding to dimer proportions of 2.9%, 5.1%, 7.9% and 11.1%, respectively.[20] The effect of dimerisation could not be discounted and therefore, the K_D values and the known molar absorbances of the monomeric and dimeric forms[20] were used to aid in the fitting of the experimental data to derive the complexation constants.

The effect of dimerisation was not considered for H_2TSPP^{4-} as the dimer proportion was calculated to be <3% at 298.2 K, assuming a K_D of 1.54 × 10^4 dm^3 mol^{-1}.[23] Furthermore, McTernan demonstrated that the UV-vis absorption spectrum of H_2TSPP^{4-} in aqueous phosphate buffer (pH 7.0, I = 0.10 mol dm^{-3}) showed only minor changes in the λ_{max} and ε_{max} over the 288.2 – 308.2 K temperature range, indicating little influence of dimerisation.[20] Similarly, the effect of dimerisation was not considered for H_2TMAP^{4+} and H_2TMPyP^{4+} as they do not aggregate under the experimental conditions of the present study.[10,17,22,24,25]

4.2.1.3.1 UV-vis spectroscopic study of the Complexation of H_2TSPP^{4-} by β-CD

The variation of the absorption spectrum of an aqueous solution of H_2TSPP^{4-} as an aqueous solution of β-CD is titrated into it at 298.2 K is shown in Figure 4.22 a). (The conditions for the titration are given in the Figure captions.) The lack of an isobestic point in Figure 4.22 a) suggests that at least two complexes of H_2TSPP^{4-} form with different absorption spectra. Thus, it was unsurprising that an algorithm for the formation of a 1:1 β-CD·H_2TSPP^{4-} complex alone fitted the variation of the absorption spectrum poorly (Figure 4.49 and Figure 4.50 in 4.5 Appendix), whilst an algorithm for the sequential formation of 1:1 β-CD·H_2TSPP^{4-} and 2:1 (β-CD)$_2$·H_2TSPP^{4-} complexes (Equations 4.3 – 4.6) fitted the variation of the absorption spectrum well, as is seen in Figure 4.22 b). The derived spectra of β-CD·H_2TSPP^{4-} and (β-CD)$_2$·H_2TSPP^{4-} and the variation of their concentrations appear in Figure 4.22 c) and d). Similarly, good fits were obtained at 278.2 K, 288.2 K and 308.2 K (Figure 4.39 and Figure 4.40 in 4.5 Appendix). The derived K_{11}, K_{21}, ΔH^{o}_{11} and $T\Delta S^{o}_{11}$ appear in Table 4.13. The ΔH^{o}_{11} and $T\Delta S^{o}_{11}$ for this and the other four systems characterised were determined from van't Hoff plots as is discussed below.

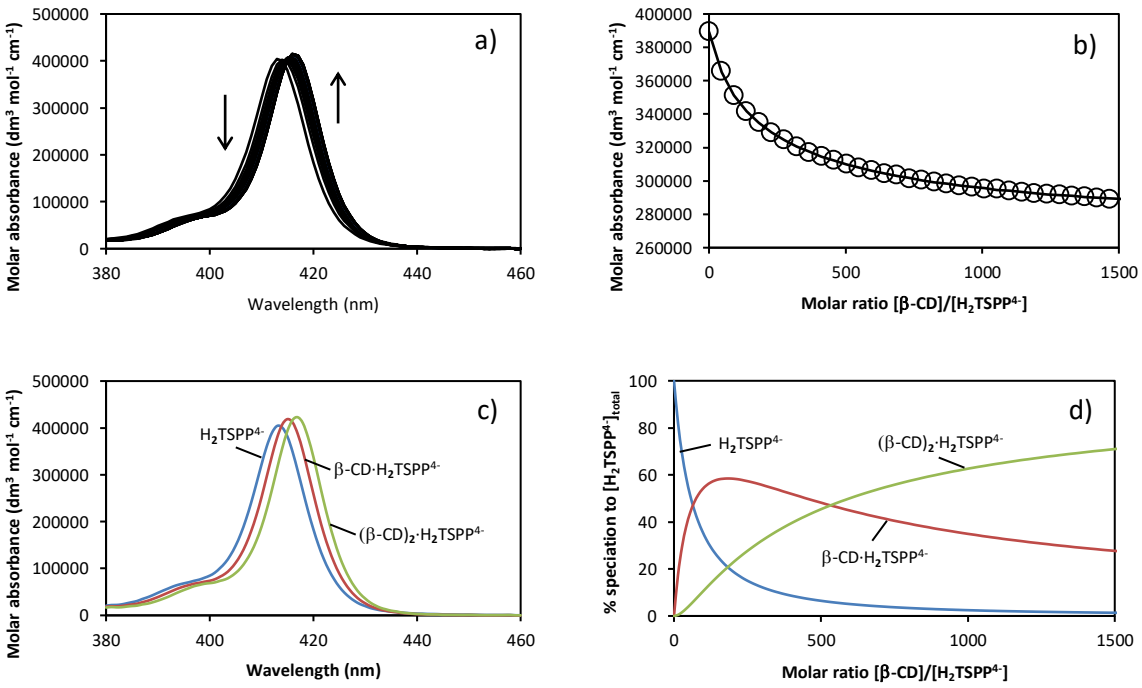

Figure 4.22: UV-vis absorbance data for H_2TSPP^{4-} (initial concentration 1.2 × 10^{-6} mol dm^{-3}) with increasing concentrations of β-CD (0 – 1.6 × 10^{-3} mol dm^{-3}) in aqueous phosphate buffer at pH 7.0 and I = 0.10 mol dm^{-3} at 298.2 K, showing a) the molar absorption spectra, the arrows indicating the direction of change, b) the experimental (circles) and best-fit (line) molar absorbances at 412 nm (fitted at 1 nm intervals over the range 400 – 425 nm) of the 1:1 β-CD·H_2TSPP^{4-} and 2:1 (β-CD)$_2$·H_2TSPP^{4-} complexes, c) the experimental molar absorbances of free H_2TSPP^{4-} and calculated molar absorbances of complexed H_2TSPP^{4-} and d) the calculated speciation of free and complexed H_2TSPP^{4-}. The concentration of β-CD was 0.011 mol dm^{-3}, and was titrated as 10 mm^3 aliquots into 2 cm^3 of a solution of H_2TSPP^{4-} in a 1 cm path length cell.

The equilibria characterising the β-CD/H_2TSPP^{4-} system are shown in Figure 4.23, where the orientation of the complexing β-CD as shown appears the most likely as deduced from the ^1H NMR studies, but the proportions of the *anti* and *syn* $(\beta\text{-CD})_2 \cdot H_2TSPP^{4-}$ complexes is uncertain.

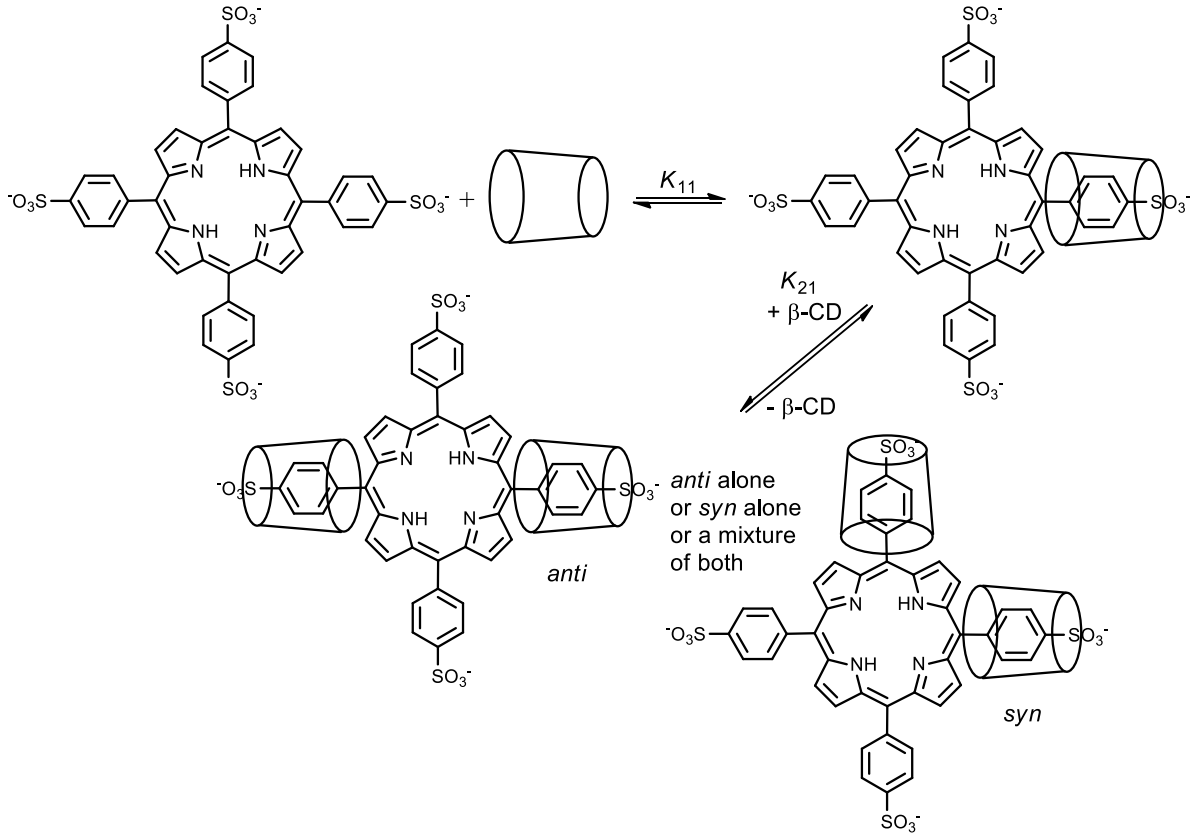

Figure 4.23: Equilibria characterising the β-CD/H_2TSPP^{4-} system.

4.2.1.3.2 UV-Vis Spectroscopic Study of the Complexation of $H_3TCPP^{3-}/H_2TCPP^{4-}$ by β-CD

The variation of the spectrum of an aqueous solution of $H_3TCPP^{3-}/H_2TCPP^{4-}$ as an aqueous solution of β-CD is titrated into it at 298.2 K is shown in Figure 4.24 a). The concentrations of H_3TCPP^{3-} and H_2TCPP^{4-} were calculated from the known dimerisation constant, K_D,[20] and incorporated into an algorithm for the formation of a 1:1 β-CD·$H_3TCPP^{3-}/H_2TCPP^{4-}$ complex (Equations 4.3 and 4.4) which fitted the variation of the spectrum well, as seen in Figure 4.24 b). The known spectra[20] of H_3TCPP^{3-} and H_2TCPP^{4-} and derived spectrum of the β-CD·$H_3TCPP^{3-}/H_2TCPP^{4-}$ complex and the variation of their concentrations appear in Figure 4.24 c) and d). Similarly, good fits were obtained at 278.2 K, 288.2 K and 308.2 K (Figure 4.41 and Figure 4.42 in 4.5 Appendix.). The derived K_{11}, ΔH^{o}_{11} and $T\Delta S^{o}_{11}$ appear in Table 4.13.

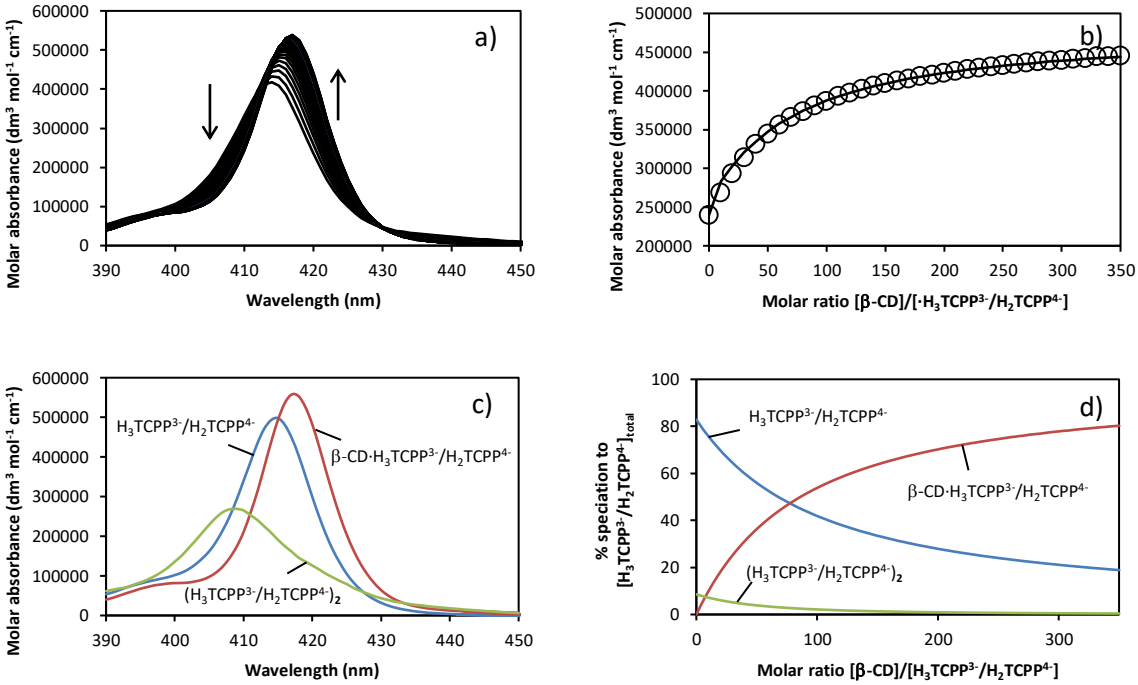

Figure 4.24: UV-vis absorbance data of $H_3TCPP^{3-}/H_2TCPP^{4-}$ (initial concentration 1.5×10^{-6} mol dm^{-3}) with increasing concentrations of β-CD ($0 - 3.6 \times 10^{-4}$ mol dm^{-3}) in aqueous phosphate buffer (pH 7.0 and I = 0.10 mol dm^{-3}), showing a) the molar absorption spectrum, the arrows indicating the direction of change, b) the experimental (circles) and best-fit (line) molar absorbances at 420 nm (fitted at 1 nm intervals over the range 400 – 425 nm) for a 1:1 β-CDab·$H_3TCPP^{3-}/H_2TCPP^{4-}$ complex, c) the experimental molar absorbances of free monomeric and dimeric $H_3TCPP^{3-}/H_2TCPP^{4-}$ and calculated molar absorbances of complexed $H_3TCPP^{3-}/H_2TCPP^{4-}$ and d) the calculated speciation of free and complexed $H_3TCPP^{3-}/H_2TCPP^{4-}$. The concentration of β-CD was 4.5×10^{-3} mol dm^{-3}, and was titrated as 5 mm^3 aliquots into 2 cm^3 of solution of $H_3TCPP^{3-}/H_2TCPP^{4-}$ in a 1 cm path length cell.

The equilibrium characterising the formation of the β-CD·H_2TCPP^{4-} complex is shown in Figure 4.25, where the orientation of the complexing β-CD as shown appears the most likely as deduced from the ^1H NMR studies. It is expected that the formation of the β-CD·H_3TCPP^{3-} complex occurs similarly.

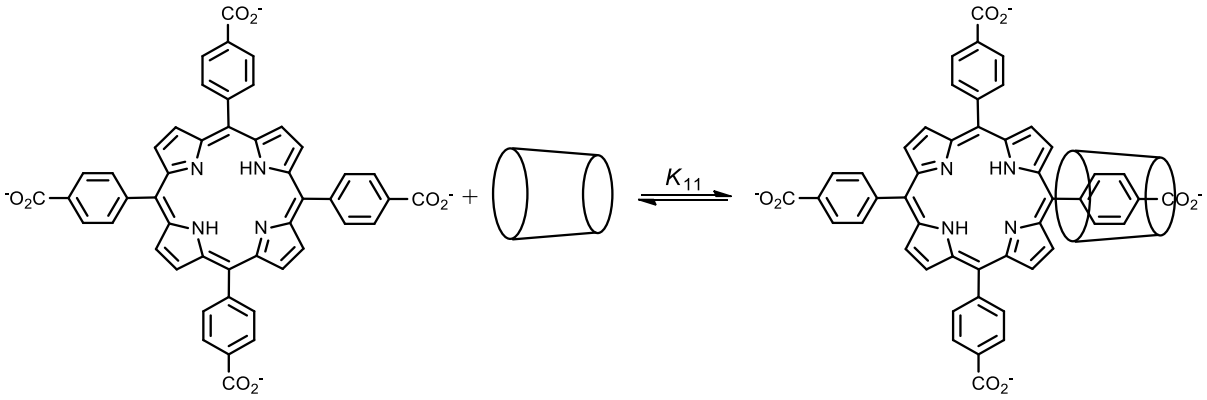

Figure 4.25: Equilibria characterising the β-CD/H_2TCPP^{4-} system. The formation of β-CD·H_3TCPP^{3-} is expected to occur similarly.

In order to determine the complexation properties of H_2TCPP^{4-} alone, attempts were made to determine the complexation at pH 10. At pH 10, TCPP would likely exist dominantly as a free base, H_2TCPP^{4-}, and therefore, reliable complexation constants and thermodynamic parameters may be derived.

Experiments using aqueous carbonate buffer (pH 10.0, I = 0.10 mol dm^{-3}) were attempted, following previous studies by Hamai and Ohshida.[45] However, it was noted that at pH 10, the absorbance of H_2TCPP^{4-} alone decreases over a 20 minute period at 308.2 and 298.2 K, as shown in Figure 4.26, likely as a result of decomposition. As a typical titration experiment requires at least 1 hour, the experiment could not be continued and therefore, the complexation properties of H_2TCPP^{4-} at pH 10 were not determined.

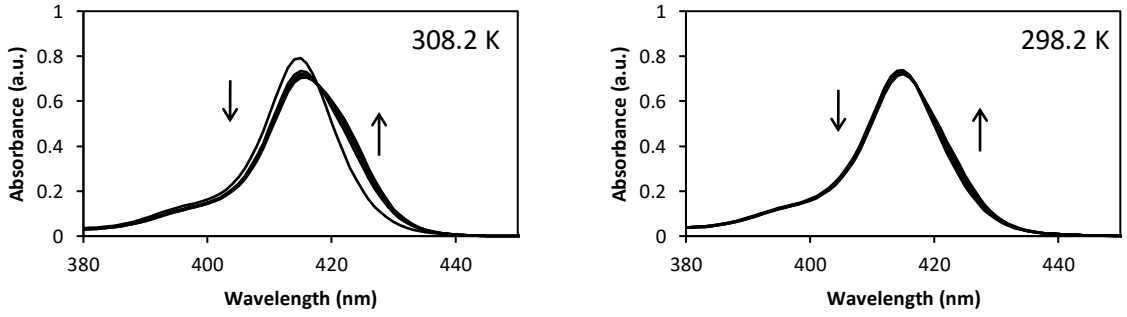

Figure 4.26: Absorbance of H_2TCPP^{4-} (2.0×10^{-6} mol dm^{-3}) in aqueous carbonate buffer (pH 10.0 and I = 0.10 mol dm^{-3}) over a 20-minute time period. The arrows indicate the direction of change.

4.2.1.3.3 UV-Vis Spectroscopic Study of the Complexation of H_2TMAP^{4+} and H_2TMPyP^{4-} by β-CD

The variation of the spectra of aqueous solutions of H_2TMAP^{4+} and H_2TMPyP^{4+} as an aqueous solution of β-CD is titrated into them at 298.2 K is shown in Figure 4.27 a) and b), respectively, consistent with complexation occurring as also evidenced by NMR spectroscopy. The change in the spectrum of H_2TMAP^{4-} is particularly small and it was not possible to fit an algorithm for either the formation of a 1:1 β-CD·H_2TMAP^{4+} complex alone (Equations 4.3 and 4.4) or together with the formation of the 2:1 $(\beta\text{-CD})_2\cdot H_2TMAP^{4+}$ complex (Equations 4.3 – 4.6). A similar situation prevailed for the β-CD/H_2TMPyP^{4+} system. It appears that the stabilities of the complexes may be too low to quantify under the experimental conditions. In the case of the β-CD/H_2TMAP^{4+} system, the absorption spectra of free and complexed H_2TMAP^{4+} may be too similar for quantitative characterisation of complexation. The unsatisfactory fitting for the 1:1 β-CD·H_2TMAP^{4-} and β-CD·H_2TMPyP^{4+} complexes are shown in Figure 4.51 and Figure 4.52 in 4.5 Appendix, respectively. This is further discussion in Section 4.2.1.3.11.

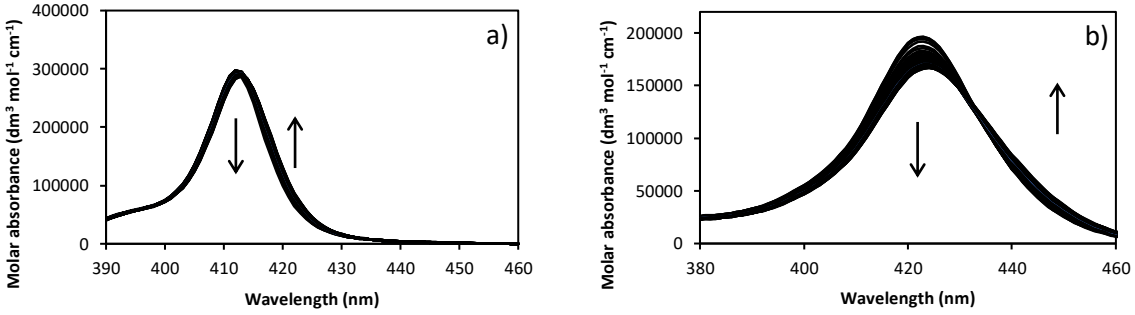

Figure 4.27: a) Molar absorbance of H_2TMAP^{4+} (2.5×10^{-6} mol dm^{-3}) with increasing concentrations of β-CD ($0 – 1.9 \times 10^{-3}$ mol dm^{-3}) in aqueous phosphate buffer (pH 7.0 and *I* = 0.10 mol dm^{-3}) at 298.2 K. The concentration of β-CD was 0.013 mol dm^{-3}, and was titrated as 10 mm^3 aliquots to a 2 cm^3 solution of H_2TMAP^{4+} in a 1 cm path length cell. b) Molar absorbance of H_2TMPyP^{4+} (2.5×10^{-6} mol dm^{-3}) with increasing concentrations of β-CD ($0 – 9.7 \times 10^{-4}$ mol dm^{-3}) in aqueous phosphate buffer (pH 7.0 and *I* = 0.10 mol dm^{-3}) at 298.2 K. The concentration of β-CD was 0.012 mol dm^{-3}, and was titrated as 10 mm^3 aliquots into 2 cm^3 solution of H_2TMPyP^{4+} in a 1 cm path length cell. The arrows indicate the direction of change.

4.2.1.3.4 UV-Vis Spectroscopic Study of the Complexation of H_2TSPP^{4-} by β-CDab

The variation of the spectrum of an aqueous solution of H_2TSPP^{4-} as an aqueous solution of β-CDab is titrated into it at 298.2 K is shown in Figure 4.28 a). The lack of an isobestic point in Figure 4.28 a) suggests that at least two complexes of H_2TSPP^{4-} with different absorption spectra form. An algorithm for the sequential formation of 1:1 β-CDab·H_2TSPP^{4-} and 2:1 (β-CDab)$_2$·H_2TSPP^{4-} complexes (Equations 4.3 – 4.6) fitted the variation of the absorption spectrum well, as is seen in Figure 4.28 b). The derived spectra of β-CDab·H_2TSPP^{4-} and (β-CDab)$_2$·H_2TSPP^{4-} and the variation of their concentrations appear in Figure 4.28 c) and d). Similarly, good fits were obtained at 278.2 K, 288.2 K and 308.2 K (Figure 4.43 and Figure 4.44 in 4.5 Appendix). The derived K_{11}, ΔH^{o}_{11} and $T\Delta S^{o}_{11}$ appear in Table 4.13.

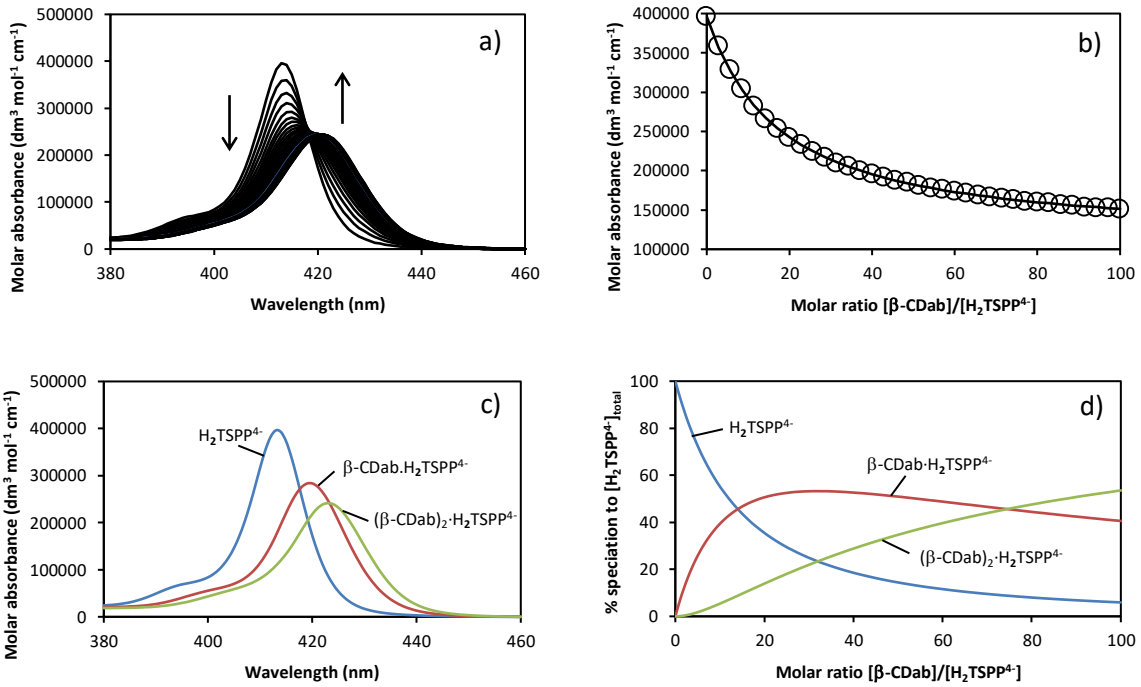

Figure 4.28: UV-vis absorbance data for H_2TSPP^{4-} (initial concentration 1.4×10^{-6} mol dm^{-3}) with increasing concentrations of β-CDab (0 – 1.3×10^{-4} mol dm^{-3}) in aqueous phosphate buffer (pH 7.0 and I = 0.10 mol dm^{-3}), showing a) the molar absorption spectra where the arrows indicate the direction of change, b) the experimental (circles) and best-fit (line) molar absorbances at 413 nm (fitted at 1 nm intervals over the range 400 – 430 nm) for 1:1 β-CDab·H_2TSPP^{4-} and 2:1 (β-CDab)$_2$·H_2TSPP^{4-} complexes, c) the experimental molar absorbances of free H_2TSPP^{4-} and calculated molar absorbances complexed H_2TSPP^{4-}, and d) the calculated speciation of free and complexed H_2TSPP^{4-}. The concentration of β-CDab was 1.6×10^{-3} mol dm^{-3}, and was titrated as 5 mm^3 aliquots into 2 cm^3 of the solution of H_2TSPP^{4-} in a 1 cm path length cell.

The equilibria characterising the formation of the β-CDab·H_2TSPP^{4-} and the (β-CDab)$_2$·H_2TSPP^{4-} complexes are shown in Figure 4.29, where the orientation of the complexing β-CDab shown appears the most likely as deduced from the ^{1}H NMR studies, but the proportions of the *anti* and *syn* (β-CDab)$_2$·H_2TSPP^{4-} complexes is uncertain.

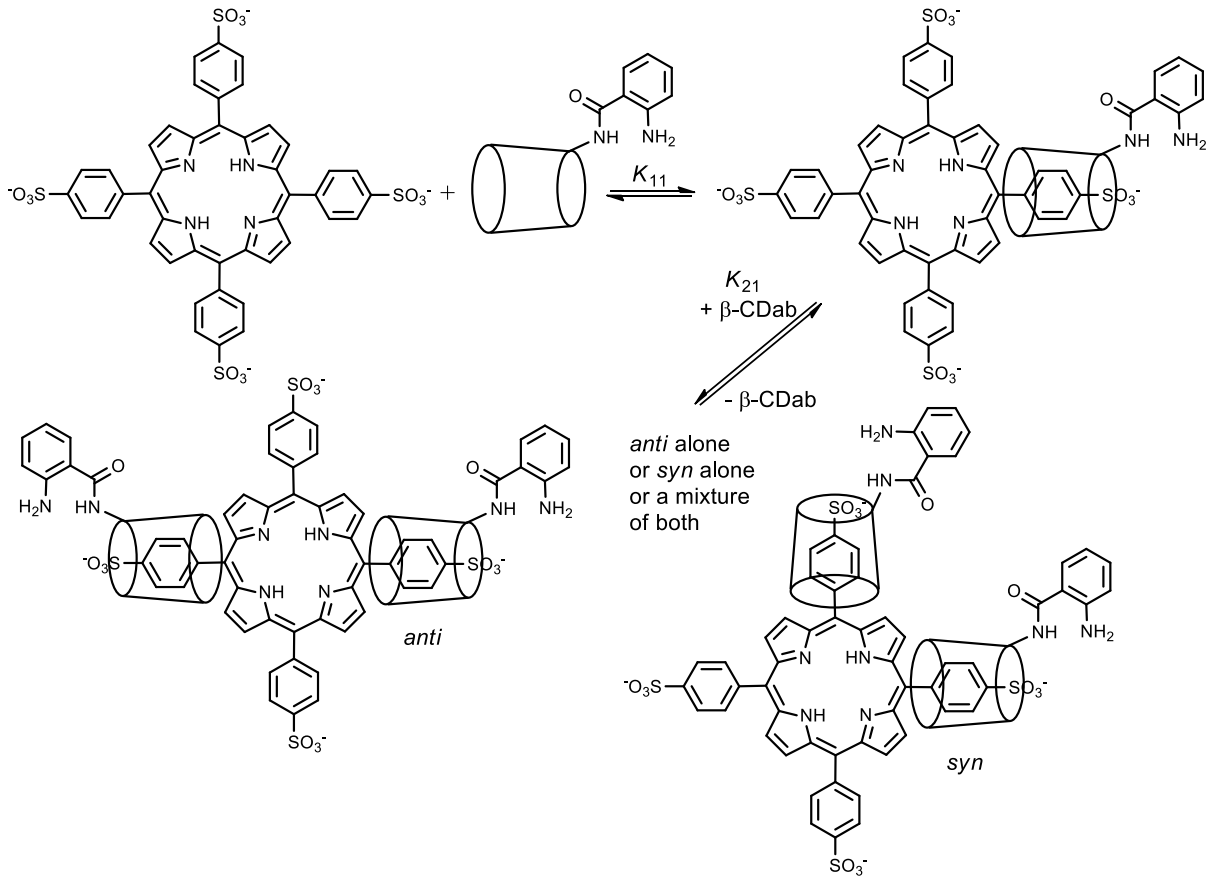

Figure 4.29: Equilibria characterising the β-CDab/H_2TSPP^{4-} system.

4.2.1.3.5 UV-Vis Spectroscopic Study of the Complexation of $H_3TCPP^{3-}/H_2TCPP^{4-}$ by β-CDab

The variation of the spectrum of an aqueous solution of $H_3TCPP^{3-}/H_2TCPP^{4-}$ as an aqueous solution of β-CDab is titrated into it at 298.2 K is shown in Figure 4.30 a). The concentrations of H_3TCPP^{3-} and H_2TCPP^{4-} were calculated from the known dimerisation constant K_D[20] and incorporated into an algorithm for the formation of a 1:1 β-CDab·$H_3TCPP^{3-}/H_2TCPP^{4-}$ complex (Equations 4.3 and 4.4) which fitted the variation of the spectrum well as seen in Figure 4.30 b). The known spectra[20] of H_3TCPP^{3-} and H_2TCPP^{4-} and derived spectrum of β-CDab·$H_3TCPP^{3-}/H_2TCPP^{4-}$ complex and the variation of their concentrations appear in Figure 4.30 c) and d). Similarly, good fits were obtained at 278.2 K, 288.2 K and 308.2 K (Figure 4.45 and Figure 4.46 in 4.5 Appendix). The derived K_{11}, ΔH^{o}_{11} and $T\Delta S^{o}_{11}$ appear in Table 4.13.

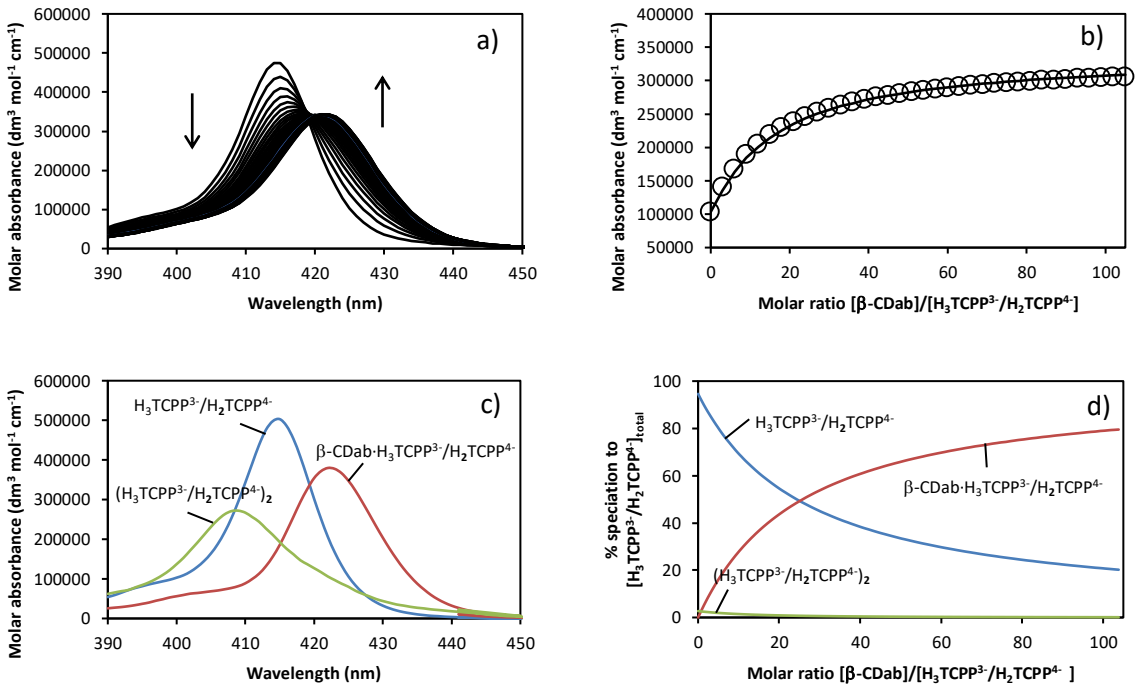

Figure 4.30: UV-vis absorbance data of $H_3TCPP^{3-}/H_2TCPP^{4-}$ (initial concentration 1.5×10^{-6} mol dm^{-3}) with increasing concentrations of β-CDab (0 – 1.4×10^{-4} mol dm^{-3}) in aqueous phosphate buffer (pH 7.0 and I = 0.10 mol dm^{-3}), showing a) the molar absorption spectrum, the arrows indicating the direction of change, b) the experimental (circles) and best-fit (line) molar absorbances at 425 nm (fitted at 1 nm intervals over the range 400 – 430 nm) for a 1:1 β-CDab·$H_3TCPP^{3-}/H_2TCPP^{4-}$ complex, c) the experimental molar absorbances of free monomeric and dimeric $H_3TCPP^{3-}/H_2TCPP^{4-}$ and the calculated molar absorbance complexed $H_3TCPP^{3-}/H_2TCPP^{4-}$, and d) the calculated speciation of free and complexed $H_3TCPP^{3-}/H_2TCPP^{4-}$. The concentration of β-CDab was 1.8×10^{-3} mol dm^{-3}, and was titrated as 5 mm^3 aliquots into 2 cm^3 of a solution of $H_3TCPP^{3-}/H_2TCPP^{4-}$ in a 1 cm path length cell.

The equilibrium characterising the formation of the β-CDab·H_2TCPP^{4-} complex is shown in Figure 4.31, where the orientation of the complexing β-CDab as shown appears the most likely as deduced from the ^1H NMR studies. It is anticipated that the formation of β-CDab·H_3TCPP^{3-} occurs similarly.

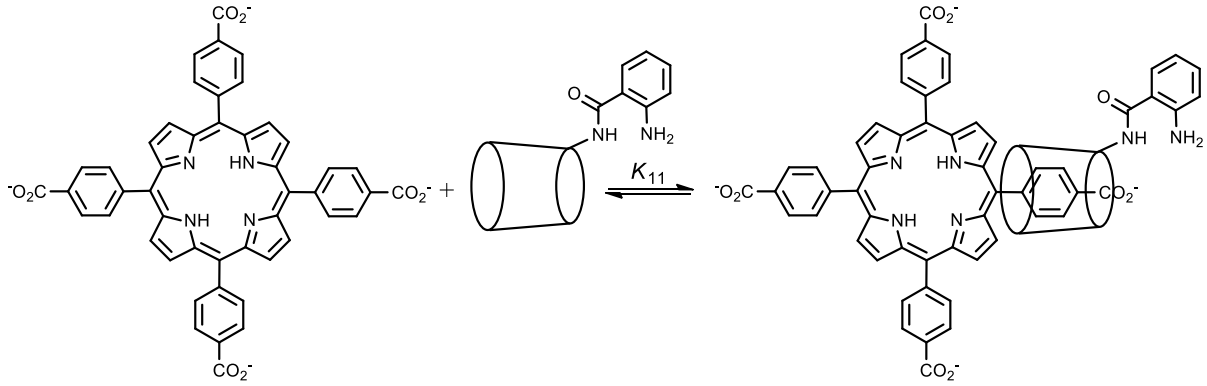

Figure 4.31: Equilibria characterising the β-CDab/H_2TCPP^{4-} system. The formation of β-CDab·H_3TCPP^{3-} is expected to occur similarly.

4.2.1.3.6 UV-Vis Spectroscopic Study of the Complexation of H_2TMAP^{4+} by β-CDab

The variation of the spectrum of an aqueous solution of of H_2TMAP^{4+} as an aqueous solution of β-CDab is titrated into it at 298.2 K is shown in Figure 4.32 a). An algorithm for the formation of a 1:1 β-CDab·H_2TMAP^{4+} complex (Equation 4.3 and 4.4) fitted the variation of the absorption spectrum well as seen in Figure 4.32 b). The molar absorbance spectra of the β-CDab/H_2TMAP^{4+} system showed a slight broadening of the apparent isobestic point with a decrease in temperature (Figure 4.47 and Figure 4.48 in 4.5 Appendix). However, it was not possible to fit the data to an algorithm characterising the sequential formation of 1:1 β-CDab·H_2TMAP^{4+} and 2:1 $(\beta\text{-CDab})_2\cdot H_2TMAP^{4+}$ complexes. Thus, while the 2:1 complex may exist, the stability of the complex may be too weak to characterise or the molar absorbance spectrum of the $(\beta\text{-CDab})_2\cdot H_2TMAP^{4+}$ complex is too similar to either H_2TMAP^{4+} or β-CDab·H_2TMAP^{4+}. The known spectrum of H_2TMAP^{4+} and derived spectrum of the β-CDab·H_2TMAP^{4+} complex and the variation of their concentrations appear in Figure 4.32 c) and d). Similarly, good fits were obtained at 278.2 K, 288.2 K and 308.2 K (Figure 4.47 and Figure 4.48 in 4.5 Appendix). The derived K_{11}, ΔH^{o}_{11} and $T\Delta S^{o}_{11}$ appear in Table 4.13.

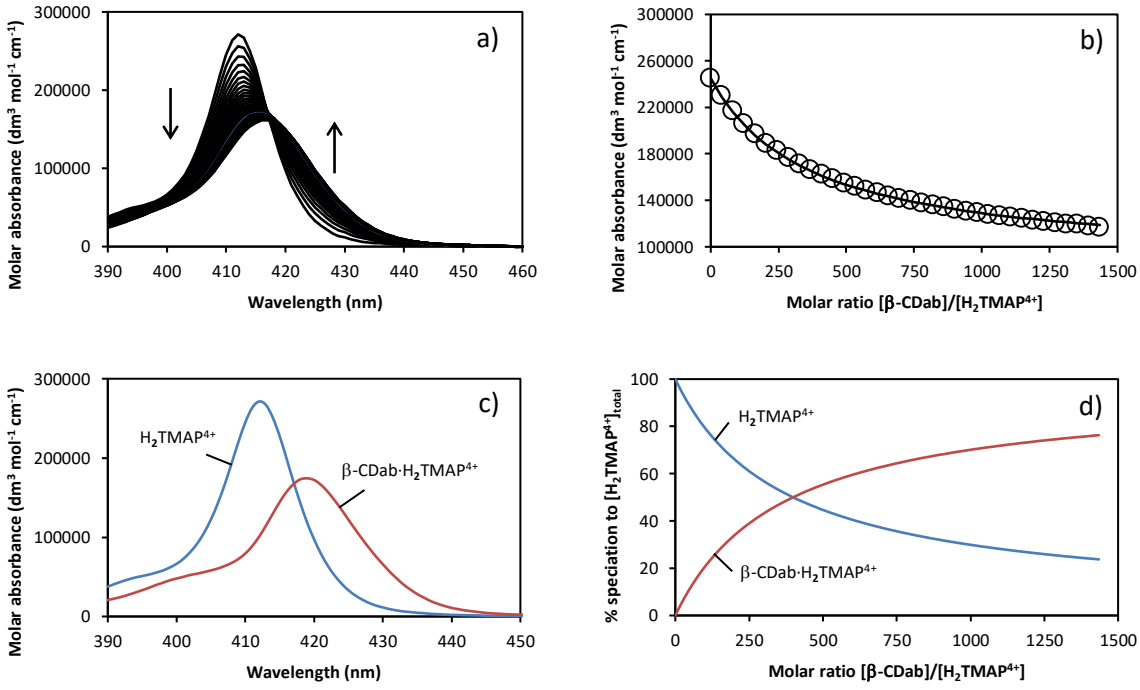

Figure 4.32: UV-vis absorbance data of H_2TMAP^{4+} (initial concentration 2.5×10^{-6} mol dm^{-3}) with increasing β-CDab ($0 - 3.0 \times 10^{-3}$ mol dm^{-3}) in aqueous phosphate buffer (pH 7.0 and I = 0.10 mol dm^{-3}), showing a) the molar absorption spectrum, arrows indicate direction of change, b) the experimental (circles) and best-fit (line) molar absorbances at 410 nm (fitted at 1 nm intervals over 400 – 430 nm) for a 1:1 β-CDab·H_2TMAP^{4+} complex, c) the experimental molar absorbances of free H_2TMAP^{4+} and the calculated molar absorbance of complexed H_2TMAP^{4+} and d) the calculated speciation of free and complexed H_2TMAP^{4+}. The concentration of β-CDab was 2.0×10^{-3} mol dm^{-3} and was titrated as 10 mm^3 aliquots into 2 cm^3 of a solution of H_2TMAP^{4+} in a 1 cm path length cell.

The equilibrium characterising the formation of the β-CDab·H_2TMAP^{4-} complex is shown in Figure 4.33, where the orientation of the complexing β-CDab as shown appears the most likely as deduced from the ^{1}H NMR studies.

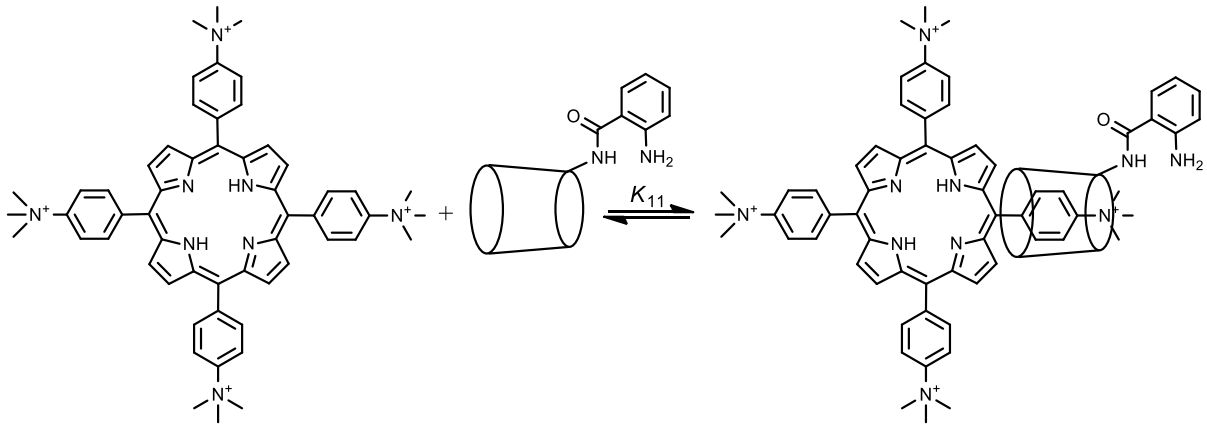

Figure 4.33: Equilibria characterising the β-CD/H_2TMAP^{4+} system.

4.2.1.3.7 UV-Vis Spectroscopic Study of the Complexation of H_2TMPyP^{4-} by β-CDab

The variation of the spectra of aqueous solutions of H_2TMPyP^{4+} as an aqueous solution of β-CDab is titrated into it at 308.2 K is shown in Figure 4.34. The change in the spectrum of the H_2TMPyP^{4+} is small and it was not possible to fit an algorithm for either the formation of a 1:1 β-CDab·H_2TMPyP^{4+} complex alone (Equations 4.3 and 4.4) or together with the formation of the 2:1 (β-CDab)$_2$·H_2TMPyP^{4+} complex (Equations 4.3 – 4.6). It appears that the stabilities of the complexes may be too low to quantify under the experimental conditions. The unsatisfactory fitting for the 1:1 β-CDab·H_2TMPyP^{4+} complex is shown in Figure 4.53 in 4.5 Appendix. This is further discussed in Section 4.2.1.3.15.

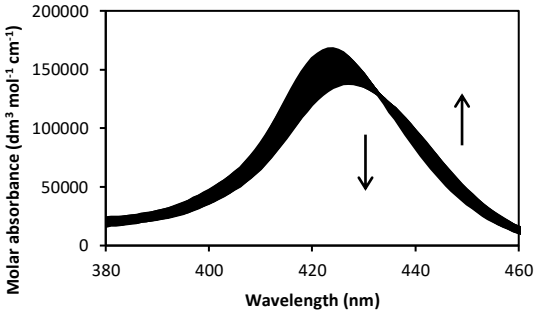

Figure 4.34: Molar absorbance of H_2TMPyP^{4+} (2.5×10^{-6} mol dm^{-3}) with increasing concentrations β-CDab ($0 – 2.4 \times 10^{-3}$ mol dm^{-3}) in aqueous phosphate buffer (pH 7.0 and I = 0.10 mol dm^{-3}) at 308.2 K. The concentration of β-CDab was 0.016 mol dm^{-3}, titrating with 10 mm^3 aliquots to a 2 cm^3 solution of H_2TMPyP^{4+} in a 1 cm path length cell. The arrows indicate the direction of change.

4.2.1.3.8 Determination of thermodynamic parameters

The complexation constants for the 1:1 host·porphyrin complexes, K_{11}, determined at 278.2 K, 288.2 K, 298.2 K and 308.2 K were used to construct van't Hoff plots and derive ΔG_{11}, ΔH_{11} and ΔS_{11} of complexation. The van't Hoff plots arising from the complexation of H_2TSPP^{4-}, $H_3TCPP^{3-}/H_2TCPP^{4-}$ and H_2TMAP^{4+} by β-CD and β-CDab are shown in Figure 4.35. An algorithm for the van't Hoff equation was best-fitted to the K_{11} data using the *GraphPad Prism* protocol.[46] A summary of the complexation constants and thermodynamic parameters for each system is given in Table 4.13.

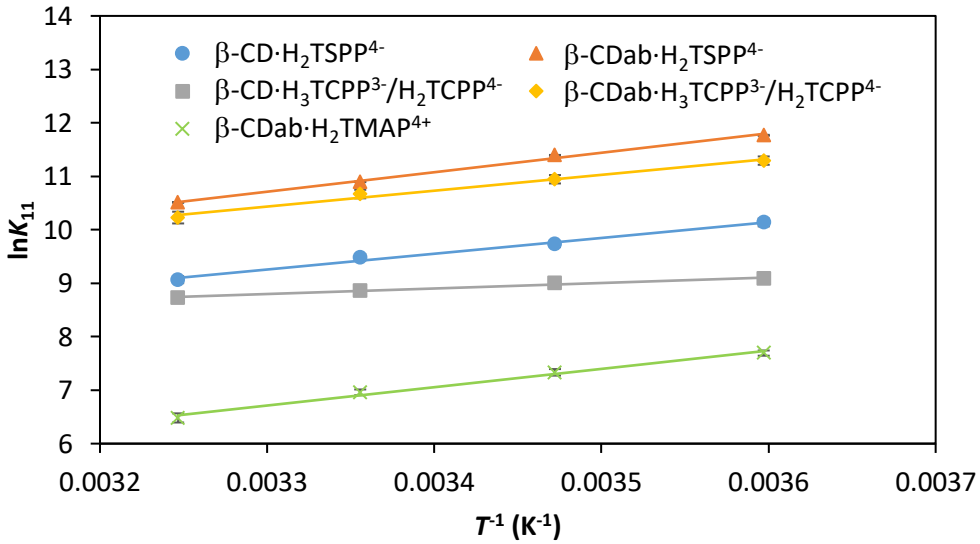

Figure 4.35: Plots of lnK_{11}, as determined by UV-vis spectroscopy at various temperatures, against T^{-1} for the β-CD·H_2TSPP^{4-} complex (R^2 = 0.989), the β-CDab·H_2TSPP^{4-} complex (R^2 = 0.996), the β-CD·$H_3TCPP^{3-}/H_2TCPP^{4-}$ complex (R^2 = 0.982), the β-CDab·$H_3TCPP^{3-}/H_2TCPP^{4-}$ complex (R^2 = 0.988) and the β-CDab·H_2TMAP^{4+} complex (R^2 = 0.990). The icons represent the experimental data and the solid lines represent the best-fit of the van't Hoff equation to the K_{11} data derived using the *GraphPad Prism* protocol.[46] The R^2 values refer to the fit of Equation 4.9 to the K_{11} data. The error bars represent the fitting errors.

Table 4.13: Complexation constants and thermodynamic parameters for the complexation of H_2TSPP^{4-}, $H_3TCPP^{3-}/H_2TCPP^{4-}$, H_2TMAP^{4+} or H_2TMPyP^{4+} with either β-CD or β-CDab in aqueous phosphate buffer (pH 7.0 and I = 0.10 mol dm^{-3}) at varying temperatures.

System	T (K)	10^{-3} K_{11}[a] (dm mol^{-1})	10^{-3} K_{21}[a] (dm mol^{-1})	$\Delta G°_{11}$[b] (kJ mol^{-1})	$\Delta H°_{11}$[c] (kJ mol^{-1})	$T\Delta S°_{11}$[d] (kJ K^{-1} mol^{-1})
β-CD·H_2TSPP^{4-}	308.2	8.67 ± 0.01	1.46 ± 0.01	-23.3 ± 0.1	-24.6 ± 1.8	-1.27 ± 0.09
	298.2	13.2 ± 0.1	1.69 ± 0.01	-23.3 ± 0.1	-24.6 ± 1.8	-1.23 ± 0.09
	288.2	16.8 ± 0.1	2.44 ± 0.01	-23.4 ± 0.1	-24.6 ± 1.8	-1.19 ± 0.09
	278.2	25.2 ± 0.1	3.45 ± 0.01	-23.4 ± 0.1	-24.6 ± 1.8	-1.15 ± 0.08
β-CDab·H_2TSPP^{4-}	308.2	36.7 ± 0.1	5.32 ± 0.02	-26.9 ± 0.1	-30.3 ± 1.4	-3.40 ± 0.16
	298.2	54.0 ± 0.1	10.4 ± 0.1	-27.0 ± 0.1	-30.3 ± 1.4	-3.29 ± 0.16
	288.2	88.6 ± 0.1	16.2 ± 0.1	-27.2 ± 0.1	-30.3 ± 1.4	-3.18 ± 0.15
	278.2	129 ± 1	21.3 ± 0.1	-27.3 ± 0.1	-30.3 ± 1.4	-3.07 ± 0.15
β-CD·H_3TCPP^{3-} /H_2TCPP^{4-}	308.2	6.18 ± 0.01	-	-22.4 ± 0.1	-8.56 ± 0.81	13.8 ± 1.3
	298.2	7.07 ± 0.01	-	-22.0 ± 0.1	-8.56 ± 0.81	13.4 ± 1.3
	288.2	8.11 ± 0.01	-	-21.5 ± 0.1	-8.56 ± 0.81	12.9 ± 1.2
	278.2	8.83 ± 0.01	-	-21.1 ± 0.1	-8.56 ± 0.81	12.5 ± 1.2
β-CDab·H_3TCPP^{3-} /H_2TCPP^{4-}	308.2	27.7 ± 0.1	-	-26.3 ± 0.1	-24.7 ± 1.9	1.61 ± 0.13
	298.2	42.9 ± 0.1	-	-26.3 ± 0.1	-24.7 ± 1.9	1.55 ± 0.12
	288.2	56.7 ± 0.1	-	-26.2 ± 0.1	-24.7 ± 1.9	1.50 ± 0.12
	278.2	80.3 ± 0.1	-	-26.2 ± 0.1	-24.7 ± 1.9	1.45 ± 0.11
β-CDab·H_2TMAP^{4+}	308.2	0.65 ± 0.01	-	-16.7 ± 0.1	-28.5 ± 2.0	-11.8 ± 0.8
	298.2	1.05 ± 0.1	-	-17.1 ± 0.1	-28.5 ± 2.0	-11.4 ± 0.8
	288.2	1.53 ± 0.1	-	-17.5 ± 0.1	-28.5 ± 2.0	-11.0 ± 0.8
	278.2	2.19 ± 1.7	-	-17.9 ± 0.1	-28.5 ± 2.0	-10.6 ± 0.7

[a] Errors calculated from UV-vis titration data using *HypSpec* fitting program and rounded up to the last significant figure. [b] Errors calculated using the errors of K_{11} and the equation $\Delta G_{11} = -RT\ln K_{11}$ and rounded up the last significant figure [c] Errors calculated from the van't Hoff plot using *GraphPad Prism* software. [d] Errors calculated from the sum of the relative errors in ΔG_{11} and ΔH_{11}, derived from van't Hoff plots of $\ln K_{11}$ against $1/T$. The errors do not take into account experimental, estimated to be ≤ 5% for K_{11} and ≤ 10% for K_{21}.

4.2.1.3.9 Complexation of H_2TSPP^{4-} by β-CD

The addition of β-CD to a solution of H_2TSPP^{4-} results in a red shift in λ_{max} of 2 nm at 298.2 K, and an increase in the overall ε_{max} from 4.04 × 10^{-6} mol dm^{-1} cm^{-1} to 4.19 × 10^{-6} mol dm^{-1} cm^{-1}. The experimental absorbance spectra did not yield a sharp isobestic point and thus, both 1:1 and 2:1 complexes were identified and the K_{11} and K_{21} were derived.

The magnitude of the K_{21} is only 12.8% of the K_{11} at 298.2 K, which is expected as the probability of a favourable collision leading to reaction is decreased as one *p*-sulfonatophenyl group of H_2TSPP^{4-} is already complexed in the β-CD·H_2TSPP^{4-} precursor complex. The geometry of the 2:1 β-CD_2·H_2TSPP^{4-} complex is unknown. The 1D and 2D NMR spectra of the 1:1 β-CD·H_2TSPP^{4-} complex indicated that the *p*-sulfonatophenyl groups of H_2TSPP^{4-} enter the β-CD cavity through the secondary face. However, the second β-CD may adopt either an *anti-* or *syn*-conformation, adding through the primary or secondary face of β-CD. Further in-depth studies would be needed to determine the preferred geometry, although Kano *et al.* has suggested that a dominant *anti*-conformation for the complexation of H_2TSPP^{4-} by β-CD[34] is likely, due to the reduction in steric clash between β-CD groups.

The $T\Delta S_{11}$ value for the β-CD·H_2TSPP^{4-} complex is negative, indicating that the entropic loss associated with the formation of a complex offsets the entropic gain from the expulsion of water molecules from the β-CD cavity upon complexation. These thermodynamic values, however, contrast previous studies. Kano *et al.* and Reinhoudt *et al.* determined a positive entropic contribution of the β-CD·H_2TSPP^{4-} complex in water at 298 K, using UV-vis spectroscopy and isothermal titration calorimetry (ITC), respectively, owing to the displacement of water molecules from both the β-CD cavity and porphyrin.[32,34,47] The results may differ from those conducted in this study due to slight experimental differences such as the presence of a buffer, pH and solute concentrations. For example, the higher porphyrin concentrations required for ITC must take into consideration the heat release profiles associated with aggregation.

4.2.1.3.10 Complexation of H_3TCPP^{3-}/H_2TCPP^{4-} by β-CD

The complexation of H_3TCPP^{3-}/H_2TCPP^{4-} by β-CD has some similarities to H_2TSPP^{4-}. The trends in the λ_{max} and ε_{max} of H_3TCPP^{3-}/H_2TCPP^{4-} upon complexation with β-CD are the same as those established by H_2TSPP^{4-}, as is the magnitude of the K_{11}. Therefore, it is likely that β-CD complexes H_3TCPP^{3-}/H_2TCPP^{4-} through the secondary face.

It is important to remember that any further analysis must take into consideration the distribution of the di-acid, mono-acid and free base forms of TCPP present in a solution at pH 7. Solutions in this study consisted of 3% H_4TCPP^{2-}, 27% H_3TCPP^{3-} and 70% H_2TCPP^{4-}. Therefore, the derived K_{11} for the

β-CD/H_3TCPP^{3-}/H_2TCPP^{4-} system represents the weighted mean of the two K_{11} pertaining to β-CD·H_3TCPP^{3-} and β-CD·H_2TCPP^{4-}. As H_4TSPP^{2-} and H_2TSPP^{4-} have been shown to complex β-CD with different K_{11} complexation constants,[15] H_3TCPP^{3-} and H_2TCPP^{4-} are not expected to complex β-CD or β-CDab with similar K_{11}.

Additionally, the relative ratios of H_3TCPP^{3-} and H_2TCPP^{4-} may alter across the four temperatures studied as the pK_a values of the porphyrin change with temperature. It has been reported that the pK_a values of common organic bases increase by 0.05 – 0.3 pH units per 10 K temperature rise,[48,49] while the addition of a β-CD host may also alter the pK_a values.[15] The low pK_a values for the protonation of H_2TSPP^{4-} (pK_{a1} = 4.85 and pK_{a2} = 4.91 at 298.2 K),[18] H_2TMAP^{4+} (pK_{a1} = 2.3 and pK_{a2} = 3.6 at 298.2 K)[17] and H_2TMPyP^{4+} (pK_{a1} = <1 and pK_{a2} = 1.4 at 298.2 K)[19] ensures that the porphyrins remain almost exclusively as free bases at pH 7.0 over the temperature range studied. However, the higher pK_a values for H_2TCPP^{4-} (pK_{a1} = 6.0 and pK_{a2} = 6.6 at 298.2 K)[17] indicate that significant variation of the ionic states may occur across the four temperatures. Assuming the largest change of 0.3 pH units per 10 K increase in temperature, the pK_a values of H_2TCPP^{4-} may significantly vary: pK_{a1} = 5.7 – 6.6 and pK_{a2} = 6.3 – 7.2. Hence, there may be significant variation in the proportion of H_3TCPP^{3-} and H_2TCPP^{4-} across the four temperatures rendering the derived thermodynamic parameters erroneous. Thus, no further analysis is performed.

It was not possible to derive the individual complexation constants and thermodynamic parameters for β-CD·H_3TCPP^{3-} and β-CD·H_2TCPP^{4-} complexes. The attempts to determine the complexation at pH 10 were not successful due to the significant degradation of H_2TCPP^{4-}.

4.2.1.3.11 Complexation of H_2TMAP^{4+} and H_2TMPyP^{4+} by β-CD

The complexation properties of the two cationic porphyrins, H_2TMAP^{4+} and H_2TMPyP^{4+}, are significantly different to the anionic porphyrins. The complexation constants for the β-CD·H_2TMAP^{4+} and β-CDab·H_2TMPyP^{4+} complexes could not be derived. This was unsurprising, given that both the 1D and 2D ^{1}H NMR spectra suggested that only weak complexes form. It would be difficult to quantify the K_{11} of a weak complex using UV-vis spectroscopy as a high host:porphyrin ratio would be required, which is beyond the solubility limits of β-CD. Additionally, K_{11} are difficult to derive for complexes that have similar absorption spectra to the uncomplexed guest.

The addition of β-CD to solutions of H_2TMAP^{4+} and H_2TMPyP^{4+} did not significantly vary the absorbance. The wavelengths chosen for study by UV-vis spectroscopy occur due to the Soret Band and therefore, significant variation of the phenyl or pyrrole protons of the porphyrins must occur upon complexation with the host. However, if the complexes are weak or characterised by

interactions between the alkyl groups of the porphyrin and the β-CD cavity, the chemical environment surrounding the phenyl and pyrrole protons of the porphyrin would not significantly vary. This is evident by the change in the UV-vis spectrum of both H_2TMAP^{4+} and H_2TMPyP^{4+} upon addition of β-CD, which shows a shift in λ_{max} of only 1 nm for both systems. Therefore, UV-vis spectroscopy or other experiments relying on optical properties may not be suitable to determine the complexation properties of cationic porphyrins.

The lack of K_{11} derivation of the β-CD/H_2TMAP^{4+} and β-CD/H_2TMPyP^{4+} systems demonstrates that the nature of the porphyrin charge is an important consideration. Kano *et al.* has previously discussed that the partially positive internal cavity of CD would favour the complexation of negatively charged species.[34] This statement appears to be validated by this research.

4.2.1.3.12 Complexation of H_2TSPP^{4-} by β-CDab

Generally, the addition of β-CDab to a solution of a porphyrin resulted in a greater change in the absorption spectra of that porphyrin. The larger spectral change is associated with the interaction between the aminophenyl substitutent of β-CDab and the phenyl and pyrrole groups of the porphyrin. Thus, the local hydrophobicity of the phenyl and pyrrole groups of the porphyrin show more significant variation for the β-CDab systems by comparison with the β-CD systems.

The addition of β-CDab to a solution of H_2TSPP^{4-} results in a red shift in λ_{max} of 7 nm at 298.2 K and a decrease in the overall ε_{max} from 4.04×10^{-6} mol dm^{-1} cm^{-1} to 2.83×10^{-6} mol dm^{-1} cm^{-1}. As the addition of β-CD to a solution of H_2TSPP^{4-} resulted in an increase in ε_{max}, the β-CDab·H_2TSPP^{4-} complex is likely to have a different complexation geometry to the β-CD·H_2TSPP^{4-} complex. The 1D and 2D NMR spectra of the β-CD·H_2TSPP^{4-} complex indicated that the *p*-sulfonatophenyl groups of H_2TSPP^{4-} enter the β-CD cavity through the secondary face. Therefore, β-CDab·H_2TSPP^{4-} may be characterised by a primary face preference instead. This orientation would allow the aminophenyl groups of β-CDab to interact with tetrapyrrole core of H_2TSPP^{4-}, increasing the stability of the complex through π-π interactions. This is evident by the three-fold increase in the K_{11} at 298.2 K of the β-CDab·H_2TSPP^{4-} complex and decrease in ΔH_{11} by comparison with the β-CD·H_2TSPP^{4-} complex. A preferential primary face orientation for the β-CDab·H_2TSPP^{4-} complex indicates that the strength of the favourable aminophenyl – pyrrole interaction overcomes the unfavourable parallel alignment of dipole moments of β-CDab and H_2TSPP^{4-}.

The $T\Delta S_{11}$ values for the β-CDab·H_2TSPP^{4-} complex is negative, indicating that the entropic loss associated with the formation of a complex offsets the entropic gain from the expulsion of water molecules from the β-CD cavity upon complexation. Similar to the β-CD·H_2TSPP^{4-} complex, these

thermodynamic values contrast studies by Kano *et al.* and Reinhoudt *et al.* who determined a positive entropic contribution for a β-CD·H_2TSPP^{4-} complex in water at 298 K. The differences are likely due to the experimental differences between the studies.

The 2:1 complex, characterised by K_{21}, was also detected for the β-CDab/H_2TSPP^{4-} system. The magnitude of the K_{21} is only 19.3% of the K_{11} at 298.2 K, which is expected as the probability of a favourable collision leading to reaction is decreased as one *p*-sulfonatophenyl group of H_2TSPP^{4-} is already complexed in the β-CDab·H_2TSPP^{4-} precursor complex. Furthermore, the K_{21} of the (β-CDab)$_2$·H_2TSPP^{4-} complex is a similar magnitude to the K_{11} of the β-CD·H_2TSPP^{4-} complex system. Therefore, the second β-CDab may complex through the secondary face of β-CD to minimise unfavourable steric interactions between the aminophenyl substituent of the first β-CDab. Thus, the K_{21} is not characterised by π-π interactions between the aminophenyl substituent of the second β-CDab and the pyrrole and phenyl groups of H_2TSPP^{4-}.

4.2.1.3.13 Complexation of H_3TCPP^{3-}/H_2TCPP^{4-} by β-CDab

The trends in the λ_{max} and ε_{max} of H_3TCPP^{3-}/H_2TCPP^{4-} upon complexation with β-CDab are the same as those established by H_2TSPP^{4-}. The K_{11} of the β-CDab·H_3TCPP^{3-}/H_2TCPP^{4-} complex is 6 times greater than the K_{11} for the β-CD·H_3TCPP^{3-}/H_2TCPP^{4-} complex, consistent with β-CDab complexing H_3TCPP^{3-}/H_2TCPP^{4-} through the primary face, maximising the interaction between the aminophenyl substituents of β-CDab and the phenyl and pyrrole groups of H_3TCPP^{3-}/H_2TCPP^{4-}. This extra stabilising interaction also corresponds to a more negative ΔH_{11} and more positive $T\Delta S_{11}$ for the β-CDab·H_3TCPP^{3-}/H_2TCPP^{4-} complex by comparison with the β-CD·H_3TCPP^{3-}/H_2TCPP^{4-} complex.

Similar to the β-CD/H_3TCPP^{3-}/H_2TCPP^{4-} system, any further analysis must take into consideration the relative proportions of the di-acid, mono-acid and free base of TCPP. The variation in the proportions of the three species across the four temperatures renders the derived complexation constants and thermodynamic parameters erroneous. Thus, no further in-depth analysis is performed.

4.2.1.3.14 Complexation of H_2TMAP^{4+} by β-CDab

The addition of β-CDab to a solution of H_2TMAP^{4+} showed a greater variation in the absorption spectra than β-CD, thus the data could be fit to the appropriate algorithm. The complexation constants and thermodynamic parameters could be derived for a 1:1 β-CDab·H_2TMAP^{4+} complex. The reliable fitting of the β-CDab/H_2TMAP^{4+} system demonstrates that the substitution of β-CD with an aminophenyl substituent can substantially alter the complexation capabilities.

In the absence of derived complexation constants and thermodynamic parameters for the β-CD/H_2TMAP^{4+} system, the β-CDab/H_2TMAP^{4+} system is compared against the H_2TSPP^{4-} and H_3TCPP^{3-}/H_2TCPP^{4-} systems. The K_{11} of the β-CDab·H_2TMAP^{4+} complex is twelve and sixteen times less than the K_{11} for the β-CD·H_2TSPP^{4-} and β-CD·H_3TCPP^{3-}/H_2TCPP^{4-} systems indicating a weakly formed 1:1 complex.

The ΔH_{11} value of the β-CDab·H_2TMAP^{4+} complex is similar to the β-CD·H_2TSPP^{4-} complex, indicating that there is some enthalpic stabilisation due to the π-π interactions between the aminophenyl substituent of β-CDab and the phenyl or pyrrole core of H_2TMAP^{4+}. However, the $T\Delta S_{11}$ is the most negative out of all of the systems studied, indicating that the entropic loss associated with the formation of a complex overcomes the entropic gain from the expulsion of water molecules from the β-CD cavity. This may indicate that H_2TMAP^{4+} only partially penetrates the β-CD cavity, resulting in some water molecules that are not expelled. This scenario is possible if the β-CD cavity resides dominantly over the alkyl groups of H_2TMAP^{4+}, rather than the phenyl groups, which is consistent with the low K_{11} value. The preference for complexation of the alkyl groups rather than the phenyl groups of H_2TMAP^{4+} is likely to be related to the charge of the porphyrin. The interaction between the β-CD and the positive charge of H_2TMAP^{4+} would be minimised due to the partially-polarised internal cavity of β-CD.[34]

4.2.1.3.15 Complexation of H_2TMPyP^{4+} by β-CDab

The complexation constants for the β-CDab·H_2TMPyP^{4+} complex could not be derived, similar to the β-CD/H_2TMAP^{4+} and β-CD/H_2TMPyP^{4+} systems. The addition of β-CDab to a solution of H_2TMPyP^{4+} caused a shift in λ_{max} of only 4 nm. Furthermore, the change in absorbance of H_2TMPyP^{4+} upon successive additions of β-CDab did not show a significant departure from linearity up to the maximum host:guest ratio (1120:1) that could be achieved given the solubility limits of β-CDab. Thus, the spectra could not be fit to the appropriate algorithm.

As with the β-CD/H_2TMAP^{4+} and β-CD/H_2TMPyP^{4+} systems, weak complexes characterised by low K_{11} that also show only minor changes in the absorption spectra are difficult to study. Therefore, UV-vis spectroscopy or other experiments relying on optical properties may not be suitable to determine the complexation properties of cationic porphyrins.

4.2.1.3.16 Enthalpy-entropy linear relationship

For a substantial number of CD studies, it has been found that a linear relationship exists between $T\Delta S_{11}$ and ΔH_{11} for the complexation by α-CD, β-CD and γ-CD hosts of a wide range of guest species to form 1:1 host-guest complexes.[50] Thus, the relationship is shown by Equation 4.10,

$$T\Delta S_{11} = \alpha\Delta H_{11} + T\Delta S_{11,0} \tag{4.10}$$

where $T\Delta S_{11}$ and ΔH_{11} are experimental data; α is the slope of a plot of $T\Delta S_{11}$ against ΔH_{11} and $T\Delta S_{11,0}$ is obtained when ΔH_{11} = 0 ($\Delta H_{11,0}$) at the zero intercept.

The size of α indicates the extent to which changes in complex stability (proportional to ΔG_{11}) occur through enthalpic stabilisation, $\Delta\Delta H_{11}$, caused by variation of the identity of the host are cancelled through entropic loss, $\Delta\Delta S_{11}$, as shown in Equation 4.11,

$$\Delta G = (1 - \alpha)\Delta\Delta H_{11} \tag{4.11}$$

such that only (1 - α) of the enthalpic increase can add to the host-guest complex stabilisation. Thus, $T\Delta S_{11,0}$ is the inherent host-guest complex stability, $\Delta G_{11,0}$, when ΔH_{11} = 0 ($\Delta H_{11,0}$). (It should be noted that Equation 4.10 and Equation 4.11 do not represent a necessary relationship, but is one observed for a variety of equilibria involving CDs.)

A plot of $T\Delta S_{11}$ and ΔH_{11} literature data for the complexation of a wide range of guests by β-CD, modified β-CD and β-CD dimers for the formation of 1:1 host-guest complexes is shown in Figure 4.36 and is characterised by α = 0.80 and 0.99 and $T\Delta S_{11,0}$ = 11 kJ mol^{-1} and 15 kJ mol^{-1} for β-CD and modified β-CD, respectively.[50] The enthalpy-entropy linear relationship for the 1:1 host·porphyrin complexes of β-CD·H_2TSPP^{4-}, β-CD·H_3TCPP^{3-}/H_2TCPP^{4-}, β-CDab·H_2TSPP^{4-}, β-CDab·H_3TCPP^{3-}/H_2TCPP4^{-} and β-CDab·H_2TMAP^{4+} are also shown in Figure 4.36.

The α value, which describes the extent of entropic compensation caused by modification of the host or porphyrin, as well as the $T\Delta S_0$, which represents the inherent complex stability (see Chapter 3) was not quantified due to the limited number of reliable data points. Therefore, the extent of enthalpy-entropy compensation in the systems of this study could only analysed by comparing against existing literature data.

The thermodynamic values for the systems in this study correspond with those in the literature, suggesting that complexation is largely influenced by the β-CD group itself, rather than modifications to β-CD or differences between the porphyrins. In particular, the values are within the range of the thermodynamic parameters of analogous systems involving H_2TSPP^{4-} and a variety of modified γ-CD compounds.[20,42,50,51]

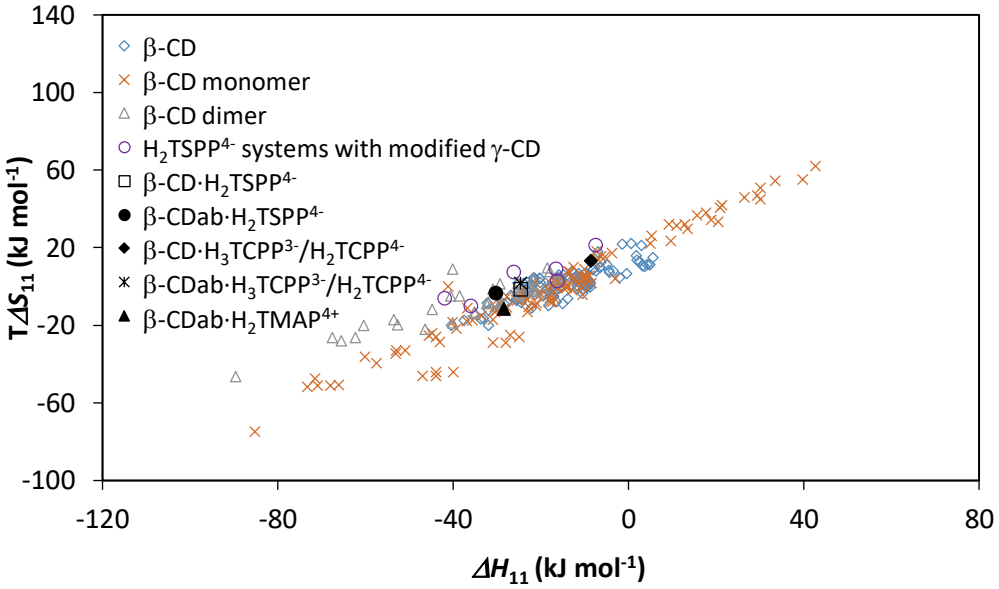

Figure 4.36: Linear relationship between ΔH_{11} and $T\Delta S_{11}$ for the 1:1 complexation of various guests and modified β-CDs and γ-CDs at 298 K, as determined from this study and the literature.[20,42,50,51]

4.2.1.4 Molecular Modelling of Complexes

Molecular modelling studies were undertaken to gain greater insight into the possible stereochemical modes of complexation for the host-porphyrin complexes, which neither the NMR or UV-vis studies could reveal. Molecular models were constructed for 1:1 complexes of β-CD·H_2TSPP^{4-}, β-CD·H_2TCPP^{4-}, β-CD·H_2TMAP^{4+} and β-CD·H_2TMPyP^{4+}. Molecular models were also constructed for 2:1 complexes of β-CD_2·H_2TSPP^{4-}, β-CD_2·H_2TCPP^{4-}, β-CD_2·H_2TMAP^{4+} and β-CD_2·H_2TMPyP^{4+}, characterised by either the *anti*- or *syn*-conformation, with β-CD hosts complexing through both of the primary faces, both of the secondary faces or one primary and one secondary face. The structures were energy minimised using the PM7 semiempirical method via MOPAC2012.[52] The di-acid of TCPP was constructed to simplify the analysis. The models are exemplified by 1:1 β-CD·H_2TSPP^{4-} and 2:1 β-CD_2·H_2TSPP^{4-} complexes, as shown in Figure 4.37 and Figure 4.38, respectively, while all other complexes are given in Figure 4.54 – Figure 4.59 in 4.5 Appendix. A summary of the gas phase heats of formation, *E*, for each complex is given in Table 4.14.

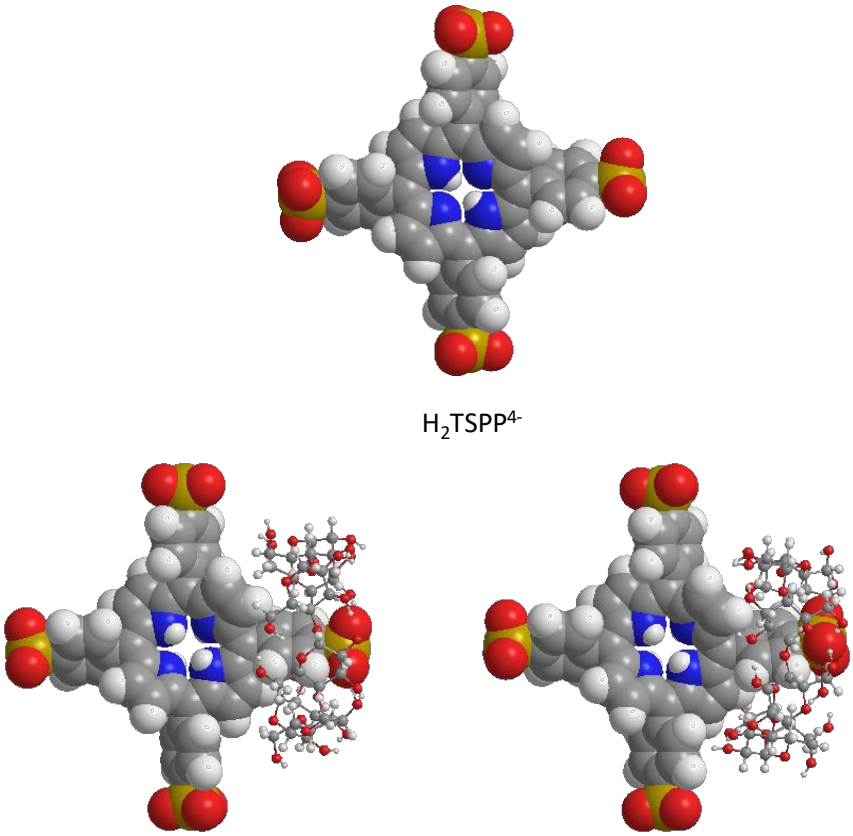

H_2TSPP^{4-}

β-CD·H_2TSPP^{4-} primary face

β-CD·H_2TSPP^{4-} secondary face

Figure 4.37: Energy minimised molecular models of H_2TSPP^{4-} alone and in a 1:1 complex with β-CD, derived using the PM7 semiempirical method on MOPAC2012 software. Note: β-CD = ball and stick, H_2TSPP^{4-} = space filling. Carbon = grey, nitrogen = blue, oxygen = red, sulfur = yellow and hydrogen = white.

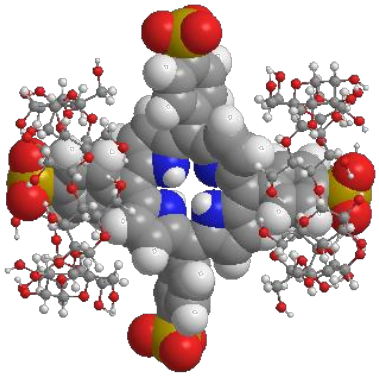

β-CD_2·H_2TSPP^{4-} *anti*, primary – primary

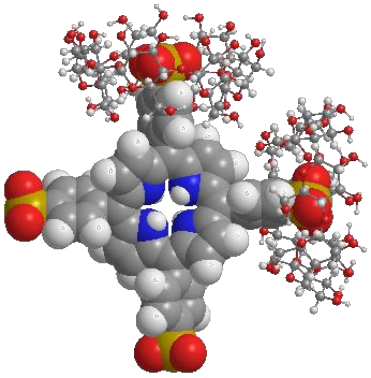

β-CD_2·H_2TSPP^{4-} *syn*, primary – primary

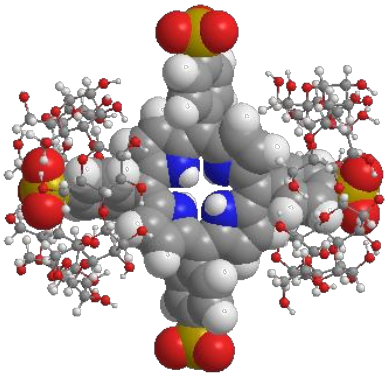

β-CD_2·H_2TSPP^{4-}· *anti*, primary – secondary

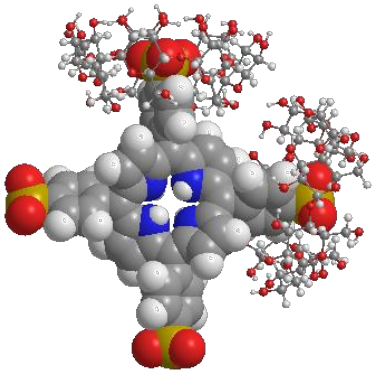

β-CD_2·H_2TSPP^{4-} *syn*, primary – secondary

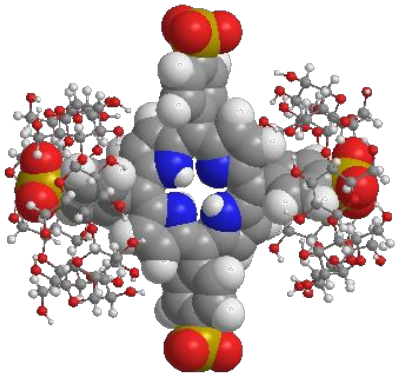

β-CD_2·H_2TSPP^{4-} *anti*, secondary – secondary

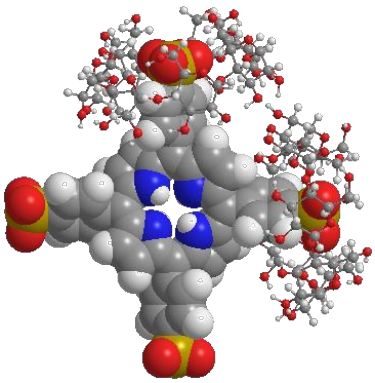

β-CD_2·H_2TSPP^{4-} *syn*, secondary – secondary

Figure 4.38: Energy minimised molecular models of 2:1 β-CD_2·H_2TSPP^{4-} complexes of various conformations, derived using the PM7 semiempirical method on MOPAC2012 software. Note: β-CD = ball and stick, H_2TSPP^{4-} = space filling. Carbon = grey, nitrogen = blue, oxygen = red, sulfur = yellow and hydrogen = white.

Table 4.14: Heats of formation, *E*, (kJ mol^{-1}) for complexes of porphyrins with β-CD in a range of host-guest ratios and orientations, calculated through MOPAC2012.[52]

Ratio and orientation		H_2TSPP^{4-}	H_2TCPP^{4-}	H_2TMAP^{4+}	H_2TMPyP^{4+}
1:1	alone	-1027	-276	4240	4529
	primary	-8128	-7116	-2568	-2163
	secondary	-8132	-7080	-2488	-2196
2:1 *anti*	primary – primary	-15148	-13850	-9372	-8919
	primary – secondary	-15023	-13871	-9328	-8919
	secondary – secondary	-15044	-13930	-9311	-9052
2:1 *syn*	primary – primary	-14909	-13853	-9242	-9135
	primary – secondary	-14926	-13966	-9365	-9012
	secondary – secondary	-14985	-13807	-9217	-8959.

The PM7 semiempirical method did not appear to be suitable to determine the preferential geometry of the host·porphyrin complexes. The experimental data does not correlate with the calculated heats of formation. For example, ^{1}H NMR spectroscopy revealed that the complexation of H_3TCPP^{3-}/H_2TCPP^{4-} by β-CD occurred through the secondary face. However, molecular modelling indicated that the heat of formation was lower for the primary face orientation by 33 kJ mol^{-1}. Similarly, NMR spectroscopy indicated no facial preference for the complexation of the cationic porphyrins by β-CD. However, there was a difference of 80 kJ mol^{-1} and 33 kJ mol^{-1} between the primary and secondary face orientations for the β-CD·H_2TMAP^{4+} and β-CD·H_2TMPyP^{4+} complexes, respectively.

As CD complexation is reliant upon an aqueous solvent media, the PM7 semiempirical method, which omits solvent molecular interactions, is not suitable for analysis of CD complexes.[53] While some non-covalent interactions are included in the calculation, the overall main driving force for CD complexation is the displacement of water molecules from the CD cavity.[54] Therefore, the calculations were not reliable and further calculations using β-CDab as the host were not undertaken.

4.3 Conclusion

The complexation of two anionic porphyrins, H_2TSPP^{4-} and $H_3TCPP^{3-}/H_2TCPP^{4-}$, and two cationic porphyrins, H_2TMAP^{4+} and H_2TMPyP^{4+} by native β-CD and β-CDab were investigated by NMR and UV-vis spectroscopy. Investigations by 1D and 2D ^1H NMR spectroscopy indicated that H_2TSPP^{4-} and $H_3TCPP^{3-}/H_2TCPP^{4-}$ preferred to complex through the secondary face of β-CD due, in part, to the anti-parallel alignment of dipole moments of both the porphyrin and β-CD. However, there was no such facial preference for the H_2TMAP^{4+} and H_2TMPyP^{4+} systems. The complexation of a β-CD host also disrupts the aggregation of the anionic porphyrins as only one of the phenyl groups of the porphyrin may reside within the β-CD cavity.

Complexation constants and thermodynamics parameters could only reliably be determined for the β-CD·H_2TSPP^{4-}, β-CDab·H_2TSPP^{4-} and β-CDab·H_2TMAP^{4+} complexes. While complexation constants were derived for the β-CD·$H_3TCPP^{3-}/H_2TCPP^{4-}$ and β-CDab·$H_3TCPP^{3-}/H_2TCPP^{4-}$ complexes, the values are unreliable due to a large amount of both the mono-acid and free base of TCPP existing at pH 7, the proportions of which may alter across the four temperatures studied. Complexation constants could also not be derived for the β-CD·H_2TMAP^{4+}, β-CD·H_2TMPyP^{4+} and β-CDab·H_2TMPyP^{4+} complexes. Generally, anionic porphyrins are likely to form stronger complexes with β-CD hosts than cationic porphyrins as the internal cavity of β-CD is partially positive.

The substitution of native β-CD with an aminophenyl substituent greatly improved the complexation properties with porphyrins. The complexation of the porphyrins with β-CDab were generally higher, owing to the additional π-π interactions between the aminophenyl substituent of β-CDab and the phenyl or pyrrole groups of the porphyrins.

Attempts were made to gain further insight in to the complex geometry of the porphyrins with the β-CD hosts by considering molecular models of each complex. However, the calculated heats of formation did not correlate with the experimental data and hence, no further analysis was performed.

This research is a step towards a full understanding of the factors that influence the complexation of porphyrins by β-CD compounds, and will aid in the utility of porphyrins in biological settings. Additionally, much like the results from Chapter 3, the results from this chapter, when analysed within the larger scope of CD complexation studies, should help to inform the design of future CD systems.

4.4 References

(1) Biesaga, M.; Pyrzynska, K.; Trojanowicz, M. *Talanta* **2000**, *51*, 209.
(2) Li, L.-L.; Diau, E. W.-G. *Chem. Soc. Rev.* **2013**, *42*, 291.
(3) Ethirajan, M.; Chen, Y.; Joshi, P.; Pandey, R. K. *Chem. Soc. Rev.* **2011**, *40*, 340.
(4) Sternberg, E. D.; Dolphin, D.; Bruckner, C. *Tetrahedron* **1998**, *54*, 4151.
(5) Miyamoto, T.; Zhu, Q.; Igrashi, M.; Kodama, R.; Maeno, S.; Fukushima, M. *J. Mol. Catal. B: Enzym.* **2015**, *119*, 64.
(6) Boehm, P.; Groeger, H. *Chemcatchem* **2015**, *7*, 22.
(7) Bonnett, R. *Chem. Soc. Rev.* **1995**, *24*, 19.
(8) Kalyanasundaram, K.; Neumannspallart, M. *J. Phys. Chem.* **1982**, *86*, 5163.
(9) Kadish, K. M.; Maiya, G. B.; Araullo, C.; Guilard, R. *Inorg. Chem.* **1989**, *28*, 2725.
(10) Pasternack. R. F.; Centuro, G. C.; Boyd, P.; Hinds, L. D.; Huber, P. R.; Francesc.L; Fasella, P.; Engasser, G.; Gibbs, E. *J. Am. Chem. Soc.* **1972**, *94*, 4511.
(11) Ma, H.-M.; Chen, X.; Zhang, N.; Han, Y.-Y.; Wu, D.; Du, B.; Wei, Q. *Spectrochim. Acta Mol. Biomol. Spectrosc.* **2009**, *72*, 465.
(12) Ghaderi, M.; Bathaie, S. Z.; Saboury, A.-A.; Sharghi, H.; Tangestaninejad, S. *Int. J. Biol. Macromol.* **2007**, *41*, 173.
(13) Merchat, M.; Spikes, J. D.; Bertoloni, G.; Jori, G. *J. Photochem. Photobiol., B* **1996**, *35*, 149.
(14) Gandini, S. C. M.; Borissevitch, I. E.; Perussi, J. R.; Imasato, H.; Tabak, M. *J. Lumin.* **1998**, *78*, 53.
(15) Mosinger, J.; Slavetinska, L.; Lang, K.; Coufal, P.; Kubat, P. *Org. Biomol. Chem.* **2009**, *7*, 3797.
(16) Lang, K.; Kubat, P.; Lhotak, P.; Mosinger, J.; Wagnerova, D. M. *Photochem. Photobiol.* **2001**, *74*, 558.
(17) Sobczynski, J.; Tonnesen, H. H.; Kristensen, S. *Pharmazie* **2013**, *68*, 100.
(18) Farajtabar, A.; Gharib, F.; Jamaat, P.; Safari, N. *J. Chem. Eng. Data* **2008**, *53*, 350.
(19) Baker, H.; Wagner, L.; Hambrigh.P *J. Am. Chem. Soc.* **1973**, *95*, 5942.
(20) McTernan, H. L., From Polymers to Porphyrins: Supramolecular Control Asserted by Cyclodextrin Oligomers, PhD Thesis, University of Adelaide, **2016.**
(21) Krishnamurthy, M.; Sutter, J. R.; Hambright, P. *J. Chem. Soc., Chem. Commun.* **1975**, 13.
(22) Iosif, A.; Grummt, U. W. *J. Prakt. Chem. /Chem-Ztg* **1997**, *339*, 420.
(23) Corsini, A.; Herrmann, O. *Talanta* **1986**, *33*, 335.
(24) Kalyanasundaram, K. *J. Chem. Soc., Perkin Trans. 2* **1983**, *79*, 1365.
(25) Kano, K.; Minamizono, H.; Kitae, T.; Negi, S. *J. Phys. Chem. A* **1997**, *101*, 6118.
(26) Kano, K.; Fukuda, K.; Wakami, H.; Nishiyabu, R.; Pasternack, R. F. *J. Am. Chem. Soc.* **2000**, *122*, 7494.
(27) Kano, K.; Takei, M.; Hashimoto, S. *J. Phys. Chem.* **1990**, *94*, 2181.
(28) Lang, K.; Mosinger, J.; Wagnerova, D. M. *Coord. Chem. Rev.* **2004**, *248*, 321.
(29) Kryjewski, M.; Goslinski, T.; Mielcarek, J. *Coord. Chem. Rev.* **2015**, *300*, 101.
(30) Bonchio, M.; Carofiglio, T.; Carraro, M.; Fornasier, R.; Tonellato, U. *Org. Lett.* **2002**, *4*, 4635.
(31) Venema, F.; Rowan, A. E.; Nolte, R. J. M. *J. Am. Chem. Soc.* **1996**, *118*, 257.
(32) Mulder, A.; Jukovic, A.; van Leeuwen, F. W. B.; Kooijman, H.; Spek, A. L.; Huskens, J.; Reinhoudt, D. N. *Chem. Eur. J.* **2004**, *10*, 1114.
(33) Mosinger, J.; Deumie, M.; Lang, K.; Kubat, P.; Wagnerova, D. M. *J. Photochem. Photobiol., A* **2000**, *130*, 13.
(34) Kano, K.; Nishiyabu, R.; Asada, T.; Kuroda, Y. *J. Am. Chem. Soc.* **2002**, *124*, 9937.
(35) Wang, X. P.; Pan, J. H.; Shuang, S. M.; Zhang, Y. *Supramol. Chem.* **2003**, *15*, 245.
(36) Wang, X. P.; Pan, J. H.; Yang, X. D.; Niu, C. D.; Zhang, Y.; Shuang, S. M. *Anal. Bioanal. Chem.* **2002**, *374*, 445.
(37) Ribo, J. M.; Farrera, J. A.; Valero, M. L.; Virgili, A. *Tetrahedron* **1995**, *51*, 3705.
(38) Schneider, H. J.; Hacket, F.; Rudiger, V.; Ikeda, H. *Chem. Rev.* **1998**, *98*, 1755.
(39) Gandini, S. C. M.; Yushmanov, V. E.; Borissevitch, I. E.; Tabak, M. *Langmuir* **1999**, *15*, 6233.

(40) Saenger, W. R.; Jacob, J.; Gessler, K.; Steiner, T.; Hoffmann, D.; Sanbe, H.; Koizumi, K.; Smith, S. M.; Takaha, T. *Chem. Rev.* **1998**, *98*, 1787.
(41) Kitagawa, M.; Hoshi, H.; Sakurai, M.; Inoue, Y.; Chujo, R. *Carbohydr. Res.* **1987**, *163*, C1.
(42) Nguyen, H. T.; Pham, D. T.; Easton, C. J.; Lincoln, S. F. *Aust. J. Chem.* **2013**, *66*, 1057.
(43) Harada, T.; Pham, D. T.; Leung, M. H. M.; Huy, T. N.; Lincoln, S. F.; Easton, C. J.; Kee, T. W. *J. Phys. Chem. B* **2011**, *115*, 1268.
(44) Wang, J.; Duc-Truc, P.; Kee, T. W.; Clafton, S. N.; Guo, X.; Clements, P.; Lincoln, S. F.; Prud'homme, R. K.; Easton, C. J. *Macromolecules* **2011**, *44*, 9782.
(45) Hamai, S.; Ohshida, T. *J. Inclusion Phenom. Macrocyclic Chem.* **2004**, *50*, 209.
(46) Motulsky, H. J.; Christopoulos, A. *Fitting models to biological data using linear and nonlinear regression: A practical guide to curve fitting*; GraphPad Prism Software Inc., San Diego, CA, **2003**.
(47) Mulder, A.; Jukovic, A.; Huskens, J.; Reinhoudt, D. N. *Org. Biomol. Chem.* **2004**, *2*, 1748.
(48) Reijenga, J. C.; Gagliardi, L. G.; Kenndler, E. *J. Chromatogr. A* **2007**, *1155*, 142.
(49) Perrin, D. D. *Aust. J. Chem.* **1964**, *17*, 484.
(50) Rekharsky, M. V.; Inoue, Y. *Chem. Rev.* **1998**, *98*, 1875.
(51) Zhang, B. L.; Breslow, R. *J. Am. Chem. Soc.* **1993**, *115*, 9353.
(52) Stewart, J. J. P. *J. Mol. Model.* **2013**, *19*, 1.
(53) Lipkowitz, K. B. *Chem. Rev.* **1998**, *98*, 1829.
(54) Del Valle, E. M. M. *Process Biochem.* **2004**, *39*, 1033.

4.5 Appendix

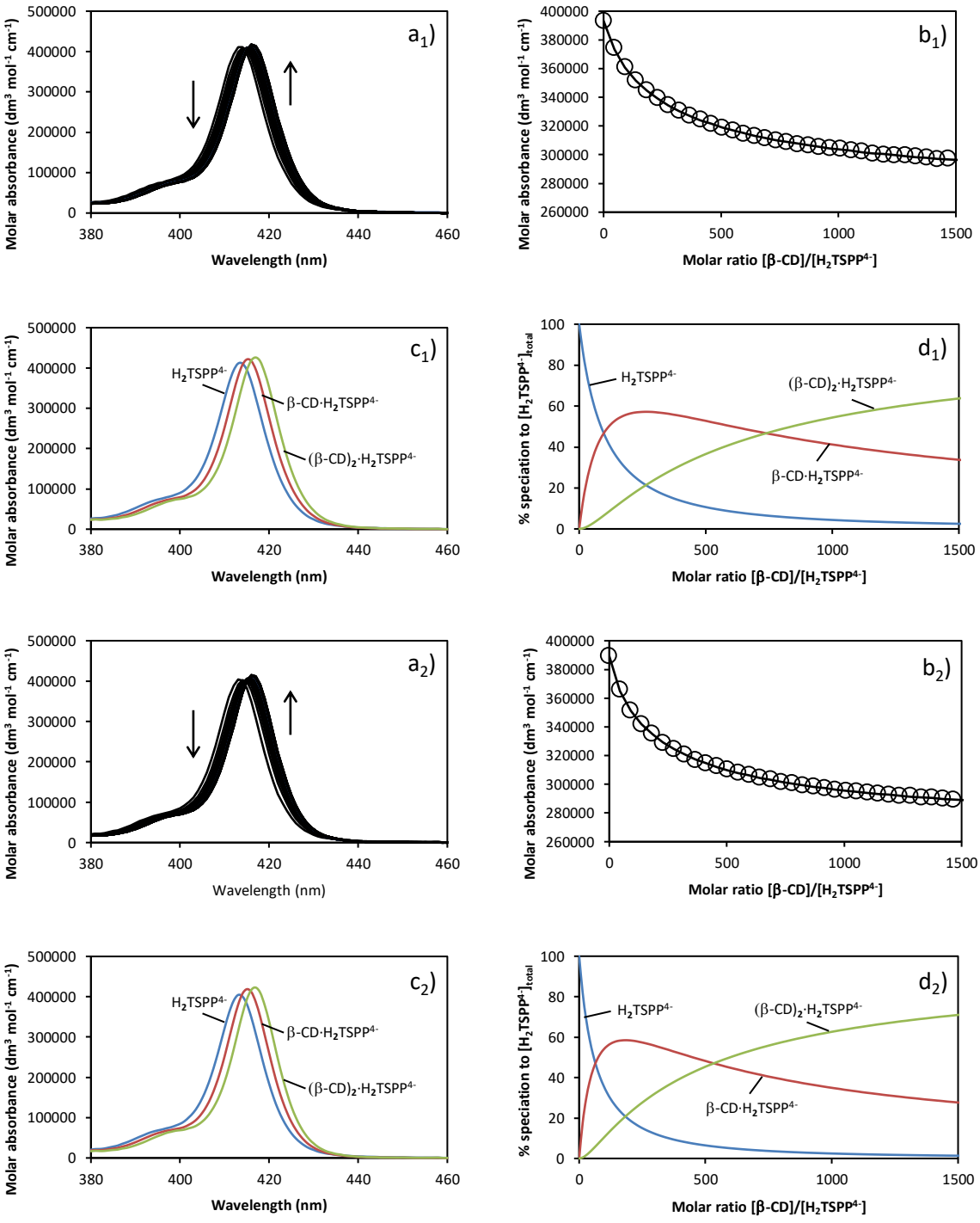

Figure 4.39: UV-vis absorbance data of H_2TSPP^{4-} (initial concentration 1.2×10^{-6} mol dm^{-3}) with increasing β-CD (0 – 1.6×10^{-3} mol dm^{-3}) in aqueous phosphate buffer (pH 7.0 and I = 0.10 mol dm^{-3}), showing a) molar absorption spectrum, arrows show direction of change, b) experimental (circles) and best-fit (line) molar absorbances at 412 nm (fitted at 1 nm intervals over 400 – 425 nm) for 1:1 β-CD·H_2TSPP^{4-} and 2:1 $(\beta\text{-CD})_2\cdot H_2TSPP^{4-}$ complexes, c) experimental and calculated molar absorbances of free and complexed H_2TSPP^{4-} and d) calculated speciation of free and complexed H_2TSPP^{4-}. Concentration of β-CD was 0.011 mol dm^{-3}, titrating with 10 mm^3 aliquots to a 2 cm^3 solution of H_2TSPP^{4-} in a 1 cm cell. Note: a_1-d_1 and a_2-d_2 refers to 308.2 K and 298.2 K, respectively.

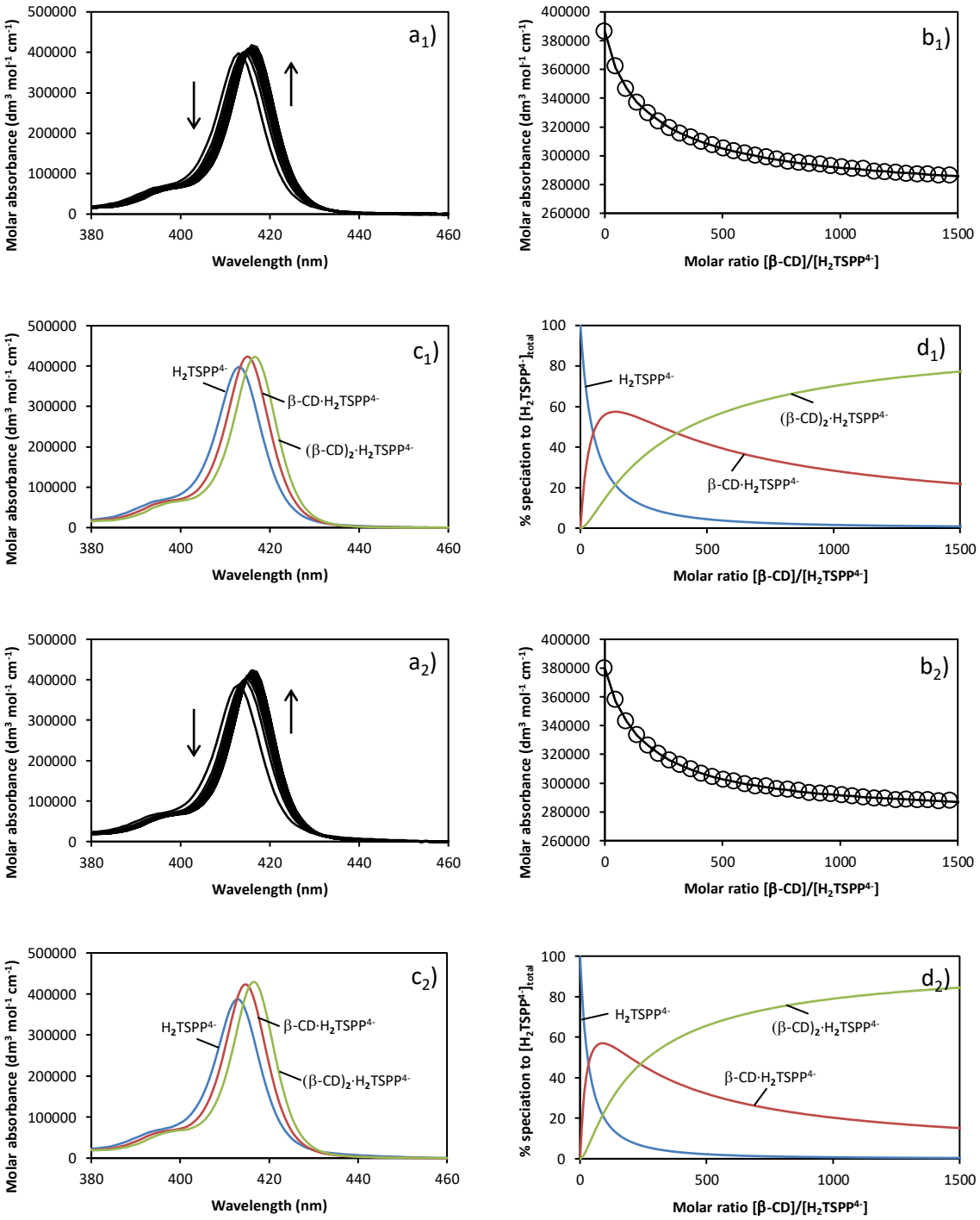

Figure 4.40: UV-vis absorbance data of H_2TSPP^{4-} (initial concentration 1.2×10^{-6} mol dm^{-3}) with increasing concentrations of β-CD (0 – 1.6×10^{-3} mol dm^{-3}) in aqueous phosphate buffer (pH 7.0 and I = 0.10 mol dm^{-3}), showing a) the molar absorption spectrum, the arrows indicating the direction of change, b) the experimental (circles) and best-fit (line) molar absorbances at 412 nm (fitted at 1 nm intervals over the range 400 – 425 nm) for 1:1 β-CD·H_2TSPP^{4-} and 2:1 $(β\text{-CD})_2$·H_2TSPP^{4-} complexes, c) the experimental molar absorbances of free H_2TSPP^{4-} and calculated molar absorbances of complexed H_2TSPP^{4-} and d) the calculated speciation of free and complexed H_2TSPP^{4-}. The concentration of β-CD was 0.011 mol dm^{-3}, titrating with 10 mm^3 aliquots to a 2 cm^3 solution of H_2TSPP^{4-} in a 1 cm path length cell. Note: a_1-d_1 and a_2-d_2 refers to 288.2 K and 278.2 K, respectively.

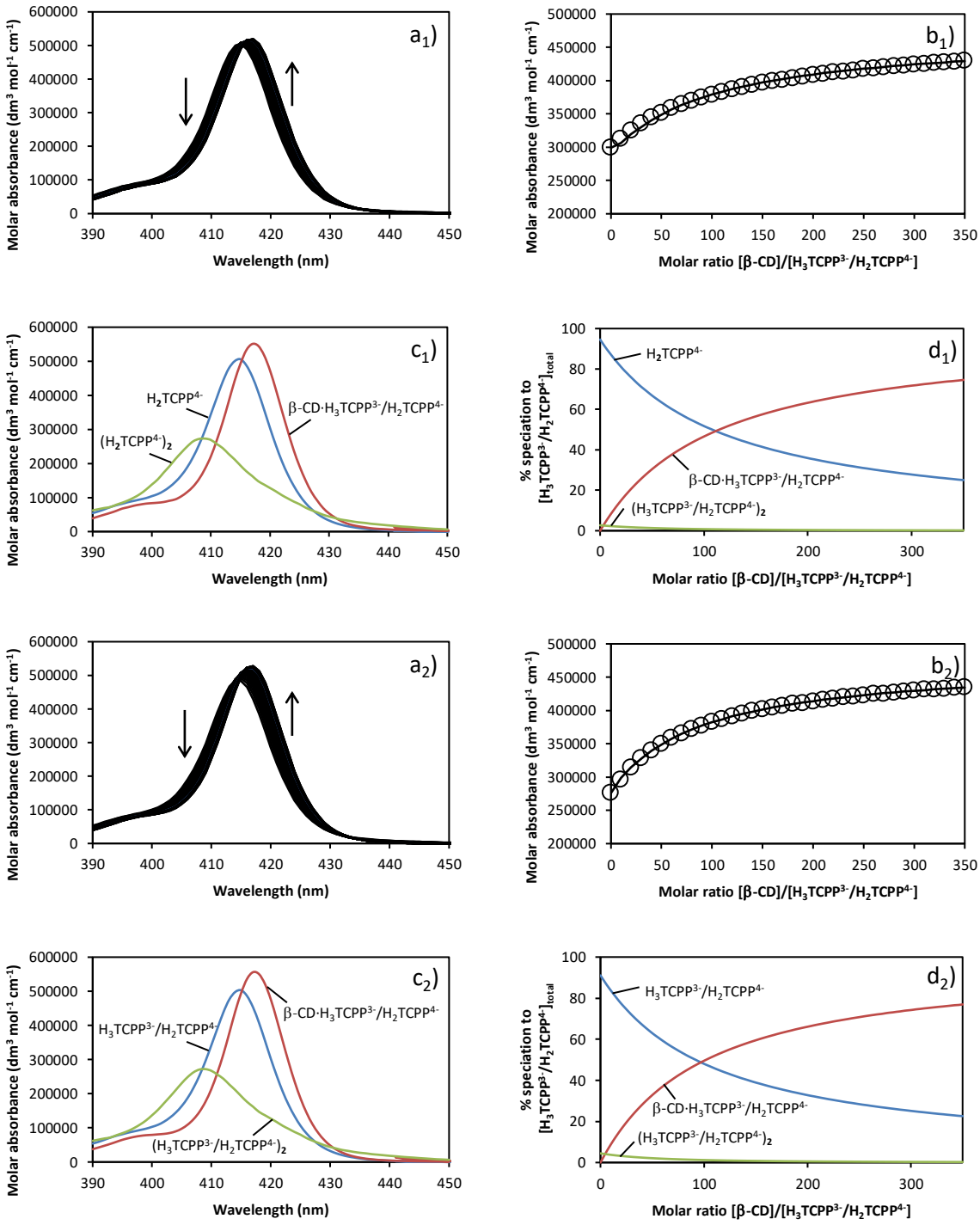

Figure 4.41: UV-vis absorbance data of $H_3TCPP^{3-}/H_2TCPP^{4-}$ (initial concentration 1.5×10^{-6} mol dm^{-3}) with increasing concentrations of β-CD (0 – 3.6×10^{-4} mol dm^{-3}) in aqueous phosphate buffer (pH 7.0 and I = 0.10 mol dm^{-3}), showing a) the molar absorption spectrum, the arrows indicating the direction of change, b) the experimental (circles) and best-fit (line) molar absorbances at 420 nm (fitted at 1 nm intervals over the range 400 – 425 nm) for a 1:1 β-CD·$H_3TCPP^{3-}/H_2TCPP^{4-}$ complex, c) the experimental molar absorbances of free monomeric and dimeric $H_3TCPP^{3-}/H_2TCPP^{4-}$ and calculated molar absorbances of complexed $H_3TCPP^{3-}/H_2TCPP^{4-}$ and d) the calculated speciation of free and complexed $H_3TCPP^{3-}/H_2TCPP^{4-}$. The concentration of β-CD was 4.5×10^{-3} mol dm^{-3}, titrating with 5 mm^3 aliquots to a 2 cm^3 solution of $H_3TCPP^{3-}/H_2TCPP^{4-}$ in a 1 cm path length cell. Note: a_1-d_1 and a_2-d_2 refers to 308.2 K and 298.2 K, respectively.

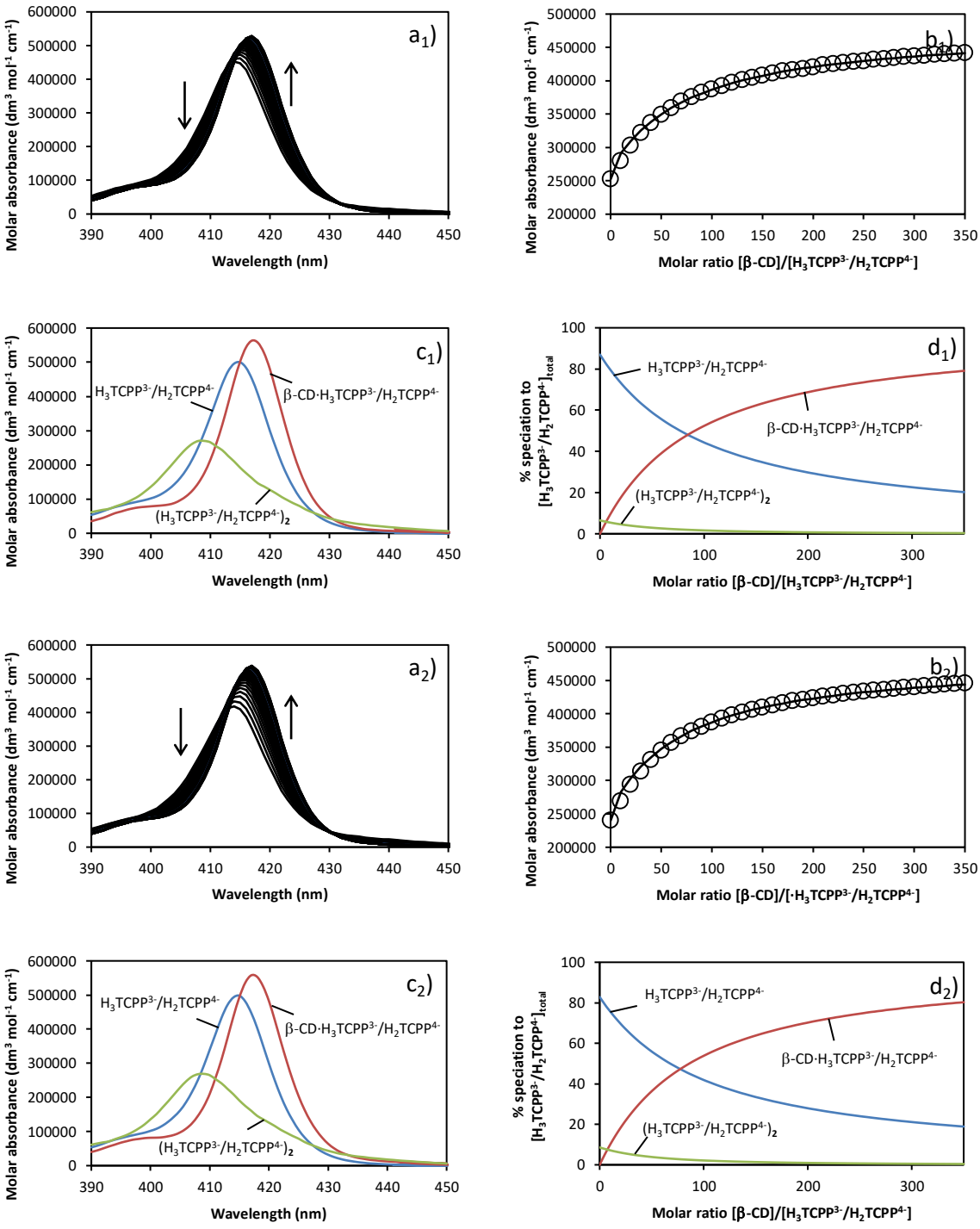

Figure 4.42: UV-vis absorbance data of $H_3TCPP^{3-}/H_2TCPP^{4-}$ (initial concentration 1.5×10^{-6} mol dm^{-3}) with increasing concentrations of β-CD (0 – 3.6×10^{-4} mol dm^{-3}) in aqueous phosphate buffer (pH 7.0 and I = 0.10 mol dm^{-3}), showing a) the molar absorption spectrum, the arrows indicating the direction of change, b) the experimental (circles) and best-fit (line) molar absorbances at 420 nm (fitted at 1 nm intervals over the range 400 – 425 nm) for a 1:1 β-CD·$H_3TCPP^{3-}/H_2TCPP^{4-}$ complex, c) the experimental molar absorbances of free monomeric and dimeric $H_3TCPP^{3-}/H_2TCPP^{4-}$ and calculated molar absorbances of complexed $H_3TCPP^{3-}/H_2TCPP^{4-}$ and d) the calculated speciation of free and complexed $H_3TCPP^{3-}/H_2TCPP^{4-}$. The concentration of β-CD was 4.5×10^{-3} mol dm^{-3}, titrating with 5 mm^3 aliquots to a 2 cm^3 solution of $H_3TCPP^{3-}/H_2TCPP^{4-}$ in a 1 cm path length cell. Note: a_1-d_1 and a_2-d_2 refers to 288.2 K and 278.2 K, respectively.

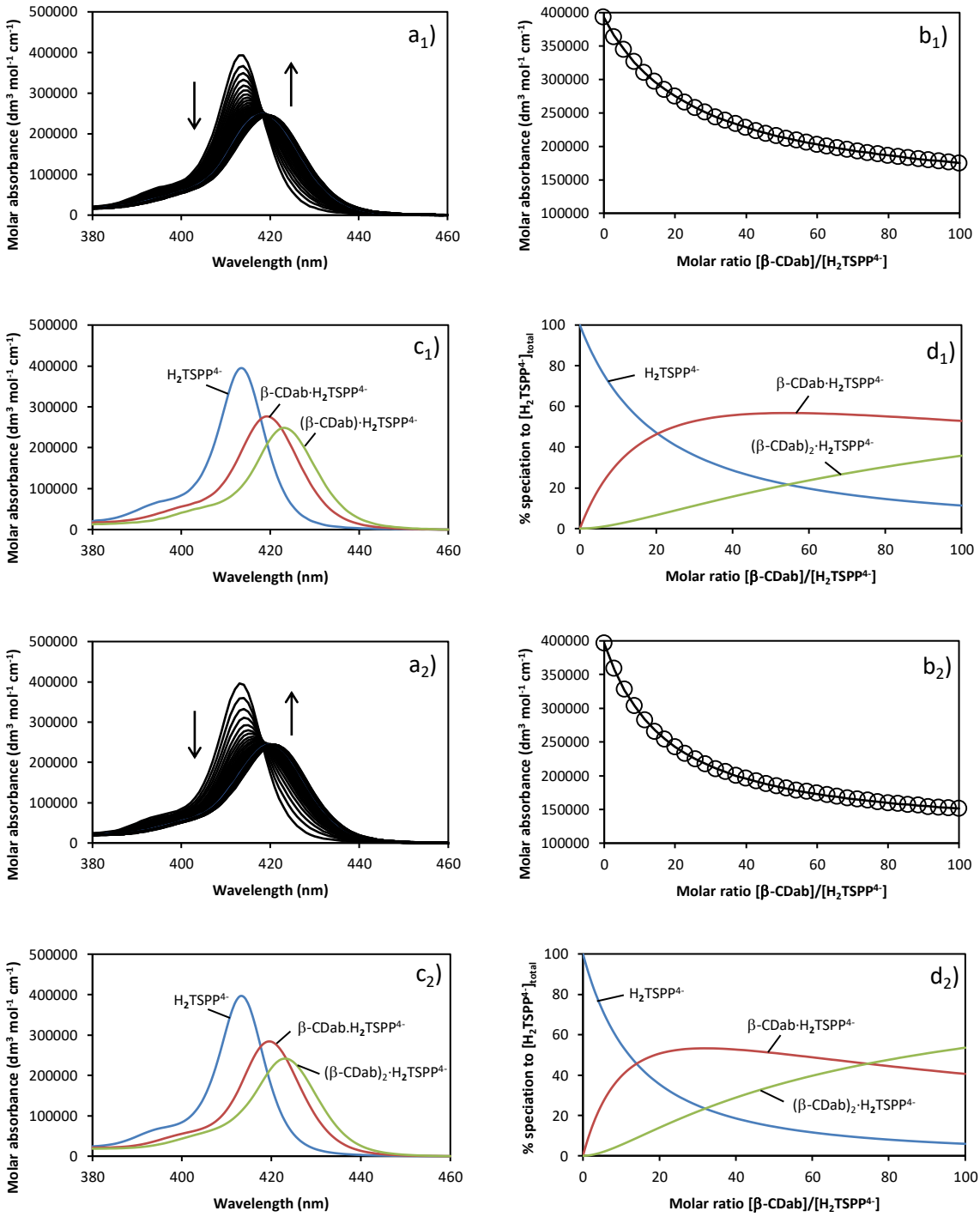

Figure 4.43: UV-vis absorbance data of H_2TSPP^{4-} (initial concentration 1.4×10^{-6} mol dm^{-3}) with increasing concentrations of β-CDab (0 – 1.3×10^{-4} mol dm^{-3}) in aqueous phosphate buffer (pH 7.0 and I = 0.10 mol dm^{-3}), showing a) the molar absorption spectrum, the arrows indicating the direction of change, b) the experimental (circles) and best-fit (line) molar absorbances at 413 nm (fitted at 1 nm intervals over the range 400 – 430 nm) for a 1:1 β-CDab·H_2TSPP^{4-} and a 2:1 (β-CDab)$_2$·H_2TSPP^{4-} complex, c) the experimental molar absorbances of free H_2TSPP^{4-} and calculated molar absorbances of complexed H_2TSPP^{4-} and d) the calculated speciation of free and complexed H_2TSPP^{4-}. The concentration of β-CDab was 1.6×10^{-3} mol dm^{-3}, titrating with 5 mm^3 aliquots to a 2 cm^3 solution of H_2TSPP^{4-} in a 1 cm path length cell. Note: a_1-d_1 and a_2-d_2 refer to 308.2 K and 298.2 K, respectively.

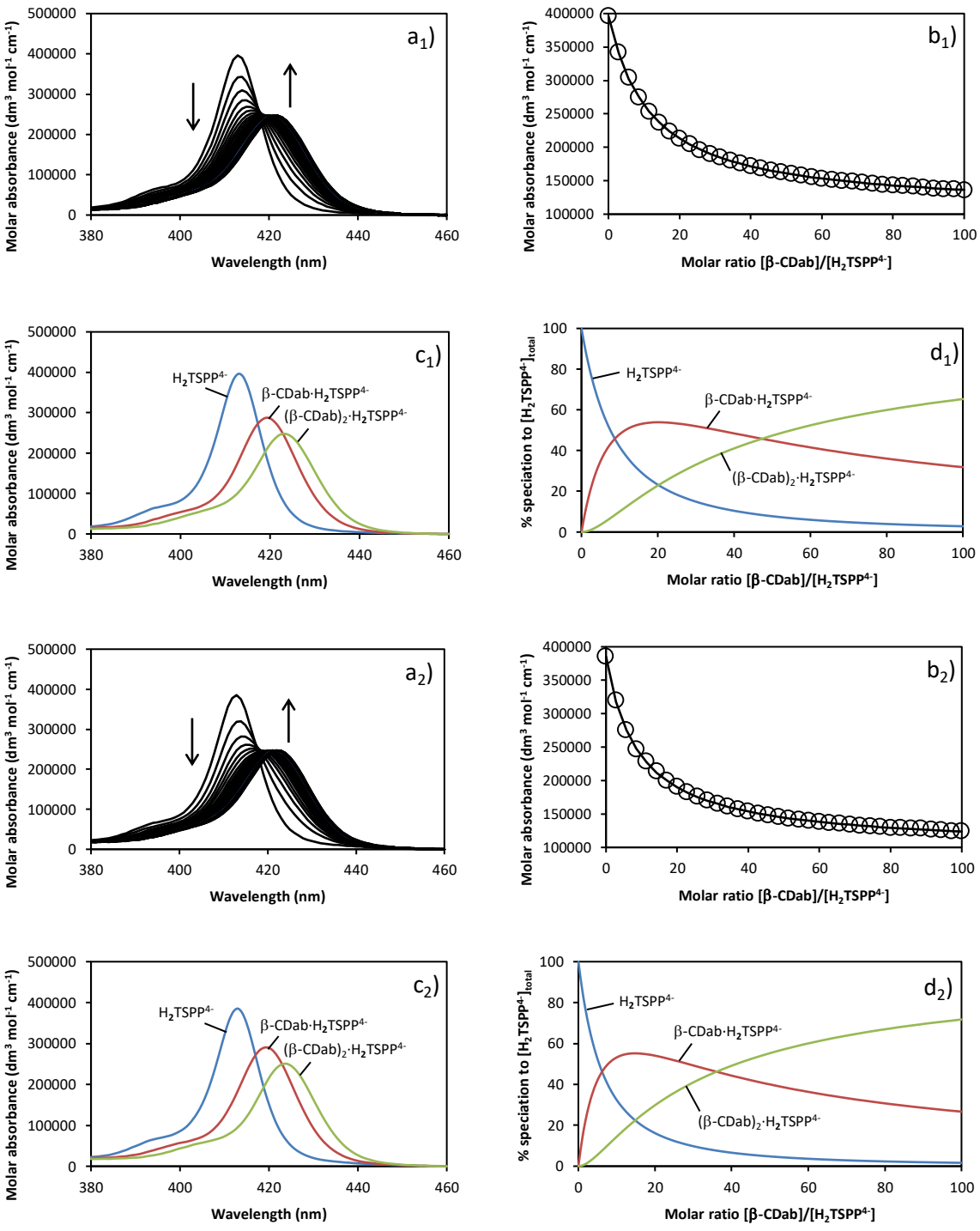

Figure 4.44: UV-vis absorbance data of H_2TSPP^{4-} (initial concentration 1.4×10^{-6} mol dm^{-3}) with increasing concentrations of β-CDab (0 – 1.3×10^{-4} mol dm^{-3}) in aqueous phosphate buffer (pH 7.0 and I = 0.10 mol dm^{-3}), showing a) the molar absorption spectrum, the arrows indicating the direction of change, b) the experimental (circles) and best-fit (line) molar absorbances at 413 nm (fitted at 1 nm intervals over the range 400 – 430 nm) for a 1:1 β-CDab·H_2TSPP^{4-} and a 2:1 $(\beta\text{-CDab})_2$·H_2TSPP^{4-} complex, c) the experimental molar absorbances of free H_2TSPP^{4-} and calculated molar absorbances of complexed H_2TSPP^{4-} and d) the calculated speciation of free and complexed H_2TSPP^{4-}. The concentration of β-CDab was 1.6×10^{-3} mol dm^{-3}, titrating with 5 mm^3 aliquots to a 2 cm^3 solution of H_2TSPP^{4-} in a 1 cm path length cell. Note: a_1-d_1 and a_2-d_2 refer to 288.2 K and 278.2 K, respectively.

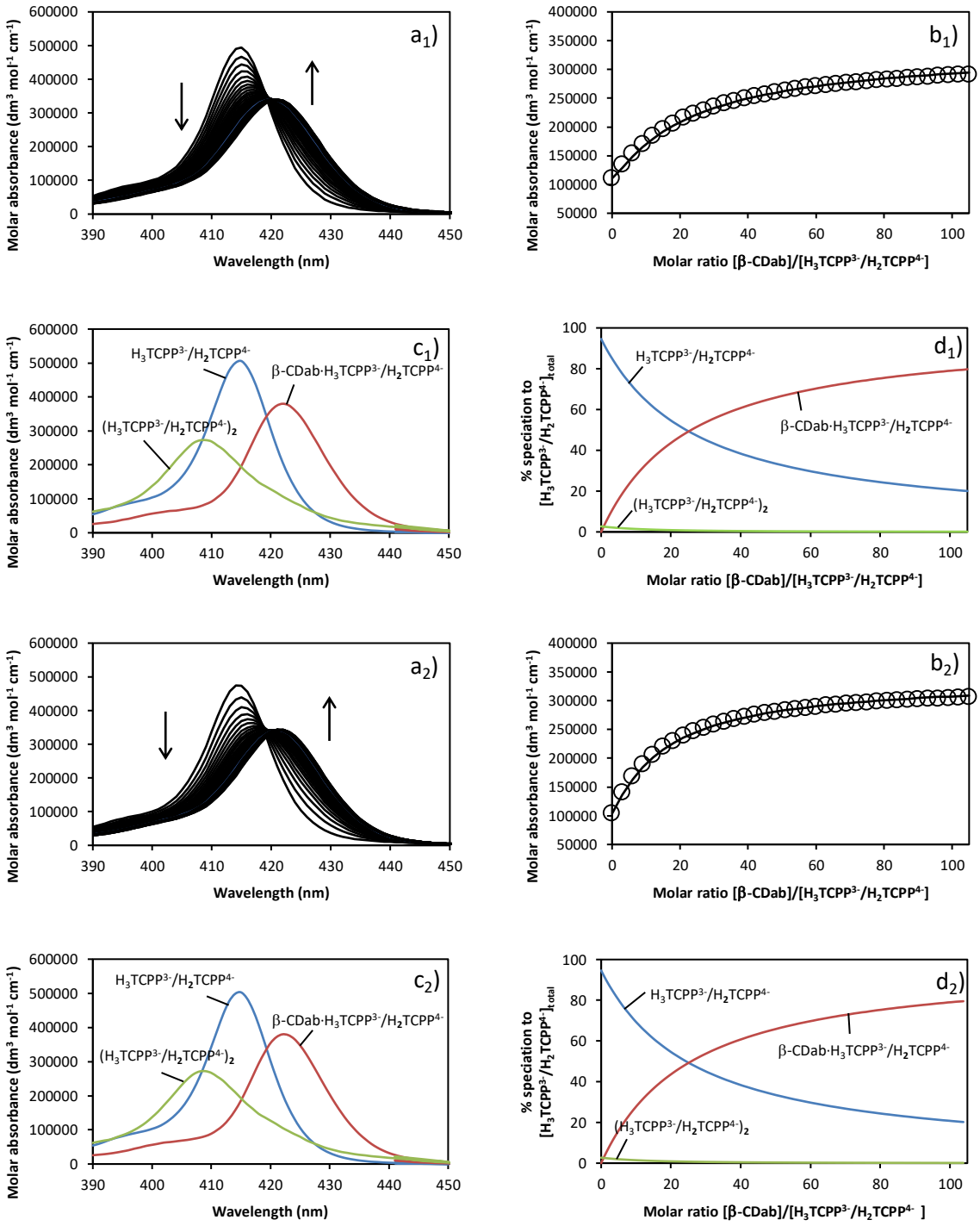

Figure 4.45: UV-vis absorbance data of $H_3TCPP^{3-}/H_2TCPP^{4-}$ (initial concentration 1.5×10^{-6} mol dm^{-3}) with increasing concentrations of β-CDab (0 – 1.4×10^{-4} mol dm^{-3}) in aqueous phosphate buffer (pH 7.0 and I = 0.10 mol dm^{-3}), showing a) the molar absorption spectrum, the arrows indicating the direction of change, b) the experimental (circles) and best-fit (line) molar absorbances at 425 nm (fitted at 1 nm intervals over the range 400 – 430 nm) for a 1:1 β-CDab·$H_3TCPP^{3-}/H_2TCPP^{4-}$ complex, c) the experimental molar absorbances of free monomeric and dimeric $H_3TCPP^{3-}/H_2TCPP^{4-}$ and calculated molar absorbances of complexed $H_3TCPP^{3-}/H_2TCPP^{4-}$ and d) the calculated speciation of free and complexed $H_3TCPP^{3-}/H_2TCPP^{4-}$. The concentration of β-CDab was 1.8×10^{-3} mol dm^{-3}, titrating with 5 mm^3 aliquots to a 2 cm^3 solution of $H_3TCPP^{3-}/H_2TCPP^{4-}$ in a 1 cm path length cell. Note: a_1-d_1 and a_2-d_2 refers to 308.2 K and 298.2 K, respectively.

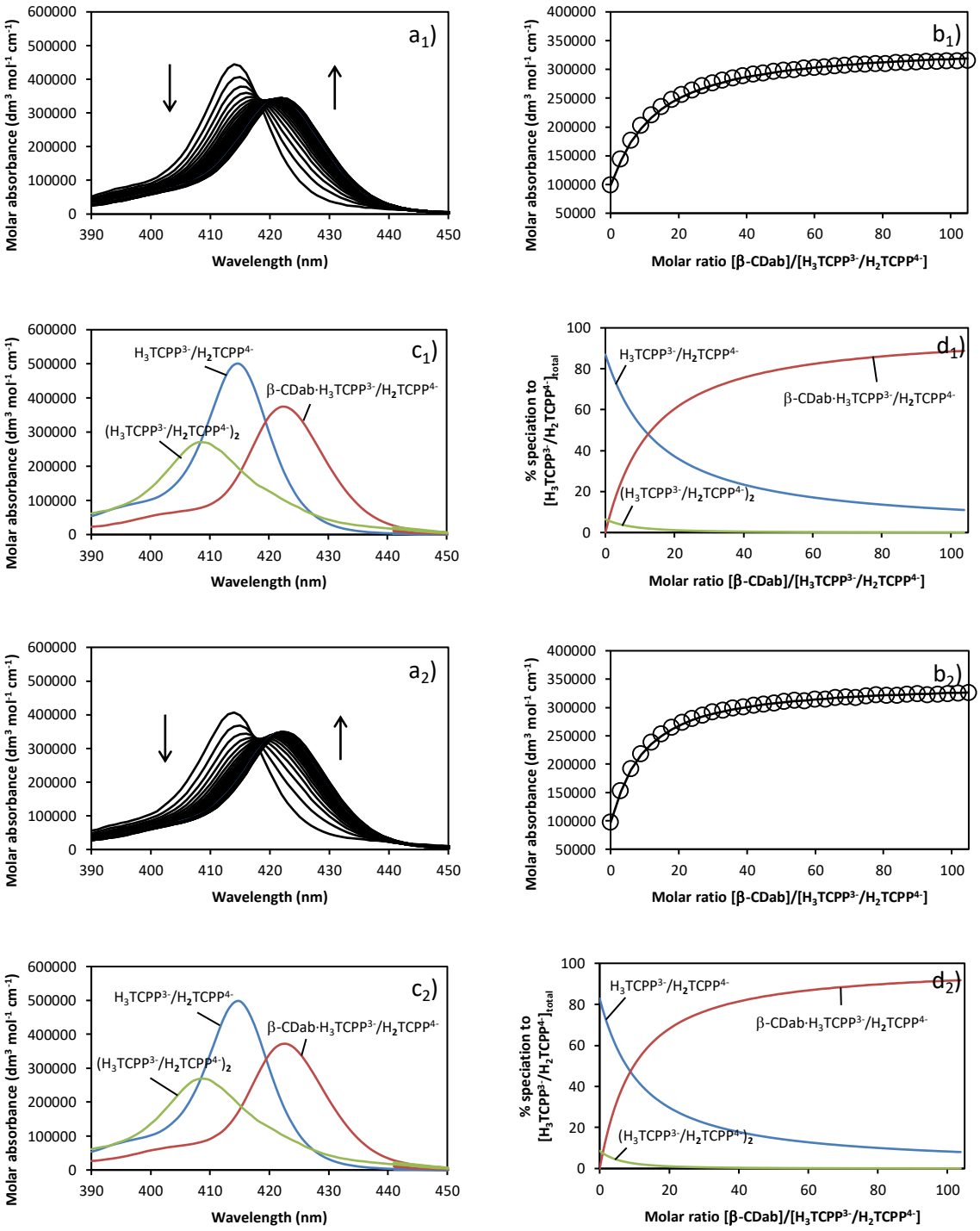

Figure 4.46: UV-vis absorbance data of $H_3TCPP^{3-}/H_2TCPP^{4-}$ (initial concentration 1.5×10^{-6} mol dm^{-3}) with increasing concentrations of β-CDab (0 – 1.4×10^{-4} mol dm^{-3}) in aqueous phosphate buffer (pH 7.0 and I = 0.10 mol dm^{-3}), showing a) the molar absorption spectrum, the arrows indicating the direction of change b) the experimental (circles) and best-fit (line) molar absorbances at 425 nm (fitted at 1 nm intervals over the range 400 – 430 nm) for a 1:1 β-CDab·$H_3TCPP^{3-}/H_2TCPP^{4-}$ complex, c) the experimental molar absorbances of free monomeric and dimeric $H_3TCPP^{3-}/H_2TCPP^{4-}$ and calculated molar absorbances of complexed $H_3TCPP^{3-}/H_2TCPP^{4-}$ and d) the calculated speciation of free and complexed $H_3TCPP^{3-}/H_2TCPP^{4-}$. The concentration of β-CDab was 1.8×10^{-3} mol dm^{-3}, titrating with 5 mm^3 aliquots to a 2 cm^3 solution of $H_3TCPP^{3-}/H_2TCPP^{4-}$ in a 1 cm path length cell. Note: a_1-d_1 and a_2-d_2 refers to 288.2 K and 278.2 K, respectively.

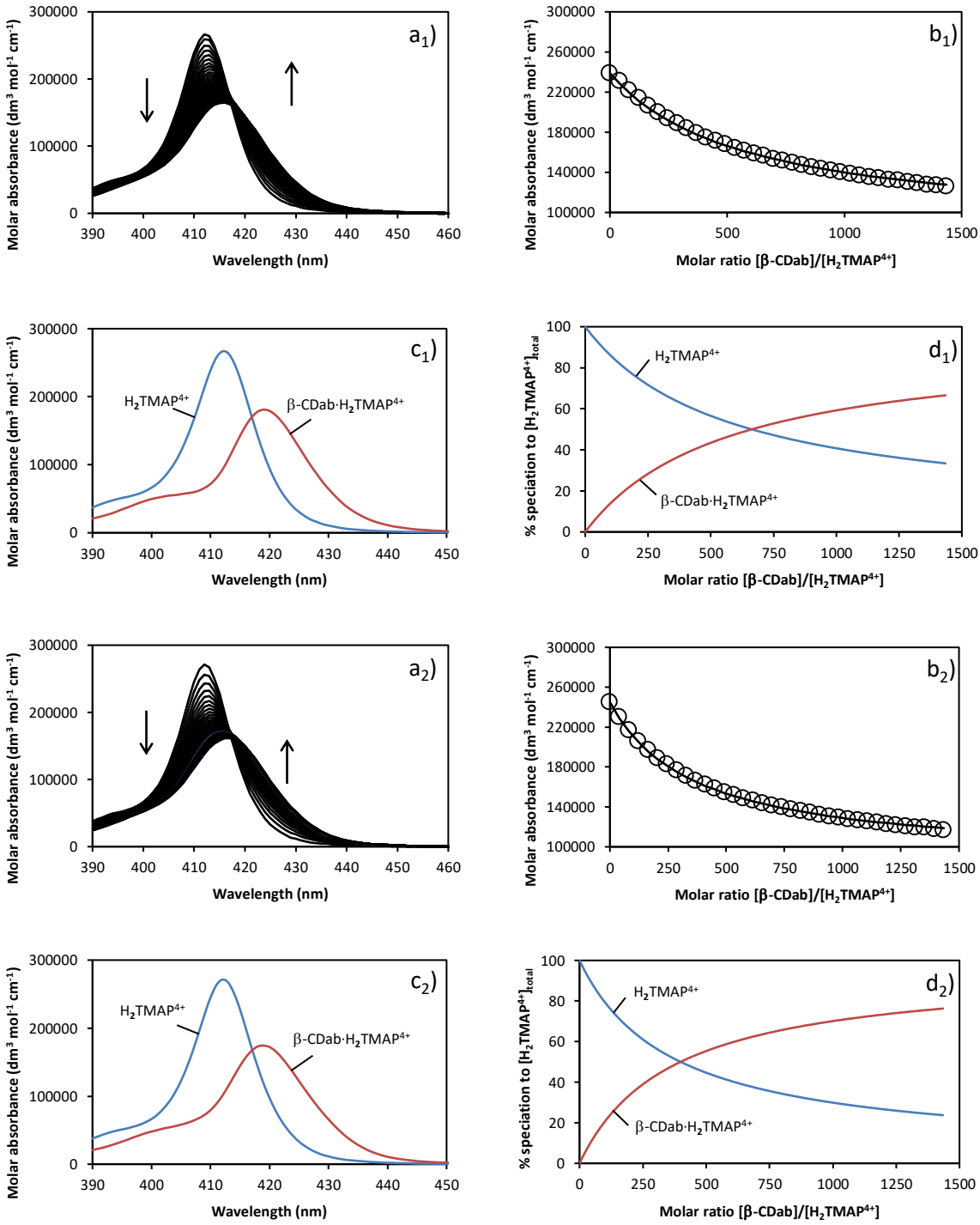

Figure 4.47: UV-vis absorbance data of H_2TMAP^{4+} (initial concentration 2.5×10^{-6} mol dm^{-3}) with increasing concentrations of β-CDab (0 – 3.0×10^{-3} mol dm^{-3}) in aqueous phosphate buffer (pH 7.0 and I = 0.10 mol dm^{-3}), showing a) the molar absorption spectrum, the arrows indicating the direction of change, b) the experimental (circles) and best-fit (line) molar absorbances at 410 nm (fitted at 1 nm intervals over the range 400 – 430 nm) for a 1:1 β-CDab·H_2TMAP^{4+} complex,, c) the experimental molar absorbances of free H_2TMAP^{4+} and calculated molar absorbances of complexed H_2TMAP^{4+} and d) the calculated speciation of free and complexed H_2TMAP^{4+}. The concentration of β-CDab was 2.0×10^{-3} mol dm^{-3}, titrating with 10 mm^3 aliquots to a 2 cm^3 solution of H_2TMAP^{4+} in a 1 cm path length cell. Note: a_1-d_1 and a_2-d_2 refers to 308.2 K and 298.2 K, respectively.

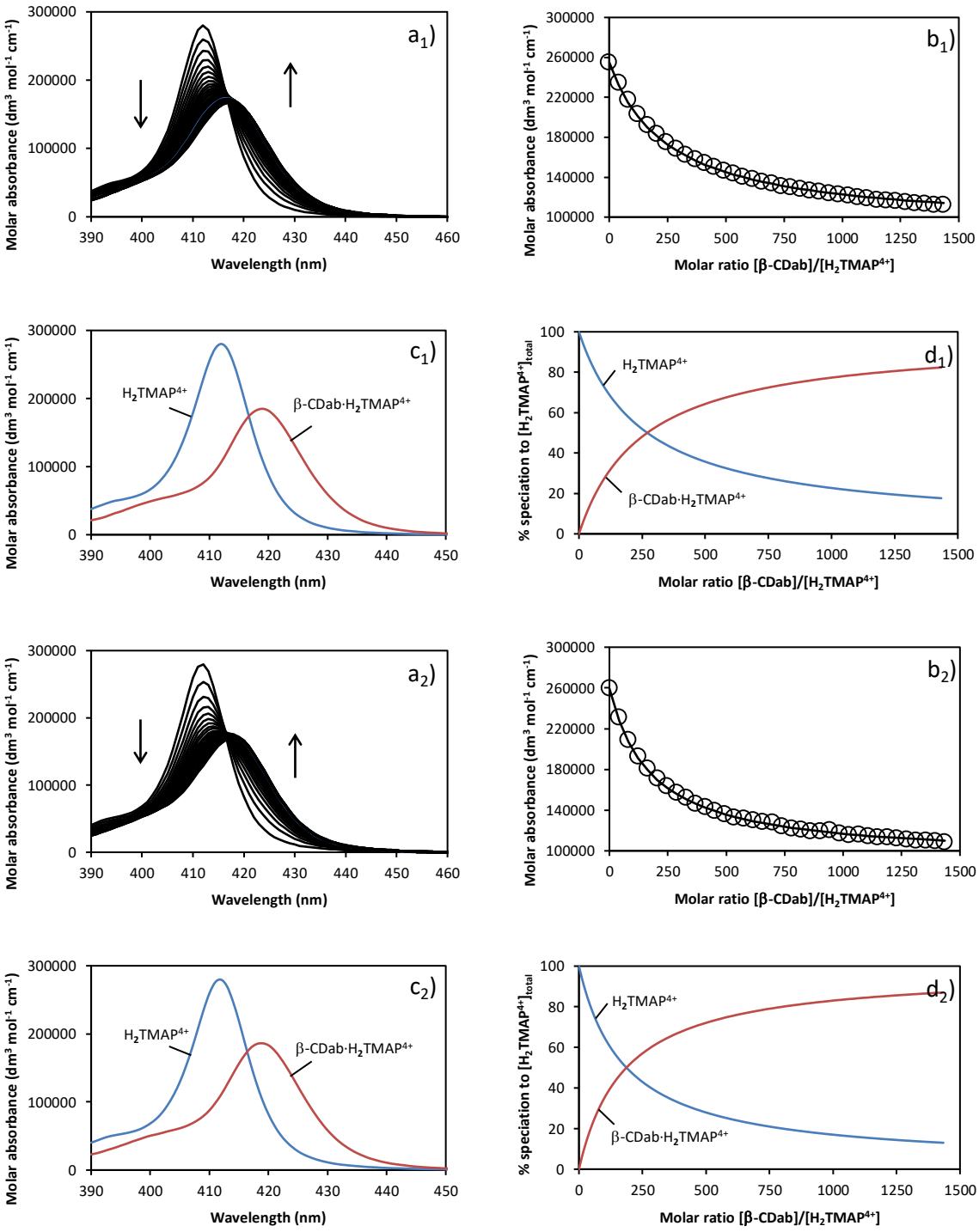

Figure 4.48: UV-vis absorbance data of H_2TMAP^{4+} (initial concentration 2.5×10^{-6} mol dm^{-3}) with increasing concentrations of β-CDab ($0 – 3.0 \times 10^{-3}$ mol dm^{-3}) in aqueous phosphate buffer (pH 7.0 and I = 0.10 mol dm^{-3}), showing a) the molar absorption spectrum, the arrows indicating the direction of change, b) the experimental (circles) and best-fit (line) molar absorbances at 410 nm (fitted at 1 nm intervals over the range 400 – 430 nm) for a 1:1 β-CDab·H_2TMAP^{4+} complex, c) the experimental molar absorbances of free H_2TMAP^{4+} and calculated molar absorbances of complexed H_2TMAP^{4+} and d) the calculated speciation of free and complexed H_2TMAP^{4+}. The concentration of β-CDab was 2.0×10^{-3} mol dm^{-3}, titrating with 10 mm^3 aliquots to a 2 cm^3 solution of H_2TMAP^{4+} in a 1 cm path length cell. Note: a_1-d_1 and a_2-d_2 refers to 288.2 K and 278.2 K, respectively.

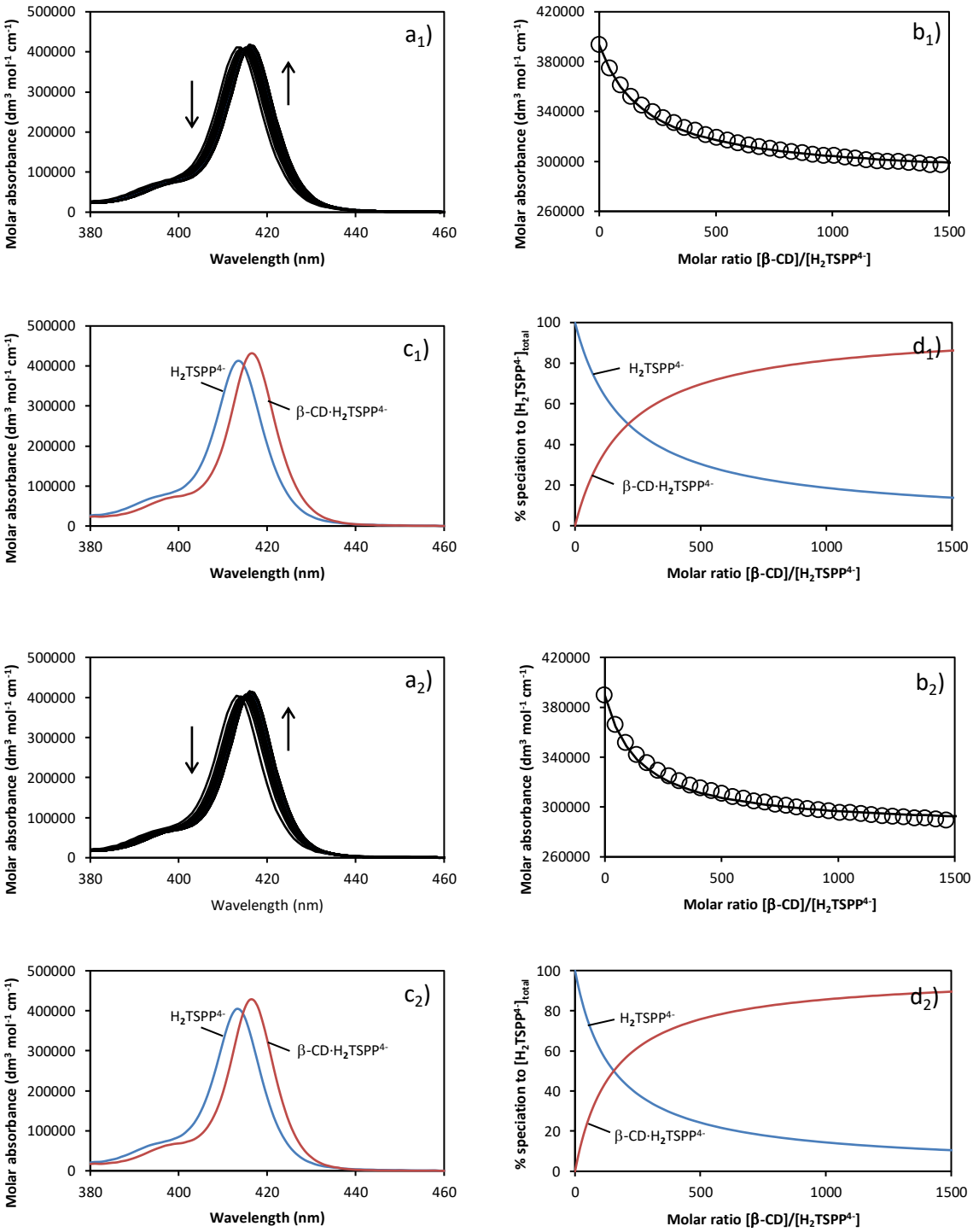

Figure 4.49: UV-vis absorbance data of H_2TSPP^{4-} (initial concentration 1.2×10^{-6} mol dm^{-3}) with increasing concentrations of β-CD ($0 - 1.6 \times 10^{-3}$ mol dm^{-3}) in aqueous phosphate buffer (pH 7.0 and I = 0.10 mol dm^{-3}), showing a) the molar absorption spectrum, the arrows indicating the direction of change, b) the experimental (circles) and best-fit (line) molar absorbances at 412 nm (unsatisfactorily fitted at 1 nm intervals over the range 400 – 425 nm) for a 1:1 β-CD·H_2TSPP^{4-} complex, c) the experimental molar absorbances of free H_2TSPP^{4-} and calculated molar absorbances of complexed H_2TSPP^{4-} and d) the calculated speciation of free and complexed H_2TSPP^{4-}. The concentration of β-CD was 0.011 mol dm^{-3}, titrating with 10 mm^3 aliquots to a 2 cm^3 solution of H_2TSPP^{4-} in a 1 cm path length cell. Note: a_1-d_1 and a_2-d_2 refers to 308.2 K and 298.2 K, respectively.

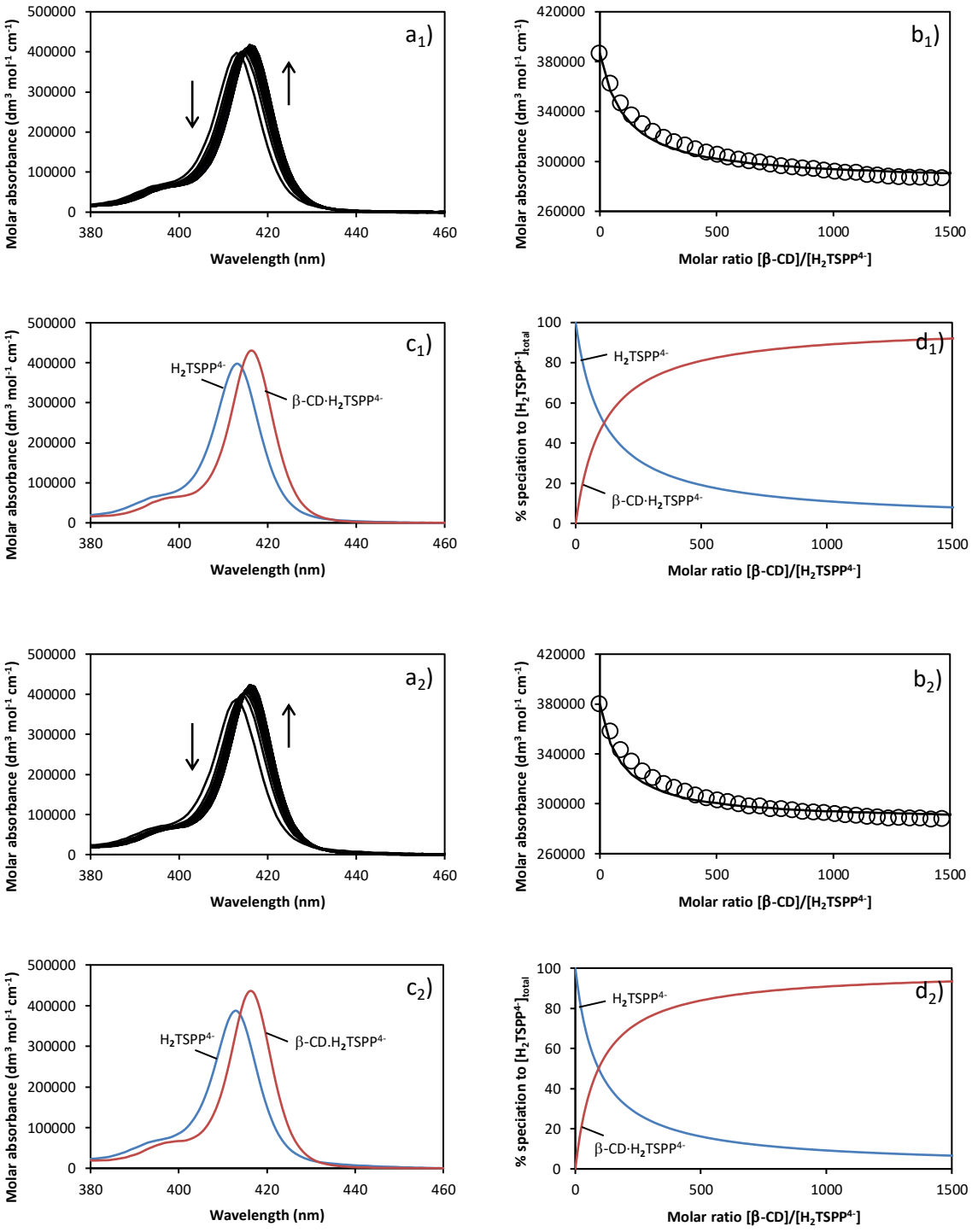

Figure 4.50: UV-vis absorbance data of H_2TSPP^{4-} (initial concentration 1.2×10^{-6} mol dm^{-3}) with increasing concentrations of β-CD ($0 - 1.6 \times 10^{-3}$ mol dm^{-3}) in aqueous phosphate buffer (pH 7.0 and I = 0.10 mol dm^{-3}), showing a) the molar absorption spectrum, the arrows indicating the direction of change, b) the experimental (circles) and best-fit (line) molar absorbances at 412 nm (unsatisfactorily fitted at 1 nm intervals over the range 400 – 430 nm) for a 1:1 β-CD·H_2TSPP^{4-} complex, c) the experimental molar absorbances of free H_2TSPP^{4-} and calculated molar absorbances of complexed H_2TSPP^{4-} and d) the calculated speciation of free and complexed H_2TSPP^{4-}. The concentration of β-CD was 0.011 mol dm^{-3}, titrating with 10 mm^3 aliquots to a 2 cm^3 solution of H_2TSPP^{4-} in a 1 cm path length cell. Note: a_1-d_1 and a_2-d_2 refers to 288.2 K and 278.2 K, respectively.

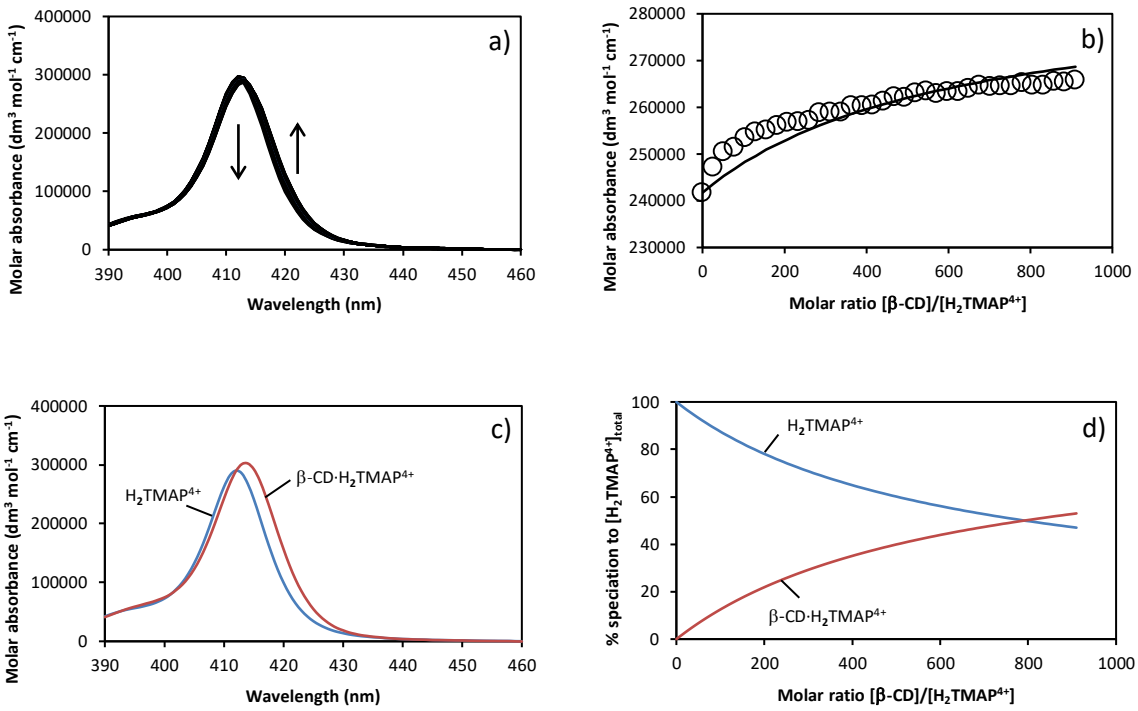

Figure 4.51: Molar absorbance of H_2TMAP^{4+} (2.5×10^{-6} mol dm^{-3}) with increasing concentrations of β-CD ($0 – 1.9 \times 10^{-3}$ mol dm^{-3}) in aqueous phosphate buffer (pH 7.0 and I = 0.10 mol dm^{-3}) at 298.2 K, showing a) the molar absorption spectrum, the arrows indicating the direction of change, b) the experimental (circles) and best-fit (line) molar absorbances at 415 nm (unsatisfactorily fitted at 1 nm intervals over the range 400 – 420 nm) for a 1:1 β-CD·H_2TMAP^{4+} complex, c) the experimental molar absorbances of free H_2TMAP^{4+} and calculated molar absorbances of complexed H_2TMAP^{4+} and d) the calculated speciation of free and complexed H_2TMAP^{4+}. The concentration of β-CD was 0.013 mol dm^{-3}, titrating with 10 mm^3 aliquots to a 2 cm^3 solution of H_2TMAP^{4+} in a 1 cm path length cell.

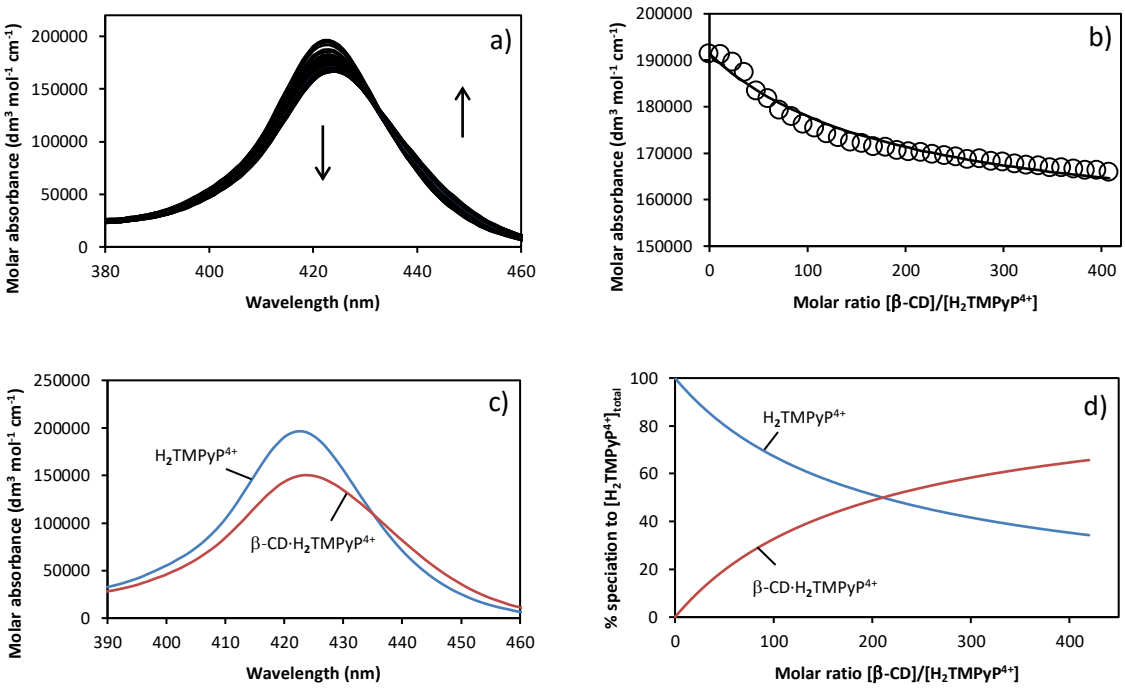

Figure 4.52: Molar absorbance of H_2TMPyP^{4+} (2.5×10^{-6} mol dm^{-3}) with increasing concentrations of β-CD (0 – 9.7×10^{-4} mol dm^{-3}) in aqueous phosphate buffer (pH 7.0 and I = 0.10 mol dm^{-3}) at 298.2 K, showing a) the molar absorption spectrum, the arrows indicating the direction of change b) the experimental (circles) and best-fit (line) molar absorbances at 425 nm (unsatisfactorily fitted at 1 nm intervals over the range 400 – 440 nm) for a 1:1 β-CD·H_2TMPyP^{4+} complex, c) the experimental molar absorbances of free H_2TMPyP^{4+} and calculated molar absorbances of complexed H_2TMPyP^{4+} and d) the calculated speciation of free and complexed H_2TMPyP^{4+}. The concentration of β-CD was 0.012 mol dm^{-3}, titrating with 10 mm^3 aliquots to a 2 cm^3 solution of H_2TMPyP^{4+} in a 1 cm path length cell.

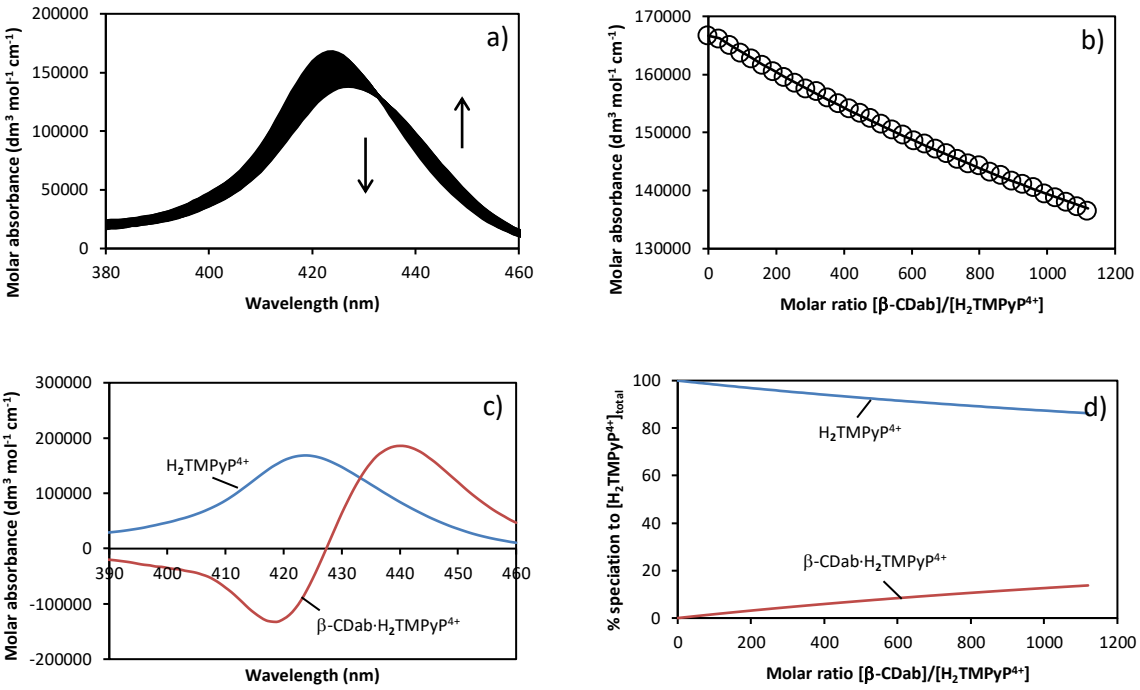

Figure 4.53: Molar absorbance of H_2TMPyP^{4+} (2.5×10^{-6} mol dm^{-3}) with increasing concentrations of β-CDab ($0 – 2.4 \times 10^{-3}$ mol dm^{-3}) in aqueous phosphate buffer (pH 7.0 and I = 0.10 mol dm^{-3}) at 308.2 K, showing a) the molar absorption spectrum, the arrows indicating the direction of change, b) the experimental (circles) and best-fit (line) molar absorbances at 425 nm (unsatisfactorily fitted at 1 nm intervals over the range 400 – 450 nm) for a 1:1 β-CDab·H_2TMPyP^{4+} complex, c) the experimental molar absorbances of free H_2TMPyP^{4+} and calculated molar absorbances of complexed H_2TMPyP^{4+} and d) the calculated speciation of free and complexed H_2TMPyP^{4+}. The concentration of β-CDab was 0.016 mol dm^{-3}, titrating with 10 mm^3 aliquots to a 2 cm^3 solution of H_2TMPyP^{4+} in a 1 cm path length cell.

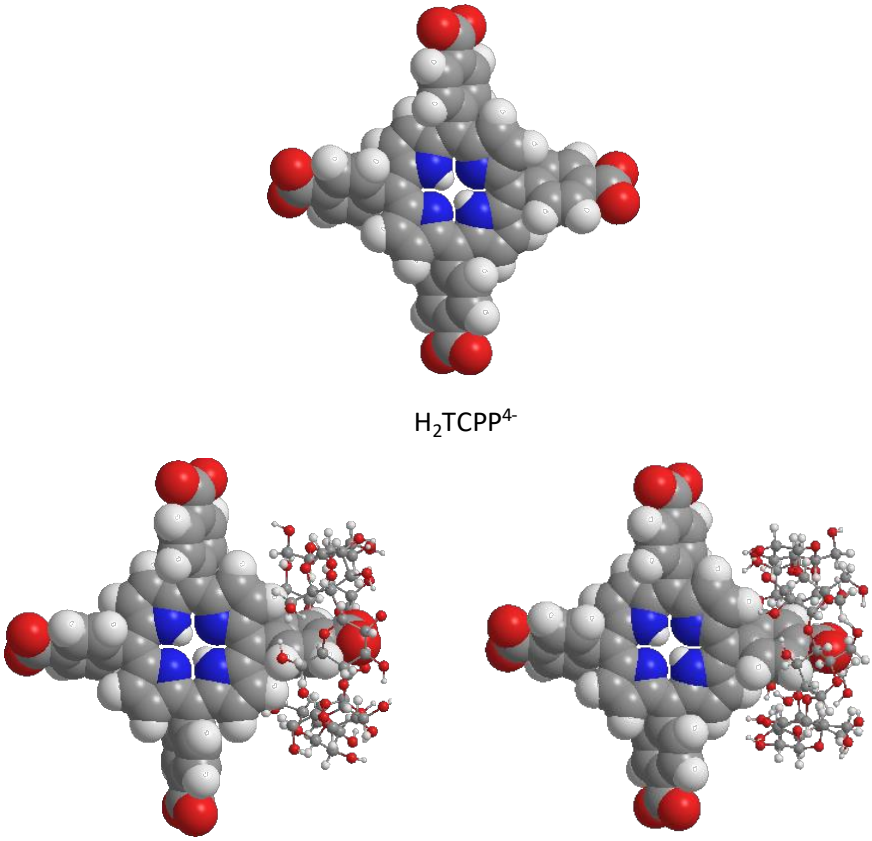

H_2TCPP^{4-}

β-CD·H_2TCPP^{4-}· primary face

β-CD·H_2TCPP^{4-} secondary face

Figure 4.54: Energy minimised molecular models of H_2TCPP^{4-} alone and in a 1:1 complex with β-CD, derived using the PM7 method on MOPAC software. The carbon, nitrogen, oxygen, and hydrogen atoms are shown in grey, blue, red, and white, respectively. Note: β-CD = ball and stick, H_2TCPP^{4-} = space filling. Carbon = grey, nitrogen = blue, oxygen = red and hydrogen = white.

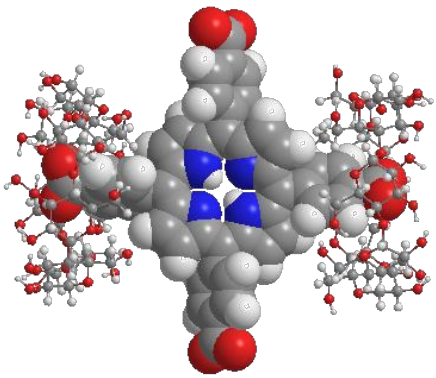

β-CD_2·H_2TCPP^{4-} *anti*, primary – primary

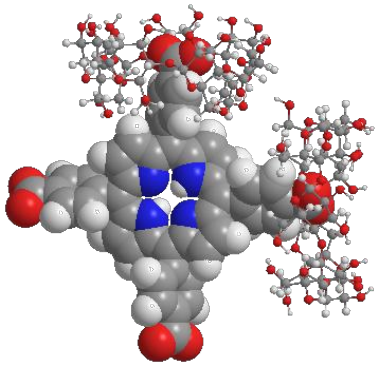

β-CD_2·H_2TCPP^{4-} *syn*, primary – primary

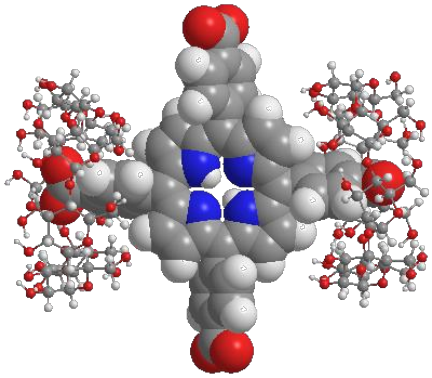

β-CD_2·H_2TCPP^{4-} *anti*, primary – secondary

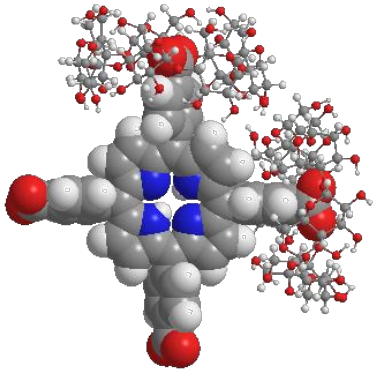

β-CD_2·H_2TCPP^{4-} *syn*, primary – secondary

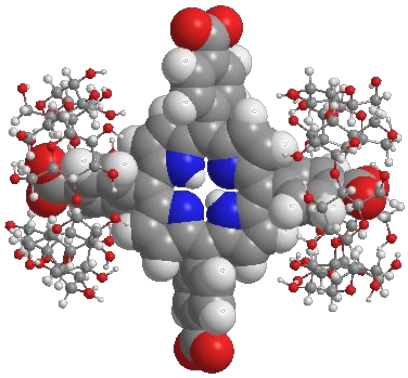

β-CD_2·H_2TCPP^{4-} *anti*, secondary – secondary

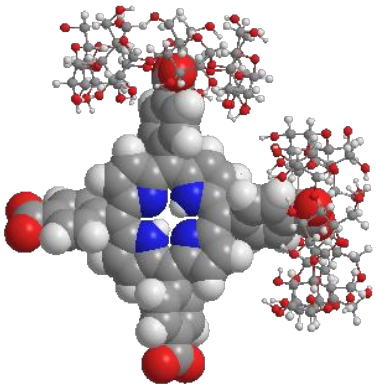

β-CD_2·H_2TCPP^{4-} *syn*, secondary – secondary

Figure 4.55: Energy minimised molecular models of 2:1 β-CD_2·H_2TCPP^{4-} complexes of various conformations, derived using the PM7 method on MOPAC software. The carbon, nitrogen, oxygen, and hydrogen atoms are shown in grey, blue, red, and white, respectively. Note: β-CD = ball and stick, H_2TCPP^{4-} = space filling. Carbon = grey, nitrogen = blue, oxygen = red and hydrogen = white.

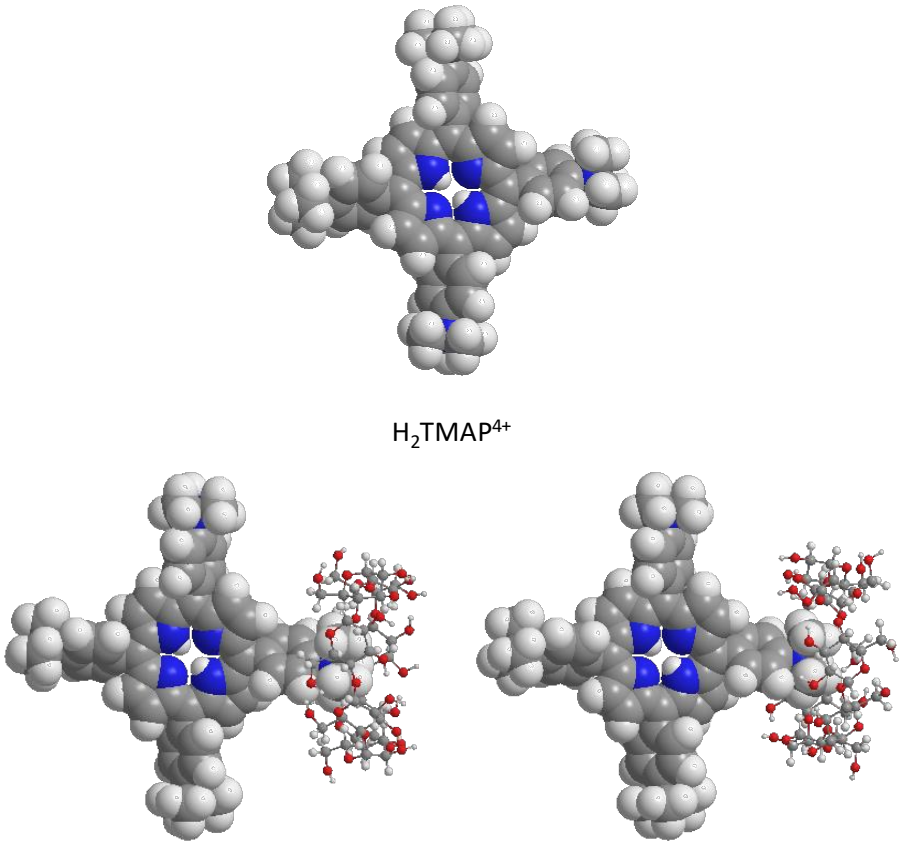

H_2TMAP^{4+}

β-CD·H_2TMAP^{4+} primary face

β-CD·H_2TMAP^{4+} secondary face

Figure 4.56: Energy minimised molecular models of H_2TMAP^{4+} alone and in a 1:1 complex with β-CD, derived using the PM7 method on MOPAC software. The carbon, nitrogen, oxygen, and hydrogen atoms are shown in grey, blue, red, and white, respectively. Note: β-CD = ball and stick, H_2TMAP^{4+} = space filling. Carbon = grey, nitrogen = blue, oxygen = red and hydrogen = white.

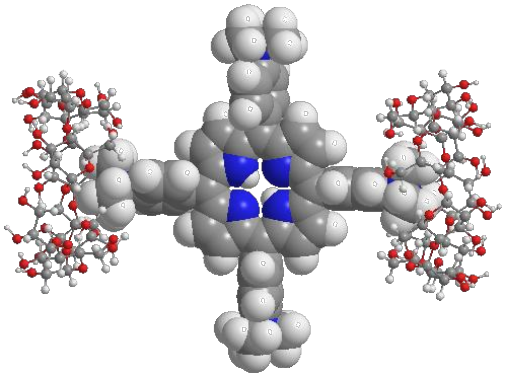

β-CD_2·H_2TMAP^{4+} *anti*, primary – primary

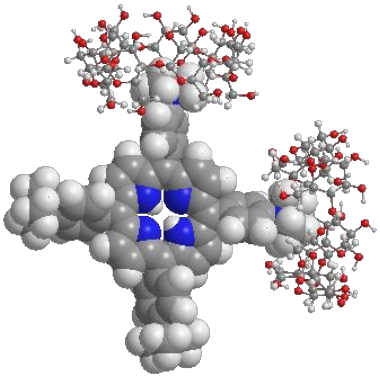

β-CD_2·H_2TMAP^{4+} *syn*, primary – primary

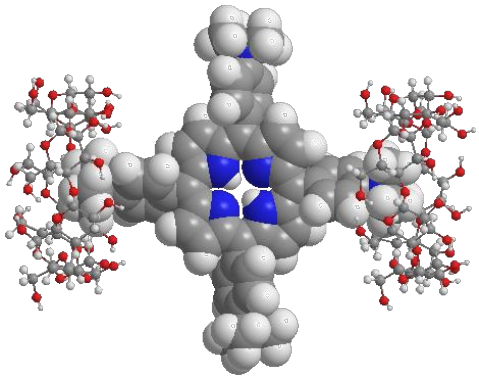

β-CD_2·H_2TMAP^{4+} *anti*, primary – secondary

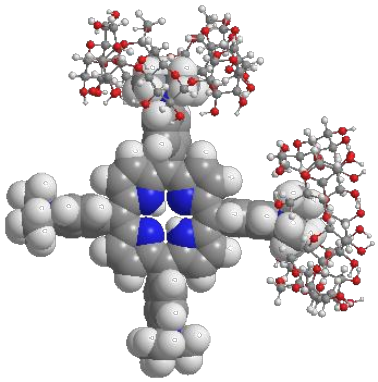

β-CD_2·H_2TMAP^{4+} *syn*, primary – secondary

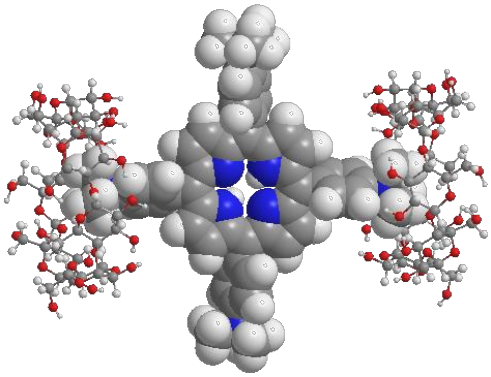

β-CD_2·H_2TMAP^{4+} *anti*, secondary – secondary

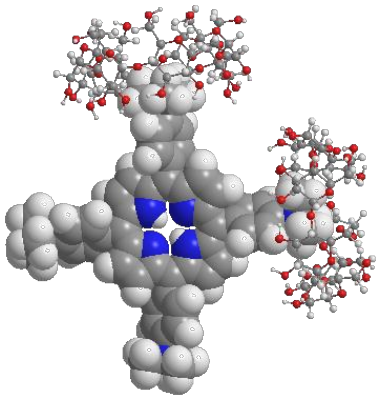

β-CD_2·H_2TMAP^{4+} *syn*, secondary – secondary

Figure 4.57: Energy minimised molecular models of 2:1 β-CD_2·H_2TMAP^{4+} complexes of various conformations, derived using the PM7 method on MOPAC software. The carbon, nitrogen, oxygen, and hydrogen atoms are shown in grey, blue, red, and white, respectively. Note: β-CD = ball and stick, H_2TMAP^{4+} = space filling. Carbon = grey, nitrogen = blue, oxygen = red and hydrogen = white.

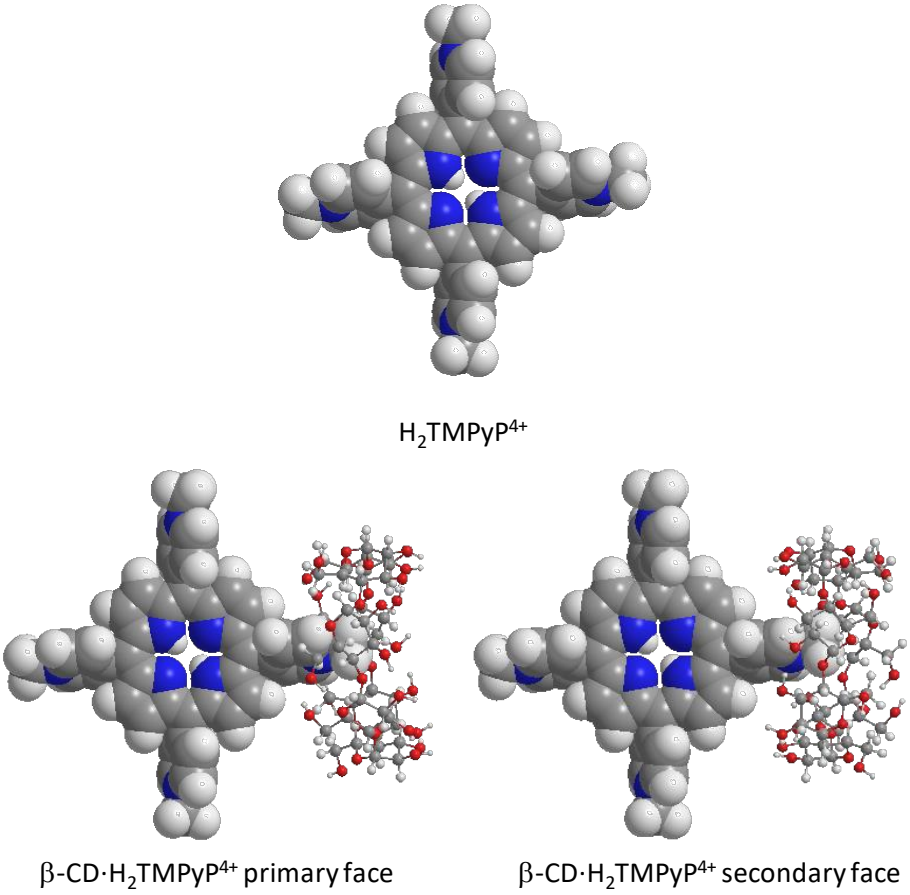

Figure 4.58: Energy minimised molecular models of H_2TMPyP^{4+} alone and in a 1:1 complex with β-CD, derived using the PM7 method on MOPAC software. The carbon, nitrogen, oxygen, and hydrogen atoms are shown in grey, blue, red, and white, respectively. Note: β-CD = ball and stick, H_2TMPyP^{4+} = space filling. Carbon = grey, nitrogen = blue, oxygen = red and hydrogen = white.

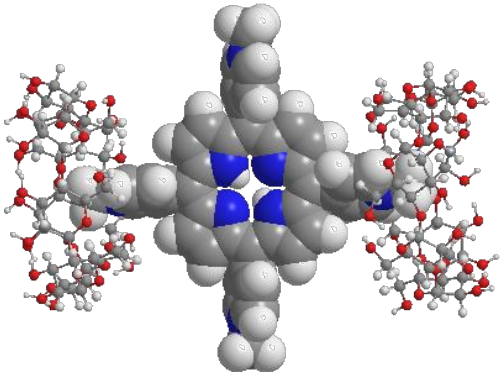

β-CD_2·H_2TMPyP^{4+} *anti*, primary – primary

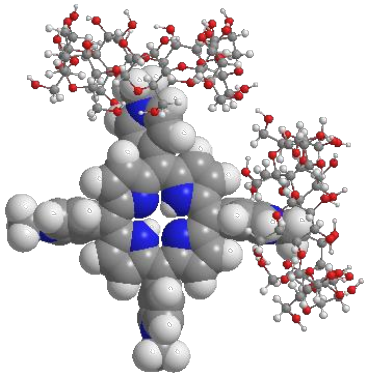

β-CD_2·H_2TMPyP^{4+} *syn*, primary – primary

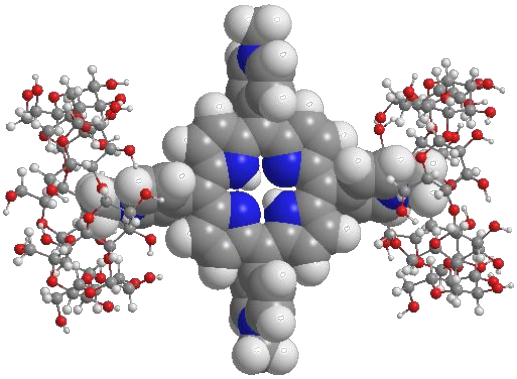

β-CD_2·H_2TMPyP^{4+} *anti*, primary – secondary

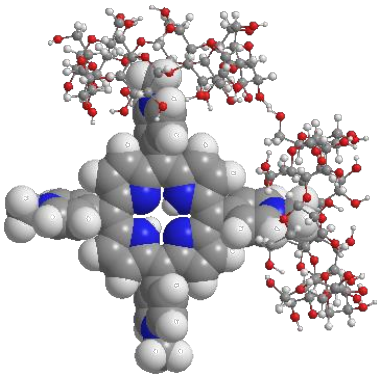

β-CD_2·H_2TMPyP^{4+} *syn*, primary – secondary

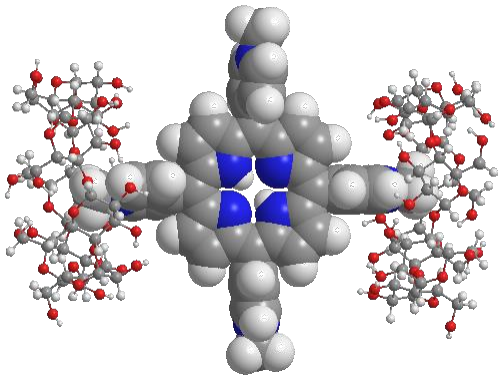

β-CD_2·H_2TMPyP^{4+} *anti*, secondary – secondary

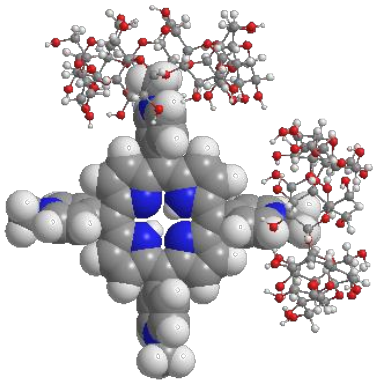

β-CD_2·H_2TMPyP^{4+} *syn*, secondary – secondary

Figure 4.59: Energy minimised molecular models of 2:1 β-CD_2·H_2TMPyP^{4+} complexes of various conformations, derived using the PM7 method on MOPAC software. Note: β-CD = ball and stick, H_2TMPyP^{4+} = space filling. Carbon = grey, nitrogen = blue, oxygen = red and hydrogen = white.

CHAPTER 5

Investigation of Polymeric Hydrogels using β-Cyclodextrin Oligomers and Adamantane- and Alkyl-substituted Poly(acrylate)s

5.1 Introduction to Polymeric Hydrogels

Polymeric hydrogels are 3D networks of polymers capable of entrapping large proportions of water. The applications of polymeric hydrogels are numerous and include drug delivery and tissue engineering.[1-7] Polymeric hydrogels are typically composed of hydrophobe-substituted water-soluble polymers. The formation of 3D networks occurs through the cross-linking of hydrophobic substituents of the polymer by hydrophobic association or a cross-linking agent.

β-Cyclodextrin oligomers may act as cross-linking agents.[8-13] In solution, the β-CD oligomers may form host-guest complexes with the hydrophobic substituents of adjacent polymer strands, giving rise to a network and, at adequate concentrations, a hydrogel. The nature of the interaction between the β-CD oligomer and hydrophobic substituents of the polymer may dictate the macroscopic properties of a hydrogel. Thus, understanding these interactions is fundamental to designing hydrogel systems with predictable traits.

The use of β-CD dimers in the formation of polymeric hydrogels has previously been established. Lincoln *et al.* designed polymeric networks based upon poly(acrylate)s (PAA) 3% randomly substituted with adamantyl (AD) or alkyl groups.[14-21] The PAA backbone is hydrophilic and readily soluble in aqueous solution, allowing the dissolution of the normally hydrophobic AD and alkyl substituents. Additionally, AD and the cavity of β-CD share similar size and shape profiles, making them suitable as host-guest counterparts. Therefore, the addition of β-CD dimers into an aqueous solution of AD- or alkyl-substituted PAAs forms a polymeric network from the complexation between β-CD groups of the dimer and hydrophobic substituents on adjacent polymer strands. The complexation is exemplified in Figure 5.1, using a urea-linked β-CD dimer as the cross-linking agent and an AD-modified PAA as the polymer.

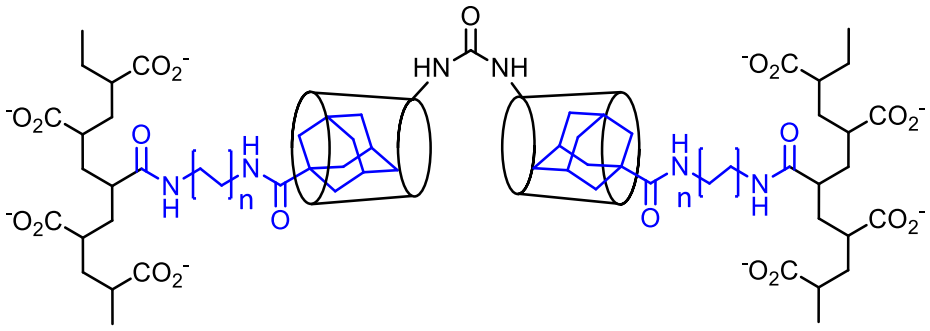

Figure 5.1: Host-guest complexation between the β-CD groups of a urea-linked β-CD dimer and the AD substituents of an AD-substituted PAA. The number of *n* subunits of the alkyl tether connecting the AD substituent to the PAA backbone may be fine-tuned.

Various stoichiometries and orientations typify the interactions between the β-CD dimers and hydrophobe-substituted PAAs, as shown in Figure 5.2. Cross-links may form due to the association of hydrophobic substituents of PAA or the formation of 1:2 host:guest complexes. Additionally, the cross-links that form may be between substituents on a single polymer strand (intra-strand cross-links) or between substituents on adjacent polymer strands (inter-strand cross-links). Aside from cross-links, monofunctional 1:1 host:guest complexes may also form.

The competition between these various interactions may be controlled by the solution concentrations. Dilute solutions favour intra-strand cross-links, resulting in the formation of small aggregates, while more concentrated solutions favour inter-strand cross-links, resulting in the formation of expansive polymer networks. Additionally, the prevalence of monofunctional complexes may be dictated by the length of the hydrophobe substituent, the structure of the β-CD oligomer and the host:guest ratio.

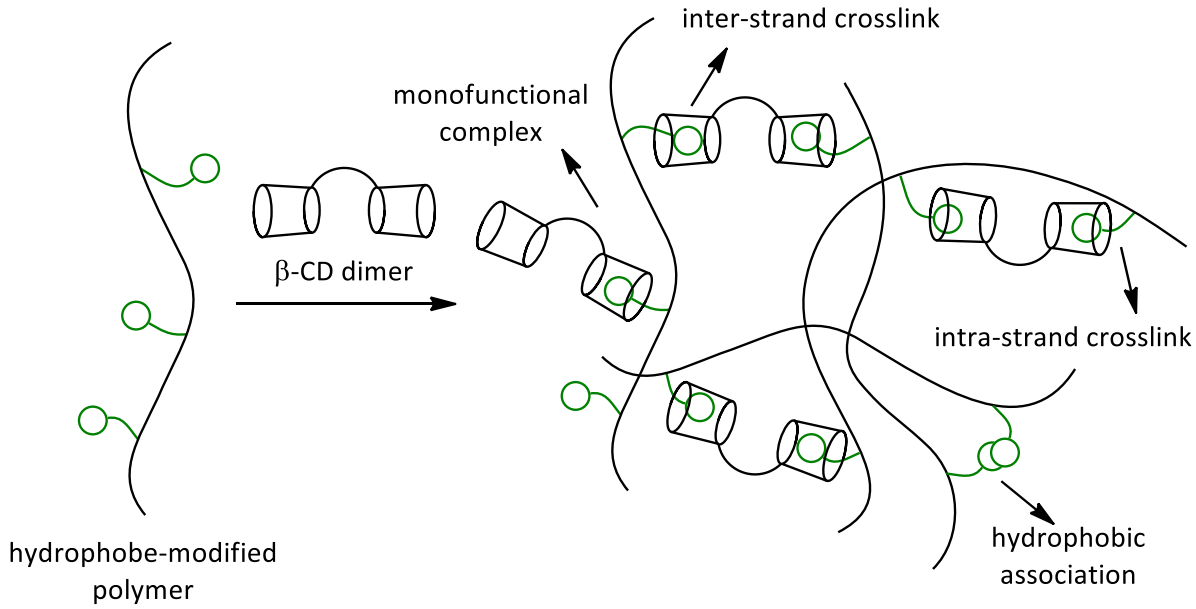

Figure 5.2: Formation of a host-guest linked hydrogel from the interactions between hydrophobe-modified polymers and β-CD dimers. The polymer is depicted by the solid curved lines and the hydrophobes are depicted as green circles.

The effect of structural isomerisation on β-CD complexation may be extended to polymeric networks. The β-CD dimers described in Chapter 2 may be used as cross-linking agents in the formation of polymeric hydrogels. The formation of polymeric networks using the two structural isomers of azobenzene-linked β-CD dimers, *E-p*-β-CD_2az and *E/Z-m*-β-CD_2az, may yield a greater understanding of the factors that influence the properties of polymeric hydrogels. Additionally, the photoisomerisation properties of *E-p*-β-CD_2az and *E/Z-m*-β-CD_2az may be utilised to affect the macroscopic properties of the hydrogel, such as the solution viscosity.[22]

5.1.1 Aims of this study

The aim of this research is to investigate the interactions between four β-CD hosts and four hydrophobe-substituted PAAs. The four β-CD hosts are native β-CD, β-CDab, *E-p*-β-CD_2az and *E/Z-m*-β-CD_2az, as shown in Figure 5.3.

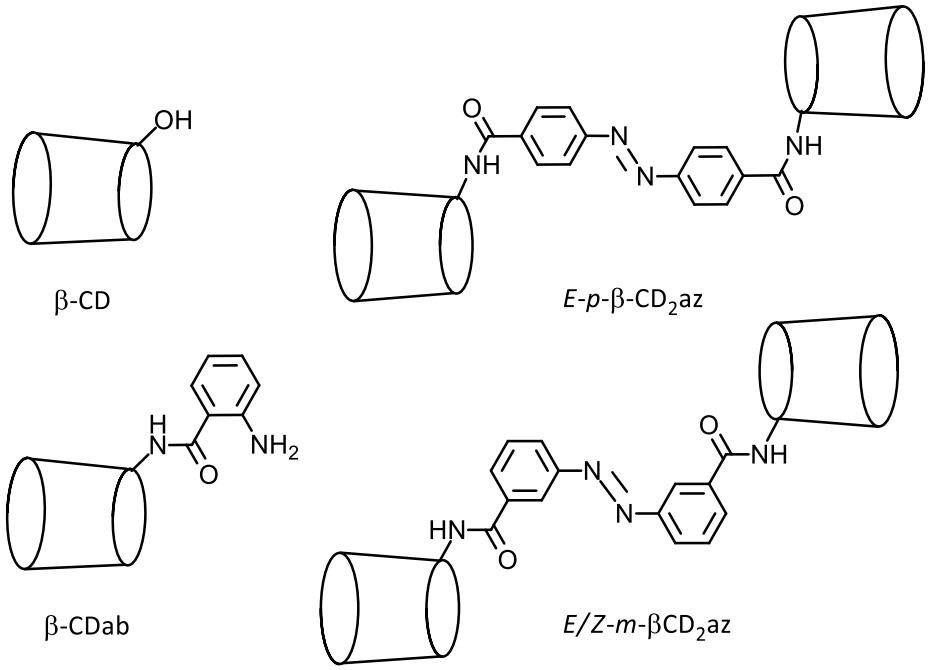

Figure 5.3: Structures of β-CD, β-CDab, *E-p*-β-CD_2az and *E/Z-m*-β-CD_2az. Note that only the *E* isomer of *E/Z-m*-β-CD_2az has been shown.

The four hydrophobe-substituted PAAs will use AD and alkyl groups as the hydrophobic substituents. Three AD-substituted PAAs and one alkyl-substitued PAA will be synthesised. The AD groups will be attached to the PAA backbone through an ethyl (en), hexyl (hn) and dodecyl (ddn) tether to form 1-(2-aminoethyl)-adamantane-1-carboxyamide poly(acrylate)s (PAAADen), 1-(6-aminohexyl)-adamantane-1-carboxyamide poly(acrylate)s (PAAADhn) and 1-(12-aminododecyl)-adamantane-1-carboxyamide poly(acrylate)s (PAAADddn), respectively. One alkyl-substituted PAA will be synthesised using a dodecyl (C12) group to form dodecyl-substituted poly(acrylate)s (PAAC12). Each substituted PAA will be synthesised with approximately 3% random substitution of the hydrophobe onto the polymer backbone. The structures of PAAADen, PAAADhn, PAAADddn and PAAC12 are shown in Figure 5.4.

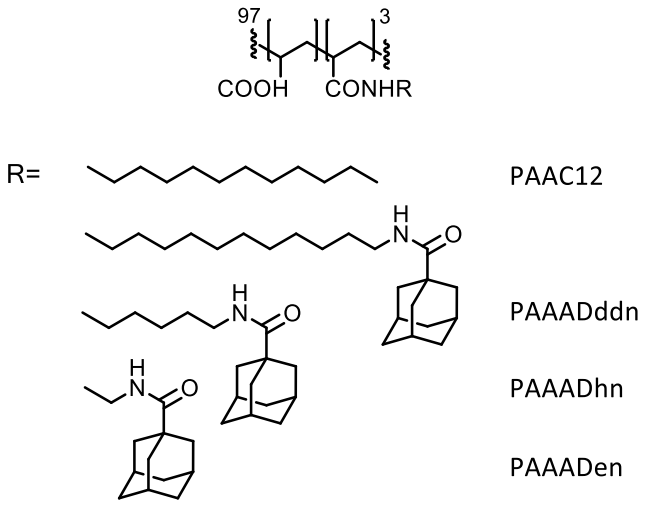

Figure 5.4: Structure of PAA 3% randomly substituted with AD- or alkyl-substituents.

The formation of a polymeric network from the interaction between the β-CD hosts and substituted PAAs, yielding 16 systems in total, will be investigated. The complexation properties will be qualitatively characterised by 2D NMR spectroscopy and quantitatively studied using isothermal titration calorimetry (ITC) to determine the complexation constants and thermodynamic parameters. The macroscopic properties will then be investigated by rheological studies. The effect of photoisomerisation of *E-p*-β-CD_2az and *E/Z-m*-β-CD_2az will also be investigated by rheology. This research will identify the effects of β-CD modification, structural isomerisation and photoisomerisation on the complexation properties and bulk-material properties of polymeric hydrogels.

5.2 Results and Discussion

5.2.1 Synthesis of polymers

The synthesis of PAAADen, PAAADhn, PAAADddn and PAAC12 followed procedures outlined in the literature,[15,19,23,24] beginning with the synthesis of the hydrophobic substituents. The ethyl-, hexyl- and dodecyl-modified AD substituents were synthesised by the modification of 1-adamantane-carboxylic acid (ADCA) with 4-nitrophenol to form 1-(4-nitrophenyloxylcarbonyl)adamantane (ADnp). Each alkyl-modified AD substituent was then synthesised through modification of ADnp with 1,2-diaminoethane, 1,6-diaminohexane and 1,12-diaminododecane to form *N*-(2-aminoethyl)-adamantane-1-carboxyamide (ADen), *N*-(2-aminohexyl)-adamantane-1-carboxyamide (ADhn), *N*-(2-aminododecyl)-adamantane-1-carboxyamide (ADddn), respectively, as shown in Figure 5.5. 1,12-diaminododecane (C12) was obtained commercially.

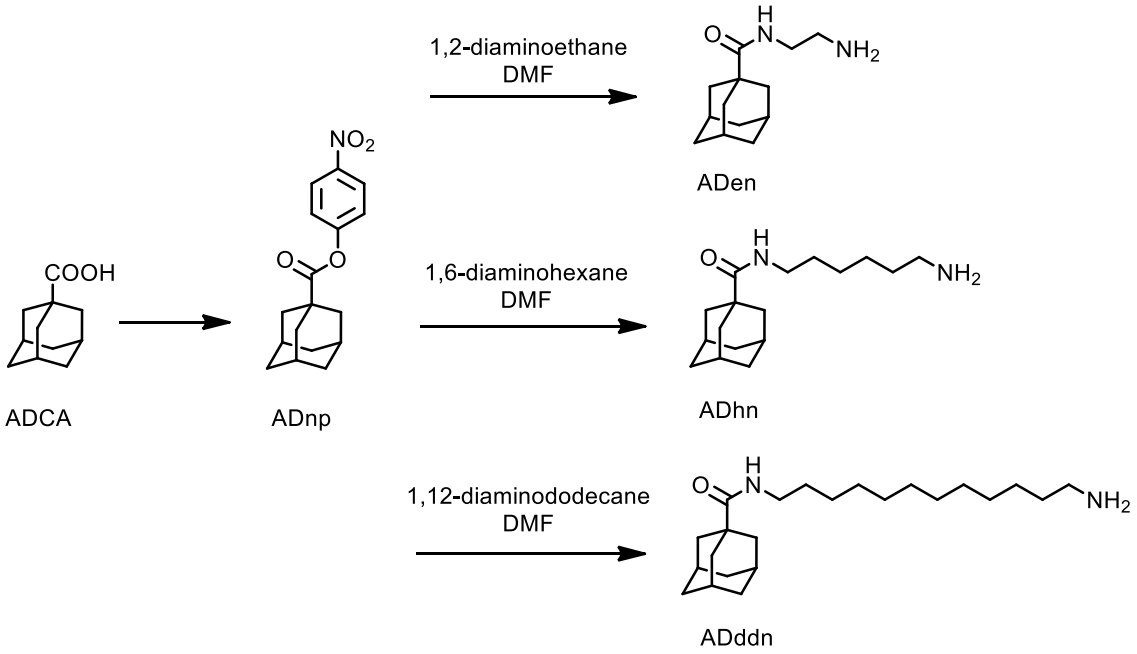

Figure 5.5: Synthesis of ethyl-, hexyl and dodecyl-modified AD.

The hydropobic substituents ADen, ADhn, ADddn and C12 were attached to the PAA backbone by direct substitution to form PAAADen, PAAADhn, PAAADddn and PAAC12, respectively, as shown in Figure 5.6. The desired degree of substitution was achieved by controlling the mole fraction of either ADen, ADhn, ADddn or C12 added to each sodium acrylate unit of PAA. The degree of hydrophobe-substitution onto the PAA backbone was determined by ^{1}H NMR spectroscopy according to literature methods[25] by comparing the areas of integration of ADen, ADhn, ADddn or C12 resonances with PAA CH_2 resonances. The degrees of substitution for PAAADen, PAAADhn, PAAADddn and PAAC12 were determined to be 2.0 ± 0.2 %, 2.7 ± 0.3 %, 2.0 ± 0.2 % and 1.8 ± 0.2 %, respectively. The complete experimental details are given in Chapter 7.

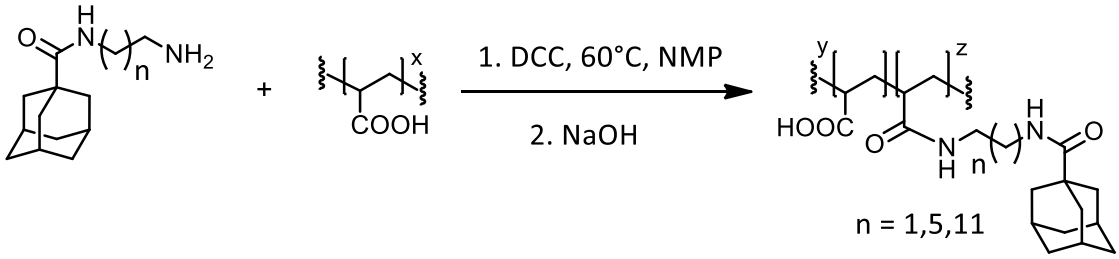

a)

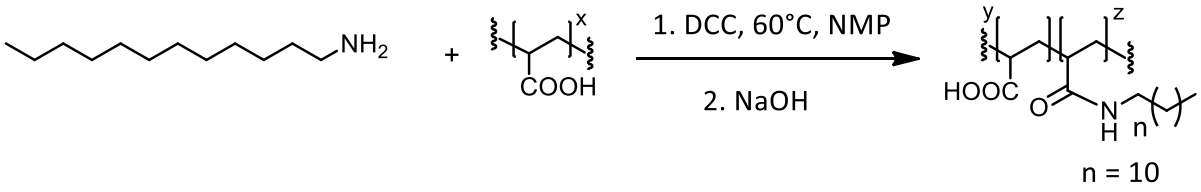

b)

Figure 5.6: Synthesis of a) AD-modified PAA, where n = 1, 5, 11 correspond to PAAADen, PAAADhn and PAAADddn, respectively, and b) PAAC12.

5.2.2 Complexation of PAAADen, PAAADhn, PAAADddn and PAAC12 by β-CD, β-CDab, *E-p*-β-CD_2az and *E/Z-m*-β-CD_2az

The complexation of the hydrophobic substituents of PAAADen, PAAADhn, PAAADddn and PAAC12 by β-CD, β-CDab, *E-p*-β-CD_2az, and *E/Z-m*-β-CD_2az was studied qualitatively and quantitatively. 2D ^{1}H NOESY NMR spectroscopy was used to determine the qualitative complexation behavior, while ITC was used to quantitatively describe the complexation constants and thermodynamic parameters which govern complexation.

5.2.2.1 Qualitative Investigation by 2D ^{1}H NOESY NMR Spectroscopy

The complexation of the hydrophobic substituents of PAAADen, PAAADhn, PAAADddn and PAAC12 by β-CD, β-CDab, *E-p*-β-CD_2az, and *E/Z-m*-β-CD_2az was determined by 2D ^{1}H NOESY NMR spectroscopy. Solutions of each host-polymer combination were prepared in D_2O phosphate buffer (pD 7.0, I = 0.10 mol dm^{-3}) at 298.2 K. The 2D ^{1}H NOESY NMR spectrum for all host-polymer combinations are given in Figure 5.7 – Figure 5.22

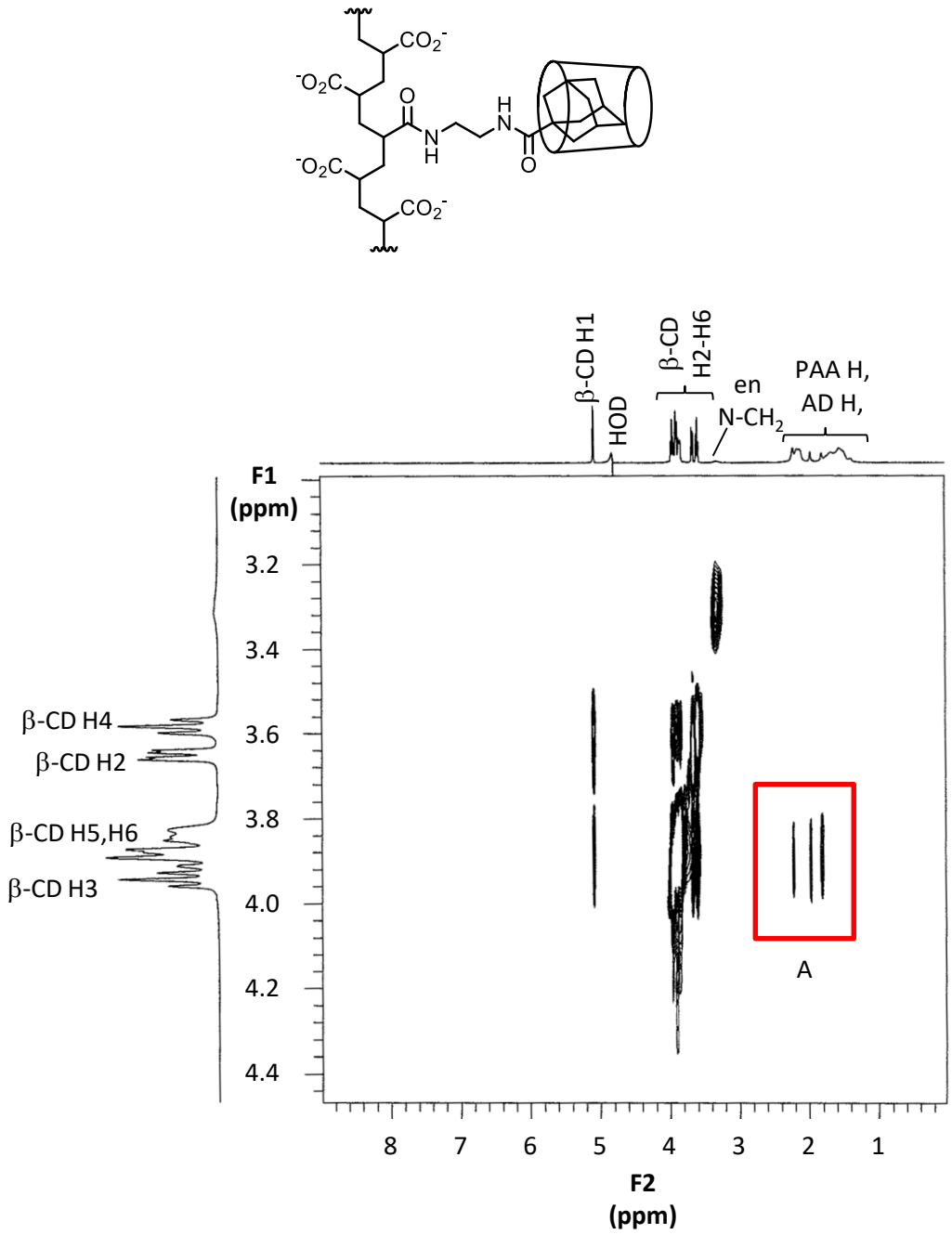

Figure 5.7: 2D ^{1}H NOESY NMR spectrum of 0.98 wt% PAAADen ([ADen] = 2.0×10^{-3} mol dm^{-3}) and β-CD (3.0×10^{-3} mol dm^{-3}) prepared in D_2O phosphate buffer (pD 7.0, I = 0.10 mol dm^{-3}) at 298.2 K. Rectangle A highlights cross-peaks arising from NOE interactions of the annular protons of β-CD with protons of ADen. A possible structure showing a portion of PAAADen forming a 1:1 complex is shown above.

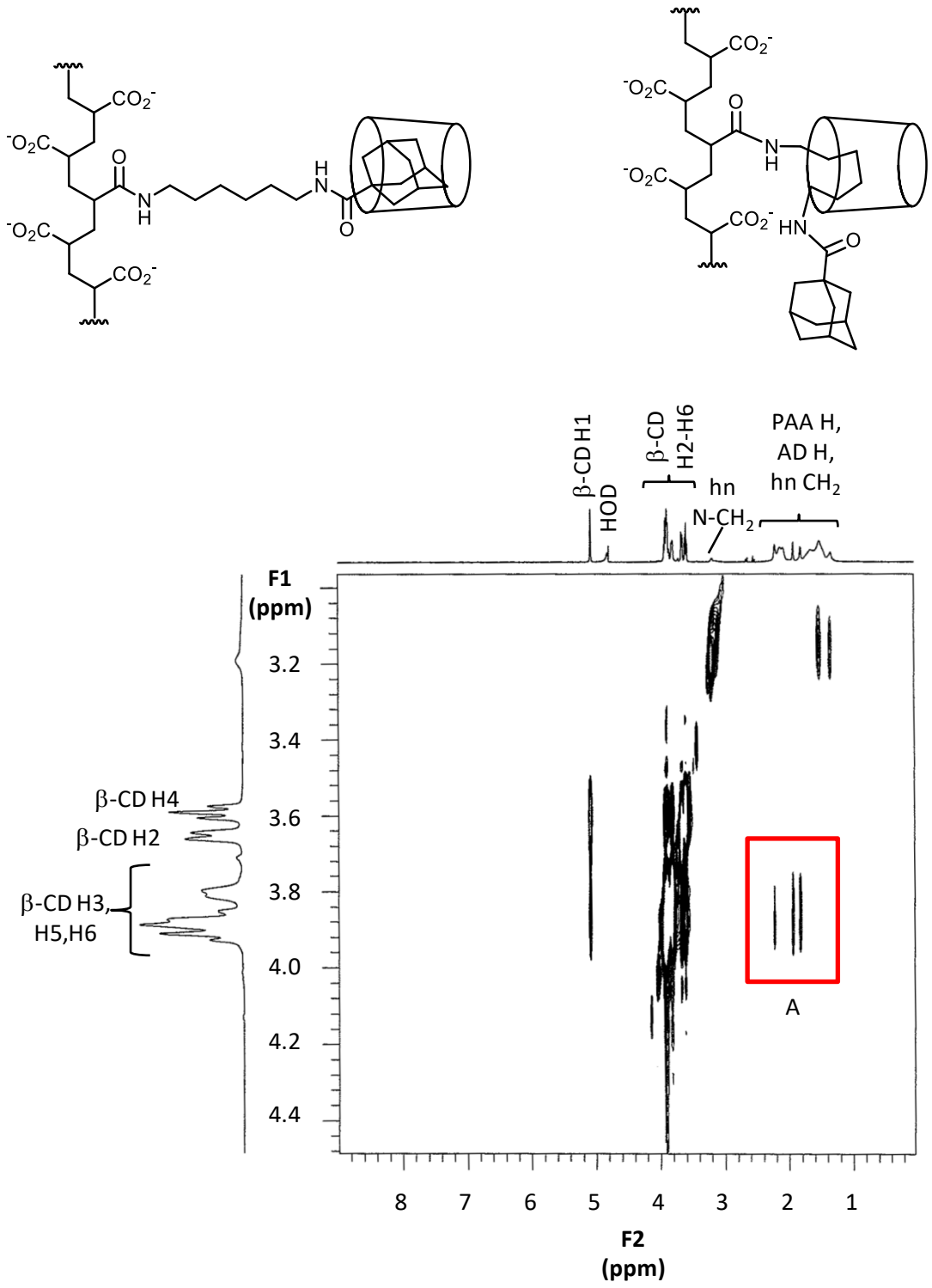

Figure 5.8: 2D ^{1}H NOESY NMR spectrum of 0.74 wt% PAAADhn ([ADhn] = 2.0×10^{-3} mol dm^{-3}) and β-CD (3.0×10^{-3} mol dm^{-3}) prepared in D_2O phosphate buffer (pD 7.0, I = 0.10 mol dm^{-3}) at 298.2 K. Rectangle A highlights cross-peaks arising from NOE interactions of the annular protons of β-CD with protons of ADhn. Possible structures showing a portion of PAAADhn forming 1:1 complexes are shown above.

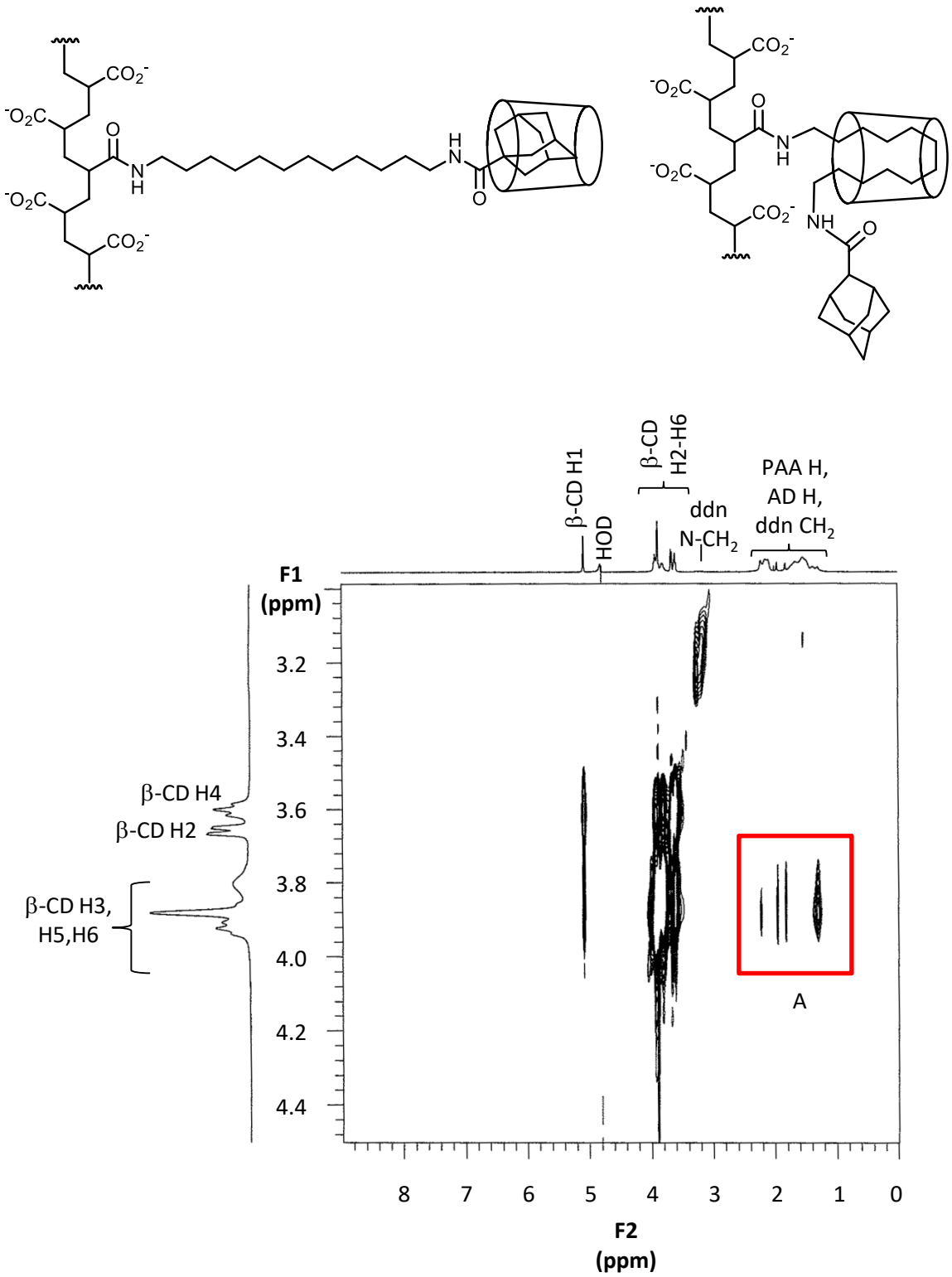

Figure 5.9: 2D ^{1}H NOESY NMR spectrum of 1.00 wt% PAAADddn ([ADddn] = 2.0 × 10^{-3} mol dm^{-3}) and β-CD (3.0 × 10^{-3} mol dm^{-3}) prepared in D_2O phosphate buffer (pD 7.0, *I* = 0.10 mol dm^{-3}) at 298.2 K. Rectangle A highlights cross-peaks arising from NOE interactions of the annular protons of β-CD with protons of ADddn. Possible structures showing a portion of PAAADddn forming 1:1 complexes are shown above.

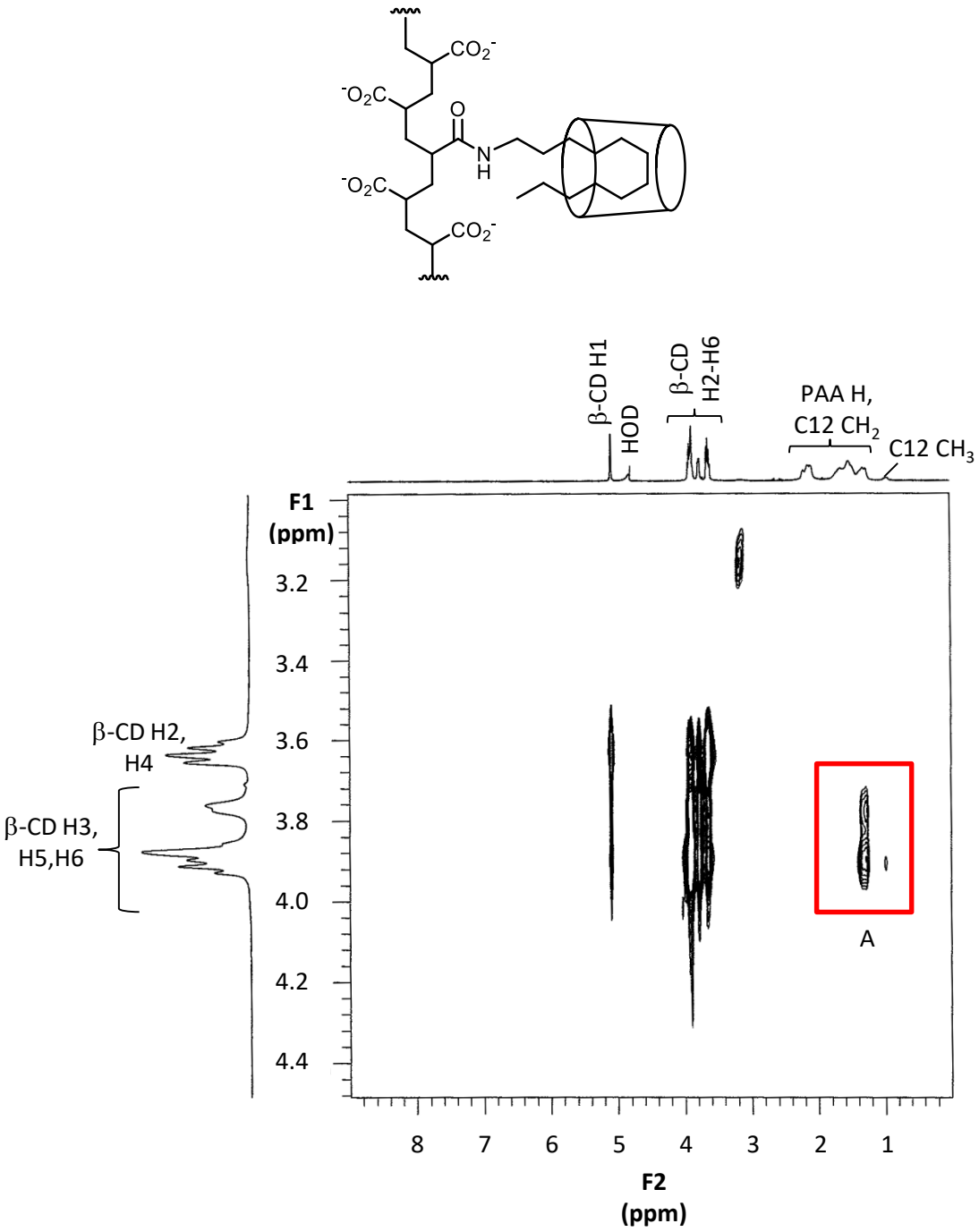

Figure 5.10: 2D ^{1}H NOESY NMR spectrum of 1.07 wt% PAAC12 ([C12] = 2.0 × 10^{-3} mol dm^{-3}) and β-CD (3.0 × 10^{-3} mol dm^{-3}) prepared in D_2O phosphate buffer (pD 7.0, *I* = 0.10 mol dm^{-3}) at 298.2 K. Rectangle A highlights cross-peaks arising from NOE interactions of the annular protons of β-CD with protons of C12. A possible structure showing a portion of PAAC12 forming a 1:1 complex is shown above.

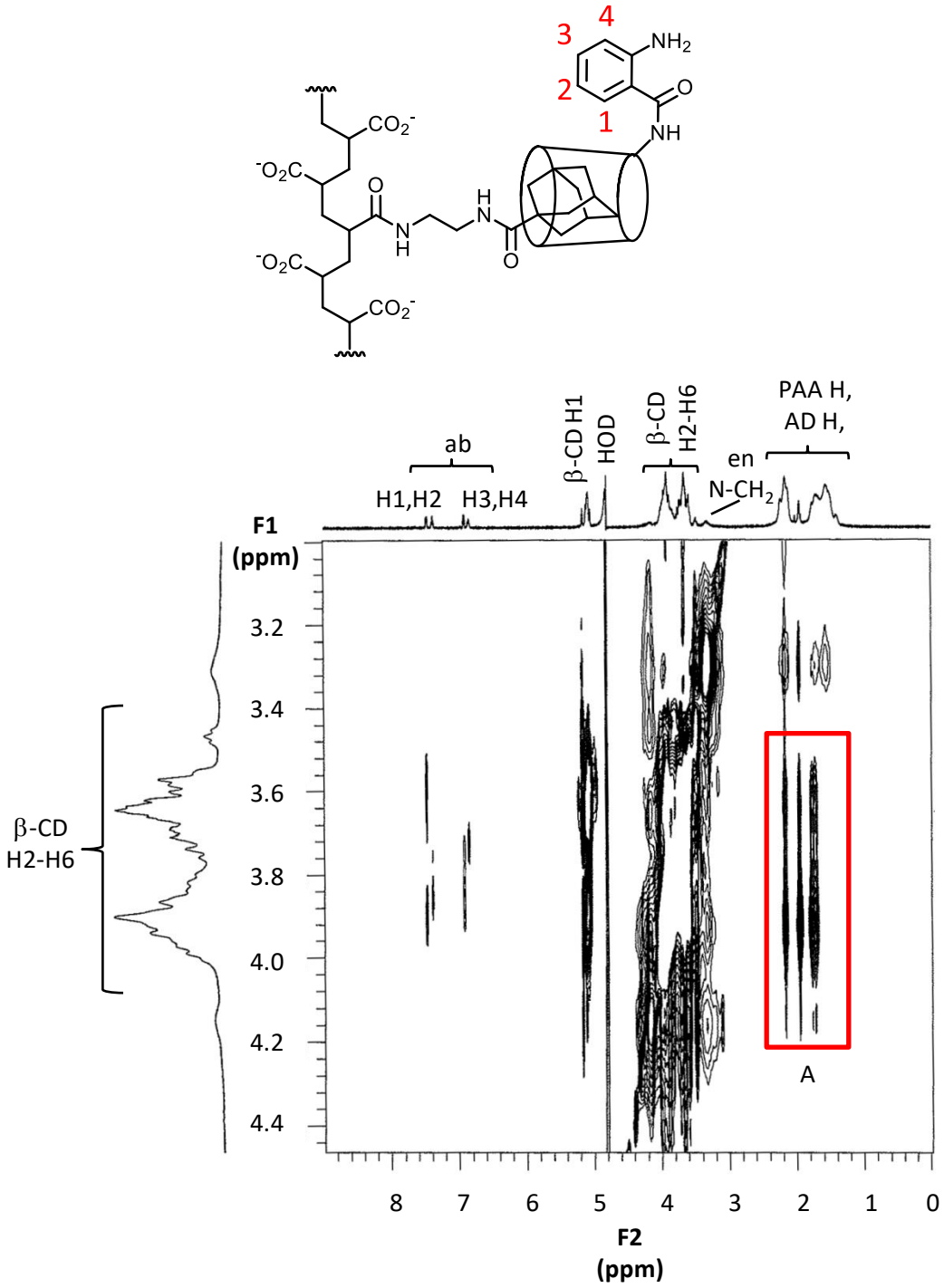

Figure 5.11: 2D ^{1}H NOESY NMR spectrum of 0.98 wt% PAAADen ([ADen] = 2.0×10^{-3} mol dm^{-3}) and β-CDab (3.0×10^{-3} mol dm^{-3}) prepared in D_2O phosphate buffer (pD 7.0, I = 0.10 mol dm^{-3}) at 298.2 K. Rectangle A highlights cross-peaks arising from NOE interactions of the annular protons of β-CD with protons of ADen. A possible structure showing a portion of PAAADen forming a 1:1 complex is shown above. The abbreviation 'ab' refers to the aminophenyl substituent of β-CDab.

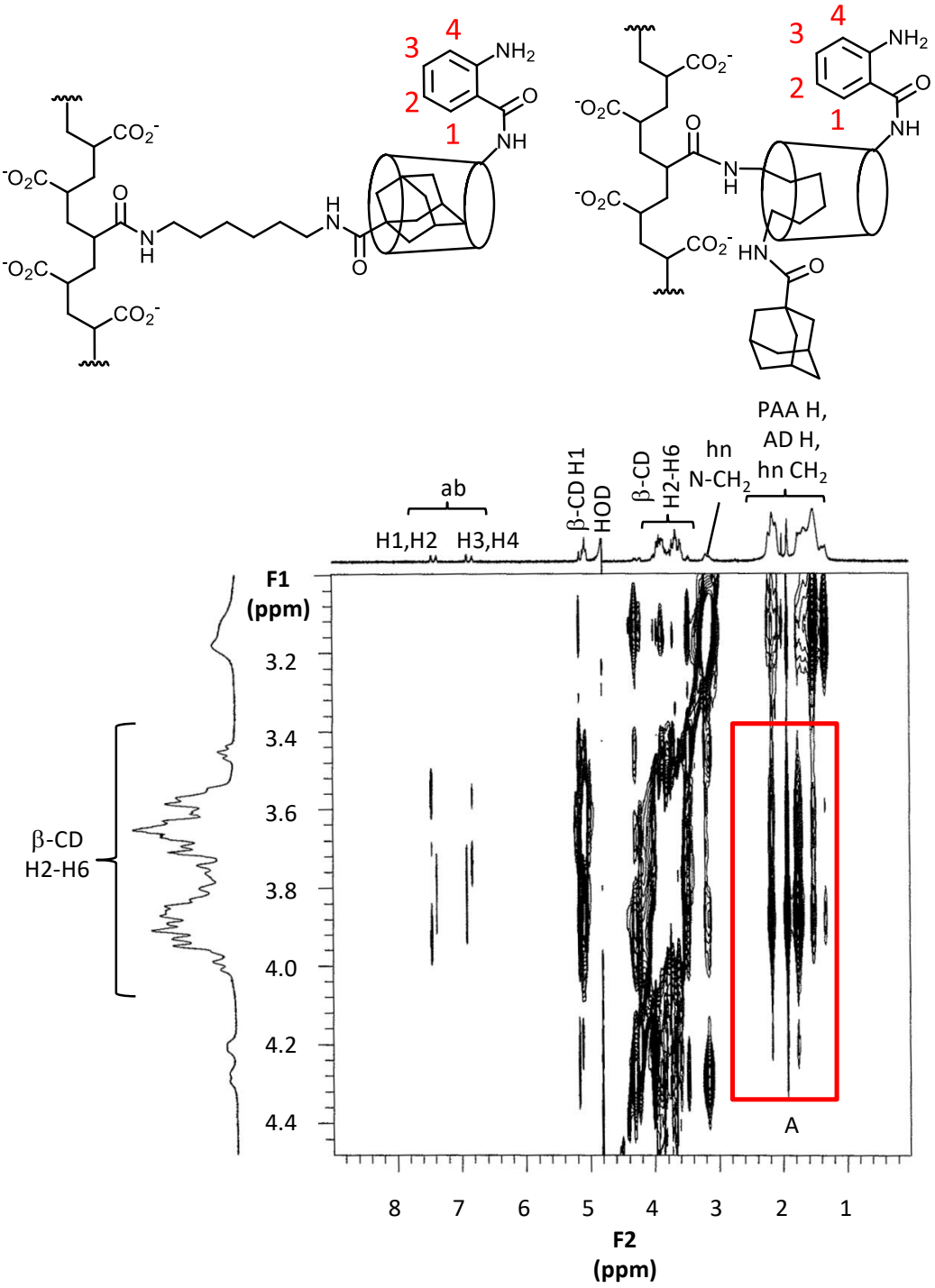

Figure 5.12: 2D ^{1}H NOESY NMR spectrum of 0.74 wt% PAAADhn ([ADhn] = 2.0 × 10^{-3} mol dm^{-3}) and β-CDab (3.0 × 10^{-3} mol dm^{-3}) prepared in D_2O phosphate buffer (pD 7.0, *I* = 0.10 mol dm^{-3}) at 298.2 K. Rectangle A highlights cross-peaks arising from NOE interactions of the annular protons of β-CD with protons of ADhn. Possible structures showing a portion of PAAADhn forming 1:1 complexes are shown above. The abbreviation 'ab' refers to the aminophenyl substituent of β-CDab.

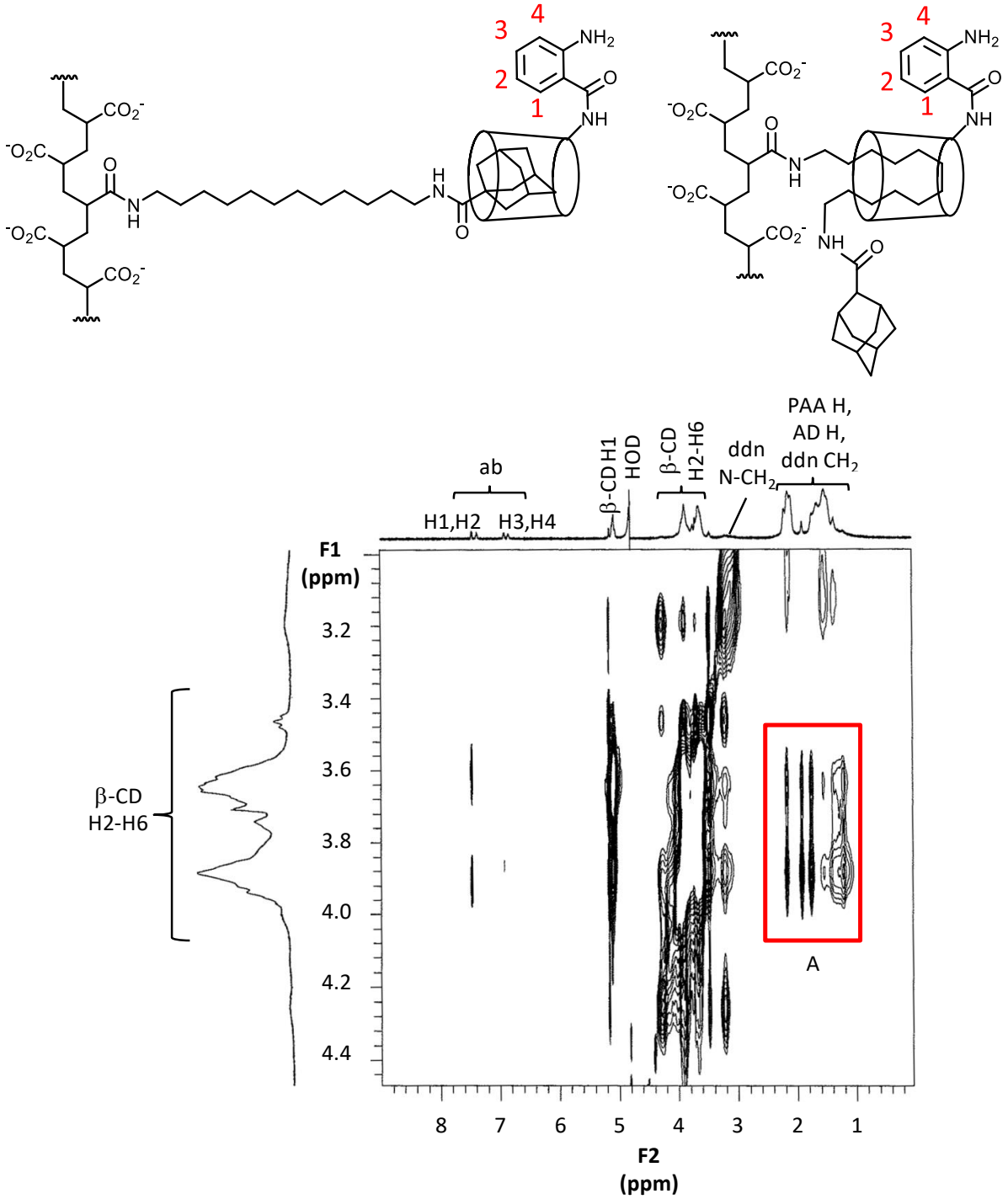

Figure 5.13: 2D ^{1}H NOESY NMR spectrum of 1.00 wt% PAAADddn ([ADddn] = 2.0×10^{-3} mol dm^{-3}) and β-CDab (3.0×10^{-3} mol dm^{-3}) prepared in D_2O phosphate buffer (pD 7.0, I = 0.10 mol dm^{-3}) at 298.2 K. Rectangle A highlights cross-peaks arising from NOE interactions of the annular protons of β-CD with protons of ADddn. Possible structures showing a portion of PAAADddn forming 1:1 complexes are shown above. The abbreviation 'ab' refers to the aminophenyl substituent of β-CDab.

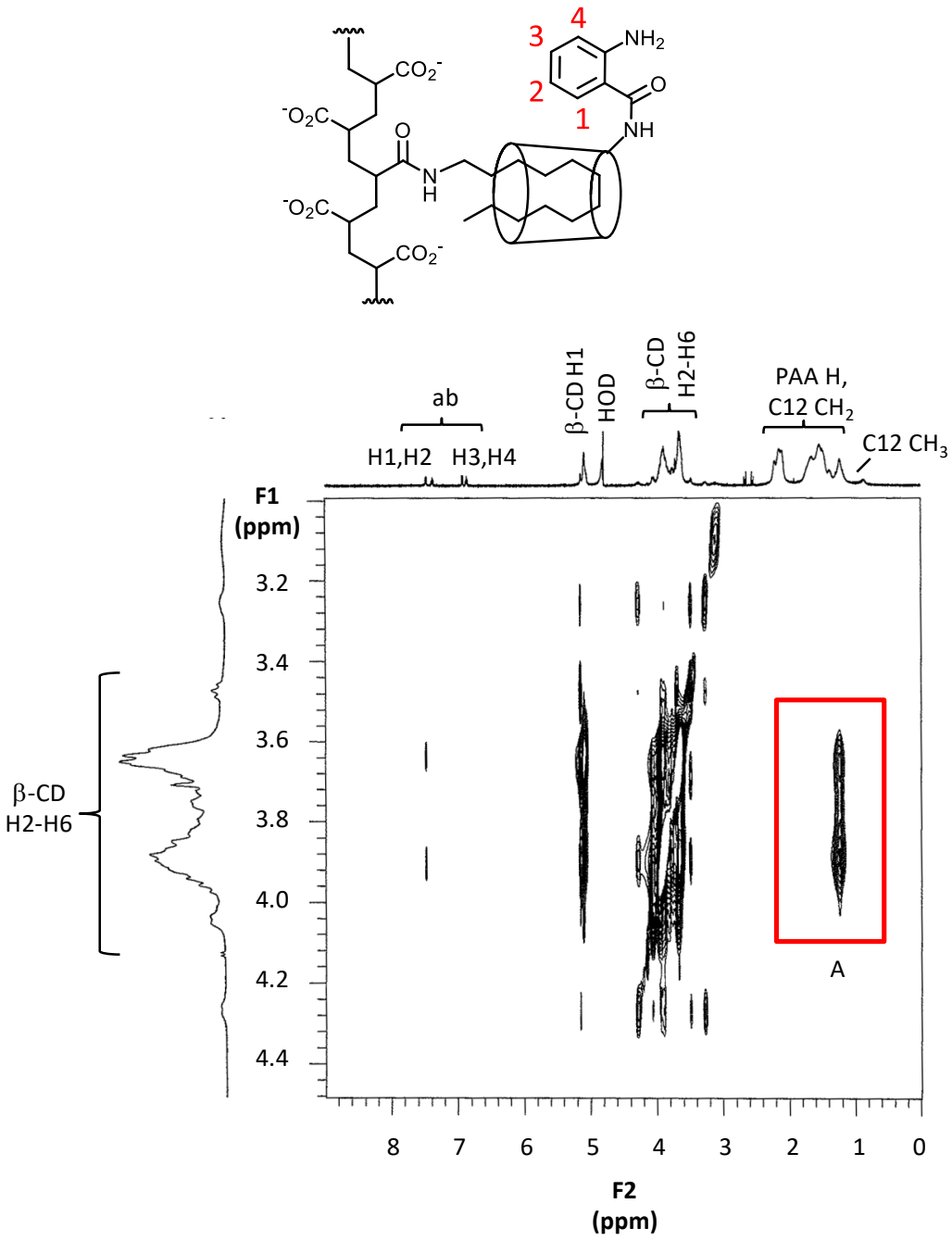

Figure 5.14: 2D ^{1}H NOESY NMR spectrum of 1.07 wt% PAAC12 ([C12] = 2.0×10^{-3} mol dm^{-3}) and β-CDab (3.0×10^{-3} mol dm^{-3}) prepared in D_2O phosphate buffer (pD 7.0, I = 0.10 mol dm^{-3}) at 298.2 K. Rectangle A highlights cross-peaks arising from NOE interactions of the annular protons of β-CD with protons of C12. A possible structure showing a portion of PAAC12 forming a 1:1 complex is shown above. The abbreviation 'ab' refers to the aminophenyl substituent of β-CDab

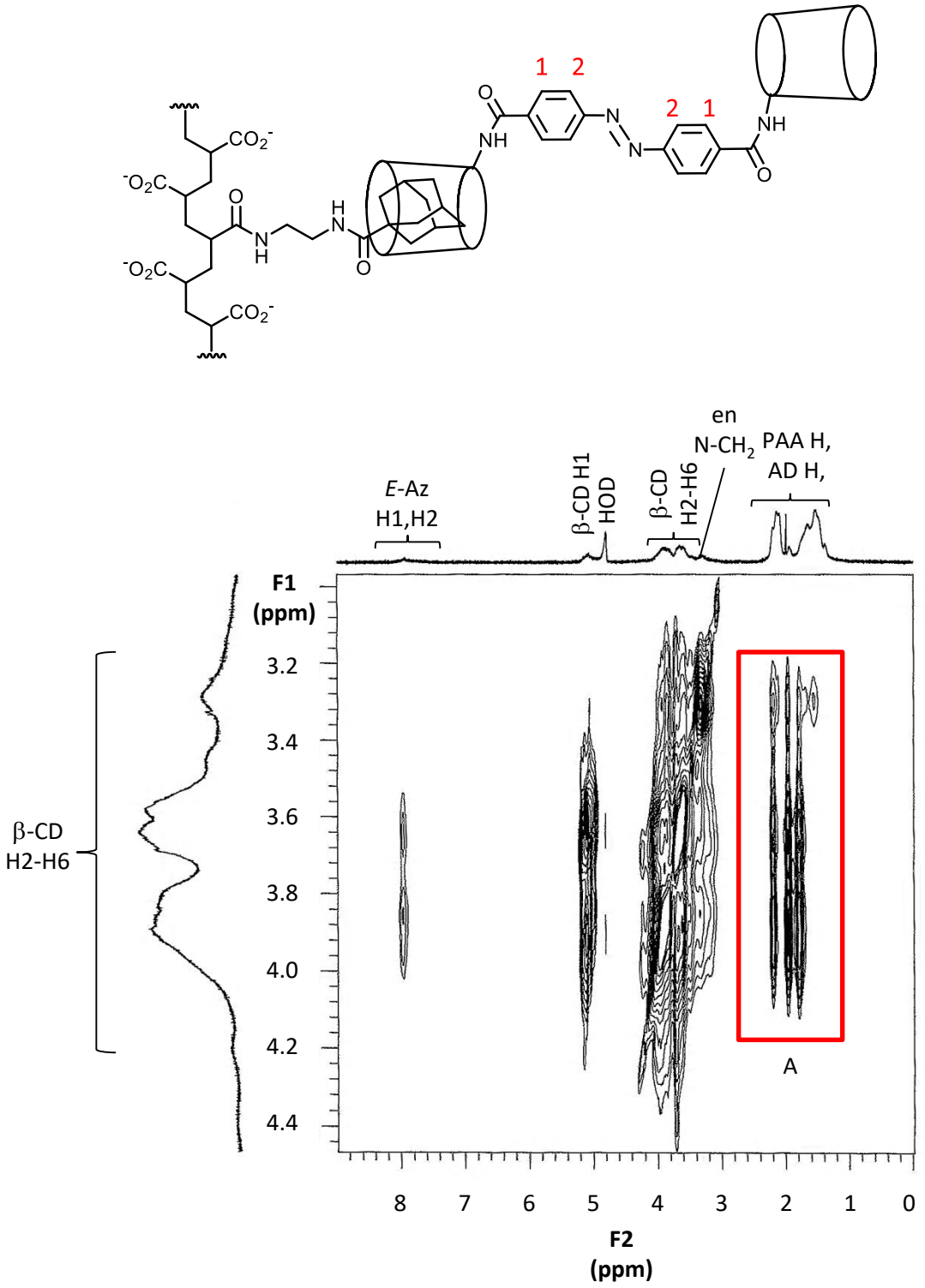

Figure 5.15: 2D ^{1}H NOESY NMR spectrum of 0.98 wt% PAAADen ([ADen] = 2.0×10^{-3} mol dm^{-3}) and *E*-*p*-β-CD_2az (1.5×10^{-3} mol dm^{-3}) prepared in D_2O phosphate buffer (pD 7.0, I = 0.10 mol dm^{-3}) at 298.2 K. Rectangle A highlights cross-peaks arising from NOE interactions of the annular protons of β-CD with protons of ADen. A possible structure showing a portion of PAAADen and *E*-*p*-β-CD_2az forming a 1:1 complex is shown above.

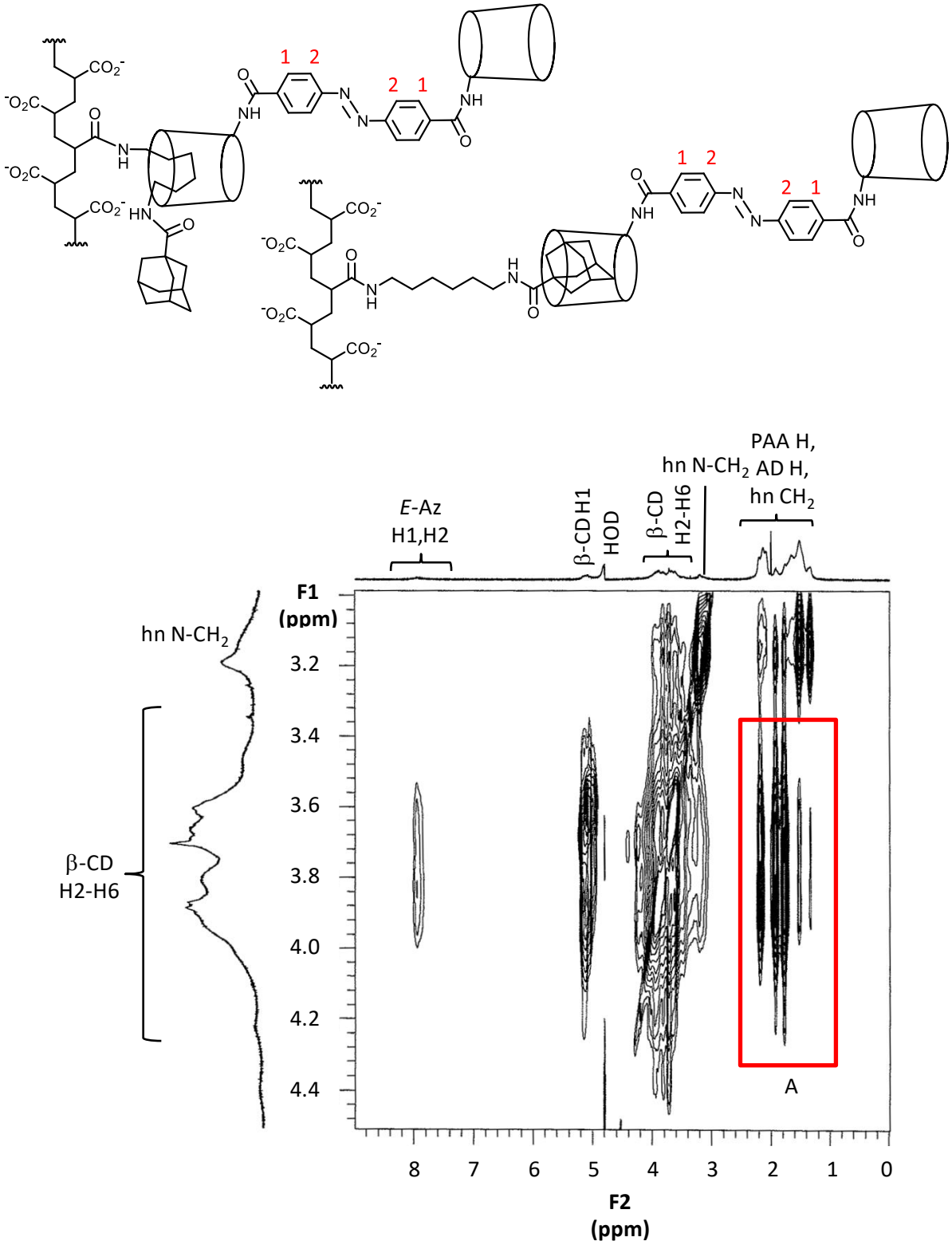

Figure 5.16: 2D ^{1}H NOESY NMR spectrum of 0.74 wt% PAAADhn ([ADhn] = 2.0×10^{-3} mol dm^{-3}) and *E*-*p*-β-CD$_2$az (1.5×10^{-3} mol dm^{-3}) prepared in D_2O phosphate buffer (pD 7.0, I = 0.10 mol dm^{-3}) at 298.2 K. Rectangle A highlights cross-peaks arising from NOE interactions of the annular protons of β-CD with protons of ADhn. Possible structures showing a portion of PAAADhn and *E*-*p*-β-CD$_2$az forming 1:1 monotopic complexes are shown above.

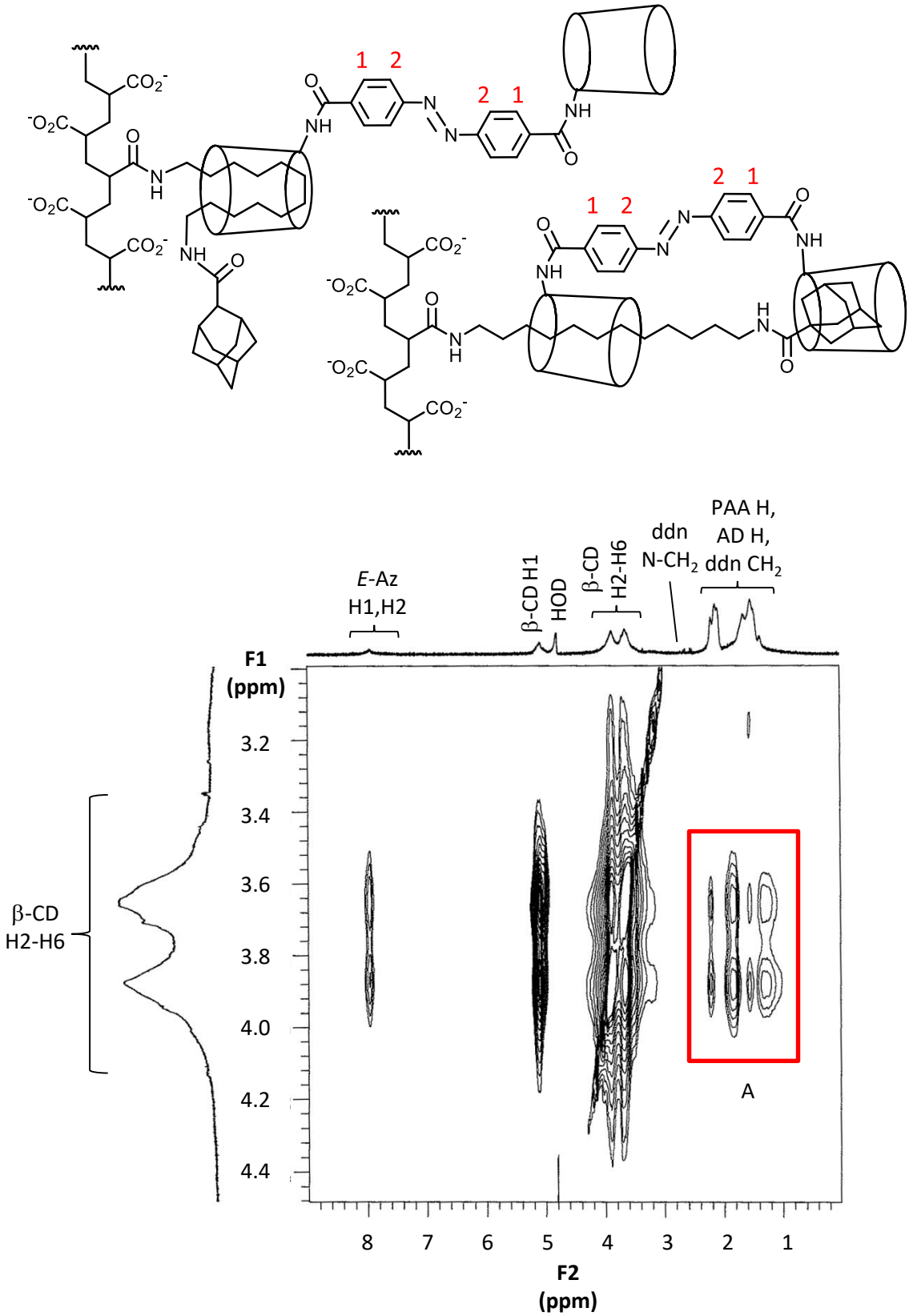

Figure 5.17: 2D ^{1}H NOESY NMR spectrum of 1.00 wt% PAAADddn ([ADddn] = 2.0×10^{-3} mol dm^{-3}) and *E*-*p*-β-CD$_2$az (1.5×10^{-3} mol dm^{-3}) prepared in D_2O phosphate buffer (pD 7.0, *I* = 0.10 mol dm^{-3}) at 298.2 K. Rectangle A highlights cross-peaks arising from NOE interactions of the annular protons of β-CD with protons of ADddn. Possible structures showing a portion of PAAADddn forming 1:1 complexes are shown above.

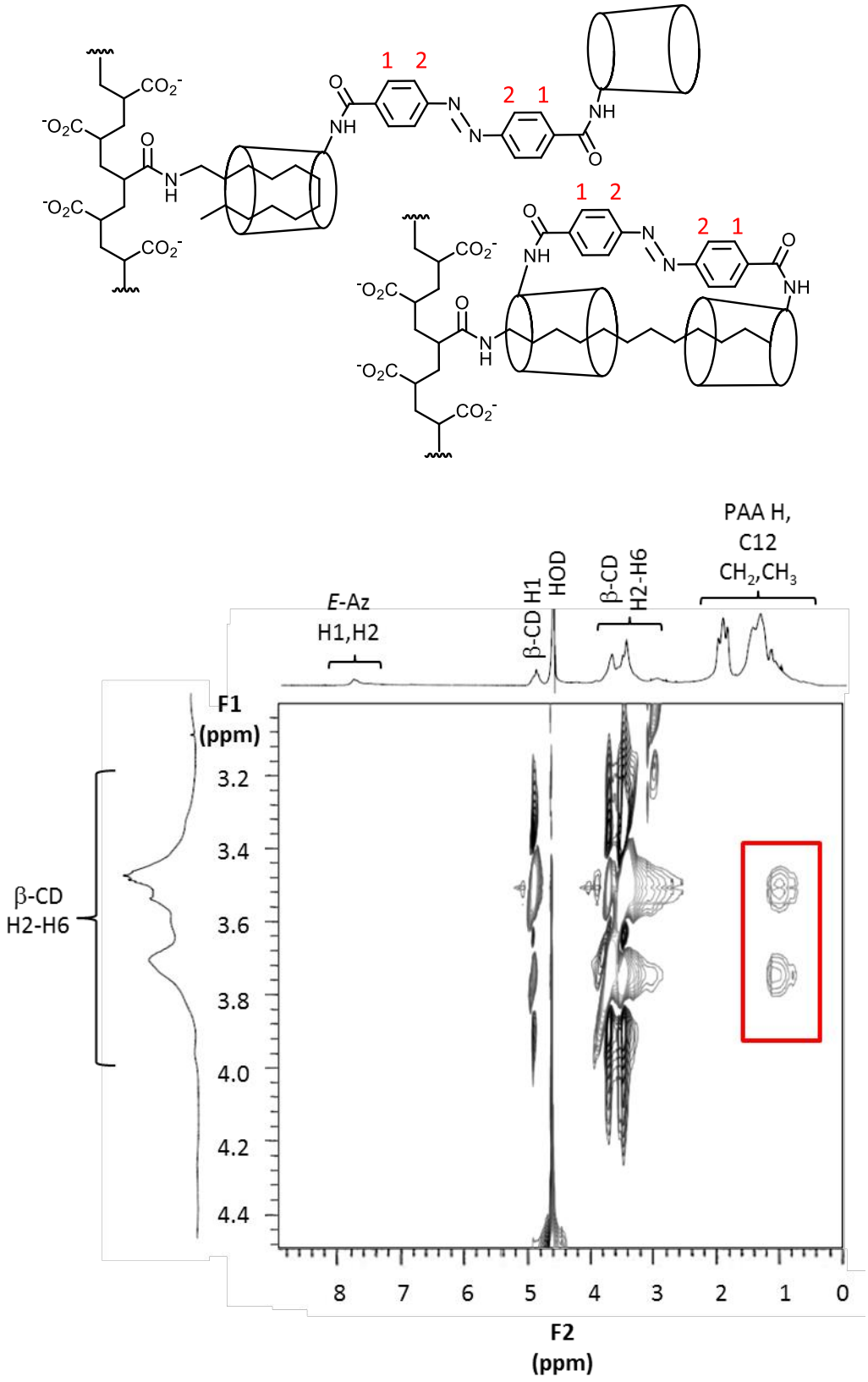

Figure 5.18: 2D ^{1}H NOESY NMR spectrum of 1.07 wt% PAAC12 ([C12] = 2.0 × 10^{-3} mol dm^{-3}) and *E-p*-β-CD_2az (1.5 × 10^{-3} mol dm^{-3}) prepared in D_2O phosphate buffer (pD 7.0, *I* = 0.10 mol dm^{-3}) at 298.2 K. Rectangle A highlights cross-peaks arising from NOE interactions of the annular protons of β-CD with protons of C12. Possible structures showing a portion of PAAC12 and *E-p*-β-CD_2az forming 1:1 monotopic complexes are shown above.

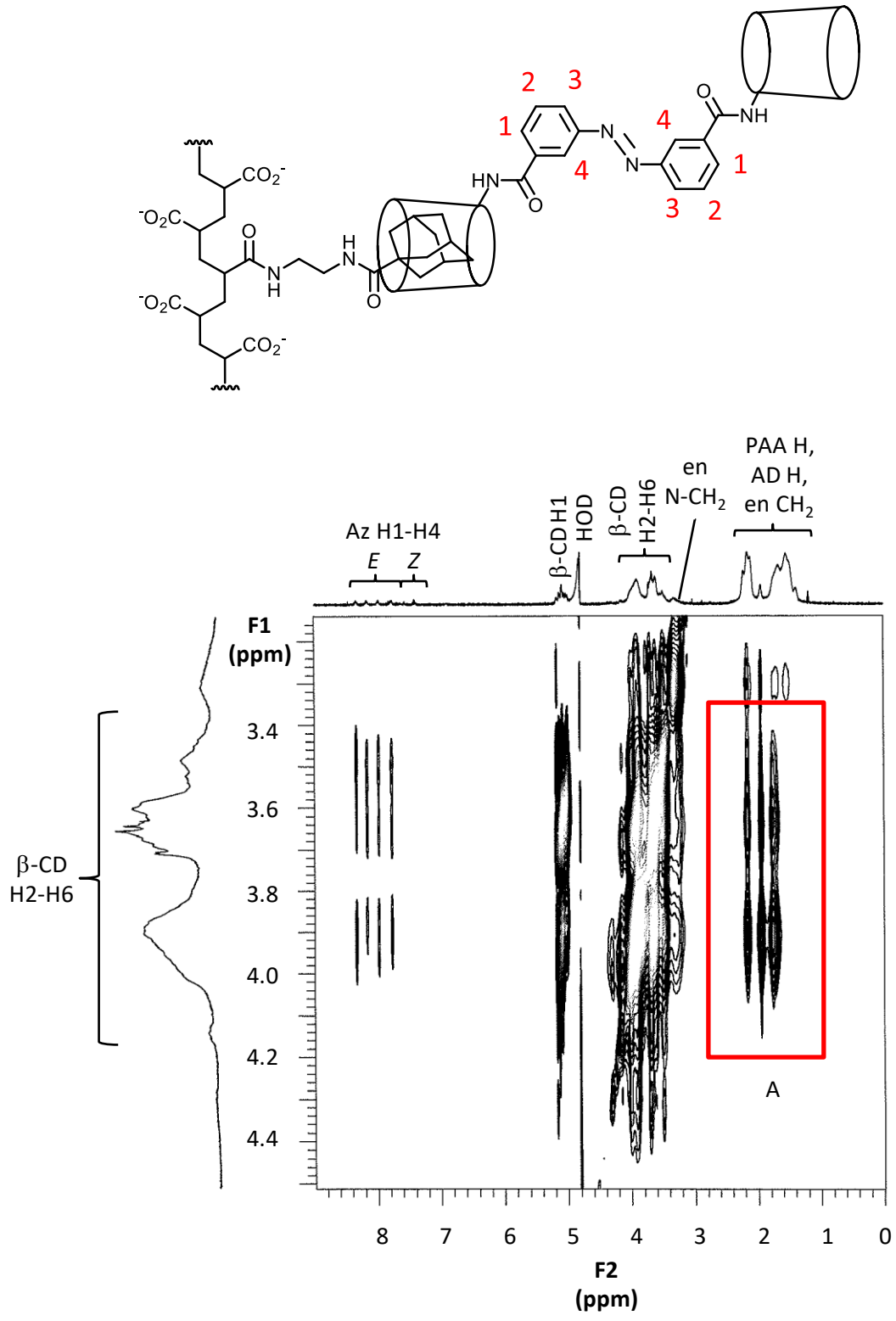

Figure 5.19: 2D ^{1}H NOESY NMR spectrum of 0.98 wt% PAAADen ([ADen] = 2.0×10^{-3} mol dm^{-3}) and *E/Z-m*-β-CD_2az (1.5×10^{-3} mol dm^{-3}) prepared in D_2O phosphate buffer (pD 7.0, I = 0.10 mol dm^{-3}) at 298.2 K. Rectangle A highlights cross-peaks arising from NOE interactions of the annular protons of β-CD with protons of ADen. A possible structure showing a portion of the PAAADen forming a 1:1 complex is shown above.

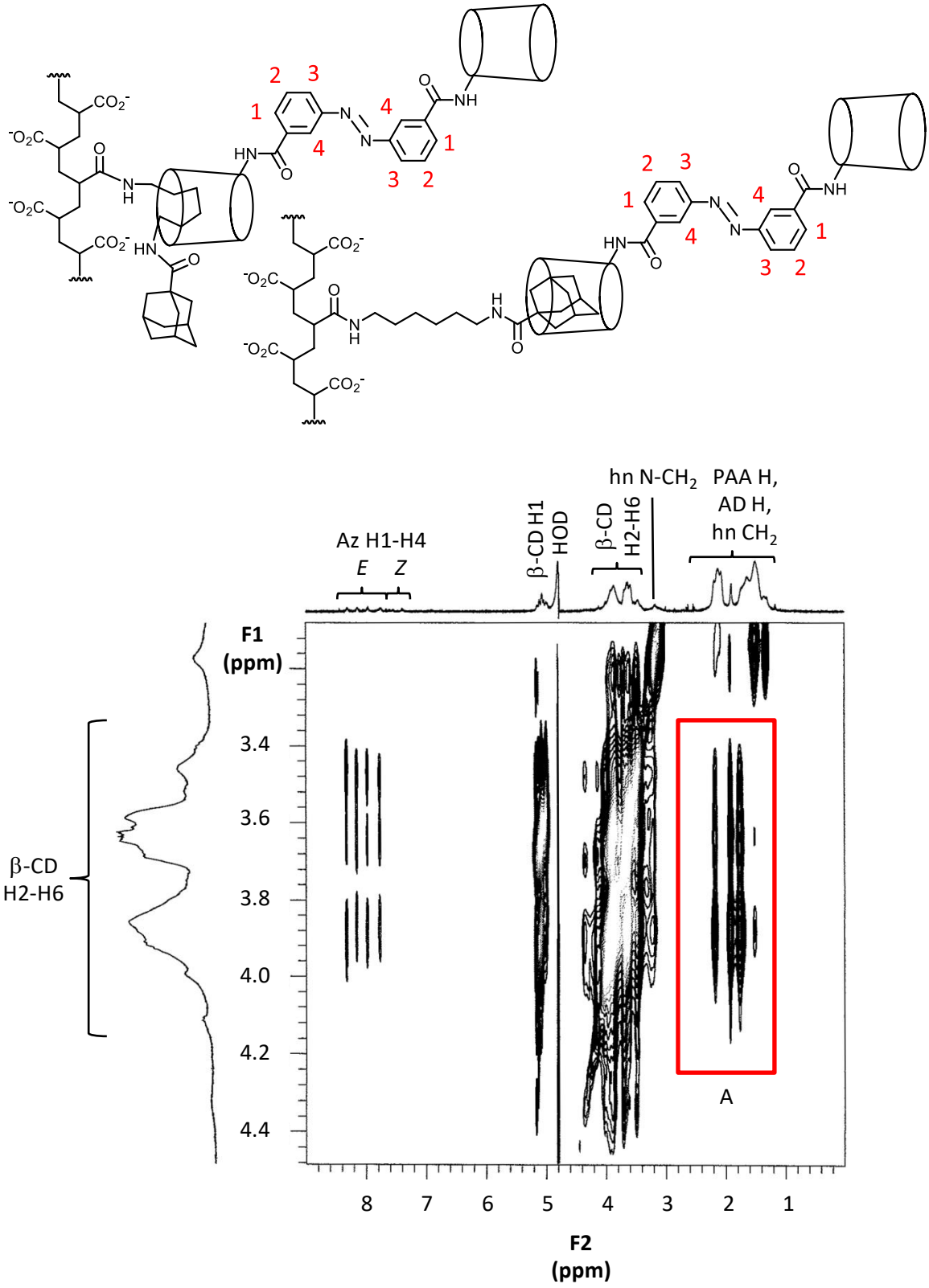

Figure 5.20: 2D ^{1}H NOESY NMR spectrum of 0.74 wt% PAAADhn ([ADhn] = 2.0 × 10^{-3} mol dm^{-3}) and *E/Z-m*-β-CD_2az (1.5 × 10^{-3} mol dm^{-3}) prepared in D_2O phosphate buffer (pD 7.0, *I* = 0.10 mol dm^{-3}) at 298.2 K. Rectangle A highlights cross-peaks arising from NOE interactions of the annular protons of β-CD with protons of ADhn. Possible structures showing a portion of PAAADhn forming 1:1 complexes are shown above.

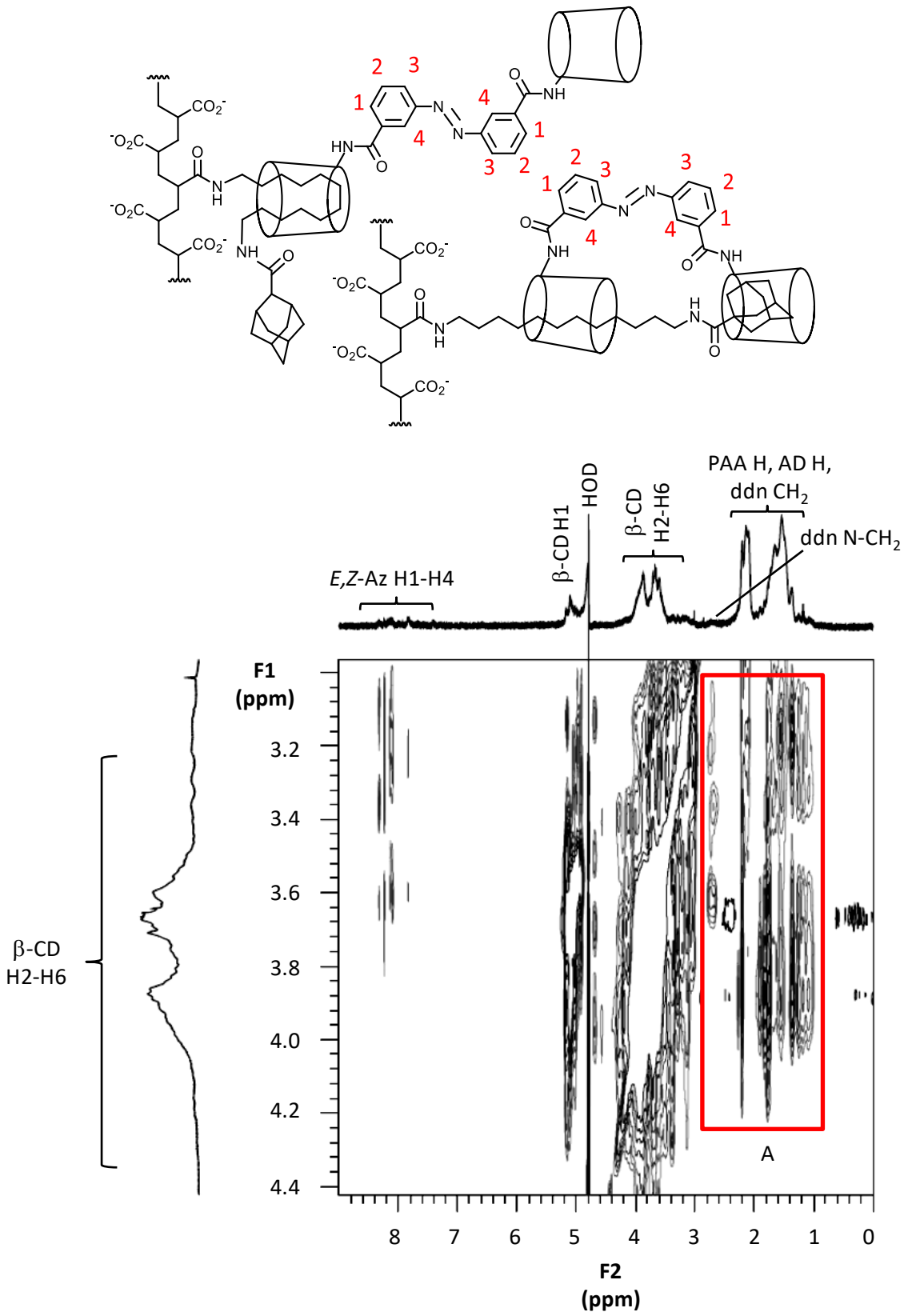

Figure 5.21: 2D ^{1}H NOESY NMR spectrum of 1.00 wt% PAAADddn ([ADddn] = 2.0×10^{-3} mol dm^{-3}) and *E/Z-m*-β-CD$_2$az (1.5×10^{-3} mol dm^{-3}) prepared in D_2O phosphate buffer (pD 7.0, I = 0.10 mol dm^{-3}) at 298.2 K. Rectangle A highlights cross-peaks arising from NOE interactions of the annular protons of β-CD with protons of ADddn. Possible structures showing a portion of PAAADddn forming 1:1 complexes are shown above.

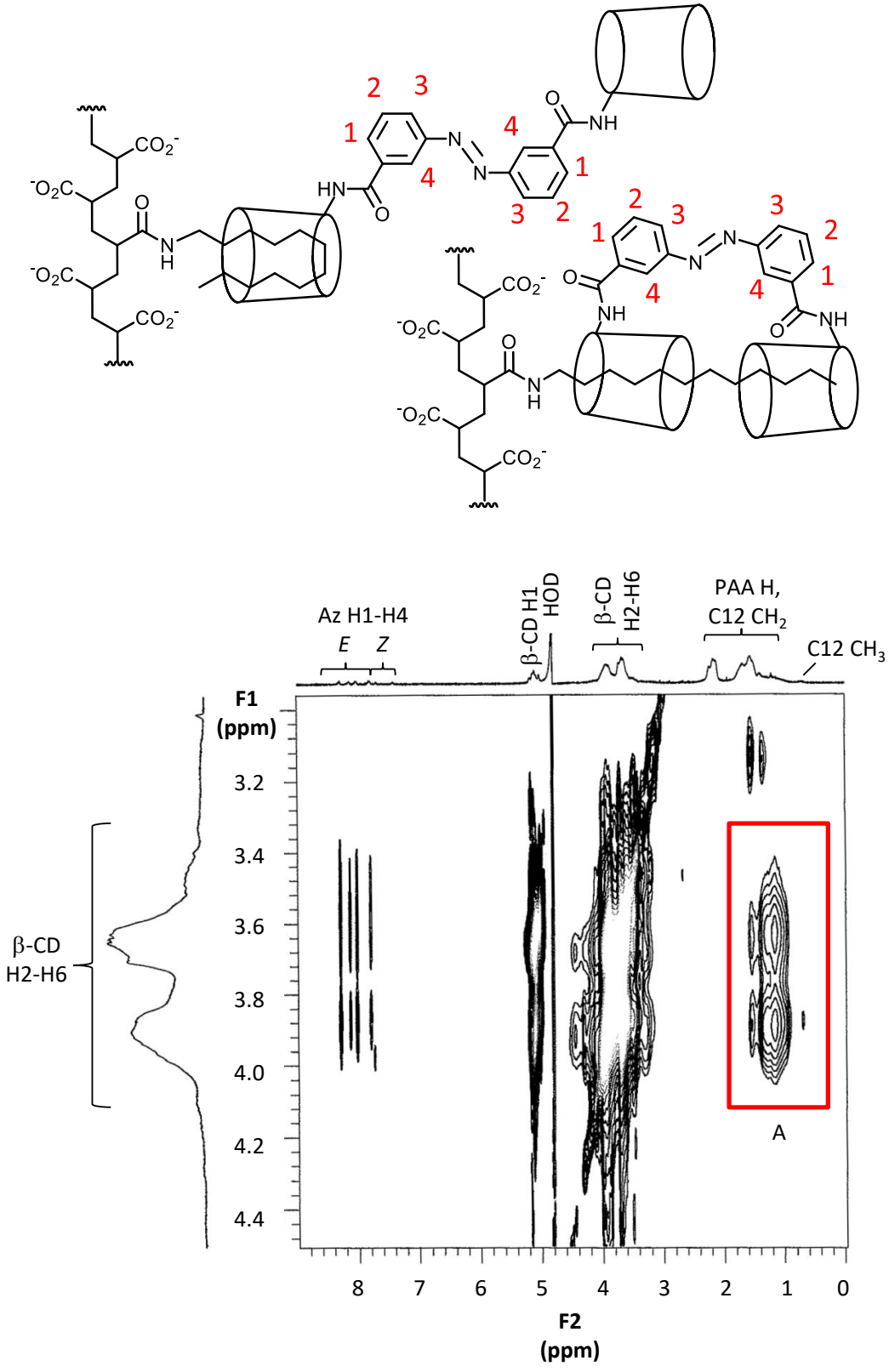

Figure 5.22: 2D ^{1}H NOESY NMR spectrum of 1.07 wt% PAAC12 ([C12] = 2.0 × 10^{-3} mol dm^{-3}) and *E/Z*-*m*-β-CD_2az (1.5 × 10^{-3} mol dm^{-3}) prepared in D_2O phosphate buffer (pD 7.0, *I* = 0.10 mol dm^{-3}) at 298.2 K. Rectangle A highlights cross-peaks arising from NOE interactions of the annular protons of β-CD with protons of C12. Possible structures showing a portion of PAAC12 forming 1:1 complexes are shown above.

The 2D ^{1}H NOESY NMR spectra of all the modified PAAs in all systems produces AD, alkyl and PAA backbone resonances that are overlapped in the region ranging from 1.0 – 2.5 ppm. As the backbone of PAA consists of charged carboxylate groups, they are not expected to form host-guest complexes with β-CD hosts. Additionally, the modification of β-CD to form *E-p*-β-CD_2az, *E/Z-m*-β-CD_2az and β-CDab causes the glucopyranose subunits to be chemically and magnetically inequivalent and hence, the H2 – H6 resonances of β-CD are broadened and overlapped. Despite the overlap in resonances, cross-peaks arising between the H2 – H6 resonances of β-CD and the resonances of the modified PAAs are generally indicative of complexes arising between the AD and/or alkyl groups of the modified PAAs and the β-CD hosts.

The 2D ^{1}H NOESY NMR spectra of all the systems studied show similar results. The spectra for the complexation of PAAADen, PAAADhn, PAAADddn and PAAC12 by native β-CD produced cross-peaks between the AD and alkyl resonances of the modified PAAs and the H3, H5 and H6 resonances of β-CD, indicating complexation.[26] Similarly, cross-peaks are produced between the H2 – H6 resonances of β-CD in either *E-p*-β-CD_2az, *E/Z-m*-β-CD_2az or β-CDab and the AD and alkyl resonances of PAAADen, PAAADhn, PAAADddn and PAAC12, indicating complexation.

In the systems involving PAAADen, PAAADhn and PAAADddn, we would expect the complexation to dominantly favour the encapsulation of the AD substituent, rather than the alkyl tether, by the β-CD host. AD is known to form a strong complex with β-CD, characterised by a 1:1 host-guest equilibrium constant, *K*, of 1400 dm mol^{-1}.[27]

While the 2D ^{1}H NOESY NMR spectra confirm the complexation of the AD and alkyl groups of the modified PAAs by the β-CD hosts, the orientation and stoichiometry of these complexes are difficult to interpret. In principle, 1:1 host-guest complexes are expected for β-CD and β-CDab, while additional 1:2 complexes are possible for *E-p*-β-CD_2az and *E/Z-m*-β-CD_2az. The 1:1 complexes between the modified PAAs and the β-CD dimers may also be characterised by monotopic or ditopic complexes, while 1:2 complexes may form intra-strand or inter-strand cross-links, depending on the concentration of the solution. The possible complexation modes of 1:1 and 1:2 complexes are shown in Figure 5.23, exemplified using PAAADddn as the polymer and *E-p*-β-CD_2az as the host. In order to confirm the stoichiometry of the complexes formed, ITC studies were performed.

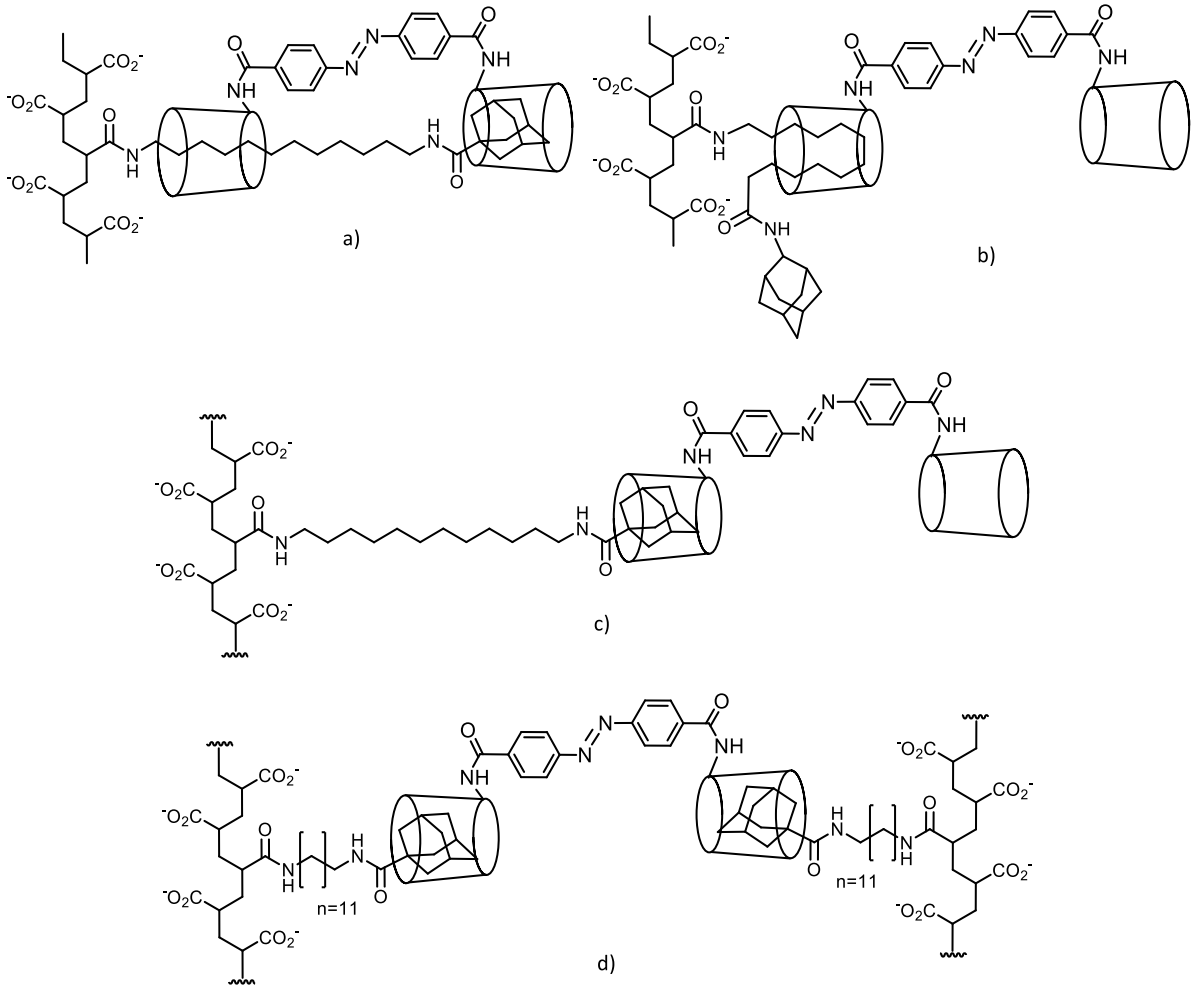

Figure 5.23: Host-guest complexes of various stoichiometries and orientations including a) 1:1 *E*-*p*-β-CD_2az·ADddn cooperative complex through both the dodecyl and AD groups of PAAADddn, b) 1:1 *E*-*p*-β-CD_2az·ADddn non-cooperative complex through the dodecyl group of PAAADddn, c) 1:1 *E*-*p*-β-CD_2az·ADddn non-cooperative complex through the AD group of PAAADddn and d) 1:2 *E*-*p*-β-CD_2az·$(ADddn)_2$ non-cooperative complex through the AD groups of adjacent PAAADddn strands, forming an intra- or inter-strand cross-link.

5.2.2.2 Quantitative Investigation of Complexation by Isothermal Titration Calorimetry

The complexation constants and thermodynamic parameters for the complexation of the hydrophobic-substitutients of PAAADen, PAAADhn, PAAADddn and PAAC12 by native β-CD, β-CDab, *E-p*-β-CD_2az and *E/Z-m*-β-CD_2az were determined by ITC. Calorimetry is the only method that can directly measure the thermodynamic parameters of a system and is particularly useful in the analysis of spectroscopically silent compounds. Therefore, ITC is a useful technique for the study of AD- and alkyl-substituted PAAs.[28,29]

Isothermal titration calorimetry measures the heat change (measured as a temperature change) upon the sequential titration of a solution containing a ligand into a solution containing a receptor.[28-34] Under constant pressure, the heat evolution or consumption represents the change in enthalpy, ΔH, which is dependent upon the interaction between the ligand and receptor. Given that this change is universal, the equilibrium constant, *K*, and stoichiometric ratio of ligand to receptor, *N*, can also be derived from the heat changes. Equation 5.1 and Equation 5.2 can then be used to determine $\Delta G°$ and $\Delta S°$.

$$\Delta G° = -RTlnK \tag{5.1}$$

$$\Delta G° = \Delta H° - T\Delta S° \tag{5.2}$$

Hence, given an appropriate ligand-receptor model, exemplified by Equation 5.3 for a 1:1 ligand·receptor complex, non-linear least squares fitting can be employed to extract *K*, *N* and the thermodynamic parameters of complexation from a single titration experiment.

$$\text{ligand} + \text{receptor} \underset{}{\overset{K_{11}}{\rightleftharpoons}} \text{ligand·receptor} \tag{5.3}$$

An optimal ITC experiment results in an isotherm with a sigmoidal shape. However, the shape of the isotherm is dependent upon the magnitude of the complexation constant and the concentration of the receptor species. Therefore, the equilibrium constant and thermodynamic parameters may only be extracted from the calorimetric data under certain concentration-dependent conditions. For this reason, the dimensionless Wiseman parameter, *c,* has been used to quantify the validity of an ITC experiment.[35] The *c* value is given by Equation 5.4,

$$c = nK[M] \tag{5.4}$$

where *n* is the number of binding sites per receptor, *M*, and *K* is the equilibrium constant describing the ligand-receptor equilibrium given in Equation 5.3. The *c* value is an indicator of the shape of the isotherm. Experiments resulting in *c* values of 10 – 500 are considered optimal as they are correlated

with isotherms that have a complete sigmoidal shape.[35] In principle, the *c* value may be moderated by changing the concentration of the receptor. However, changing the concentration may introduce further errors. For example, increasing or decreasing the concentration of the ligand or receptor may result heat change profiles that are saturated or insufficiently noisy, respectively.

The experimental ITC isotherms for systems in this study describe the complexation equilibrium of one host with one hydrophobic substituent, according to Equation 5.5,

$$\text{host} + \text{hydrophobe} \overset{K_{11}}{\rightleftharpoons} \text{host}\cdot\text{hydrophobe} \tag{5.5}$$

where the host refers to either native β-CD, β-CDab, *E-p*-βCD$_2$az or *E/Z-m*-βCD$_2$az and the hydrophobe refers to ADen, ADhn, ADddn or C12 of PAAADen, PAAADhn, PAAADddn and PAAC12, respectively. The equation for the complexation constant, K_{11}, is given by Equation 5.6.

$$K_{11} = \frac{[host \cdot hydrophobe]}{[host][hydrophobe]} \tag{5.6}$$

In principle, a host may also form a complex with a second hydrophobic substituent. The equilibrium expression for the 1:2 complexation of a second hydrophobe to an existing 1:1 host-hydrophobe complex is given by Equation 5.7,

$$\text{host}\cdot\text{hydrophobe} + \text{hydrophobe} \overset{K_{12}}{\rightleftharpoons} \text{host}\cdot\text{hydrophobe}_2 \tag{5.7}$$

The equation for the second complexation constant, K_{12}, is given by Equation 5.8,

$$K_{12} = \frac{[host \cdot hydrophobe_2]}{[host \cdot hydrophobe][hydrophobe]} \tag{5.8}$$

The K_{12} represents a step-wise addition of a second hydrophobic substituent to an existing 1:1 host:hydrophobe complex, rather than a concerted addition of two hydrophobic substituents. An ITC experiment for a system with a step-wise K_{12} equilibrium is likely to yield a distinct heat-release profile, distinguishable from the K_{11} equilibrium. Thus, the magnitude of the K_{12} may be determined. However, by comparison, the heat release profile associated with the concerted addition of two hydrophobic substituents to one host is likely to be similar to the heat release profile associated with the K_{11} equilibrium. Thus, it would not be possible to quantitatively evaluate the magnitude of a concerted K_{12} equilibrium. This is further discussed in the context of individual isotherms in Section 5.2.2.2.1 - 5.2.2.2.4.

The complexation of PAAADen, PAAADhn, PAAADddn and PAAC12 by native β-CD, β-CDab, *E-p*-β-CD_2az and *E/Z-m*-β-CD_2az was determined by ITC in aqueous phosphate buffer (pH 7.0, *I* = 0.10 mol dm^{-3}) at 298.2 K, using a MicroCal VP isothermal titration calorimeter. Heat changes were measured upon addition of 10 mm^3 aliquots of the β-CD host into a cell containing the hydrophobe-substituted PAA. The aliquots of the β-CD host were titrated by a computer-controlled micro-syringe at 210 – 270 s intervals. The initial cell volume containing the hydrophobe-substituted PAA was 1.46 cm^3. Concentration corrections for displaced volume effects which occur with each injection were calculated by Origin 70 MicroCal protocol.[36]

Heat changes resulting from the dilution of native β-CD, β-CDab and *E/Z-m*-βCD_2az were found to be insignificant. However, the heat of dilution of *E-p*-βCD_2az represented at least 10% of the heat change associated with complexation. Therefore, the heat of dilution of *E-p*-β-CD_2az into aqueous phosphate buffer solution (pH 7.0, *I* = 0.10 mol dm^{-3}) was measured and subtracted from the heat changes corresponding to all systems containing *E-p*-β-CD_2az, following the Origin 70 MicroCal protocol.[36] The heat of dilution of *E-p*-β-CD_2az corresponds to the dissociation of *E-p*-β-CD_2az dimers, as described in Equation 5.9. The ITC isotherm for the dilution of *E-p*-β-CD_2az into aqueous phosphate buffer is given in Figure 5.24.

$$(E\text{-}p\text{-}\beta\text{-}CD_2az)_2 \rightleftharpoons 2\ E\text{-}p\text{-}\beta\text{-}CD_2az \qquad (5.9)$$

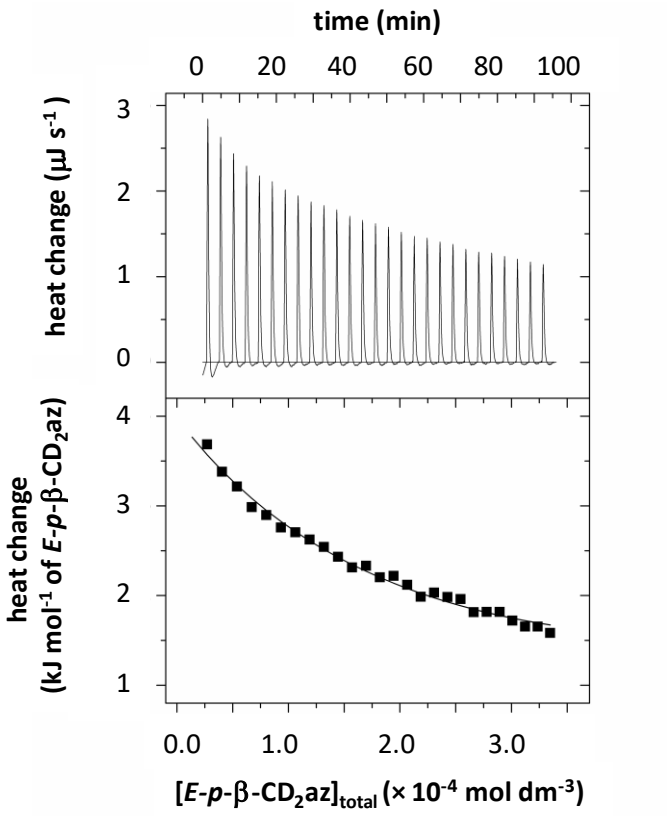

Figure 5.24: ITC isotherm for the dilution of *E*-*p*-βCD$_2$az (2.0×10^{-3} mol dm^{-3}) in aqueous phosphate buffer (pH 7.0, I = 0.10 mol dm^{-3}) at 298.2 K. The top section shows the raw ITC heat release profile with time. The bottom sections shows the experimental heat released with each addition of *E*-*p*-βCD$_2$az (squares) and the line of best-fit of an algorithm for the dissociation of a *E*-*p*-βCD$_2$az dimer (solid line), analogous to that shown in Equation 5.9.

The appropriate equilibrium describing the complexation of the hydrophobic-substituents of PAAADen, PAAADhn, PAAADddn and PAAC12 by native β-CD, β-CDab, *E*-*p*-β-CD_2az and *E/Z*-*m*-β-CD_2az was used to fit the experimental isotherms. The experimental data were best fit using the Origin 7.0 MicroCal protocol to yield K_{xy}, ΔH_{xy}, $T\Delta S_{xy}$ and the stoichiometry of host to hydrophobe, *N*. Each system was fitted to the appropriate host:guest model, based upon the shape of the isotherm and the structure of the β-CD host, as is now discussed.

5.2.2.2.1 ITC Study of the Complexation of PAAADen by β-CD, β-CDab, *E*-*p*-β-CD_2az and *E/Z*-*m*-β-CD_2az

The heat change profile of an aqueous solution of PAAADen as an aqueous solution of either β-CD, β-CDab, *E*-*p*-β-CD_2az or *E/Z*-*m*-β-CD_2az is titrated into it at 298.2 K is consistent with complexation occurring, as also evidenced by NMR spectroscopy. The isotherms for the β-CD/PAAADen, β-CDab/PAAADen, *E*-*p*-β-CD_2az/PAAADen and *E/Z*-*m*-β-CD_2az/PAAADen systems are shown in Figure 5.25 a) – Figure 5.28 a), respectively. The heat release associated with the dissociation of *E*-*p*-β-CD_2az aggregates (Figure 5.24) was subtracted from the total heat release profile of the *E*-*p*-β-CD_2az/PAAADen system (Figure 5.27 a)).

Each system produced a monophasic isotherm, suggesting the formation of a 1:1 complex. An algorithm for the formation of 1:1 host·ADen complexes (Equation 5.5 and Equation 5.6) fitted the isotherms well. The variation of the concentrations of the 1:1 β-CD·ADen, β-CDab·Aden, *E*-*p*-β-CD_2az·Aden and *E/Z*-*m*-β-CD_2az·ADen complexes are shown in Figure 5.25 b) – Figure 5.28 b), respectively. The derived K_{11}, ΔG°_{11}, ΔH°_{11} and $T\Delta S^\circ_{11}$ appear in Table 5.1.

As the *E/Z*-*m*-β-CD_2az/PAAADen system consisted of a mixture of *E* and *Z* isomers of *m*-β-CD_2az, it was anticipated that the isotherm may be biphasic, accounting for the formation of 1:1 *E*-*m*-β-CD_2az·ADen and *Z*-*m*-β-CD_2az·ADen complexes. However, as the *E/Z*-*m*-β-CD_2az/PAAADen system produced a monophasic isotherm, *E*-*m*-β-CD_2az and *Z*-*m*-β-CD_2az are likely to have similar complexation properties. Thus, the K_{11} for the *E/Z*-*m*-β-CD_2az·ADen complex represents the weighted average of the K_{11} corresponding to the *E*-*m*-β-CD_2az·ADen and *Z*-*m*-β-CD_2az·ADen complexes. Similarly, the derived thermodynamic parameters represent the weighted average of the thermodynamic parameters corresponding to 1:1 *E*-*m*-β-CD_2az·ADen and *Z*-*m*-β-CD_2az·ADen complexes.

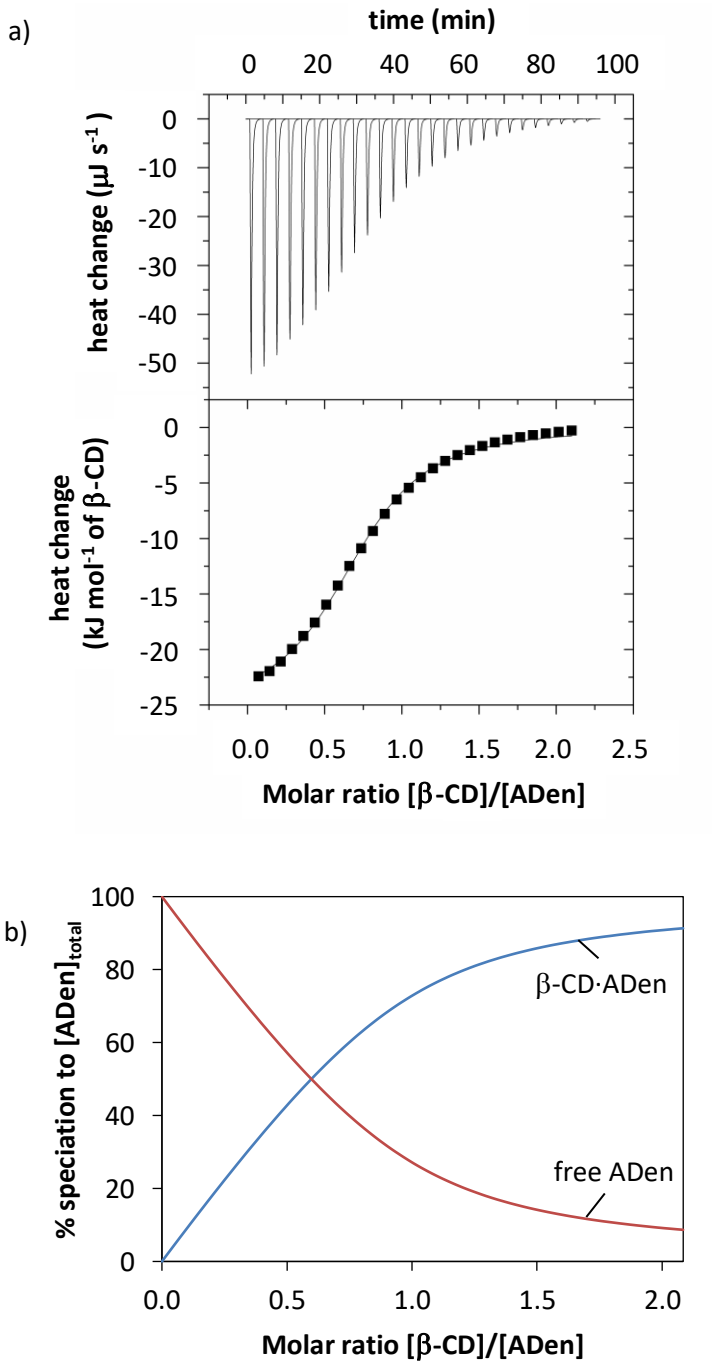

Figure 5.25: ITC data for 0.34 wt% PAAADen ([ADen] = 7.0×10^{-4} mol dm^{-3}) with β-CD (7.3×10^{-3} mol dm^{-3}) in aqueous phosphate buffer (pH 7.0, I = 0.10 mol dm^{-3}) at 298.2 K. a) The top section shows the raw ITC heat release profile with time. The bottom section shows the experimental heat released with each addition of β-CD (squares) and the best-fit of an algorithm for a 1:1 β-CD·ADen complex (solid line), analogous to that shown in Equation 5.5. b) Speciation plot showing the variation in the proportion of free and complexed ADen-substituent as [β-CD]/[ADen] increases.

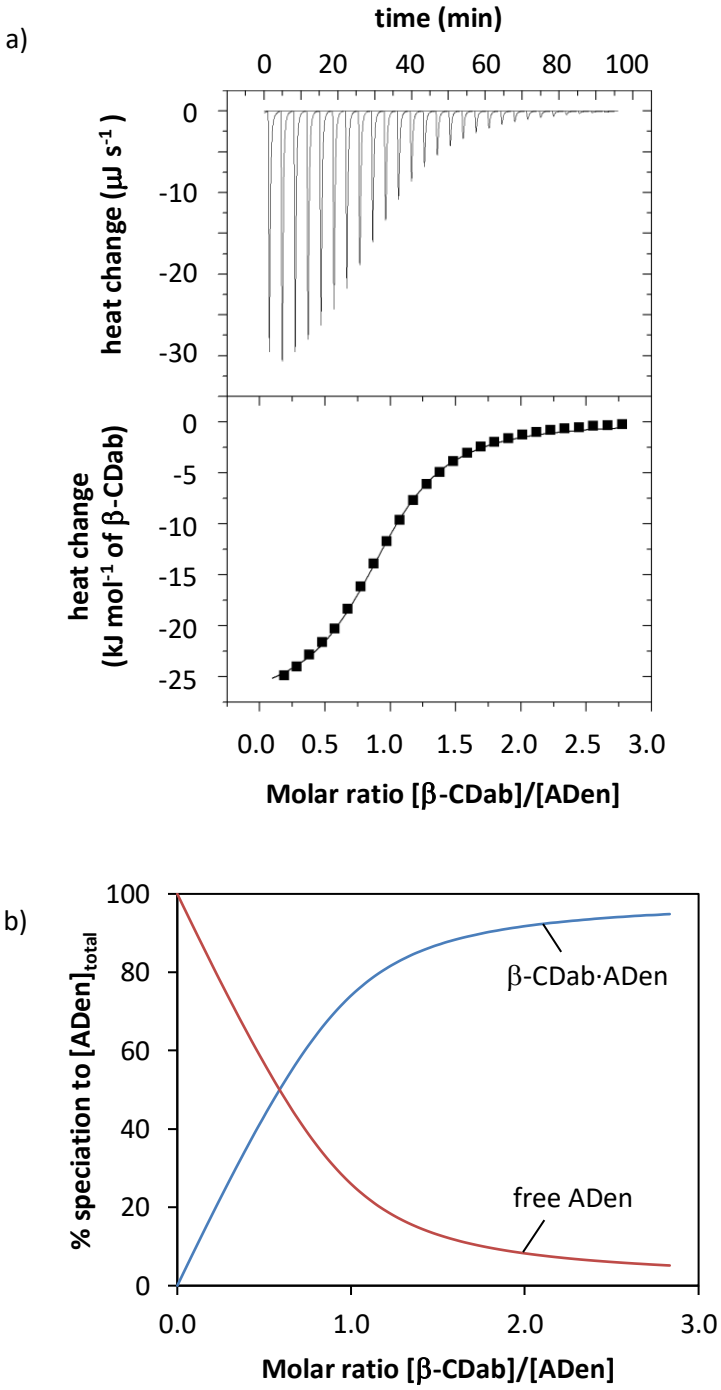

Figure 5.26: ITC data for 0.14 wt% PAAADen ([ADen] = 2.9×10^{-4} mol dm^{-3}) with β-CDab (4.0×10^{-3} mol dm^{-3}) in aqueous phosphate buffer (pH 7.0, I = 0.10 mol dm^{-3}) at 298.2 K. a) The top section shows the raw ITC heat release profile with time. The bottom section shows the experimental heat released with each addition of β-CDab (squares) and the best-fit of an algorithm for a 1:1 β-CDab·ADen complex (solid line), analogous to that shown in Equation 5.5. b) Speciation plot showing the variation in the proportion of free and complexed ADen-substituent as [β-CDab]/[ADen] increases.

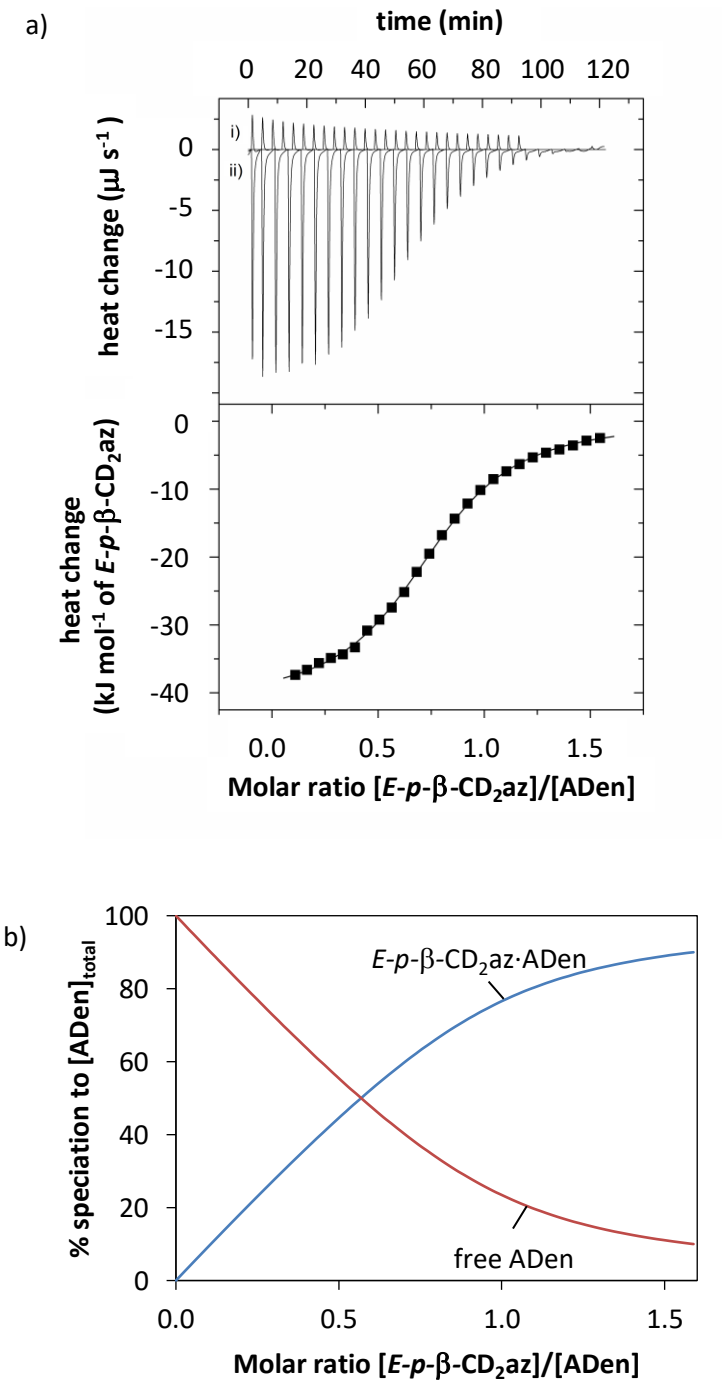

Figure 5.27: ITC data for 0.12 wt% PAAADen ([ADen] = 2.5×10^{-4} mol dm^{-3}) with *E*-*p*-β-CD_2az (2.0×10^{-3} mol dm^{-3}) in aqueous phosphate buffer (pH 7.0, I = 0.10 mol dm^{-3}) at 298.2 K. a) The top section shows the raw ITC heat release profile with time, where i) is the *E*-*p*-β-CD_2az dilution data and ii) is the titration data. The bottom section shows the experimental heat released with each addition of E-*p*-β-CD_2az, subtracting the heat of dilution of *E*-*p*-β-CD_2az (squares) and the best-fit of an algorithm for a 1:1 *E*-*p*-β-CD_2az·ADen complex (solid line), analogous to that shown in Equation 5.5. b) Speciation plot showing the variation in the proportion of free and complexed ADen-substituent as [*E*-*p*-β-CD_2az]/[ADen] increases.

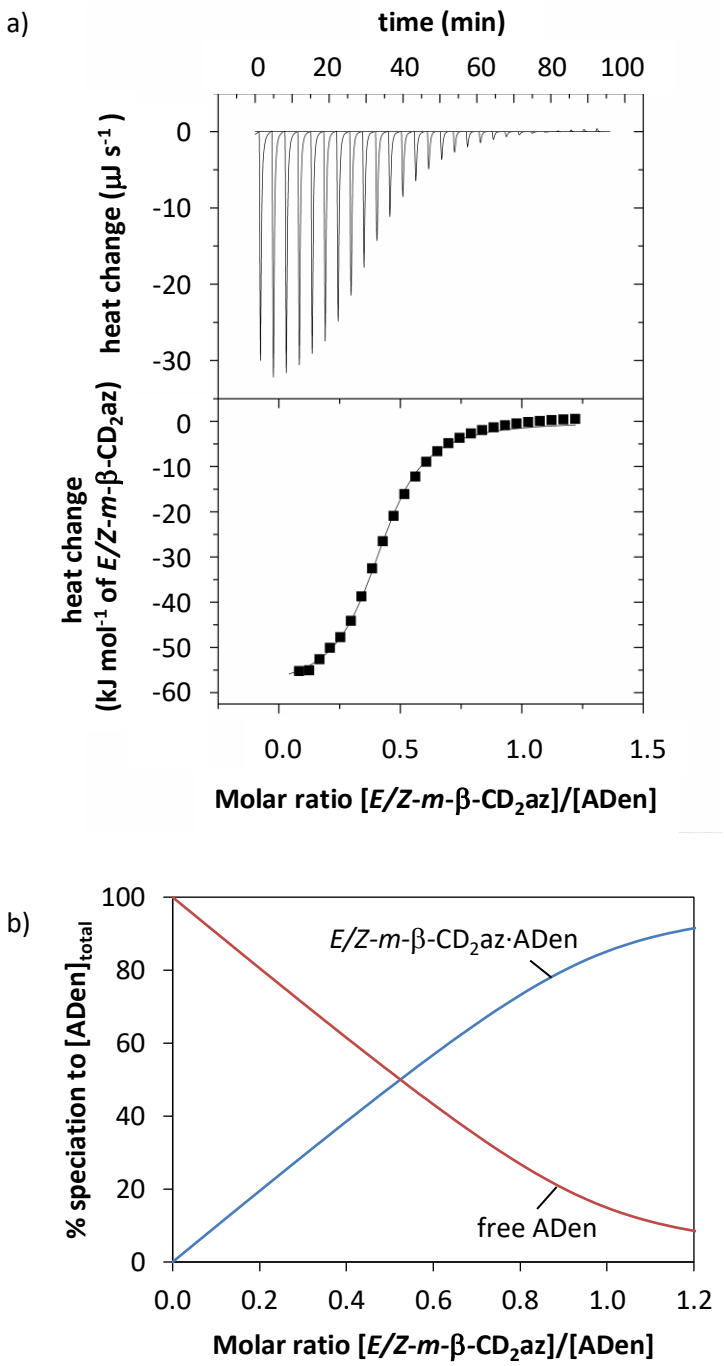

Figure 5.28: ITC data for 0.16% wt% PAAADen ([ADen] = 3.3×10^{-4} mol dm^{-3}) with *E/Z-m*-β-CD_2az (2.0×10^{-3} mol dm^{-3}) in aqueous phosphate buffer (pH 7.0, I = 0.10 mol dm^{-3}) at 298.2 K. a) The top section shows the raw ITC heat release profile with time. The bottom section shows the experimental heat released with each addition of *E/Z-m*-β-CD_2az (squares) and the best-fit of an algorithm for a 1:1 *E/Z-m*-β-CD_2az·ADen complex (solid line), analogous to that shown in Equation 5.5. b) Speciation plot showing the variation in the proportion of free and complexed ADen-substituent as [*E/Z-m*-β-CD_2az] /[ADen] increases.

5.2.2.2.2 ITC Study of the Complexation of PAAADhn by β-CD, β-CDab, *E*-*p*-β-CD_2az and *E/Z*-*m*-β-CD_2az

The heat change profile of an aqueous solution of PAAADhn as an aqueous solution of either β-CD, β-CDab, *E*-*p*-β-CD_2az or *E/Z*-*m*-β-CD_2az is titrated into it at 298.2 K is consistent with complexation occurring, as also evidenced by NMR spectroscopy. The isotherms for the β-CD/PAAADhn, β-CDab/PAAADhn, *E*-*p*-β-CD_2az/PAAADhn and *E/Z*-*m*-β-CD_2az/PAAADhn systems are shown in Figure 5.29 a) – Figure 5.32 a), respectively. The heat release associated with the dissociation of *E*-*p*-β-CD_2az aggregates (Figure 5.24) was subtracted from the total heat release profile of the *E*-*p*-β-CD_2az/PAAADhn system (Figure 5.31 a)).

Each system produced a monophasic isotherm, suggesting the formation of a 1:1 complex. An algorithm for the formation of 1:1 host·ADhn complex (Equation 5.5 and Equation 5.6) fitted the isotherms well. The variation of the concentrations of the 1:1 β-CD·ADhn, β-CDab·ADhn, *E*-*p*-β-CD_2az·ADhn and *E/Z*-*m*-β-CD_2az·ADhn complexes are shown in Figure 5.29 b) – Figure 5.32 b), respectively. The derived K_{11}, ΔG°_{11}, ΔH°_{11} and $T\Delta S^\circ_{11}$ appear in Table 5.1.

As the *E/Z*-*m*-β-CD_2az/PAAADhn system consisted of a mixture of *E* and *Z* isomers of *m*-β-CD_2az, it was anticipated that the isotherm may be biphasic, accounting for the formation of 1:1 *E*-*m*-β-CD_2az·ADhn and *Z*-*m*-β-CD_2az·ADhn complexes. However, as the *E/Z*-*m*-β-CD_2az/PAAADhn system produced a monophasic isotherm, *E*-*m*-β-CD_2az and *Z*-*m*-β-CD_2az are likely to have similar complexation properties. Thus, the K_{11} for the *E/Z*-*m*-β-CD_2az·ADhn complex represents the weighted average of the K_{11} corresponding to the *E*-*m*-β-CD_2az·ADhn and *Z*-*m*-β-CD_2az·ADhn complexes. Similarly, the derived thermodynamic parameters represent the weighted average of the thermodynamic parameters corresponding to 1:1 *E*-*m*-β-CD_2az·ADhn and *Z*-*m*-β-CD_2az·ADhn complexes.

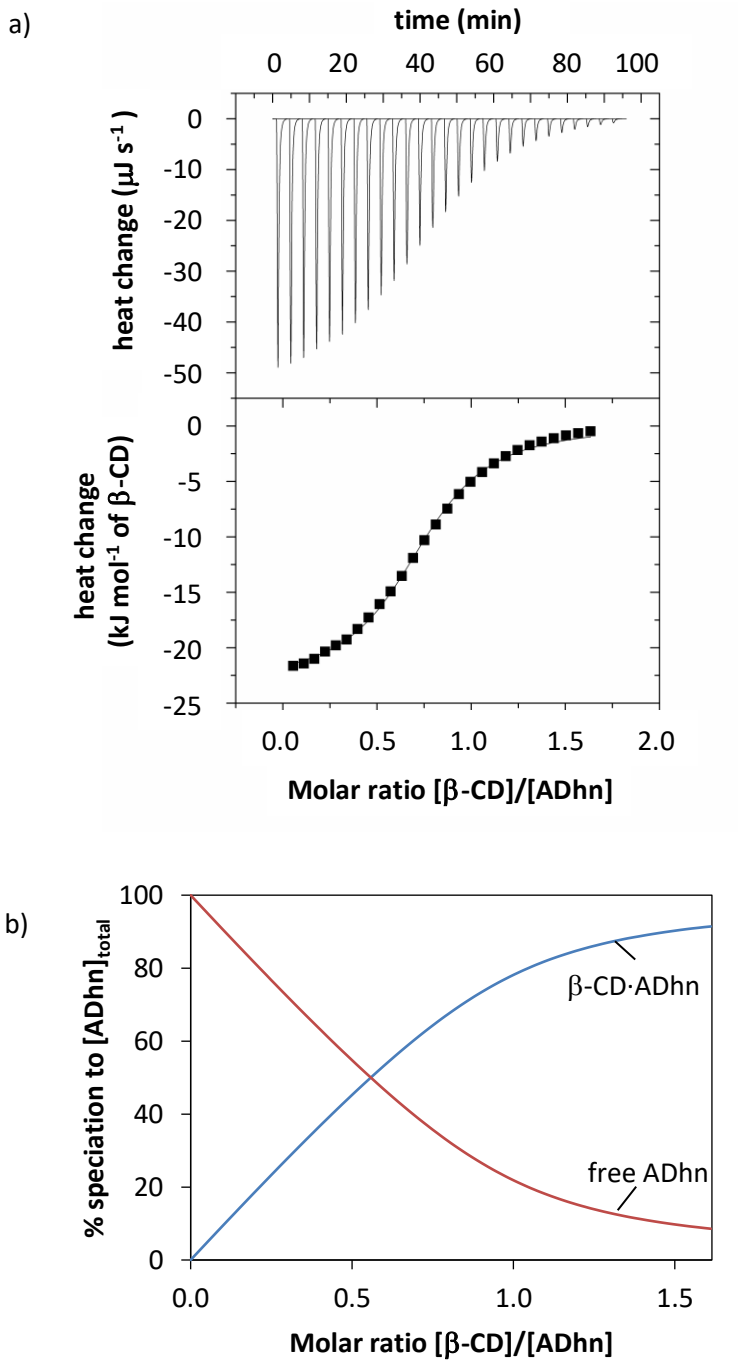

Figure 5.29: ITC data for 0.33 wt% PAAADhn ([ADhn] = 9.0×10^{-4} mol dm^{-3}) with β-CD (7.3×10^{-3} mol dm^{-3}) in aqueous phosphate buffer (pH 7.0, I = 0.10 mol dm^{-3}) at 298.2 K. a) The top section shows the raw ITC heat release profile with time. The bottom section shows the experimental heat released with each addition of β-CD (squares) and the best-fit of an algorithm for a 1:1 β-CD·ADhn complex (solid line), analogous to that shown in Equation 5.5. b) Speciation plot showing the variation in the proportion of free and complexed ADhn-substituent as [β-CD]/[ADhn] increases.

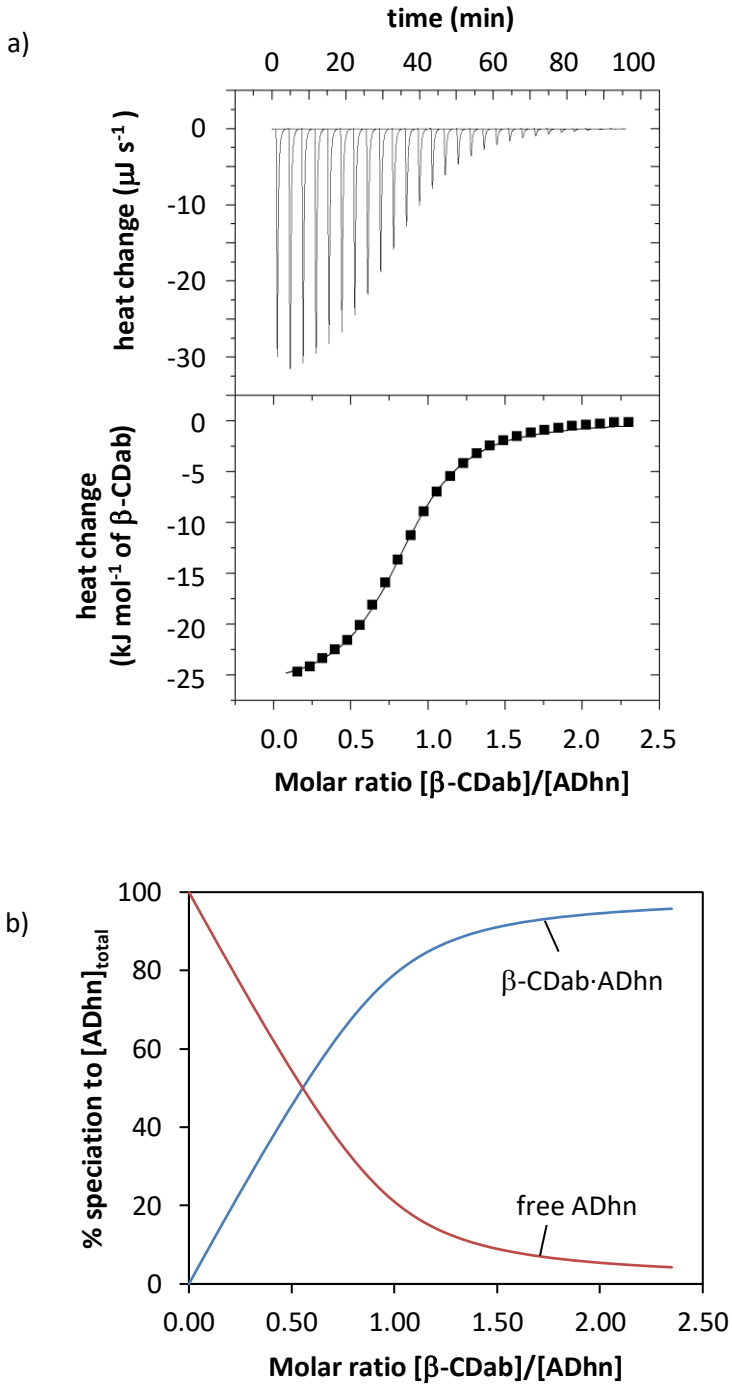

Figure 5.30: ITC data for 0.13 wt% PAAADhn ([ADhn] = 3.5×10^{-4} mol dm^{-3}) with β-CDab (4.0×10^{-3} mol dm^{-3}) in aqueous phosphate buffer (pH 7.0, I = 0.10 mol dm^{-3}) at 298.2 K. a) The top section shows the raw ITC heat release profile with time. The bottom section shows the experimental heat released with each addition of β-CDab (squares) and the best-fit of an algorithm for a 1:1 β-CDab·ADh complex (solid line), analogous to that shown in Equation 5.5. b) Speciation plot showing the variation in the proportion of free and complexed ADhn-substituent as [β-CDab]/[ADhn] increases.

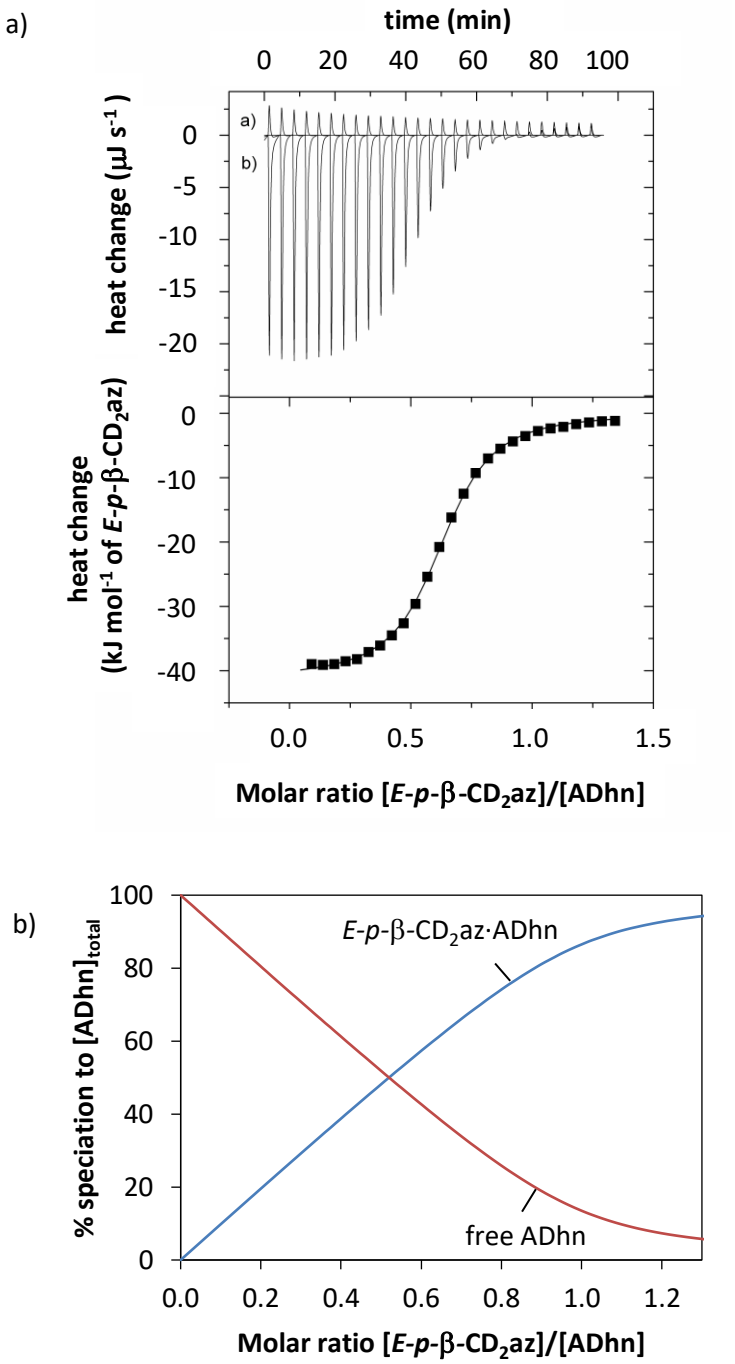

Figure 5.31: ITC data for 0.11 wt% PAAADhn ([ADhn] = 3.0×10^{-4} mol dm^{-3}) with *E*-*p*-β-CD_2az (2.0×10^{-3} mol dm^{-3}) in aqueous phosphate buffer (pH 7.0, I = 0.10 mol dm^{-3}) at 298.2 K. a) The top section shows the raw ITC heat release profile with time, where i) is the *E*-*p*-β-CD_2az dilution data and ii) is the titration data. The bottom section shows the experimental heat released with each addition *E*-*p*-β-CD_2az, subtracting the heat of dilution of *E*-*p*-β-CD_2az (squares) and the best-fit of an algorithm for 1:1 *E*-*p*-β-CD_2az·ADhn complex (solid line), analogous to that shown in Equation 5.5. b) Speciation plot showing the variation in the proportion of free and complexed ADhn-substituent as [*E*-*p*-β-CD_2az]/[ADhn] increases.

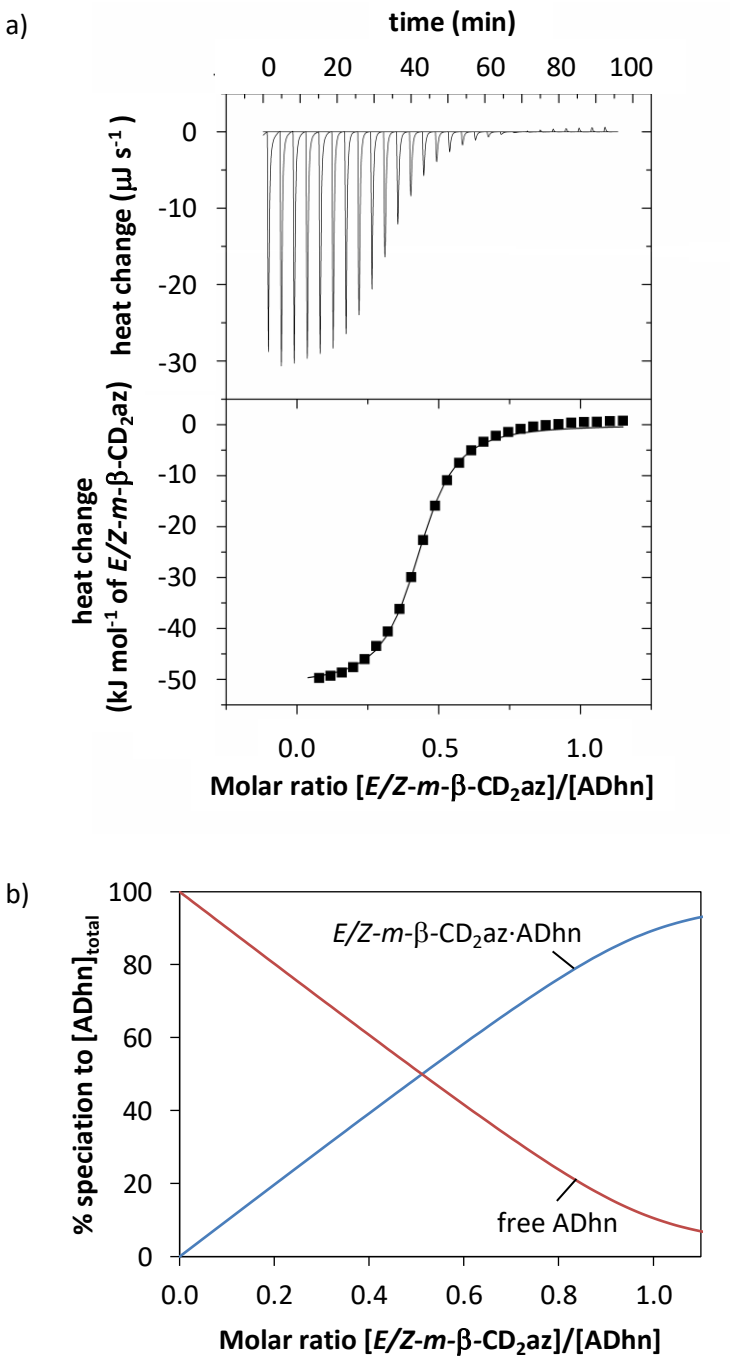

Figure 5.32: ITC data for 0.13 wt% PAAADhn ([ADhn] = 3.5×10^{-4} mol dm^{-3}) with *E/Z-m*-β-CD_2az (2.0×10^{-3} mol dm^{-3}) in aqueous phosphate buffer (pH 7.0, I = 0.10 mol dm^{-3}) at 298.2 K. a) The top section shows the raw ITC heat release profile with time. The bottom section shows the experimental heat released with each addition of *E/Z-m*-βCD_2az (squares) and the best-fit of an algorithm for a 1:1 *E/Z-m*-β-CD_2az·ADhn complex (solid line), analogous to that shown in Equation 5.5. b) Speciation plot showing the variation in the proportion of free and complexed ADhn-substituent as [*E/Z-m*-β-CD_2az]/[ADhn] increases.

5.2.2.2.3 ITC Study of the Complexation of PAAADddn by β-CD, β-CDab, *E-p*-β-CD_2az and *E/Z-m*-β-CD_2az

The heat change profile of an aqueous solution of PAAADddn as an aqueous solution of either β-CD, β-CDab, *E-p*-β-CD_2az or *E/Z-m*-β-CD_2az is titrated into it at 298.2 K is consistent with complexation occurring, as also evidenced by NMR spectroscopy. The isotherms for the β-CD/PAAADddn, β-CDab/PAAADddn, *E-p*-β-CD_2az/PAAADddn and *E/Z-m*-β-CD_2az/PAAADddn systems are shown in Figure 5.33 a) – Figure 5.36 a), respectively. The heat release associated with the dissociation of *E-p*-β-CD_2az aggregates (Figure 5.24) was subtracted from the heat release profile of the *E-p*-β-CD_2az/PAAADddn system (Figure 5.35 a)).

The β-CD/PAAADddn and β-CDab/PAAADddn systems produced monophasic isotherms, suggesting the formation of 1:1 complexes. An algorithm for the formation of 1:1 host·ADddn complexes (Equation 5.5 and Equation 5.6) fitted the isotherms well. The variation of the concentrations of the 1:1 β-CD·ADddn and β-CDab·ADddn complexes are shown in Figure 5.33 b) and Figure 5.34 b), respectively. The derived K_{11}, ΔG°_{11}, ΔH°_{11} and $T\Delta S^\circ_{11}$ appear in Table 5.1.

The *E-p*-β-CD_2az/PAAADddn system produced an isotherm which was not clearly monophasic. An algorithm for the formation of a 1:1 *E-p*-β-CD_2az·ADddn complex (Equation 5.5 and Equation 5.6) unsatisfactorily fitted the data, as shown in Figure 5.57 a) in 5.5 Appendix. Therefore, an algorithm for the sequential formation of 1:1 *E-p*-β-CD_2az·ADddn and 1:2 *E-p*-β-CD_2az·$(ADddn)_2$ complexes (Equation 5.5 – Equation 5.8) was fitted to the isotherm. The fitting was satisfactory, as shown in Figure 5.35 a). The variation of the concentrations of the 1:1 *E-p*-β-CD_2az·ADddn and 1:2 *E-p*-β-CD_2az·$(ADddn)_2$ complexes are shown in Figure 5.35 b). The derived K_{11}, K_{12}, ΔG°_{11}, ΔG°_{12}, ΔH°_{11}, ΔH°_{12}, $T\Delta S^\circ_{11}$ and $T\Delta S^\circ_{12}$ appear in Table 5.1.

The *E/Z-m*-β-CD_2az/PAAADddn system produced a biphasic isotherm, suggesting the formation of two complexes. The two complexes are unlikely to be 1:1 *E-m*-β-CD_2az·ADen and *Z-m*-β-CD_2az·ADen complexes as the *E/Z-m*-β-CD_2az/PAAADen and *E/Z-m*-β-CD_2az/PAAADhn systems indicated similar complexation properties for both *E-m*-β-CD_2az and *Z-m*-β-CD_2az. Thus, the biphasic isotherm of the *E/Z-m*-β-CD_2az/PAAADddn system represents the formation of 1:1 and 1:2 complexes.

An algorithm for the sequential formation of 1:1 *E/Z-m*-β-CD_2az·ADddn and 1:2 *E/Z-m*-β-CD_2az·$(ADddn)_2$ complexes (Equation 5.5 – Equation 5.8) fitted the isotherm well. The variation of the concentrations of the 1:1 *E/Z-m*-β-CD_2az·ADddn and 1:2 *E/Z-m*-β-CD_2az·$(ADddn)_2$ complexes are shown in Figure 5.36 b). The derived K_{11}, K_{12}, $\Delta G°_{11}$, $\Delta G°_{12}$, $\Delta H°_{11}$, $\Delta H°_{12}$, $T\Delta S°_{11}$ and $T\Delta S°_{12}$ appear in Table 5.1. The K_{11} for the *E/Z-m*-β-CD_2az·ADddn complex represents the weighted average of the K_{11} corresponding to the *E-m*-β-CD_2az·ADddn and *Z-m*-β-CD_2az·ADddn complexes, while the K_{12} for the *E/Z-m*-β-CD_2az·$(ADddn)_2$ complex represents the weighted average of the K_{12} corresponding to the *E-m*-β-CD_2az·$(ADddn)_2$ and *Z-m*-β-CD_2az·$(ADddn)_2$ complexes. Similarly, the derived thermodynamic parameters represent a weighted average of the thermodynamic parameters of the analogous 1:1 and 1:2 complexes.

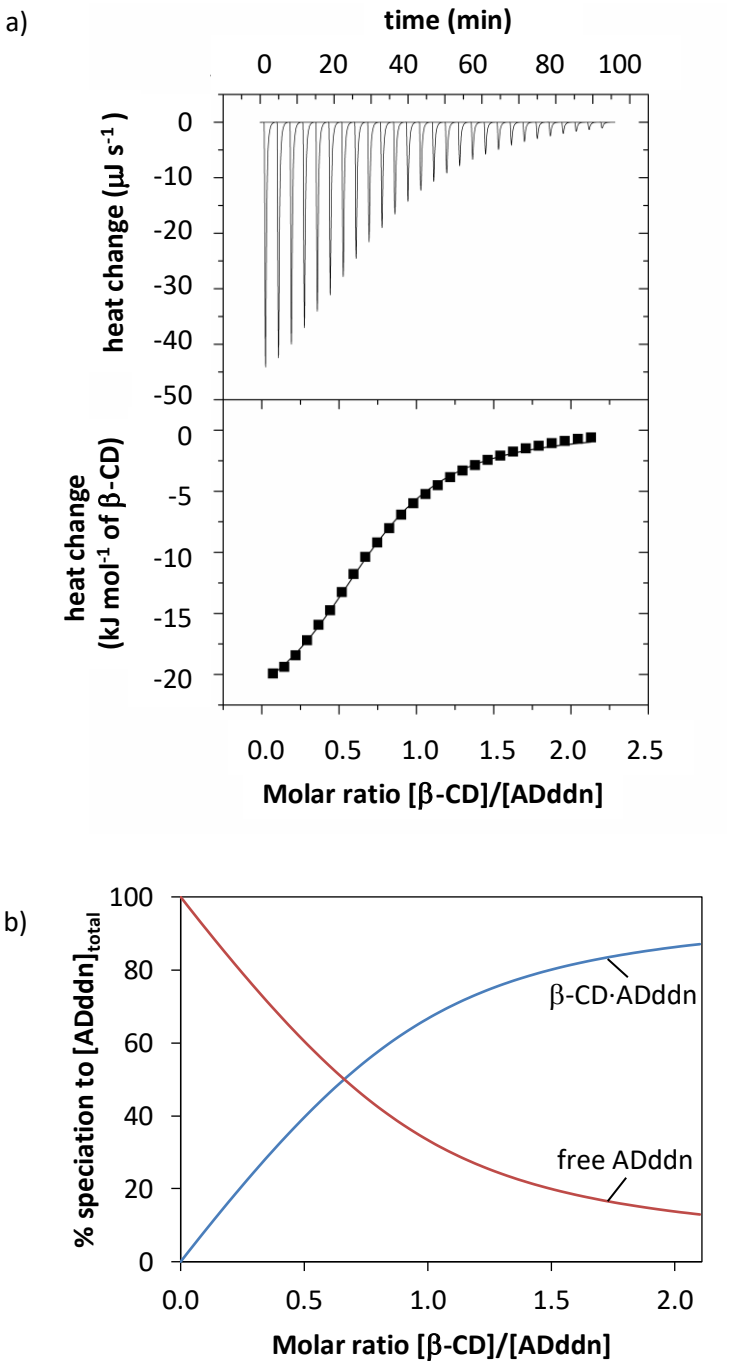

Figure 5.33: ITC data for 0.35 wt% PAAADddn ([ADddn] = 6.9×10^{-4} mol dm^{-3}) with β-CD (7.3×10^{-3} mol dm^{-3}) in aqueous phosphate buffer (pH 7.0, I = 0.10 mol dm^{-3}) at 298.2 K. a) The top section shows the raw ITC heat release profile with time. The bottom section shows the experimental heat released with each addition of β-CD (squares) and the best-fit of an algorithm for a 1:1 β-CD·ADddn complex (solid line), analogous to that shown in Equation 5.5. b) Speciation plot showing the variation in the proportion of free and complexed ADddn-substituent as [β-CD]/[ADddn] increases.

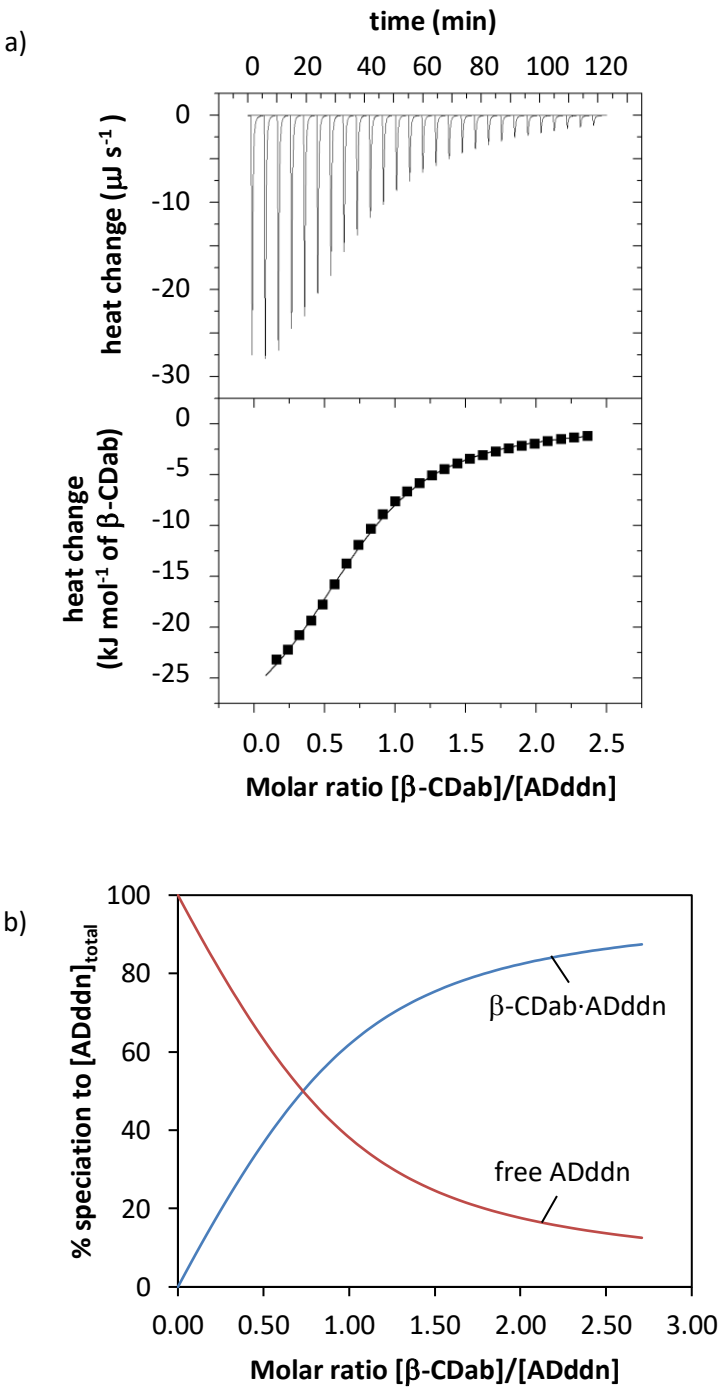

Figure 5.34: ITC data for 0.17 wt% PAAADddn ([ADddn] = 3.0×10^{-4} mol dm^{-3}) with β-CDab (4.0×10^{-3} mol dm^{-3}) in aqueous phosphate buffer (pH 7.0, I = 0.10 mol dm^{-3}) at 298.2 K. a) The top section shows the raw ITC heat release profile with time. The bottom section shows the experimental heat released with each addition of β-CDab (squares) and the best-fit of an algorithm for a 1:1 β-CDab·ADddn complex (solid line), analogous to that shown in Equation 5.5. b) Speciation plot showing the variation in the proportion of free and complexed ADddn-substituent as [β-CDab]/[ADddn] increases.

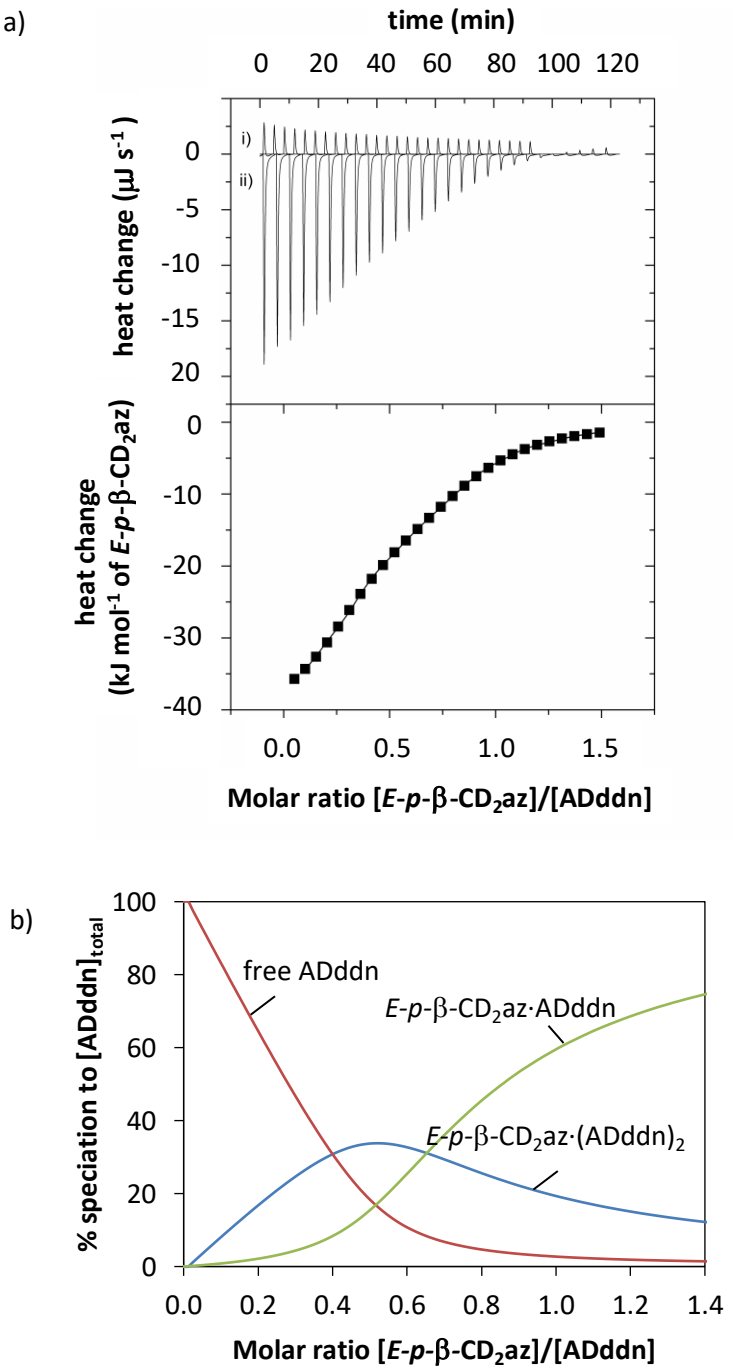

Figure 5.35: ITC data for 0.14 wt% PAAADddn ([ADddn] = 2.7×10^{-4} mol dm^{-3}) with *E*-*p*-β-CD$_2$az (2.0×10^{-3} mol dm^{-3}) in aqueous phosphate buffer (pH 7.0, I = 0.10 mol dm^{-3}) at 298.2 K. a) The top section shows the raw ITC heat release profile with time, where i) is the *E*-*p*-β-CD$_2$az dilution data and ii) is the titration data. The bottom section shows the experimental heat released with each addition of *E*-*p*-β-CD$_2$az, subtracting the heat of dilution of *E*-*p*-β-CD$_2$az (squares) and the best-fit of an algorithm for 1:1 *E*-*p*-β-CD$_2$az·ADddn and 1:2 *E*-*p*-β-CD$_2$az·(ADddn)$_2$ complexes (solid line), analogous to that shown in Equation 5.5 and Equation 5.7, respectively. b) Speciation plot showing the variation in the proportion of free and complexed ADddn-substituent as [*E*-*p*-β-CD$_2$az]/[ADddn] increases.

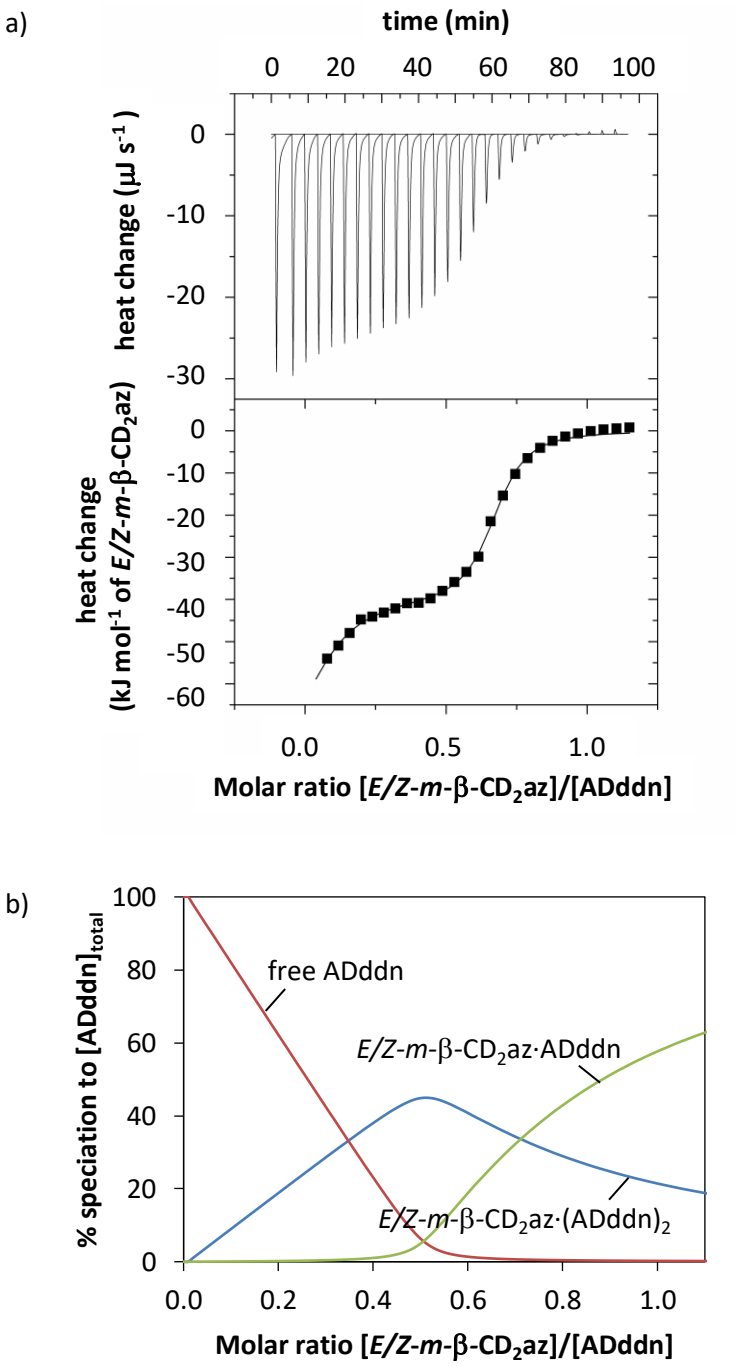

Figure 5.36: ITC data for 0.18 wt% PAAADddn ([ADddn] = 3.5×10^{-4} mol dm^{-3}) with *E/Z-m*-β-CD_2az (2.0×10^{-3} mol dm^{-3}) in aqueous phosphate buffer (pH 7.0, I = 0.10 mol dm^{-3}) at 298.2 K. a) The top section shows the raw ITC heat release profile with time. The bottom section shows the experimental heat released with each addition of *E/Z-m*-β-CD_2az (squares) and the best-fit of an algorithm for 1:1 *E/Z-m*-β-CD_2az·ADddn and 1:2 *E/Z-m*-β-CD_2az·$(ADddn)_2$ complexes (solid line), analogous to that shown in Equation 5.5 and Equation 5.7, respectively. b) Speciation plot showing the variation in the proportion of free and complexed ADddn-substituent as [*E/Z-m*-β-CD_2az]/[ADddn]increases.

5.2.2.2.4 ITC Study of the Complexation of PAAC12 by β-CD, β-CDab, *E-p*-β-CD_2az and *E/Z-m*-β-CD_2az

The heat change profile of an aqueous solution of PAAC12 as an aqueous solution of either β-CD, β-CDab, *E-p*-β-CD_2az or *E/Z-m*-β-CD_2az is titrated into it at 298.2 K is consistent with complexation occurring, as also evidenced by NMR spectroscopy. The isotherms for the β-CD/PAAC12, β-CDab/PAAC12, *E-p*-β-CD_2az/PAAC12 and *E/Z-m*-β-CD_2az/PAAC12 systems are shown in Figure 5.37 a) – Figure 5.40 a), respectively. The heat release associated with the dissociation of *E-p*-β-CD_2az aggregates (Figure 5.24) was subtracted from the heat release profile of the *E-p*-β-CD_2az/PAAC12 system (Figure 5.39 a)).

The β-CD/PAAC12 and β-CDab/PAAC12 systems produced monophasic isotherms, suggesting the formation of a 1:1 complex. An algorithm for the formation of 1:1 host·C12 complexes (Equation 5.5 and Equation 5.6) fitted the isotherms well. The variation of the concentrations of the 1:1 β-CD·C12 and β-CDab·C12 complexes are shown in Figure 5.37 b) – Figure 5.38 b), respectively. The derived K_{11}, ΔG°_{11}, ΔH°_{11} and $T\Delta S^\circ_{11}$ appear in Table 5.1.

The *E-p*-β-CD_2az/PAAC12 system produced a biphasic isotherm, suggesting the formation of two complexes. An algorithm for the sequential formation of 1:1 *E-p*-β-CD_2az·C12 and 1:2 *E-p*-β-CD_2az·$(C12)_2$ complexes (Equation 5.5 – Equation 5.8) fitted the isotherm well. The variation of the concentrations of the 1:1 *E-p*-β-CD_2az·C12 and 1:2 *E-p*-β-CD_2az·$(C12)_2$ complexes are shown in Figure 5.39 b). The derived K_{11}, K_{12}, ΔG°_{11}, ΔG°_{12}, ΔH°_{11}, ΔH°_{12}, $T\Delta S^\circ_{11}$ and $T\Delta S^\circ_{12}$ appear in Table 5.1.

The *E/Z-m*-β-CD_2az/PAAC12 system produced a biphasic isotherm, suggesting the formation of two complexes. The two complexes are unlikely to be 1:1 *E-m*-β-CD_2az·C12 and *Z-m*-β-CD_2az·C12 complexes as the *E/Z-m*-β-CD_2az/PAAADen and *E/Z-m*-β-CD_2az/PAAADhn systems indicated similar complexation properties for both *E-m*-β-CD_2az and *Z-m*-β-CD_2az. Thus, the biphasic isotherm of the *E/Z-m*-β-CD_2az/PAAC12 system is likely to represent the formation of 1:1 and 1:2 complexes.

An algorithm for the sequential formation of 1:1 *E/Z-m*-β-CD_2az·C12 and 1:2 *E/Z-m*-β-CD_2az·$(C12)_2$ complexes (Equation 5.5 – Equation 5.8) fitted the isotherm well. The variation of the concentrations of the 1:1 *E/Z-m*-β-CD_2az·C12 and 1:2 *E/Z-m*-β-CD_2az·$(C12)_2$ complexes are shown in Figure 5.40 b). The derived K_{11}, K_{12}, ΔG°_{11}, ΔG°_{12}, ΔH°_{11}, ΔH°_{12}, $T\Delta S^\circ_{11}$ and $T\Delta S^\circ_{12}$ appear in Table 5.1. The K_{11} for the *E/Z-m*-β-CD_2az·C12 complex represents the weighted average of the K_{11} corresponding to the *E-m*-β-CD_2az·C12 and *Z-m*-β-CD_2az·C12 complexes, while the K_{12} for the *E/Z-m*-β-CD_2az·$(C12)_2$ complex represents the weighted average of the K_{12} corresponding to the *E-m*-β-CD_2az·$(C12)_2$ and *Z-m*-β-CD_2az·$(C12)_2$ complexes. Similarly, the derived thermodynamic parameters represent the weighted average of the analogous 1:1 and 1:2 complexes.

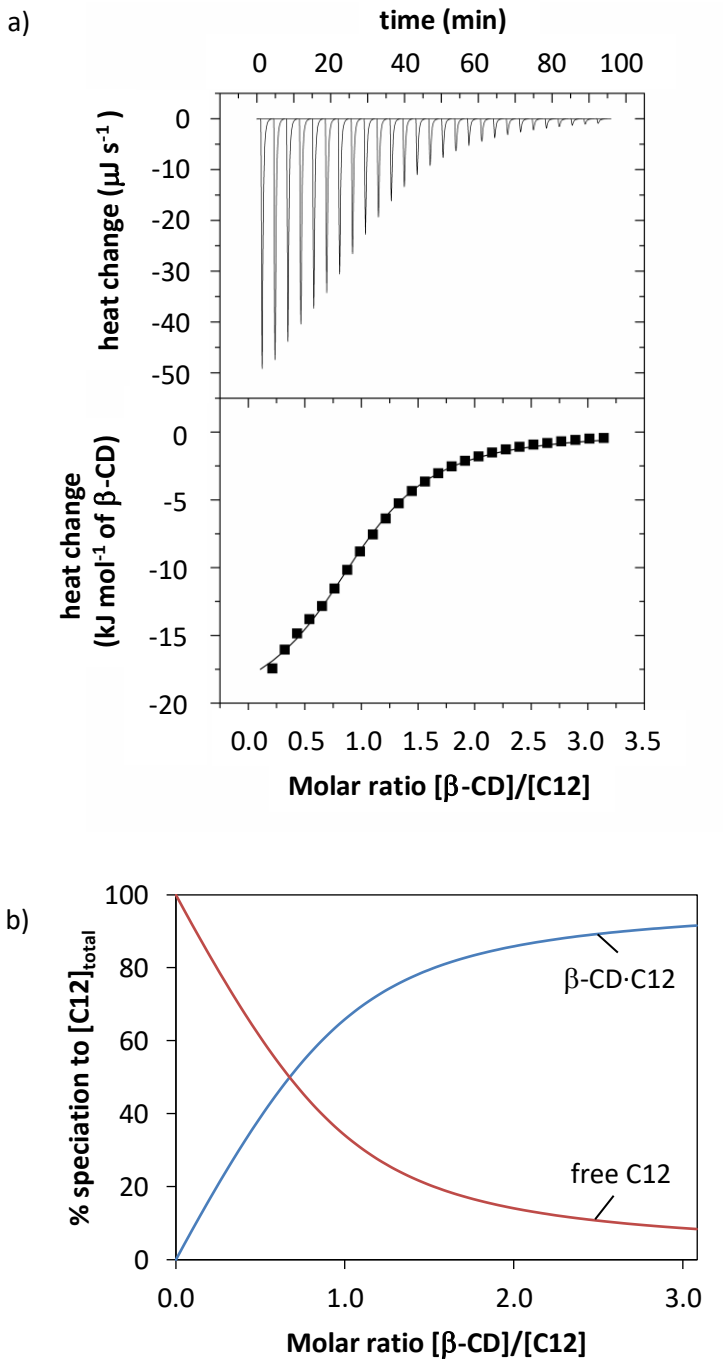

Figure 5.37: ITC data for 0.31 wt% PAAC12 ([C12] = 5.8 × 10^{-4} mol dm^{-3}) with β-CD (9.0 × 10^{-3} mol dm^{-3}) in aqueous phosphate buffer (pH 7.0, I = 0.10 mol dm^{-3}) at 298.2 K. a) The top section shows the raw ITC heat release profile with time. The bottom section shows the experimental heat released with each addition of β-CD (squares) and the best-fit of an algorithm for a 1:1 β-CD·C12 complex (solid line), analogous to that shown in Equation 5.5. b) Speciation plot showing the variation in the proportion of free and complexed C12-substituent as [β-CD]/[C12] increases.

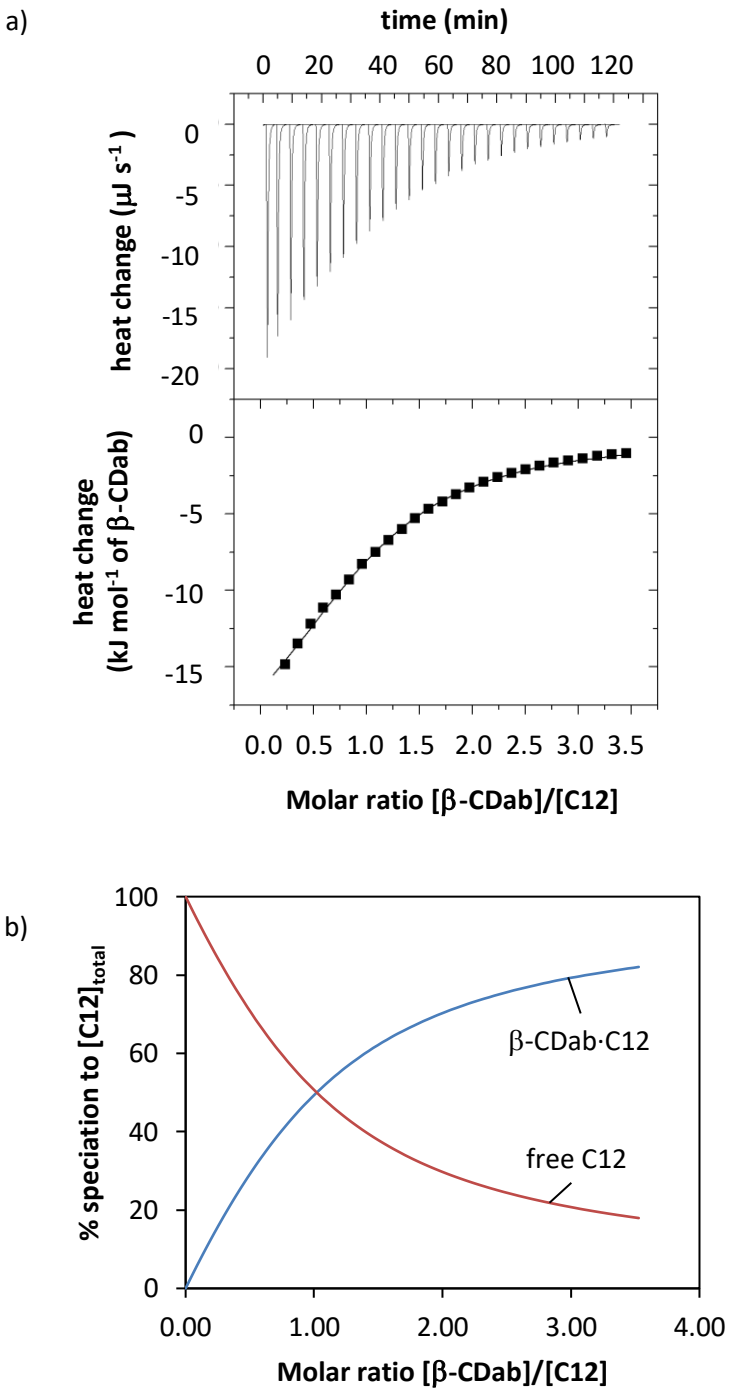

Figure 5.38: ITC data for 0.13 wt% PAAC12 ([C12] = 2.3×10^{-4} mol dm^{-3}) with β-CDab (4.0×10^{-3} mol dm^{-3}) in aqueous phosphate buffer (pH 7.0, I = 0.10 mol dm^{-3}) at 298.2 K. b) The top section shows the raw ITC heat release profile with time. The bottom section shows the experimental heat released with each addition of β-CDab (squares) and the best-fit of an algorithm for a 1:1 β-CDab·C12 complex (solid line), analogous to that shown in Equation 5.5. b) Speciation plot showing the variation in the proportion of free and complexed C12-substituent as [β-CDab]/[C12] increases.

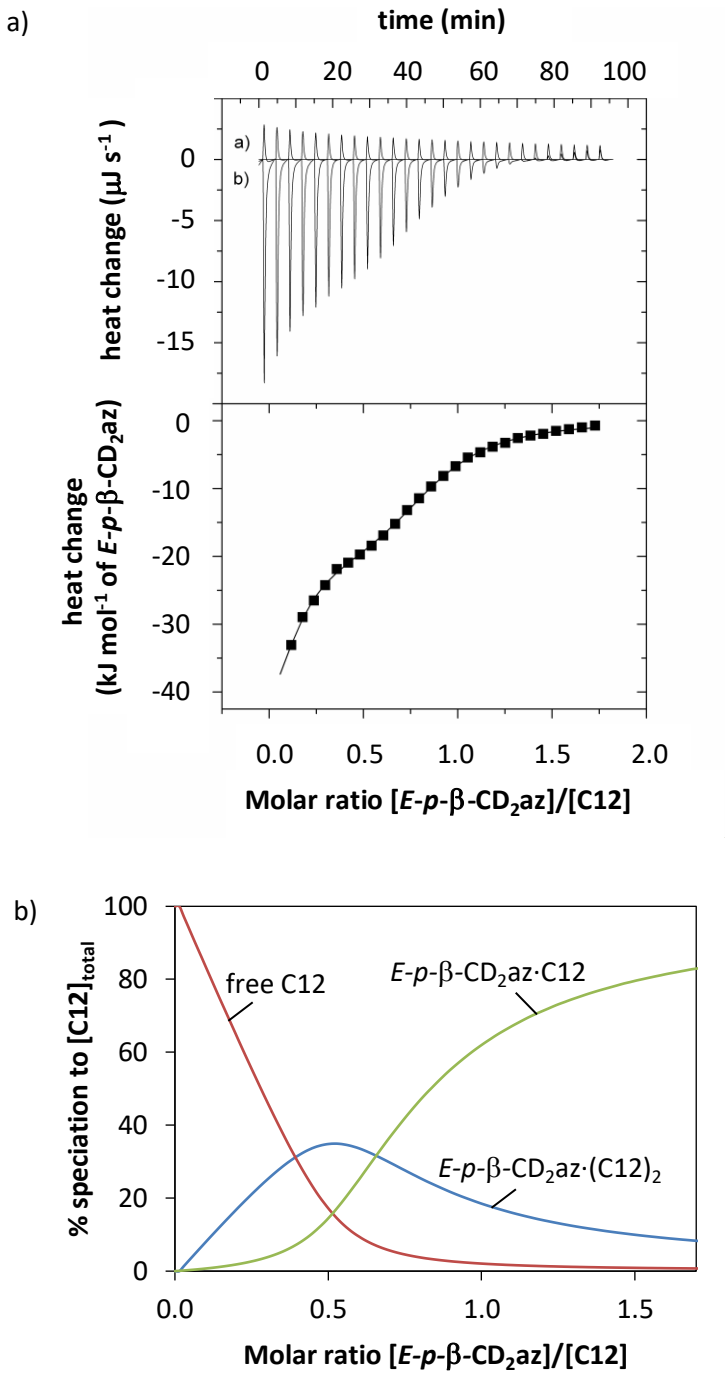

Figure 5.39: ITC data for 0.13 wt% PAAC12 ([C12] = 2.3×10^{-4} mol dm^{-3}) with *E*-*p*-β-CD_2az (2.0×10^{-3} mol dm^{-3}) in aqueous phosphate buffer (pH 7.0, I = 0.10 mol dm^{-3}) at 298.2 K. a) The top section shows the raw ITC heat release profile with time, where i) is the *E*-*p*-β-CD_2az dilution data and ii) is the titration data. The bottom section shows the experimental heat released with each addition of *E*-*p*-β-CD_2az, subtracting the heat of dilution of *E*-*p*-β-CD_2az (squares) and the best-fit of an algorithm for 1:1 *E*-*p*-β-CD_2az·C12 and 1:2 *E*-*p*-β-CD_2az·$(C12)_2$ complexes (solid line), analogous to that shown in Equation 5.5 and Equation 5.7, respectively. b) Speciation plot showing the variation in proportion of free and complexed C12-substituent as [*E*-*p*-β-CD_2az]/[C12] increases.

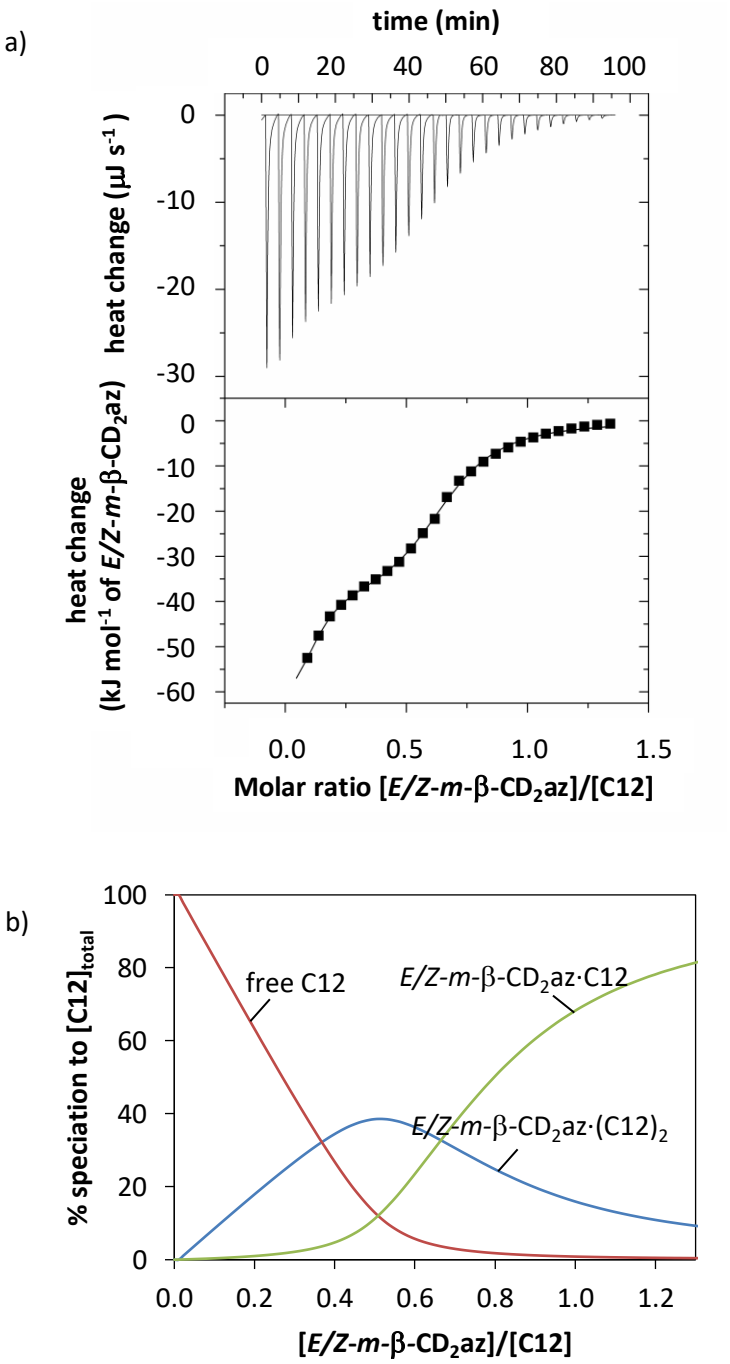

Figure 5.40: ITC data for 0.16 wt% PAAC12 ([C12] = 3.0×10^{-4} mol dm^{-3}) with *E/Z-m*-β-CD_2az (2.0×10^{-3} mol dm^{-3}) in aqueous phosphate buffer (pH 7.0, I = 0.10 mol dm^{-3}) at 298.2 K. a) The top section shows the raw ITC heat release profile with time. The bottom section shows the experimental heat released with each addition of *E/Z m*-βCD_2az (squares) and the best-fit of an algorithm for 1:1 *E/Z-m*-β-CD_2az·C12 and 1:2 *E/Z-m*-β-CD_2az·$(C12)_2$ complexes (solid line), analogous to that shown in Equation 5.5 and Equation 5.7, respectively. b) Speciation plot showing the variation in the proportion of free and complexed C12-substituent as [*E/Z-m*-β-CD_2az]/[C12] increases.

5.2.2.2.5 Summary of Complexation Constants and Thermodynamic Parameters

A summary of the complexation constants and thermodynamic parameters for the complexation of PAAADen, PAAADhn, PAAADddn and PAAC12 by β-CD, β-CDab, *E-p*-β-CD_2az and *E/Z-m*-β-CD_2az are given in Table 5.1. The *N* value for the biphasic systems has been excluded as two complexation processes are occurring, corresponding to K_{11} and K_{12}. Thus, there is an overlap of heat release profiles and the *N* value cannot be simply interpreted.

Table 5.1: Complexation constants and thermodynamic parameters for the complexation between the hydrophobic-substitutients of PAAADen, PAAADhn, PAAADddn and PAAC12 by β-CD, β-CDab, *E-p*-β-CD_2az and *E/Z-m*-β-CD_2az in aqueous phosphate buffer (pH 7.0, I = 0.10 mol dm^{-3}) at 298.2 K as derived from ITC measurements.

System		10^{-4} K_{xy}[a] (dm mol^{-1})	$\Delta G°_{xy}$[b] (kJ mol^{-1})	$\Delta H°_{xy}$[a] (kJ mol^{-1})	$T\Delta S°_{xy}$[c] (kJ mol^{-1})	N[a]
β-CD/PAAADen	K_{11}	1.55 ± 0.08	-23.9 ± 0.1	-25.4 ± 0.3	-1.50 ± 0.03	0.73 ± 0.01
β-CDab/PAAADen	K_{11}	4.06 ± 0.16	-26.3 ± 0.1	-27.7 ± 0.3	-1.42 ± 0.02	0.93 ± 0.01
E-p-β-CD_2az/PAAADen	K_{11}	6.27 ± 0.16	-27.4 ± 0.1	-41.1 ± 0.2	-13.8 ± 0.10	0.77 ± 0.01
E/Z-m-β-CD_2az/PAAADen	K_{11}	13.6 ± 1.0	-29.3 ± 0.2	-59.1 ± 0.7	-28.7 ± 0.5	0.41 ± 0.01
β-CD/PAAADhn	K_{11}	2.04 ± 0.10	-24.6 ± 0.1	-23.1 ± 0.2	1.48 ± 0.02	0.74 ± 0.01
β-CDab/PAAADhn	K_{11}	5.58 ± 0.23	-27.1 ± 0.1	-26.5 ± 0.2	0.59 ± 0.01	0.84 ± 0.01
E-p-β-CD_2az/PAAADhn	K_{11}	18.2 ± 0.6	-30.0 ± 0.1	-41.1 ± 0.2	-11.1 ± 0.1	0.62 ± 0.01
E/Z-m-β-CD_2az/PAAADhn	K_{11}	27.0 ± 2.0	-31.0 ± 0.2	-50.9 ± 0.5	-19.9 ± 0.3	0.42 ± 0.01
β-CD/PAAADddn	K_{11}	0.95 ± 0.04	-22.7 ± 0.1	-24.7 ± 0.3	-1.97 ± 0.04	0.71 ± 0.01
β-CDab/PAAADddn	K_{11}	1.51 ± 0.05	-23.9 ± 0.1	-32.0 ± 0.5	-8.13 ± 0.05	0.73 ± 0.01
E-p-β-CD_2az /PAAADddn	K_{11}	44.2 ± 4.7	-32.2 ± 0.3	-41.6 ± 1.1	-9.44 ± 0.32	-
	K_{12}	5.09 ± 0.21	-26.9 ± 0.1	-17.8 ± 1.2	9.09 ± 0.63	-
E/Z-m-β-CD_2az /PAAADddn	K_{11}	408 ± 174	-37.7 ± 1.1	-85.1 ± 46.8	-47.4 ± 27.5	-
	K_{12}	55.0 ± 22.1	-32.8 ± 1.1	-40.1 ± 2.0	-7.25 ± 0.60	-
β-CD/PAAC12	K_{11}	1.04 ± 0.05	-22.9 ± 0.1	-20.7 ± 0.3	2.19 ± 0.05	0.99 ± 0.01
β-CDab/PAAC12	K_{11}	0.873 ± 0.036	-22.5 ± 0.1	-23.9 ± 0.6	-1.40 ± 0.04	0.99 ± 0.01
E-p-β-CD_2az/PAAC12	K_{11}	75.7 ± 31.7	-33.6 ± 1.1	-50.5 ± 13.1	-16.9 ± 5.0	-
	K_{12}	7.1 ± 0.7	-27.7 ± 0.3	-23.0 ± 1.2	4.65 ± 0.29	-
E/Z-m-β-CD_2az/PAAC12	K_{11}	196 ± 1	-35.9 ± 1.4	-64.4 ± 8.4	-28.5 ± 4.8	-
	K_{12}	10.6 ± 1.0	-28.7 ± 0.2	-40.3 ± 1.2	-11.7 ± 0.6	-

[a]Errors given as fitting errors from ITC fitting program. [b]Errors calculated using the errors in K_{xy} and the equation $\Delta G_{xy} = -RT\ln K_{xy}$. [c]Errors are the sum of the relative errors in ΔG and ΔH. The errors are rounded up to the last significant figure. The errors do not take into account experimental estimated to be ≤ 5% for K_{11}.and ≤ 10% for K_{21}.

The reliability of the derived complexation constants and thermodynamic parameters was assessed by considering the *c* value for each system. The *c* values for monophasic isotherms were calculated using Equation 5.4. While *c* values are a useful measure for monophasic isotherms, it is not suitable for biphasic systems as there are overlapping heat release profiles. Thus, *c* values were not

calculated for the *E*-*p*-β-CD_2az/PAAADddn, *E/Z*-*m*-β-CD_2az/PAAADddn, *E*-*p*-β-CD_2az/PAAC12 and *E/Z*-*m*-β-CD_2az/PAAC12 systems. The calculated *c* values appear in Table 5.2.

Table 5.2: The *c* value derived for the 1:1 complexation between the hydrophobic-substitutients of PAAADen, PAAADhn, PAAADddn and PAAC12 by β-CD, β-CDab, *E*-*p*-β-CD_2az and *E/Z*-*m*-β-CD_2az in aqueous phosphate buffer (pH 7.0, I = 0.10 mol dm^{-3}) at 298.2 K as derived from ITC measurements. The *c* values for the *E*-*p*-β-CD_2az/PAAADddn, *E/Z*-*m*-β-CD_2az/PAAADddn, *E*-*p*-β-CD_2az/PAAC12 and *E/Z*-*m*-β-CD_2az/PAAC12 systems have been omitted as the associated isotherms are biphasic.

System	*c* value
β-CD/PAAADen	10.9
β-CDab/PAAADen	11.8
E-*p*-β-CD_2az/PAAADen	15.7
E/Z-*m*-β-CD_2az/PAAADen	44.9
β-CD/PAAADhn	18.4
β-CDab/PAAADhn	19.5
E-*p*-β-CD_2az/PAAADhn	54.6
E/Z-*m*-β-CD_2az/PAAADhn	94.5
β-CD/PAAADddn	6.55
β-CDab/PAAADddn	5.13
E-*p*-β-CD_2az/PAAADddn	-
E/Z-*m*-β-CD_2az/PAAADddn	-
β-CD/PAAC12	6.03
β-CDab/PAAC12	2.01
E-*p*-β-CD_2az/PAAC12	-
E/Z-*m*-β-CD_2az/PAAC12	-

An ITC experiment that has a *c* value between 10 – 500 is generally considered to produce reliable complexation constants and thermodynamic parameters, while experiments with *c* values < 10 are more likely to generate erroneous results.[35] A *c* value of <10 generally corresponds to an isotherm with an incomplete sigmoidal curve.

However, low affinity systems characterised by low *c* values may be accurately studied given known concentrations of species, known stoichiometries, a low noise level and a sufficient portion of the isotherm is used for fitting. Therefore, a system characterised by a low *c* value may be considered valid at the discretion of the experimenter.[35]

All systems comprising PAAADen (Figure 5.25 – Figure 5.28) and PAAADhn (Figure 5.29 – Figure 5.32) had *c* values within the range of 10.9 – 94.5. Only the β-CD/PAAADddn (Figure 5.33), β-CDab/PAAADddn (Figure 5.34), β-CD/PAAC12 (Figure 5.37) and β-CDab/PAAC12 (Figure 5.38) systems produced *c* values < 10. However, in these cases, the concentrations of the hydrophobic

substituents and β-CD compounds were well known, the level of noise was low and the complete isotherm was used for fitting. The equilibrium was also well known as both β-CD and β-CDab are only capable of complexing a single AD moiety or alkyl tether of the modified PAA. Therefore, despite the low *c* values, the results derived for these low affinity system are considered reliable.

As *c* values may not be used to assess the reliability of biphasic isotherms, the overall shape of the isotherms must be taken into account. The biphasic isotherms of the *E*-*p*-β-CD_2az/PAAADddn (Figure 5.35), *E/Z*-*m*-β-CD_2az/PAAADddn (Figure 5.36), *E*-*p*-β-CD_2az/PAAC12 (Figure 5.39) and *E/Z*-*m*-β-CD_2az/PAAC12 (Figure 5.40) systems correspond to two equilibria (Equation 5.5 – 5.8). However, complete sigmoidal curves for both equilibria were not observed in any biphasic system. Thus, the complexation constants and thermodynamic parameters derived are subject to significant errors. Significant fitting errors were observed for the *E/Z*-*m*-β-CD_2az/PAAADddn and *E*-*p*-β-CD_2az/PAAC12 systems.

The error in the K_{11} and K_{12} for the *E/Z*-*m*-β-CD_2az/PAAADddn system is 42.6% and 40.2%, respectively, while the error in the K_{11} for the *E*-*p*-β-CD_2az/PAAC12 system is 41.8%. Thus, while the K_{11} and K_{12} equilibria of the *E/Z*-*m*-β-CD_2az/PAAADddn and *E*-*p*-β-CD_2az/PAAC12 systems are likely to exist, the magnitude of the equilibrium constants is unreliable. The thermodynamic parameters derived from these systems are also erroneous, with errors ranging from 29.6% to 55.0%.

The high errors are likely to arise from the smaller number of data points characterising the K_{11} and K_{12} equilibria in biphasic isotherms by comparison with monophasic isotherms. In principle, the fitting error may be reduced by increasing the number of experimental data points. However, increasing the number of data points to improve the resolution of the sigmoidal isotherm requires a decrease in the titrant volume. This would cause a decrease in the heat change of the system, thus increasing the level of noise.[35] This may be compensated by increasing the concentration of both the modified PAA and the β-CD host. However, the concentrations of PAAADddn and PAAC12 in the *E/Z*-*m*-β-CD_2az/PAAADddn and *E*-*p*-β-CD_2az/PAAC12 systems, respectively, were deliberately low to discourage the formation of inter-strand cross-links. Thus, increasing the concentration of either PAAADddn and PAAC12 would encourage polymeric network formation and incur further inaccuracies as to the type of complexation mode being either intra-strand or inter-strand.

While the complexation constants and thermodynamic parameters for the *E/Z-m*-β-CD_2az/PAAADddn and *E-p*-β-CD_2az/PAAC12 systems produced significant errors, the biphasic isotherms that characterised both systems (Figure 5.36 and Figure 5.39, respectively) indicate the presence of both 1:1 and 1:2 complexes. Thus, while it may not be appropriate to compare the magnitude of the complexation constants and thermodynamic parameters of these systems, the prevalence of K_{11} and K_{12} equilibria can be discussed, albeit carefully.

5.2.2.2.6 Complexation of PAAADen by β-CD, β-CDab, *E-p*-β-CD_2az and *E/Z-m*-β-CD_2az

The complexation of PAAADen by β-CD and β-CDab produced monophasic isotherms (Figure 5.25 and Figure 5.26, respectively) and therefore, 1:1 complexes are expected to dominate in solution. This corresponds to the structure of the hosts as both β-CD and β-CDab may only complex a single AD moiety. The likely equilibrium characterising the formation of the β-CD·ADen and β-CDab·ADen complexes are shown in Figure 5.41.

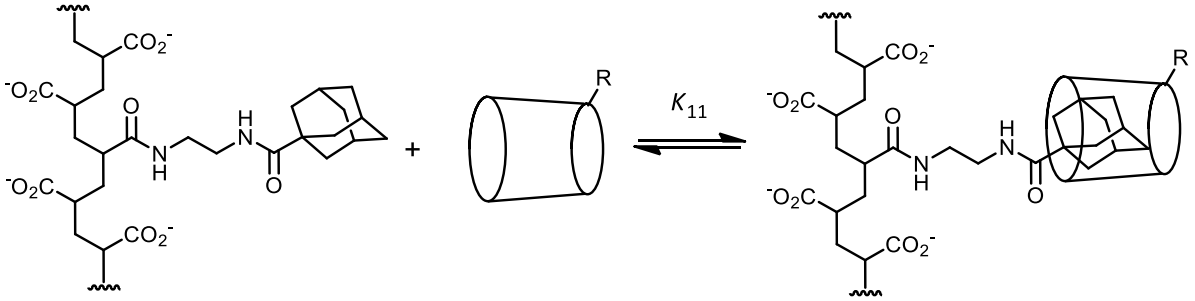

Figure 5.41: Equilibrium characterising the 1:1 complexation of PAAADen by β-CD and β-CDab. The R group refers to the hydroxy and aminophenyl substituents of β-CD and β-CDab, respectively.

As a dominant 1:1 complex is expected for both β-CD/PAAADen and β-CDab/PAAADen systems, the expected *N* value is 1. However, the *N* values of the β-CD·ADen and β-CDab·ADen complexes are 0.73 and 0.93, respectively. The deviation from unity may be due to the unfavourable steric interactions between the complexed β-CD and the polymer backbone.[14,15] Additionally, there may be some competition from the hydrophobic association between AD groups of adjacent polymer strands. However, given the dilute concentrations used, hydrophobic association is unlikely to be a significant factor. As the *N* value of the β-CDab·ADen complex is closer to 1 than the β-CD·ADen complex, the effect of the unfavourable steric interactions between the host and polymer backbone is diminished by the aminophenyl substituent of β-CDab. The strength of the unfavourable steric interaction between the host and polymer backbone may be overcome by favourable hydrogen-bonding interactions between the carboxylate group of PAAADen and the amino group on the aminophenyl substituent of β-CDab.

The effect of the aminophenyl substituent of β-CDab is also reflected in the K_{11} value of the β-CDab·ADen complex, which is 2.6 times larger than the K_{11} for the β-CD·ADen complex, indicating some extra stability, possibly from hydrogen-bonding interactions between the amino group of β-CDab and the carboxylate groups of the polymer backbone. However, the ΔH_{11} and $T\Delta S_{11}$ of the two complexes are similar and therefore, the thermodynamic controls of the system are largely independent of the aminophenyl substituent of β-CDab.

By contrast to the two β-CD monomers, the complexation of PAAADen by *E-p*-βCD_2az and *E/Z-m*-βCD_2az is expected to result in both 1:1 and 1:2 complexes forming. Each β-CD dimer possess two β-CD groups, thus enabling the formation of 1:2 host-guest complexes. Under the relatively dilute conditions used in the ITC experiments, the 1:2 host-guest complexes would form intra-strand cross-links.[37]

A dominant 1:2 complex would expectedly produce a biphasic isotherm, however, both the *E-p*-β-CD_2az/PAAADen and *E/Z-m*-β-CD_2az/PAAADen systems are monophasic (Figure 5.27 and Figure 5.28, respectively), suggesting a dominant 1:1 complex. However, the K_{11} of the *E-p*-β-CD_2az·PAAADen and *E/Z-m*-β-CD_2az·ADen complexes are four and nine times greater than the K_{11} of the β-CD·ADen complex and therefore, additional 1:2 complexes are likely. This is also supported by the thermodynamic parameters.

The ΔH_{11} of the *E-p*-β-CD_2az·ADen and *E/Z-m*-β-CD_2az·ADen complexes are -41.1 kJ mol^{-1} and -59.1 kJ mol^{-1}, respectively, substantially more negative than the ΔH_{11} of the β-CD·ADen complex, which is -25.4 kJ mol^{-1}. The $T\Delta S_{11}$ of the *E-p*-β-CD_2az·ADen and *E/Z-m*-β-CD_2az·ADen complexes are -13.8 kJ mol^{-1} and -28.7 kJ mol^{-1}, which is substantially more negative than the $T\Delta S_{11}$ of the β-CD·ADen complex, which is -1.50 kJ mol^{-1}. The difference suggests that the *E-p*-β-CD_2az/PAAADen and *E/Z-m*-β-CD_2az/PAAADen systems comprise additional 1:2 intra-strand cross-links. Therefore, the monophasic isotherms of the *E-p*-β-CD_2az/PAAADen and *E/Z-m*-β-CD_2az/PAAADen systems indicate that the first and second equilibria exhibit identical or similar heat profiles and complexation modes. Thus, the monophasic isotherm can be characterised by an initial complexation of one AD substituent of PAAADen by one β-CD group of either *E-p*-β-CD_2az or *E/Z-m*-β-CD_2az, followed by the rapid and sequential complexation of a second AD substituent by the second β-CD group of the dimer to yield a single *K*, analogous to the complexation between a multi-dentate ligand and a metal ion.[15] The likely equilibria characterising the formation of 1:1 and 1:2 complexes of the *E-p*-βCD_2az/PAAADen and *E/Z-m*-βCD_2az/PAAADen systems are shown in Figure 5.42.

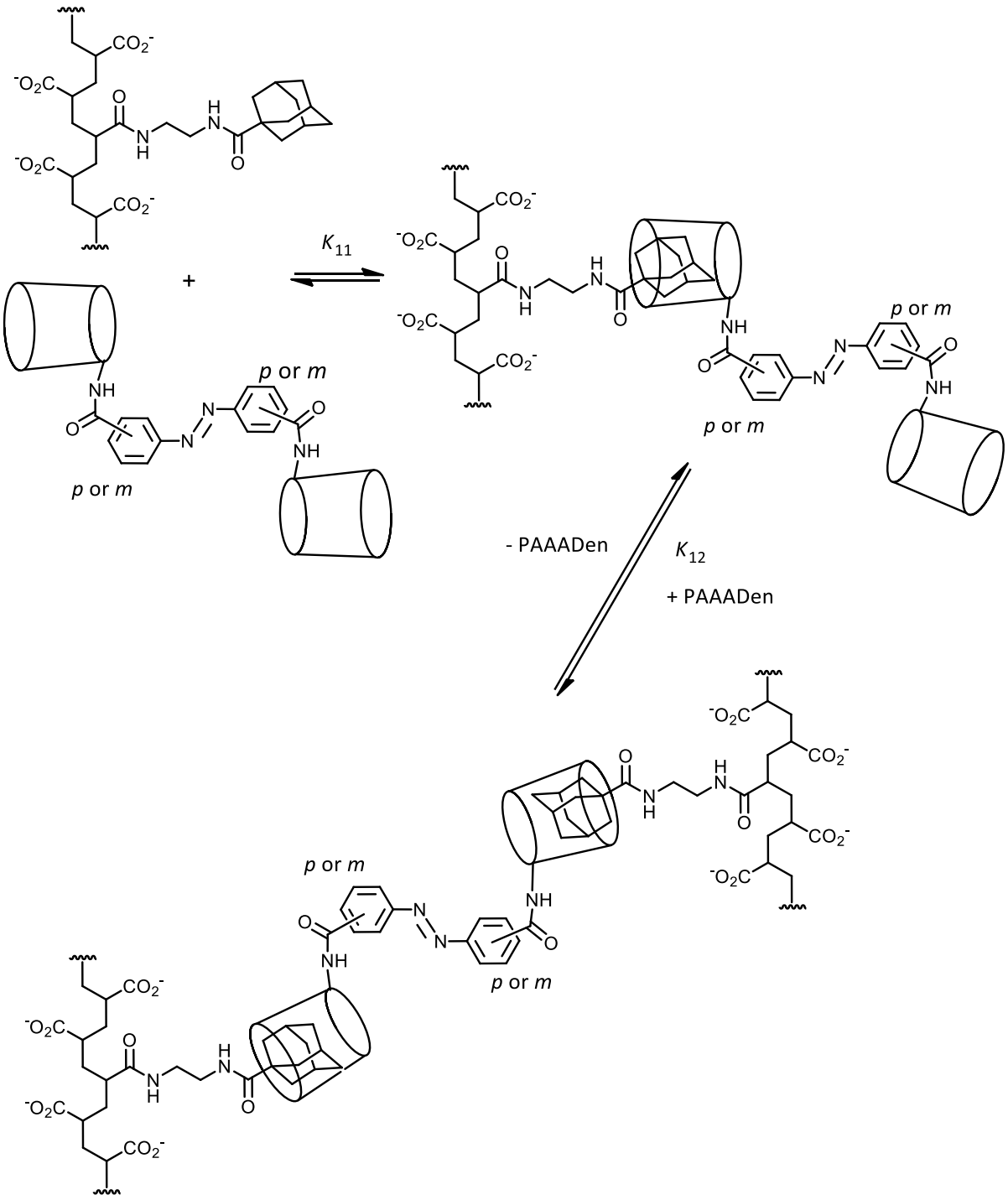

Figure 5.42: Equilibria characterising the 1:1 and 1:2 complexation of PAAADen by *E*-*p*-β-CD_2az and *E*-*m*-β-CD_2az. The complexation by *Z*-*m*-β-CD_2az is expected to occur similarly.

The effect of structural isomerisation on the complexation properties may be determined by comparing the *N*, K_{11}, ΔH_{11} and $T\Delta S_{11}$ between the *E*-*p*-β-CD_2az·ADen and *E/Z*-*m*-β-CD_2az·ADen complexes. The K_{11} of the *E/Z*-*m*-β-CD_2az·ADen complex is twice that of the *E*-*p*-β-CD_2az·ADen complex. The ΔH_{11} and $T\Delta S_{11}$ of the *E/Z*-*m*-β-CD_2az·ADen complex are also more negative than the *E*-

p-β-CD_2az·ADen complex, while the *N* value of the *E/Z-m*-β-CD_2az·ADen complex is closer to 0.5 Thus, *E/Z-m*-β-CD_2az forms stronger 1:2 intra-strand cross-links than *E-p*-β-CD_2az.

Given that *E/Z-m*-β-CD_2az consists of both the *E* and *Z* isomers and the K_{11} is a weighted average of both isomers, the stronger 1:2 intra-strand cross-links may be due to either the effect of structural isomerisation or photoisomerisation. However, as the complexation of PAAADen by *E/Z-m*-β-CD_2az produced a monophasic isotherm, it is reasonable to suggest that *E-m*-β-CD_2az and *Z-m*-β-CD_2az have similar complexation properties corresponding to similar K_{11} values. Therefore, the difference in K_{11} and thermodynamic parameters between the *E/Z-m*-β-CD_2az·ADen and *E-p*-β-CD_2az·ADen complexes are likely due to the effect of structural isomerisation. The shorter azobenzene-linker of *E/Z-m*-β-CD_2az may reduce the flexibility of the 1:2 intra-strand cross-link, corresponding to a more stable complex.

The differences between the magnitude of the K_{11} of the *E/Z-m*-β-CD_2az·ADen complex and K_{11} of the *E-p*-β-CD_2az·ADen complex may also be due to the effect of β-CD dimer aggregation. During the ITC experiment, it was noted that the titration of *E-p*-β-CD_2az into the solution containing PAAADen produced some heat output, which correlated to the presence of *E-p*-β-CD_2az aggregates. It is possible that this extra competing interaction may diminish the strength of a *E-p*-β-CD_2az·ADen complex. The aggregation of *E/Z-m*-β-CD_2az was not observed during this experiment.

5.2.2.2.7 Complexation of PAAADhn by β-CD, β-CDab, *E-p*-β-CD_2az and *E/Z-m*-β-CD_2az

The complexation of PAAADhn by β-CD and β-CDab produced monophasic isotherms (Figure 5.29 and Figure 5.30, respectively). The *N* and K_{11} values for the β-CD·ADhn and β-CDab·ADhn complexes are similar to their analogous PAAADen complexes and therefore, both are characterised by a dominant 1:1 monotopic complex. Due to the *N* values of the β-CD·ADhn and β-CDab·ADhn complexes being less than 1, there are some unfavourable steric interactions between the polymeric backbone and complexed β-CD.[14,15]

The length of the tether appears to be suitably long to facilitate the complexation of β-CD through both the AD and alkyl groups of PAAADhn. However, the thermodynamic parameters indicate that complexation via the AD group of PAAADhn is dominant. The ΔH_{11} value of the β-CD·ADhn and β-CDab·ADhn complexes are similar to their analogous PAAADen systems. As complexation may only occur through the AD groups of PAAADen, the similar ΔH_{11} values indicate similar complexation modes. The likely equilibria characterising the formation of the β-CD·ADhn and β-CDab·ADhn complexes are shown in Figure 5.43.

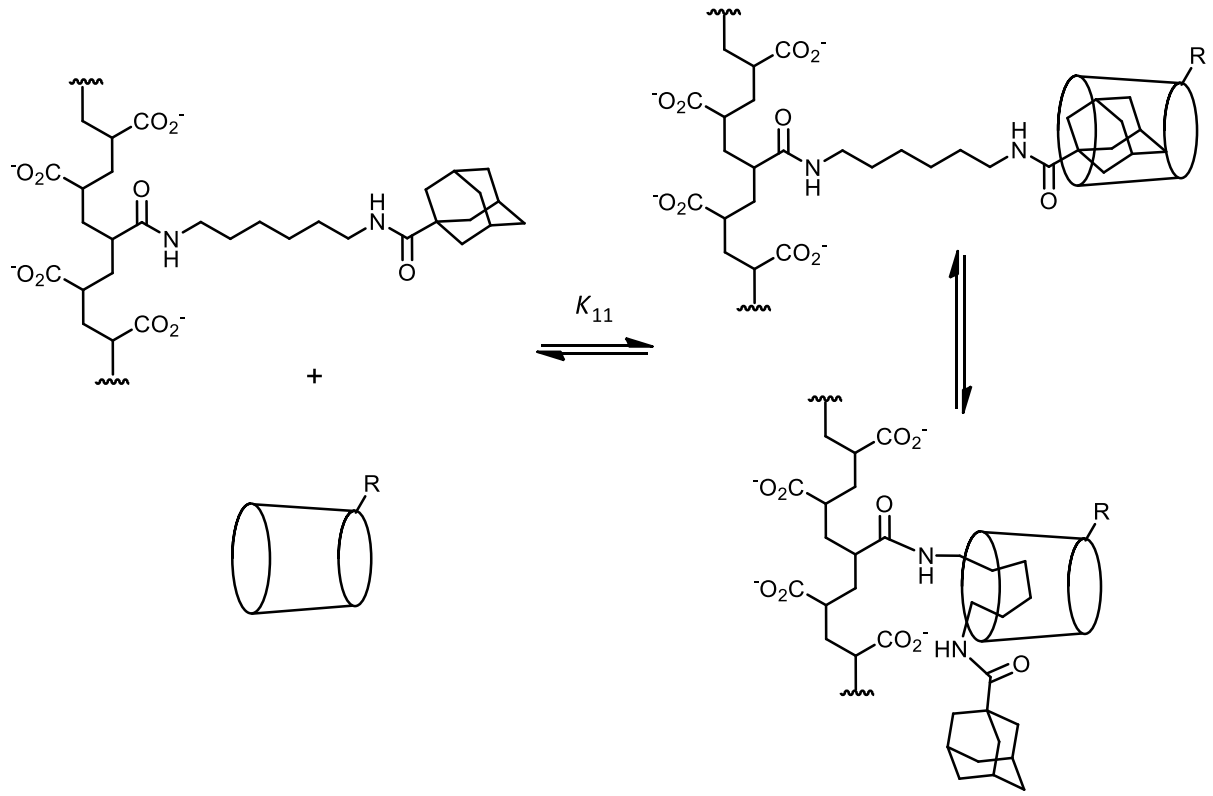

Figure 5.43: Equilibrium characterising the 1:1 complexation of PAAADhn by β-CD and β-CDab. The R group refers to the hydroxy and aminophenyl substituents of β-CD and β-CDab, respectively.

The complexation of PAAADhn by *E-p*-β-CD_2az and *E/Z-m*-β-CD_2az produced monophasic isotherms (Figure 5.31 and Figure 5.32, respectively), similar to the analogous PAAADen systems. The *N* values for the *E-p*-β-CD_2az/ADhn and *E/Z-m*-β-CD_2az/ADhn systems are 0.62 and 0.42, respectively and therefore, both 1:1 and 1:2 complexes exist in solution. As both isotherms are monophasic, the 1:1 and 1:2 complexes have similar complexation modes. The complexation process can therefore be characterised by the initial complexation of one AD substituent of one β-CD group of either *E-p*-β-CD_2az or *E/Z-m*-β-CD_2az, followed by the rapid and sequential complexation of a second AD substituent on an adjacent polymer strand by the second β-CD group of the dimer.

As with the β-CD·ADhn and β-CDab·ADhn complexes, the 1:1 *E/Z-m*-β-CD_2az·ADhn and *E-p*-β-CD_2az·ADhn complexes are dominated by interactions between the β-CD hosts and the AD group of PAAADhn, although complexation through the alkyl group may be possible. This is supported by the thermodynamic parameters which shows that the ΔH_{11} of the *E-p*-β-CD_2az·ADhn complex is identical to the *E-p*-β-CD_2az·ADen complex, while the ΔH_{11} of the *E/Z-m*-β-CD_2az·ADhn is only slightly more positive than the ΔH_{11} for the *E/Z-m*-β-CD_2az·ADen complex. The likely equilibria characterising the complexation of PAAADhn by *E-p*-β-CD_2az and *E/Z-m*-β-CD_2az is given in Figure 5.44.

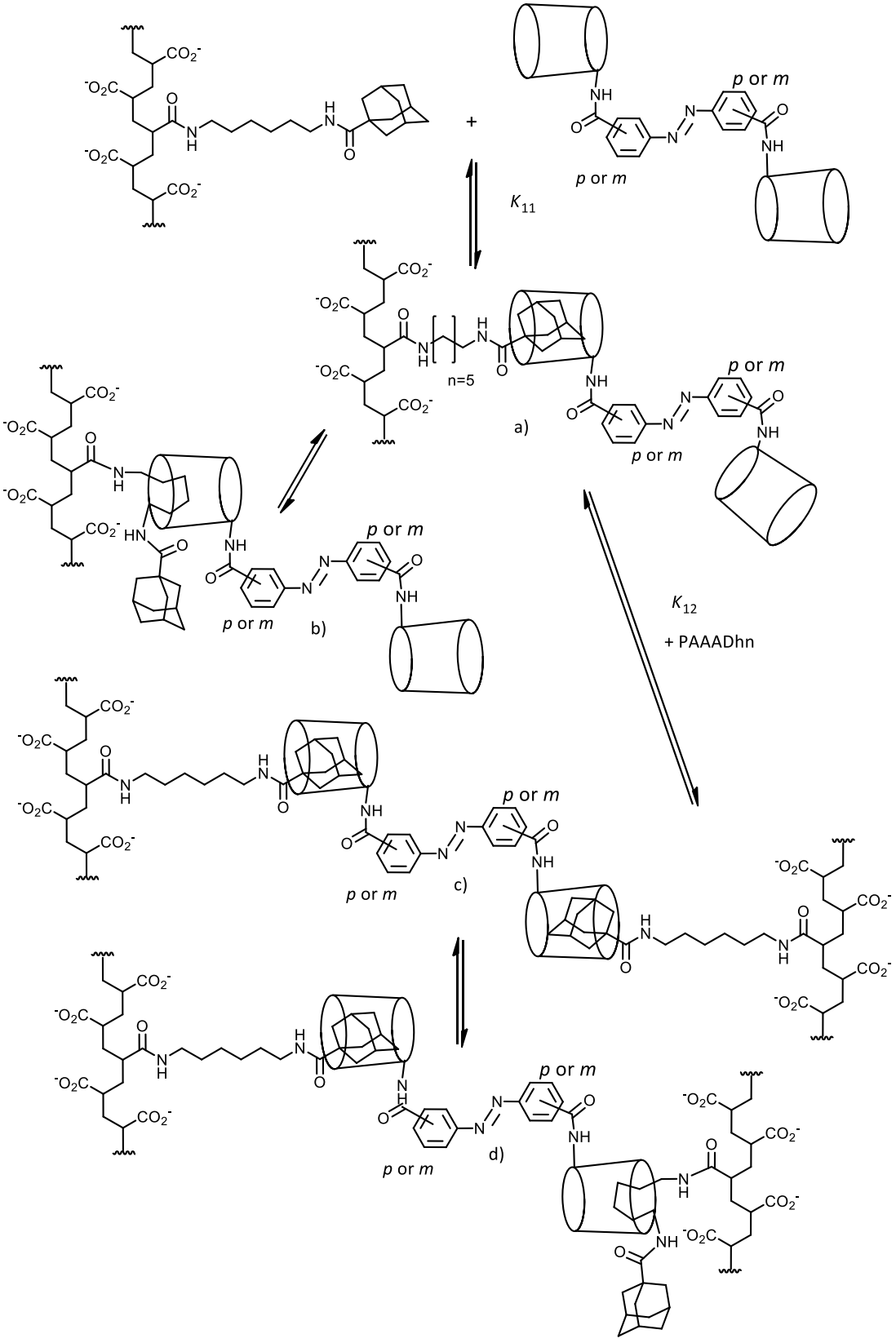

Figure 5.44: Equilibria characterising the 1:1 and 1:2 complexation of PAAADhn by *E*-*p*-β-CD_2az and *E*-*m*-β-CD_2az. The β-CD dimers may form a) 1:1 complex through the AD group, b) 1:1 complex through the alkyl group, c) 1:2 cross-link between the AD groups on adjacent polymer strands and d) 1:2 cross-link between the AD and alkyl groups of adjacent polymer strands. The complexation by *Z*-*m*-β-CD_2az is expected to occur similarly.

The K_{11} of the *E*-*p*-β-CD_2az·ADhn and *E/Z*-*m*-β-CD_2az·ADhn complexes are nine and thirteen times greater than the K_{11} for the β-CD·ADhn complex. The length of the tether of PAAADhn is too short to facilitate cooperative complexation and therefore, the increase in K_{11} is due to the enhanced probability of collision from having two β-CD groups within a dimer, as well as the formation of 1:2 cross-links. The longer tether length of PAAADhn may also reduce steric interaction between the complexed β-CD and the polymeric backbone, further increasing the strength of the complex. This is reflected in the $T\Delta S_{11}$ in all PAAADhn systems, which are more positive than their analogous PAAADen systems.

The K_{11} of the *E/Z*-*m*-β-CD_2az·ADhn complex is greater than the K_{11} of the *E*-*p*-β-CD_2az·ADhn, similar to the analogous PAAADen systems. The difference is due to the effect of structural isomerisation. The *E/Z*-*m*-β-CD_2az/PAAADhn and *E*-*p*-β-CD_2az/PAAADhn systems comprise additional 1:2 intra-strand cross-links. The shorter azobenzene-linker of *E/Z*-*m*-β-CD_2az reduces the flexibility of the 1:2 complex, increasing the complex stability.

5.2.2.2.8 Complexation of PAAADddn by β-CD, β-CDab, *E*-*p*-β-CD_2az and *E/Z*-*m*-β-CD_2az

The isotherms for the complexation of PAAADddn by native β-CD and β-CDab are monophasic (Figure 5.33 and Figure 5.34, respectively), indicating a dominant 1:1 complex, similar to the analogous PAAADen and PAAADhn systems. Due to the long length of the dodecyl tether of PAAADddn, the β-CD hosts may complex through the AD or alkyl groups. However, the similarity in the ΔH_{11} of the β-CD·ADddn and β-CDab·ADddn complexes and their analogous PAAADen complexes indicates that complexation through the AD groups are favoured. The likely equilibria characterising the complexation of PAAADddn by β-CD and β-CDab is given in Figure 5.45.

The K_{11} values for the β-CD·ADddn and β-CDab·ADddn complexes are similar and therefore, the aminophenyl substituent of β-CDab does not significantly alter the strength of the complex. However, the thermodynamic parameters differ. The $T\Delta S_{11}$ of the β-CDab·ADddn complex is more than four times negative than the $T\Delta S_{11}$ of the β-CD·ADddn complex. It is probable that there are some unfavourable steric interactions occurring between the uncomplexed alkyl tether and the aminophenyl substituent of the complexed β-CDab.

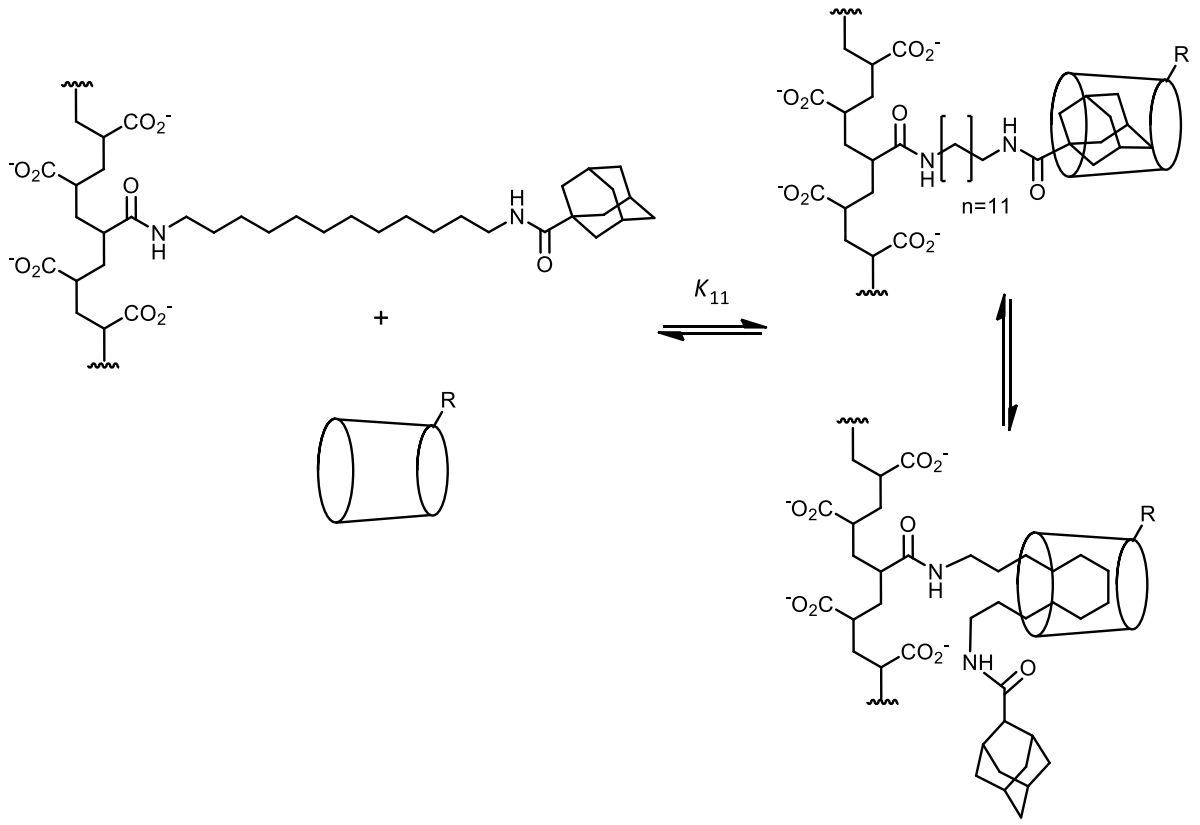

Figure 5.45: Equilibrium characterising the 1:1 complexation of PAAADddn by β-CD and β-CDab. The R group refers to the hydroxy and aminophenyl substituents of β-CD and β-CDab, respectively.

The complexation of PAAADddn by *E-p*-β-CD_2az and *E/Z-m*-β-CD_2az are in stark contrast to the analogous PAAADen and PAAADhn systems. Both *E-p*-β-CD_2az/PAAADddn and *E/Z-m*-β-CD_2az/PAAADddn systems produced biphasic isotherms (Figure 5.35 and Figure 5.36, respectively), yielding distinct K_{11} and K_{12} values corresponding to Equation 5.5 and Equation 5.7, respectively. During the experiment, the first sigmoidal change in the heat release profile corresponds to the K_{12} equilibrium as the host:AD ratio is low. As the host:AD ratio increases, the prevalence of the K_{11} equilibrium increases.[38]

The appearance of a biphasic isotherm suggests that the first and second complexation equilibria exhibit very different complexation modes and heat release profiles. The longer dodecyl tether of PAAADddn facilitates the cooperative complexation of both the AD and alkyl groups of PAAADddn by both β-CD groups of either *E-p*-β-CD_2az or *E/Z-m*-β-CD_2az. The K_{12} equilibrium would therefore be substantially different, as each β-CD group non-cooperatively complexes AD substituents on adjacent polymer strands.[24] The likely equilibria characterising the complexation of PAAADdn by *E-p*-β-CD_2az and *E/Z-m*-β-CD_2az are given in Figure 5.46.

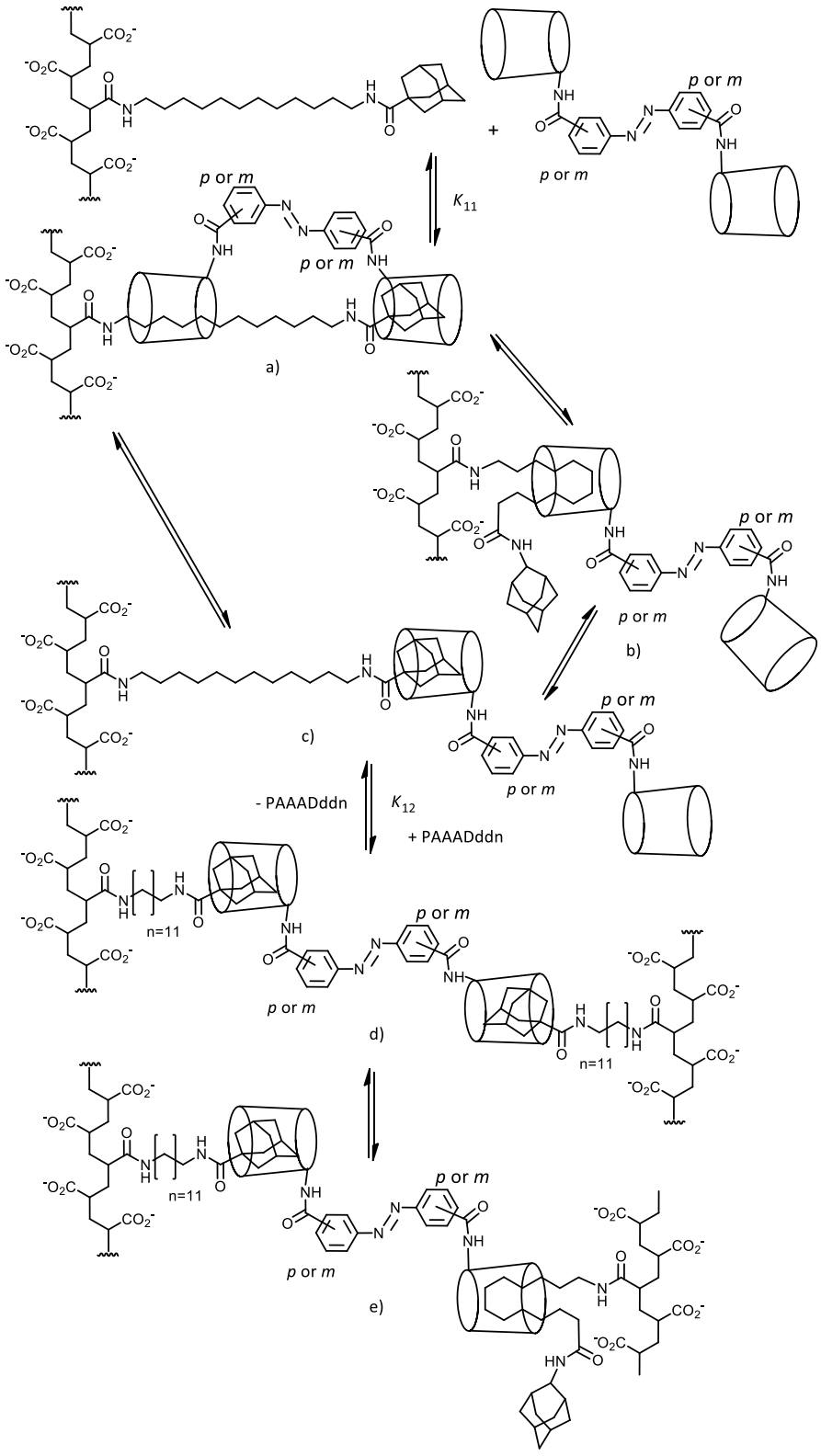

Figure 5.46: Equilibria characterising the 1:1 and 1:2 complexation of PAAADddn by *E*-*p*-β-CD_2az and *E*-*m*-β-CD_2az. The β-CD dimers may form either a) 1:1 cooperative complex, b) 1:1 non-cooperative complex through the alkyl group, c) 1:1 non-cooperative complex through the AD group, d) 1:2 cross-link between AD groups on adjacent polymer strands and e) 1:2 cross-link between the AD and alkyl groups of adjacent polymer strands. The complexation by *Z*-*m*-β-CD_2az is expected to occur similarly.

The formation of a 1:1 complex characterised by cooperative complexation is supported by the magnitude of K_{11}. The *E-p*-β-CD_2az·ADddn and *E/Z-m*-β-CD_2az·ADddn complexes have derived K_{11} values that are 46 and 430 times larger than the K_{11} for the β-CD·ADddn complex, respectively. While the K_{11} of the *E/Z-m*-β-CD_2az·ADddn complex has a 42% error, cooperative complexation is still expected due to the long dodecyl tether of PAAADddn. The thermodynamic parameters also support the formation of cooperative complexes, with both the ΔH_{11} and $T\Delta S_{11}$ of the *E-p*-β-CD_2az·ADddn and *E/Z-m*-βCD_2az·ADddn complexes being substantially more negative than the ΔH_{11} and $T\Delta S_{11}$ for the β-CD·ADddn complex. It must be reiterated that the analysis of the *E/Z-m*-β-CD_2az·ADddn complex is tentative as the ITC analysis produced high errors for the K_{11} and thermodynamic parameters of this system. Given the large error in the K_{11} of the *E/Z-m*-β-CD_2az·ADddn complex, it is not possible to compare the relative stability of the *E-p*-β-CD_2az·ADddn and *E/Z-m*-β-CD_2az·ADddn complexes.

The K_{12} values of the *E-p*-β-CD_2az·$(ADddn)_2$ and *E/Z-m*-β-CD_2az·$(ADddn)_2$ complexes are significantly less than their K_{11} values, which reflects the non-cooperative nature of the 1:2 complexes. This is also reflected in the thermodynamic terms, which show a more positive $T\Delta S_{12}$ and ΔH_{12} values, by comparison with the positive $T\Delta S_{11}$ and ΔH_{11}, respectively. The K_{12} of the *E/Z-m*-β-CD_2az·$(ADddn)_2$ complex has a 40% error and thus, analysis is tentative. However, we may expect that the shorter azobenzene length that connects the two β-CD groups of *E/Z-m*-β-CD_2az reduces the flexibility of the 1:2 intra-strand cross-link. Thus, the K_{12} of the *E/Z-m*-β-CD_2az·$(ADddn)_2$ complex is expected to be greater than the K_{12} of the *E-p*-β-CD_2az·$(ADddn)_2$ complex.

5.2.2.2.9 Complexation of PAAC12 by β-CD, β-CDab, *E-p*-β-CD_2az and *E/Z-m*-β-CD_2az

The isotherms for the complexation of PAAC12 by native β-CD, β-CDab, *E-p*-β-CD_2az and *E/Z-m*-β-CD_2az are similar to the analogous PAAADddn systems. The β-CD/PAAC12 and β-CDab/PAAC12 systems yield monophasic isotherms (Figure 5.37 and Figure 5.38, respectively) characterised by *N* values of 0.99, indicative of a dominant 1:1 complex in solution. As the *N* value is close to the optimum value of 1, there are only minor competing interactions. Nguyen *et al.* previously reported that the dodecyl tethers of PAAC12 systems do not significantly aggregate.[39] The likely equilibria characterising the complexation of PAAC12 by β-CD and β-CDab is given in Figure 5.47.

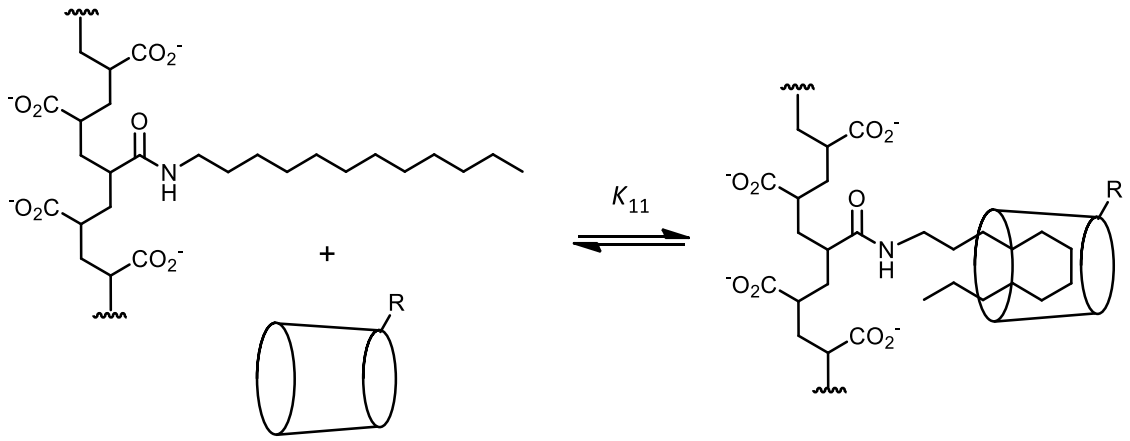

Figure 5.47: Equilibrium characterising the 1:1 complexation of PAAC12 by β-CD and β-CDab. The R group refers to the hydroxy and aminophenyl substituents of β-CD and β-CDab, respectively.

There is very little difference between the K_{11} of the β-CD·C12 and β-CDab·C12 complexes. However, the $T\Delta S_{11}$ of the β-CD·C12 complex is positive, while the $T\Delta S_{11}$ of the β-CDab·C12 complex is negative. It is probable that the aminophenyl substituent may interact with a portion of the uncomplexed C12 substituent, corresponding to a decrease in entropy.

Similar to the PAAADddn systems, the *E*-*p*-β-CD_2az/PAAC12 and *E*/*Z*-*m*-β-CD_2az/PAAC12 systems yield biphasic isotherms (Figure 5.39 and Figure 5.40, respectively). This suggests that both 1:1 and 1:2 complexes exist in equilibrium, exhibiting very different complexation modes. The 1:1 complexes likely exhibit cooperative complexation of two sites of the long dodecyl tether of PAAC12, while the 1:2 complexes are characterised by non-cooperative intra-strand cross-links. The likely equilibria characterising the complexation of PAAC12 by *E*-*p*-β-CD_2az and *E*/*Z*-*m*-β-CD_2az are given in Figure 5.48.

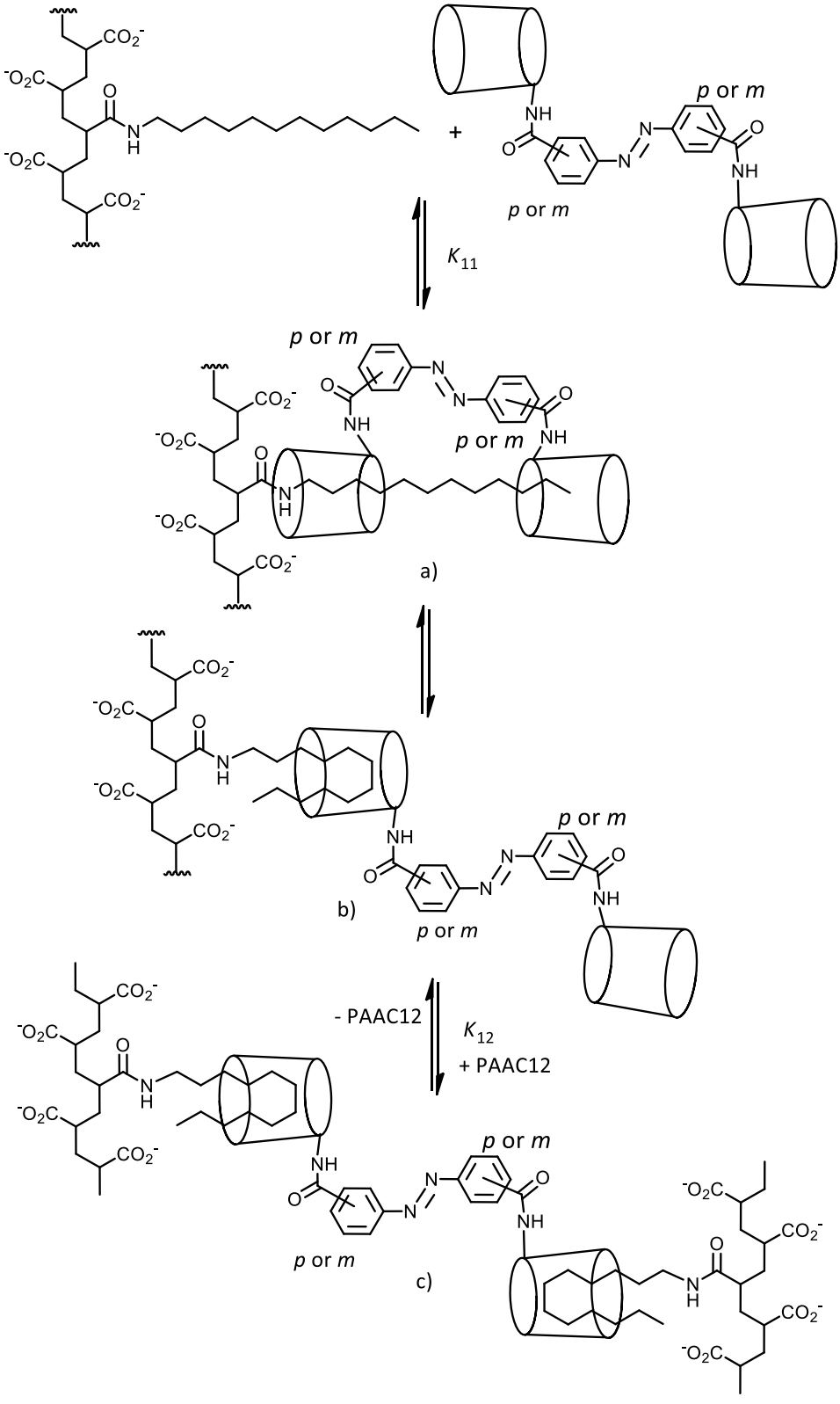

Figure 5.48: Equilibria characterising the 1:1 and 1:2 complexation of PAAC12 by *E*-*p*-β-CD_2az and *E/m*-β-CD_2az. The β-CD dimers may form a) 1:1 cooperative complex, b) 1:1 monotopic complex and c) 1:2 cross-link between dodecyl groups on adjacent polymer strands. The complexation by *Z*-*m*-β-CD_2az is expected to occur similarly.

The K_{11} of *E-p*-β-CD_2az·C12 and *E/Z-m*-β-CD_2az·C12 complexes are 72 and 188 times greater than the K_{11} of the β-CD·C12 complex, indicative of cooperative complexation. The K_{11} of the *E-p*-β-CD_2az·C12 has a 42% error, and thus, the analysis is only tentative. However, cooperative complexation is expected given the relatively long dodecyl substituent of PAAC12. Cooperative complexation is also reflected in the more negative ΔH_{11} and $T\Delta S_{11}$ values by comparison with the β-CD·C12 complex.

The K_{12} of the *E-p*-β-CD_2az·$(C12)_2$ and *E/Z-m*-β-CD_2az·$(C12)_2$ complexes are significantly less than the analogous K_{11}, due to the non-cooperative complexation of two adjacent C12 groups by two β-CD groups of the dimers. The non-cooperative nature of the 1:2 complex may also explain the increase in both ΔH_{12} and $T\Delta S_{12}$. The transition from cooperative complex to non-cooperative complex reintroduces flexibility to the C12 substituent, thereby increasing $T\Delta S_{12}$, while the disruption of a cooperative complex increases the ΔH_{12}.

The K_{12} of the *E/Z-m*-β-CD_2az·$(C12)_2$ complex is slightly greater than the K_{12} of the *E-p*-β-CD_2az·$(C12)_2$ complex. The enhanced stability of the *E/Z-m*-β-CD_2az·$(C12)_2$ may arise due to the shorter azobenzene length of *E/Z-m*-β-CD_2az. The shorter length would reduce the flexibility of an intra-strand cross-link, thus increasing the stability of the complex.

5.2.2.2.10 Enthalpy-entropy linear relationship

The change in enthalpy and entropy between each host-polymer system was characterised using the enthalpy-entropy linear relationship, given in Equation 5.10,

$$T\Delta S_{11} = \alpha\Delta H_{11} + T\Delta S_{11,0} \tag{5.10}$$

where α (the slope) quantifies the extent of entropic compensation caused by modifications to the host or guest and $T\Delta S_{11,0}$ (the intercept) represents the inherent complex stability (ΔG_{11}) when ΔH_{11} = 0. The α value can further be described in terms of ΔG_{11}, given in Equation 5.11, which describes the extent to which $\Delta\Delta H_{11}$ is compensated by $\Delta\Delta S_{11}$ in terms of the α value to contribute to the overall ΔG_{11}. It should be noted that Equation 5.10 and Equation 5.11 do not represent a necessary relationship, but is one observed for a variety of equilibria involving CDs.

$$\Delta G = (1 - \alpha)\Delta\Delta H_{11} \tag{5.11}$$

The enthalpy-entropy linear relationship for the complexation of PAAADen, PAAADhn, PAAADddn and PAAC12 by β-CD, β-CDab, *E-p*-β-CD_2az and *E/Z-m*-β-CD_2az is given in Figure 5.49. The entropy and enthalpy of complexation for the systems in this study were also compared against literature values,[40-42] as shown in Figure 5.50.

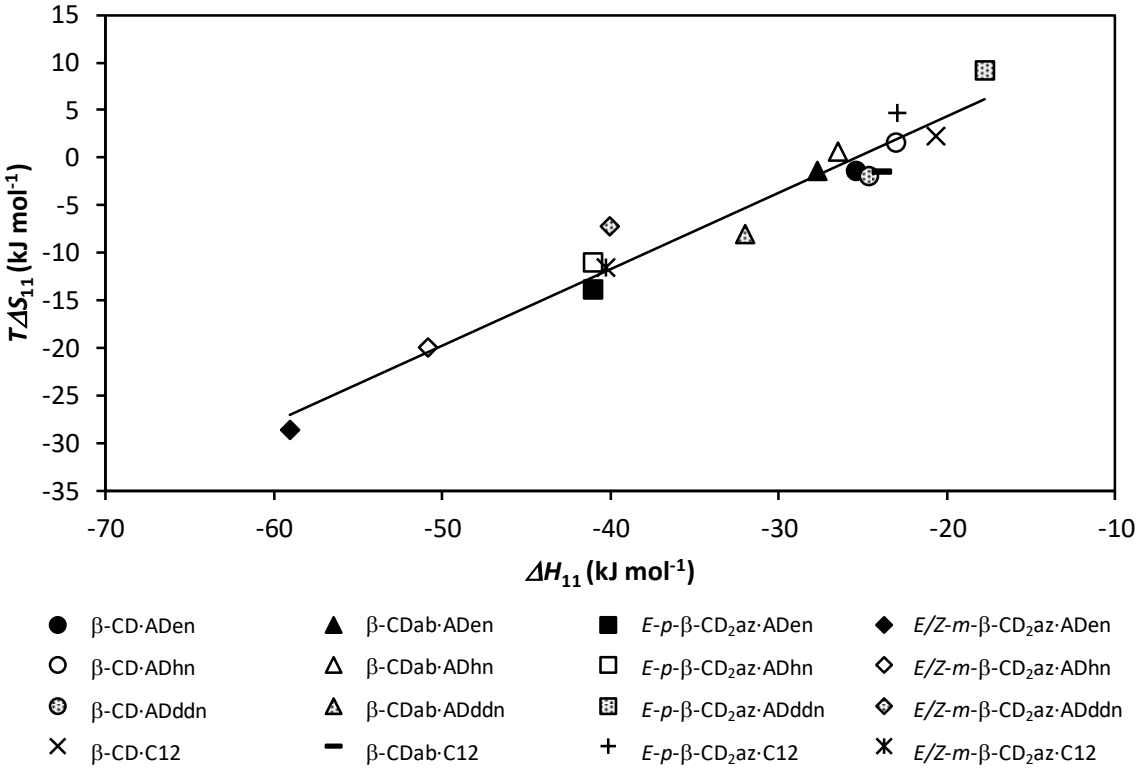

Figure 5.49: Linear relationship between ΔH_{11} and $T\Delta S_{11}$ for the 1:1 complexation of of PAAADen, PAAADhn, PAAADddn and PAAC12 by β-CD, β-CDab, *E*-*p*-β-CD$_2$az and *E*/*Z*-*m*-β-CD$_2$az in aqueous phosphate buffer (pH 7.0 and I = 0.10 mol dm^{-3}) at 298.2 K (R^2 = 0.949). The icons represent the experimental data and the solid lines represent the best fit of Equation 5.10 to the thermodynamic parameters, derived using the *Graphpad Prism* protocol.[47] The R^2 value refers to the fit of Equation 5.10 to the data.

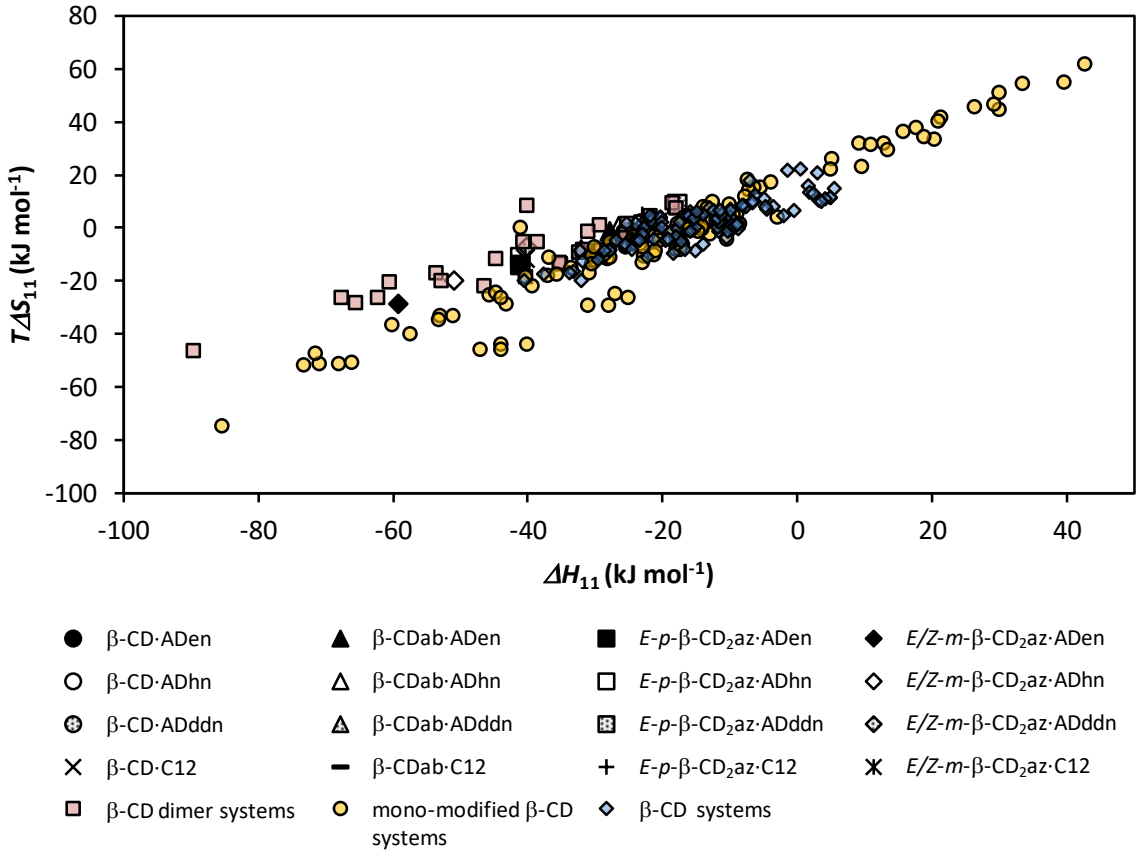

Figure 5.50: Linear relationship between ΔH_{11} and $T\Delta S_{11}$ for the 1:1 complexation of various guests by native and modified β-CDs at 298 K obtained from the literature, along with the systems in this study.[40-42]

The enthalpy-entropy linear relationship for the β-CD compounds in this study generated a $T\Delta S_0$ value of 23.0 kJ mol^{-1}, indicating entropic stabilisation in the absence of any enthalpic change. This may arise from the expulsion of water molecules from the β-CD cavity upon complexation.[40] The α value of 0.80 indicates that approximately 80% of the $\Delta\Delta H_{11}$ is compensated by the $\Delta\Delta S_{11}$. This value is identical to the α value for host-guest systems characterised by β-CD alone.[40] Therefore, most of the thermodynamic parameters that govern the complexation of the modified PAAs by the β-CD compounds may be explained by the properties of β-CD itself, rather than modifications to β-CD, or experimental differences.[14,15]

The polymer does not appear to significantly influence the complexation thermodynamics. We may have expected the freedom of motion of the polymeric backbone to be restricted upon complexation of the hydrophobic moieties by the β-CD cavity, especially upon the formation of intra-strand crosslinks. However, the polymers have a low percentage substitution of the hydrophobic groups and thus, the backbone is flexible enough to allow for freedom of motion upon complexation.

5.2.3 Macroscopic properties studies

The macroscopic properties of solutions containing of PAAADen, PAAADhn, PAAADddn and PAAC12 alone and with β-CD, β-CDab, *E*-*p*-β-CD_2az and *E/Z*-*m*-β-CD_2az were studied by rheology to determine the solution viscosity. The high concentration solutions required for rheological measurements favour the formation of 3D polymeric networks, which occur due to the inter-strand cross-linking of polymer strands.

5.2.3.1 Rheological Studies

The viscosities of solutions containing PAAADen, PAAADhn, PAAADddn and PAAC12 alone and with native β-CD, *E*-*p*-β-CD_2az, *E/Z*-*m*-β-CD_2az and β-CDab were studied by rheology. The rheologicaly determined visocities provide insight into the extent to which inter-strand cross-linking occurs between AD- or alkyl-substituted PAA strands in the presence of β-CD hosts. Therefore, the viscosities of 5.3 wt% solutions of PAAADen, PAAADhn, PAAADddn and PAAC12 alone and in the presence of β-CD, *E*-*p*-β-CD_2az, *E/Z*-*m*-β-CD_2az and β-CDab were determined over a shear-rate range to give extrapolated zero-shear viscosities.

The viscosities were measured using a Physica MCR 501 (Anton Par GmbH) stress-controlled rheometer with a 25 mm cone and plate geometry, using a Peltier plate temperature controller set to 298.2 ± 0.1 K. Measurements were performed using 5.3 wt% solution of PAAADen ([ADen] = 0.010 mol dm^{-3}), PAAADhn ([ADhn] = 0.014 mol dm^{-3}), PAAADddn ([ADddn] = 0.011 mol dm^{-3}) and PAAC12 ([C12] = 0.010 mol dm^{-3}) alone and with native β-CD (0.016 mol dm^{-3}), *E*-*p*-β-CD_2az (0.007 mol dm^{-3}), *E/Z*-*m*-β-CD_2az (0.007 mol dm^{-3}) and β-CDab (0.014 mol dm^{-3}) in 0.10 mol dm^{-3} aqueous NaCl solution, adjusted to pH 7.0 using 0.10 mol dm^{-3} aqueous NaOH solution. Solutions containing *E*-*p*-βCD_2az and *E/Z*-*m*-βCD_2az were also irradiated at 300 – 355 nm for 12 hours prior to experimentation to determine the influence of photoisomerisation on the rheological properties. The rheological experiments were performed by Wang Meng Xue at East China University of Science and Technology, under the supervision of Professor Xuhong Guo.

The variation in the viscosities of each solution with shear rates for PAAADen, PAAADhn, PAAADddn and PAAC12 alone and in combination with β-CD, *E*-*p*-β-CD_2az, *E/Z*-*m*-β-CD_2az and β-CDab are shown in Figure 5.51 – Figure 5.54. The zero-shear viscosities of each solution (in the absence of irradiation), corresponding to the viscosities extrapolated from those observed at the lowest shear rates, are given in Figure 5.55. The extrapolated zero-shear viscosities of irradiated solutions are compared against the parent solutions in Figure 5.56. The values for the extrapolated zero-shear viscosities for all systems are given in Table 5.3.

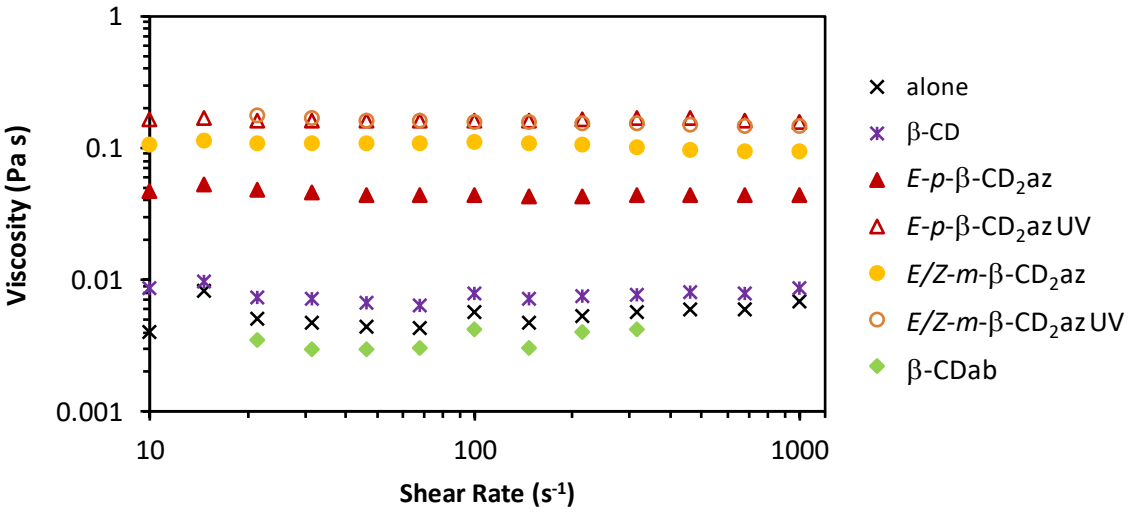

Figure 5.51: Viscosity variations with shear rate of 5.3 wt% PAAADen ([ADen] = 0.010 mol dm^{-3}) alone and with β-CD (0.016 mol dm^{-3}), *E-p*-β-CD_2az (0.007 mol dm^{-3}), *E/Z-m*-β-CD_2az (0.007 mol dm^{-3}) and β-CDab (0.014 mol dm^{-3}) in 0.10 mol dm^{-3} aqueous NaCl solution (pH = 7.0) at 298.2 K. Solutions containing *E-p*-β-CD_2az and *E/Z-m*-β-CD_2az were also irradiated at 300 – 355 nm for 12 hours prior to experimentation.

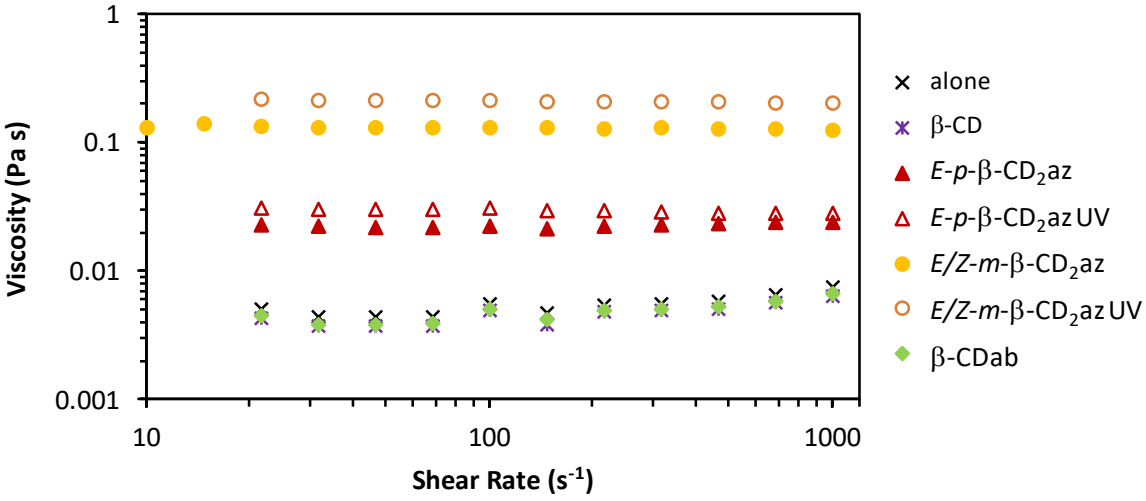

Figure 5.52: Viscosity variations with shear rate of 5.3 wt% PAAADhn ([ADhn] = 0.014 mol dm^{-3}) alone and with β-CD (0.016 mol dm^{-3}), *E-p*-β-CD_2az (0.007 mol dm^{-3}), *E/Z-m*-β-CD_2az (0.007 mol dm^{-3}) and β-CDab (0.014 mol dm^{-3}) in 0.10 mol dm^{-3} aqueous NaCl solution (pH = 7.0) at 298.2 K. Solutions containing *E-p*-β-CD_2az and *E/Z-m*-β-CD_2az were also irradiated at 300 – 355 nm for 12 hours prior to experimentation.

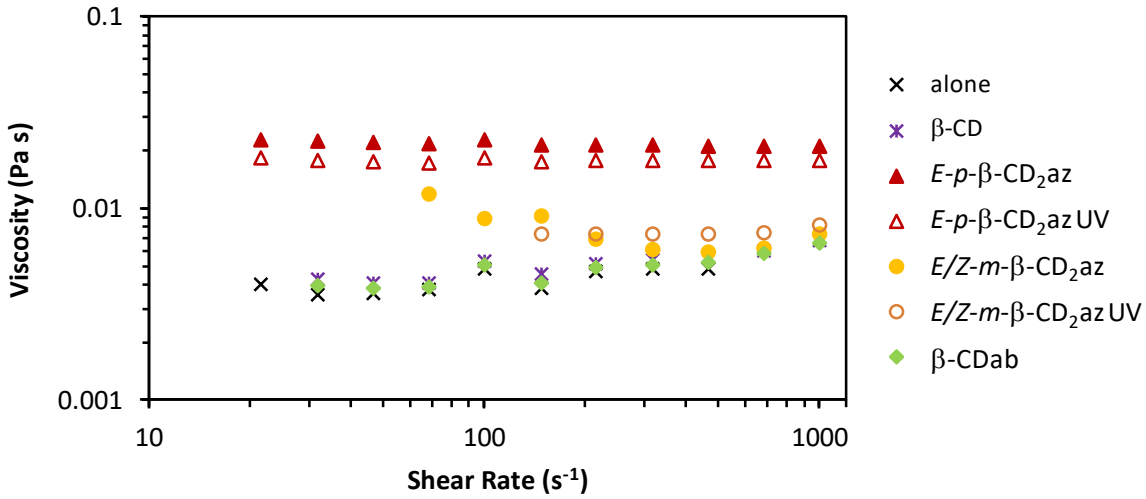

Figure 5.53: Viscosity variations with shear rate of 5.3 wt% PAAADddn ([ADddn] = 0.011 mol dm^{-3}) alone and with β-CD (0.016 mol dm^{-3}), *E-p*-β-CD_2az (0.007 mol dm^{-3}), *E/Z-m*-β-CD_2az (0.007 mol dm^{-3}) and β-CDab (0.014 mol dm^{-3}) in 0.10 mol dm^{-3} aqueous NaCl solution (pH = 7.0) at 298.2 K. Solutions containing *E-p*-β-CD_2az and *E/Z-m*-β-CD_2az were also irradiated at 300 – 355 nm for 12 hours prior to experimentation.

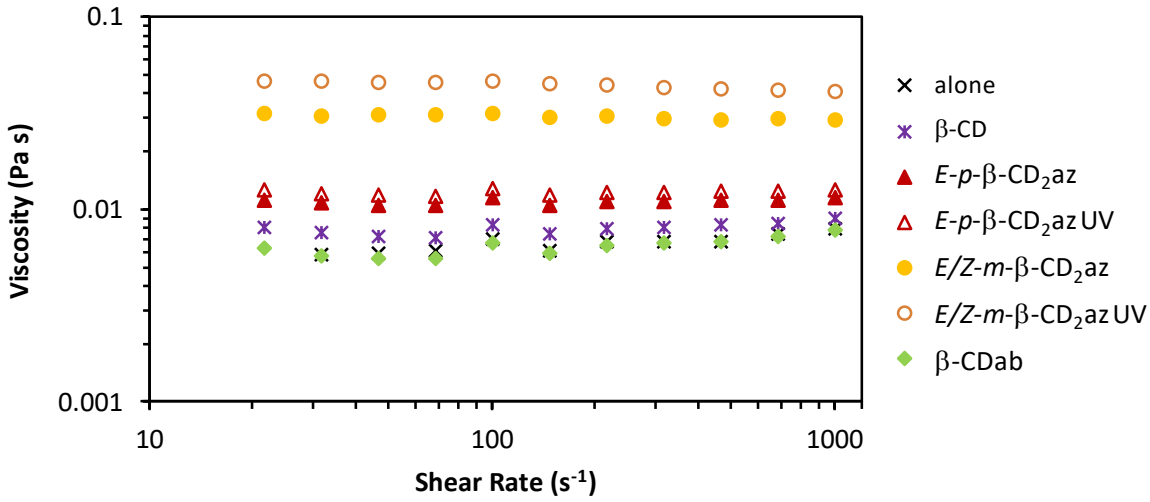

Figure 5.54: Viscosity variations with shear rate of 5.3 wt% PAAC12 ([C12] = 0.010 mol dm^{-3}) alone and with β-CD (0.016 mol dm^{-3}), *E-p*-β-CD_2az (0.007 mol dm^{-3}), *E/Z-m*-β-CD_2az (0.007 mol dm^{-3}) and β-CDab (0.014 mol dm^{-3}) in 0.10 mol dm^{-3} aqueous NaCl solution (pH = 7.0) at 298.2 K. Solutions containing *E-p*-β-CD_2az and *E/Z-m*-β-CD_2az were also irradiated at 300 – 355 nm for 12 hours prior to experimentation.

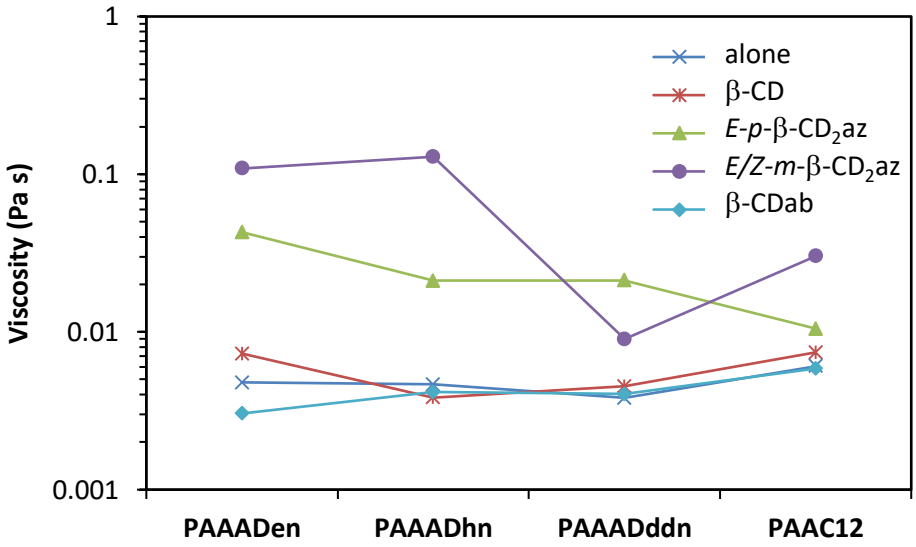

Figure 5.55: Variations of zero-shear viscosities of 5.3 wt% PAAADen ([ADen] = 0.010 mol dm^{-3}), PAAADhn ([ADhn] = 0.014 mol dm^{-3}), PAAADddn ([ADddn] = 0.011 mol dm^{-3}) and PAAC12 ([C12] = 0.010 mol dm^{-3}) alone and with β-CD (0.016 mol dm^{-3}), *E-p*-β-CD_2az (0.007 mol dm^{-3}), *E/Z-m*-β-CD_2az (0.007 mol dm^{-3}) and β-CDab (0.014 mol dm^{-3}) in 0.10 mol dm^{-3} aqueous NaCl solution (pH = 7.0) at 298.2 K.

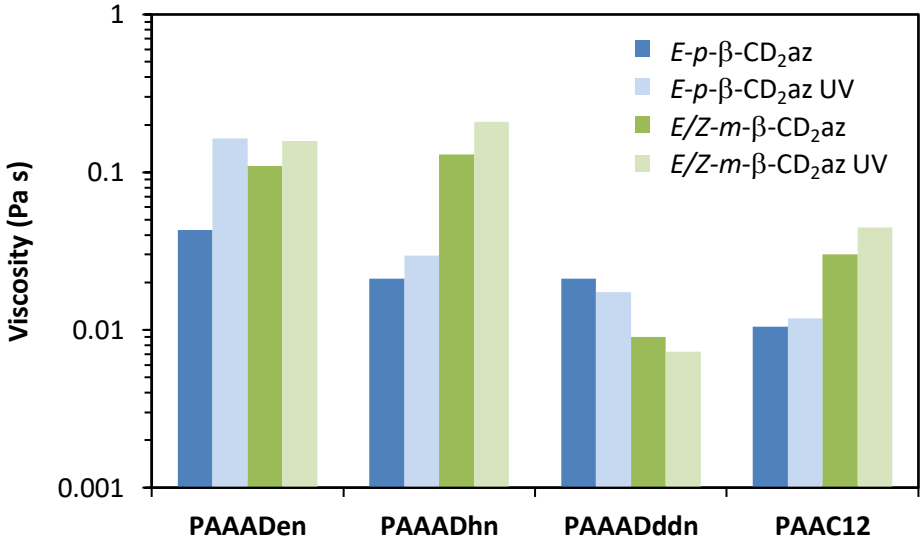

Figure 5.56: Variations of zero-shear viscosities of 5.3 wt% PAAADen ([ADen] = 0.010 mol dm^{-3}), PAAADhn ([ADhn] = 0.014 mol dm^{-3}), PAAADddn ([ADddn] = 0.011 mol dm^{-3}) and PAAC12 ([C12] = 0.010 mol dm^{-3}) and with *E-p*-β-CD_2az (0.007 mol dm^{-3}) and *E/Z-m*-β-CD_2az (0.007 mol dm^{-3}) in 0.10 mol dm^{-3} aqueous NaCl solution (pH = 7.0) at 298.2 K, before and after irradiation at 300 – 355 nm.

Table 5.3: Zero-shear viscosities (× 10^{-3} Pa s) of 5.3 wt% PAAADen ([ADen] = 0.010 mol dm^{-3}), PAAADhn ([ADhn] = 0.014 mol dm^{-3}), PAAADddn ([ADddn] = 0.011 mol dm^{-3}) and PAAC12 ([C12] = 0.010 mol dm^{-3}) alone and with *E*-*p*-β-CD_2az (0.007 mol dm^{-3}) and *E/Z*-*m*-β-CD_2az (0.007 mol dm^{-3}) in 0.10 mol dm^{-3} aqueous NaCl solution (pH = 7.0) at 298.2 K. The zero-shear viscosities of solutions containing *E*-*p*-β-CD_2az or *E/Z*-*m*-β-CD_2az were also measured following irradiation at 300 – 355 nm. The experimental error associated with the measurements is estimated to be 5%.

Polymer / Host	PAAADen	PAAADhn	PAAADddn	PAAC12
alone	4.08 ± 0.02	4.67 ± 0.23	4.00 ± 0.20	5.63 ± 0.28
β-CD	13.3 ± 0.7	4.13 ± 0.21	4.03 ± 0.20	7.56 ± 0.38
β-CDab	3.32 ± 0.16	4.20 ± 0.21	3.66 ± 0.18	6.21 ± 0.31
***E*-*p*-β-CD_2az**	56.8 ± 2.8	24.8 ± 1.2	22.8 ± 1.1	10.7 ± 0.54
***E*-*p*-β-CD_2az UV**	163 ± 8	30.4 ± 1.5	17.8 ± 0.9	12.1 ± 0.61
***E/Z*-*m*-β-CD_2az**	110 ± 6	142 ± 7	9.45 ± 0.47	30.8 ± 1.5
***E/Z*-*m*-β-CD_2az UV**	178 ± 9	216 ± 11	7.04 ± 0.35	44.9 ± 2.2

The zero shear viscosities range from 3.32 × 10^{-3} Pa s for a solution of 5.3 wt% of PAAADen in the presence of β-CDab to 0.216 Pa s for 5.3 wt% of PAAADhn in the presence of *E/Z*-*m*-β-CD_2az and irradiated at 300 – 355 nm, a 67-fold range. The solution viscosities are influenced by the competition between 1:1 monofunctional complexes, 1:2 intra-strand cross-links and 1:2 inter-strand cross-links. The solution viscosities derived from rheology may be compared with the complexation constants from the ITC studies to investigate the influence of molecular scale properties of the solutions on the bulk material properties. However, as the solutions used for rheology are relatively concentrated (5.3 wt%) by comparison with the solutions used for ITC studies (0.12 – 0.35 wt%), there will be greater competition between the 1:2 intra- and inter-strand cross-links. The variation in solution viscosities with shear rate is first discussed, followed by the variation in zero-shear viscosities of non-irradiated and irradiated solutions.

5.2.3.1.1 Variation in the solution viscosities with shear-rate

There is little variation in the solution viscosities with shear-rate of the modified PAAs alone and with the addition of native β-CD, β-CDab, *E*-*p*-β-CD_2az or *E/Z*-*m*-β-CD_2az. However, the *E/Z*-*m*-β-CD_2az/PAAADddn system (Figure 5.53) showed some shear thinning. An increase in the shear-rate corresponds to an extension of the polymer strands. Correspondingly, the cooperative complexation of the AD substituent and dodecyl tether of PAAADddn by both β-CD groups of *E/Z*-*m*-β-CD_2az may be favoured with increased shear-rate. Thus, a decrease in the proportion of inter-strand cross-links is observed, along with a decrease in the solution viscosity. This scenario may not occur for the *E*-*p*-β-CD_2az/PAAADddn system as the length of the azobenzene linker of *E*-*p*-β-CD_2az is longer and may diminish strength of the cooperative complex.

5.2.3.1.2 Variation in the zero-shear viscosities

The addition of either β-CD or β-CDab to solutions of the modified PAAs did not significantly change the solution viscosities. It was expected that the addition of β-CD or β-CDab would cause a decrease in the solution viscosity as a result of the disruption of hydrophobic association between AD or alkyl substituents of PAAADen, PAAADhn, PAAADddn and PAAC12. Thus, the lack of solution viscosity change indicates that the AD and alkyl substituents of the modified PAAs do not exhibit significant hydrophobic association.

The addition of either *E-p*-β-CD_2az or *E/Z-m*-β-CD_2az to solutions of the modified PAAs resulted in an increase in solution viscosities. The solution viscosities range from 1.07×10^{-2} Pa s for the *E-p*-β-CD_2az/PAAC12 system to 0.142 Pa s for the *E/Z-m*-β-CD_2az/PAAADhn. The increase in solution viscosities correspond to the formation of 1:2 inter-strand complexes. Generally, solutions containing *E/Z-m*-β-CD_2az produced larger viscosities than solutions with *E-p*-β-CD_2az (Figure 5.56). The larger viscosities of the *E/Z-m*-β-CD_2az solutions may be a result of the shorter azobenzene linker, which would reduce the flexibility of the 1:2 inter-strand cross-links.

The relative solution viscosities of the modified PAAs with either *E-p*-β-CD_2az or *E/Z-m*-β-CD_2az generally correlated with the relative magnitudes in K_{11} observed for the complexes in dilute solutions (from ITC studies), with the exception of PAAADddn systems. The K_{11} of the *E/Z-m*-β-CD_2az·ADen, *E/Z-m*-β-CD_2az·ADhn, and *E/Z-m*-β-CD_2az·C12 complexes are 2.2, 1.5 and 2.6 times larger than the analogous K_{11} of the *E-p*-β-CD_2az complexes. The zero-shear viscosities of the *E/Z-m*-β-CD_2az/PAAADen, *E/Z-m*-β-CD_2az/PAAADhn and *E/Z-m*-β-CD_2az/PAAC12 systems are 1.9, 5.7 and 2.9 times larger than the analogous systems involving *E-p*-β-CD_2az. Therefore, the stereochemical factors that control the molecular-scale complexation properties influence the macroscopic rheological properties to a similar extent. However, given the differences in solution concentration in the ITC studies (0.12 – 0.35 wt%) by comparison with the rheological studies (5.3 wt%), some additional stereochemical factors must be considered.

The ITC studies revealed that *E-p*-β-CD_2az has a tendency to aggregate in solution, which, in solutions containing modified PAAs, would compete with the formation of 1:1 and 1:2 complexes. This competition would be greater in the more concentrated solutions used for rheology. Thus, solutions containing the modified PAAs and *E-p*-β-CD_2az would have a decreased proportion of 1:2 cross-links by comparison with solutions containing *E/Z-m*-β-CD_2az, resulting in a lower viscosity.

The trends in solution viscosity do not hold for the PAAADddn systems. The K_{11} of the *E/Z-m*-β-CD_2az·ADddn complex is 9.2 times greater than the K_{11} for the *E-p*-β-CD_2az·ADddn complex. Thus we would expect that the viscosity of the *E/Z-m*-β-CD_2az/PAAADddn solution to be greater than the *E-p*-

β-CD_2az/PAAADddn solution. However, the viscosity of the *E-p*-β-CD_2az/PAAADddn solution is 2.4 times greater than the *E/Z-m*-β-CD_2az/PAAADddn solution. This may be explained by the balance between the 1:1 and 1:2 complexes. The large K_{11} of the *E/Z-m*-β-CD_2az·PAAADddn complex is characterised by cooperative complexation of the AD and alkyl substituents of PAAADddn. The high stability of this 1:1 cooperative complex may disfavor the formation of 1:2 complexes, thus reducing the number of inter-strand cross-links, correlating to a lower than expected solution viscosity. It must be reiterated that this analysis is tentative, due to the high errors associated with the ITC data for the *E/Z-m*-β-CD_2az/PAAADddn system.

5.2.3.1.3 Variation in zero-shear viscosities of irradiated solutions

The viscosities of solutions comprising either *E-p*-β-CD_2az or *E/Z-m*-β-CD_2az did not significantly change upon irradiation at 300 – 355 nm, although a general trend has emerged. Generally, irradiation caused a slight increase in solution viscosity of between 1.1 – 2.9 times. The change in solution viscosities of irradiated systems is due to the change in *E*:*Z* isomer ratio of *E-p*-β-CD_2az and *E/Z-m*-β-CD_2az. The proportion of *Z-p*-β-CD_2az and *Z-m*-β-CD_2az increase from 5% to 20% and 24% to 61% upon irradiation at 300 – 355 nm, respectively. The effective length of the azobenzene linker of the *Z* isomers is shorter than the *E* isomers. Thus, irradiation causes a decrease in the flexibility of 1:2 inter-strand cross-links and an increase in the solution viscosity.

However, this explanation does not apply for the *E/Z-m*-β-CD_2az/PAAADddn and *E-p*-β-CD_2az/PAAADddn systems, which show a decrease in solution viscosity upon irradiation. This implies that there is a greater proportion of 1:1 complexes. Thus, the *Z* isomers of *E/Z-m*-β-CD_2az and *E-p*-β-CD_2az preference the cooperative complexation of the AD and alkyl substituents of PAAADddn. The length of the *Z*-azobenzene linker is likely to be comparable to the length of the tether of PAAADddn, thus increasing the strength of 1:1 cooperative complexes.

Although the solutions studied did not yield viscosities high enough to form a hydrogel, the study does indicate that molecular-scale properties of the solutions influence the macroscopic properties. In this study, the distance between the two β-CD groups of the dimers influences the formation of inter-strand cross-links. By altering the length and rigidity of the spacer/linker, the flexibility of the inter-strand cross-link can be changed, which influences the solution viscosity. This may be achieved by structural isomerisation or photoisomerisation. This could be the key to controlling the formation of AD and alkyl substituted PAA hydrogels with β-CD dimers.

5.3 Conclusions

The difference in the complexation and macroscopic properties of solutions containing PAAADen, PAAADhn, PAAADddn and PAAC12 with either native β-CD, *E-p*-β-CD_2az, *E/Z-m*-β-CD_2az and β-CDab were studied. The complexation properties between the modified PAAs and β-CD compounds were determined by 2D ^{1}H NOESY NMR spectroscopy and ITC and the macroscopic properties were studied by rheology.

2D ^{1}H NOESY NMR spectroscopy indicated successful complexation between the AD or alkyl substituents of modified PAAs and the β-CD groups of native β-CD, *E-p*-β-CD_2az, *E/Z-m*-β-CD_2az and β-CDab, while ITC determined the complexation constants and thermodynamic parameters of complexation. Native β-CD and β-CDab were characterised by 1:1 monofunctional complexes in all systems, while the dimers were characterised by a mixture of 1:1 monofunctional complexes and 1:2 intra-strand crosslinks. Generally, the complexation by *E/Z-m*-β-CD_2az was stronger than the complexation by *E-p*-β-CD_2az. The shorter-azobenzene linker of *E/Z-m*-β-CD_2az reduces the flexibility of a complex, particularly 1:2 complexes, enhancing the stability.

Rheological experiments provided insight into the solution viscosities. Generally, the solution viscosities correlated with the complexation constants derived from ITC studies. Solutions comprising *E-p*-β-CD_2az and *E/Z-m*-β-CD_2az with the modified PAAs showed higher viscosities by comparison with solutions of the modified PAAs alone or with β-CD/β-CDab due to the formation of inter-strand cross-links. Solutions containing *E/Z-m*-β-CD_2az generally gave the highest solution viscosities due to the shorter azobenzene length connecting the two β-CD groups, which reduce the flexibility of the inter-strand cross-links.

This explanation also applies to the observation that the irradiation of solutions containing *E-p*-β-CD_2az and *E/Z-m*-β-CD_2az generally increased the solution viscosities. Irradiation causes an increase in the proportion of the *Z* isomer, reducing the effective length of the azobenzene linker that connects the two β-CD groups. The shorter azobenzene linker reduces the flexibility of the 1:2 inter-strand cross-links, thus increasing the solution viscosity. Therefore, both structural isomerisation and photoisomerisation influences the rheological properties.

Importantly, this research demonstrates that the molecular-scale properties of polymer solutions with β-CD hosts influence the bulk-material properties. Thus, the design of β-CD linked polymer hydrogels with specific, intended macroscopic properties should take into account the structure and properties of the individual molecular constituents.

5.4 References

(1) Hoffman, A. S. *Adv. Drug Delivery Rev.* **2002**, *54*, 3.
(2) Hoare, T. R.; Kohane, D. S. *Polymer* **2008**, *49*, 1993.
(3) Sangeetha, N. M.; Maitra, U. *Chem. Soc. Rev.* **2005**, *34*, 821.
(4) Appel, E. A.; del Barrio, J.; Loh, X. J.; Scherman, O. A. *Chem. Soc. Rev.* **2012**, *41*, 6195.
(5) Loethen, S.; Kim, J.-M.; Thompson, D. H. *Polym. Rev.* **2007**, *47*, 383.
(6) Kopecek, J. *Biomaterials* **2007**, *28*, 5185.
(7) Lee, K. Y.; Mooney, D. J. *Chem. Rev.* **2001**, *101*, 1869.
(8) Li, J. *NPG Asia Mater.* **2010**, *2*, 112.
(9) van de Manakker, F.; Vermonden, T.; van Nostrum, C. F.; Hennink, W. E. *Biomacromolecules* **2009**, *10*, 3157.
(10) Tan, S.; Ladewig, K.; Fu, Q.; Blencowe, A.; Qiao, G. G. *Macromol. Rapid Commun.* **2014**, *35*, 1166.
(11) Guan, Y.; Zhao, H.-B.; Yu, L.-X.; Chen, S.-C.; Wang, Y.-Z. *RSC Adv.* **2014**, *4*, 4955.
(12) Kretschmann, O.; Choi, S. W.; Miyauchi, M.; Tomatsu, I.; Harada, A.; Ritter, H. *Angew. Chem.* **2006**, *45*, 4361.
(13) Lecourt, T.; Bleriot, Y.; Auzely-Velty, R.; Sollogoub, M. *Chem. Commun.* **2010**, *46*, 2238.
(14) Guo, X. H.; Wang, J.; Li, L.; Pham, D. T.; Clements, P.; Lincoln, S. F.; May, B. L.; Chen, Q. C.; Zheng, L.; Prud'homme, R. K. *J. Polym. Sci. Part B Polym. Phys.* **2010**, *48*, 1818.
(15) Hanh-Trang, N.; Duc-Truc, P.; Lincoln, S. F.; Wang, J.; Guo, X.; Easton, C. J.; Prud'homme, R. K. *Polym. Chem.* **2013**, *4*, 820.
(16) Guo, X.; Abdala, A. A.; May, B. L.; Lincoln, S. F.; Khan, S. A.; Prud'homme, R. K. *Polymer* **2006**, *47*, 2976.
(17) Guo, X. H.; Wang, J.; Li, L.; Chen, Q. C.; Zheng, L.; Pham, D. T.; Lincoln, S. F.; May, B. L.; Prud'homme, R. K.; Easton, C. J. *AIChE J.* **2010**, *56*, 3021.
(18) Li, L.; Guo, X.; Fu, L.; Prud'homme, R. K.; Lincoln, S. F. *Langmuir* **2008**, *24*, 8290.
(19) Li, L.; Guo, X.; Wang, J.; Liu, P.; Prud'homme, R. K.; May, B. L.; Lincoln, S. F. *Macromolecules* **2008**, *41*, 8677.
(20) Guo, X. H.; Wang, J.; Li, L.; Pham, D. T.; Clements, P.; Lincoln, S. F.; May, B. L.; Chen, Q. C.; Zheng, L.; Prud'homme, R. K. *Macromol. Rapid Commun.* **2010**, *31*, 300.
(21) Wang, J.; Li, L.; Guo, X.; Zheng, L.; Pham, D.-T.; Lincoln, S. F.; Ngo, H. T.; Clements, P.; May, B. L.; Prud'homme, R. K.; Easton, C. J. *Ind. Eng. Chem. Res.* **2011**, *50*, 7566.
(22) Tomatsu, I.; Peng, K.; Kros, A. *Adv. Drug Delivery Rev.* **2011**, *63*, 1257.
(23) Wang, J.; Main, D. T.; Guo, X. H.; Li, L.; Lincoln, S. F.; Luo, Z. F.; Ke, H. L.; Zheng, L.; Prud'homme, R. K. *Ind. Eng. Chem. Res.* **2010**, *49*, 609.
(24) Wang, J.; Xu, Y. S.; Wang, Y. M.; Liu, J. J.; Xu, J.; Li, L.; Nguyen, H. T.; Pham, D. T.; Lincoln, S. F.; Guo, X. H. *RSC Adv.* **2015**, *5*, 46067.
(25) Guo, X. H.; Abdala, A. A.; May, B. L.; Lincoln, S. F.; Khan, S. A.; Prud'homme, R. K. *Macromolecules* **2005**, *38*, 3037.
(26) Schneider, H. J.; Hacket, F.; Rudiger, V.; Ikeda, H. *Chem. Rev.* **1998**, *98*, 1755.
(27) Tosner, Z.; Aski, S. N.; Kowalewski, J. *J. Inclusion Phenom. Macrocyclic Chem.* **2006**, *55*, 59.
(28) Bouchemal, K.; Mazzaferro, S. *Drug Discovery Today* **2012**, *17*, 623.
(29) Chiad, K.; Stelzig, S. H.; Gropeanu, R.; Weil, T.; Klapper, M.; Muellen, K. *Macromolecules* **2009**, *42*, 7545.
(30) Bertaut, E.; Landy, D. *Beilstein J. Org. Chem.* **2014**, *10*, 2630.
(31) Wszelaka-Rylik, M.; Gierycz, P. *J. Therm. Anal. Calorim.* **2013**, *111*, 2029.
(32) Pierce, M. M.; Raman, C. S.; Nall, B. T. *Methods* **1999**, *19*, 213.
(33) Ababou, A.; Ladbury, J. E. *J. Mol. Recognit.* **2006**, *19*, 79.
(34) Falconer, R. J.; Collins, B. M. *J. Mol. Recognit.* **2011**, *24*, 1.
(35) Turnbull, W. B.; Daranas, A. H. *J. Am. Chem. Soc.* **2003**, *125*, 14859.
(36) Origin Lab, Northampton, MA, 01060, USA

(37) Wang, J.; Duc-Truc, P.; Kee, T. W.; Clafton, S. N.; Guo, X.; Clements, P.; Lincoln, S. F.; Prud'homme, R. K.; Easton, C. J. *Macromolecules* **2011**, *44*, 9782.
(38) Trang, H., T, Linked β-cyclodextrin trimers: from molecular recognition to polymer network hydrogels, University of Adelaide, **2013**.
(39) Duc-Truc, P.; Hanh-Trang, N.; Lincoln, S. F.; Wang, J.; Guo, X.; Easton, C. J.; Prud'homme, R. K. *Journal of Polymer Science Part a-Polymer Chemistry* **2015**, *53*, 1278.
(40) Rekharsky, M. V.; Inoue, Y. *Chem. Rev.* **1998**, *98*, 1875.
(41) Zhang, B. L.; Breslow, R. *J. Am. Chem. Soc.* **1993**, *115*, 9353.
(42) Nguyen, H. T.; Pham, D. T.; Easton, C. J.; Lincoln, S. F. *Aust. J. Chem.* **2013**, *66*, 1057.
(43) Hameed, N.; Guo, Q. *Polymer* **2008**, *49*, 5268.
(44) Ravi, P.; Wang, C.; Dai, S.; Tam, K. C. *Langmuir* **2006**, *22*, 7167.
(45) Wang, C.; Tam, K. C. *J. Phys. Chem. B* **2005**, *109*, 5156.
(46) Grieshaber, S. E.; Paik, B. A.; Bai, S.; Kiick, K. L.; Jia, X. *Soft Matter* **2013**, *9*, 1589.
(47) Padua, G. W.; Wang, Q. *Nanotechnology research methods for foods and bioproducts*, **2012**.
(48) Shibayama, M.; Karino, T.; Okabe, S. *Polymer* **2006**, *47*, 6446.
(49) Forster, S.; Schmidt, M.; Antonietti, M. *Polymer* **1990**, *31*, 781.
(50) Li, Y. J.; Xia, J. L.; Dubin, P. L. *Macromolecules* **1994**, *27*, 7049.
(51) Forster, S.; Hermsdorf, N.; Bottcher, C.; Lindner, P. *Macromolecules* **2002**, *35*, 4096.
(52) Lu, T.; Vesterinen, E.; Tenhu, H. *Polymer* **1998**, *39*, 641.

5.5 Appendix

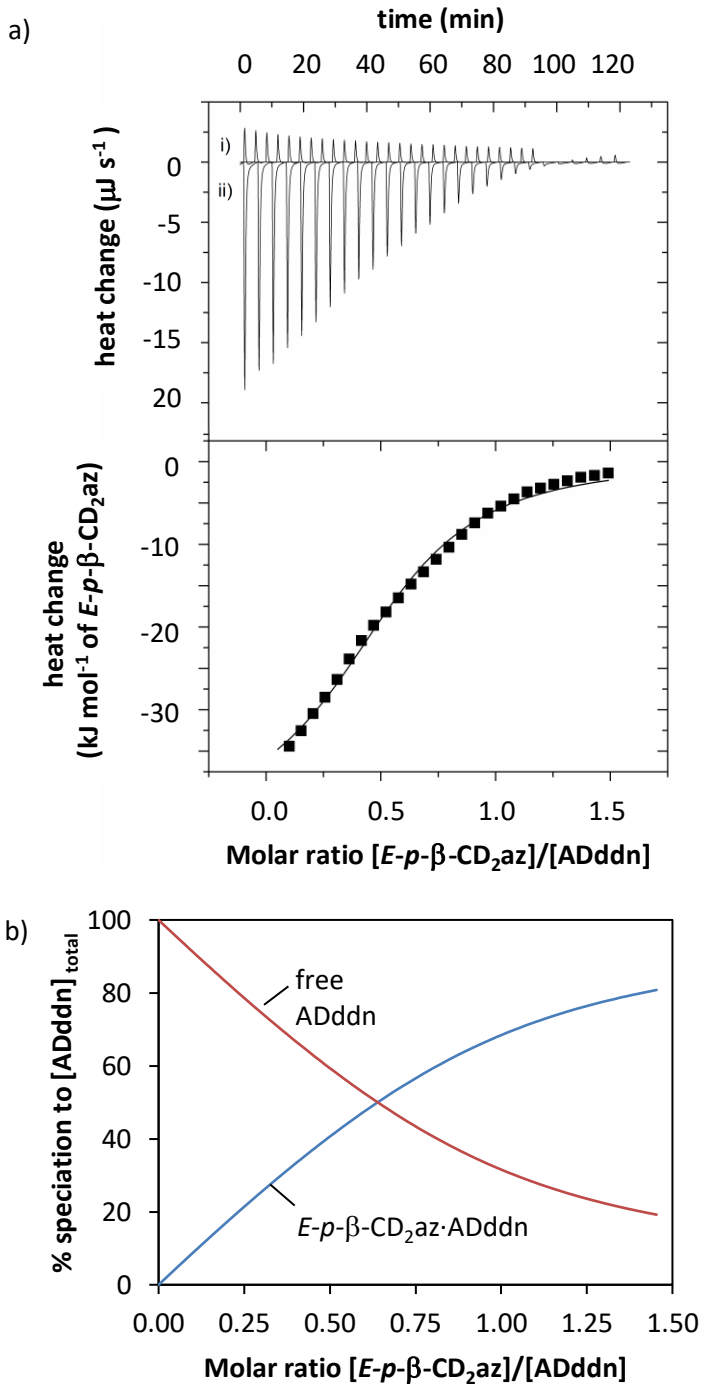

Figure 5.57: ITC data for 0.14 wt% PAAADddn ([ADddn] = 2.7×10^{-4} mol dm^{-3}) with *E*-*p*-β-CD_2az (2.0×10^{-3} mol dm^{-3}) in aqueous phosphate buffer (pH 7.0, I = 0.10 mol dm^{-3}) at 298.2 K. a) The top section shows the raw ITC heat release profile with time, where i) is the *E*-*p*-β-CD_2az dilution data and ii) is the titration data. The bottom section shows the experimental heat released with each addition of *E*-*p*-β-CD_2az (squares) and the best-fit of an algorithm for a 1:1 *E*-*p*-β-CD_2az·ADddn complex (solid line), as shown in Equation 5.5. b) Speciation plot showing the variation in the proportion of free and complexed ADddn-substituent as [*E*-*p*-β-CD_2az]/[ADddn] increases.

This page is intentionally left blank

CHAPTER 6

Synthesis of β-Cyclodextrin-based Molecular Muscles

6.1 Introduction

6.1.1 Molecular Muscles

Molecular devices are sets of interrelated molecules, not necessarily covalently linked, that perform a function when exposed to an external stimulus.[1-4] Research into molecular devices aims to offer a new approach to improving the efficiency and functionality of technological devices by using the 'bottom-up' approach, that is, through mastering molecular information. Various molecular devices have been synthesised including molecular rotors,[5,6] molecular shuttles,[7-10] molecular tweezers,[11] molecular elevators,[12] logic gates[13] and molecular walkers.[14] The importance of molecular device research was recognised through the 2016 Nobel Prize in Chemistry, which was awarded to pioneers Jean-Pierre Sauvage, Sir J. Fraser Stoddart and Bernard L. Feringa.

Molecular devices are typically constructed using mechanically-interlocked molecules (MIM), compounds that consist of multiple components that are linked by mechanical bonds,[15] rather than covalent bonds (see Chapter 1). The most common examples of MIMs are rotaxanes and catenanes.[16] Cyclodextrins have routinely been employed as components of molecular devices owing to their complexation capabilities.

Molecular muscles are a type of molecular device, characterised by expansion and contraction movements controlled by an external stimulus.[8,17-19] A variety of CD-based molecular muscles have been synthesised in the literature, often using α-CD.[20-23]

Cyclodextrin-based molecular muscles typically consist of four components: a CD host, a photocontrollable moiety, an alkyl tether and a blocking group. The formation of a CD-based molecular muscle begins with the modification of CD with the photocontrollable moiety. Azobenzene and stilbene are typically chosen as photocontrollable groups as they expand and contract upon photoisomerisation from the *E* to the *Z* isomer and *vice versa*, and have similar size profiles to the internal cavity of α-CD and β-CD. After modification of CD with the photocontrollable moiety, an alkyl tether is added. Alkyl tethers provide additional spacing to the molecule, which is required for expansion and contraction of the final molecular muscle.

The modification of CD with the photocontrollable moiety and alkyl tether forms a heteroditopic compound, named due to the molecule possessing both host and guest components. The heteroditopic compound is capable of self-assembling into a Janus (see Chapter 1) in aqueous solution. Upon formation of a Janus, a blocking group is added to mechanically lock in the formation. The main requirement for a blocking group is that it must be sufficiently larger than the annulus of CD. Figure 6.1 describes the synthesis of an α-CD-based molecular muscle using stilbene as the photocontrollable moiety.[23]

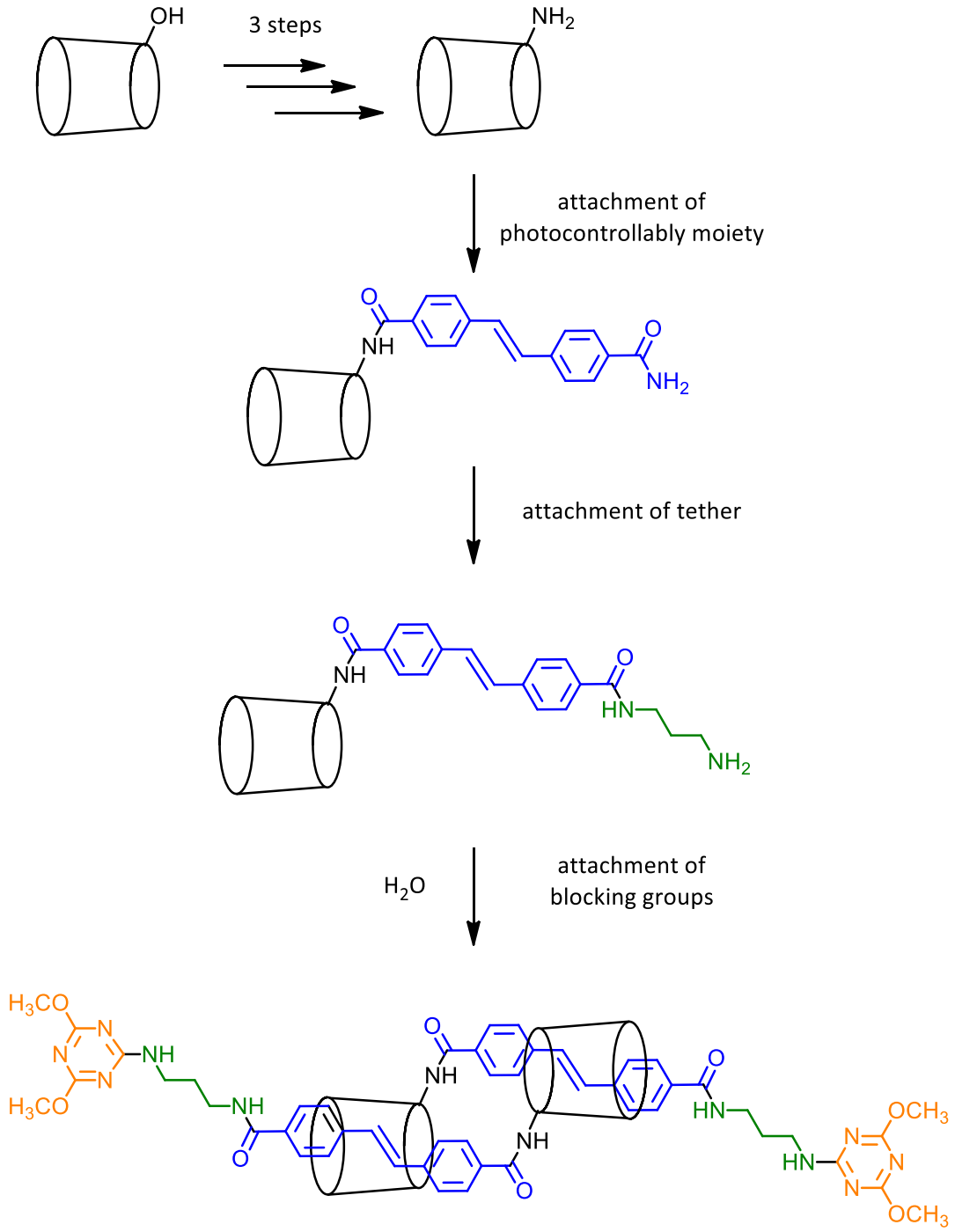

Figure 6.1: Synthesis of a molecular muscle based on stilbene-modified α-CD Janus with dimethoxy-triazine blocking groups.[23] The photcontrollable moiety (stilbene) is shown in blue, the alkyl tether (propyl group) is shown in green and the blocking group (dimethoxy-triazine) is shown in orange.

The utility of CD-based molecular muscles is achieved through photoirradiation to isomerise the azobenzene or stilbene moiety from the *E* to *Z* isomer. The *E* isomers of azobenzene and stilbene are longer than their respective *Z* isomers. Thus, photoirradiation from one isomer to another is accompanied by an expansion or contraction of the entire compound. Figure 6.2 demonstrates the utility of an α-CD-based molecular muscle using stilbene as the photocontrollable moiety.[23]

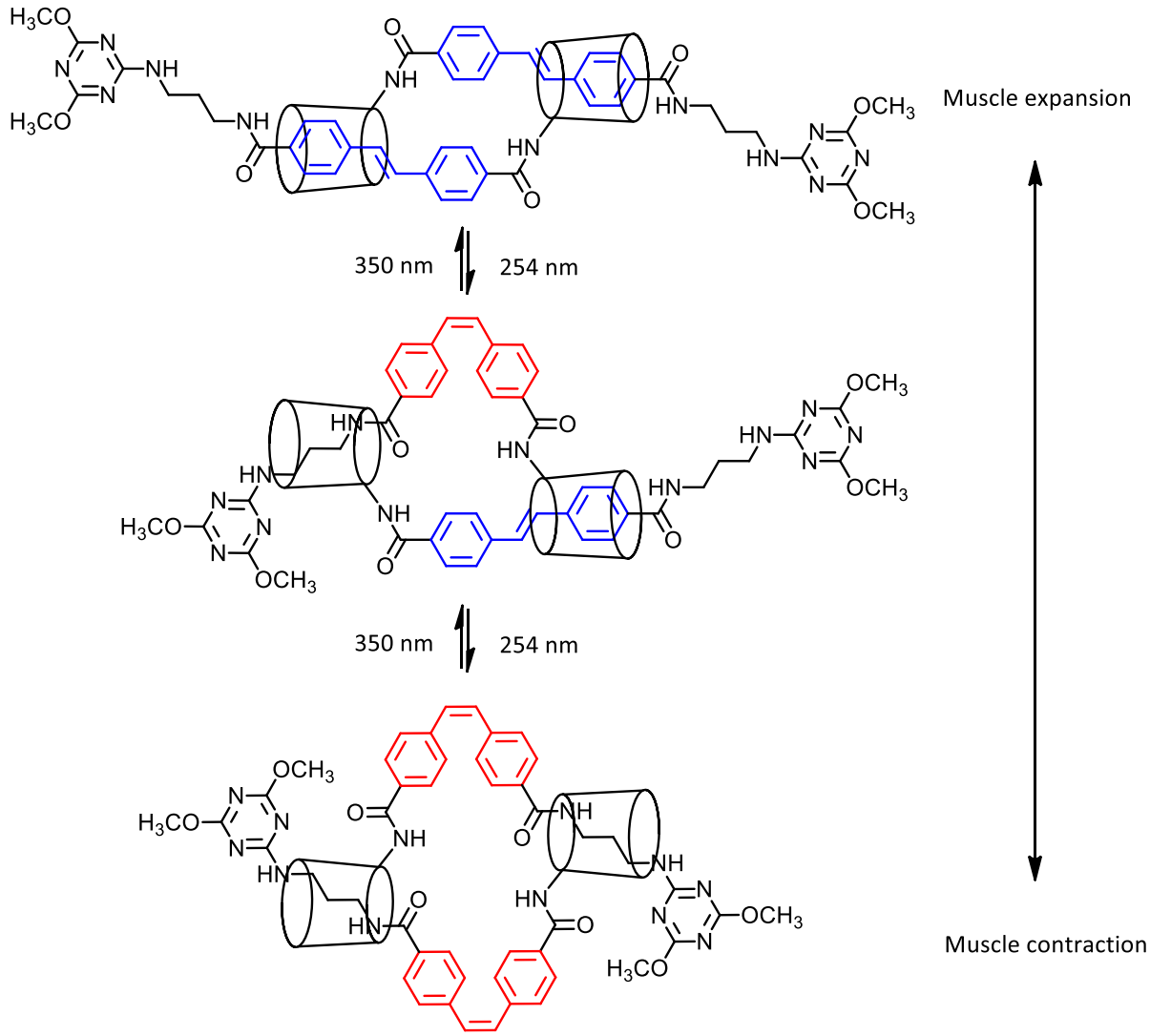

Figure 6.2: Operation of a molecular muscle based on a stilbene-modified α-CD Janus, which expands and contracts upon photoirradiation.[23]

Many of the CD-based molecular muscles published in the literature use α-CD as the macrocycle. However, studying β-CD- or γ-CD-based molecular muscles could elucidate additional factors that influence the formation and utility of molecular muscles. One area of interest for further study is the self-assembly process. A heteroditopic compound may self-assemble into a Janus or acyclic daisy chain, however, the preference into one or the other is not well-understood.[24] Thus, the study of

molecular muscles with various types of components can assist in understanding the self-assembly process.

The role of the blocking group has also not been thoroughly explored. Most blocking groups are chosen based on size, for purely mechanical means. However, different mechanisms of blocking could be used. It may be possible to lock a Janus through host-guest complexation rather than steric bulk. A stable complex formed between the host and blocking group may be strong enough to stabilise a Janus upon photoirradiation. A more accurate term for a blocking group acting through complexation rather than steric bulk would be a 'psuedo-blocking group'.

Blocking groups that possess additional functionality could also be explored. Lanthanide-bound ligands offer potential in providing structural information as well as the requisite blocking mechanism. Determining the geometry of a self-assembled systems remains challenging. While NMR spectroscopy can give some structural information, the unambiguous assignment of protons is challenging due to overlapping chemical shifts and thus, the structure of a self-assembled system is difficult to elucidate. Lanthanides are useful in this respect as they may be used as shift reagents in NMR spectroscopy.[25]

Lanthanides can induce large chemical shifts to extend the normal range of a ^{1}H NMR spectra beyond 0 – 10 ppm.[26] Lanthanide-induced shifts arise from through-space interactions between a paramagnetic lanthanide and a bound ligand, due to the anisotropic effect.[26,27] As the effect of anisotropy is distant dependent, nuclei closer in space to the lanthanide will exhibit a larger shift. Lanthanide-bound blocking groups may therefore be able to more definitively determine the geometry of a self-assembled system being either a Janus or acyclic daisy chain.[25,28]

As supramolecular chemistry becomes more and more sophisticated, new synthetic routes are required to continually expand the field. Thus, it remains important to explore new ways to construct molecular devices. Molecular muscles constructed with non-conventional blocking groups and different macrocycles may provide extra functionality to the system, open up simpler synthetic routes and provide a more nuanced understanding of the self-assembly process. It is important to remain innovative in the approach to molecular device design to understand the complete potential of these systems.

6.1.2 Aims of this study

The aim of this research is to synthesise and characterise three molecular muscles, differing by the type of blocking group. The three molecular muscles are based upon (*E*)-*N*-(6^{A}-deoxy-β-cyclodextrin-6^{A}-yl)-4-aminocarbonyl-4'-carboxyazobenzene (β-CDazpr), as shown in Figure 6.3. β-CD is chosen as the host, azobenzene is used as the photocontrollable moiety, while a propyl group serves as the tether. As β-CDazpr possess both host and guest components, it is a heteroditopic molecule capable of self-assembling in water to form a Janus or acyclic daisy chain.

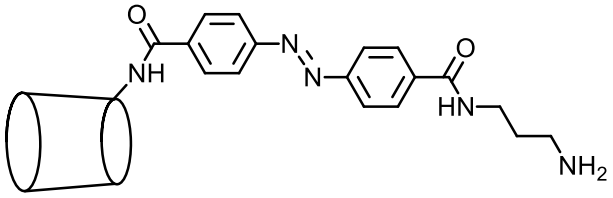

Figure 6.3: Structure of β-CDazpr.

The self-assembly of β-CDazpr into either a Janus or acyclic daisy chain will first be determined. The successful formation of a self-assembled structure will be followed by the addition of three different blocking groups to mechanically lock in the formation. Adamantane (AD), aza-18-crown-6 and 1,4,7,10-tetraazacyclododecane-1,4,7,10-tetraacetic acid (DOTA) will be used as blocking groups to synthesise [(*E*)-N-(6^{A}-deoxy-β-cyclodextrin-6^{A}-yl)-4-aminocarbonyl-4'-(3-(1-aminocarbonyl-adamantane) propylaminocarbonyl) azobenzene]-[c2]-[daisy chain] (**2**), [(*E*)-*N*-(6^{A}-deoxy-β-cyclodextrin-6^{A}-yl)-4-aminocarbonyl-4'-(3-(2-aminocarbonyl-(1,4,7,10,13-pentaoxa-16-azacyclooctadecan-16-yl)propylaminocarbonyl) azobenzene]-[c2]-[daisy chain] (**3**) and [(*E*)-*N*-(6^{A}-deoxy-β-cyclodextrin-6^{A}-yl)-4-aminocarbonyl-4'-(3-(1,4,7,10-tetraazacyclododecane-1-aminocarbonyl-4,7,10-tetraacetic acid)propylaminocarbonyl)azobenzene]-[c2]-[daisy chain] (**4**), respectively, as shown in Figure 6.4. The complete structure of molecular muscles **2**, **3** and **4** will then be determined to confirm the Janus geometry and ability to act as molecular muscles.

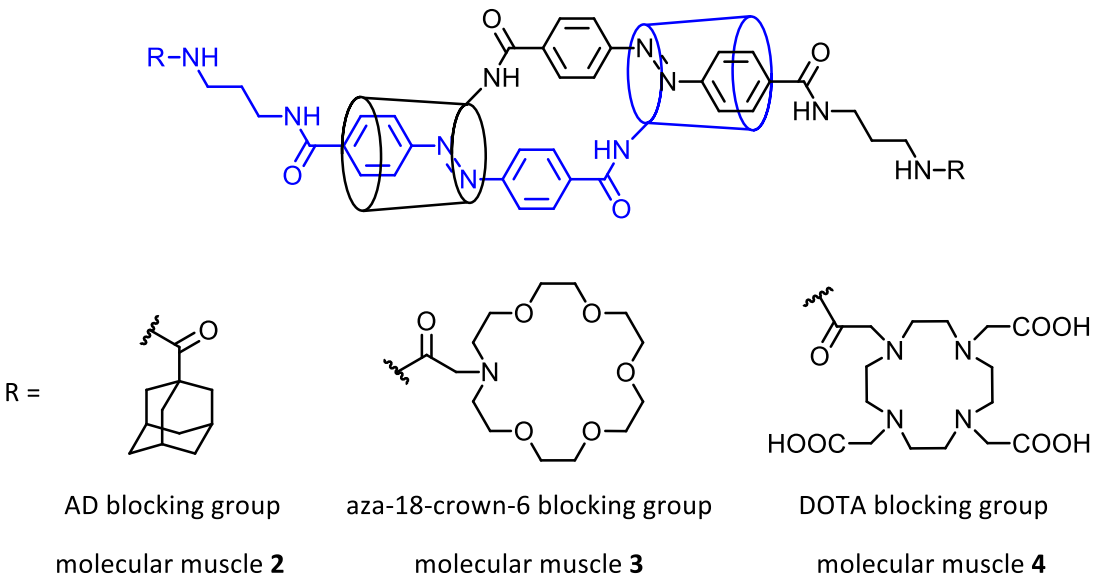

AD blocking group molecular muscle **2**

aza-18-crown-6 blocking group molecular muscle **3**

DOTA blocking group molecular muscle **4**

Figure 6.4: Structures of molecular muscles **2**, **3** and **4**.

The three blocking groups were considered based on their size and lanthanide-binding capabilities. Aza-18-crown-6 and DOTA were chosen as blocking groups as they form stable complexes with europium.[29,30] The incorporation of a lanthanide in molecular muscles **3** and **4** will provide additional structural information through lanthanide-shift ^{1}H NMR spectroscopy. Thus, the self-assembled structure of molecular muscles **3** and **4** as either a Janus or acyclic daisy chain can be studied.

Unlike aza-18-crown-6 and DOTA, AD was chosen as a pseudo-blocking group. The size of AD is similar to the cavity of β-CD and thus, a host-guest complex may be formed characterised by an equilibrium constant of K = 1400 dm mol^{-1}.[31] The formation of a strong host-guest complex between β-CD and AD may enable a Janus to be locked through complexation, rather than steric bulk, as shown in Figure 6.5. The structure is not expected to dissociate upon irradiation.

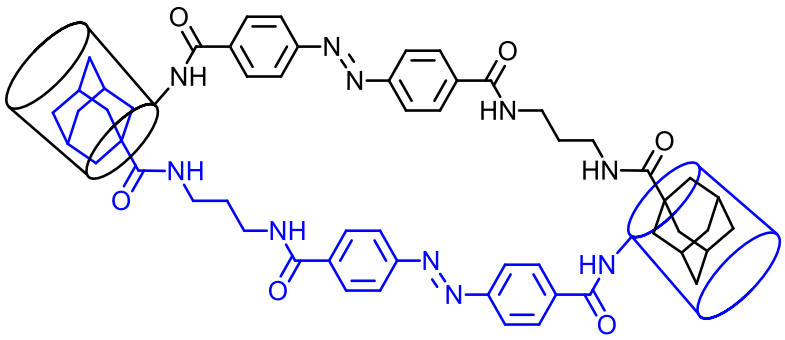

Figure 6.5: Structure of molecular muscle **2** in aqueous solution using AD as a pseudo-blocking group.

6.2 Results and Discussion

6.2.1 Synthesis of β-CDazpr

The molecular muscles **2**, **3** and **4** were prepared by first synthesising β-CDazpr. The first step of the synthesis was the formation of 6β-CDNH$_2$ by literature methods.[32,33] The azobenzene moiety was introduced by amide coupling 6β-CDNH$_2$ and *para*-*E*-azobenzene-dicarboxylic acid (*E*-*p*-AzCOOH) to form (*E*)-*N*-(6^A-deoxy-β-cyclodextrin-6^A-yl)-4-aminocarbonyl-4'-carboxyazobenzene (β-CDaz) using 1-hydroxybenzatriazole (HoBT) and N,N'-dicyclohexylcarbodiimide (DCC) as coupling reagents. The final step in the synthesis was the addition of a propyl group as a tether. 1,3-diaminopropane was amide coupled to β-CDaz using BOP reagent, to form β-CDazpr. The syntheses were confirmed by TLC, ^{1}H NMR spectroscopy and mass spectrometry. The syntheses are described in Figure 6.6 and the full synthetic details are in Chapter 7.

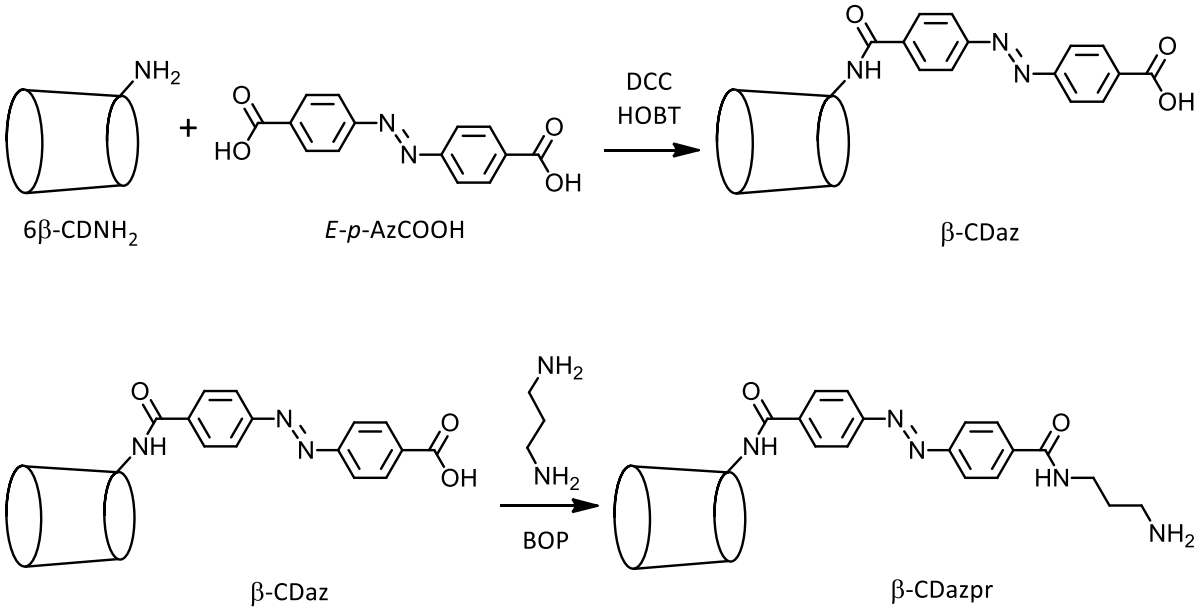

Figure 6.6: Synthesis of β-CDazpr.

6.2.2 Self-Assembly of β-CDazpr

The self-assembly of β-CDazpr in aqueous solution may lead to the formation of a Janus or acyclic daisy chain, as shown in Figure 6.7. The self-assembled structures may exist either alone or in equilibrium. It is difficult to determine the exact geometry of the self-assembled structure as there are no blocking groups to mechanically lock the structure. However, it is pertinent to confirm that β-CDazpr does self-assemble in aqueous solution before attaching the blocking groups. The self-assembly behaviour was studied by 2D ^{1}H NMR spectroscopy.

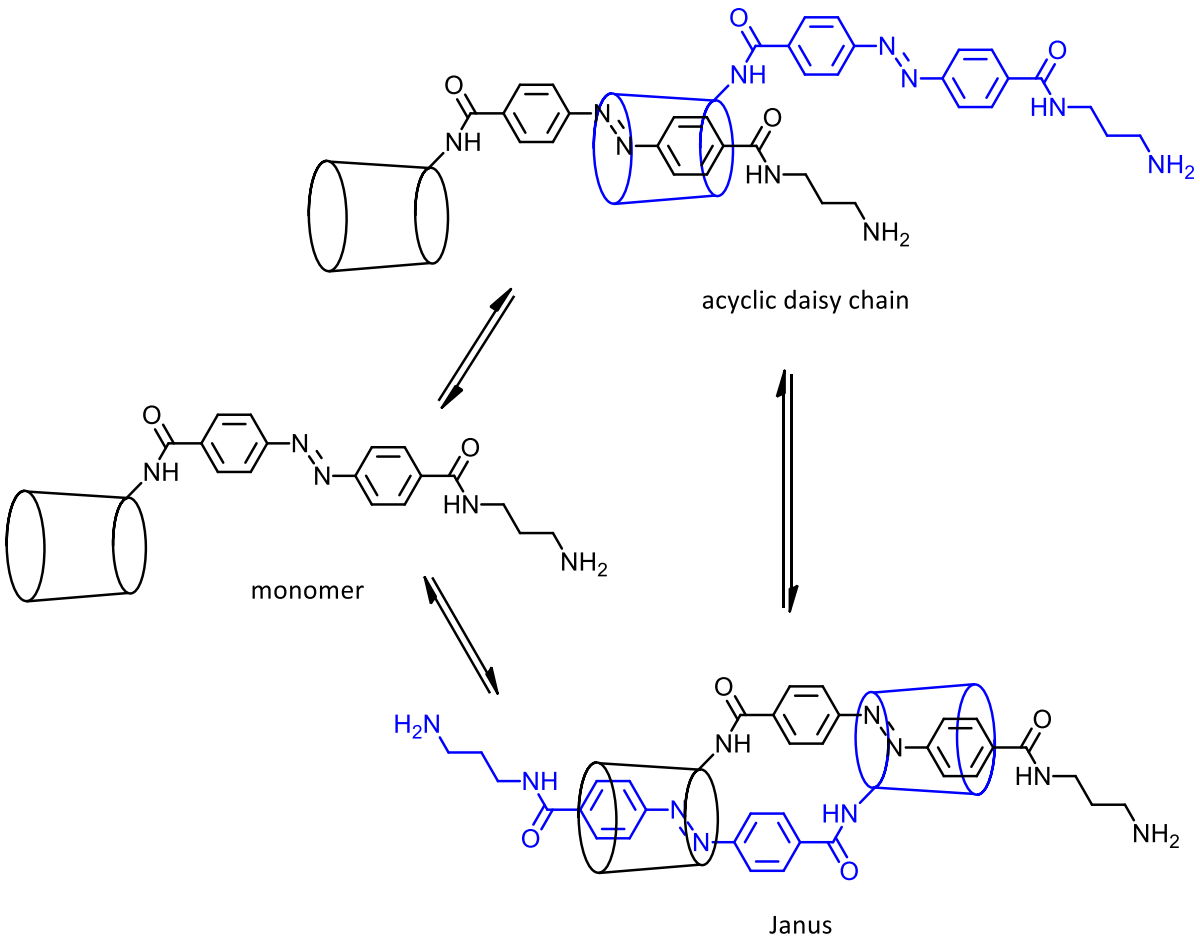

Figure 6.7: Equilibrium of the self-assembly of β-CDazpr in aqueous solution to form a Janus or acylic daisy chain. The acyclic daisy chain may consist of more than 2 monomeric units.

6.2.2.1 2D ^{1}H ROESY NMR spectroscopy of β-CDazpr

The self-assembly behaviour of β-CDazpr was studied by 2D ^{1}H ROESY NMR spectroscopy. The 2D ^{1}H ROESY NMR spectrum of β-CDazpr (2.0×10^{-3} mol dm^{-3}) in D_2O phosphate buffer (pD 7.0, I = 0.10 mol dm^{-3}) at 298.2 K is shown in Figure 6.8. Cross-peaks between the annular protons of β-CD and protons of azobenzene or the propyl tether indicate complexation.[34]

The 2D ^{1}H ROESY NMR spectrum shows cross-peaks between the H1 – H4 protons of the azobenzene group and the H2 – H6 protons of the β-CD group. There are also cross-peaks between the H6 protons of the propyl tether and the H2 – H6 protons of β-CD. As the azobenzene group is connected to β-CD through an amide link, it is incapable of internal complexation. Thus, NOE interactions indicate that azobenzene and the propyl tether of one β-CDazpr molecule are complexing within a β-CD cavity of an adjacent β-CDazpr molecule. The NMR spectrum does not indicate whether the self-assembly reflects a Janus or acyclic daisy chain.

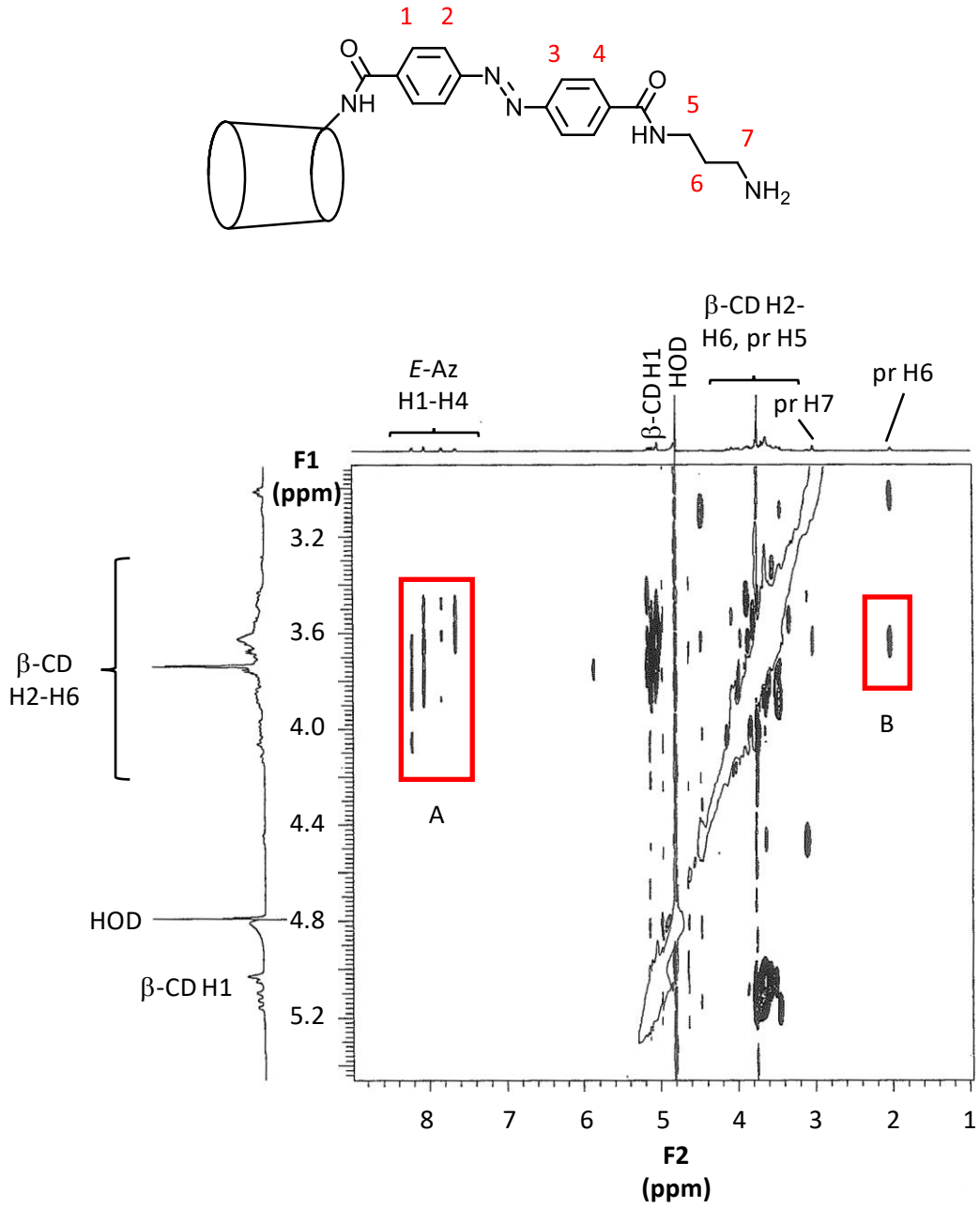

Figure 6.8: 2D ^{1}H ROESY NMR spectrum of β-CDazpr (2.0×10^{-3} mol dm^{-3}) in D_2O phosphate buffer (pD 7.0, I = 0.10 mol dm^{-3}) at 298.2 K. The abbreviation '*E*-Az' and 'pr' refers to the *E*-azobenzene and propyl groups of β-CDazpr, respectively. An annotated structure of β-CDazpr is shown above.

6.2.3 Synthesis of Molecular Muscles

The synthesis of molecular muscles **2**, **3** and **4** were attempted by modifying β-CDazpr with blocking groups AD, aza-18-crown-6 and DOTA, respectively.

6.2.3.1 Synthesis of Molecular Muscle 2

The synthesis of molecular muscle **2** was attempted by first synthesising monomeric **2**. The synthesis of monomeric **2** and the self-assembly into the Janus are shown in Figure 6.9 and Figure 6.10, respectively. The synthesis of monomeric 2 was achieved by amide coupling the AD pseudo-blocking group to β-CDazpr by direct substitution. The full experimental details are given in Chapter 7.

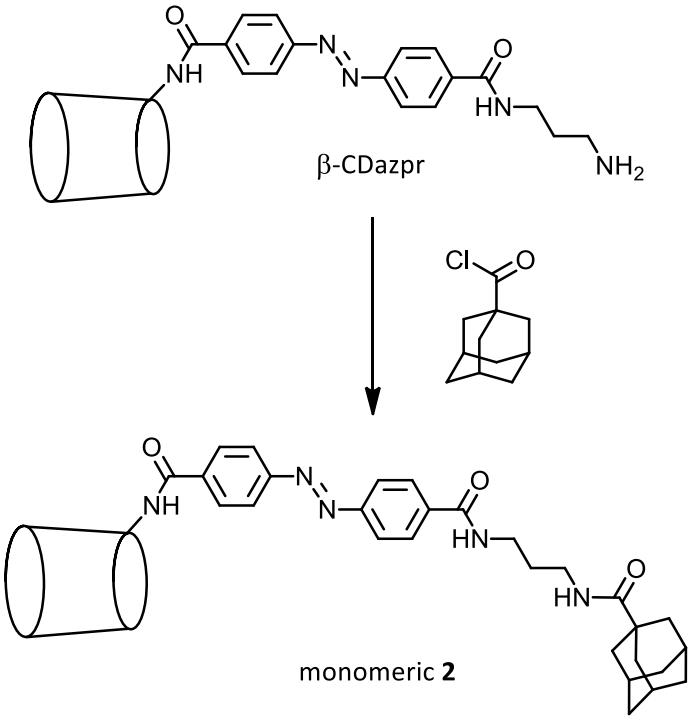

Figure 6.9: Synthesis of monomeric **2**.

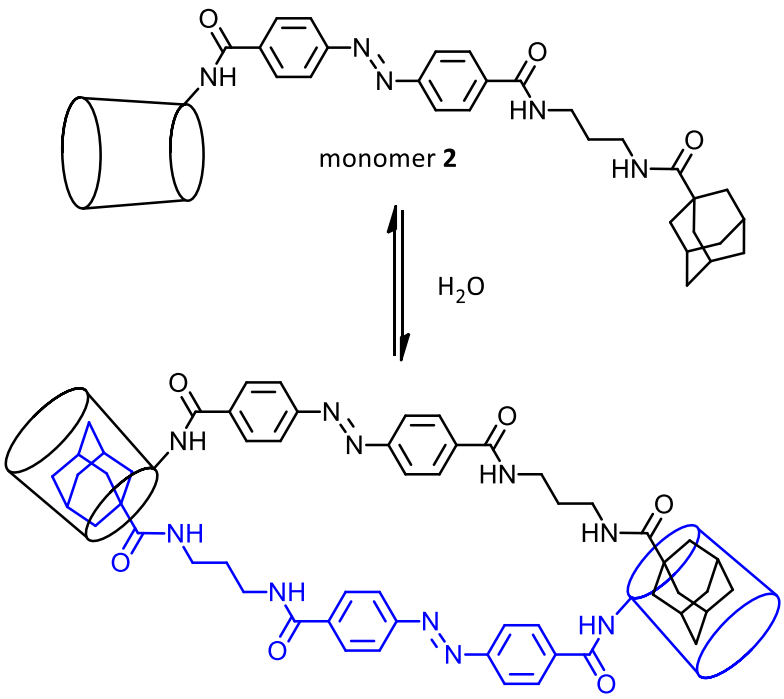

Figure 6.10: Proposed equilibrium of **2** in water as a monomer and molecular muscle.

The product was confirmed by ^{1}H NMR spectroscopy. The ^{1}H NMR spectrum of the product in DMSO-d_6 is given in Figure 6.11. A summary of the resonances is given in Table 6.1. Resonances A, B and D are likely to refer to *Z*-azobenzene protons H1 – H4, while resonance C is likely to refer to *E*-azobenzene protons H1 – H4, based largely upon the chemical shifts being similar to the analogous protons of β-CDazpr. Additionally, *E*-azobenzene protons are typically downfield of *Z*-azobenzene protons.[35,36]

Resonances F, G, H and I have been well-characterised and correspond to OH^{2-3}, H1, OH^6 and H2 – H6 resonances of β-CD, respectively. The protons corresponding to the H5 – H7 propyl tether protons appear to be superimposed with the H2 – H6 resonances of β-CD. Resonances J, K and L correspond to H10, H8 and H9 protons of the AD pseudo-blocking group, respectively, which would expectedly give rise to quintet, doublet and triplet multiplicities. However, as resonances J, K and L are singlets, it indicates that the coupling constants have tended towards zero as a result of modification with β-CD.

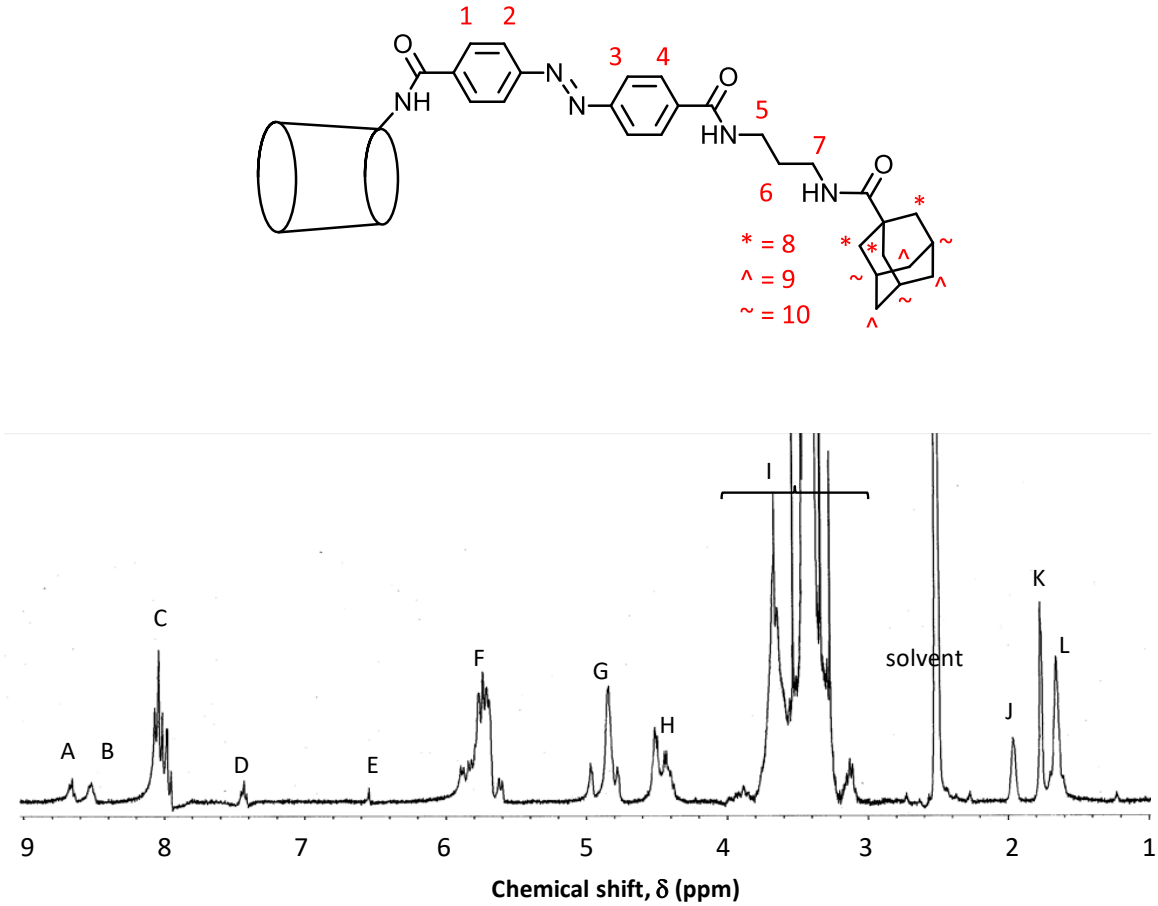

Figure 6.11: ^{1}H NMR spectrum of monomer **2** (2.0×10^{-3} mol dm^{-3}) in DMSO-d_6 at 298.2 K.

Table 6.1: Summary of ^{1}H NMR resonances of monomer **2** (2.0×10^{-3} mol dm^{-3}) in DMSO-d_6 at 298.2 K. The type of resonance is not specified for low intensity peaks as the assignment is ambiguous.

Resonance	Shift (ppm)	Type
A	8.64	-
B	8.52	-
C	8.07	m
D	7.43	-
E	6.54	-
F	5.60 – 5.89	m
G	4.78 – 4.97	m
H	4.43 – 4.51	m
I	3.13 – 3.66	m
J	1.96	s
K	1.77	s
L	1.65	s

While the ^{1}H NMR spectrum of monomer **2** indicated that the synthesis may be successful, mass spectroscopy did not give definitive results. The calculated exact mass of monomer **2** ($M+H^{+}$) is 1604.628 m/z. The MALDI-TOF spectrum gave a parent ion at 1603.85 *m/z*, which was beyond the margin of error for the instrument. Furthermore, the final product was found to be insoluble in water. Thus, while the synthesis of monomer **2** may have been successful, the insolubility in water would not enable self-assembly of monomer **2** into molecular muscle **2**. Therefore, the synthesis of molecular muscle **2** was not further continued. The unsuccessful synthesis of molecular muscle **2** is further discussed in Section 6.2.4.

6.2.3.2 Synthesis of Molecular Muscle 3

The blocking group required for the formation of molecular muscle **3** was first synthesised by modifying aza-18-crown-6 with a carboxylic acid group to form 2-(1,4,7,10,13-pentaoxa-16-azacyclooctadecan-16-yl)acetic acid (aza-18-crown-6-COOH),[37] as shown in Figure 6.12. The synthesis of molecular muscle **3** was then attempted by first forming the self-assembled Janus of β-CDazpr in aqueous solution. The Janus was then mechanically locked by amide coupling aza-18-crown-6-COOH to the terminal amine of β-CDazpr using 4-(4,6-dimethoxy-1,3,5-triazin-2-yl)-4-methylmorpholinium chloride (DMT-MM), as shown in Figure 6.13. This approach was previously reported by Harada *et al.* in the construction of an azobenzene- and α-CD-based molecular muscle.[20] The full experimental details are given in Chapter 7.

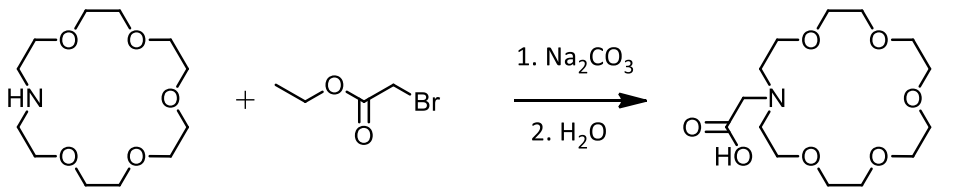

aza-18-crown-6 aza-18-crown-6-COOH

Figure 6.12: Synthesis of aza-18-crown-6-COOH

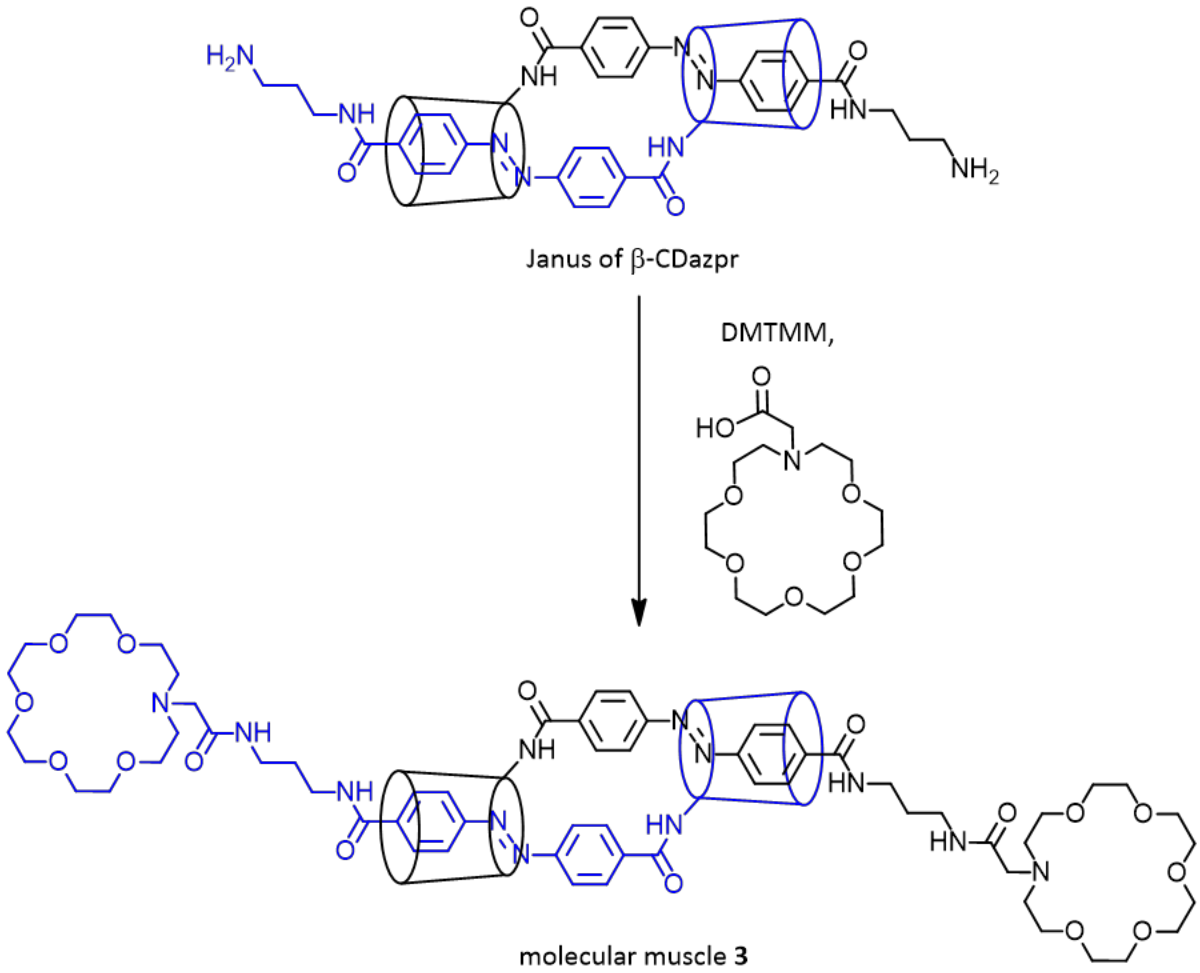

Figure 6.13: Attempted synthesis of molecular muscle **3**.

Despite repeated attempts, molecular muscle **3** could not be obtained. The short length of the propyl tether of β-CDazpr may be responsible for the lack of reactivity. Access to the terminal amine by DMT-MM may be hindered due to the close proximity of the propyl tether of one β-CDazpr to the secondary face of the adjacent β-CD group. Thus, the synthesis of molecular muscle **3** was not further attempted. The unsuccessful synthesis of molecular muscle **3** is further discussed in Section 6.2.4.

6.2.3.3 Synthesis of Molecular Muscle 4

The synthesis of molecular muscle **4** was attempted by first forming the self-assembled Janus of β-CDazpr in aqueous solution. The Janus was then mechanically locked by amide coupling DOTA to the terminal end of β-CDazpr using DMT-MM, as shown in Figure 6.14. The full experimental details are given in Chapter 7.

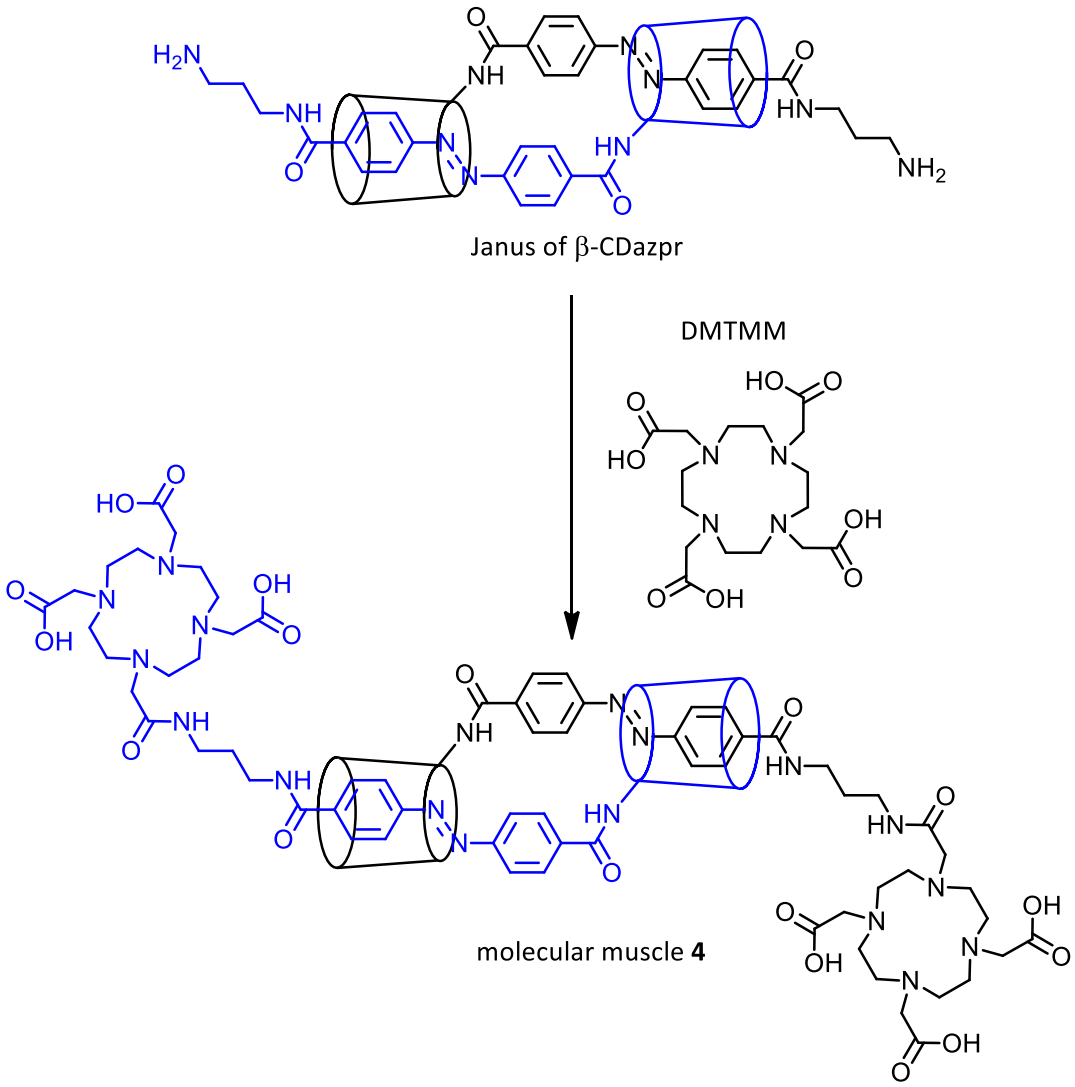

Figure 6.14: Attempted synthesis of molecular muscle **4**.

The synthesis was performed using similar conditions as molecular muscle **3**. As DOTA possesses four carboxylic acid groups, it was hypothesised that the coupling may be more successful than the synthesis of molecular muscle **3**. However, repeated attempts did not yield molecular muscle **4**, indicating that a more reactive coupling reagent or new synthetic route is required. Thus, the synthesis of molecular muscle **4** was not further attempted. The unsuccessful synthesis of molecular muscle **4** is further discussed in Section 6.2.4.

6.2.4 Molecular Muscle Design Considerations

The failed syntheses of molecular muscles **2**, **3** and **4** require an overhaul of the initial design. The choice of β-CD as the host may itself be an impedance to this work. While the aim of this research was to investigate the effect of β-CD in the construction of molecular muscles, it seems prudent to acknowledge the difficulty in determining the self-assembled structure of β-CDazpr. The solubility of β-CD is 0.016 mol dm^{-3}, which is significantly lower than the solubilities of both α-CD (0.15 mol dm^{-3}) and γ-CD (0.18 mol dm^{-3}).[38] This lower solubility limits the types of experiments that may be performed to understand the self-assembly behaviour.

Previously, Harada *et al.* synthesised supramolecular polymers based upon cinnamide-modified α-CD.[39] The self-assembled structure was determined as a polymeric daisy chain using vapour pressure osmometry (VPO). However, the solubility requirements of VPO are high and thus, VPO is not suitable for experiments with β-CD compounds. While γ-CD could be explored instead of β-CD as a point of difference to the already established α-CD-based molecular muscles, the comparatively larger annulus size makes it difficult to find suitable blocking groups.

The length of the tether must also be addressed. The coupling reagent used to amide couple the tether with the blocking group may have been sterically hindered by the β-CD host. Therefore, longer tethers may be employed to extend the distance between the terminal end of the tether and β-CD. Harada *et al.* previously synthesised an azobenzene-based α-CD molecular muscle using polyethylene glycol as a tether.[20] The Janus form was successively locked using AD as a blocking group and DMT-MM as a coupling reagent in aqueous solution. A polyethylene glycol tether may be suitable for β-CD based molecular muscles as it may also increase the solubility of the compound. Enhanced solubility would be particularly important for monomer **2**, which was insoluble in water.

While the length of the tether may be altered to address issues with the coupling reagent, it may be pertinent to avoid coupling reagents altogether. Lincoln *et al.* mechanically locked-in the Janus of a stilbene and α-CD-based molecular muscle using direct attachment of a dimethoxychlorotriazine blocking group in aqueous solution.[23] However, this option utilised an aromatic group to facilitate the coupling, which this project deliberately avoided. The presence of aromatic groups other than azobenzene or stilbene can decrease the photoisomerisation yields during irradiation of a molecular muscle. The presence of extra resonances in the aromatic region of a ^{1}H NMR spectra can also lead to incorrect reporting of *E* and *Z* isomers of the molecular muscle upon irradiation.

The use of lanthanides to probe the self-assembled structure may also need further consideration. While the incorporation of the lanthanide was not tested in this research, various issues are foreseen. For example, as aza-18-crown-6 and DOTA are only slightly larger in diameter than the secondary face of β-CD, the Janus may dissociate during lanthanide chelation. It may be more suitable to chelate the lanthanide to the ligand before attaching the blocking group, however, this may further impede the synthesis to attach the blocking group using a coupling reagent.

6.3 Conclusion

The precursor to the molecular muscles, β-CDazpr, was successfully synthesised. The self-assembly behaviour of β-CDazpr in aqueous solution was confirmed by 2D ^{1}H ROESY NMR spectroscopy. The synthesis of molecular muscles **2**, **3** and **4** were attempted. Monomeric **2** was likely successfully synthesised. However, monomeric **2** was insoluble in water and thus, a Janus would not be able to self-assemble in aqueous solution. Thus, the synthesis of molecular muscle **2** was not successful. The syntheses of molecular muscles **3** and **4** were also not successful.

The design of the molecular muscles would need to be overhauled to determine the effect of β-CD on the self-assembly processes of molecular muscles. The low solubility of β-CD, the short length of the propyl tether and the use of DMT-MM as a coupling reagent may have contributed to the unsuccessful syntheses.

6.4 References

(1) Lehn, J. M. *Angew. Chem. Int. Ed. Engl.* **1988**, *27*, 89.
(2) Balzani, V.; Credi, A.; Ferrer, B.; Silvi, S.; Venturi, M. In *Molecular Machines*; Kelly, T. R., Ed. 2005; Vol. 262, p 1.
(3) Lucia, U. *Chem. Phys. Lett.* **2013**, *556*, 242.
(4) Niess, F.; Duplan, V.; Sauvage, J. P. *Chem. Lett.* **2014**, *43*, 964.
(5) Koumura, N.; Zijlstra, R. W. J.; van Delden, R. A.; Harada, N.; Feringa, B. L. *Nature* **1999**, *401*, 152.
(6) Puigmarti-Luis, J.; Saletra, W. J.; Gonzalez, A.; Amabilino, D. B.; Perez-Garcia, L. *Chem. Commun.* **2014**, *50*, 82.
(7) Ashton, P. R.; Ballardini, R.; Balzani, V.; Baxter, I.; Credi, A.; Fyfe, M. C. T.; Gandolfi, M. T.; Gomez-Lopez, M.; Martinez-Diaz, M. V.; Piersanti, A.; Spencer, N.; Stoddart, J. F.; Venturi, M.; White, A. J. P.; Williams, D. J. *J. Am. Chem. Soc.* **1998**, *120*, 11932.
(8) Collin, J. P.; Dietrich-Buchecker, C.; Gavina, P.; Jimenez-Molero, M. C.; Sauvage, J. P. *Acc. Chem. Res.* **2001**, *34*, 477.
(9) Berna, J.; Leigh, D. A.; Lubomska, M.; Mendoza, S. M.; Perez, E. M.; Rudolf, P.; Teobaldi, G.; Zerbetto, F. *Nature Mater.* **2005**, *4*, 704.
(10) Silvi, S.; Venturi, M.; Credi, A. *J. Mater. Chem.* **2009**, *19*, 2279.
(11) Leblond, J.; Petitjean, A. *Chemphyschem* **2011**, *12*, 1043.
(12) Badjic, J. D.; Ronconi, C. M.; Stoddart, J. F.; Balzani, V.; Silvi, S.; Credi, A. *J. Am. Chem. Soc.* **2006**, *128*, 1489.
(13) Li, A. F.; Ruan, Y. B.; Jiang, Q. Q.; He, W. B.; Jiang, Y. B. *Chem. Eur. J.* **2010**, *16*, 5794.
(14) von Delius, M.; Leigh, D. A. *Chem. Soc. Rev.* **2011**, *40*, 3656.
(15) Bruns, C. J.; Stoddart, J. F. In *Beauty in Chemistry: Artistry in the Creation of New Molecules*; Fabbrizzi, L., Ed. 2012; Vol. 323, p 19.
(16) Nepogodiev, S. A.; Stoddart, J. F. *Chem. Rev.* **1998**, *98*, 1959.
(17) Liu, Y.; Flood, A. H.; Bonvallett, P. A.; Vignon, S. A.; Northrop, B. H.; Tseng, H. R.; Jeppesen, J. O.; Huang, T. J.; Brough, B.; Baller, M.; Magonov, S.; Solares, S. D.; Goddard, W. A.; Ho, C. M.; Stoddart, J. F. *J. Am. Chem. Soc.* **2005**, *127*, 9745.
(18) Bruns, C. J.; Stoddart, J. F. *Acc. Chem. Res.* **2014**, *47*, 2186.
(19) Jimenez, M. C.; Dietrich-Buchecker, C.; Sauvage, J. P. *Angew. Chem.* **2000**, *39*, 3284.
(20) Li, S. J.; Taura, D.; Hashidzume, A.; Harada, A. *Chem. Asian J.* **2010**, *5*, 2281.
(21) Tsuda, S.; Aso, Y.; Kaneda, T. *Chem. Commun.* **2006**, 3072.
(22) Fujimoto, T.; Sakata, Y.; Kaneda, T. *Chem. Commun.* **2000**, 2143.
(23) Dawson, R. E.; Lincoln, S. F.; Easton, C. J. *Chem. Commun.* **2008**, 3980.
(24) Rotzler, J.; Mayor, M. *Chem. Soc. Rev.* **2013**, *42*, 44.
(25) Hinckley, C. C. *J. Am. Chem. Soc.* **1969**, *91*, 5160.
(26) Sanders, J. K. M.; Williams, D. H. *Nature* **1972**, *240*, 385.
(27) Cockeril.Af; Davies, G. L. O.; Harden, R. C.; Rackham, D. M. *Chem. Rev.* **1973**, *73*, 553.
(28) Lee, L.; Sykes, B. D. *Biophys. J.* **1980**, *32*, 193.
(29) Liu, Y.; Han, B. H.; Chen, Y. T. *Coord. Chem. Rev.* **2000**, *200*, 53.
(30) Marques, M. P. M.; Geraldes, C.; Sherry, A. D.; Merbach, A. E.; Powell, H.; Pubanz, D.; Aime, S.; Botta, M. *J. Alloys Compd.* **1995**, *225*, 303.
(31) Tosner, Z.; Aski, S. N.; Kowalewski, J. *J. Inclusion Phenom. Macrocyclic Chem.* **2006**, *55*, 59.
(32) Kretschmann, O.; Choi, S. W.; Miyauchi, M.; Tomatsu, I.; Harada, A.; Ritter, H. *Angew. Chem.* **2006**, *45*, 4361.
(33) Brown, S. E.; Coates, J. H.; Coghlan, D. R.; Easton, C. J.; Vaneyk, S. J.; Janowski, W.; Lepore, A.; Lincoln, S. F.; Luo, Y.; May, B. L.; Schiesser, D. S.; Wang, P.; Williams, M. L. *Aust. J. Chem.* **1993**, *46*, 953.
(34) Schneider, H. J.; Hacket, F.; Rudiger, V.; Ikeda, H. *Chem. Rev.* **1998**, *98*, 1755.

(35) Tait, K. M.; Parkinson, J. A.; Bates, S. P.; Ebenezer, W. J.; Jones, A. C. *J. Photochem. Photobiol., A* **2003**, *154*, 179.
(36) Norikane, Y.; Katoh, R.; Tamaoki, N. *Chem. Commun.* **2008**, 1898.
(37) Lock, J. S., Cyclodextrins : molecular wheels for supramolecular chemistry, PhD Thesis, University of Adelaide, **2004**.
(38) Li, S.; Purdy, W. C. *Chem. Rev.* **1992**, *92*, 1457.
(39) Miyauchi, M.; Kawaguchi, Y.; Harada, A. *J. Inclusion Phenom. Macrocyclic Chem.* **2004**, *50*, 57.

This page is intentionally left blank

CHAPTER 7

Experimental

7.1 General Experimental

Thin layer chromatography (TLC) was carried out on Merck Kieselgel 60 F_{254} on aluminium-backed sheets. For analysis of CD derivatives, plates were developed with 7:7:5:4 v/v ethylacetate/propan-2-ol/1 mol dm^{-3} ammonia solution/water. Compounds were visualised by drying the plate, dipping it into a 1% sulphuric acid in ethanol solution and heating it with a heat gun. For the preparations described in Section 7.2 – Section 7.6, R_c represents the R_f of a modified β-CD relative to the R_f of the parent native β-CD.

Routine nuclear magnetic resonance (NMR) spectra were recorded on a Varian Gemini ACP-300 spectrometer (300 MHz) and Agilent 500 MHz NMR spectrometer (500 MHz). 2D ROESY and NOESY ^{1}H NMR spectra were recorded on a Agilent 600 (600 MHz) spectrometer, using a standard sequence with a mixing time of 300 ms at 298.2 K.

Solutions for NMR were prepared in either deuterium oxide (D_2O), dimethylsulfoxide-d_6 (DMSO-d_6) or D_2O phosphate buffer (pD 7.0, I = 0.10 mol dm^{-3}). Chemical shifts are reported on the δ scale in parts per million (ppm) and were referenced to residual peaks of non-deuterated solvents: D_2O, (4.79 ppm), D_2O phosphate buffer (4.79 ppm) and DMSO-d_6 (2.54 ppm). The following abbreviations are used to report multiplicity: s, singlet; d, doublet; t, triplet; q, quartet; m, multiplet; br, broad. The δ value at the centre of the multiplet resonance is recorded except for signals where a multiplet is well resolved, in which case the δ values for all individual multiplet components are given.

UV-visible absorbance spectra were recorded using a Varian CARY 5000 UV-VIS-NIR spectrophotometer equipped with matched 1.0 cm path length quartz cells over a range of required wavelengths at 1 nm intervals. Each solution was run against a reference solution containing all components of the solution of interest except the absorbing compound. Solutions were pre-equilibrated at 298.2 ± 0.2 K, unless stated otherwise, and maintained at this temperature during measurement by means of a thermostatted cell block. All solutions were freshly prepared prior to measurement.

Irradiation was performed using a 500 W Xe Lamp (Ushio Inc.) equipped with cutoff filters for UV light (Hoya UV 34) and visible light (Hoya Y45). Samples were irradiated in a 1 cm path length quartz cell while stirring.

Quadrupole Time of Flight (QTOF) mass spectra were run on a Micromass Q-ToF 2 (Waters/Micromass, Manchester, UK) mass spectrometer. Electrospray ionisation mass spectra (ESI-MS) were recorded on a Finnigan MAT ion trap LC-Q octapole mass spectrometer. Gas chromatography - mass spectrometry (GC-MS) data were obtained using a Shimadzu GC-MS

spectrometer. Samples were dissolved in either Milli-Q water, HPLC grade methanol or a mixture of both at a concentration of 0.5 mg cm^{-3}. Analyses was performed in the positive mode.

Matrix-assisted laser desorption/ionisation time of flight (MALDI TOF) mass spectra were acquired using a Bruker Ultrafle Xtreme MALDI TOF mass spectrometer (Bruker Daltonik GmbH) operating in linear mode under the control of Flex Control software (Version 3.3, Bruker Daltonik GmbH). External calibration was carried out using peptide standards (Bruker Daltonik GmbH), over a range of 800 to 4500 D, which was analysed under the same conditions as that of the sample. Spectra were obtained at various locations over the surface of the matrix spot at an intensity determined by the operator. The sample was dissolved in 1 cm^3 water and diluted to 100 µg cm^{-3} with an aqueous 0.1% trifluoroacetic acid (TFA) solution. A 1 mm^3 portion was mixed with 1 mm^3 sinapinic acid in water/acetonitrile/TFA (V/V/V) (10/90/0.1) solution and 1 mm^3 of this mixture was applied to an 800 µm Anchor Chip target plate (Bruker Daltonik GmbH, Bremen, Germany) and air dried. Analysis was performed in both positive and negative mode. The MS spectra obtained were analysed using Flex Analysis software (Version 3.3, Bruker Daltonik GmbH) employing smoothing, background subtractions and peak detection algorithms. MALDI TOF mass spectra were performed by the Adelaide Proteomics Centre.

Isothermal Titration Calorimetry (ITC) measurements were recorded on a MicroCal VP Isothermal Titration Calorimeter. Solutions were degassed and thermostatted to 298.2 K using ThermoVac. Solutions were prepared in aqueous phosphate buffer (pH 7.0, I = 0.10 mol dm^{-3}) immediately prior to experiment. The initial cell volume was 1.46 cm^3. The concentration correction for displaced volume effects due to each injection (10 mm^3) were calculated by Origin 7.0 MicroCal Protocol.[1] In each case, 1.46 cm^3 volume of the substituted poly(acrylate)s were titrated by adding 10 mm^3 aliquots of the host solutions from a computer-controlled micro-syringe at intervals of 210 s.

Rheological measurements were carried out at the State Key Laboratory of Chemical Engineering, East China University of Science and Technology, Shanghai 00237, China using a Physica MCR 501 (Anton Parr GmbH) stress-controlled rheometer with a 25 mm cone and plate geometry. Temperature was controlled at 209.2 K ± 0.1 K by a Peltier plate. Rheological samples were prepared in 0.10 mol dm^{-3} aqueous sodium chloride solution adjusted to pH 7.0 with 0.10 mol dm^{-3} aqueous sodium hydroxide solution. The rheological experiments were performed by Wang Meng Xue under the supervision of Professor Xuhong Guo.

7.1.1 Materials

Deionised water was prepared using a Milli-Q-Reagent system to give a resistivity of >15 MΩ cm. Aqueous phosphate buffer (pH 7.0, I = 0.10 mol dm^{-3}) was prepared from sodium hydrogen phosphate and potassium phosphate as described in the literature.[2]

Column chromatography was carried out using Bio-Rex 70 resin, which was purchased from Bio-Rad Laborators, Inc., CA and converted to the acid form using 3 mol dm^{-3} hydrochloric acid.

β-Cyclodextrin was obtained from Nihon Shokuhin Kako Co. β-CD was dried to a constant weight under vacuum and stored in the dark under refrigeration. *N,N*-Dimethylformamide (DMF) was obtained from APS and D_2O and DMSO-d_6 were obtained from Cambridge Isotope Laboratory. Crystal violet (CV^+) as the chloride salt (95%, BDH), rhodamine B (RB) as the chloride salt (95%, Sigma) and ethyl orange (EO^-) as the sodium salt (95%, Sigma) were twice recrystallised from water and dried to constant weight under high vacuum, prior to use. The porphyrins *meso*-tetra(4-sulfonatophenyl)porphine dihydrochloride (TSPP), *meso*-tetra(4-carboxyphenyl)porphine (TCPP), *meso*-tetra(4-*N*,*N*,*N*-trimethylanilinium)porphine tetrachloride (TMAP) and *meso*-tetra(*N*-methyl-4-pyridyl)porphine tetrachloride (TMPyP) were obtained from Frontier Scientific and used without further purification. Poly(acrylic acid) (PAA) was purchased from Sigma Aldrich as a 35 wt% aqueous solution and lyophilised to a constant weight. 1,4,7,10-Tetraazacyclododecane-1,4,7,10-tetraacetic acid (DOTA) was purchased from Bioscientific and 1,4,7,10-tetraazacyclododecane (cyclen) was purchased from Tokyo Chemical Industry. All other reagents and solvents were obtained from Sigma Aldrich and were used without further purification, unless otherwise stated.

7.2 Chapter 2 Experimental

7.2.1 Syntheses

The synthesis of 6^A-O-*p*-toluenesulfonyl-β-cylodextrin (6β-CDTs),[3] 6^A-amino-6^A-deoxy-β-cyclodextrin (6β-$CDNH_2$)[4,5] and (*E*)-azobenzene-4,4'-dicarboxylic acid (*E*-*p*-AzCOOH)[6] followed literature methods.

7.2.1.1 Synthesis of *bis*(6^A-deoxy-β-cyclodextrin-6^A-yl)-4,4'-aminocarbonylazobenzene (*E*-*p*-β-CD_2az)

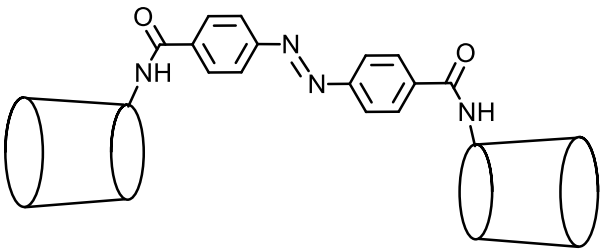

The synthesis of *E*-*p*-β-CD_2az followed a modified literature procedure.[7] *E*-*p*-AzCOOH (1.0 g, 3.8 mmol) was dissolved in anhydrous DMF (200 cm^3). 1-Hydroxybenzatriazole (0.17 g, 1.25 mmol) and *N,N'*-dicyclohexylcarbodiimide (0.26 g 1.25 mmol) was added to the solution. A solution of 6β-$CDNH_2$ (1.43 g, 1.26 mmol) in DMF (40 cm^3) was added dropwise to the solution over 4 hours while stirring. The solution was stirred for 72 hours at 25 °C and filtered under vacuum. The filtrate was added to acetone (2 dm^3) to give a precipitate. The precipitate was isolated by centrifugation and dissolved in water (25 cm^3). The solution was added to acetone (500 cm^3) to reform the precipitate. The precipitate was isolated by centrifugation, dissolved in water (3 cm^3) and purified by column chromatography (Bio-rex 70 (H^+), 10:1 to 0:1 gradient of H_2O:1 mol dm^{-3} ammonia solution) to yield *E*-*p*-β-CD_2az as an orange powder (162 mg, 10 %). R_c = 0.48. ^{1}H NMR: (300 MHz, D_2O) δ 7.96 (s, 1H, Ar H); 5.25 – 5.07 (m, 7H, β-CD H1); 4.26 – 3.17 (m, 42H, β-CD H2-H6). ^{13}C NMR: (125 MHz, D_2O) δ 165.7 (amide C=O), 153.3 (Ar C-C=O), 136.9 (Ar C-H), 130.5 (Ar C-H), 128.7 (Ar C-H), 122.5 (Ar C-H), 102.3 – 101.9 (β-CD C1), 101.4 (β-CD C1), 84.4 (β-CD C4), 81.4 – 81.6 (β-CD C2 – C4), 80.9 (β-CD C2 – C4), 71.9 – 73.3 (β-CD C2, C3, C5), 69.7 (β-CD C2, C3, C5), 60.1 – 59.8 (β-CD C6), 59.2 (β-CD C6). MALDI-TOF MS *m/z:* Calculated $C_{98}H_{148}N_4O_{70}$ ($M + Na^+$) 2523.80, found 2523.83. The spectroscopic data matched that given in the literature.[8]

7.2.1.2 Synthesis of *E*-azobenzene-3,3'-dicarboxylic acid (*E*-*m*-AzCOOH)

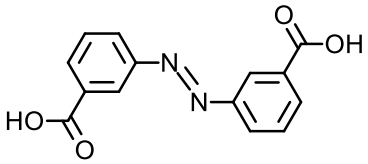

The synthesis of *E*-*m*-AzCOOH followed a modified literature procedure.[6] 3-nitrobenzoic acid (5.0 g, 0.03 mol) was added to a solution of sodium hydroxide (10 g) in water (90 cm^3) and heated to 50 °C. An 80 °C solution of α-*D*-glucose (40 g, 0.2 mol) in water (30 cm^3) was added dropwise to the solution over 40 minutes while stirring vigorously. The solution was stirred for 2 hours at 50 °C. Air was bubbled through the solution for 24 hours at 25 °C while stirring. Acetic acid was then added to the solution until pH 6, to produce a precipitate. The precipitate was filtered and collected (12.7 g). The precipitate was made into a slurry with hot water and hot filtered. The precipitate was hot filtered again and collected (2.8 g). Hot methanol was added to the precipitate to make a slurry. The precipitate was collected by centrifugation to yield *E*-*m*-AzCOOH as an orange solid (2.1 g, 52 %). R_f (4:1 DCM:MeOH) = 0.28. ^{1}H NMR: (300 MHz, DMSO-d_6) δ 8.41 (t, *J* = 1.5 Hz, 2H, Ar H); 8.18 (m, 4H, Ar H); 7.76 (t, *J* = 8.1 Hz, 2H, Ar H).

7.2.1.3 Synthesis of *bis*(6^{A}-deoxy-β-cyclodextrin-6^{A}-yl)-3,3'-aminocarbonyl azobenzene (*E/Z-m*-βCD$_2$az)

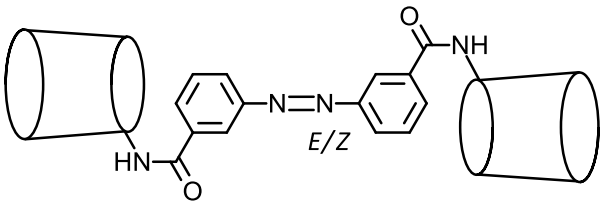

The synthesis of *E/Z-m*-β-CD$_2$az followed a modified literature procedure.[7] 6β-CDNH$_2$ (500 mg, 0.44 mol) was dissolved in DMF (40 cm^3). *N,N'*-Dicyclohexylcarbodiimide (91 mg, 0.44 mmol) and 1-hydroxybenzatriazole (59.5 mg, 0.44 mmol) were added to the solution. *E-m*-AzCOOH (47.5 mg, 0.18 mmol) was added in two portions over a 1 hour period. The solution was stirred for 3 days at 25 °C. The solution was added dropwise to acetone (400 cm^3) and stirred for 2 hours at 25 °C. The resultant precipitate was then isolated by centrifugation. The precipitate was dissolved in water (20 cm^3), added to acetone (200 cm^3) and stirred for 24 hours at 25 °C. The precipitate was isolated by centrifugation. The precipitate was purified by column chromatography (Bio-rex 70 (H^+), 10:1 to 0:1 gradient of H_2O:1 mol dm^{-3} ammonia solution) to yield *E/Z-m*-β-CD$_2$az as an orange powder (153 mg, 28 %) as a mixture of *E* and *Z* isomers (78:22). R_c = 0.35. *E* isomer ^{1}H NMR: (300 MHz, D_2O) δ 8.27 (s, 2H, Ar H); 8.12 (d, *J* = 8.1 Hz, 2H, Ar H), 7.97 (d, *J* = 7.8, 2H, Ar H); 7.75 (t, *J* = 8.1, 2H, Ar H); 5.1 – 4.7 (m, 7H, β-CD H1); 4.2 – 3.0 (m, 42H, β-CD H2 – H6). *Z* isomer ^{1}H NMR: δ(300 MHz, D2O) 7.64 (d, *J* = 8.1 Hz, 2H, Ar H); 7.55 (s, 2H, Ar H); 7.37 (t, *J* = 7.8 Hz, 2H, Ar H); 6.90 (d, *J* = 7.5, 2H, Ar H); 5.1 – 4.7 (m, 7H, β-CD H1); 4.2 – 3.0 (m, 42H, β-CD H2 – H6). ^{13}C NMR: (125 MHz, D_2O) δ 165.76 (amide C=O), 151.7 (C-C=O), 135.8 (Ar C-H), 130.3 (Ar C-H), 129.4 (Ar C-H), 124.8 (Ar C-H), 121.9 (Ar C-H), 111.9 (Ar C-H), 102.3 – 101.9 (β-CD C1), 101.5 (β-CD C1), 84.2 (β-CD C4), 81.7 – 81.4 (β-CD C2 – C4), 80.9 (β-CD C2 – C4), 73.2 – 71.9 (β-CD C2, C3, C5), 69.6 (β-CD C2, C3, C5), 60.0 – 59.7 (β-CD C6), 59.3 (β-CD C6). QTOF MS *m/z:* Calculated $C_{98}H_{148}N_4O_{70}$ (M + Na^+) 2523.80, found 2524.15.

7.2.1.4 Synthesis of 2-amino-benzoic acid

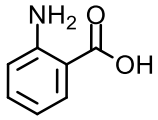

2-Nitrobenzoic acid (5.2 g, 0.03 mol) was added to a solution of sodium hydroxide (10 g) in water (90 cm^3) and heated to 50 °C. A 50 °C solution of α-*D*-glucose (40 g, 0.22 mol) in water (30 cm^3) was added dropwise over 40 minutes while stirring. The solution was stirred for 24 hours at 50 °C. The solution was cooled to 25 °C and air was bubbled through the solution for 24 hours. The solution was acidified using glacial acetic acid and added to acetone (200 cm^3) to form a precipitate. The precipitate was removed by filtration and the filtrate was evaporated to dryness. Dichloromethane was added to the dry solid and the remaining precipitate was removed by filtration. The filtrate was evaporated to dryness and recrystallised with dichloromethane to yield 2-amino-benzoic acid as yellow crystals (1.1 g, 26 %). R_f (1:9 MeOH:DCM) = 0.51. ^{1}H NMR: (300 MHz, DMSO-d_6) δ 9.29 (br, 1H, COOH); 7.74 (d, *J* = 8.1 Hz, 1H, Ar H); 7.29 – 7.20 (m, 1H, Ar H); 6.78 (d, *J* = 8.1 Hz, 1H, Ar H); 6.57 – 6.49 (m, 1H, Ar H).

7.2.1.5 Synthesis of 4-nitrophenyl-2-aminobenzoate

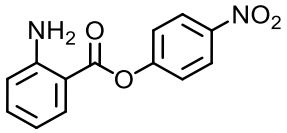

2-Aminobenzoic acid (500 mg, 1.85 mmol) and *N,N'*-dicyclohexylcarbodiimide (762 mg, 3.70 mmol) were dissolved in dichloromethane (25 cm^3) and stirred at room temperature. 4-Nitrophenol (514 mg, 3.70 mmol) was added to the solution and stirred for 24 hours at 25 °C. The solution was purified by squat column chromatography (SiO_2, neat dichloromethane). Fractions containing the ester were combined and washed with 5 % sodium bicarbonate solution to yield 4-nitrophenyl-2-aminobenzoate as a yellow powder (190 mg, 40 %). R_f (1:19 hexane:DCM) = 0.47. ^{1}H NMR: (300 MHz, DMSO) δ 8.34 (d, *J* = 6.9, 2H, Ar H nitrophenyl); 7.93 (d, *J* = 8.1 Hz, 1H, Ar H); 7.55 (d, *J* = 6.6 Hz, 2H, Ar H nitrophenyl); 7.36 (t, *J* = 7.5 Hz, 1H, Ar H); 6.84 (d, *J* = 8.7 Hz, 1H Ar H); 6.62 (t, *J* = 6.9 Hz, 1H, Ar H).

7.2.1.6 Synthesis of (6^A-deoxy-β-cyclodextrin-6^A-yl)-4-nitrophenyl-2-aminobenzoate (β-CDab)

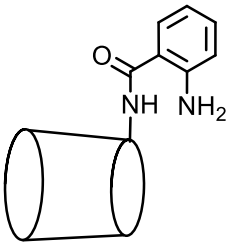

To a solution of 6β-CDNH$_2$(500 mg, 0.44 mmol) in pyridine (15 cm^3) at 25 °C was added 4-nitrophenyl-2-aminobenzoate (92 mg, 0.36 mmol) in two portions over 1 hour. The reaction mixture was then stirred for 48 hours at 25 °C. The mixture was then added dropwise to acetone (150 cm^3) with vigorous stirring. The resultant precipitate was collected by centrifugation and dissolved in water (10 cm^3). The solution was added dropwise to acetone (200 cm^3) and stirred for 24 hours 25 °C. The precipitate was collected by centrifugation and purified by column chromatography (Bio-rex 70 (H+), water and 1 mol dm^{-3} ammonia solution) to yield β-CDab as a pale yellow powder (120 mg, 26 %). R_c = 1.2. ^{1}H NMR: (300 MHz, D_2O) δ 7.47 (d, *J* = 8.1 Hz, 1H, Ar H); 7.37 (t, *J* =7.8 Hz, 1H, Ar H); 6.91 (d, *J* = 8.1 Hz, 1H, Ar H); 6.86 (t, *J* = 8.1 Hz, 1H, Ar H), 5.15 – 5.03 (m, 7H, β-CD H1); 4.11 – 3.9 (m, 42H, β-CD H2 – H6). ^{13}C NMR: (500 MHz, DMSO) δ 169.1 (amide C=O), 149.5 (Ar C-NH$_2$), 131.6 (Ar C-C=O), 128.2 (Ar C-H), 116.2 (Ar C-H), 114.9 (Ar C-H), 114.6 (Ar C-H), 102.4 – 102.0 (β-CD C1), 81.9 – 81.4 (β-CD C4), 73.1 – 71.1 (β-CD C2, C3, C5), 60.2 – 59.2 (β-CD C6). QTOF MS *m/z:* Calculated $C_{49}H_{76}N_2O_{35}$ (M + H$^+$) 1253.42, found 1253.60.

7.2.2 Sample Preparation

7.2.2.1 Preparation of solutions for photoisomerisation studies by UV-vis absorption spectroscopy

Solutions of *p*-βCD$_2$az (2.5×10^{-3} mol dm^{-3}) and *m*-βCD$_2$az (5.0×10^{-3} mol dm^{-3}) were prepared in aqueous phosphate buffer (pH 7.0, I = 0.10 mol dm^{-3}). Samples were allowed to equilibrate at the thermostatted probe temperature of 298.2 K for 10 minutes prior to recording the spectra.

7.2.2.2 Preparation of solutions for photoisomerisation studies by ^{1}H NMR spectroscopy

Solutions of *p*-βCD$_2$az (2.0×10^{-3} mol dm^{-3}) and *m*-βCD$_2$az (2.0×10^{-3} mol dm^{-3}) were prepared in D_2O phosphate buffer (pD 7.0, I = 0.10 mol dm^{-3}). Samples were irradiated for 1 hour in a 1 cm path length quartz cell with at 300 – 355 nm or > 400 nm using a lamp with cutoff filters.

7.2.2.3 Preparation of solutions for complexation studies by 2D ^{1}H ROESY NMR spectroscopy

Solutions of ADC (1.0×10^{-2} mol dm^{-3}) were prepared in the presence of one molar equivalent of β-CD groups of *p*-βCD$_2$az and *m*-βCD$_2$az in D_2O phosphate buffer (pD 7.0, I = 0.10 mol dm^{-3}).

7.2.2.4 Preparation of solutions for complexation and photoisomerisation studies by ^{1}H NMR spectroscopy

Solutions of ADC (1.2×10^{-2} mol dm^{-3}) were prepared in the presence of one molar equivalent of β-CD groups of *p*-βCD$_2$az and *m*-βCD$_2$az in D_2O phosphate buffer (pD 7.0, I = 0.10 mol dm^{-3}). Samples were irradiated for 1 hour in a 1 cm path length quartz cell with either UV or visible light using a lamp with cutoff filters.

7.3 Chapter 3 Experimental

7.3.1 Sample Preparation

7.3.1.1 Preparation of solutions for complexation studies by 2D ^{1}H ROESY NMR spectroscopy

Solutions of CV^+, RB and EO^- (5.0×10^{-3} mol dm^{-3}) were prepared in the presence of one molar equivalent of native β-CD, β-CDab or *E*-*p*-βCD_2az in D_2O phosphate buffer (pH 7.0, I = 0.10 mol dm^{-3}).

7.3.1.2 Preparation of solutions for complexation studies by UV-vis spectroscopy

Stock solutions of CV^+ (2.5×10^{-5} mol dm^{-3}), RB (2.0×10^{-5} mol dm^{-3}) and EO^- (4.0×10^{-5} mol dm^{-3}) were prepared in aqueous phosphate buffer (pH 7.0, I = 0.10 mol dm^{-3}) and diluted to 8.0×10^{-6} mol dm^{-3}, 8.0×10^{-6} mol dm^{-3} and 2.0×10^{-5} mol dm^{-3}, respectively. Samples were analysed at four different temperatures ranging from 278.2 K to 308.2 K in 10 K increments. Samples were equilibrated at each temperature for 10 minutes before measurement. Stock solutions of hosts β-CD (1.2×10^{-2} mol dm^{-3} for EO^- only), *E*-*p*-βCD_2az (1.0×10^{-3} mol dm^{-3}, 3.0×10^{-3} mol dm^{-3} and 6.0×10^{-3} mol dm^{-3}) and β-CDab (8.0×10^{-3} mol dm^{-3}, 1.4×10^{-2} mol dm^{-3} and 1.0×10^{-2} mol dm^{-3}) were titrated into the CV^+, RB and EO^- solutions, respectively. Recordings were taken after sequential injections (10 mm^3) of host, while stirring, into the dye and reference solutions. A total of 35-40 injections were made for each system, with 1 minute of stirring between injections.

7.4 Chapter 4 Experimental

7.4.1 Sample Preparation

7.4.1.1 Preparation of solutions for complexation studies by ^{1}H NMR spectroscopy

Solutions of H_2TSPP^{4-}, $H_3TCPP^{3-}/H_2TCPP^{4-}$, H_2TMAP^{4+} and H_2TMPyP^{4+} (4.8×10^{-3} mol dm^{-3}) were prepared alone and with one molar equivalent of β-CD and two molar equivalents of β-CDab in D_2O phosphate buffer (pD 7.0, I = 0.10 mol dm^{-3}). Solutions of β-CD (4.8×10^{-3} mol dm^{-3}) and β-CDab (9.6×10^{-3} mol dm^{-3}) were also prepared.

7.4.1.2 Preparation of solutions for complexation studies by 2D ^{1}H ROESY NMR spectroscopy

Solutions of H_2TSPP^{4-}, $H_3TCPP^{3-}/H_2TCPP^{4-}$, H_2TMAP^{4+} and H_2TMPyP^{4+} (4.8×10^{-3} mol dm^{-3}) were prepared in the presence of one molar equivalent of β-CD and two molar equivalent of β-CDab in D_2O phosphate buffer (pD 7.0, I = 0.10 mol dm^{-3}).

7.4.1.3 Preparation of solutions for complexation studies by UV-vis spectroscopy

Stock solutions of H_2TSPP^{4-} (2.4×10^{-4} mol dm^{-3}), $H_3TCPP^{3-}/H_2TCPP^{4-}$ (4.0×10^{-5} mol dm^{-3}) H_2TMAP^{4+} (2.5×10^{-4} mol dm^{-3}) and H_2TMPyP^{4+} (5.0×10^{-4} mol dm^{-3}) were prepared in aqueous phosphate buffer (pH 7.0, I = 0.10 mol dm^{-3}) and diluted to the required concentrations. Samples were analysed at four different temperatures ranging from 278.2 K to 308.2 K in 10 K increments. Samples were equilibrated at each temperature for 10 minutes before measurement. Stock solutions of hosts β-CD (1.1×10^{-2} mol dm^{-3}, 4.5×10^{-3} mol dm^{-3}, 1.3×10^{-2} mol dm^{-3} and 1.2×10^{-2} mol dm^{-3}) and β-CDab (1.6×10^{-3} mol dm^{-3}, 1.8×10^{-3} mol dm^{-3}, 2.0×10^{-3} mol dm^{-3} and 1.6×10^{-3} mol dm^{-}) were titrated into the H_2TSPP^{4-}, $H_3TCPP^{3-}/H_2TCPP^{4-}$, H_2TMAP^{4+} and H_2TMPyP^{4+} solutions, respectively. Recordings were taken after sequential injections (10 mm^3) of host, while stirring, into the porphyrin and reference solutions. A total of 35 injections were made for each system.

7.5 Chapter 5 Experimental

7.5.1 Syntheses

The synthesis of 1-(4-nitrophenylcarbonyl)adamantane (ADnp),[9] *N*-(2,aminoethyl)-adamantane-1-carboxyamide (ADen),[10] 1-(6-aminohexyl)adamantane-1-carboxyamide (ADhn)[11] and 1-(12-aminododecyl) adamantane-1-carboxyamide (ADddn)[11] followed literature methods.

7.5.1.1 General methods for preparing modified PAAs

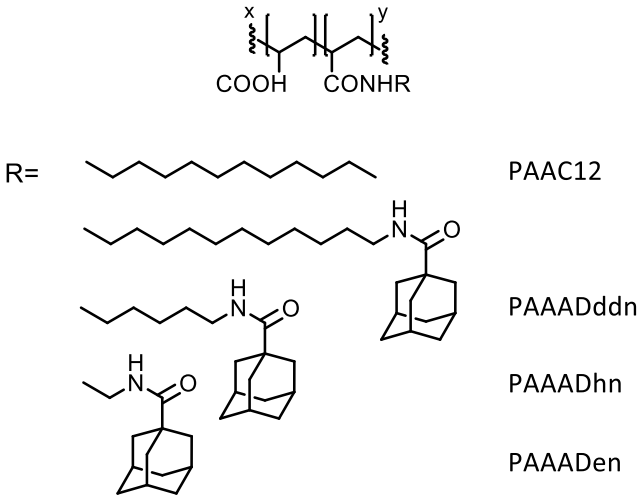

The synthesis of PAAADen, PAAADhn, PAAADddn and PAAC12 followed literature methods.[11,12] A solution of poly(acrylic acid) (1 g, 13.88 mmol) in *N*-methyl-2-pyrrolidone (35 cm^3) was stirred for 48 hours at 60°C. A solution of either ADen, ADhn, ADddn or C12 (0.42 mmol) in *N*-methyl-2-pyrrolidone (3.5 cm^3) and a solution of *N,N'*-dicyclohexylcarbodiimide (112 mg, 0.54 mmol) in *N*-methyl-2-pyrrolidone (3.5 cm^3) were added dropwise to the PAA solution. The solution was stirred for 96 hours at 60°C. The solution was cooled to 25 °C and 40 wt% sodium hydroxide solution (35 cm^3) was added to form a precipitate. The solution was filtered and washed with *N*-methyl-2-pyrrolidone (2 × 15 cm^3) and methanol (20 cm^3). The precipitate was dissolved in water (20 cm^3) and added dropwise to methanol (200 cm^3) to reform the precipitate (three times). The precipitate was collected by vacuum filtration and dissolved in water (20 cm^3) and dialysed (Spectra/Por 3 tubing, molecular weight cutoff 3500 g mol^{-1}) against deionised water until the conductivity of the water outside the tube remained constant. The final solution was lyophilised to yield a white powder.

The percentage substitution for PAAADen, PAAADhn and PAAADddn was determined by ^{1}H NMR spectroscopy using literature methods[13] according to Equation 7.1,

$$\text{substitution (mol \%)} = \frac{\text{A1}}{\text{A2} - \frac{\text{A1}}{4}(2m+15)} \times 100 \qquad (7.1)$$

where A1 is the area of integration for the N-CH_2-C groups (connected to amide or amine group) of the alkyl tether, A2 is the area of integration of the CH_2 groups of the PAA backbone as well as the C-CH_2-C (not connected to amide or amine groups) and AD groups of the substituent and *m* is the number C-CH_2-C groups (not connected to amide or amine groups) of the alkyl tether.

The percentage substitution for PAAC12 was determined by ^{1}H NMR spectroscopy using literature methods[13] according to Equation 7.2,

$$\text{substitution (mol \%)} = \frac{\text{A3}}{\text{A2} - \frac{2m\text{A3}}{3}} \times 100 \qquad (7.2)$$

where A3 is the area of integration of the CH_3 group of the C12 substituent. The percentage substitution for PAAADen, PAAADhn, PAAADddn and PAAC12 were determined to be 2.0 ± 0.2 %, 2.7 ± 0.3 %, 2.0 ± 0.2 % and 1.8 ± 0.2 %, respectively.

The molecular weight of each compound was determined by Equation 7.3, according to literature methods.[14]

$$\text{MW(modified PAA)} = \frac{(\text{M1} \times (100 - \%\text{subs})) + (\text{M2} \times \%\text{subs})}{\%\text{subs}} \qquad (7.3)$$

where M1 is the molecular mass of $CH_2CHCOO^-Na^+$, M2 is the molecular mass of the substituent (either ADen, ADhn, ADddn or C12) and %subs is the percentage substitution of the modified PAA. The molecular weights of PAAADen, PAAADhn, PAAADddn and PAAC12 were determined to be 3315.7 g mol^{-1}, 3371.7 g mol^{-1}, 3455.9 g mol^{-1} and 3278.3 g mol^{-1}, respectively.

7.5.2 Sample Preparation

7.5.2.1.1 Preparation of solutions for complexation studies by 2D ^{1}H NOESY NMR spectroscopy

Solutions of 0.98 wt% PAAADen ([AD] = 2.0×10^{-3} mol dm^{-3}), 0.74 wt% PAAADhn ([AD] = 2.0×10^{-3} mol dm^{-3}), 1.00 wt% PAAADddn ([AD] = 2.0×10^{-3} mol dm^{-3}) and 1.07 wt% PAAC12 ([C12] = 2.0×10^{-3} mol dm^{-3}) were prepared alone and with β-CD (3.0×10^{-3} mol dm^{-3}), β-CDab (3.0×10^{-3} mol dm^{-3}), *E*-*p*-βCD$_2$az (1.5×10^{-3} mol dm^{-3}) or *E/Z*-*m*-βCD$_2$az (1.5×10^{-3} mol dm^{-3}) in D_2O phosphate buffer (pD 7.0, I = 0.10 mol dm^{-3}).

7.5.2.1.2 Preparation of solutions for complexation studies by ITC

Stock solutions of β-CD (7.3×10^{-3} mol dm^{-3}), β-CDab (4.0×10^{-3} mol dm^{-3}), *E*-*p*-βCD$_2$az (2.0×10^{-3} mol dm^{-3}) and *E/Z*-*m*-βCD$_2$az (2.0×10^{-3} mol dm^{-3}) were prepared in aqueous phosphate buffer (pH 7.0, I = 0.10 mol dm^{-3}). The concentration of each polymer was varied, as indicated in the Figure captions in Chapter 5 (Figure 5.24 – Figure 5.39). Aliquots (10 mm^3) of host were added to a solution of the substituted PAA (1.46 cm^3) using a computer-controlled micro-syringe at 210 s intervals. The concentration corrections for displaced volume effects, which occur with each injection, were calculated by Origin 7.0 MicroCal protocol.[1]

7.6 Chapter 6 Experimental

7.6.1 Syntheses

The synthesis of 6^A-O-*p*-toluenesulfonyl-β-cyclodextrin (6β-CDTs),[3] 6^A-amino-6^A-deoxy-β-cyclodextrin (6β-$CDNH_2$)[4,5] and 2-(1,4,7,10,13-pentaoxa-16-azacyclooctadecan-16-yl)acetic acid[15] (aza-18-crown-6-COOH) was achieved by literature methods.

7.6.1.1 Synthesis of (*E*)-*N*-(6^A-deoxy-β-cyclodextrin-6^A-yl)-4-aminocarbonyl-4'-carboxyazobenzene (β-CDaz)

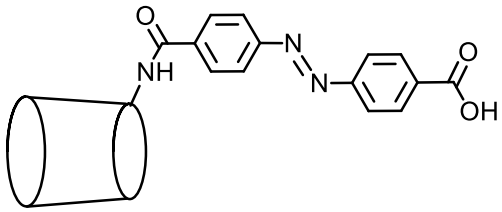

The synthesis of β-CDaz followed a modified literature procedure.[7] 4,4-Dicarboxyazobenzene (1.0 g, 3.70 mmol) was dissolved in anhydrous DMF (200 cm^3). 1-Hydroxybenzatriazole (0.18 g, 1.26 mmol) and *N,N'*-dicyclohexylcarbodiimide (0.26 g, 1.26 mmol) were added to the solution. A solution of 6β-$CDNH_2$ (1.4 g, 1.2 mmol) in DMF (40 cm^3) was added dropwise to the solution over 4 hours while stirring. The solution was stirred for 72 hours at 25 °C and filtered under vacuum. The filtrate was added to acetone (2 dm^3) to give a precipitate. The precipitate was isolated by centrifugation and dissolved in water (25 cm^3). The solution was added to acetone (500 cm^3) to reform the precipitate. The precipitate was isolated by centrifugation and purified by column chromatography (Bio-rex 70 (H^+), water and 1 mol dm^{-3} ammonia solution) to yield β-CDaz as an orange powder (129 mg, 21 %). R_c = 1.19. ^{1}H NMR (600MHz): δ (D_2O) 8.37 (d, *J* = 7.8Hz, 2H, ArH); 7.95 (d, *J* = 8.4Hz, 2H, ArH); 7.75 (d, *J* = 7.2Hz, 2H, ArH); 7.60 (d, *J* = 7.8Hz, 2H, ArH); 5.21 – 4.97 (m, 7H, β-CD H1); 4.21 – 2.91 (m, 42H, β-CD H2 – H6). ^{13}C NMR (125 MHz): (DMSO-d_6) δ 165.6 (COOH), 153.2 (amide C=O), 136.7 (Ar C-C=O), 130.3 (Ar C-H), 128.5 (Ar C-H), 122.4 (Ar C-H) 122.3 (Ar C-H), 102.4 – 101.9 (β-CD C1), 101.3 (β-CD C1), 84.4 (β-CD C4), 81.7 – 81.4 (β-CD C2 – C4), 80.7 (β-CD C2, C3, C5), 73.3 – 71.9 (β-CD C2, C3, C5), 60.2 – 59.8 (β-CD C6), 59.1 (β-CD C6). MALDI-TOF MS *m/z:* Calculated $C_{56}H_{79}N_3O_{37}$ ($M + Na^+$) 1408.43, found 1408.45.

7.6.1.2 Synthesis of (*E*)-N-(6^{A}-deoxy-β-cyclodextrin-6^{A}-yl)-4-aminocarbonyl-4-(3-aminopropylaminocarbonyl) azobenzene (β-CDazpr)

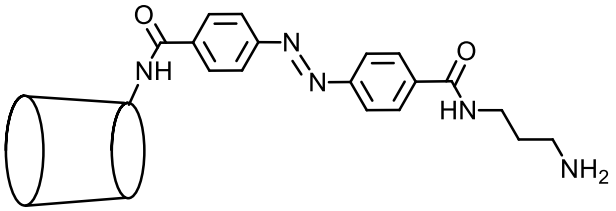

(*E*)-*N*-(6^{A}-Deoxy-β-cyclodextrin-6^{A}-yl)-4-aminocarbonyl-4'-carboxyazobenzene (100 mg, 0.07 mmol), 1,3-diaminopropane (0.06 mL, 0.72 mmol) and BOP reagent (95 mg, 0.22 mmol) were added to DMF (10 cm^3). The solution was stirred under nitrogen and triethylamine (0.21 cm^3, 0.22 mmol) was added. The solution was stirred under nitrogen for 72 hours at 25 °C. The solution was added to acetone (150 cm^3) and centrifuged to collect a precipitate. The precipitate was dissolved in water (5 cm^3) and added to acetone (200 cm^3) and centrifuged to collect a precipitate. The precipitate was purified by column chromatography (Bio-rex 70 (H^+), water and 0.5 mol dm^{-3} ammonia solution) to yield β-CDazpr as a white precipitate (70 mg, 70 %). R_c: 0.75. ^{1}H NMR: (300 MHz, D_2O) δ 8.20 (d, *J* = 8.7 Hz, 2H, Ar H); 8.03 (d, *J* = 8.4 Hz, 2H, Ar H); 7.79 (d, *J* = 8.7Hz, 2H, Ar H); 7.61 (d, *J* = 8.4 Hz, 2H, Ar H); 5.15 – 4.98 (m, 7H, β-CD H1); 4.06 – 3.16 (m, 42H, β-CD H2 – H6); 3.14 (t, *J* = 7.8 Hz, 4H, pr H5, H7); 2.08 (quintet, *J* = 7.5 Hz, 2H, pr H6). ^{13}C NMR (125 MHz): (DMSO-d_6) δ 153.2 (amide C=O), 134.0 (Ar C-C=O), 128.6 (Ar C-H), 128.5 (Ar C-H), 122.6 (Ar C-H), 122.4 (Ar C-H), 102.3 – 101.9 (β-CD C1), 81.6 – 81.4 (β-CD C2 – C4), 73.1 – 72.0 (β-CD C2, C3, C5), 60.1 – 59.8 (β-CD C6), 37.3 (pr C-H), 32.8 (pr C-H), 29.0 (pr C-H). ESI MS *m/z*: Calculated $C_{59}H_{87}N_5O_{36}$ ($M + H^+$) 1442.52, found 1442.30.

7.6.1.3 Attempted synthesis of [(*E*)-*N*-(6^A-deoxy-β-cyclodextrin-6^A-yl)-4-aminocarbonyl-4'-(3-(1-aminocarbonyl-adamantane) propylaminocarbonyl)azobenzene (monomer 2)

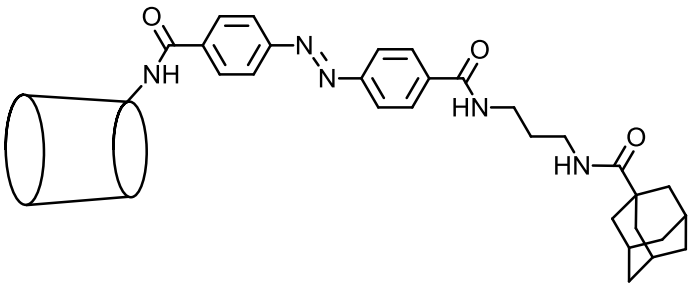

(*E*)-*N*-(6^A-deoxy-β-cyclodextrin-6^A-yl)-4-aminocarbonyl-4-(3-aminopropylaminocarbonyl)azobenzene (413 mg, 28.5 mmol) was dissolved in DMF (40 cm^3). Triethylamine was added to the solution until pH 9 was reached. 1-adamantanecarbonyl chloride (57 mg, 28.5 mmol) was added to the solution and the suspension was stirred for 4 days at 25 °C. The solution was added to acetone (100 cm^3) and stirred for 2 hours at 25 °C. The resultant precipitate was collected by centrifugation. The precipitate was purified by column chromatography (Bio-rex 70 (H^+), water and 1 mol dm^{-3} ammonia solution) to yield monomer **2** as an orange powder (24 mg, 5 %). R_c = 1.2. ^{1}H NMR: δ(300 MHz, D_2O) 8.07 (m, 8H, Ar H), 5.89 – 5.60 (m, 14H, β-CD OH$^{2-3}$), 4.97 – 4.78 (m, 7H, β-CD H1), 4.51 – 4.43 (m, 14H, β-CD OH^6), 3.66 – 3.13 (m, 48H, β-CD H2 – H6, pr H5 – H7), 1.96 (m, 3H, AD H10), 1.77 (m, 6H, AD H8), 1.65 (m, 6H, AD H9). Calculated $C_{70}H_{101}N_5O_{37}$ (M + H^+) 1604.63, found 1603.85. The title compound was not confirmed by mass spectrometry.

7.7 References

(1) Origin Lab, Northampton, MA, 01060, USA

(2) *Biochemist Handbook / Compiled by One Hundred and Seventy-One Contributors*; Long, C., Ed.; Spon, London, **1971**.

(3) Brady, B.; Lynam, N.; O'Sullivan, T.; Ahern, C.; Darcy, R. *Org. Synth.* **2000**, *77*, 220.

(4) Kretschmann, O.; Choi, S. W.; Miyauchi, M.; Tomatsu, I.; Harada, A.; Ritter, H. *Angew. Chem.* **2006**, *45*, 4361.

(5) Brown, S. E.; Coates, J. H.; Coghlan, D. R.; Easton, C. J.; Vaneyk, S. J.; Janowski, W.; Lepore, A.; Lincoln, S. F.; Luo, Y.; May, B. L.; Schiesser, D. S.; Wang, P.; Williams, M. L. *Aust. J. Chem.* **1993**, *46*, 953.

(6) Liu, D. B.; Xie, Y. Y.; Shao, H. W.; Jiang, X. Y. *Angew. Chem.* **2009**, *48*, 4406.

(7) Dawson, R. E.; Lincoln, S. F.; Easton, C. J. *Chem. Commun.* **2008**, 3980.

(8) Hamon, F.; Blaszkiewicz, C.; Buchotte, M.; Banaszak-Leonard, E.; Bricout, H.; Tilloy, S.; Monflier, E.; Cezard, C.; Bouteiller, L.; Len, C.; Djedaini-Pilard, F. *Beilstein J. Org. Chem.* **2014**, *10*, 2874.

(9) May, B. L.; Clements, P.; Tsanaktsidis, J.; Easton, C. J.; Lincoln, S. F. *J. Chem. Soc. Perkin Trans. 1 1* **2000**, 463.

(10) Li, L.; Guo, X.; Wang, J.; Liu, P.; Prud'homme, R. K.; May, B. L.; Lincoln, S. F. *Macromolecules* **2008**, *41*, 8677.

(11) Guo, X. H.; Wang, J.; Li, L.; Pham, D. T.; Clements, P.; Lincoln, S. F.; May, B. L.; Chen, Q. C.; Zheng, L.; Prud'homme, R. K. *J. Polym. Sci. Part B Polym. Phys.* **2010**, *48*, 1818.

(12) Hanh-Trang, N.; Duc-Truc, P.; Lincoln, S. F.; Wang, J.; Guo, X.; Easton, C. J.; Prud'homme, R. K. *Polym. Chem.* **2013**, *4*, 820.

(13) Guo, X. H.; Abdala, A. A.; May, B. L.; Lincoln, S. F.; Khan, S. A.; Prud'homme, R. K. *Macromolecules* **2005**, *38*, 3037.

(14) McTernan, H. L., From Polymers to Porphyrins: Supramolecular Control Asserted by Cyclodextrin Oligomers, PhD Thesis, University of Adelaide, **2016**.

(15) Lock, J. S., Cyclodextrins : molecular wheels for supramolecular chemistry, PhD Thesis, University of Adelaide, **2004**.

CHAPTER 8

Conclusion

8.1 Conclusion and Future Directions

This thesis demonstrated the use of azobenzene-modified β-cyclodextrin (CD) compounds on the oligomeric, material and molecular device scale. CDs are commonly used in these areas of chemistry, as examined in Chapter 1, but identical or similar compounds are seldom used across multiple facets of chemistry. The studies herein illustrated that simply design CD systems may be applied creatively as host-guest systems on the molecular level, components of polymeric hydrogels and as the basis of molecular muscles.

Chapter 2 described the synthesis of azobenzene-modified β-CD compounds, differing by the position of the β-CD group towards the azobenzene, either at the *para*- (*p*-β-CD_2az), *meta*- (*m*-β-CD_2az) or *ortho*-position (*o*-β-CD_2az). The *para*- and *meta*-substituted isomers were successfully synthesised, however, synthesis of the *ortho*-isomer was not successful, yielding instead an aminophenyl-modified β-CD monomer (β-CDab). The photochemical properties of *p*-β-CD_2az and *m*-β-CD_2az were examined by UV-vis and NMR spectroscopy, which showed differences in the photostationary states.

Chapters 3 and 4 examined the host-guest properties of *E*-*p*-β-CD_2az, β-CDab and native β-CD using model dye systems (crystal violet, rhodamine B and ethyl orange) and porphyrins, respectively. The aim of this research was to explore the host-guest properties of the hosts on the oligomeric level, demonstrating their potential use in biological systems. The effect of β-CD modification was examined in both chapters by comparing complexation constants and thermodynamic parameters of each host-guest system.

Chapter 5 explored the use of *E*-*p*-β-CD_2az, *E/Z*-*m*-β-CD_2az and β-CDab as components in polymeric hydrogels. Adamantane- and alkyl-substituted poly(acrylate)s were synthesised and complexed with the β-CD hosts, creating polymeric networks that could serve as hydrogels. Each host-polymer combination was examined on the molecular scale through determination of complexation constants and thermodynamic parameters, and on the macromolecular scale, through rheological studies. The molecular-scale interactions between each host and polymer could be used to predict the rheological properties.

Chapter 6 described the attempted synthesis of a molecular muscle, based upon an azobenzene-modified β-CD compound, the structure of which had clear similarities to *p*-β-CD_2az and *m*-β-CD_2az. Unfortunately, the synthesis of the molecular muscle was not successful.

Each chapter in the thesis featured identical or similar modified β-CD compounds, demonstrating the potential for simple β-CD systems to be applied across multiple hierarchies of chemistry. As such, the future of this research can be taken in multiple directions. A logical next step would be to apply the azobenzene-modified β-CD compounds in other aspects of chemistry, again demonstrating their versatility. However, future research could also aim to gain further insight into the use of β-CD compounds as hosts in biological systems or in hydrogel design. Research could also be performed to fully synthesise an operable molecular device.